

OPTIMIZATION OF RIDE COMFORT FOR VEHICLES EQUIPPED WITH
PASSIVE AND ACTIVE HYDRO-PNEUMATIC SUSPENSIONS

A THESIS SUBMITTED TO
THE GRADUATE SCHOOL OF NATURAL AND APPLIED SCIENCES
OF
MIDDLE EAST TECHNICAL UNIVERSITY

BY

FERHAT SAĞLAM

IN PARTIAL FULFILLMENT OF THE REQUIREMENTS
FOR
THE DEGREE OF DOCTOR OF PHILOSOPHY
IN
MECHANICAL ENGINEERING

FEBRUARY 2016

Approval of the thesis:

**OPTIMIZATION OF RIDE COMFORT FOR VEHICLES EQUIPPED WITH
PASSIVE AND ACTIVE HYDRO-PNEUMATIC SUSPENSIONS**

submitted by **FERHAT SAĞLAM** in partial fulfillment of the requirements for the degree of **Doctor of Philosophy in Mechanical Engineering Department, Middle East Technical University** by,

Prof. Dr. Gülbin Dural Ünver
Dean, Graduate School of **Natural and Applied Sciences**

Prof. Dr. R.Tuna Balkan
Head of Department, **Mechanical Engineering**

Prof. Dr. Y. Samim Ünlüsoy
Supervisor, **Mechanical Engineering Dept., METU**

Examining Committee Members:

Prof. Dr. Tuna Balkan
Mechanical Engineering Dept., METU

Prof. Dr. Y. Samim Ünlüsoy
Mechanical Engineering Dept., METU

Assoc. Prof. Dr. Yiğit Yazıcıoğlu
Mechanical Engineering Dept., METU

Assoc. Prof. Dr. S. Çağlar Başlamışlı
Mechanical Engineering Dept., Hacettepe University

Asst. Prof. Dr. Kutluk Bilge Arıkan
Mechatronic Engineering Dept., Atılım University

Date:

02.02.2016

I hereby declare that all information in this document has been obtained and presented in accordance with academic rules and ethical conduct. I also declare that, as required by these rules and conduct, I have fully cited and referenced all material and results that are not original to this work.

Name, Last name: Ferhat SAĞLAM

Signature :

ABSTRACT

OPTIMIZATION OF RIDE COMFORT FOR VEHICLES EQUIPPED WITH PASSIVE AND ACTIVE HYDRO-PNEUMATIC SUSPENSIONS

Sağlam, Ferhat

Ph.D., Department of Mechanical Engineering

Supervisor: Prof. Dr. Y. Samim Ünlüsoy

February 2016, 443 pages

The main objective of this study is the optimization of ride comfort performance of vehicles equipped with Hydro-Pneumatic (HP) suspension systems. In order to improve ride comfort performance together with handling behavior as a constraint, active-passive, and unconnected-interconnected HP suspension systems are included in the study.

The basic HP suspension model is developed and validated by experiments. Various HP suspension systems of increasing complexity are modeled, and their dynamic characteristics are analyzed and compared with each other. Nonlinear models of the active HP suspension system are derived and nonlinear active suspension controllers are designed in order to improve ride comfort, to control vehicle attitude, and to get safe driving conditions, using a quarter car model with active HP suspension system. Similarly, modeling and active suspension control of the half and full vehicle models with active HP suspension systems are carried out. A nonlinear feedback control method, State Dependent Riccati Equation (SDRE) control, is used for the design of

the active controllers. Performance of the active suspension systems have been examined by time and frequency domain simulations. Simulation results show that, the active HP suspension systems improve ride comfort and vehicle attitude performance together with vehicle handling characteristics.

As the next step of the study, analysis and design of the interconnected HP suspension systems for multi-axle vehicles are performed. Interconnections are enumerated for pitch plane of a three-axle vehicle and then, various interconnection layouts for roll, pitch, and coupled roll and pitch planes of the three axle-vehicles are examined. Stiffness and damping characteristics of different interconnections are obtained and compared with each other. Performances of vehicles with interconnected HP suspension system are evaluated by simulations. Simulation results have shown that, interconnected HP suspension systems improve vehicle handling considerably, together with slightly degraded ride comfort performance, as compared to the unconnected HP suspension systems. A general interconnected suspension design guideline is developed for the systematic parametric design of the HP suspension system for multi-axle vehicles.

Finally, suspension system parameters for a three-axle vehicle equipped with unconnected and interconnected HP suspension systems are optimized for ride comfort with handling constraint. Optimization results show that, even though both unconnected and interconnected HP suspension systems improve the ride comfort, interconnected HP suspension system results in additional performance improvement in ride comfort and vehicle handling as compared to the unconnected HP suspension system, due to increased stiffness and damping performance in the roll and pitch planes.

Keywords: Hydro-Pneumatic Suspension, Ride Comfort, Active Suspension, Nonlinear Control, State Dependent Riccati Equation Control, Suspension Optimization, Interconnected Suspension

ÖZ

PASİF VE AKTİF HİDROPNÖMATİK SÜSPANSİYONLU ARAÇLARIN SÜRÜŞ KONFORUNUN OPTİMİZASYONU

Sağlam, Ferhat

Doktora, Makina Mühendisliği Bölümü

Tez Yöneticisi: Prof. Dr. Y. Samim Ünlüsoy

Şubat 2016, 443 sayfa

Bu çalışmanın temel amacı, aktif ve pasif Hidro-Pnömatik (HP) süspansiyon sistemlerine sahip araçların sürüş konforu için optimizasyonudur. Sürüş konforu performansı iyileştirilirken, sürüş güvenliliği araç yol tutuş performansı sınırlandırılarak ve iyileştirilerek göz önüne alınmıştır. İyileştirilmiş sürüş konforu performansını elde etmek için aktif-pasif ve bağlı-bağımsız süspansiyon sistemleri kullanılmıştır.

Temel HP süspansiyon modeli geliştirilmiş ve deneylerle doğrulanmıştır. Değişik tiplerdeki HP süspansiyon sistemleri modellenmiş, dinamik karakteristikleri incelenmiş ve birbirleri ile karşılaştırılmıştır. Doğrusal olmayan aktif HP süspansiyon sistemi türetilmiş ve sürüş konforunu, araç yükseklik kontrolünü ve güvenli sürüş durumunu iyileştirmek için çeşitli doğrusal olmayan aktif süspansiyon kontrolcileri tasarlanmıştır. Benzer şekilde, aktif HP süspansiyonlara sahip yarım ve tam araç modellerinin modellenmesi ve aktif süspansiyon kontrolü tasarımı gerçekleştirilmiştir. Aktif kontrolcülerin tasarlanmasında, doğrusal olmayan geribeslemeli bir kontrol yöntemi olan Durum Bağımlı Riccati Denklemi kontrolü

kullanılmıştır. Aktif süspansiyonların performansı zaman ve frekans tabanlı benzetimlerle incelenmiştir. Benzetim sonuçları, aktif süspansiyonun, yol tutuş performansı ile birlikte sürüş konforu ve araç yükseklik performanslarını iyileştirdiğini göstermiştir.

Çalışmanın ikinci basamağı olarak, çok akslı araçlar için bağlı HP süspansiyon sistemlerinin analizi ve tasarımı gerçekleştirilmiştir. Önce üç akslı bir aracın yunuslama düzlemi için değişik bağlantı yerleşimleri belirtilmiş ve daha sonra aracın yalpa, yunuslama ve birleşik yalpa ve yunuslama düzlemleri için çeşitli bağlantı şekilleri incelenmiştir. Bu çeşitli bağlı süspansiyonların direngenlik ve sönümleme karakteristikleri elde edilmiş ve birbirleriyle karşılaştırılmıştır. Bağlı HP süspansiyon sistemine sahip aracın performansı benzetim çalışmalarıyla incelenmiştir. Benzetim sonuçları, bağlı HP süspansiyonun, aracın yol tutuş performansını önemli ölçüde iyileştirdiğini ve bağımsız HP süspansiyona göre azda olsa bozulmuş araç sürüş konforu performansına sahip olduğunu göstermiştir. Çok akslı araçlar için bağlı HP süspansiyonların parametrik tasarımları için genel bir bağlı süspansiyon tasarım rehberi geliştirilmiştir.

En son olarak, bağlı ve bağımsız HP süspansiyonlara sahip araçların süspansiyon parametreleri sürüş konforu performansı, yol tutuş sınırlamasıyla birlikte eniyileştirilmiştir. Eniyileştirme sonuçları, hem bağımsız hem de bağımlı süspansiyonların sürüş konforunu iyileştirmesine rağmen, bağlı süspansiyon sisteminin yalpa ve yunuslama düzlemindeki artan direngenlik ve sönümleme performansı sebebiyle ek bir sürüş konforu performansı artışına olanak verdiğini göstermiştir.

Anahtar Kelimeler: Hidro-Pnömatik Süspansiyon, Sürüş Konforu, Aktif Süspansiyon, Doğrusal Olmayan Kontrol, Durum Bağımlı Riccati Denklemi Kontrolü, Süspansiyon Eniyileştirmesi, Bağlı Süspansiyon

To my family,

ACKNOWLEDGEMENTS

First, I would like to express my gratitude to my Supervisor Prof. Dr. Y. Samim Ünlüsoy for his support, guidance, and encouragement during my thesis study.

I would like to state my appreciation to Prof. Dr. Tuna Balkan and to Asst. Prof. Dr. Kutluk Bilge Arıkan for their assistance and advice in improving the quality of this study. I am thankful to my company ASELSAN Inc. for supporting my work. Financial support of TÜBİTAK is also gratefully acknowledged.

Finally I would like to thank to my family for their endless support, encouragement, and guidance.

TABLE OF CONTENTS

ABSTRACT.....	v
ÖZ	vii
ACKNOWLEDGEMENTS	x
TABLE OF CONTENTS	xi
LIST OF TABLES	xix
LIST OF FIGURES	xxiii
LIST OF ABBREVIATIONS	xxxvii
NOMENCLATURE.....	xxxviii
CHAPTERS	
1. INTRODUCTION	1
2. LITERATURE SURVEY	7
2.1. INTRODUCTION	7
2.2. LITERATURE SURVEY	7
2.3. MOTIVATION	25
2.3.1. Development of Single Unit HP Suspension Systems.....	25
2.3.2. Active HP Suspension Design	25
2.3.3. Interconnection of the HP Suspension Systems.....	26
2.3.4. Optimization of the HP suspension system.....	27
3. MODELLING OF THE HP SUSPENSION SYSTEMS.....	29
3.1. MODELING OF THE HP SUSPENSION	29

3.1.1.	Modeling of the HP Suspension System with Incompressible Oil Assumption.....	29
3.1.2.	Modeling of the HP Suspension with Compressible Oil Model	34
3.1.3.	Static Analysis.....	36
3.1.4.	Effect of Compressibility on the Dynamics of the Suspension.....	37
3.2.	ANALYSIS OF THE HP SUSPENSION SYSTEM.....	39
3.2.1.	Stiffness and Damping Characteristics of the HP Suspension.....	39
3.2.1.1.	Stiffness Characteristics	39
3.2.1.2.	Comparisons of Stiffness Characteristics.....	42
3.2.1.3.	Damping Characteristics	42
3.2.2.	Parameter Sensitivity Study	44
3.2.3.	Sensitivity Analysis in Frequency Domain.....	47
3.2.3.1.	Piston Area	49
3.2.3.2.	Initial Gas Volume	51
3.2.3.3.	Orifice Opening.....	53
3.2.3.4.	Input Amplitude	55
3.3.	COMPARISON OF DIFFERENT HP SUSPENSION SYSTEM.....	57
3.3.1.	Modeling of the HP Suspension System with Double Gas Chambers... ..	57
3.3.2.	Static Analysis of the Double Gas Chamber HP Suspension System	60
3.3.3.	Stiffness Characteristics of the Double Gas Chamber HP Suspension System	60
3.3.4.	Damping Characteristics of the Double Gas Chamber HP Suspension System	62
3.4.	EXPERIMENTAL VERIFICATION OF THE HP SUSPENSION UNIT	62
3.4.1.	Test Setup.....	63
3.4.2.	Experiments.....	67
3.5.	TUNING OF THE PARAMETERS OF HP SUSPENSION SYSTEM....	73
4.	ACTIVE HP SUSPENSION SYSTEM	75

4.1.	INTRODUCTION	75
4.2.	QUARTER CAR MODEL WITH ACTIVE HP SUSPENSION SYSTEM.	77
4.2.1.	State Dependent Riccati Equation (SDRE) Control.....	78
4.2.2.	Quarter Car with Active HP Suspension System.....	81
4.2.2.1.	Modeling of the Quarter Car Model with Active HP Suspension System	81
4.2.3.	Controller Design for Active HP Suspension System	88
4.2.3.1.	Active Controller without the Integral State	89
4.2.3.2.	Active Controller with the Integral State	89
4.2.3.3.	Active Controller with the Adaptive Integral Controller	91
4.2.4.	Simulations.....	91
4.2.4.1.	Simulations with Active Controller without Integral Controller ...	92
4.2.4.2.	Simulations of the Active System with the Integral Controller	98
4.3.	ACTIVE CONTROL OF ROLL PLANE HALF VEHICLE MODEL WITH THE HP SUSPENSION SYSTEM	124
4.3.1.1.	Modeling of Half Vehicle Roll Model with Active HP Suspension System	125
4.3.1.2.	Static Analysis of the Suspension System	128
4.3.1.3.	Stiffness Characteristics	128
4.3.1.4.	State Space Representation of the Linearized Half Vehicle Model with the HP Suspensions.....	130
4.3.1.5.	Design of an Active Controller for Half Vehicle Model with the Active HP Suspension System.....	134
4.3.1.6.	Simulations.....	137
4.3.2.	Conclusion	147
4.4.	FULL VEHICLE MODEL WITH ACTIVE HP SUSPENSION SYSTEM.	148
4.4.1.	Modeling of the Full Vehicle Model with Active HP Suspension System	148

4.4.2.	Static Analysis of the Full Vehicle Model with HP Suspension System	151
4.4.3.	Vertical Stiffness of the Full Vehicle Model	151
4.4.4.	Roll Stiffness of the Full Vehicle Model	152
4.4.5.	Pitch Stiffness of the Full Vehicle Model	154
4.4.6.	State Dependent Linear Model of the Full Vehicle Model with the Active HP Suspension System	155
4.4.7.	Design of the Controller for the Full Vehicle Model with Active HP Suspensions	161
4.4.8.	Simulations.....	163
4.4.8.1.	Simulation with Random Road Displacement Input.....	163
4.4.8.2.	Braking In Cornering Simulation.....	165
4.5.	CONCLUSION	174
5.	INTERCONNECTED HP SUSPENSION SYSTEMS.....	177
5.1.	INTRODUCTION.....	177
5.2.	SOLVABILITY OF THE SUSPENSION FORCES AND THE SUSPENSION PRESSURES.....	179
5.3.	EXAMINATION OF THE POSSIBLE HP INTERCONNECTIONS FOR A VEHICLE WITH THREE AXLES.....	180
5.3.1.	One Degree of Freedom Interconnections	182
5.3.2.	Two Degrees of Freedom Interconnections	182
5.3.3.	Three Degrees of Freedom Interconnections	183
5.4.	CONCLUSION	184
6.	ANALYSIS AND DESIGN OF A PITCH INTERCONNECTED HP SUSPENSION SYSTEM FOR THREE-AXLE VEHICLES	187
6.1.	INTRODUCTION.....	187
6.2.	DEVELOPMENT OF A THREE-AXLE VEHICLE MODEL IN PITCH PLANE.....	190

6.3.	MODELING OF A PITCH INTERCONNECTED HP SUSPENSION SYSTEM FOR A THREE AXLE VEHICLE.....	195
6.3.1.	Possible Interconnected Suspension Layout	196
6.3.2.	Mathematical Modeling of the Pitch Interconnected HP Suspension Systems	200
6.3.2.1.	Modeling of the First Suspension Configuration.....	201
6.3.2.2.	Stiffness Characteristics	205
6.3.2.3.	Damping Characteristics	209
6.4.	A GENERAL FORMULA FOR THE PITCH INTERCONNECTED HP SUSPENSION SYSTEM FOR THE THREE AXLE VEHICLES	211
6.4.1.	Stiffness Properties	212
6.4.2.	Damping Properties.....	213
6.5.	COMPARISON OF THE STIFFNESS PROPERTIES OF THE DIFFERENT INTERCONNECTED SUSPENSION CONFIGURATIONS.....	213
6.6.	COMPARISON OF THE DAMPING PROPERTIES OF DIFFERENT SUSPENSION CONFIGURATIONS	218
6.7.	LOAD-LEVELING, STATIC DEFLECTION, AND SUSPENSION FORCE CHARACTERISTICS	221
6.8.	SIMULATIONS.....	223
6.8.1.	Simulations with Random Road	224
6.8.2.	Simulation with Bump Input.....	227
6.8.3.	Simulations with Body Disturbance Inputs	239
6.8.3.1.	Simulation with Braking Input.....	239
6.8.3.2.	Simulation with Firing Shock Input.....	248
6.9.	COMPARISON OF SUSPENSION CONFIGURATIONS	257
6.10.	PARAMETER SENSITIVITY ANALYSIS	258
6.10.1.	Change of the Vertical Stiffness with the Piston Area, Rod Area, and Initial Gas Volume	258
6.10.2.	Change of the Pitch Stiffness with the Piston Area, Rod Area, and Initial Gas Volume	260

6.10.3.	Change of the Vertical Damping with the Piston Area, Rod Area, and Damper Valve Parameters.....	262
6.10.4.	Change of the Pitch Damping with the Piston Area, Rod Area, and Damper Valve Parameters.....	264
6.10.5.	Braking Simulation	266
6.10.6.	Random Road Simulation	282
6.11.	CONCLUSION.....	283
7.	ANALYSIS AND DESIGN OF THE FULL INTERCONNECTED HP SUSPENSION SYSTEM FOR THREE-AXLE VEHICLES	287
7.1.	INTRODUCTION.....	287
7.2.	FULL VEHICLE MODEL.....	288
7.2.1.	Modeling of the Nine Degree of Freedom Full Vehicle Model	290
7.3.	MODELING OF THE EIGHTEEN DEGREE OF FREEDOM FULL VEHICLE MODEL.....	291
7.3.1.	Interconnected Suspension Layouts	303
7.3.1.1.	Solvability of the Suspension Forces and the Suspension Pressures	304
7.3.1.2.	Mathematical Degree of Freedom of Interconnected HP Suspension Systems	308
7.3.1.3.	Type of the Interconnected HP Suspension System.....	308
7.3.1.4.	Determination of the Full Interconnections	309
7.3.1.5.	Determination of the Semi-interconnections.....	310
7.4.	MODELING OF THE INTERCONNECTED HP SUSPENSION SYSTEM FOR THE FULL VEHICLE MODEL WITH THREE AXLES	327
7.4.1.	1 st Interconnected Suspension Configuration.....	328
7.4.1.1.	Static Analysis.....	328
7.4.1.2.	Stiffness Characteristics	329
7.4.1.3.	Damping Properties.....	333
7.4.1.4.	Warp Moment	337

7.5.	COMPARISON OF STIFFNESS PROPERTIES OF THE INTERCONNECTED HP SUSPENSION SYSTEM.....	338
7.5.1.	Case 1: $A_r=0.6A_p$	338
7.5.2.	Case 2: $A_r=0.8A_p$	344
7.6.	COMPARISON OF DAMPING PROPERTIES OF THE INTERCONNECTED HP SUSPENSION SYSTEM.....	349
7.6.1.	Case 1: $A_r=0.6A_p$	349
7.6.2.	Case 2: $A_r=0.8 A_p$	353
7.7.	COMPARISON OF WARP MOMENT CHARACTERISTICS OF THE INTERCONNECTED HP SUSPENSION SYSTEM.....	356
7.7.1.	Case 1: $A_r=0.6A_p$	357
7.7.2.	Case 2: $A_r=0.8A_p$	358
7.8.	COMPARING THE SUSPENSION CONFIGURATIONS FOR ROLL AND PITCH PERFORMANCE.....	359
7.9.	SENSITIVITY STUDY: EFFECT OF THE SUSPENSION PARAMETERS ON THE STIFFNESS AND DAMPING CHARACTERISTICS OF THE INTERCONNECTED SUSPENSION SYSTEMS.....	360
7.9.1.	Stiffness Sensitivity Study	361
7.9.1.1.	Effect of Piston Area.....	361
7.9.1.2.	Effect of Initial Gas Volume	363
7.9.1.3.	Effect of Piston Rod Area	364
7.9.2.	Damping Sensitivity Study	367
7.9.2.1.	Effect of Maximum Valve Opening.....	367
7.9.2.2.	Effect of Piston Area.....	369
7.9.2.3.	Effect of Rod Area	370
7.10.	SIMULATIONS.....	372
7.10.1.	Ride Comfort Simulations	373
7.10.2.	Vehicle Handling Simulation.....	374
7.10.3.	Firing Shock Simulation	380
7.11.	CONCLUSION.....	385

8. DESIGN OF THE PITCH INTERCONNECTED HP SUSPENSION SYSTEM FOR MULTI-AXLE VEHICLE	389
8.1. INTRODUCTION.....	389
8.2. INTERCONNECTED HP SUSPENSION SYSTEM FOR A MULTI-AXLE VEHICLE	390
8.3. CONCLUSION	398
9. OPTIMIZATION OF HP SUSPENSION SYSTEMS.....	399
9.1. INTRODUCTION.....	399
9.2. SUSPENSION OPTIMIZATION	401
9.3. SENSITIVITY STUDY	406
9.4. OPTIMIZATION RESULTS	415
9.5. CONCLUSION	419
10. CONCLUSION	421
REFERENCES.....	427
APPENDICES	
A. STATE DEPENDENT MATRICES OF HALF VEHICLE MODEL WITH ACTIVE HP SUSPENSION SYSTEM	437
CURRICULUM VITAE	441

LIST OF TABLES

TABLES

Table 3.1: Vehicle and Suspension Parameters	36
Table 4.1: rms Values of Performance Variables with the Active and Passive HP Suspensions	98
Table 4.2: Weighting Coefficient Sets	117
Table 4.3: rms Values for Random Road Simulations for 50 kph	118
Table 4.4: rms Values for Random Road Simulations for 60 kph	118
Table 4.5: rms Values for Random Road Simulations for 70 kph	119
Table 4.6: rms Values for Random Road Simulations for 80 kph	119
Table 4.7: rms Values for Random Road Simulations for 90 kph	119
Table 4.8: Suspension and Vehicle Parameters for Half Vehicle Model.....	134
Table 4.9: Controller Weighting Parameters	137
Table 4.10. rms Values for Performance Variables for 60 kph	137
Table 4.11. rms Values for Performance Variables for 70 kph	138
Table 4.12. rms Values for Performance Variables for 80 kph	138
Table 4.13. rms Values for Performance Variables for 90 kph	138
Table 4.14: Suspension and Vehicle Parameters for Full Vehicle Model	160
Table 4.15: Controller Weighting Parameters	163
Table 4.16: rms Values of Responses for the Active and Passive Suspensions at V=60 kph.....	163
Table 4.17: rms Values of Responses for the Active and Passive Suspensions at V=70 kph.....	164
Table 4.18: rms Values of Responses for the Active and Passive Suspensions at V=80 kph.....	164

Table 4.19: rms Values of Responses for the Active and Passive Suspensions at V=90 kph.....	165
Table 6.1: Definition of variable	193
Table 6.2: Definition of Parameters	193
Table 6.3: Vehicle Parameters	196
Table 6.4: Definition of Parameters	200
Table 6.5: Definition of Variables Used in Derivation	201
Table 6.6: Suspension Parameters.....	211
Table 6.7: Suspension Parameters.....	214
Table 6.8: Suspension Parameters.....	216
Table 6.9: Static Equilibrium for $A_r=0.6A_p$, $\Delta L=0.6m$ and $\Delta M=2000kg$	222
Table 6.10: Static Equilibriums for $A_r=0.8A_p$, $\Delta L=0.6m$ and $\Delta M=2000kg$	222
Table 6.11: Static Equilibrium for $A_r=0.6A_p$, $\Delta L=-0.6m$ and $\Delta M=2000kg$	223
Table 6.12: Static Equilibriums for $A_r=0.8A_p$, $\Delta L=-0.6m$ and $\Delta M=2000kg$	223
Table 6.13: Random Road Simulations for V=60kph.....	224
Table 6.14: Random Road Simulations for V=70kph.....	224
Table 6.15: Random Road Simulations for V=80kph.....	224
Table 6.16: Random Road Simulations for V=90kph.....	225
Table 6.17: Random Road Simulations for V=60kph.....	225
Table 6.18: Random Road Simulations for V=70kph.....	226
Table 6.19: Random Road Simulations for V=80kph.....	226
Table 6.20: Random Road Simulations for V=90kph.....	226
Table 6.21: Maximum Values of the Performance Variables	232
Table 6.22: Minimum Values of the Performance Variables.....	233
Table 6.23: Maximum Values of the Performance Variables	238
Table 6.24: Minimum Values of the Performance Variables.....	239
Table 6.25: Maximum Values of the Performance Variables	248
Table 6.26: Minimum Values of the Performance Variables.....	256
Table 6.27: Weighting Factors Used For a Military Vehicles	257
Table 6.28: Calculated Suspension Metrics for Military Vehicles	258

Table 6.29: Vertical and Pitch Acceleration rms for Different Piston Areas.....	282
Table 6.30: Vertical and Pitch Acceleration rms for Different Piston Rod Areas ...	282
Table 6.31: Vertical and Pitch Acceleration rms for Different Initial Gas Volumes	282
Table 6.32: Vertical and Pitch Acceleration rms for Different Maximum Valve Openings	283
Table 7.1: Variable Definition	289
Table 7.2: Definition Parameters/Variables for Magic Formula Tire Model	300
Table 7.3: Vehicle Parameters	303
Table 7.4: Initial Oil Pressure at Static Equilibrium for Different Interconnected Configurations.....	339
Table 7.5: Gas Volumes of Front, Intermediate, and Rear Suspension Volumes....	339
Table 7.6: Roll and Pitch Stiffness Characteristics of Different Interconnections ..	344
Table 7.7: Initial Oil Pressure at Static Equilibrium for Different Interconnected Configurations.....	345
Table 7.8: Gas Volumes of Front, Intermediate, and Rear Suspension Volumes....	345
Table 7.9: Roll and Pitch Stiffness Characteristics of Different Interconnections ..	348
Table 7.10: Integral of Roll and Pitch Damping of Different Interconnections	353
Table 7.11: Integral of Roll and Pitch Damping Characteristics of Different Interconnections	356
Table 7.12: Integral of Warp Moment for Different Interconnections	357
Table 7.13: Integral of Warp Moment for Different Interconnections	358
Table 7.14: Suspension Metrics of Different Interconnected Configurations	360
Table 7.15: rms Values for Random Road Simulation at 60 kph Longitudinal Velocity.....	373
Table 7.16: rms Values for Random Road Simulation at 70 kph Longitudinal Velocity.....	373
Table 7.17: rms Values for Random Road Simulation at 80 kph Longitudinal Velocity.....	373

Table 7.18: rms Values for Random Road Simulation at 90 kph Longitudinal Velocity	373
Table 9.1: Optimized and Design Parameters	404
Table 9.2: Optimization Results	415
Table 9.3: Optimum Parameter Sets	415
Table 9.4: Optimization Results	417
Table 9.5: Optimum Parameter Sets for Ride Comfort Optimization.....	417
Table 9.6: Optimum Parameter Sets for Handling Optimization.....	418

LIST OF FIGURES

FIGURES

Figure 1.1: General Structure of HP Suspension System	1
Figure 2.1: HP Suspension System [2]	8
Figure 2.2: HP Suspension System [3]	9
Figure 2.3: Test Rig for the Validation of the HP Suspension Model [3]	10
Figure 2.4: Active HP Suspension System [3].....	10
Figure 2.5: Semi-Active HP Suspension System [4]	11
Figure 2.6: Coupled Controller and Vehicle Model [5].....	12
Figure 2.7: Structure of the HP Suspension Systems [6].....	14
Figure 2.8: Test Rig for HP Suspension System [6]	14
Figure 2.9: HP Suspension System and Flow Control Valve [7].....	15
Figure 2.10: Active Suspension Control [7]	16
Figure 2.11: Two State Switchable Semi-active HP Suspension System [8]	17
Figure 2.12: Quarter Car Model with Passive HP Suspension System [9].....	17
Figure 2.13: Quarter Car Model with HP Suspension System with Two Accumulators [9].....	18
Figure 2.14: Semi-active HP Suspension System [9]	18
Figure 2.15: HP Suspension System [10]	19
Figure 2.16: HP Suspension System [14]	21
Figure 3.1: Quarter Car Model with HP Suspension System	30
Figure 3.2: Hard Stop Force Characteristics	31
Figure 3.3: Sprung Mass Accelerations Obtained from HP Suspension with Compressible and Incompressible Oil	37

Figure 3.4: Suspension Deflections Obtained from HP Suspension with Compressible and Incompressible Oil.....	38
Figure 3.5: Tire Deflections Obtained from HP Suspension with Compressible and Incompressible Oil	38
Figure 3.6: HP Suspension Layout Used in Analysis	39
Figure 3.7: Effect of Oil Compressibility in the Suspension Stiffness	42
Figure 3.8: Combined Damper Model	44
Figure 3.9: Change of the Valve Opening with the Pressure Drop.....	44
Figure 3.10: Variation of Suspension Stiffness with Piston Area.....	45
Figure 3.11: Variation of Suspension Stiffness with Initial Gas Volume.....	45
Figure 3.12: Variation of Damping Force with Piston Area	46
Figure 3.13: Variation of Damping Force with Orifice Opening.....	47
Figure 3.14: Amplitude vs Frequency Plot of the Road Displacement Sine Input	48
Figure 3.15: Variation of Sprung Mass Acceleration with Piston Area.....	49
Figure 3.16: Variation of Suspension Deflection with Piston Area.....	50
Figure 3.17: Variation of the Tire Deflection with Piston Area.....	50
Figure 3.18: Variation of Sprung Mass Acceleration with Initial Gas Volume.....	51
Figure 3.19: Variation of Suspension Deflection with Initial Gas Volume	52
Figure 3.20: Variation of Tire Deflection with Initial Gas Volume.....	52
Figure 3.21: Variation of the Sprung Mass Acceleration with the Valve Opening ...	53
Figure 3.22: Variation of Suspension Deflection with Valve Opening	54
Figure 3.23: Variation of Tire Deflection with Valve Opening.....	54
Figure 3.24: Variation of Sprung Mass Acceleration with Input Amplitude.....	55
Figure 3.25: Variation of Suspension Deflection with Input Amplitude	56
Figure 3.26: Variation of Tire Deflection with Input Amplitude.....	56
Figure 3.27. Double Gas Chamber HP Suspension	57
Figure 3.28: Variation of Gas Stiffness with Relative Displacement	61
Figure 3.29: HP Suspension Test Setup	63
Figure 3.30: HP Suspension Test Setup	64
Figure 3.31: Schematic of the HP Suspension System	65

Figure 3.32: Hydraulic Cylinder	66
Figure 3.33: Fox 0.7 L Membrane Type Hydraulic Accumulator [50]	66
Figure 3.34: Parker 9MV600S Needle Valve [51].....	67
Figure 3.35: Measured vs Simulated Gas Force for $P_i=25.8$ bar.....	68
Figure 3.36: Measured vs Simulated Gas Force for $P_i=33$ bar	68
Figure 3.37: Measured vs Simulated Gas Force for $P_i=45$ bar	69
Figure 3.38: Measured vs Simulated Gas Force for $P_i=25.8$ bar, $A=35$ mm, $f=1$ Hz	70
Figure 3.39: Measured vs Simulated Gas Force for $P_i=25.8$ bar $A=35$ mm, $f=1$ Hz .	70
Figure 3.40: Measured vs Simulated Gas Force for $P_i=25.8$ bar $A=35$ mm, $f=1$ Hz .	71
Figure 3.41: Measured vs Simulated Gas Force for $P_i=25.8$ bar $A=35$ mm, $f=1.5$ Hz	71
Figure 3.42: Measured vs Simulated Gas Force for $P_i=25.8$ bar, $A=25$ mm $f=2.5$ Hz	72
Figure 3.43: Measured vs Simulated Gas Force for $P_i=25.8$ bar, $A=25$ mm $f=3$ Hz .	72
Figure 4.1: Active HP Suspension Design by SDRE Control	80
Figure 4.2: Quarter Car Model with the active HP Suspension System	82
Figure 4.3: Polynomial Model of Polytropic Gas Equation.....	83
Figure 4.4: Saturation Function-Saturation of the Oil Flow Rate.....	88
Figure 4.5: Acceleration FRF.....	93
Figure 4.6: Tire Deflection FRF	93
Figure 4.7: Suspension Deflection FRF.....	94
Figure 4.8: rms Value of the Oil Flow Rate.....	94
Figure 4.9: Power Spectral Densities of Random Road Displacement Input At Different Velocities	95
Figure 4.10: Random Road Input at 50 kph.....	95
Figure 4.11: Acceleration Response	96
Figure 4.12: Suspension Deflection Response.....	96
Figure 4.13: Tire Deflection Response	97
Figure 4.14: Oil Flow Rate.....	97
Figure 4.15: Acceleration FRF.....	99

Figure 4.16: Suspension Deflection FRF	100
Figure 4.17: Tire Deflection FRF.....	101
Figure 4.18: rms of the Oil Flow Rate	101
Figure 4.19: Acceleration FRF.....	102
Figure 4.20: Tire Deflection FRF.....	103
Figure 4.21: Suspension Deflection FRF	103
Figure 4.22: rms of the Oil Flow Rate	104
Figure 4.23: Acceleration FRF.....	105
Figure 4.24: Suspension Deflection FRF	105
Figure 4.25: Tire Deflection FRF.....	106
Figure 4.26: RMS of the Oil Flow Rate	106
Figure 4.27: rms of the Acceleration.....	107
Figure 4.28: rms of the Suspension Deflection	107
Figure 4.29: rms of the Tire Deflection.....	108
Figure 4.30: rms of the Flow Rate.....	108
Figure 4.31: Suspension Deflection	109
Figure 4.32: Oil Flow Rate.....	110
Figure 4.33: Suspension Deflection	110
Figure 4.34: Oil Flow Rate.....	111
Figure 4.35: Suspension Deflection	111
Figure 4.36: Oil Flow Rate.....	112
Figure 4.37: Suspension Deflection	113
Figure 4.38: Oil Flow Rate.....	113
Figure 4.39: Suspension Deflection	114
Figure 4.40: Oil Flow Rate.....	114
Figure 4.41: Suspension Deflection	115
Figure 4.42: Oil Flow Rate.....	115
Figure 4.43: Change of Integral Controller Coefficient with Suspension Deflection	117
Figure 4.44: Suspension Deflection	120

Figure 4.45: Oil Flow Rate.....	121
Figure 4.46: Suspension Deflection	122
Figure 4.47: Oil Flow Rate.....	122
Figure 4.48: Suspension Deflection	123
Figure 4.49: Oil Flow Rate.....	124
Figure 4.50. Half Vehicle Roll Model with Active HP Suspension System.....	126
Figure 4.51: Lateral Acceleration	139
Figure 4.52: Left Suspension Deflection	139
Figure 4.53: Right Suspension Deflection	140
Figure 4.54: Roll Angle	140
Figure 4.55: Left Tire Deflection	141
Figure 4.56: Right Tire Deflection.....	141
Figure 4.57: Left Suspension Flow Rate.....	142
Figure 4.58: Right Suspension Flow Rate	142
Figure 4.59: Lateral Acceleration	143
Figure 4.60: Left Suspension Deflection	144
Figure 4.61: Right Suspension Deflection	144
Figure 4.62: Roll Angle	145
Figure 4.63: Left Tire Deflection	145
Figure 4.64: Right Tire Deflection.....	146
Figure 4.65: Left Suspension Flow Rate.....	146
Figure 4.66: Right Suspension Flow Rate	147
Figure 4.67. Full Vehicle Model with Active Suspension.....	150
Figure 4.68: Longitudinal Acceleration	166
Figure 4.69: Lateral Acceleration	167
Figure 4.70: Roll Angle	167
Figure 4.71: Pitch Angle	168
Figure 4.72: Front Left Suspension Deflection.....	168
Figure 4.73: Front Right Suspension Deflection	169
Figure 4.74: Rear Left Suspension Deflection.....	169

Figure 4.75: Rear Right Suspension Deflection	170
Figure 4.76: Front Left Tire Deflection	170
Figure 4.77: Front Right Tire Deflection	171
Figure 4.78: Rear Left Tire Deflection.....	171
Figure 4.79: Rear Right Tire Deflection	172
Figure 4.80: Front Left Flow Rate	172
Figure 4.81: Front Right Flow Rate	173
Figure 4.82: Rear Left Flow Rate.....	173
Figure 4.83: Rear Right Flow Rate	174
Figure 5.1: A Military Vehicle with Three-Axles [67]	178
Figure 5.2: Pitch Plane Vehicle Model	178
Figure 5.3: One Possible Interconnection Configuration in the Pitch Plane.....	179
Figure 5.4: Unfeasible Interconnection Configurations	181
Figure 5.5: Two Degrees of Interconnections	183
Figure 5.6: Three Degrees of freedom Interconnection	184
Figure 6.1: Pitch Plane Model of a Three-Axle Vehicle.....	190
Figure 6.2: Free Body Diagram of the Tires and the Vehicle Sprung Mass	191
Figure 6.3: Magic Formula Tire Characteristics	195
Figure 6.4: First Possible Full Interconnection	197
Figure 6.5: Second Possible Full Interconnection.....	197
Figure 6.6: First Possible Semi-Interconnection	198
Figure 6.7: Second Possible Semi-Interconnection.....	198
Figure 6.8: Third Possible Semi-Interconnection	199
Figure 6.9: Unconnected Suspension Configuration.....	199
Figure 6.10: Vertical Stiffness of Different Suspension Configurations	215
Figure 6.11: Pitch Stiffness of Different Suspension Configurations for $A_r=0.6A_p$	215
Figure 6.12: Vertical Stiffness of Different Suspension Configurations	217
Figure 6.13: Pitch Stiffness of Different Suspension Configurations for $A_r=0.8A_p$	217
Figure 6.14: Vertical Damping Force for Suspension Configurations.....	219

Figure 6.15: Pitch Damping Moment for Interconnected Suspension Configurations	220
Figure 6.16: Vertical Damping Force for Suspension Configurations	220
Figure 6.17: Pitch Damping Moment for Suspension Configurations.....	221
Figure 6.18: Ramp Input	227
Figure 6.19: Sprung Mass Vertical Acceleration.....	228
Figure 6.20: Pitch Acceleration.....	228
Figure 6.21: Front Suspension Deflection	229
Figure 6.22: Intermediate Suspension Deflection	229
Figure 6.23: Rear Suspension Deflection	230
Figure 6.24: Pitch Angle	230
Figure 6.25: Front Tire Force.....	231
Figure 6.26: Intermediate Tire Force	231
Figure 6.27: Rear Tire Force.....	232
Figure 6.28: Sprung Mass Vertical Acceleration.....	234
Figure 6.29: Pitch Acceleration.....	234
Figure 6.30: Front Suspension Deflection	235
Figure 6.31: Intermediate Suspension Deflection	235
Figure 6.32: Rear Suspension Deflection	236
Figure 6.33: Pitch Angle Response.....	236
Figure 6.34: Front Tire Force.....	237
Figure 6.35: Intermediate Tire Force	237
Figure 6.36: Rear Tire Force.....	238
Figure 6.37: Brake Torque Input.....	240
Figure 6.38: Front Suspension Deflection	240
Figure 6.39: Intermediate Suspension Deflection	241
Figure 6.40: Rear Suspension Deflection	241
Figure 6.41: Pitch Angle	242
Figure 6.42: Front Tire Force.....	242
Figure 6.43: Intermediate Tire Force	243

Figure 6.44: Rear Tire Force	243
Figure 6.45: Front Suspension Deflection.....	244
Figure 6.46: Intermediate Suspension Deflection	245
Figure 6.47: Rear Suspension Deflection.....	245
Figure 6.48: Pitch Angle	246
Figure 6.49: Front Tire Force	246
Figure 6.50: Intermediate Tire Force	247
Figure 6.51: Rear Tire Force	247
Figure 6.52: Firing Shock Input	248
Figure 6.53: Front Suspension Deflection.....	249
Figure 6.54: Intermediate Suspension Deflection	249
Figure 6.55: Rear Suspension Deflection.....	250
Figure 6.56: Pitch Angle Response	250
Figure 6.57: Front Tire Force	251
Figure 6.58: Intermediate Tire Force	251
Figure 6.59: Rear Tire Force	252
Figure 6.60: Front Suspension Deflection.....	253
Figure 6.61: Intermediate Suspension Deflection	253
Figure 6.62: Rear Suspension Deflection.....	254
Figure 6.63: Pitch Angle Response	254
Figure 6.64: Front Tire Force	255
Figure 6.65: Intermediate Tire Force	255
Figure 6.66: Rear Tire Force	256
Figure 6.67: Change of the Vertical Stiffness with the Piston Area	259
Figure 6.68: Change of the Vertical Stiffness with the Initial Gas Volume	259
Figure 6.69: Change of the Vertical Stiffness with the Rod Area.....	260
Figure 6.70: Change of the Pitch Stiffness with the Piston Area.....	261
Figure 6.71: Change of the Pitch Stiffness with the Piston Area.....	261
Figure 6.72: Change of the Pitch Stiffness with the Piston Rod Area	262
Figure 6.73: Change of the Vertical Damping Force with the Piston Area	263

Figure 6.74: Change of the Vertical Damping Force with the Piston Area	263
Figure 6.75: Change of the Vertical Damping Force with the Maximum Valve Opening	264
Figure 6.76: Change of the Pitch Damping Moment with the Piston Area	265
Figure 6.77: Change of the Pitch Damping Moment with the Piston Rod Area.....	265
Figure 6.78: Change of the Pitch Damping Moment with the Maximum Valve Opening.....	266
Figure 6.79: Change of Front Suspension Deflection with Piston Area	267
Figure 6.80: Change of Intermediate Suspension Deflection with Piston Area	267
Figure 6.81: Change of Rear Suspension Deflection with Piston Area	268
Figure 6.82: Change of Pitch Angle with Piston Area.....	268
Figure 6.83: Change of Front Tire Force with Piston Area	269
Figure 6.84: Change of Intermediate Tire Force with Piston Area.....	269
Figure 6.85: Change of Rear Tire Force with Piston Area	270
Figure 6.86: Change of Front Suspension Deflection with Piston Area	271
Figure 6.87: Change of Intermediate Suspension Deflection with Piston Area	271
Figure 6.88: Change of Rear Suspension Deflection with Piston Area	272
Figure 6.89: Change of Pitch Angle with Piston Area.....	272
Figure 6.90: Change of Front Tire Force with Piston Area	273
Figure 6.91: Change of Intermediate Tire Force with Piston Area.....	273
Figure 6.92: Change of Rear Tire Force with Piston Area	274
Figure 6.93: Change of Front Suspension Deflection with Initial Gas Volume	275
Figure 6.94: Change of Intermediate Suspension Deflection with Initial Gas Volume	275
Figure 6.95: Change of Rear Suspension Deflection with Initial Gas Volume	276
Figure 6.96: Change of Pitch Angle with Initial Gas Volume	276
Figure 6.97: Change of Front Tire Force with Initial Gas Volume	277
Figure 6.98: Change of Intermediate Tire Force with Initial Gas Volume	277
Figure 6.99: Change of Rear Tire Force with Initial Gas Volume.....	278
Figure 6.100: Change of Front Suspension Deflection with Valve Opening	278

Figure 6.101: Change of Intermediate Suspension Deflection with Valve Opening	279
Figure 6.102: Change of Rear Suspension Deflection with Valve Opening	279
Figure 6.103: Change of Pitch Angle with Valve Opening	280
Figure 6.104: Change of Front Tire Force with Valve Opening	280
Figure 6.105: Change of Intermediate Tire Force with Valve Opening	281
Figure 6.106: Change of Rear Tire Force with Valve Opening	281
Figure 7.1: Nine Degree of Freedom Full Vehicle Model	291
Figure 7.2: Full Vehicle Model - Sprung Mass Free Body Diagram	293
Figure 7.3: Free body Diagrams of Tires	294
Figure 7.4: Slip Angle Definitions	295
Figure 7.5: Cornering Force vs Slip Angle Characteristics for Different Vertical Tire Load at zero Longitudinal Slip	301
Figure 7.6: Longitudinal Force vs Longitudinal Slip Characteristics for Different Vertical Tire Load at Zero Slip Angle	301
Figure 7.7: Change of Cornering Force with Slip Angle and Longitudinal Slip	302
Figure 7.8: Change of Longitudinal Force with Slip Angle and Longitudinal Slip	302
Figure 7.9: First Interconnected HP Suspension System for a Three Axle Vehicle	311
Figure 7.10: Second Interconnected HP Suspension System for a Three Axle Vehicle	312
Figure 7.11: Third Interconnected HP Suspension System for a Three Axle Vehicle	313
Figure 7.12: Fourth Interconnected HP Suspension System for a Three Axle Vehicle	314
Figure 7.13: Fifth Interconnected HP Suspension System for a Three Axle Vehicle	315
Figure 7.14: Sixth Interconnected HP Suspension System for a Three Axle Vehicle	316
Figure 7.15: Seventh Interconnected HP Suspension System for a Three Axle Vehicle	317

Figure 7.16: Eighth Interconnected HP Suspension System for a Three Axle Vehicle	318
Figure 7.17: Ninth Interconnected HP Suspension System for a Three Axle Vehicle	319
Figure 7.18: Tenth Interconnected HP Suspension System for a Three Axle Vehicle	320
Figure 7.19: Eleventh Interconnected HP Suspension System for a Three Axle Vehicle	321
Figure 7.20: Twelfth Interconnected HP Suspension System for a Three Axle Vehicle	322
Figure 7.21: Thirteenth HP Suspension System for a Three Axle Vehicle- Unconnected HP Suspension Configuration.....	323
Figure 7.22: Infeasible Interconnected HP Suspension System for a Three Axle Vehicle	326
Figure 7.23: Vertical Stiffness of Different Interconnections.....	340
Figure 7.24: Roll Stiffness of Different Interconnections.....	341
Figure 7.25: Pitch Stiffness of Different Interconnections	341
Figure 7.26: Integral of Roll Stiffness.....	342
Figure 7.27: Integral of Pitch Stiffness	343
Figure 7.28: Vertical Stiffness of Different Interconnections.....	346
Figure 7.29: Roll Stiffness of Different Interconnections.....	346
Figure 7.30: Pitch Stiffness of Different Interconnections	347
Figure 7.31: Integral of Roll Stiffness.....	347
Figure 7.32: Integral of Pitch Stiffness	348
Figure 7.33: Vertical Damping of Different Interconnections.....	349
Figure 7.34: Roll Damping of Different Interconnections.....	350
Figure 7.35: Pitch Damping of Different Interconnections	351
Figure 7.36: Integral of Roll Damping of Different Interconnections	351
Figure 7.37: Integral of Pitch Damping of Different Interconnections.....	352
Figure 7.38: Vertical Damping of Different Interconnections.....	353

Figure 7.39: Roll Damping of Different Interconnections	354
Figure 7.40: Pitch Damping of Different Interconnections.....	354
Figure 7.41: Integral of Roll Damping of Different Interconnections	355
Figure 7.42: Integral of Pitch Damping of Different Interconnections.....	355
Figure 7.43: Warp Moment of Different Interconnections	357
Figure 7.44: Warp Moment of Different Interconnections	358
Figure 7.45: Change of the Vertical Stiffness with Piston Area for $A_r=0.6A_p$	361
Figure 7.46: Change of the Roll Stiffness with Piston Area for $A_r=0.6A_p$	362
Figure 7.47: Change of the Pitch Stiffness with Piston Area for $A_r=0.6A_p$	362
Figure 7.48: Change of the Vertical Stiffness with Initial Gas Volume for $A_r=0.6A_p$	363
Figure 7.49: Change of the Roll Stiffness with Initial Gas Volume for $A_r=0.6A_p$..	363
Figure 7.50: Change of the Pitch Stiffness with Initial Gas Volume for $A_r=0.6A_p$.	364
Figure 7.51: Change of the Vertical Stiffness with Rod Area	365
Figure 7.52: Change of the Roll Stiffness with Rod Area	366
Figure 7.53: Change of the Pitch Stiffness with Rod Area	366
Figure 7.54: Change of the Vertical Damping with Maximum Valve Opening	367
Figure 7.55: Change of the Roll Damping with Maximum Valve Opening	368
Figure 7.56: Change of the Pitch Damping with Maximum Valve Opening.....	368
Figure 7.57: Change of the Vertical Damping with Piston Area	369
Figure 7.58: Change of the Roll Damping with Piston Area	369
Figure 7.59: Change of the Pitch Damping with Piston Area.....	370
Figure 7.60: Change of the Vertical Damping with Rod Area.....	371
Figure 7.61: Change of the Roll Damping with Rod Area.....	371
Figure 7.62: Change of the Pitch Damping with Rod Area	372
Figure 7.63: Steering Input.....	374
Figure 7.64: Braking Input	375
Figure 7.65: Front Left Suspension Deflection	376
Figure 7.66: Front Right Suspension Deflection.....	376
Figure 7.67: Intermediate Left Suspension Deflection	377

Figure 7.68: Intermediate Right Suspension Deflection	377
Figure 7.69: Rear Left Suspension Deflection	378
Figure 7.70: Rear Right Suspension Deflection.....	378
Figure 7.71: Roll Angle	379
Figure 7.72: Pitch Angle	379
Figure 7.73: Trajectory of the Vehicle	380
Figure 7.74: Firing Shock Force	381
Figure 7.75: Front Left Suspension Deflection.....	381
Figure 7.76: Front Right Suspension Deflection	382
Figure 7.77: Intermediate Left Suspension Deflection	382
Figure 7.78: Intermediate Right Suspension Deflection	383
Figure 7.79: Rear Left Suspension Deflection.....	383
Figure 7.80: Rear Right Suspension Deflection.....	384
Figure 7.81: Pitch Angle	384
Figure 7.82: Roll Angle	385
Figure 8.1: Interconnected HP Suspension System for a Three Axle Vehicle	392
Figure 8.2: Interconnected HP Suspension System for a Three Axle Vehicle	393
Figure 8.3: Interconnected Suspension Design Layout.....	395
Figure 8.4: Interconnected Suspension Design Layout.....	396
Figure 9.1: Weighting Frequency Approximation of the ISO-2631 Weighting Curve for Vertical Acceleration [85]	402
Figure 9.2: Roll Angle Constraint.....	406
Figure 9.3: rms of Vertical Acceleration.....	407
Figure 9.4: rms of Roll Acceleration	407
Figure 9.5: rms of Pitch Acceleration	408
Figure 9.6: rms of Vertical Acceleration.....	409
Figure 9.7: rms of Roll Acceleration	409
Figure 9.8: rms of Pitch Acceleration	410
Figure 9.9: rms of Vertical Acceleration.....	410
Figure 9.10: rms of Roll Acceleration	411

Figure 9.11: rms of Pitch Acceleration	411
Figure 9.12: Steering Wheel Input for Double Lane Change Maneuver	412
Figure 9.13: Roll Angle versus Volume Ratio	413
Figure 9.14: Roll Angle versus Damping Ratio	413
Figure 9.15: Roll Angle versus Piston Ratio.....	414

LIST OF ABBREVIATIONS

HP	Hydro-Pneumatic
SDRE	State Dependent Riccati Equation
rms	Root Mean Square
FRF	Frequency Response Function
PID	Proportional, Integral, Derivative
LQR	Linear Quadratic Regulator
COG	Center of Gravity
dof	Degree of Freedom
SM	Suspension Metric
SDM	State Dependent Matrix

NOMENCLATURE

F	Suspension Force
P_1	Oil Pressure in the First Oil Volume
P_2	Oil Pressure in the Second Oil Volume
P_3	Absolute Gas Pressure in Third Chamber
P_4	Absolute Gas Pressure in Fourth Chamber for Double Gas Chamber HP Suspension System or Oil Pressure in the Fourth Oil Chamber of Single Gas Chamber HP Suspension System
P_5	Oil Pressure in the Fifth Oil Chamber
P_6	Oil Pressure in the Sixth Oil Chamber
P_{3i}	Precharge Gas Pressure
P_{30}	Absolute Gas Pressure in Third Chamber at Static Equilibrium
P_{40}	Absolute Gas Pressure in Fourth Chamber at Static Equilibrium
ΔP	Pressure Difference
ΔP_{\max}	Pressure Difference at Maximum Valve Opening
P_{Atm}	Atmospheric Pressure
A_p	Piston Area
A_r	Piston Rod Area
A_{pr}	Difference between Piston and Piston Rod Area
F_{pF}	Coulomb Friction between Piston and Cylinder Wall
F_{fpF}	Coulomb Friction between Floating Piston and Cylinder Wall
F_{fpF1}	Coulomb Friction between First Floating Piston and Cylinder Wall
F_{fpF2}	Coulomb Friction between Second Floating Piston and Cylinder Wall
F_{pHS}	Hard Stop Force between Piston and Cylinder Hard Stop

F_{fpHS}	Hard Stop Force between Floating Piston and Cylinder Hard Stop
F_{fpHS1}	Hard Stop Force between First Floating Piston and Cylinder Hard Stop
F_{fpHS2}	Hard Stop Force between Second Floating Piston and Cylinder Hard Stop
M	Sprung Mass
M_{fp}	Floating Piston Mass
I_{xx}	Roll Moment of Inertia
I_{yy}	Pitch Moment of Inertia
I_{zz}	Yaw Moment of Inertia
a	Longitudinal Distance between Front Axle and Center of Gravity
b	Longitudinal Distance between Middle (Rear in Two-Axle Vehicle) Axle and Center of Gravity
c	Longitudinal Distance between Rear Axle and Center of Gravity
t	Track Width
t_f	Front Track Width
t_m	Middle Track Width
t_r	Rear Track Width
h_{zSCOG}	Vertical Distance between Gun Axis and Center of Gravity
H_{xSCOG}	Longitudinal Distance between Gun Axis and Center of Gravity
h_{COGF}	Vertical Distance between Front Wheel Hub and Center of Gravity
h_{COGM}	Vertical Distance between Middle Wheel Hub and Center of Gravity
h_{COGR}	Vertical Distance between Rear Wheel Hub and Center of Gravity
g	Gravitational Acceleration

z_p	Piston Displacement
z	Vertical Displacement
z_{fp}	Floating Piston Displacement
z_{fp1}	First Floating Piston Displacement
z_{fp2}	Second Floating Piston Displacement
z_t	Wheel Hub Displacement
z_0	Road Displacement Input
\varnothing	Roll Angle
θ	Pitch Angle
F_{pC}	Coulomb Friction Force for Piston
F_{fpC}	Coulomb Friction Force for Floating Piston
k_{pHS}	Hard Stop Spring Constant for Main Piston
k_{fpHS}	Hard Stop Spring Constant for Floating Piston
h_{pHSU}	Distance between the Piston and Upper Hard Stop at Static Equilibrium
h_{pHSL}	Distance between the Piston and Lower Hard Stop at Static Equilibrium
h_{fpHSU}	Distance between the Floating Piston and Upper Hard Stop at Static Equilibrium
h_{fpHSL}	Distance between the Floating Piston and Lower Hard Stop at Static Equilibrium
Q_{12}	Oil Flow Rate Through the Orifice between First and Second Oil Volumes
Q_{65}	Oil Flow Rate Through the Orifice between Fifth and Sixth Oil Volumes
$Q_{\beta 1}$	Flow Rate due to Oil Compressibility of First Oil Chamber
$Q_{\beta 2}$	Flow Rate due to Oil Compressibility of Second Oil Chamber
Q_1	Net Oil Flow Rate to First Chamber
Q_2	Net Oil Flow Rate to Second Chamber

Q_{4F1R}	Oil Flow Rate between The Fourth Volume of Front Suspension Unit and First Oil Volume of Rear Suspension Unit
Q_{4M1F}	Oil Flow Rate between The Fourth Volume of Middle Suspension Unit and First Oil Volume of Rear Suspension Unit
Q_{4R1M}	Oil Flow Rate between The Fourth Volume of Rear Suspension Unit and First Oil Volume of Middle Suspension Unit
R_{4F1R}	Resistance of Hydraulic Hose between Fourth Volume of Front Suspension Unit and First Volume of Rear Suspension Unit
R_{4M1F}	Resistance of Hydraulic Hose between Fourth Volume of Middle Suspension Unit and First Volume of Front Suspension Unit
R_{4R1M}	Resistance of Hydraulic Hose between Fourth Volume of Rear Suspension Unit and First Volume of Middle Suspension Unit
A_v	Orifice or Valve Opening Area
A_{vmax}	Maximum Valve Opening
C_d	Orifice Drag Coefficient
ρ	Oil Density
β	Bulk Modulus
V_1	Instantaneous Volume of First Oil Chamber
V_2	Instantaneous Volume of Second Oil Chamber
V_{10}	Initial Volume of First Oil Chamber
V_{20}	Initial Volume of Second Oil Chamber
V_{30}	Gas Volume in Third Chamber at Static Equilibrium
V_{40}	Gas Volume in Fourth Chamber at Static Equilibrium
V_{3i}	Precharge Gas Volume
V_3	Instantaneous Gas Volume
κ	Polytropic Gas Coefficient
M_t	Tire Mass
r_t	Tire Radius

I_{yyt}	Tire Mass Moment of Inertia in y Direction
I_{zzt}	Tire Mass Moment of Inertia in z Direction
k_t	Tire Stiffness
c_t	Tire Damping
k	Suspension Stiffness
k_{ϕ}	Roll Stiffness
k_{θ}	Pitch Stiffness
H_{Accl}	Sprung Mass Acceleration Frequency Response Function
$H_{TireDef}$	Tire Deflection Frequency Response Function
H_{SusDef}	Suspension Deflection Frequency Response Function
ω_{bb}	Body Bounce Frequency
ω_{roll}	Roll Frequency
z_{pt}	Relative Displacement of the Piston with Respect to Tire
z_{fpt}	Relative Displacement of the Floating Piston with respect to Tire
Q_{in}	Oil Flow Rate to Second Oil Volume- Control Input
Q_{max}	Maximum Oil Flow Rate
F_{gas}	Gas Force
F_{Damp}	Damping Force
$p's$	Polynomial Coefficient of Gas Force
x	System State
u	Control Input
A	System Matrix
B	Control Input Matrix
F_1	State Dependent Gas Force
f_1	State Dependent Gas Stiffness
f_2	State Dependent Oil Damping Coefficient
F_2	State Dependent Oil Damping Force
F_D	Vertical Disturbance Force

M_{ϕ}	Roll Disturbance Moment
M_{θ}	Pitch Disturbance Moment
F_S	Missile Shock Force
β_r	Road Displacement Model Coefficient
β_s	Angle between Missile and x Axes
w	White Noise
q's	Controller Weighting Parameters
C_{per}	Performance Matrix
r	Reference Suspension Deflection Input
T_i	Traction or Braking Torque at Tires for i^{th} Tire
F_{iO}	Vertical Reaction Force between i^{th} Tire and Ground
F_{iXO}	Traction or Braking Force at i^{th} Tire
F_{iX}	Longitudinal Reaction Force at Wheel Hub of i^{th} Tire
θ_i	Rotation Angle of i^{th} Tire
u	Longitudinal Velocity
S	Longitudinal Slip
C	Magic Formula Tire Model Parameter
D	Magic Formula Tire Model Parameter
B	Magic Formula Tire Model Parameter
E	Magic Formula Tire Model Parameter
S_h	Magic Formula Tire Model Parameter
S_v	Magic Formula Tire Model Parameter
b's	Magic Formula Tire Model Base Parameters for Longitudinal Tire Model
a's	Magic Formula Tire Model Base Parameters for Lateral Tire Model
V	Vehicle Longitudinal Velocity
F_z	Vertical Tire Load
w_{RCPV}	Weighting Factor of Vertical Acceleration for Ride Comfort

w_{RCPP}	Weighting Factor of Pitch Acceleration for Ride Comfort
w_{SPV}	Weighting Factor for the Maximum and Minimum Values of the Vertical Acceleration
w_{SPP}	Weighting Factor for the Maximum and Minimum Values of the Vertical Acceleration
w_{FSP}	Weighting Factor for Maximum Pitch Angle for Firing Shock Performance
w_{BP}	Weighting Factor for the Pitch Angle For the Braking Input
F_{yij}	Reaction Force between Suspension and Sprung Mass in y Direction
M_{ij}	Reaction Moment between Tire and Sprung Mass in z Direction
F_{Tyij}	Tire Cornering Force
δ_{ij}	Tire Steering Input
u	Longitudinal Velocity in Ground Plane
v	Lateral Velocity in Ground Plane
r	Yaw Velocity
Ψ	Yaw Angle
a_{Gx}	Acceleration of Sprung Mass COG in x Direction
a_{Gy}	Acceleration of Sprung Mass COG in y Direction
a_{Gz}	Acceleration of Sprung Mass COG in z Direction
α_{Gx}	Angular Acceleration of Sprung Mass in x Direction
α_{Gy}	Angular Acceleration of Sprung Mass in y Direction
α_{Gz}	Angular Acceleration of Sprung Mass in z Direction
ω_{Gx}	Angular Velocity of Sprung Mass in x Direction
ω_{Gy}	Angular Velocity of Sprung Mass in y Direction
ω_{Gz}	Angular Velocity of Sprung Mass in z Direction
F_x	Forces on Sprung Mass in x Direction
F_y	Forces on Sprung Mass in y Direction
F_z	Forces on Sprung Mass in z Direction

a_{txij}	Acceleration of Tire in x Direction
a_{tyij}	Acceleration of Tire in y Direction
a_{tzij}	Acceleration of Tire in z Direction
α_{tyij}	Angular Acceleration of Tire in y Direction
α_{tzij}	Angular Acceleration of Tire in z Direction
F_{tRCij}	Reaction Force on Tire due to Suspension Jacking
α_{ij}	Slip Angle
F_y	Pure Lateral Tire Force
F_x	Pure Longitudinal Tire Force
F_{x^*}	Longitudinal Tire Force in Combined Tire Model
F_{y^*}	Lateral Tire Force in Combined Tire Model
α^*	Ratio of Slip Angle to Slip Angle at which Maximum Lateral Force Occurs
s^*	Ratio of Longitudinal Slip to Longitudinal Slip at which Maximum Lateral Force Occurs
X_s	Slip Angle or Longitudinal Slip in Magic Formula Tire Model
n_{v30}	Scaled Initial Gas Volume
n_{Damp}	Scaled Orifice Damping
n_{Ar}	Scaled Piston Rod Area
V_{30n}	Initial Gas Volume to be Optimized
PQ_n	Orifice Damping to be Optimized
A_{rn}	Piston Rod Area to be Optimized

CHAPTER 1

INTRODUCTION

HP suspension systems have many advantages with respect to conventional suspension systems, and thus are commonly used in military and off-road vehicles, as well as in some passenger vehicles. In its basic structure, an HP suspension system consists of a gas volume which acts as a spring and an oil volume which provides the damping to the system by flow through an orifice and therefore acts as a damper. General structure of the HP suspension system is shown in Figure 1.1.

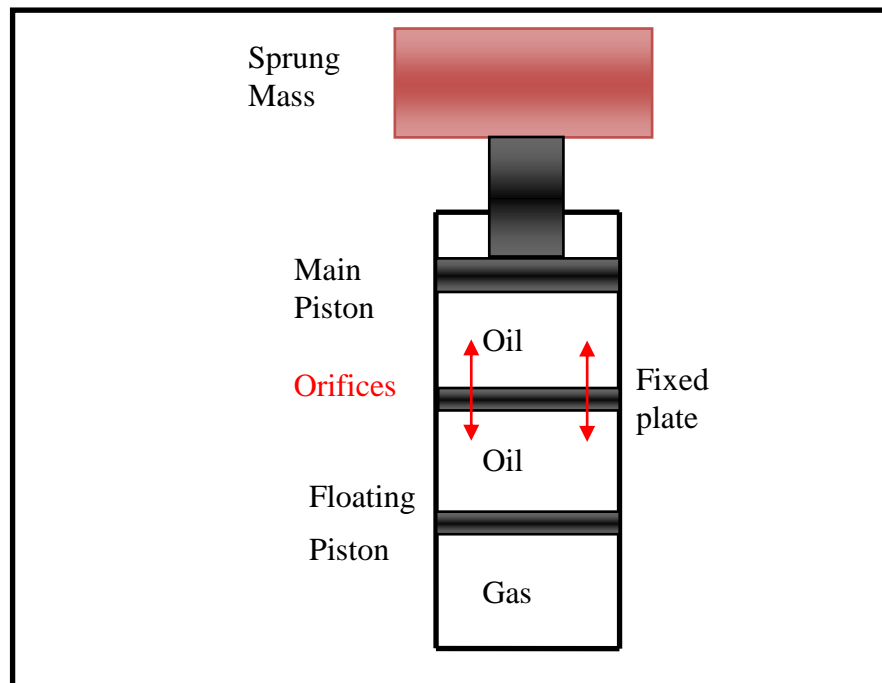


Figure 1.1: General Structure of HP Suspension System

HP suspension system shown in Figure 1.1 consists of the main piston which supports the sprung mass by the piston rod, orifices on the fixed plate which act as damper, the floating piston which separates the gas volume from oil volume, and the cylinder which houses all structural elements, hydraulic oil, and gas. When the cylinder of the HP suspension system connected to the unsprung mass is displaced, the gas compresses or expands and moves the floating piston. Then the oil goes through the orifices on the fixed plate and moves the main piston. Thus, the HP system provides the shock absorbing and damping functions of a suspension system.

HP suspensions have a number of advantages compared with the conventional suspension systems [1]. In conventional suspensions when the sprung mass is increased, since the suspension stiffness is essentially constant the bounce natural frequency of the suspension decreases. On the contrary, in HP suspension systems, when the sprung mass is increased, the stiffness of the suspension also increases and almost constant bounce natural frequency can be maintained. Leveling control of the vehicle can be easily performed with the HP suspension systems, which is difficult to implement in conventional suspension systems. By changing the orifice area and by adding gas into or removing gas from the accumulator, or by connecting or disconnecting another accumulator into the system, damping and stiffness characteristics of the HP suspension can be modified. Therefore, active or semi-active suspension applications are relatively easy in HP suspension systems. Since the gas stiffness increases with an increasing rate when it is compressed, HP suspension system prevents the unsprung mass from approaching its mechanical limits. One of the most important advantages of the HP suspension systems is that implementing interconnections in HP suspension systems are relatively straightforward. By interconnected suspensions, vehicle performance can be improved considerably. However, HP suspension systems have also some disadvantages when compared with mechanical suspensions. Due to their more complicated structure, they have high initial and maintenance costs and relatively low reliability. Nevertheless due to their significant advantages, HP suspension systems enjoy wider use in many types of vehicles including military vehicles, off-road vehicles, heavy commercial vehicles, and large mobile cranes.

An active HP suspension system can be obtained by pumping oil to hydraulic cylinder or extracting the hydraulic oil from the hydraulic cylinder. By this way, improved ride comfort characteristic can be obtained. In mechanical suspension systems with the conventional helical spring and the shock absorber, application of active suspension is somewhat difficult, since a separate actuator placed between the sprung and unsprung masses is required. On the other hand, a separate hydraulic actuator is not required for an active HP suspension system.

For off-road vehicles different vehicle height is required for off-road and on-road driving performance. On off-road conditions, a high vehicle height is required. On the contrary, on the asphalt roads a low vehicle height is required for good handling. Therefore, the suspension system should adjust the vehicle height according to the user defined suspension input. For vehicles with mechanical suspension system this requires an extra actuator. However, for a vehicle with HP suspension system, vehicle height can be adjusted by changing the oil volume in the hydraulic cylinder.

Another advantage of the HP suspension systems is that stiffness and the damping characteristic of the suspensions can be changed easily by driving the valves on the suspension hydraulic circuit. For sport utility vehicles with sport and soft driving conditions, stiff spring and damper characteristics are required for good handling, while softer spring and damper characteristics are needed for more comfortable driving conditions. Again with mechanical suspension, hard and soft driving settings cannot be obtained easily. However, with an HP suspension system, spring characteristics can be modified by increasing or decreasing the gas volume or by adding or removing extra gas volumes into the system. Similarly softer and stiffer damper characteristics can be obtained by simply opening or closing the on-off directional control valve in the system.

For road vehicles, requirements for good handling and ride comfort are in conflict. In general, good ride comfort requires a relatively soft suspension and good handling requires a stiff suspension. Therefore, in order to improve vehicle handling without degrading the ride comfort, an anti-roll bar which is a suspension stiffener in the roll plane is used. Thus, left and the right suspension units are connected to each other by

a mechanical bar. In vertical motion, anti-roll bar does not affect the vertical motion significantly. However, in roll anti-roll bar increases the roll stiffness and improves handling. Similarly, for a vehicle equipped with an HP suspension system, left and right suspension can be interconnected in a special pattern to increase the roll stiffness. By this interconnection the handling of the vehicle can be improved without affecting the vertical motion. Anti-roll bar is used in the roll plane easily, yet for pitch motion use of the anti-roll bar is not applicable due to space requirements and cost. On the other hand, for a vehicle with HP suspension systems, suspension units in roll and pitch plane can be interconnected easily by adding cheap hydraulic conductors and desired suspension performance can be obtained with different interconnection patterns. For commercial vehicles, military vehicles, and off-road vehicles with multi-axles, interconnections of the HP suspension units for performance improvements in handling, ride comfort, mobility, and the load sharing result in significant advantages.

Due to all these advantages of the HP suspension systems with respect to the commercial mechanical suspensions, they have been more and more commonly used in road and off-road vehicles. Thus, the possible approaches to the design and optimization of the HP suspension systems for ride comfort are investigated in this dissertation. While ride comfort is optimized, improvement of the handling and the mobility of the vehicle are also considered. Moreover, analysis and design of the interconnected HP suspension systems for two and multi-axle vehicles are also studied. The topics of detailed investigation are summarized below.

- ❖ Modeling of the HP suspension system unit.
- ❖ Parametric design of the HP suspension system unit.
- ❖ Active HP suspension design for ride comfort, handling, and the attitude control.
- ❖ Adaptive HP suspension design for the performance improvements of the active HP suspension system.
- ❖ Analysis and design of the interconnected HP suspension system for two and multi-axle vehicles in pitch plane.

- ❖ Analysis and design of the interconnected HP suspension system for the full vehicle model in roll and pitch planes.
- ❖ Optimization of the unconnected and the interconnected HP suspension systems for improved ride comfort together with handling constraints.

In the literature, there are a number of studies related to the modeling, simulation, and analysis of HP suspension systems. Those studies cover mainly some aspect of interest and many possible applications of the HP suspension system have not been covered to any extent. Most of the publications consider a simple model with only a single HP suspension unit without going into higher order models, and thus cannot provide insight into the interaction between suspension units of a vehicle. Some studies provide a qualitative analysis only and they lack a formal quantitative analysis. The potential of interconnected HP suspensions have received only very limited attention. The motivation of this thesis study is to contribute to the work done so far on HP suspension systems, considering a unified approach starting with the basic ideas with simple systems and then extending the investigation to more complicated higher order active and passive systems. Further, it is aimed to handle the difficult aspect of interconnected HP suspensions in a more detailed fashion.

In the thesis, second chapter presents a literature survey covering the modeling and the analysis of the HP suspension systems, studies on the active and semi-active HP suspension systems, different active HP suspension layouts, control methods, and simulation results together with the interconnected HP suspension systems. In the third chapter, a mathematical model for the basic HP suspension unit is developed and a detailed parametric design analysis is performed. In the fourth chapter, active HP suspension system design for the quarter car model, half vehicle model, and full vehicle models are studied. Firstly, the models of these active suspension systems are developed and then active suspension controllers are designed. In the fifth chapter, a general study on the interconnected HP suspension systems is given. For a vehicle with three axles, possible interconnections are determined. In sixth chapter, analysis and design of the interconnected HP suspension system for the vehicle pitch plane is carried out to increase the pitch performance. In seventh chapter, analysis and the

design of the interconnected HP suspension systems for the full vehicle model are considered. Different interconnection layouts are determined and compared to each other. In chapter eight, a general guideline for the design of the interconnected HP suspension system for the multi-axles vehicles is proposed. In chapter nine, optimization of the parameters for the interconnected HP suspension systems is made. The optimization is aimed to increase the ride comfort, yet vehicle handling is also taken into account. Effect of the performance improvements of the interconnected HP suspension on the ride comfort was illustrated by a detailed study comparing the results from the simulations of the optimized interconnected and unconnected HP suspension systems. In chapter ten, studies in this dissertation are summarized and conclusions reached are stated.

CHAPTER 2

LITERATURE SURVEY

In this chapter, previous studies on the modeling, simulation, and applications in vehicles of HP suspension systems are presented. The detailed reviews of the previous studies are given together with their contributions and limitations. Then the motivation and contribution of this study are discussed.

2.1. INTRODUCTION

There are studies in the literature on various different aspects of the HP suspension systems. The main subjects of these publications may be classified as,

- ❖ Modeling and analysis of the HP suspension systems,
- ❖ Active and semi-active HP suspension systems,
- ❖ Interconnected HP suspension systems,
- ❖ Optimization of the HP suspension systems.

In the following sections, each subject is covered in turn.

2.2. LITERATURE SURVEY

In the publications in vehicle dynamics, there is a somewhat limited number of studies taking the HP suspension system as the subject area. In the study of Deprez et al. [2], passive and semi-active Hydro-pneumatic suspension system used as a cabin suspension in an off-road vehicle was optimized to improve ride comfort. The cost function was formed as the squared difference between the desired frequency

response function and the actual frequency response function. The HP suspension system was modeled in Matlab/Simulink and its schematic representation is given in Figure 2.1.

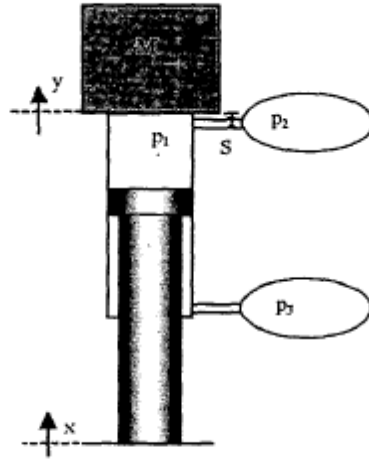


Figure 2.1: HP Suspension System [2]

In the passive model the optimized parameters were internal pressure, volume of two nitrogen bulbs, opening of the valve, and the dimensions of the hydraulic cylinder and piston. In semi-active HP suspension system, the damping force was taken as proportional to relative velocity between the input and output. The design parameters in this force model were optimized according to effective root mean square and vibration dose value. According to results, the semi-active suspensions were better than the passive suspensions, while passive suspensions reduced effective root mean square and vibration dose values by more than 60 and 80%, respectively, as compared with the no suspension condition.

In the study by Shi et al. [3] a nonlinear HP suspension model was linearized using feedback linearization and then the sliding mode control method was applied to get an active HP suspension system. The schematic of the HP suspension system is given in Figure 2.2.

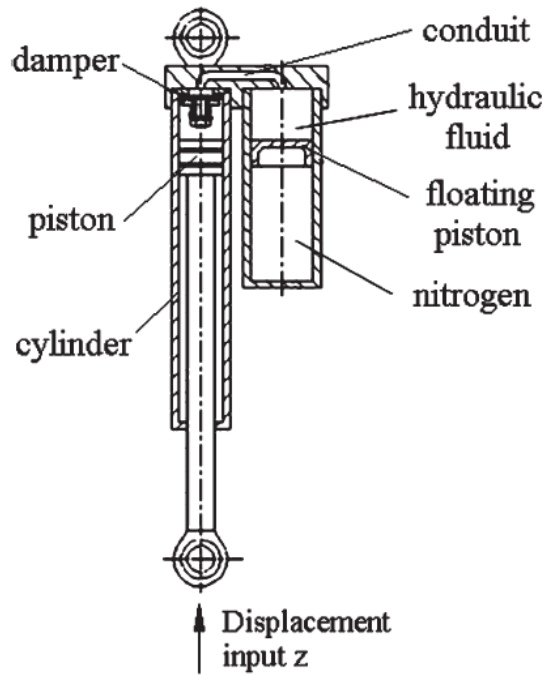


Figure 2.2: HP Suspension System [3]

In this study while modeling HP suspension system, the compressibility of the hydraulic oil was neglected. To validate this model, a test rig shown in Figure 2.3 was used. In static tests the force and displacement input are measured to obtain the static stiffness characteristics of the HP suspension system. In dynamic characteristics tests, sinusoidal displacement input is used and the relation between the force and displacement inputs is measured. After the mathematical model was validated, the active HP suspension system was formed by pumping or extracting hydraulic fluid into the system or from the system using two different pumps, one of which is small and the other of large capacity as shown in Figure 2.4. The friction between the piston and the cylinder was neglected. After the active HP suspension system was modeled, it was linearized by feedback linearization method. Then the sliding mode control method was applied to control the active system. The simulation results showed that the active system has more accurate results and robustness as compared with the passive system.



Figure 2.3: Test Rig for the Validation of the HP Suspension Model [3]

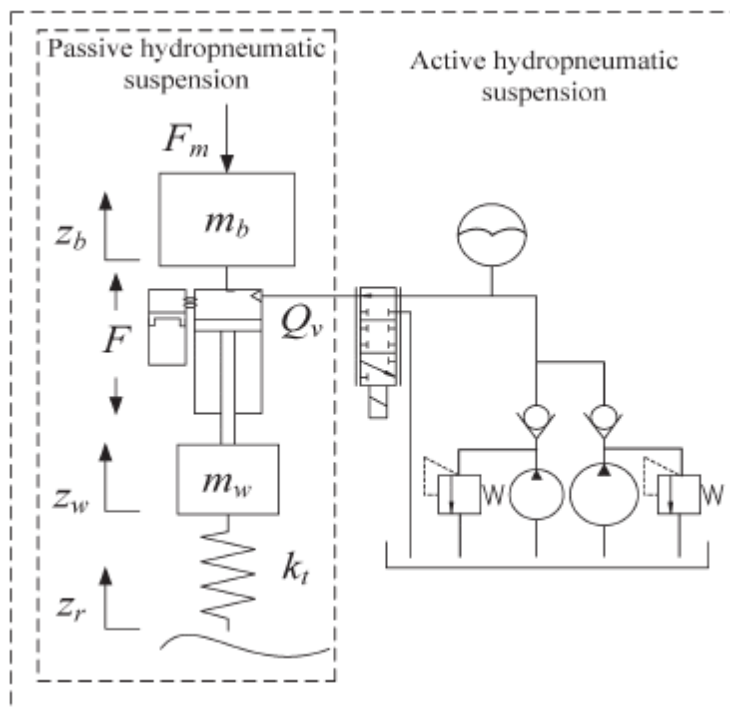


Figure 2.4: Active HP Suspension System [3]

In the paper of Gao et al. [4], a semi-active HP suspension was designed and investigated by developing the passive HP suspension. This suspension was built and investigated on the quarter car model. There are two different controllers, one of which is a two-stage controller and the other of which is continuously adjustable damping controller. The model of the suspension system is shown in Figure 2.5.

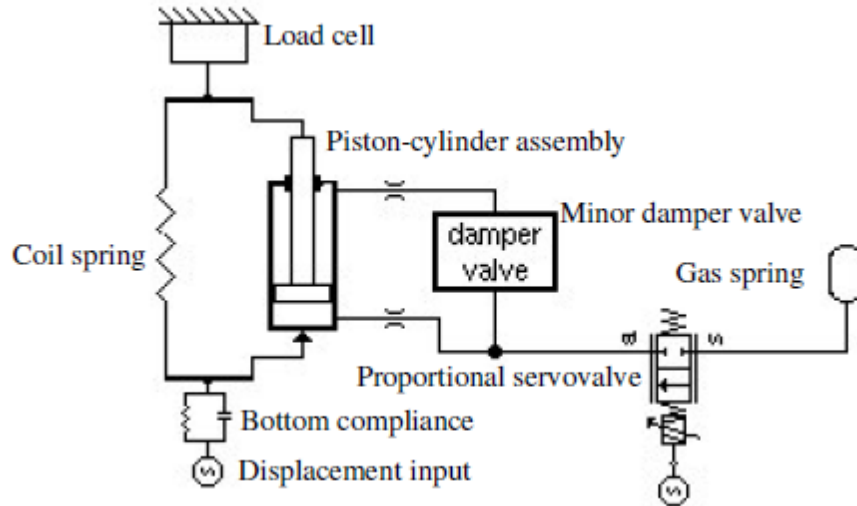


Figure 2.5: Semi-Active HP Suspension System [4]

In this study, the damping force in the hydraulic cylinder was assumed to include Coulomb friction and a velocity dependent damping. The leakage across the piston was also taken into account, and the fluid compressibility and cavitation effects were modeled. The damper valve was modeled using experimental data and it was incorporated into a look up table. In the simulation the cubic spline or linear interpolation of damper valve was used. The proportional servovalve was modeled as a second order critically damped system in which the input is the valve current and the output is the valve position. In this study the skyhook damper control was used to obtain a semi-active HP suspension system. The nominal drive current was optimized with respect to body accelerations, tire deflections and suspension deflections to find an optimum controller. After the optimization of the controller, simulations were performed. Simulation results showed that the two-stage valve caused harshness problems and in general continuously variable valve provided better performance. Since the sensors used were limited, filters were designed to

measure the body and suspension velocities using the body accelerations and suspension travel. In addition, it was shown that the valve bandwidth should be 20-30 Hz to achieve sufficient performance.

In the paper of Beno [5], a simulation-based active suspension control system was developed. The vehicle model was constructed in a Multi Body Simulation Software DADS and the suspension controller was designed on the Matlab/Simulink. Two systems were then coupled and the suspension unit of the military tank modeled in the DADS was controlled using the control unit formed in the Simulink. The coupled system is shown in Figure 2.6.

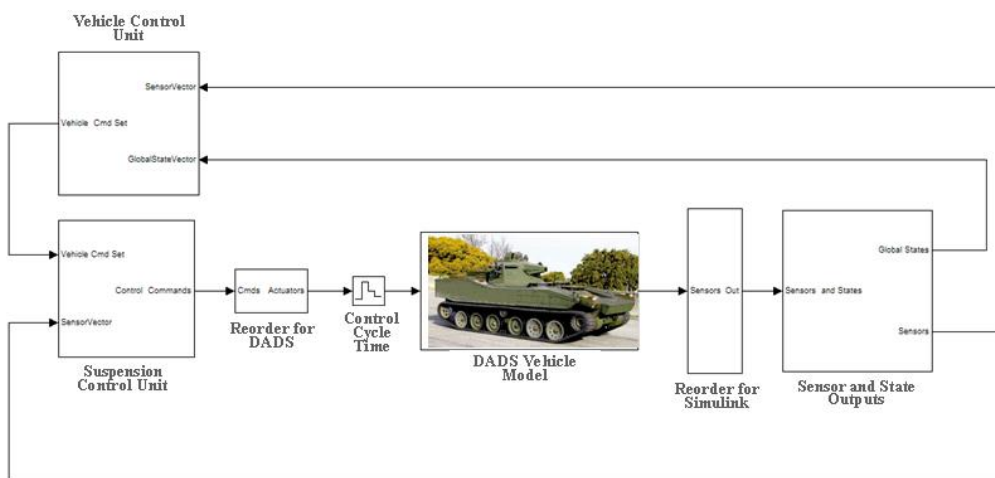


Figure 2.6: Coupled Controller and Vehicle Model [5]

Vehicle states and outputs taken from the simulations were fed into vehicle control unit and the suspension control unit. Then a control input was sent into actuator in the vehicle suspension to obtain active suspension control. To validate the vehicle and suspension model, tests were performed with the suspension system and the full vehicle.

In the paper of Gao et al. [6] the HP suspension systems were modeled in two different ways. Firstly, Bathfp software was used for detailed physical modeling of the HP systems using dynamic equations and experimental data, and then the neural network model of the system was obtained. In the neural network modeling, experimental data was used to train the model. The structure of the HP system used

in this study is shown in Figure 2.7. The test rig of the HP suspension system is shown in Figure 2.8. At the top of the HP suspension system there is a load cell which is used to measure the strut force and the displacement input is given from the bottom of the system. In the actuator model the friction was modeled as a combination of the Coulomb friction and velocity dependent friction. The compressibility of the fluid was taken into account using a first order model. Leakage across the piston was considered, yet leakage across the rod seals was not included in the model. Moreover the cavitation effect of the fluid volume was taken into consideration. In this study the identification of the friction forces were performed by the existing test setup. The damper valves were removed and then the strut was excited using 0.01-20 Hz frequency input. Then the friction model of the strut consisting both constant and the velocity dependent parts was identified. The damper valve model was identified using flow bench tests and a look up table was formed to be used in the HP suspension model. To train the neural network model, HP suspension was tested with a random road profile. The input in the test was the velocity and displacement of the strut and the output was the strut force. Then, the HP suspension was tested with the random road profile input and the same input was used in the simulation of the Bathfp and the neural network model. The results showed that neural network model gave better results than the Bathfp model. It was concluded that since the Bathfp model does not consider higher dynamics, using neural network model is more appropriate. However, since the Bathfp model was a physical model, it could be used to examine the system dynamics especially when the parameters of the system changed. The neural network model did not consider the changes in parameters since it was trained with a fixed parameter set.

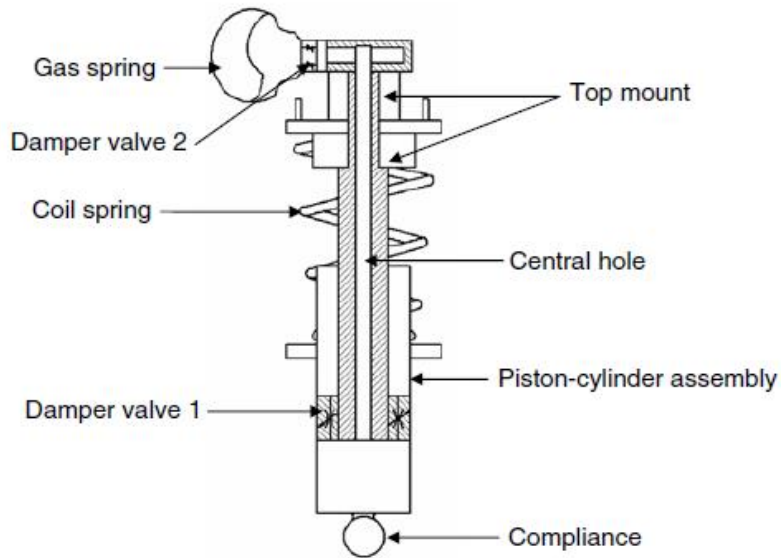


Figure 2.7: Structure of the HP Suspension Systems [6]



Figure 2.8: Test Rig for HP Suspension System [6]

In the paper of Gao et al. [7], control of active HP suspension system was described. The system consisted of an HP suspension systems and a nonlinear valve. HP

Suspension system and the three-way flow control valve were modeled in the fluid power simulation software Bathfp. The structures of the HP suspension system and the valve are shown in Figure 2.9. HP suspension model was adopted from [6]. The dynamics of the proportional valve was identified by an experimental study. The active suspension control is shown in Figure 2.10. After the model was constructed, it was validated on the four poster vehicle tester. The harmonic sine inputs and the random road profile inputs were used in the model validation. Then the system model was linearized and the model was reduced for use in control applications. The objective of the controller was disturbance rejection and the body leveling control. Linear Quadratic controller was used for disturbance rejection. For leveling control, a PID controller which uses the suspension deflection as the feedback was designed. These controllers were evaluated in Bathfp nonlinear model using simulations. In this paper, other practical issues of the active suspension systems like valve bandwidth, valve deadband, and power consumptions were also examined.

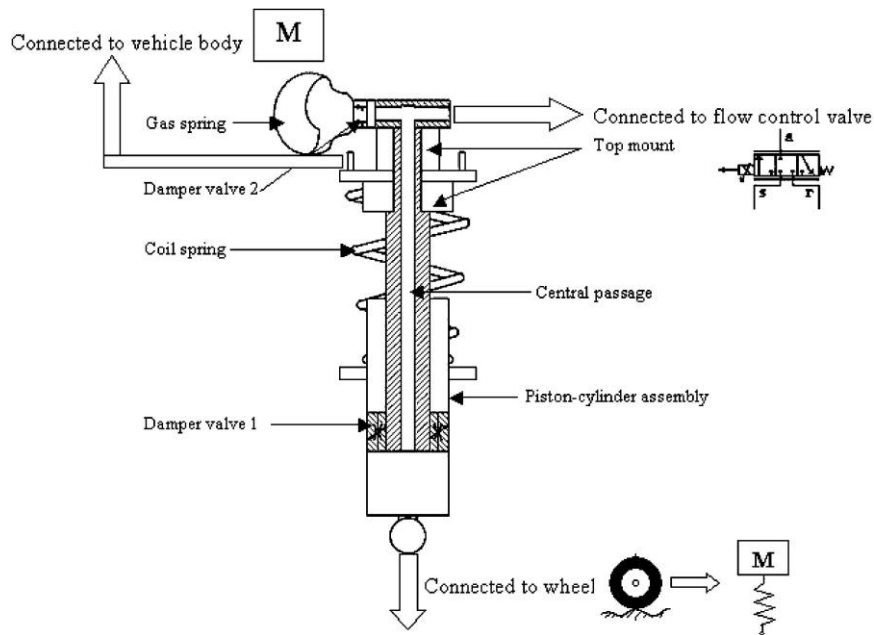


Figure 2.9: HP Suspension System and Flow Control Valve [7]

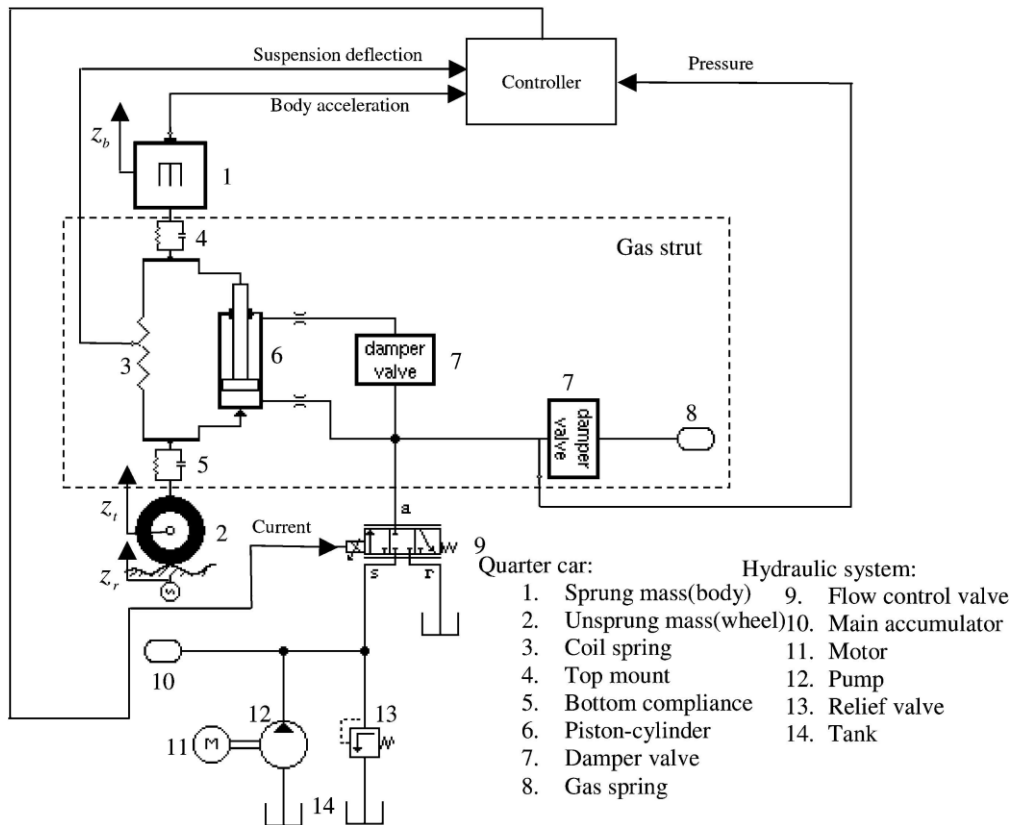


Figure 2.10: Active Suspension Control [7]

In the study of Giliomee et al. [8], a semi-active HP suspension system was designed. The semi-active HP suspension system consists of two state HP springs and two state dampers as shown in Figure 2.11. By switching between two different spring states, both good ride comfort and good vehicle handling were obtained. Similarly, by switching between two different damper states, good ride comfort was obtained in different road conditions. Therefore in this study, by changing the damper and spring states, an improved ride comfort and handling were obtained in different road and driving conditions. With this system, the height adjustment of the vehicle could also be performed.

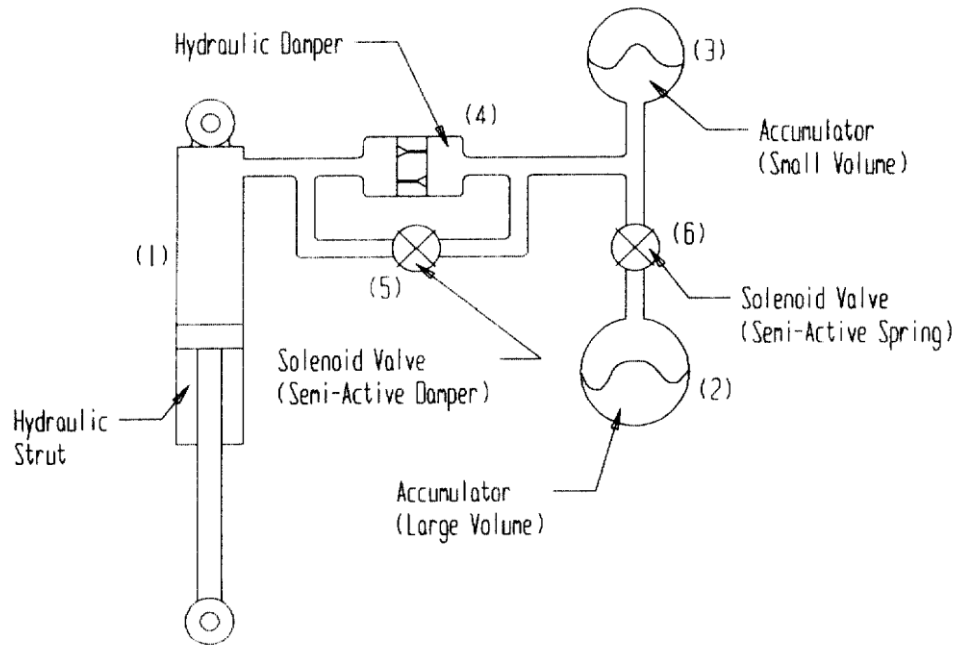


Figure 2.11: Two State Switchable Semi-active HP Suspension System [8]

In the paper of El-Tawwab [9], an advanced semi-active HP suspension system was evaluated, and it was compared with the passive HP suspension system and the twin accumulator systems. The general structure of the passive and the twin accumulator HP suspension systems were given in Figure 2.12 and Figure 2.13, respectively.

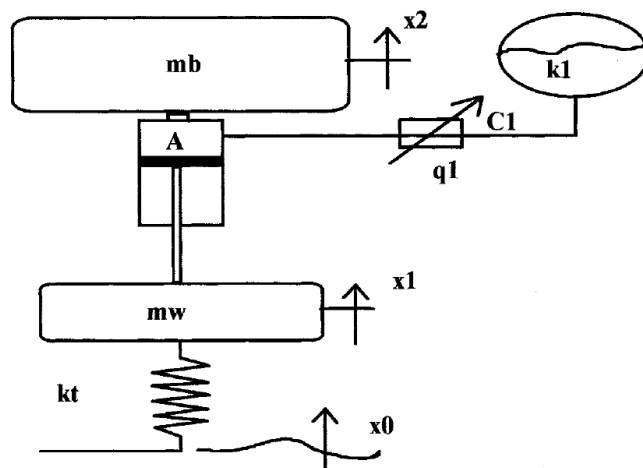


Figure 2.12: Quarter Car Model with Passive HP Suspension System [9]

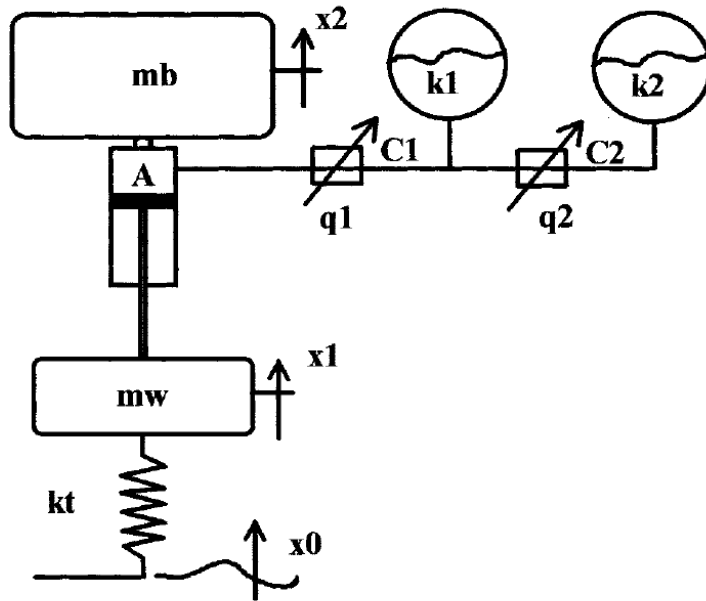


Figure 2.13: Quarter Car Model with HP Suspension System with Two Accumulators [9]

In this study, the semi-active HP suspension system was obtained by the modification of the double accumulator-HP suspension systems. The general structure of the semi-active HP suspension system is given in Figure 2.14.

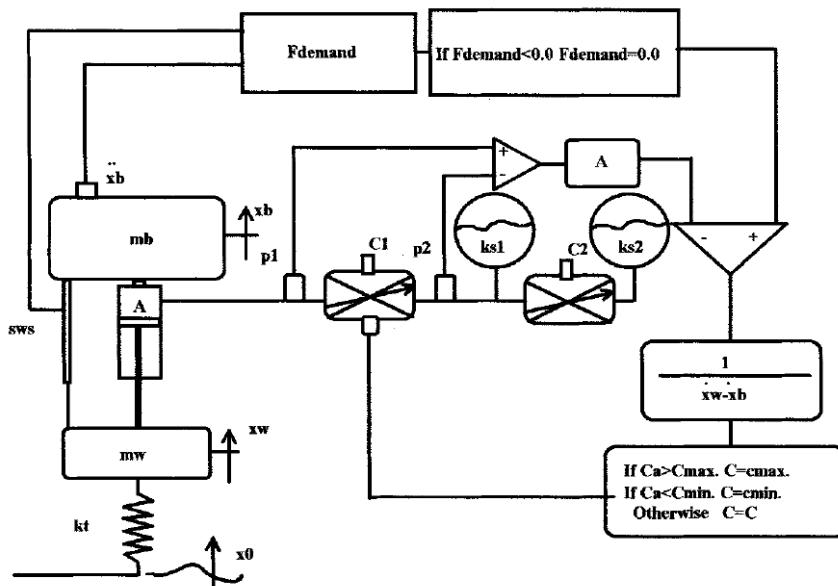


Figure 2.14: Semi-active HP Suspension System [9]

The quarter car model with twin accumulator HP suspension was simulated with a random road profile input, and the root mean square values of the body acceleration, suspension displacements, and tire loads were calculated. Simulations were repeated by changing the openings of the orifice valves. In the frequency range from 1.5 to 8.0 Hz, dynamics tire loads and the body acceleration results were improved. According to the simulation results, the best ride comfort was obtained by adjusting the openings of the first damper. Therefore, the twin accumulator suspension system gave better performance than the conventional HP suspension system. Finally the semi-active HP suspension system gave the best result of all suspensions systems.

In the paper of Sihong and Baozhan [10], a model of the HP suspension system with an adjustable damper was developed. Then the effects of the changes of parameters on the output force characteristics of the HP suspension were examined. The structure of the HP suspension system is shown in Figure 2.15. The friction between the piston and the cylinder and the compressibility of the oil were neglected.

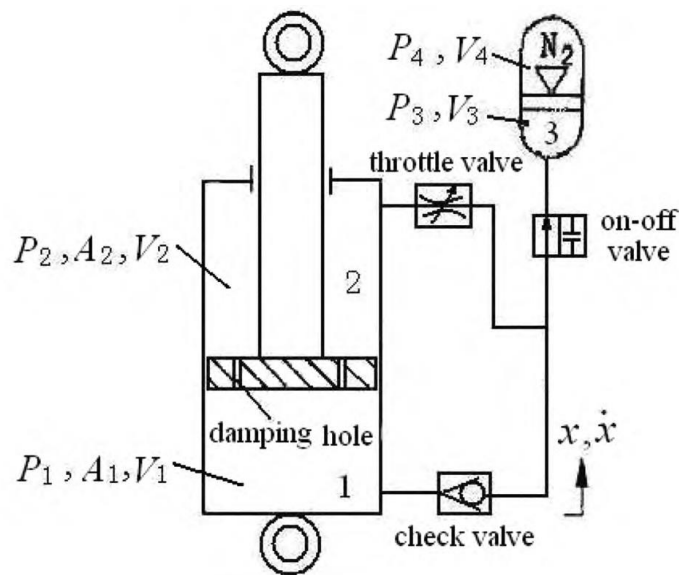


Figure 2.15: HP Suspension System [10]

The design parameters were the initial volume and pressure of the accumulator, the number and area of the valves, the diameter of the throttle and the input parameters. When the initial pressure was increased, the displacement and velocity output curves were translated upwards while the shape of the curves did not change. The effect of

the initial volume was more important in compression. Moreover, decreasing the diameter and number of orifices increased suspension force. When the diameter of the adjustable valve was small, the change in the output force was high. In addition, the sinusoidal input affected the velocity and displacement characteristics of the output force. A rise in the amplitude and frequency of the input led to a considerable rise in the output force.

In the paper by Purdy et al. [11], a mathematical model of the HP suspension system was derived and simulated. Compressibility of the hydraulic oil and the compliance of the components of the HP suspension system were also included in the model. Spring loaded orifice valves were used as dampers. Moreover, the friction between the piston and the cylinder was neglected and while deriving the equation of motion of the system, piston mass was neglected. Then the HP suspension system was incorporated into the eight degrees of freedom, six-wheel station tracked vehicle. The optimum orifice diameters were determined for different terrain inputs.

In the paper by Siminski [12], a HP suspension model was integrated into the multibody dynamics model of the 8-wheeled armored fighting vehicle. Various simulations were performed to examine the dynamics and performance of the vehicle. Similarly, in the paper of Ryu et al. [13], both torsion bar and HP suspension systems were integrated into the multibody dynamics model of the tracked military vehicle and various simulations were performed.

In the paper of Becker et al. [14], an active suspension system which used HP suspension system was designed for the active body control of a bus. The HP suspension model was validated by experiment and was used in a simple vehicle model as shown in Figure 2.16. Controllers were designed for pitch, roll, and height control of the body. The controller parameters were determined by optimization. The bus was tested in a double lane change maneuver and it was shown that with the controlled suspension, better driving safety can be obtained.

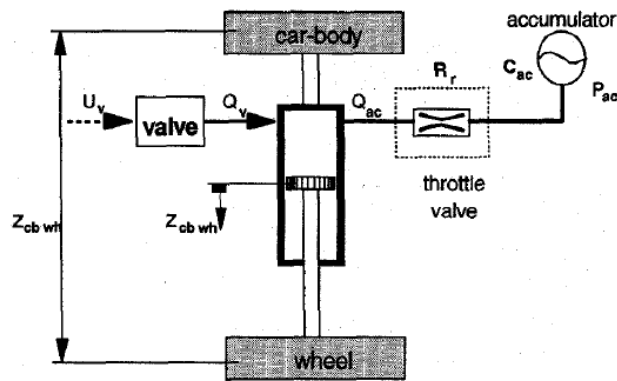


Figure 2.16: HP Suspension System [14]

El-Demerdash and Crolla [15] studied the active and slow-active HP suspension systems with preview control. They developed a linear HP suspension system and used a linear optimal control approach for the active suspension. Rosam and Darling [16] designed an active roll controller to improve the roll motion for the interconnected HP suspension system. Schuman and Anderson [17] used an optimal control law to design a controller for an active suspension to control the roll motion in an interconnected HP suspension system. The nonlinear interconnected hydragas suspension model was linearized to design the linear optimal controller.

In the thesis by Joo [18] a detailed model of the HP suspension was developed. The shock and vibration isolation potentials of the HP suspension system were examined. Then the HP suspension model was incorporated into a seven degrees of freedom tracked military vehicle model. The author reached the conclusion that the HP suspension model gave better results than the conventional suspensions as regards to vibration and shock isolations. There is also a book written about HP suspension. In the book by Bauer [1], general structures and practical considerations about the HP suspension, rather than dynamics of HP suspension system, were detailed.

The studies about the HP suspension in the literature are mostly about the modeling, simulation, and control of the single unit HP suspension systems. Mathematical model of the HP suspension system is derived and simulations are performed to examine the dynamics of the system. If a controller is to be designed, the HP suspension system is linearized, and then linear controllers are designed for semi-

active and active suspension systems. There are also studies which use full vehicle models or multibody dynamics model with HP suspension systems. In these studies, simulations are performed mostly to examine system characteristics rather than control them.

In the literature there are some studies investigating the interconnected suspension configurations [19] - [24]. In these studies, the so called X type suspension interconnection is examined. In this configuration, the aim is to increase the roll and pitch stiffness, and the roll and pitch damping for improved vehicle handling and mobility. For the pitch and the roll motion, this type of interconnection may be used to increase the stiffness and damping to get superior performance against the disturbances coming from the vehicle body. In the thesis by Cao [19], HP suspension systems including single and twin gas chambers were modeled and then roll and pitch interconnected HP suspension systems were studied. Bounce, pitch, roll, and the warp responses of the vehicle with interconnected suspensions to external excitations were examined. It was shown that hydraulically coupled vehicle suspensions enhanced the vehicle ride and handling performance of the vehicle considerably. Zhang et al. [22] derived the frequency dependent mathematical model of the hydraulically interconnected suspension system in the pitch plane. For this model, a test setup was prepared and the tests were performed in order to evaluate ride comfort. Results from the model and experiments were compared and the model was validated. Zhang et al. [23] derived the mathematical model of the full vehicle model with hydraulically interconnected suspension system. Simulations, performed for the vehicle handling, showed that hydraulically interconnected suspension systems improved vehicle handling, yet they decreased vehicle ride comfort at the same time. Ding et al. [24] studied the modeling of a vehicle with three-axles by the hydraulically interconnected suspension system in the pitch plane.

In literature, there are numerous studies about the active and semi-active control of conventional suspension systems. Basic functions of the suspensions, suspension control methodologies, and the theoretical and practical limitations of the controllable suspensions were examined in the study by Karnopp and Heess [25].

Butsuen [26] examined invariant properties of the quarter car model and analyzed different performance considerations in active suspension systems. Elmadany [27] proposed an optimal linear active suspension system controlled by multivariable integral control. Alleyne et al. [28] investigated linear and nonlinear control methods in active suspension systems. The desired active force was obtained using skyhook control methods and the realization of the control force from the hydraulic actuator was performed using Proportional, Integral, and Derivative (PID) control, feedback linearization control, and sliding control. They showed that active suspension with a nonlinear control method provided better performance than that with linear control. Pilbeam and Sharp [29] examined different active suspension system configurations with preview control together with power consumptions. Thompson and Chaplin [30] studied the inner loop force control in active suspensions. Applications of the optimal control theory in vehicle dynamics area were investigated in the study by Sharp and Peng [31]. Hudha [32] designed an active suspension system for a vehicle with firing capability. Performance of the active suspension system was examined against disturbances coming from firing shocks and the road. Youn et al. [33] designed an active suspension for the attitude and the level control of a full car model. The integral control was used to obtain zero steady state suspension deflection for ramped road and the body forces and the derivative control was used to improve the performances for the bump and braking inputs. Wang and Shen [34] studied the active suspension control for vehicle ride, and roll control for the full car model. Roll control was achieved by actively tilting the vehicle body inwards against the steering maneuvers. It was shown that integrated ride comfort and roll controls improved ride comfort and prevented possible vehicle rollover. There are other studies on active suspensions with conventional suspension systems which use control approaches such as H-infinity control [35], switched control [36] hybrid control [37] and fuzzy control [38]. Cooke et al. [39] studied the active control of vehicle ride comfort and handling. Two control strategies for ride comfort and the road holding were derived and then combined. The performance of combined controllers was tested for straight running, J-Turn test, Sine Steer Test, Double Lane Change Test. They showed that,

in general, combined controller had slightly superior performance for handling and ride comfort simultaneously.

In the literature, there are many studies on the parameter optimization of vehicle suspension system. In most of these studies, stiffness and damping parameters of the suspension units are optimized. Wong [40] examined the effects of the spring stiffness, damper damping, and the unsprung mass on the ride comfort, suspension packaging, and the road holding performance for a quarter car model. Thoresson [41] studied the optimization of the suspension system parameters of an off-road vehicle for ride comfort and handling. The parameters, damping characteristics scale coefficients, and the HP suspension gas volumes of the front and rear suspensions are optimized. Objective function for the vehicle ride comfort and handling was defined as the weighted rms of the vertical acceleration and body roll angle, respectively. Els and Uys [42] studied the optimization of the suspension system for ride comfort and handling. Parameters of the suspension system, HP suspension gas volume and damper scale factors, were optimized. The cost function to be minimized was formed as the weighted rms of the vertical acceleration in the Belgian paved road simulation, and the optimization constraint was formed as the maximum roll angle in the double lane change simulation. Then, maximum roll angle was taken as the cost function and rms of the vertical acceleration was used as the optimization constraint. According to the results, it was suggested that optimization should be performed for improved handling for better optimization results. Drehmer et al. [43] studied the optimization of the suspension system parameters for ride comfort, suspension packaging, and road holding on different roads at different longitudinal velocities. A detailed sensitivity study was performed to examine the effects of the suspension system parameters on the objective function. In the studies of Naude and Snyman [44], [45] damper parameters of the suspension system of a three axle vehicle for ride comfort were optimized. Thoresson et al. [46], [47] studied the modeling of a simplified vehicle ride and vehicle handling to be used in the vehicle suspension optimization and the full vehicle model in Msc ADAMS software. The simplified vehicle models were used for the gradient information and the full vehicle model was used for the objective function evaluation. Normalized HP suspension gas volume

and normalized damper scale factors were used as the parameters to be optimized. Optimization were performed according to ride comfort, handling, and both ride comfort and handling. As expected, for handling optimization, gas volumes were set to the lower bounds on the boundary and damper values were set to upper boundary values. For ride comfort, gas volumes were set to upper boundary values and dampers were set to lower boundary values. For combined ride comfort and handling optimization, the damper and gas volumes were set to values within the parameter space for compromised solution. Choi et al. [48] designed an optimum suspension for the best vehicle mobility. Optimum suspension parameters to minimize the stabilization time and the driver vertical acceleration were found.

2.3. MOTIVATION

In the literature, there are somewhat limited number of studies about the HP suspension systems. Most of these are concentrated on the modeling, simulation, and control of single unit HP suspension system. There are also a limited number of studies on the interconnected HP suspension systems. Studies on the interconnected HP suspension systems are mostly for vehicles with two axles. The following topics involving the HP suspension systems have not received adequate cover in the literature and will be examined in full detail in the following chapters.

2.3.1. Development of Single Unit HP Suspension Systems

In the literature, usually the simple configuration of the HP suspension system which consists of a single gas volume and orifices was modeled. However, when additional gas volume and orifices are added to the basic HP suspension system, different stiffness and the damping characteristics can be obtained. In this study, HP suspension systems with single and double gas chambers are going to be modeled, analyzed, and compared to each other. Similarly, HP suspensions systems with single and double orifices are also be examined.

2.3.2. Active HP Suspension Design

In the literature, there exists large number of studies in which a single unit HP suspension system is studied, and controllers are designed for active and semi-active

suspensions. Since the HP suspension has highly nonlinear dynamics, the model is first linearized, and then linear controllers are designed. In this study, to capture the true dynamics of the system, nonlinear controllers will be designed for the single unit HP suspension model, half vehicle model, and the full vehicle model for active suspension designs. Active controllers to improve ride comfort and attitude control are studied in only a few studies. In these studies, attitude and the ride comfort control are performed separately, and then two controllers are combined. Moreover, one of the important concepts in the controller design, stability analysis is not carried out in most of the active HP suspension system studies. In this dissertation, an active controller for both ride comfort and attitude control is examined in a detailed way, and a combined controller is directly designed. Since there is only a compromise solution for the simultaneous attitude control and ride comfort control, an adaptive active controller is designed to improve ride comfort and attitude control performances simultaneously and a mathematical analysis of the stability of the proposed controller is carried out.

2.3.3. Interconnection of the HP Suspension Systems

One of the main advantages of the HP suspension system is that the HP suspensions in full vehicles can be interconnected by hydraulically or pneumatically. By this way handling, ride comfort, and pitch and roll stability of the vehicle can be improved. The most detailed study about interconnected HP suspension systems was performed by Cao [19]. As also specified in that study, different strategies of passive interconnected suspensions can be developed. However, interconnected HP suspension systems for multi-axle vehicles are not adequately studied. In this study, interconnected HP suspension systems for multi-axle vehicles are studied in detail and a general conclusion is made.

With the results found from this study, vehicle designer can select the best interconnected suspension configuration for the specific purposes. Thus, the interconnected HP suspension system studied for the three axle vehicles is generalized for the four and multi-axle vehicle models.

2.3.4. Optimization of the HP suspension system

When a new suspension is designed, its parameters must be tuned for different objectives such as ride comfort and handling. To be able find the correct parameter set, related parameters have to be optimized for specific purposes. Similarly, when the controller is to be designed for the active and semi-active suspensions, the controller parameters can also be found by parameter optimization.

Optimization studies have been performed mostly using a quarter car model with the HP suspension system. Optimization studies can also be applied to full vehicle model or multibody dynamics model of a vehicle. In this case, the optimization can be performed with respect to roll stability, pitching, vertical ride comfort, leveling of the vehicle, and handling. Thus, the vehicle can be designed for realistic driving conditions. Therefore, in this study the HP suspension parameters will be optimized both for full vehicle model equipped with unconnected and interconnected HP suspension systems. In the literature, there are no studies on the optimization of the interconnected HP suspension systems. In this study, the parameters of the interconnected HP suspension systems are optimized to find the best ride comfort with a handling constraint. Therefore, a method of selecting the type of the interconnections and the parameters of the interconnection are proposed.

CHAPTER 3

MODELLING OF THE HP SUSPENSION SYSTEMS

In the literature, there are a number of different HP suspension models each of which is suited for a different application. In its basic form, a HP suspension model consists of a gas volume, two oil volumes, and an orifice (or damping valve). The gas volume provides system with elastic element to absorb road shocks and the flow of oil through the orifice provides system damping. However, for different applications, one or more other components can be inserted to the system.

3.1. MODELING OF THE HP SUSPENSION

In this chapter, an HP suspension system with a single gas chamber is modeled, and its static and dynamic characteristics are examined in both time and frequency domains. Then, the HP suspension system with double gas chambers and double orifices are modeled, their characteristics are examined, and they are compared with the HP suspension system having a single orifice and a single gas volume.

3.1.1. Modeling of the HP Suspension System with Incompressible Oil Assumption

The general structure of the HP suspension system considered in the following modeling phase is shown in Figure 3.1.

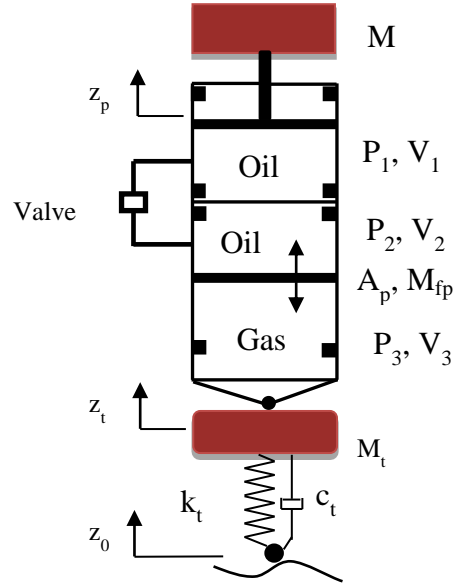


Figure 3.1: Quarter Car Model with HP Suspension System

The first step in the derivation of the mathematical model is to write the force balance to determine the force on the piston. The piston force, F , is

$$F = P_1 A_p - F_{pf} - F_{pHS} \quad (3-1)$$

where P_1 is the oil pressure in the first oil volume, A_p is the piston area, F_{pf} is the Coulomb Friction between piston and the cylinder wall, and F_{pHS} is the force between the piston and the hard stops. The equation of motion for the sprung mass can be written as

$$P_1 A_p - Mg - F_{pf} - F_{pHS} = M\ddot{z}_p \quad (3-2)$$

where M is the sprung mass, g is the gravitational acceleration, and, and z_p is the piston displacement. Friction force is expressed as

$$F_{pf} = \begin{cases} F_{pC} & \text{if } \dot{z}_p - \dot{z}_t > 0 \\ 0 & \text{if } \dot{z}_p - \dot{z}_t = 0 \\ -F_{pC} & \text{if } \dot{z}_p - \dot{z}_t < 0 \end{cases} \quad (3-3)$$

where F_{pC} is the Coulomb friction force and z_t is the wheel hub displacement. Similarly, the hard stop force is given by,

$$F_{\text{pHS}} = \begin{cases} k_{\text{pHS}} (z_p - z_t - h_{\text{pHSU}}) & \text{if } z_p - z_t > h_{\text{pHSU}} \\ 0 & \text{if } h_{\text{pHSL}} \leq z_p - z_t \leq h_{\text{pHSU}} \\ k_{\text{pHS}} (z_p - z_t - h_{\text{pHSL}}) & \text{if } z_p - z_t < h_{\text{pHSL}} \end{cases} \quad (3-4)$$

where k_{pHS} is the hard stop spring constant, h_{pHSU} is the distance between the piston and the upper hard stop at static equilibrium position, and h_{pHSL} is the distance between the piston and the lower hard stop at static equilibrium position. The assumed force deflection characteristic of the hard stop is shown in Figure 3.2.

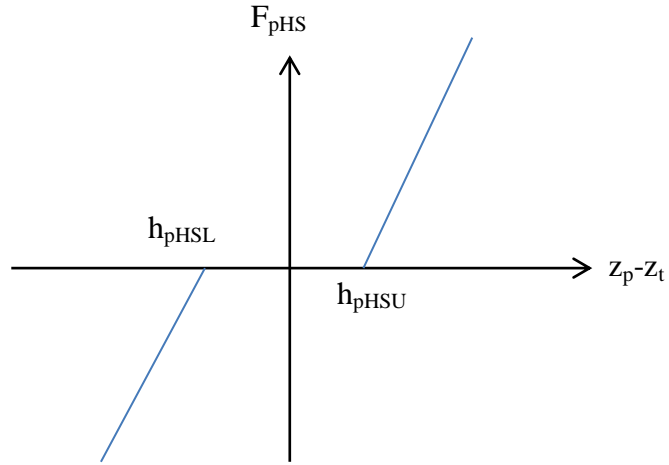


Figure 3.2: Hard Stop Force Characteristics

The equation of motion of the floating piston is

$$(P_3 - P_{\text{Atm}} - P_2)A_p - M_{\text{fp}}g - F_{\text{fpf}} - F_{\text{fpHS}} = M_{\text{fp}}\ddot{z}_{\text{fp}} \quad (3-5)$$

where P_3 is the absolute gas pressure in third chamber, P_{Atm} is the atmospheric pressure, P_2 is the oil pressure in second chamber, M_{fp} is the floating piston mass, z_{fp} is the floating piston displacement, F_{fpf} is the Coulomb friction force between floating piston and the cylinder wall, and, F_{fpHS} is the hard stop force between the floating piston and the hard stop. The Coulomb friction force is

$$F_{\text{fpf}} = \begin{cases} F_{\text{fpC}} & \text{if } \dot{z}_{\text{fp}} - \dot{z}_t > 0 \\ 0 & \text{if } \dot{z}_{\text{fp}} - \dot{z}_t = 0 \\ -F_{\text{fpC}} & \text{if } \dot{z}_{\text{fp}} - \dot{z}_t < 0 \end{cases} \quad (3-6)$$

where is F_{fpC} is the Coulomb friction force. Similarly, the hard stop force is,

$$F_{fpHS} = \begin{cases} k_{fpHS} (z_{fp} - z_t - h_{fpHSU}) & \text{if } z_{fp} - z_t > h_{fpHSU} \\ 0 & \text{if } h_{fpHSL} \leq z_{fp} - z_t \leq h_{fpHSU} \\ k_{fpHS} (z_{fp} - z_t - h_{fpHSL}) & \text{if } z_{fp} - z_t < h_{fpHSL} \end{cases} \quad (3-7)$$

where k_{fpHS} is the hard stop spring constant, h_{fpHSU} is the distance between the floating piston and the upper hard stop at static equilibrium position, and h_{fpHSL} is the distance between the floating piston and the lower hard stop at static equilibrium position. Force displacement characteristics of the hard stops are similar to one shown in Figure 3.2. When the oil is assumed as incompressible, from the continuity of the oil in first and second oil chamber:

$$z_{fp} = z_p \quad (3-8)$$

Thus, the motion of the main piston and the floating piston becomes the same. Using Equation (3-5), the pressure P_2 can be found as,

$$P_2 = P_3 - P_{atm} - \frac{M_{fp}g + M_{fp}\ddot{z}_{fp} + F_{fpf} + F_{fpHS}}{A_p} \quad (3-9)$$

Oil flow rate, Q_{12} , passing through the orifice can be found by using the orifice equation as,

$$Q_{12} = A_v C_d \sqrt{\frac{2}{\rho} |P_2 - P_1| \text{sign}(P_2 - P_1)} \quad (3-10)$$

where A_v is the orifice area, C_d is the drag coefficient, and ρ is the oil density. Equation (3-10) can also be written as,

$$Q_{12} = A_v C_d \sqrt{\frac{2}{\rho} |P_2 - P_1| \text{sign}(\dot{z}_p - \dot{z}_t)} \quad (3-11)$$

From the continuity of the oil in chamber 1,

$$Q_{12} = A_p (\dot{z}_p - \dot{z}_t) \quad (3-12)$$

The absolute gas pressure can be found using polytropic gas equation as,

$$P_{30} V_{30}^\kappa = P_3 V_3^\kappa \quad (3-13)$$

where P_{30} is the absolute gas pressure at static equilibrium (or initial gas volume), V_{30} is the gas volume at static equilibrium (or initial gas volumes), P_3 is the instantaneous absolute gas pressure, V_3 is the instantaneous gas volume, and κ is the polytropic gas coefficient. The relation between the initial gas properties and gas properties at static equilibrium can be found by using the isothermal polytropic gas equation as,

$$P_{30} V_{30} = P_{3i} V_{3i} \quad (3-14)$$

where P_{3i} is the precharge gas pressure and V_{3i} is the precharge gas volume. The instantaneous gas volume can be obtained as,

$$V_3 = \left[V_{30} + A_p (z_p - z_t) \right] \quad (3-15)$$

The instantaneous gas pressure can be obtained as

$$P_3 = \frac{P_{30} V_{30}^\kappa}{\left[V_{30} + A_p (z_p - z_t) \right]^\kappa} \quad (3-16)$$

As a result, one degree of freedom HP suspension model is obtained assuming incompressible model. Using the derived equations so far, oil pressure P_2 can be found as,

$$P_2 = \frac{P_{30} V_{30}^\kappa}{\left[V_{30} + A_p (z_p - z_t) \right]^\kappa} - P_{\text{Atm}} - \frac{M_{\text{fp}} g + M_{\text{fp}} \ddot{z}_{\text{fp}} + F_{\text{fpf}} + F_{\text{fpHS}}}{A_p} \quad (3-17)$$

Similarly, oil pressure P_1 can be found as,

$$P_1 = \frac{P_{30} V_{30}^\kappa}{\left[V_{30} + A_p (z_p - z_t) \right]^\kappa} - P_{\text{Atm}} - \frac{M_{\text{fp}} g + M_{\text{fp}} \ddot{z}_{\text{fp}} + F_{\text{fpf}} + F_{\text{fpHS}}}{A_p} - \left[\frac{A_p (\dot{z}_p - \dot{z}_t)}{A_v C_d} \right]^2 \frac{\rho}{2} \text{sign}(\dot{z}_p - \dot{z}_t) \quad (3-18)$$

Then, the suspension force F can be found as,

$$F = \left\{ \begin{array}{l} \frac{P_{30} V_{30}^\kappa}{[V_{30} + A_p (z_p - z_t)]^\kappa} - P_{Atm} - \frac{M_{fp} g + M_{fp} \ddot{z}_{fp} + F_{fpf} + F_{fpHS}}{A_p} \\ - \left[\frac{A_p (\dot{z}_p - \dot{z}_t)}{A_v C_d} \right]^2 \frac{\rho}{2} \text{sign}(\dot{z}_p - \dot{z}_t) \end{array} \right\} A_p - F_{pf} - F_{pHS} \quad (3-19)$$

The equation of motion for the tire can be written as,

$$\begin{aligned} k_t (z_0 - z_t) + c_t (\dot{z}_0 - \dot{z}_t) - (P_3 - P_{Atm}) A_p + P_2 A_p - P_1 A_p + \\ + F_{pf} + F_{fpf} + F_{pHS} + F_{fpHS} = M_t \ddot{z}_t \end{aligned} \quad (3-20)$$

where z_0 is the road displacement input, k_t is the tire stiffness, c_t is the tire damping coefficient, and M_t is the tire mass.

3.1.2. Modeling of the HP Suspension with Compressible Oil Model

In previous part HP suspension system is modeled with incompressible oil assumption. However, in real oil is somewhat compressible. Therefore, in this part, HP suspension system is to be modeled with compressible oil model. Here, the first order compressible oil model is used. When the compressibility of the oil is also taken into account, the continuity equation of the oil in first chamber becomes,

$$Q_1 = Q_{12} - Q_{\beta 1} \quad (3-21)$$

where Q_1 is the net flow rate to first chamber, Q_{12} is the flow rate through the orifice into first chamber, and $Q_{\beta 1}$ is the flow rate due to compressibility of the oil. From the compatibility relations, the net flow rate to first chamber can be found as,

$$Q_1 = A_p (\dot{z}_p - \dot{z}_t) \quad (3-22)$$

Moreover, the flow rate, $Q_{\beta 1}$, due to compressibility of the oil in first chamber can be found as,

$$Q_{\beta 1} = \frac{V_1}{\beta} \dot{P}_1 \quad (3-23)$$

where β is the oil bulk modulus, and V_1 is the instantaneous volume of the first chamber. V_1 can be found as,

$$V_1 = V_{10} + A_p (z_p - z_t) \quad (3-24)$$

where V_{10} is the initial volume of the oil in the first chamber. From these equations, the pressure P_1 can be found as,

$$\dot{P}_1 = \frac{\beta}{V_{10} + A_p (z_p - z_t)} \left[C_d A_v \sqrt{\frac{2}{\rho} |P_2 - P_1| \text{sign}(P_2 - P_1)} - A_p (\dot{z}_p - \dot{z}_t) \right] \quad (3-25)$$

Similarly, the continuity equation for the oil in second chamber becomes,

$$Q_2 = -Q_{12} - Q_{\beta 2} \quad (3-26)$$

where Q_2 is the net flow rate to second chamber, and $Q_{\beta 2}$ is the flow rate due to compressibility of the oil. From the compatibility relations, Q_2 can be found as,

$$Q_2 = A_p (-\dot{z}_{fp} + \dot{z}_t) \quad (3-27)$$

Then, the flow rate due to compressibility of the oil in second chamber becomes,

$$Q_{\beta 2} = \frac{V_2}{\beta} \dot{P}_2 \quad (3-28)$$

where V_2 is the instantaneous volume of the second chamber and is given as,

$$V_2 = V_{20} + A_p (-z_{fp} + z_t) \quad (3-29)$$

where V_{20} is the initial volume of the oil in the second chamber. Using the continuity equation of the oil in the second chamber, the pressure P_2 can be calculated as,

$$\dot{P}_2 = \frac{\beta}{V_{20} + A_p (-z_{fp} + z_t)} \left[-C_d A_v \sqrt{\frac{2}{\rho} |P_2 - P_1| \text{sign}(P_2 - P_1)} - A_p (-\dot{z}_{fp} + \dot{z}_t) \right] \quad (3-30)$$

The gas pressure can be expressed as,

$$P_3 = \frac{P_{30} V_{30}^k}{\left[V_{30} + A_p (z_{fp} - z_t) \right]^k} \quad (3-31)$$

The suspension force F is found by using the derived equations so far. However, an explicit equation cannot be found. Solving the nonlinear differential equations derived so far by numerical methods, the suspension force and other variables can be obtained. The equation of motion for the tire for the incompressible and the compressible cases are identical.

Vehicle and HP suspension model parameters are given in Table 3.1.

Table 3.1: Vehicle and Suspension Parameters

Parameter	Symbol	Value
Sprung Mass	M [kg]	1500
Floating Piston Mass	M_{fp} [kg]	1
Tire Mass	M_t [kg]	150
Orifice Opening	A_v [m ²]	2e-4
Piston Area	A_p [m ²]	0.007
Polytropic Gas Constant	κ	1.4
Orifice Drag Coefficient	C_d	0.8
Oil Density	ρ [kg/m ³]	800
Coulomb Friction Force for Piston	F_p [N]	40
Coulomb Friction Force for Floating Piston	F_{fp} [N]	20
Tire Stiffness	k_t [N/m]	6e5
Initial Gas Volume for Single Gas Chamber HP Suspension System	V_{30} [m ³]	0.0019
Initial Gas Volume for Double Gas Chamber HP Suspension System	V_{30} [m ³]	0.0031
Oil Bulk Modulus	β [Pa]	1.3e9
Gravitational Acceleration	g [m/s ²]	9.816
Atmospheric Pressure	P_{Atm} [bar]	1
Piston Rod Area	A_r [m ²]	0.004
Initial Gas Pressure at 4 th Volume for Double Gas Chamber HP Suspension	P_{40} [bar]	12
Initial Gas Volume at 4 th Gas Volume for Double Gas Chamber HP Suspension	V_{40} [m ³]	0.0008

3.1.3. Static Analysis

After the dynamic equations are derived for the HP suspension system with incompressible and the compressible oil models suspension variables are to be found at the static equilibrium. At static equilibrium, the suspension force become,

$$F = \left[P_{30} - P_{Atm} - \frac{M_{fp}g}{A_p} \right] A_p \quad (3-32)$$

Thus, absolute gas pressure at static equilibrium becomes,

$$P_{30} = \frac{(M + M_{fp})g}{A_p} + P_{Atm} \quad (3-33)$$

3.1.4. Effect of Compressibility on the Dynamics of the Suspension

To see the effect of the oil compressibility on the system dynamics, as a first attempt, time domain simulations are performed and the responses of the HP suspension with compressible and incompressible oil models are compared to each other. Previously derived HP suspension models with the compressible and the incompressible oil models are simulated by a road displacement input which is a sine sweep input in the frequency range 1-10 Hz.

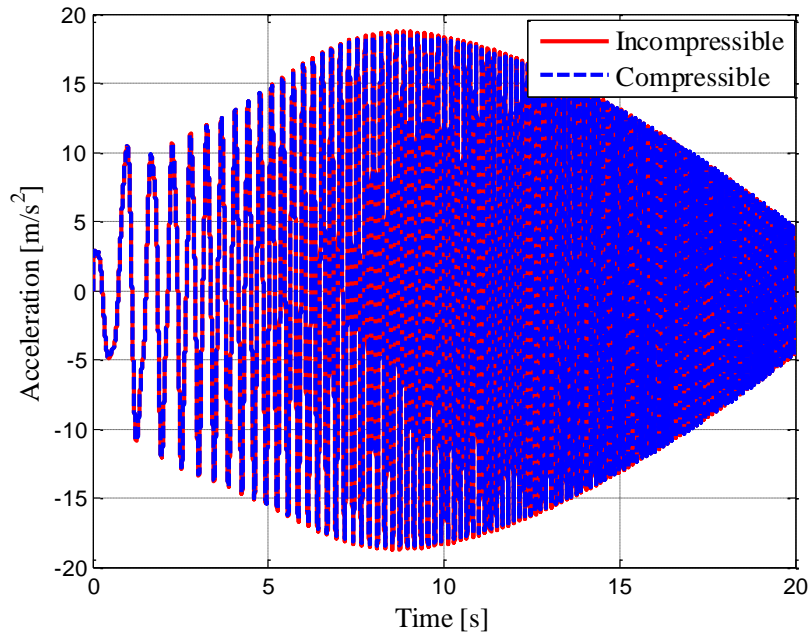


Figure 3.3: Sprung Mass Accelerations Obtained from HP Suspension with Compressible and Incompressible Oil

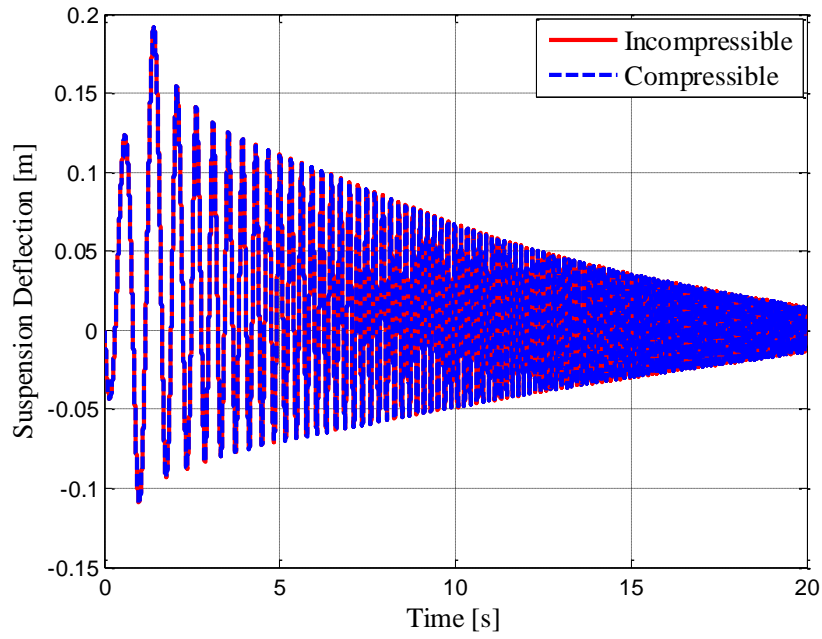


Figure 3.4: Suspension Deflections Obtained from HP Suspension with Compressible and Incompressible Oil

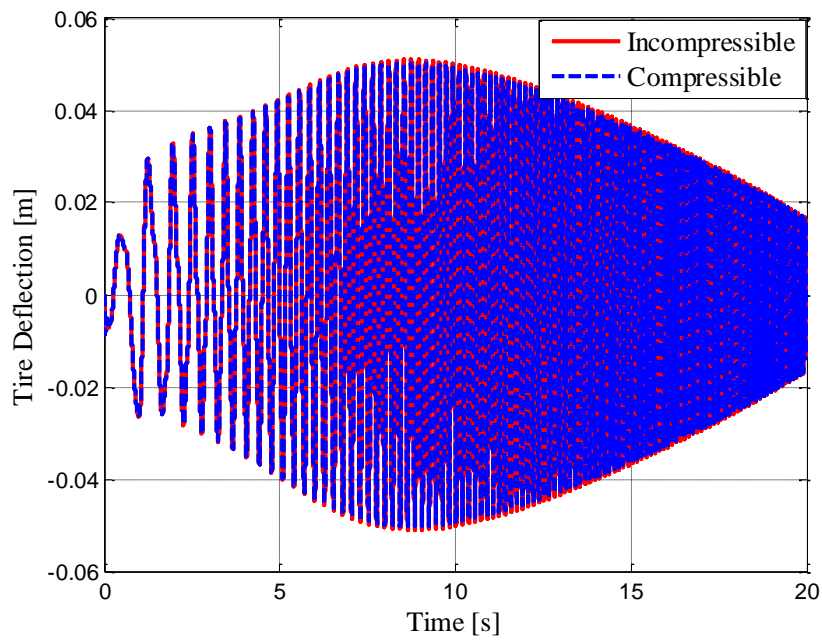


Figure 3.5: Tire Deflections Obtained from HP Suspension with Compressible and Incompressible Oil

Figure 3.3 to Figure 3.5 show the simulation outputs. As the results illustrate, for the specified input, the HP suspension model with the compressible and the incompressible oil models have similar results. In other words oil compressibility does not appreciably affect the simulation outputs. This is due to the fact that gas compressibility is much higher than the oil compressibility and thus dominates the stiffness characteristics of the HP suspension system. In the following section, the effect of the oil compressibility on the stiffness characteristics of the HP suspension system is examined.

3.2. ANALYSIS OF THE HP SUSPENSION SYSTEM

After the comparison between the HP suspension systems with compressible and incompressible oil models are performed, now the stiffness and the damping properties of the HP suspension system is to be performed and a general parametric study is to be carried out in both time and the frequency domains.

3.2.1. Stiffness and Damping Characteristics of the HP Suspension

3.2.1.1. Stiffness Characteristics

For stiffness properties of the HP suspension system, the model shown in Figure 3.6 is used. Stiffness characteristic of the HP suspension system is to be obtained for both the incompressible and the compressible oil models.

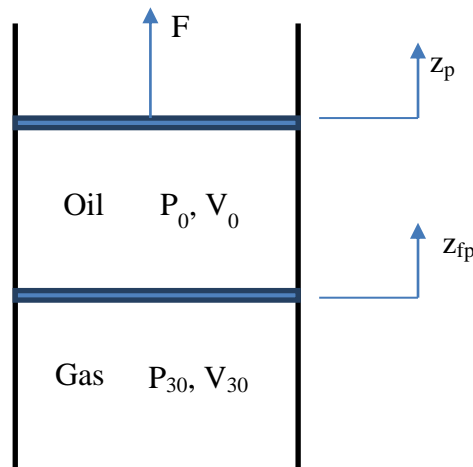


Figure 3.6: HP Suspension Layout Used in Analysis

Incompressible Oil

Stiffness of the HP suspension system changes with the relative displacement of the main piston with respect to the tire displacement. Thus suspension stiffness, k , is dependent on the relative piston displacement and can be found as,

$$k = -\frac{dF}{dz_p} \quad (3-34)$$

and F is the suspension force at steady state and is,

$$F = \frac{P_{30} V_{30}^{\kappa} A_p}{[V_{30} + A_p z_p]^{\kappa}} - P_{Atm} A_p - M_{fp} g \quad (3-35)$$

Thus suspension stiffness can be found as,

$$k = -\frac{dF}{dz_p} = -\frac{d \left[\frac{P_{30} V_{30}^{\kappa} A_p}{(V_{30} + A_p z_p)^{\kappa}} - P_{Atm} A_p - M_{fp} g \right]}{dz_p} = \frac{P_{30} V_{30}^{\kappa} A_p^2 \kappa}{(V_{30} + A_p z_p)^{\kappa+1}} \quad (3-36)$$

As can be seen from the Equation (3-36) the gas stiffness increases when z_{pt} decreases. At static equilibrium, suspension stiffness become,

$$k = \frac{P_{30} A_p^2 \kappa}{V_{30}} \quad (3-37)$$

Compressible Oil

When the incompressible oil model is used in the derivation of the HP suspension force, the motion of the floating and main piston become the same. However, when the compressible oil model is used, they are different. Therefore, another elastic medium, oil, has also an effect in the stiffness characteristic of the HP suspension system. At steady state conditions,

$$P_0 = P_{30} - P_{Atm} - \frac{M_{fp} g}{A_p} = \frac{F_0}{A_p} \quad (3-38)$$

Thus the compressibility of the oil in oil volume can be written as,

$$dP = -\beta \frac{dV}{V} \quad (3-39)$$

$$P - P_0 = -\beta \ln \left(\frac{V}{V_0} \right) = -\beta \ln \left[\frac{V_0 - A_p (z_p - z_{fp})}{V_0} \right] \quad (3-40)$$

$$z_{fp} = z_p - \frac{V_0}{A_p} \left(e^{\left(\frac{P - P_0}{-\beta} \right)} - 1 \right) \quad (3-41)$$

where

$$P = \frac{F}{A_p} \quad (3-42)$$

From the derived equations, the suspension force, F , can be found as,

$$F = \frac{P_{30} V_{30}^\kappa A_p}{\left[V_{30} + A_p \left(z_p - \frac{V_0}{A_p} \left(e^{\left(\frac{F - P_0}{-\beta} \right)} - 1 \right) \right) \right]^\kappa} - P_{Atm} A_p - M_{fp} g \quad (3-43)$$

After some manipulation, Equation (3-43) can be written as,

$$\frac{\left(\frac{P_{30} V_{30}^\kappa A_p}{F + P_{Atm} A_p + M_{fp} g} \right)^{\frac{1}{\kappa}} - V_{30} + V_0 \left(e^{\frac{F - P_0}{-\beta}} - 1 \right)}{A_p} = z_p \quad (3-44)$$

where

$$P_{30} = \frac{F_0}{A_p} + P_{Atm} + \frac{M_{fp} g}{A_p} \quad (3-45)$$

Suspension stiffness characteristics can be found from Equations (3-44) and (3-45).

3.2.1.2. Comparisons of Stiffness Characteristics

In this section, the suspension stiffness is compared for HP suspension model with compressible and incompressible oil assumptions. Figure 3.7 shows the stiffness characteristics of the HP suspension with the compressible and incompressible oil models.

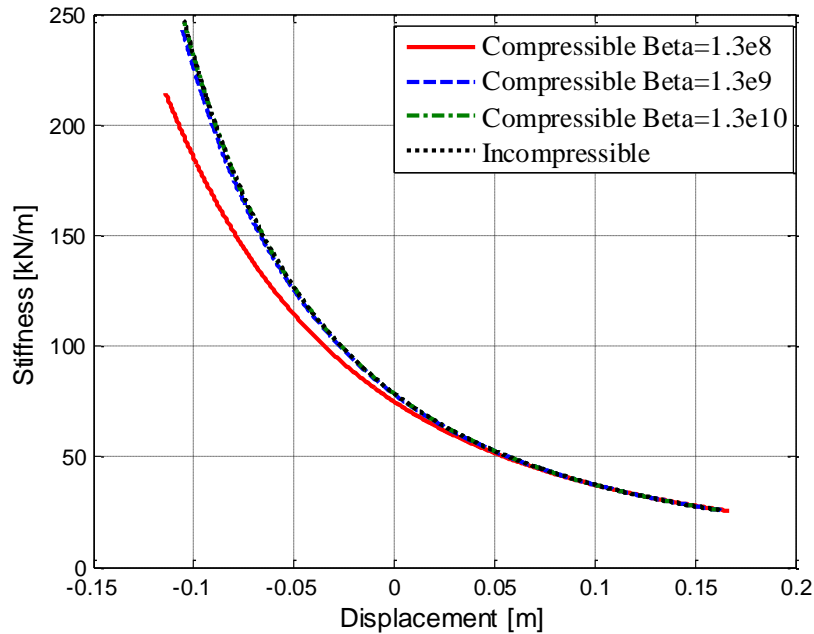


Figure 3.7: Effect of Oil Compressibility in the Suspension Stiffness

As can be seen from Figure 3.7, as the bulk modulus of the oil decreases, the stiffness values of the HP suspension also decreases. However, when the oil compressibility is high, the suspension stiffness values are nearly the same for compressible and incompressible oil models. Thus, the HP suspension system with typical hydraulic oil can be modeled with the incompressible oil assumption.

3.2.1.3. Damping Characteristics

In the HP suspension system, the damping is provided by the orifice or the damper valve. According to the pressure drop-oil flow rate characteristic of the orifice or valve, different damping characteristics can be obtained. For the HP suspension system with incompressible oil, the damping force in the typical orifice is,

$$F = A_p \left[\frac{A_p (\dot{z}_p - \dot{z}_t)}{A_v C_d} \right]^2 \frac{\rho}{2} \text{sign}(\dot{z}_p - \dot{z}_t) \quad (3-46)$$

The damping force is proportional to the amplitude of the relative velocity between the sprung and unsprung masses. At low velocities, the system has low damping and at high velocities it has high damping. As explained in the study of the Bauer [1], low damping at low velocities gives the feeling of losing contact of the tires with the road. Therefore, instead of using the direct orifice damper in the modeling, combined valve systems are used. By combination of different valve systems, the pressure drop and the flow rate or the damping force and the suspension relative velocity characteristic can be obtained. In the study of the Dixon [49], modeling of the damper valves is explained in detail. In this study, the damping characteristics are modeled by using both the orifice damping and the combined damping models. The combined damping model is shown in Figure 3.8. The mathematical representation of the combined damper model is,

$$A_v (\Delta P_E) = \begin{cases} \frac{\Delta P_E A_{v \max E}}{\Delta P_{\max E}} + A_v & \text{if } \Delta P_E \leq \Delta P_{\max E} \\ A_{v \max E} + A_v & \text{if } \Delta P_E > \Delta P_{\max E} \end{cases} \quad (3-47)$$

$$A_v (\Delta P_C) = \begin{cases} \frac{\Delta P_C A_{v \max C}}{\Delta P_{\max C}} + A_v & \text{if } \Delta P_C \leq \Delta P_{\max C} \\ A_{v \max C} + A_v & \text{if } \Delta P_C > \Delta P_{\max C} \end{cases}$$

where “E” and “C” stand for defining the parameters when the suspension expands and compresses, respectively, ΔP is the pressure difference, ΔP_{\max} is the pressure difference which results in maximum valve opening, $A_{v \max}$ is the maximum valve opening, and A_v is the constant orifice opening.

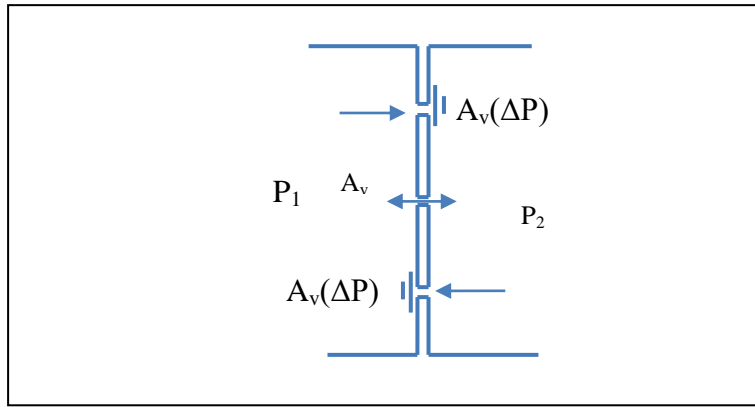


Figure 3.8: Combined Damper Model

The change of the valve opening area with the pressure drop is shown in Figure 3.9.

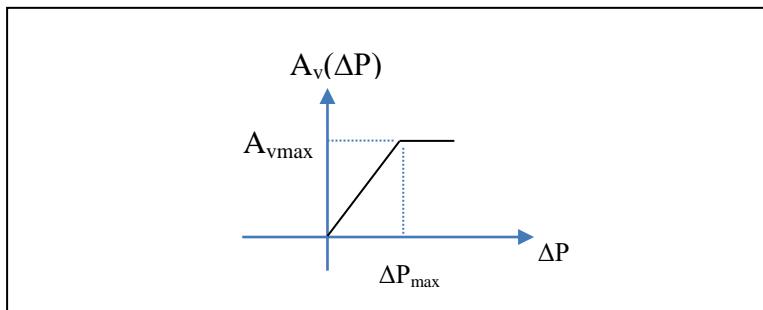


Figure 3.9: Change of the Valve Opening with the Pressure Drop

When the variable valve opening becomes maximum, the valve behaves as a constant area orifice and the damping force changes proportional to the square of the suspension velocity. However, when the valve openings are not fully open, damping force changes proportional to square root of the suspension velocity. Moreover, orifice with constant area is used as the bleed orifice.

3.2.2. Parameter Sensitivity Study

After the stiffness and the damping characteristics of the HP suspension system are derived, a parameter sensitivity study is to be performed. The stiffness characteristic of the HP suspension system with incompressible oil model is dependent on piston area, gas pressure at static equilibrium, gas volume at static equilibrium, and polytropic gas constant. Initial gas pressure is dependent on sprung mass and piston area. Therefore, the gas stiffness is dependent on the two basic suspension design

parameters, piston area, and the gas volume at static equilibrium (or initial gas volume). By changing these parameters, suspension stiffness can be tuned accordingly. The variation of the suspension stiffness with the piston area is shown in Figure 3.10 and Figure 3.11.

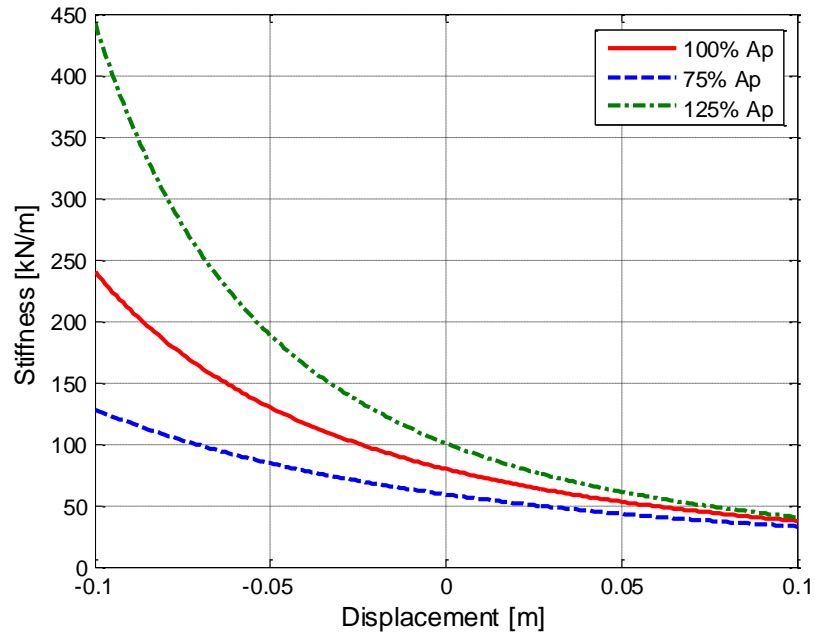


Figure 3.10: Variation of Suspension Stiffness with Piston Area

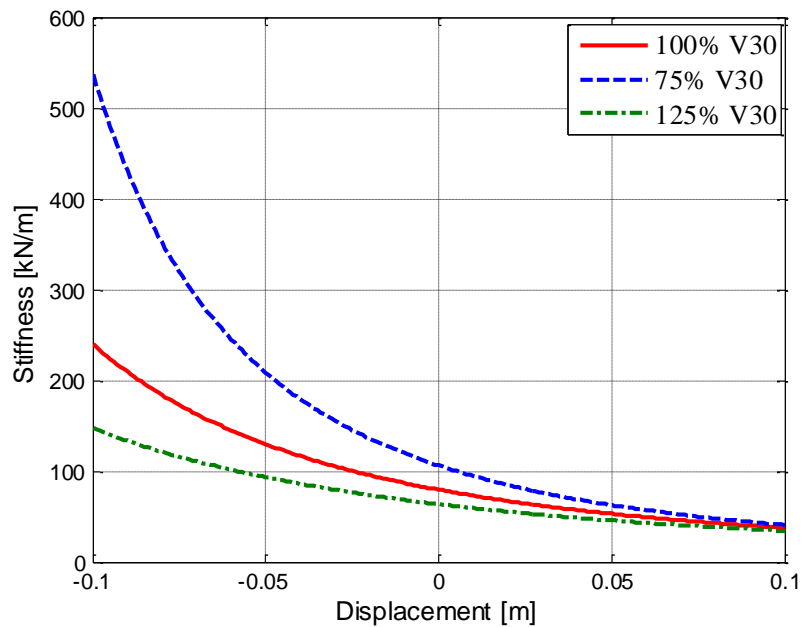


Figure 3.11: Variation of Suspension Stiffness with Initial Gas Volume

As can be seen from Figure 3.10, when the piston area is increased, the amount of displaced oil also increases and thus the stiffness increases. On the contrary, when the piston area is reduced, suspension stiffness also decreases.

As Figure 3.11 illustrates, when the initial gas volume is increased, suspension stiffness decreases and when the initial gas volume decreases, suspension stiffness increases. Further, as Figure 3.10 and Figure 3.11 illustrate, when the gas volume decreases, suspension stiffness increases with an increasing rate. On the contrary, when the gas volume increases, suspension stiffness decreases with a decreasing rate.

As can be seen from Equation (3-46), the orifice damping is dependent on the design parameters, piston area, and orifice opening. The variation of the damping force with piston area and orifice opening are shown in Figure 3.12 and Figure 3.13, respectively.

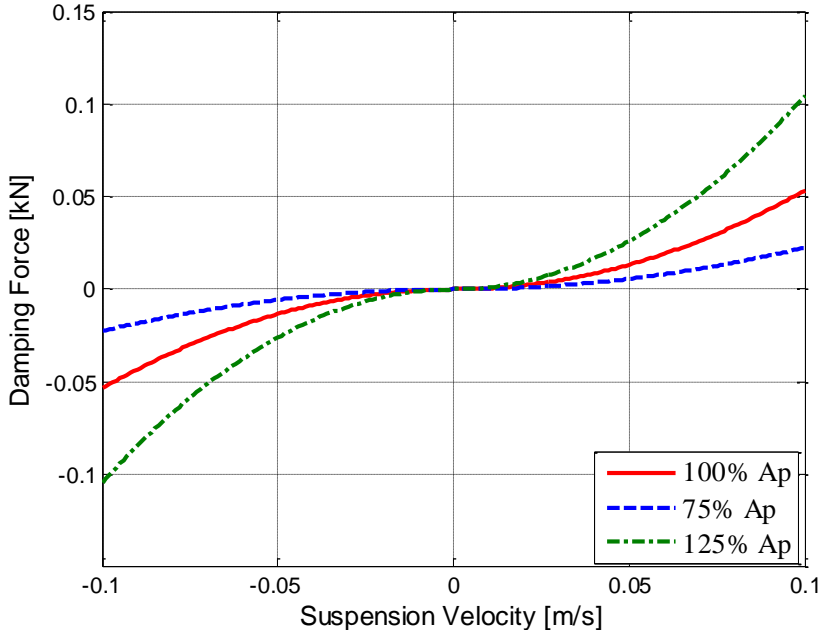


Figure 3.12: Variation of Damping Force with Piston Area

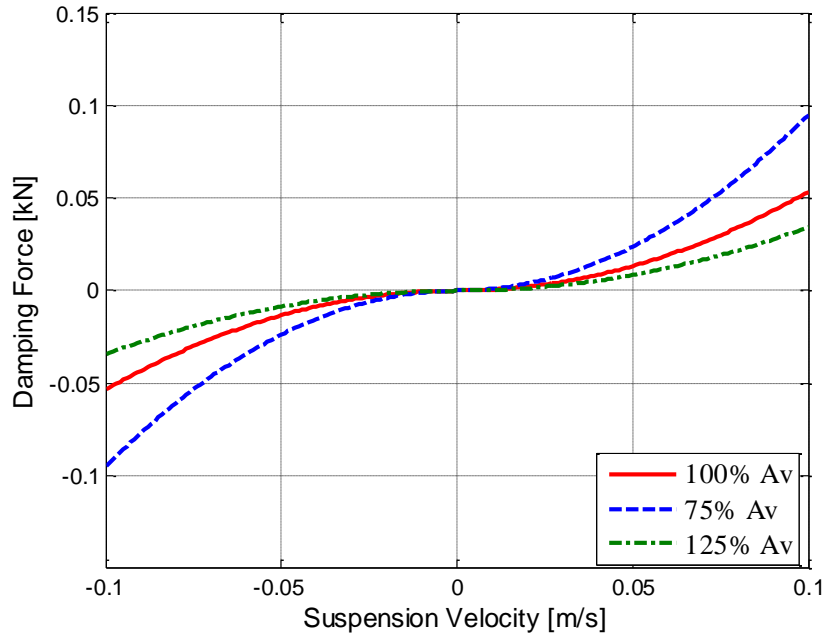


Figure 3.13: Variation of Damping Force with Orifice Opening

As can be seen from Figure 3.12 and Figure 3.13, when the piston area increases the amount of the oil forced to flow through the orifice also increases and thus the suspension force increases. Similarly, when the orifice area decreases the amount of the displaced oil through the orifice also decreases and thus suspension damping decreases. Moreover, since the damping force is proportional to the square of the suspension velocity, at low suspension velocities, damping force is also low. However, there is a sharp rise in damping force at high suspension velocities.

As a result, the stiffness of HP suspension system can be adjusted by tuning the piston area and the initial gas volume. Similarly, the damping of the HP suspension can be adjusted by varying orifice opening area and the piston area. This provides flexibility for the design of the HP suspension systems.

3.2.3. Sensitivity Analysis in Frequency Domain

To get the responses in the frequency domain, sinusoidal inputs at different amplitudes and frequencies will be used as road displacement inputs. The approximate frequency response functions (FRF) will be obtained as the ratio of the

root mean square of the response value to root mean square of the road velocity input. The frequency response functions are obtained as,

$$H_{\text{Accel}}(\omega) = \frac{\text{rms}\{\ddot{z}_p(t)\}}{\text{rms}\{\dot{z}_0(t)\}} \quad (3-48)$$

$$H_{\text{Tire Def}}(\omega) = \frac{\text{rms}\{z_{t0}(t)\}}{\text{rms}\{\dot{z}_0(t)\}} \quad (3-49)$$

$$H_{\text{Sus Def}}(\omega) = \frac{\text{rms}\{z_{pt}(t)\}}{\text{rms}\{\dot{z}_0(t)\}} \quad (3-50)$$

where $H_{\text{Accel}}(\omega)$ is the sprung mass acceleration frequency response function, $H_{\text{Tire Def}}(\omega)$ is the tire deflection frequency response function, and the $H_{\text{Sus Def}}(\omega)$ is the suspension deflection frequency response function. The road displacement input is, $z_0 = A_i \sin(2\pi f_i t)$ where $A_i \in \{0.1 \text{ m}, 0.01 \text{ m}\}$ and $f_i \in \{0.4 \text{ Hz}, 20 \text{ Hz}\}$. The amplitude of the displacement input used in the simulation is shown in Figure 3.14.

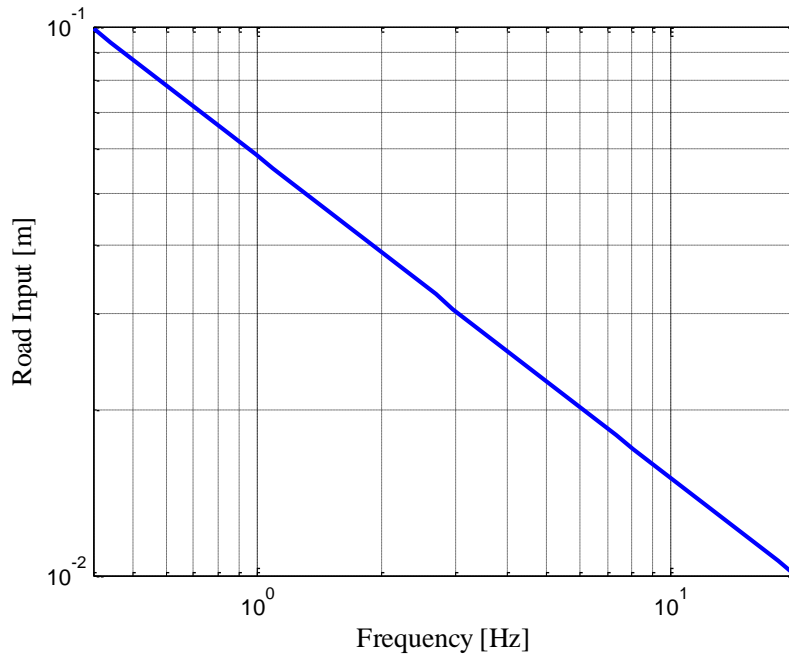


Figure 3.14: Amplitude vs Frequency Plot of the Road Displacement Sine Input

3.2.3.1. Piston Area

Variation of the acceleration, suspension deflection, and the tire deflection with the piston area in frequency domain are shown in Figure 3.15, to Figure 3.17. Variation of the FRFs of the HP suspension systems with the suspension design parameters can be interpreted in view of the stiffness and damping properties. When the piston area increases, suspension damping force also increases in proportion to third power of the piston area. Thus the FRFs, around body bounce and wheel hop frequencies decrease. Thus, ride comfort, suspension deflection, and tire deflection are improved. For the vertical acceleration and the tire deflection FRFs, in the isolation region, increasing piston area causes an increase in responses which in turn causes deterioration in ride comfort and road holding. However, for suspension deflection, piston area has no effect in the isolation region. Moreover, when the piston area is increased, suspension stiffness also increases, and body bounce frequency increases. Thus ride comfort performance is decreased. Increasing stiffness improves suspension packaging performance by decreasing suspension deflection. In summary, changing piston area changes both suspension stiffness and damping.

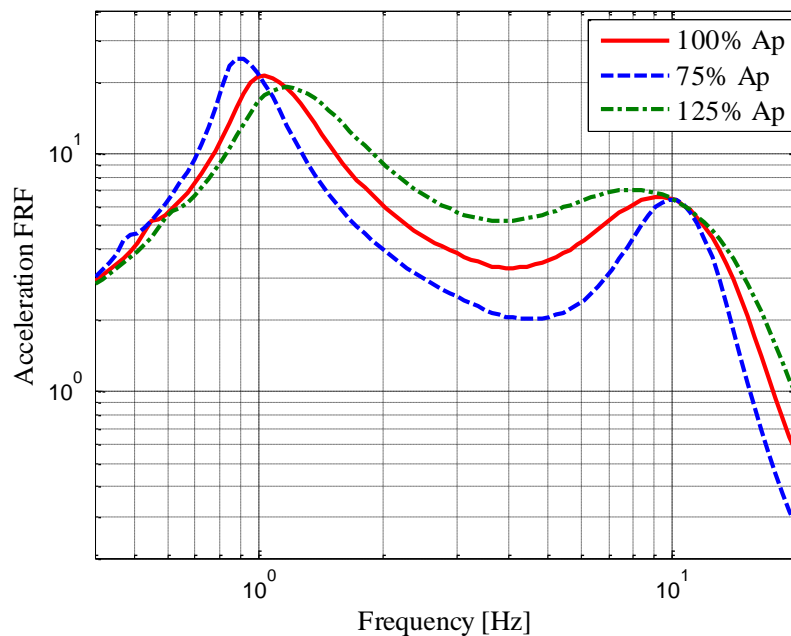


Figure 3.15: Variation of Sprung Mass Acceleration with Piston Area

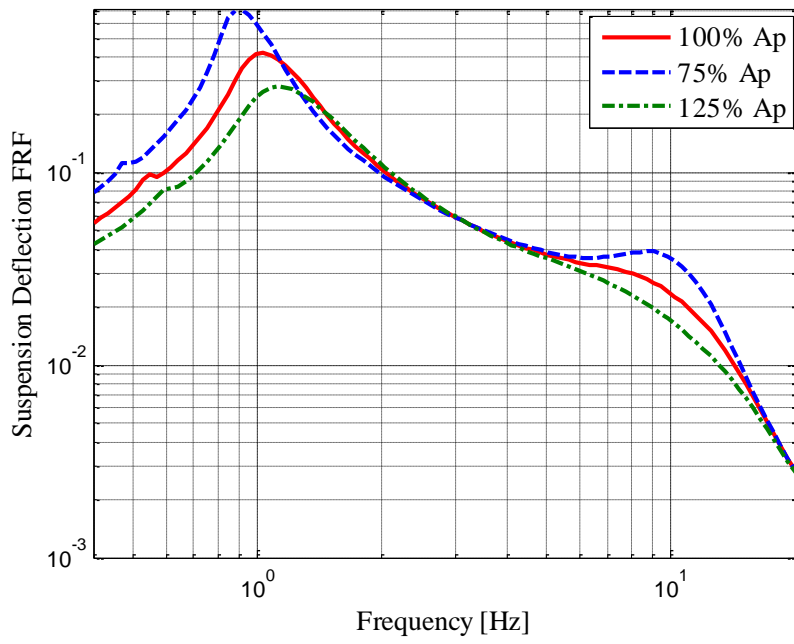


Figure 3.16: Variation of Suspension Deflection with Piston Area

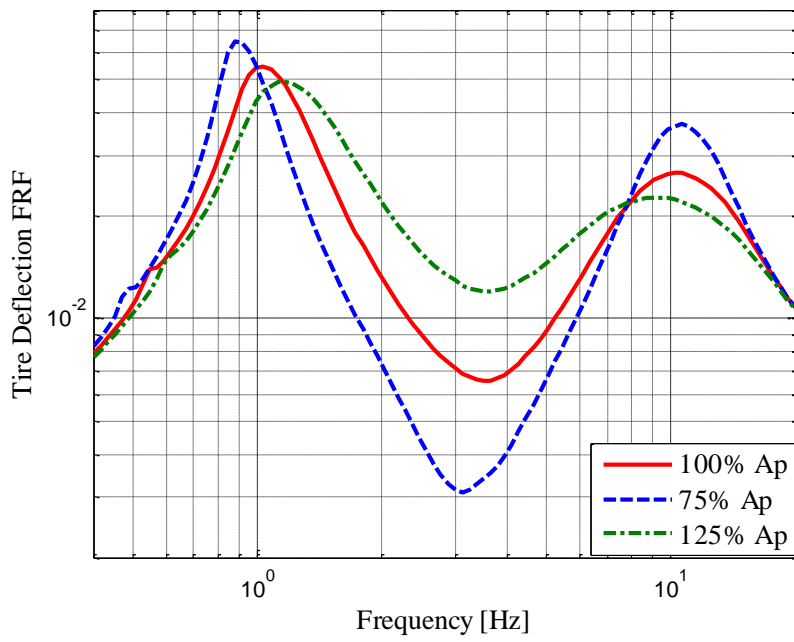


Figure 3.17: Variation of the Tire Deflection with Piston Area

3.2.3.2. Initial Gas Volume

Variation of the acceleration, suspension deflection, and tire deflection with initial gas volume are shown in Figure 3.18 to Figure 3.20. When the initial gas volume increases, suspension stiffness decreases and thus body bounce frequency is also lowered. When the initial gas volume is reduced, suspension becomes more stiff and thus body bounce frequency increases. Initial gas volume has nearly no effect on the FRFs around wheel hop frequencies. Thus increasing initial gas volume increases the acceleration response around body bounce frequency and around isolation frequencies, and thus ride comfort is degraded.

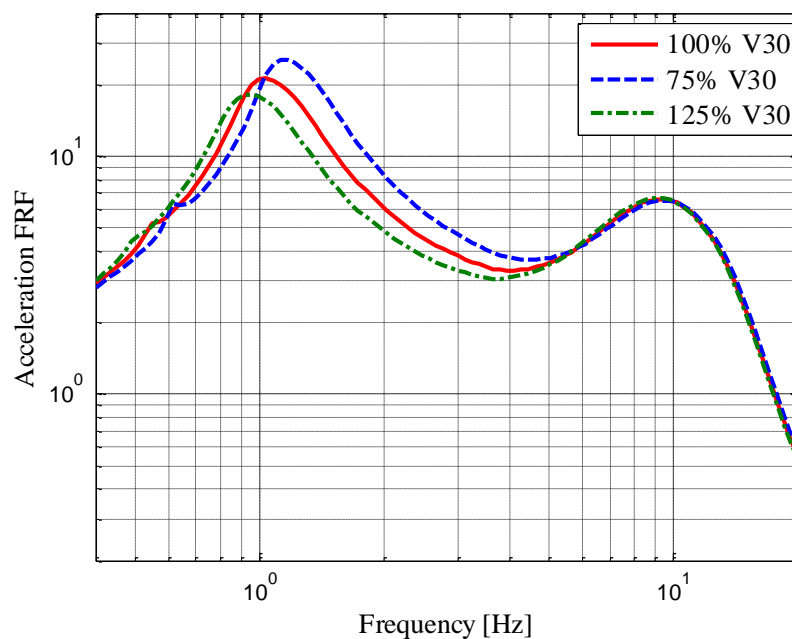


Figure 3.18: Variation of Sprung Mass Acceleration with Initial Gas Volume

On the other hand, when the initial gas volume is reduced, suspension deflection at frequencies below body bounce frequencies is reduced. Making the suspension stiffer by reducing the initial gas volume increases the tire deflection around body bounce and isolation regions, and thus road holding performance goes down. However, larger initial gas volume has inverse effect on the tire deflection around wheel hop frequency region.

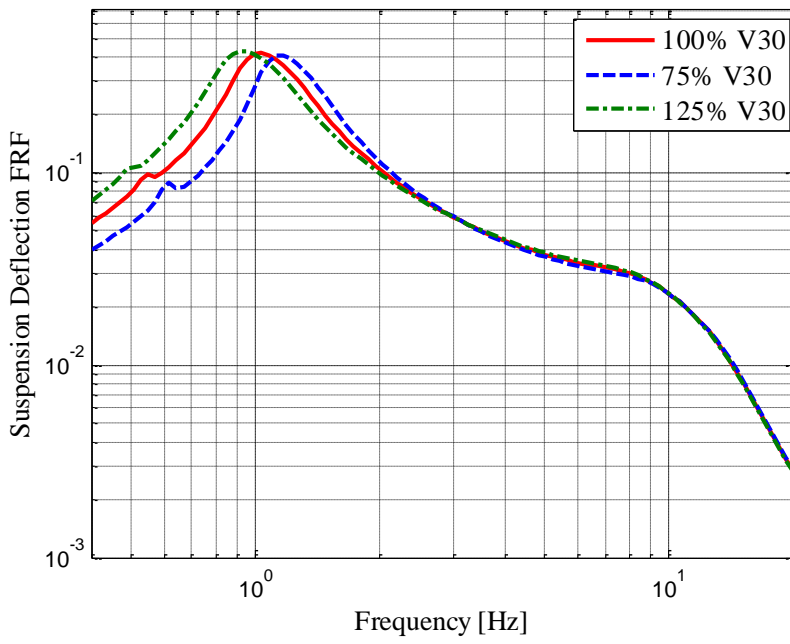


Figure 3.19: Variation of Suspension Deflection with Initial Gas Volume

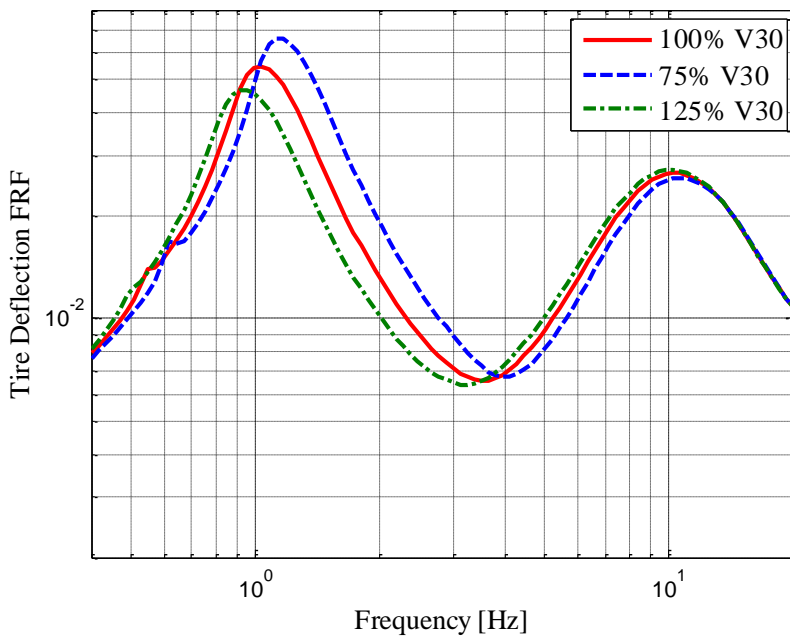


Figure 3.20: Variation of Tire Deflection with Initial Gas Volume

3.2.3.3. Orifice Opening

Variations of the sprung mass acceleration, suspension deflection, and tire deflection with orifice opening area are shown in Figure 3.21 to Figure 3.23. Variation of the vehicle performance characteristics with the orifice opening is similar to variation of the vehicle performance characteristics with the piston area with regard to damping. When the orifice opening is reduced, suspension damping increases and thus performance variables around body bounce frequency dampen out. Moreover, tire and suspension deflections around wheel hop frequencies brought down. Nonetheless, in the isolation region, vertical acceleration and tire deflection are increased.

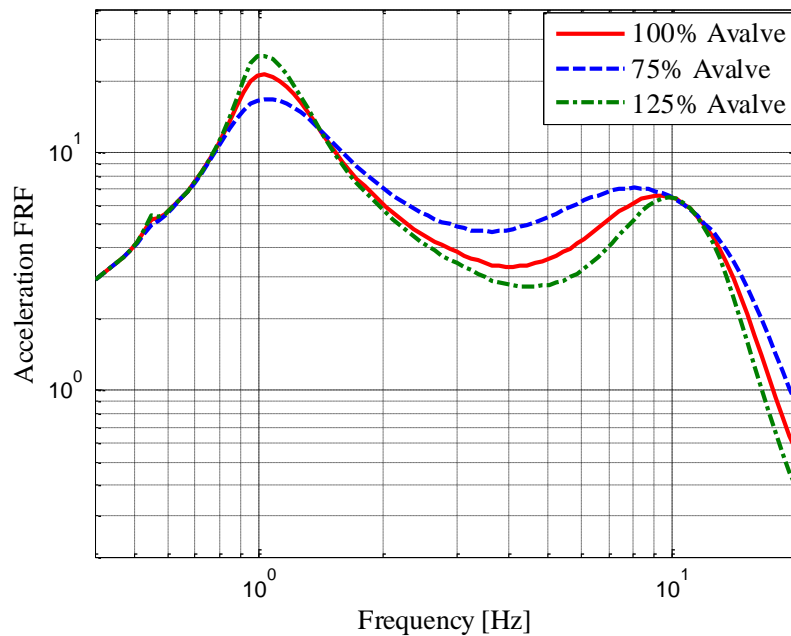


Figure 3.21: Variation of the Sprung Mass Acceleration with the Valve Opening

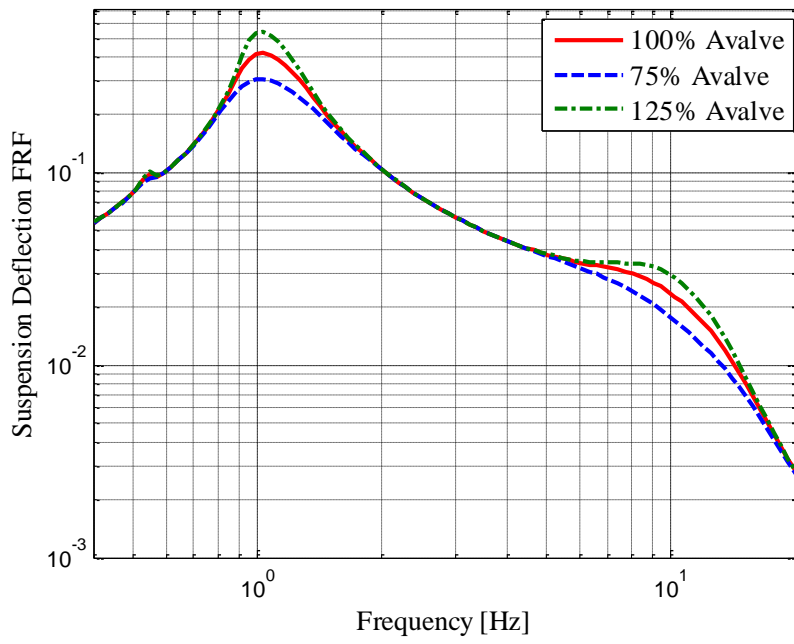


Figure 3.22: Variation of Suspension Deflection with Valve Opening

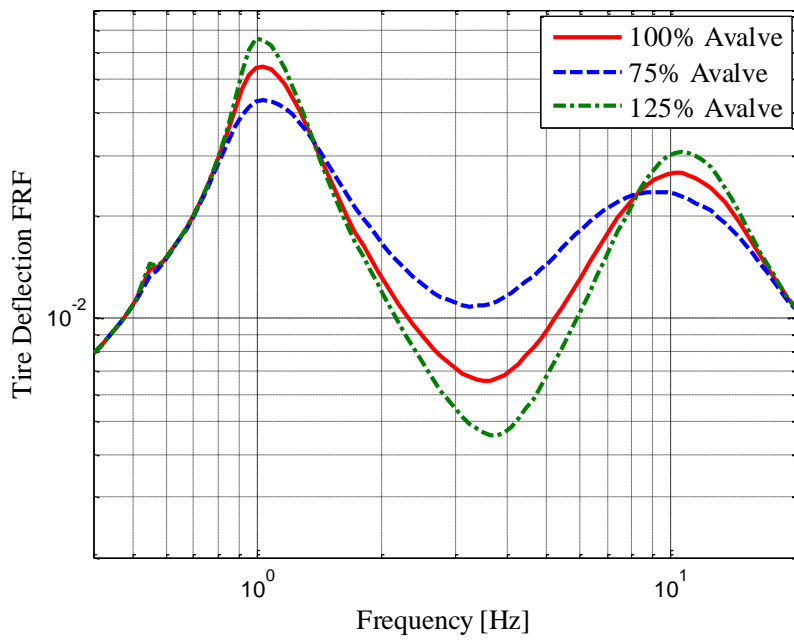


Figure 3.23: Variation of Tire Deflection with Valve Opening

3.2.3.4. Input Amplitude

Variation of the sprung mass acceleration, suspension deflection, and tire deflection with input amplitude are shown in Figure 3.24 to Figure 3.26. Since the HP suspension is a nonlinear system, FRFs are dependent on the input amplitude. Variation of the FRFs with the input amplitude again can be interpreted in accordance with the damping property. When the input amplitude increases, the damping force increases and thus performance variables around the body bounce frequency are also reduced. Moreover in the isolation region, increasing the input amplitude increases the vertical acceleration and tire deflection and ride comfort and road holding performances are degraded. Therefore, input amplitude and the orifice opening have similar effect on the response characteristics. The only difference is the degree of the effect. Damping force is proportional to square of the input velocity, and is inversely proportional to the square of the orifice opening. Thus orifice opening and suspension velocity have similar inverse effect of the response variables.

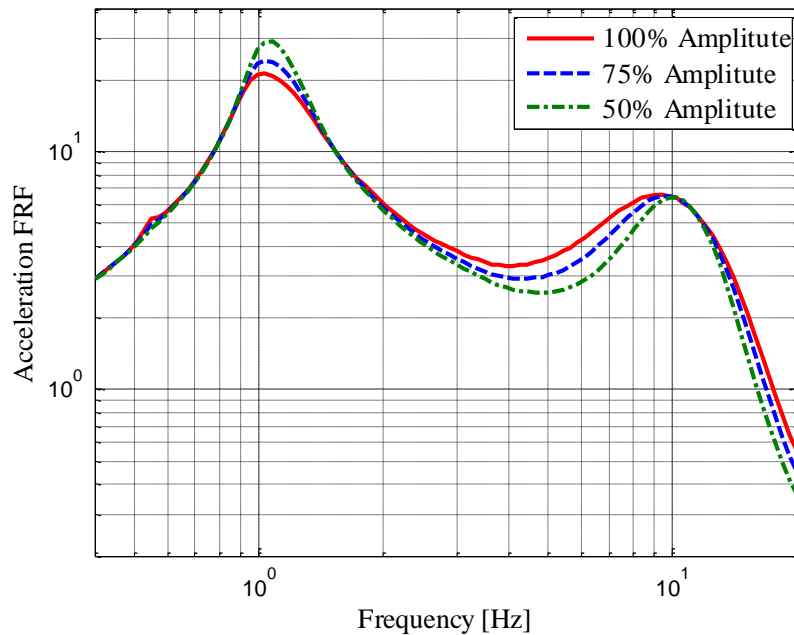


Figure 3.24: Variation of Sprung Mass Acceleration with Input Amplitude

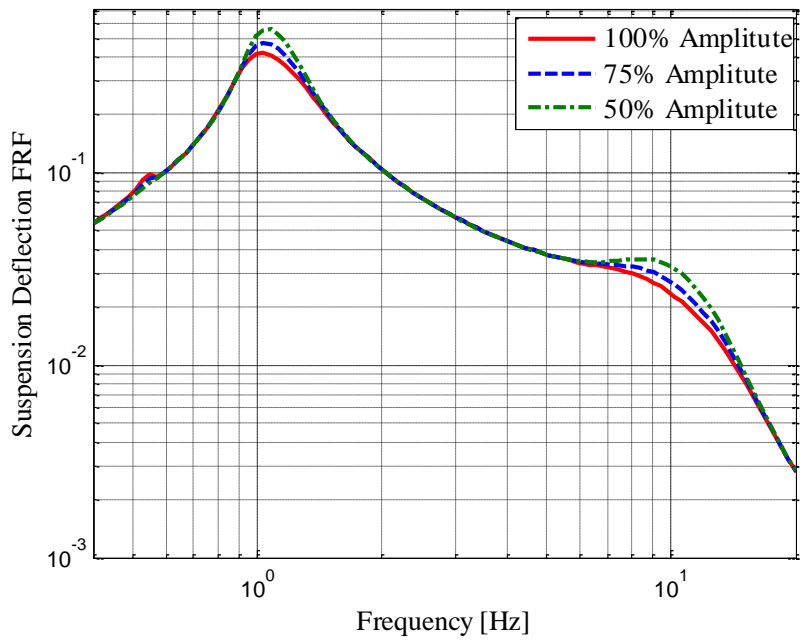


Figure 3.25: Variation of Suspension Deflection with Input Amplitude

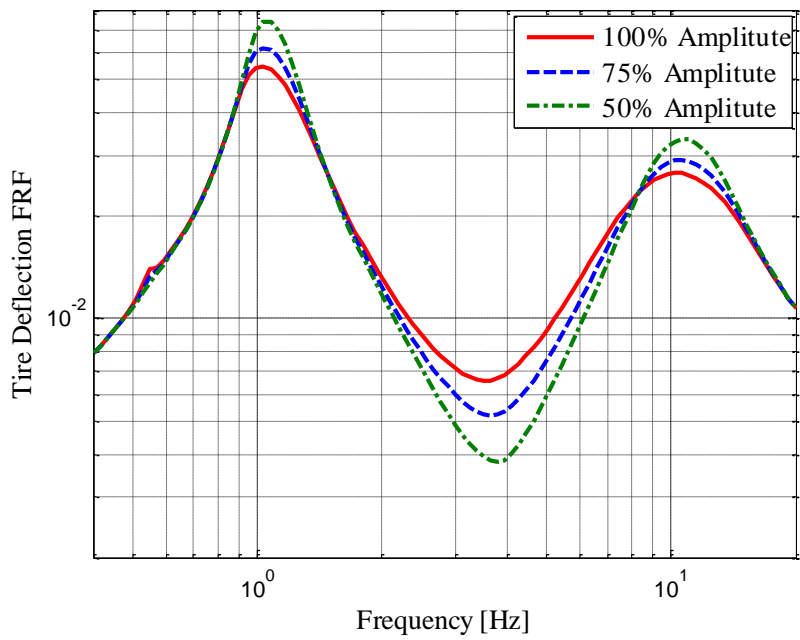


Figure 3.26: Variation of Tire Deflection with Input Amplitude

In summary, increasing piston area increases both suspension stiffness and damping, increasing initial gas volumes decreases suspension stiffness and increasing orifice opening decreases suspension damping.

3.3. COMPARISON OF DIFFERENT HP SUSPENSION SYSTEM

In this section the HP suspension system with double gas chambers will be modeled and its characteristics will be compared to those of the HP suspension system with single gas chamber.

3.3.1. Modeling of the HP Suspension System with Double Gas Chambers

With double gas chambers HP suspension, different stiffness and damping characteristics of the HP suspension system can be obtained. Therefore, more design parameters are available for suspension design. The schematic of the double gas HP suspension is given in Figure 3.27.

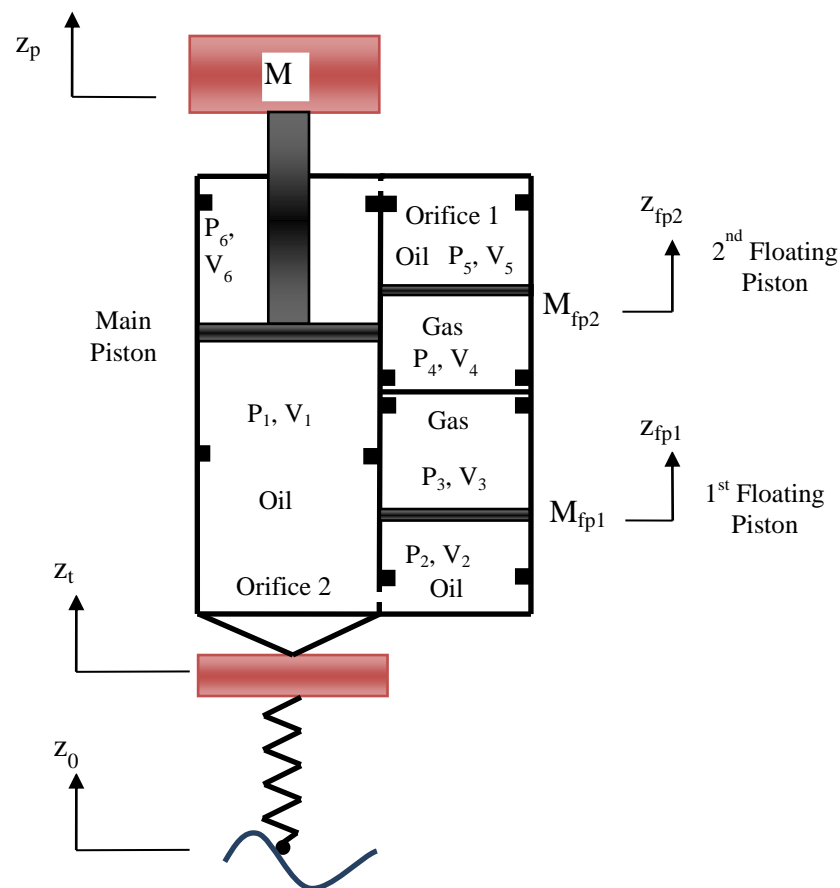


Figure 3.27. Double Gas Chamber HP Suspension

Equation of motion of the main piston can be written as

$$P_1 A_p - P_6 A_{pr} - Mg - F_{pf} - F_{pHS} = M \ddot{z}_p \quad (3-51)$$

where P_6 is the pressure at the 6th chamber, A_{pr} is the difference between the main piston area and the rod area.

Suspension force F can be written as,

$$F = P_1 A_p - P_6 A_{pr} - F_{pf} - F_{pHS} \quad (3-52)$$

Equation of the motion for the 1st floating piston can be written as,

$$P_2 A_{fp} - (P_3 - P_{Atm}) A_{fp} - M_{fp} g - F_{fpf1} - F_{fpHS1} = M_{fp} \ddot{z}_{fp1} \quad (3-53)$$

where A_{fp} is the floating piston area, F_{fpf1} is the friction force, F_{fpHS1} is the hard stop force for the first floating piston, and z_{fp1} is the displacement of the first floating piston. Similarly, the equation of motion of the second floating piston can be written as,

$$(P_4 - P_{Atm}) A_{fp} - P_5 A_{fp} - M_{fp} g - F_{fpf2} - F_{fpHS2} = M_{fp} \ddot{z}_{fp2} \quad (3-54)$$

where P_4 is the absolute gas pressure at the 4th chamber, P_5 is the oil pressure at the 5th chamber, F_{fpf2} is the friction force, F_{fpHS2} is the hard stop force for the second floating piston, and z_{fp2} is the displacement of the second floating piston.

Assuming incompressible oil, from continuity, it can be easily shown that,

$$z_{fp2} = z_t - \frac{A_{pr} (z_p - z_t)}{A_{fp}} \quad (3-55)$$

and

$$z_{fp1} = z_t - \frac{A_p (z_p - z_t)}{A_{fp}} \quad (3-56)$$

Moreover, the oil flow rate through 1st orifice is,

$$Q_{65} = C_d A_{v1} \sqrt{\frac{2}{\rho} |P_6 - P_5|} \text{sign}(\dot{z}_p - \dot{z}_t) \quad (3-57)$$

where, A_{v1} is the valve opening of the first orifice. Furthermore, Q_{65} is also equal to,

$$Q_{65} = A_{pr} (\dot{z}_p - \dot{z}_t) \quad (3-58)$$

Therefore P_6 can be found as,

$$P_6 = \left[\frac{A_{pr} (\dot{z}_p - \dot{z}_t)}{C_d A_{v1}} \right]^2 \frac{\rho}{2} \text{sign}(\dot{z}_p - \dot{z}_t) + P_5 \quad (3-59)$$

In a similar way, P_1 can be found as,

$$P_1 = P_2 - \left[\frac{A_p (\dot{z}_p - \dot{z}_t)}{C_d A_{v2}} \right]^2 \frac{\rho}{2} \text{sign}(\dot{z}_p - \dot{z}_t) \quad (3-60)$$

where A_{v2} is the valve opening of the second orifice. The gas pressure in 3rd chamber can be found from the polytropic gas equation as,

$$P_3 = \frac{P_{30} V_{30}^\kappa}{\left[V_{30} - A_{fp} (z_{fp1} - z_t) \right]^\kappa} \quad (3-61)$$

Similarly, the gas pressure in 4th chamber can be found as,

$$P_4 = \frac{P_{40} V_{40}^\kappa}{\left[V_{40} + A_{fp} (z_{fp2} - z_t) \right]^\kappa} \quad (3-62)$$

where P_{40} is the initial gas pressure at the 4th chamber and V_{40} is the initial volume of the gas in the 4th chamber. Pressures P_2 and P_5 can be found as,

$$P_2 = \frac{(P_3 - P_{Atm}) A_{fp} + M_{fp} g + F_{fpf1} + F_{fpHS1} + M_{fp} \ddot{z}_{fp1}}{A_{fp}} \quad (3-63)$$

$$P_5 = \frac{(P_4 - P_{Atm}) A_{fp} - M_{fp} g - F_{fpf2} - F_{fpHS2} - M_{fp} \ddot{z}_{fp2}}{A_{fp}} \quad (3-64)$$

After some manipulation, the pressures P_1 and P_6 are found as,

$$P_1 = \frac{\left(\frac{P_{30} V_{30}^\kappa}{[V_{30} - A_{fp}(z_{fp1} - z_t)]^\kappa} - P_{Atm} \right) A_{fp} + M_{fp}g + M_{fp}\ddot{z}_{fp1} + F_{fpf1} + F_{fpHS1}}{A_{fp}} - \quad (3-65)$$

$$- \left[\frac{A_p(\dot{z}_p - \dot{z}_t)}{C_d A_{v2}} \right]^2 \frac{\rho}{2} \text{sign}(\dot{z}_p - \dot{z}_t)$$

$$P_6 = \left[\frac{A_{pr}(\dot{z}_p - \dot{z}_t)}{C_d A_{v1}} \right]^2 \frac{\rho}{2} \text{sign}(\dot{z}_p - \dot{z}_t) + \quad (3-66)$$

$$+ \frac{\left(\frac{P_{40} V_{40}^\kappa}{[V_{40} + A_{fp}(z_{fp2} - z_t)]^\kappa} - P_{Atm} \right) A_{fp} - M_{fp}g - M_{fp}\ddot{z}_{fp2} - F_{fpf2} - F_{fpHS2}}{A_{fp}}$$

3.3.2. Static Analysis of the Double Gas Chamber HP Suspension System

At static equilibrium, the suspension force become,

$$F = \left[\frac{(P_{30} - P_{Atm})A_{fp} + M_{fp}g}{A_{fp}} \right] A_p - \left[\frac{(P_{40} - P_{Atm})A_{fp} - M_{fp}g}{A_{fp}} \right] A_{pr} = Mg \quad (3-67)$$

This force is equal to weight of the sprung mass M. Therefore, initial gas pressures P_{30} and P_{40} can be determined from Equation (3-67). However, there are two unknown initial gas pressures and one equation; there is a parameter family of solutions. To be able to determine a unique set of initial gas pressures, one of the initial gas pressures is set to a value, and the other one can be found.

3.3.3. Stiffness Characteristics of the Double Gas Chamber HP Suspension System

Since there are two gas chambers, the HP suspension system with double gas chambers has different stiffness characteristics. Let

$$z_1 = z_{fp1} - z_t = z_t - \frac{A_p(z_p - z_t)}{A_{fp}} - z_t = - \frac{A_p(z_p - z_t)}{A_{fp}} \quad (3-68)$$

and

$$z_2 = -z_{fp2} + z_t = -z_t + \frac{A_{pr}(z_p - z_t)}{A_{fp}} + z_t = \frac{A_{pr}(z_p - z_t)}{A_{fp}} \quad (3-69)$$

Then the suspension force becomes,

$$F = \left[\left(\frac{P_{30} V_{30}^\kappa}{[V_{30} + A_p(z_p - z_t)]^\kappa} - P_{Atm} \right) + \frac{M_{fp} g}{A_{fp}} \right] A_p - \left[\left(\frac{P_{40} V_{40}^\kappa}{[V_{40} - A_{pr}(z_p - z_t)]^\kappa} - P_{Atm} \right) - \frac{M_{fp} g}{A_{fp}} \right] A_{pr} \quad (3-70)$$

Then the suspension stiffness become,

$$k = -\frac{dF}{dz_{pt}} = \frac{P_{30} V_{30}^\kappa A_p^2 \kappa}{[V_{30} + A_p z_{pt}]^{\kappa+1}} + \frac{P_{40} V_{40}^\kappa A_{pr}^2 \kappa}{[V_{40} - A_{pr} z_{pt}]^{\kappa+1}} \quad (3-71)$$

At static equilibrium, the suspension stiffness can be found as

$$k = \frac{P_{30} A_p^2 \kappa}{V_{30}} + \frac{P_{40} A_{pr}^2 \kappa}{V_{40}} \quad (3-72)$$

The variation of the stiffness of double gas chamber suspension with relative displacement is shown in Figure 3.28.

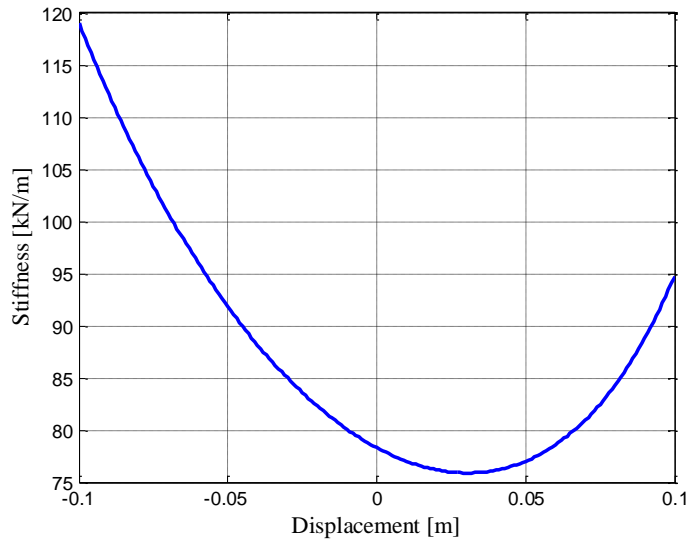


Figure 3.28: Variation of Gas Stiffness with Relative Displacement

The suspension stiffness in the double gas chamber HP suspension depends on many design parameters; initial gas volumes, V_{30} , and V_{40} , main piston area, A_p , floating piston area, A_{fp} , difference between piston and piston rod area, A_{pr} , and initial gas pressures P_{30} and P_{40} . Therefore, a more flexible tuning of suspension parameters can be obtained to satisfy suspension performance. The main difference between the suspension stiffness of the single-gas chamber and double-gas chamber HP suspension system is the shape of the stiffness curve. For the HP suspension system with single gas chamber, when the suspension displacement increases, stiffness decreases, and when the suspension displacement decreases stiffness increases. However, double gas chamber HP suspension system has a stiffness characteristic which has a minimum at some suspension displacement value. At other displacement values, increasing or decreasing suspension displacement increases suspension stiffness.

3.3.4. Damping Characteristics of the Double Gas Chamber HP Suspension System

Damping force F due to orifices in HP suspension system with double gas chamber can be written as,

$$F = A_p \left[\frac{A_p (\dot{z}_p - \dot{z}_t)}{C_d A_{v2}} \right]^2 \frac{\rho}{2} \text{sign}(\dot{z}_p - \dot{z}_t) + A_{pr} \left[\frac{A_{pr} (\dot{z}_p - \dot{z}_t)}{C_d A_{v1}} \right]^2 \frac{\rho}{2} \text{sign}(\dot{z}_p - \dot{z}_t) \quad (3-73)$$

As can be seen from Equation (3-73), the HP suspension system with double gas chamber has a damping force due to two orifices. This damping force can be provided in a HP suspension system with single gas chamber with an equivalent orifice area. On the contrary to stiffness characteristics, damping characteristics of the single and double gas chambers HP suspension system are identical.

3.4. EXPERIMENTAL VERIFICATION OF THE HP SUSPENSION UNIT

In order to validate the model of the HP suspension system used in the control and design studies, an experimental test setup is built and the HP suspension system is tested. Data collected from the experiment and model are compared to each other and

the HP suspension system is validated and the unknown parameters of the HP suspension system are determined by optimization.

3.4.1. Test Setup

HP suspension system test setup and HP suspension system are shown in Figure 3.29 and Figure 3.30 respectively.

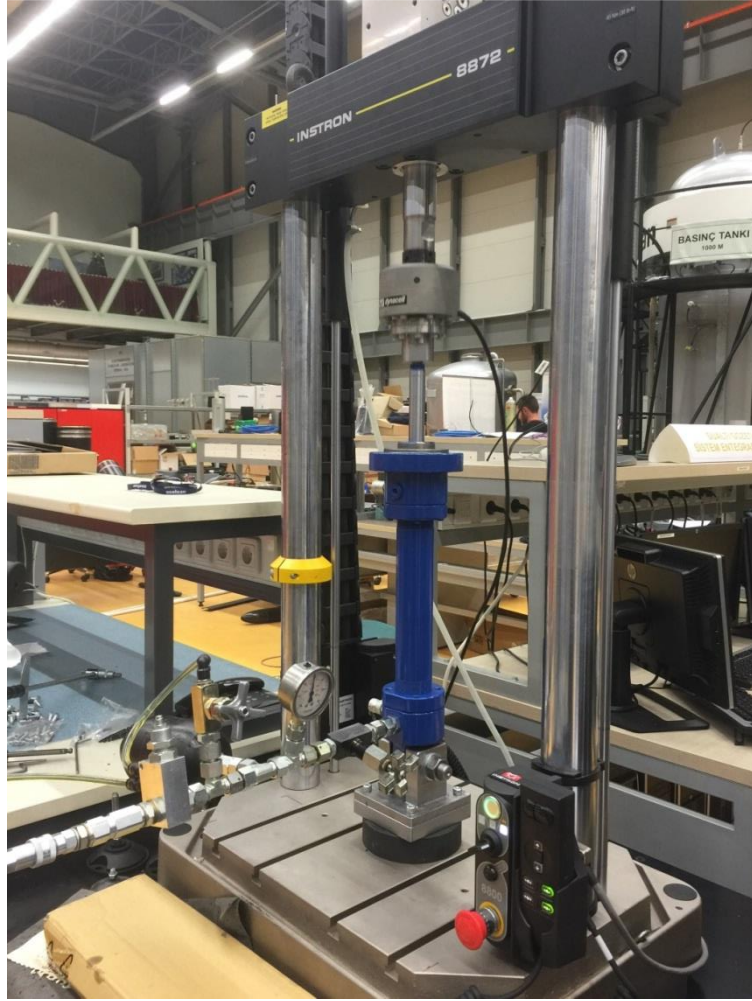


Figure 3.29: HP Suspension Test Setup

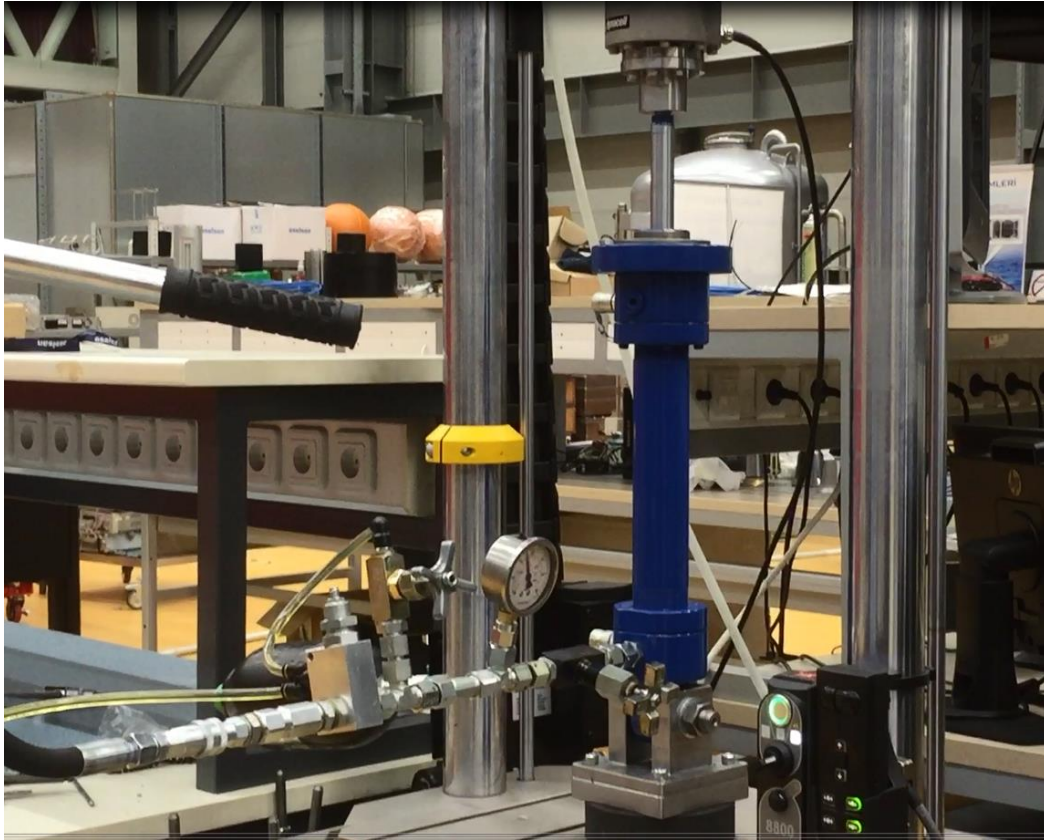


Figure 3.30: HP Suspension Test Setup

The HP suspension system can be built in different ways. In one construction, gas volume, oil volume, and orifices are all placed in the hydraulic cylinder as a whole unit. In the other construction, separate hydraulic elements are used to form the HP suspension system. In this study, separate industrial hydraulic elements are connected to each other to get a HP suspension system. The hydraulic system components making up the HP suspension system are listed below.

- ❖ Custom made $\varnothing 40\text{mm}$, 200mm stroke Hydraulic Cylinder (shown in Figure 3.32)
- ❖ Fox 0.7 liter Membrane Type Hydraulic Accumulator (shown in Figure 3.33)
- ❖ Parker Needle Valve (shown in Figure 3.34)
- ❖ Pressure Gage
- ❖ Check Valve
- ❖ Pressure Relief Valve

- ❖ Hand Pump
- ❖ Hydraulic Connectors
- ❖ Hydraulic Hoses
- ❖ Hydraulic Tank

Figure 3.31 shows the schematic of the HP suspension system used in the experiment.

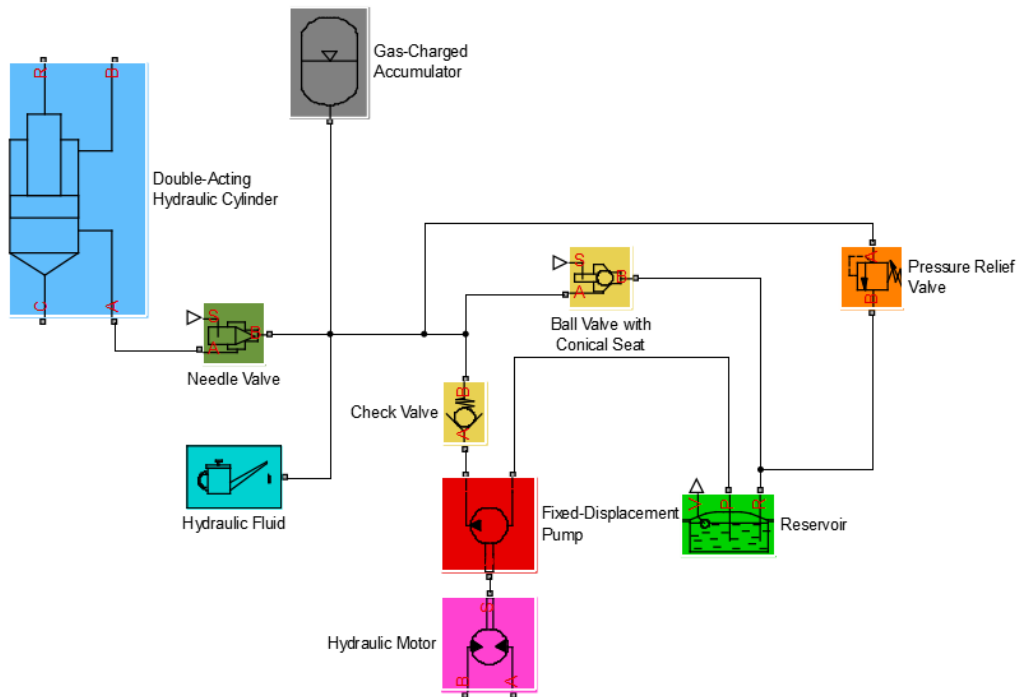


Figure 3.31: Schematic of the HP Suspension System

As shown in Figure 3.31, lower port of the hydraulic cylinder is connected to the needle valve and the needle valve is connected to the gas charged accumulator. Oil is pumped to the HP suspension system by a hand pump. In order to protect the pump from high pressure oil, a check valve is connected between the pump and the needle valve. In order to unload the system, a ball valve is connected between the main pressure line and the hydraulic reservoir. Moreover, a pressure relief valve is installed between the main pressure line and the hydraulic tank in order to protect the system against overpressure. The gas charged accumulator is used to provide the

system stiffness characteristics and the needle valve is used to provide the system damping characteristics. HP suspension system is mounted between the table and piston of the INSTRON test machine as shown in Figure 3.29. The INSTRON test machine produces the desired motion by its piston rod using a hydraulic system. Desired force and the corresponding displacement, or the desired displacement and the corresponding force can be obtained by the test machine. Both the force and the displacement of the piston are measured and recorded during the tests.



Figure 3.32: Hydraulic Cylinder



Figure 3.33: Fox 0.7 L Membrane Type Hydraulic Accumulator [50]



Figure 3.34: Parker 9MV600S Needle Valve [51].

3.4.2. Experiments

As stated before, the aim of the experiments is to validate the mathematical model of the HP suspension system. For this reason, two different types of tests are performed. In first group of tests the stiffness and in the second group of tests damping characteristics of the HP suspension system are examined. A ramp displacement input with lower ramp rate is used in the first group of tests and sinusoidal displacement inputs with different frequencies are used in the second group of tests. Then the unknown parameters of the model are estimated and responses of the model and experimental results are compared to each other. Figure 3.35 to Figure 3.37 show the comparison of the responses obtained from the tests and from the simulations of the model for different initial gas pressures.

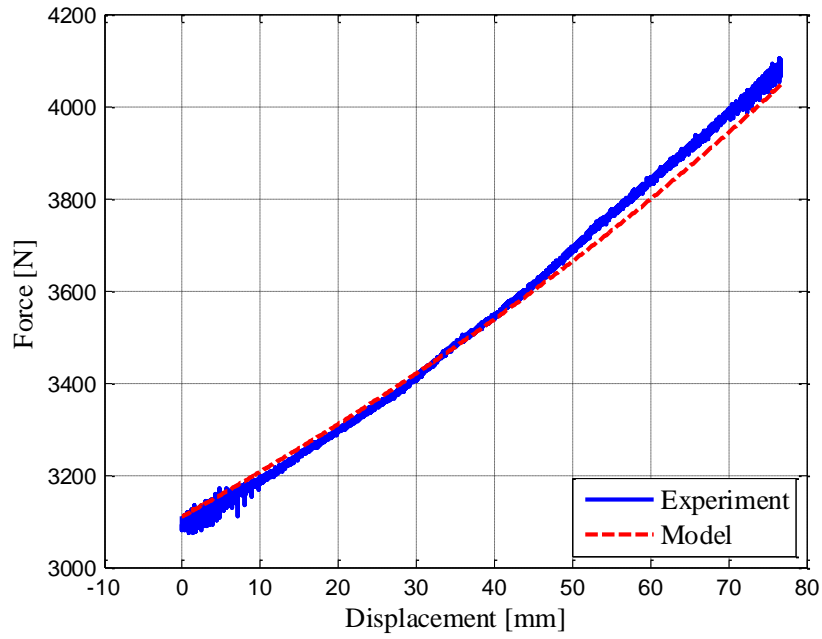


Figure 3.35: Measured vs Simulated Gas Force for $P_i=25.8$ bar

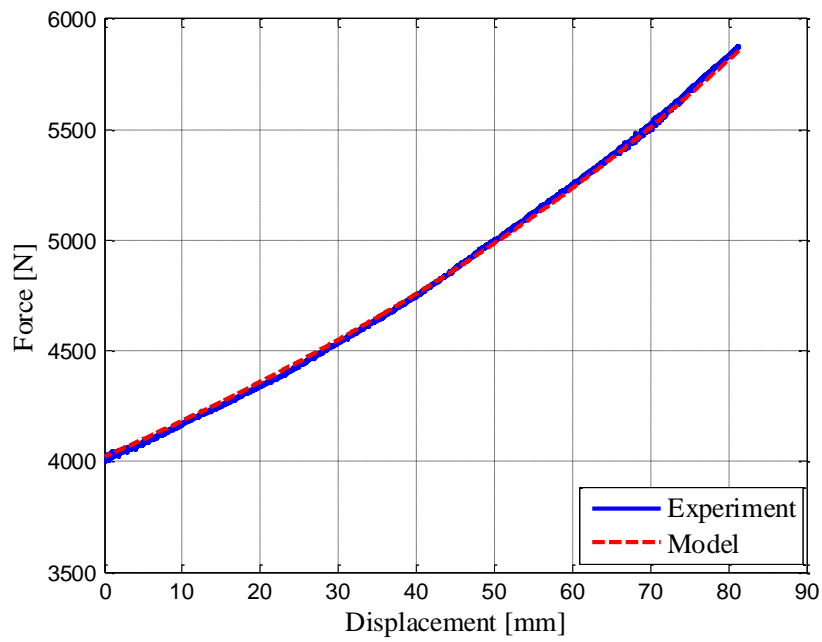


Figure 3.36: Measured vs Simulated Gas Force for $P_i=33$ bar

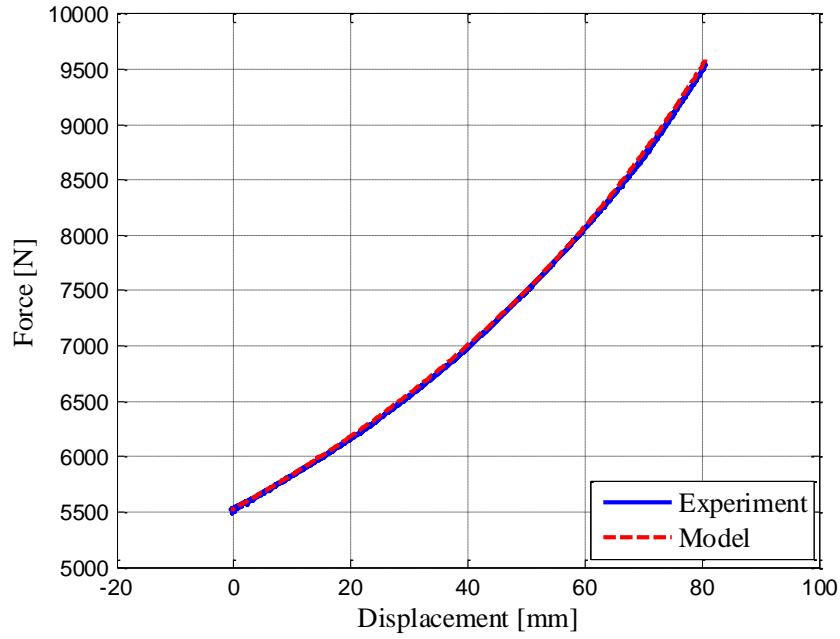


Figure 3.37: Measured vs Simulated Gas Force for $P_i=45$ bar

As Figure 3.35 to Figure 3.37 show, force-displacement characteristics of the HP suspension setup and the HP suspension model are almost identical. Since the ramp input is used with very low ramp rate, polytropic gas model is approximately on the isothermal working conditions. After the stiffness tests are performed, damping tests are conducted at different input frequencies and amplitudes. Figure 3.38 to Figure 3.43 show the comparison of the force-displacement characteristics of the HP suspension setup and the HP suspension model for different input frequencies and amplitudes, and valve openings. Figure 3.38 to Figure 3.40 show the experimental results at 1 Hz sinusoidal input for different valve openings. Since the valve opening cannot be measured during the experiment, an estimated value is used while comparing the experimental and the model results. As can be seen from the experimental results, the magnitude of the Coulomb friction, approximately 220 N, can be estimated from the results directly.

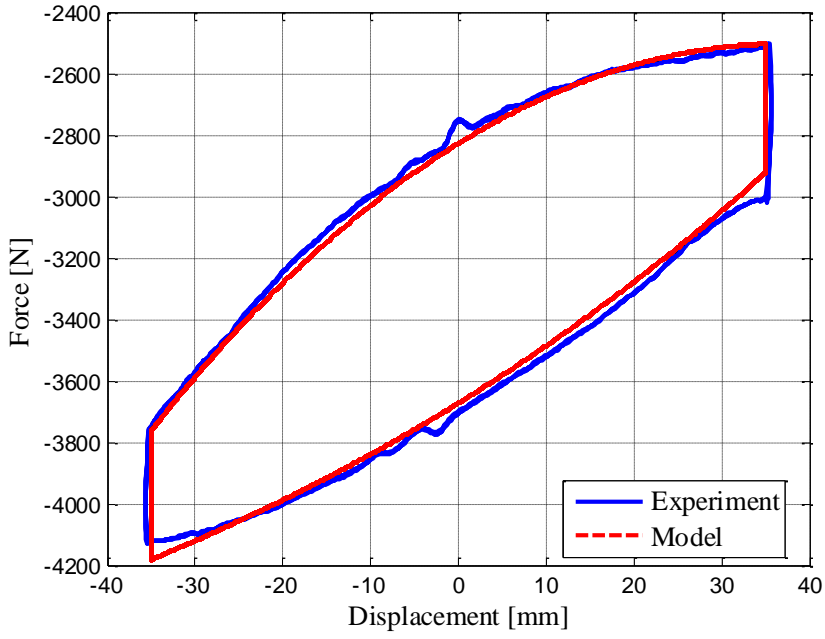


Figure 3.38: Measured vs Simulated Gas Force for $P_i=25.8$ bar, $A=35$ mm, $f=1$ Hz

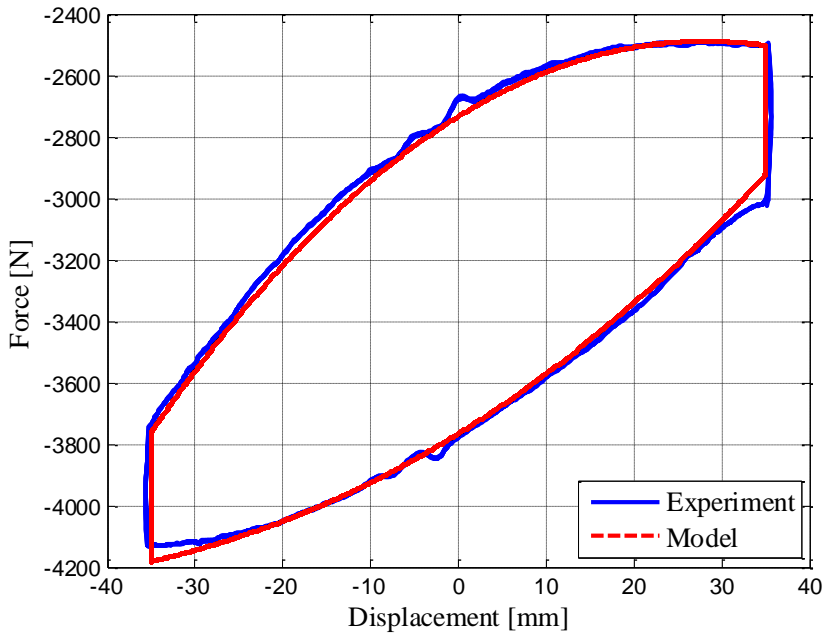


Figure 3.39: Measured vs Simulated Gas Force for $P_i=25.8$ bar $A=35$ mm, $f=1$ Hz

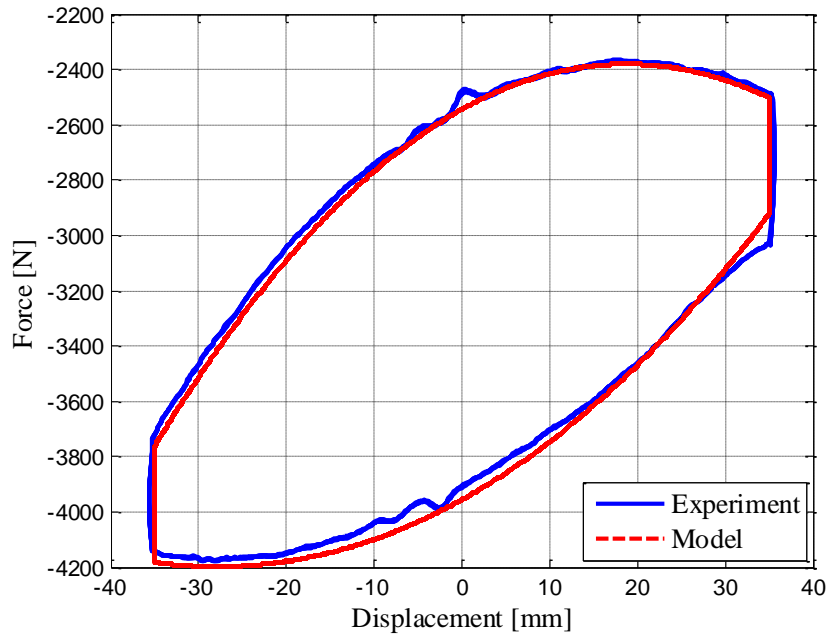


Figure 3.40: Measured vs Simulated Gas Force for $P_i=25.8$ bar $A=35$ mm, $f=1$ Hz

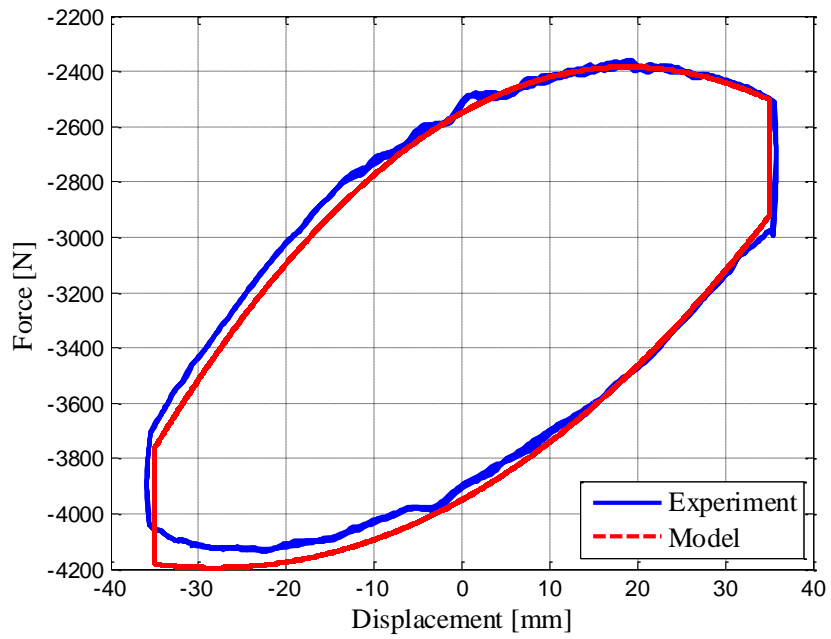


Figure 3.41: Measured vs Simulated Gas Force for $P_i=25.8$ bar $A=35$ mm, $f=1.5$ Hz

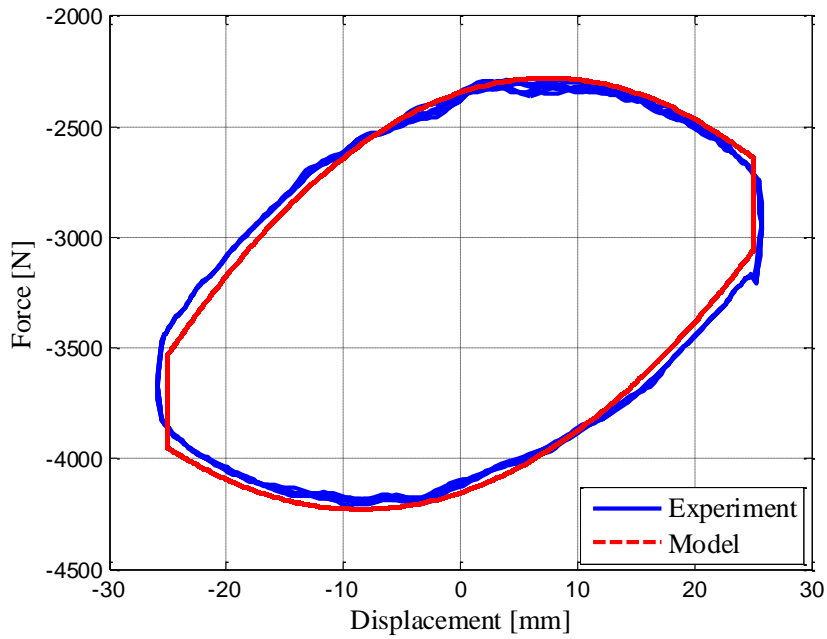


Figure 3.42: Measured vs Simulated Gas Force for $P_i=25.8$ bar, $A=25$ mm $f=2.5$ Hz

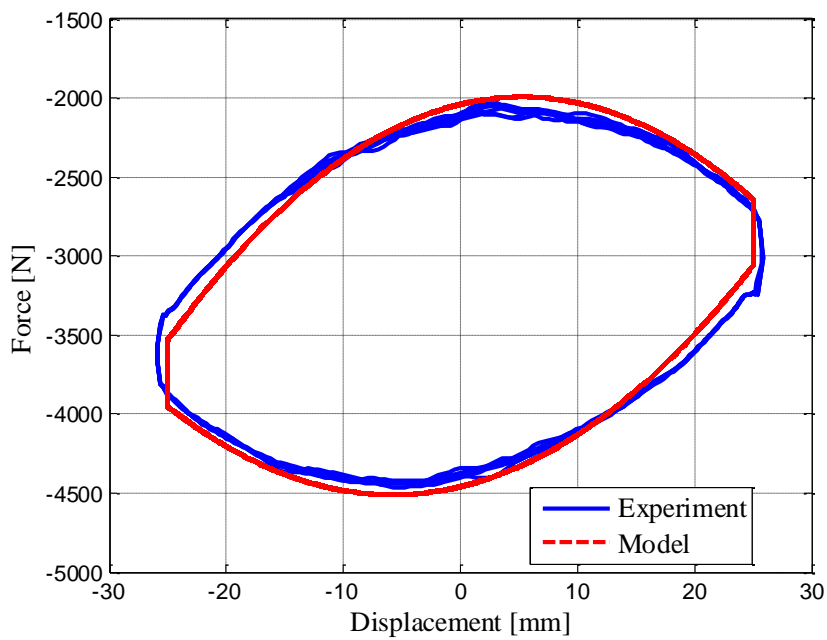


Figure 3.43: Measured vs Simulated Gas Force for $P_i=25.8$ bar, $A=25$ mm $f=3$ Hz

In the mathematical model of the HP suspension system, two important hydraulic system elements, the gas volume and orifice models, are used. Dynamics of the gas

volume is modeled by the polytropic gas model and the dynamics of the orifice is modeled by the orifice equation. Since the model and the experiment results are close to each other for the specified parameters of the test, it can be concluded that, the derived model of the HP suspension system can be used in the control, optimization, and the design studies.

3.5. TUNING OF THE PARAMETERS OF HP SUSPENSION SYSTEM

For a HP suspension system with single accumulator and single valve, the design parameters are the piston area, initial gas volume, and the orifice area. By tuning these parameters, stiffness and the damping characteristics of the HP suspension system can be determined. As stated in previous part, stiffness of the HP suspension system at static equilibrium depends on the initial gas volume and the piston area. The damping of the HP suspension system, on the other hand, depends on the piston area and the orifice opening. Therefore, for a desired stiffness and the damping characteristics, these three parameters need to be adjusted. Normally, two parameters are enough to design the suspension stiffness and the damping, yet extra one parameter provides design flexibility. By fixing the piston area, the suspension stiffness can be adjusted by changing the initial gas volume and damping can be adjusted by changing the orifice area.

For a HP suspension system with double gas chamber, the suspension parameters are the initial gas volumes, initial gas pressures, piston area, floating piston area, rod area, and orifice openings. As can be seen from Equation (3-72), the suspension stiffness depends on the initial gas volumes, initial gas pressures, main piston area, and rod areas. However, as the static equilibrium equation indicates, one of the initial gas pressures can be set and the remaining initial gas pressure can be found, i.e. one of the initial gas pressures is not an independent parameter. Thus, the suspension stiffness depends on only five design parameters which are the main piston area, rod area, initial gas volumes, and one of initial gas pressures. This case provides more design flexibility as compared with the HP suspension system with single gas chamber. Moreover, the damping force in the HP suspension system with double gas chamber depends on the main piston area, rod area, and orifice opening. There are

more design parameters for the damping force in a HP suspension system with double gas chamber as compared with the HP suspension system with single gas chamber. For a quarter car model with HP suspension system, for an approximate body bounce frequency ω_{bb} , the initial gas volume can be found for a predetermined piston area by,

$$V_{30} = \frac{P_{30} A_p^2 \kappa}{M \omega_{bb}^2} \quad (3-74)$$

This initial gas volume provides a starting value for the design of the HP suspension system. In summary, to be able to design the HP suspension system firstly, the type of the HP suspension system, either single gas volume or double gas volume, is determined. Then the piston area (and rod area) is determined according to the initial gas and the oil pressure. In order not to increase the oil pressure too much, the piston area is set to some limited range of values. When the piston area is fixed, the only design parameter which effects suspension stiffness is the initial gas volume.

In the following chapters, the HP suspension system with single gas chamber is used so that the subjects for investigation are not shadowed by the more involved characteristics of the double gas chamber HP suspension system.

CHAPTER 4

ACTIVE HP SUSPENSION SYSTEM

The HP suspension systems are more suitable for the implementation of active and semi-active suspension control compared with mechanical suspensions. In the HP suspension system, active suspension can be designed by pumping hydraulic oil into suspension, or by extracting the hydraulic oil from the suspension back to the reservoir. Similarly, the semi-active suspension can be implemented by introducing a controllable damper valve opening.

4.1. INTRODUCTION

A suspension system is expected to isolate the vehicle body from road disturbances and keep the tires in contact with the road. Ride comfort is directly associated with sprung mass acceleration, and road holding is associated with tire deflection. Passive suspension systems can satisfy ride comfort, road holding, and handling requirements only to a limited extent. To improve suspension performance, various active and semi-active suspensions have been proposed in the literature and there are numerous studies on the active control of the conventional suspension systems. Models of active systems in these studies are mostly linear and thus linear control methods have been applied to determine the desired active force. In some of the studies, hydraulic actuators which provide active force are included in the model and thus actuator dynamics are also taken into account.

It is observed that, most of the studies related to the design of controllers for active suspensions which involve conventional linear suspension systems. For these systems well-known linear control methods can be used to design the controller. There are, on the other hand, few studies about the active control of the HP suspension system with nonlinear controllers. Since the HP suspension system is inherently nonlinear due to the orifice and the gas equations, the controller should also be nonlinear to capture the system dynamics thoroughly. Linearizing the nonlinear HP suspension system for specific operating point and designing the controller for that point is not effective for the whole dynamic range of the system.

Designing a suboptimal nonlinear controller for the quarter car with a nonlinear active HP suspension in a systematic manner is the main target of this chapter. The basic concern is the design of the active HP suspension to obtain improved ride comfort together with improved handling by taking the nonlinear behavior of the system into consideration. Therefore, a state space model with state dependent matrices (SDM) of the nonlinear HP suspension system is derived by the extended linearization [52] to be used for the controller design. Polytropic gas model is rewritten as a polynomial gas equation, such that the gas force is a polynomial function of the relative gas displacement. Thus, the gas force is expressed in terms of a linear stiffness equation with a state dependent spring coefficient. Similarly, the orifice equation is written as a linear damping equation with state dependent viscous coefficient. By this way, all nonlinearities of the original nonlinear HP suspension system are preserved. Then, a nonlinear control method, State Dependent Riccati Equation (SDRE) control, is used to design the nonlinear active controller. A nonlinear active controller is designed effectively and systematically, instead of using more complicated formal nonlinear control approaches. The proposed method can also be applied to suspension systems with different types of nonlinear spring and damper characteristics easily. Further, as explained in reference [53], saturation on the oil flow rate can also be incorporated with the SDRE control. The control designers are required only to adjust the weighting parameters of the performance variables according to the aim of the control.

SDRE control is a systematic way of designing a nonlinear controller. It is similar to the Linear Quadratic Regulator (LQR) control and by applying the SDRE control as a nonlinear control method; all properties of the well-known LQR control can be exploited [53], [54]. Mracek and Cloutier [53] studied the theory of SDRE control and illustrated the applications of SDRE for nonlinear control problems. Banks et al. [54] studied the SDRE method for nonlinear control and estimation problems. Various methods for the solution of the SDRE were also covered in the study. An extensive review of the SDRE control was presented by Çimen [55]. In the literature, there are various applications of the SDRE control in different areas such as vehicle dynamics, aerospace, robotics, etc. Kanarachos et al. [56] and Jansen et al. [57] used the SDRE control for the design of the braking controller of electric vehicles. Alirezai et al. [58] developed a vehicle dynamics controller using the SDRE control and then validated the performance of the controller experimentally. There are also studies which use the SDRE control method to design nonlinear controllers for robotics, motor, and aerospace control applications [59]-[61].

4.2. QUARTER CAR MODEL WITH ACTIVE HP SUSPENSION SYSTEM

In this section, active suspension application with the HP suspension on a quarter car model is considered. Firstly, the active HP suspension with various complexity levels is modeled and then a nonlinear control method, SDRE is used for the design of the controllers. Finally, the performance of the HP suspension system is examined by simulations.

The HP suspension system has inherent nonlinear dynamics due to the gas and orifice characteristics. When the gas is compressed or expanded, it behaves according to the polytropic gas equation. Moreover, the pressure drop and oil flow rate characteristics of the damping orifice are also nonlinear. In the literature, there are many studies about the active suspension control [25]-[39]. In these studies, mostly, conventional mechanical suspension system together with a linear actuator is used. The output of the linear actuator, which is force, is used as the control input to the active suspension system. The behavior of the mechanical spring and the damper are approximated by linear relations, and a linear controller design problem is

formed. In most of these studies, the well-known linear quadratic regulator is used for the design of the controller. In some studies, actuator dynamics is also taken into account in the design of the active controller [28]-[30].

4.2.1. State Dependent Riccati Equation (SDRE) Control

In the SDRE control, the first step is to obtain a state space model of the system in which the matrices are functions of states. By this way, a linear structure of the nonlinear model is obtained and the nonlinearities in the model are fully captured in the state space formulation. Then the cost function to be minimized is formed using the SDM. Thus the Algebraic Riccati Equation is also state dependent and is solved online along the trajectory of states, and a state dependent control law is obtained.

A detailed theoretical analysis of both the control and estimation with the SDRE, which is followed with some modifications here, is presented in reference [54].

A nonlinear, input affine system,

$$\dot{x} = f(x) + B(x)u \quad (4-1)$$

$$z = C(x)x \quad (4-2)$$

can be written as

$$\dot{x} = A(x)x + B(x)u \quad (4-3)$$

where

$$A(x)x = f(x) \quad (4-4)$$

The infinite horizon cost function,

$$J = \frac{1}{2} \int_0^{\infty} (x^T Q(x)x + u^T R(x)u) dt \quad (4-5)$$

can be minimized by solving the SDRE,

$$A^T(x)P + PA(x) - PB(x)R(x)^{-1} B^T(x)P + C^T(x)C(x) = 0 \quad (4-6)$$

where $P \geq 0$ and constructing the nonlinear feedback controller,

$$u = -R^{-1}(x)B^T(x)P(x)x \quad (4-7)$$

The controllability and observability matrices associated with the state dependent linear model are defined as,

$$\text{Con}(x) = [B(x) \quad A(x)B(x) \quad \dots \quad A^{n-1}(x)B(x)] \quad (4-8)$$

$$\text{Obs}(x) = [C(x) \quad C(x)A(x) \quad \dots \quad C(x)A^{n-1}(x)] \quad (4-9)$$

respectively.

Theorem 1: If the pairs $\{A(x), B(x)\}$ and $\{C(x), A(x)\}$ are pointwise stabilizable and detectable in the linear sense for all, $x \in \Omega$ then the closed loop system is locally asymptotically stable [53].

For a vehicle, ride comfort is related to the vertical, roll, and pitch accelerations; road holding is associated with tire deflection, suspension packaging is related with the suspension deflection, and vehicle handling is related with roll and pitch angles of the vehicle body. In active suspension design, the aim is to improve the vehicle ride comfort by decreasing the vertical acceleration, to improve the road holding by decreasing the tire deflection, and to improve suspension packaging by decreasing the suspension deflection. When complete vehicle dynamics is taken into account, the active suspension should also improve vehicle ride comfort and vehicle handling by decreasing the roll and the pitch accelerations, and the roll and the pitch motion of the vehicle. The design of a controller which can fulfill all these performance requirements is a difficult task. In the active suspension control, linear quadratic regulator is a commonly used control method, since a controller which improves the performance of the weighted combination of the performance variables can be designed. According to the aim of the controller, weighting coefficients can be assigned for the specific performance requirements. Therefore, one of the reasons of the use of the SDRE for the active controller design is that, a multi-objective nonlinear controller can be designed for weighted performance variables in a systematic manner. Moreover, in multi-objective controller design, it is difficult for a

single controller to improve all the performance variables simultaneously. Sometimes, according to the magnitude of the performance variables, the controller should be targeted for different performance considerations. As will be shown in following sections, with SDRE control, weighting coefficients can be changed online according to the measured or calculated performance variables, since the controller is updated online with the changing states at each time step. By this way, different performance considerations can be satisfied according to the changing situation of the system. Moreover desired control applications such as using state constraint or input saturation can easily implemented with SDRE control. Consequently, SDRE control is selected for the controller design of the active HP suspension system.

First step in the design of the active HP suspension system, the mathematical model of the active HP suspension system must be obtained. Then, a linear state space model with state dependent matrices is to be obtained. Finally the controller is designed by using the SDRE control method. In order to obtain the linear state space model with state dependent coefficients, the gas model and the orifice equations should be linearized by called extended linearization [52] or direct parameterization [53], [54]. The schematic of the active HP suspension design is shown in Figure 4.1.

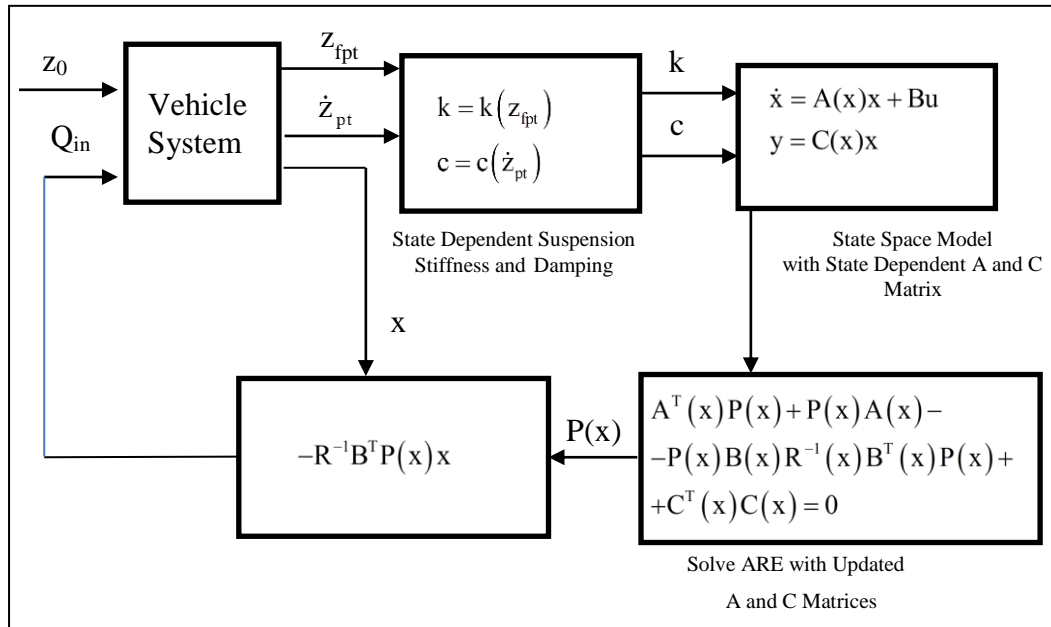


Figure 4.1: Active HP Suspension Design by SDRE Control

4.2.2. Quarter Car with Active HP Suspension System

The first active HP suspension is to be designed for the simplest vehicle ride model, i.e. the classical quarter car model.

4.2.2.1. Modeling of the Quarter Car Model with Active HP Suspension System

Linearizing the HP Suspension system about an equilibrium point yields accurate results only in the neighborhood of the equilibrium point. At other points, the results obtained from linear model deviates from reality. The schematic of the quarter car model with active HP suspension system is shown in Figure 4.2. An active oil flow rate into the second oil volume of the suspension or an oil flow rate from the second oil volume of the suspension to the hydraulic tank is introduced. Therefore, the oil flow rate is taken as the control input for the active HP suspension system. All the equations obtained while deriving the equations of motion of the single unit HP suspension system are still valid, except the continuity equation for the second oil volume. Since there is an active oil flow rate into the second oil volume, the continuity equation for the second oil volume become,

$$Q_{in} - Q_{12} = A_p (-\dot{z}_{fp} + \dot{z}_t) \quad (4-10)$$

where Q_{in} is the oil flow rate to the second oil volume Similarly, the continuity equation for the first oil volume is,

$$Q_{12} = A_p (\dot{z}_p - \dot{z}_t) \quad (4-11)$$

From Equation (4-10) and Equation (4-11), the relation between floating piston motion and the main piston motion can be found as,

$$Q_{in} = A_p (\dot{z}_p - \dot{z}_{fp}) \quad (4-12)$$

As can be seen from Equation (4-12) , the motion of the floating piston and the main piston is governed by the oil flow rate in to the system. Other equations can be adopted from the previous chapter.

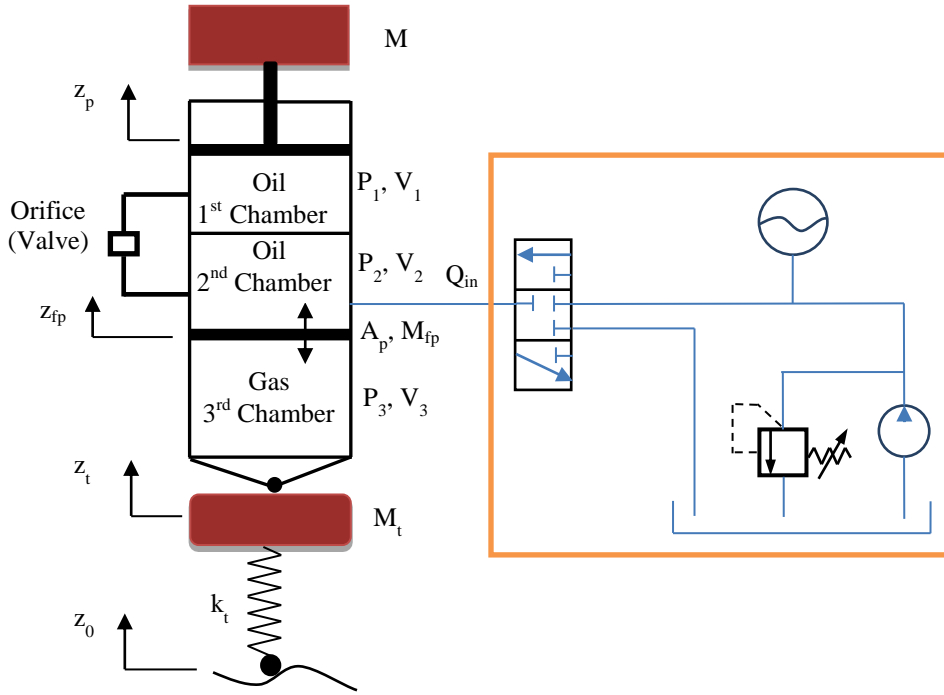


Figure 4.2: Quarter Car Model with the active HP Suspension System

To be able to get the linear state space model with state dependent coefficients of the active HP suspension system, there should be no constant terms in the nonlinear state equation. Moreover, the state coefficients should be finite when the states go to zero. There are infinitely many direct parameterization form of the given nonlinear system. In linear springs, spring force is proportional to spring deflection. In other words, spring force is a polynomial function of spring deflection with zero constant term. Mimicking the linear spring characteristics, the gas dynamics is expressed as the polynomial function of the relative floating piston displacement with zero constant term. The degree of fitted polynomial can be determined according to the domain of the fitted curve. To illustrate, a five degree polynomial is fitted to the dynamic gas force as,

$$\begin{aligned} \frac{P_{30} V_{30}^\kappa A_p}{(V_{30} + A_p z_{fpt})^\kappa} - Mg - M_{fp} g - P_{Atm} A_p = p_1 z_{fpt} + p_2 z_{fpt}^2 + p_3 z_{fpt}^3 + \\ + p_4 z_{fpt}^4 + p_5 z_{fpt}^5 = F_{gas}(z_{fpt}) \end{aligned} \quad (4-13)$$

where, z_{fpt} is the relative displacement across the gas volume and p 's are the polynomial coefficient. The fitted polynomial and the polytropic gas model are shown in Figure 4.3.

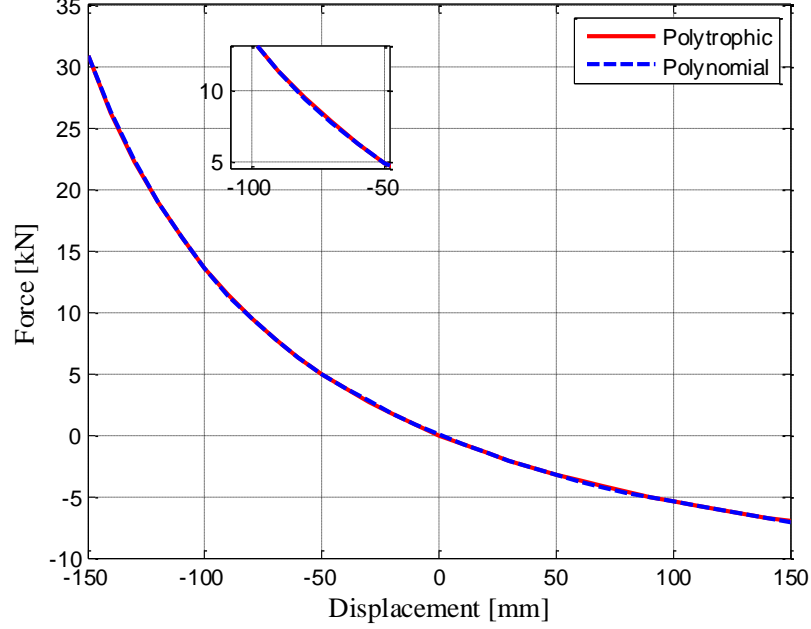


Figure 4.3: Polynomial Model of Polytropic Gas Equation

Thus, the state dependent linearized model becomes,

$$F_1(z_{fpt}) = (p_1 + p_2 z_{fpt} + p_3 z_{fpt}^2 + p_4 z_{fpt}^3 + p_5 z_{fpt}^4) z_{fpt} = f_1(z_{fpt}) z_{fpt} \quad (4-14)$$

where f_1 is the state dependent gas stiffness and is equal to,

$$f_1(z_{fpt}) = p_1 + p_2 z_{fpt} + p_3 z_{fpt}^2 + p_4 z_{fpt}^3 + p_5 z_{fpt}^4 \quad (4-15)$$

As can be seen from the Equation (4-15), when the relative gas displacement is zero, the gas stiffness is finite and there is no constant term in gas force equation. Similarly, the state dependent formulation of the orifice equation is straightforward and it can be expressed like linear damper equation. The state dependent model of the orifice equations become,

$$F_2 = A_p \left[\frac{A_p \dot{z}_{pt}}{A_v C_d} \right]^2 \frac{\rho}{2} \text{sign}(\dot{z}_{pt}) = f_2(\dot{z}_{pt}) \dot{z}_{pt} \quad (4-16)$$

where \dot{z}_{pt} is the relative suspension velocity,

$$\dot{z}_{pt} = \dot{z}_p - \dot{z}_t \quad (4-17)$$

and f_2 is the state dependent damping coefficient expressed as,

$$f_2(\dot{z}_{pt}) = \dot{z}_{pt} A_p \left[\frac{A_p}{A_v C_d} \right]^2 \frac{\rho}{2} \text{sign}(\dot{z}_{pt}) \quad (4-18)$$

After the nonlinear elements are converted into direct parameterization form, the state dependent model of the HP Suspension model can be obtained. Assume that friction forces and floating piston dynamics are negligible and assuming road velocity displacement is integrated white noise, system states can be defined as,

$$x_1 = \dot{z}_p \quad (4-19)$$

$$x_2 = z_{ip} - z_t \quad (4-20)$$

$$x_3 = z_t - z_0 \quad (4-21)$$

$$x_4 = \dot{z}_t \quad (4-22)$$

$$x_5 = z_p - z_t \quad (4-23)$$

The system states are sprung mass velocity, floating piston relative displacement, tire deflection, tire velocity, and suspension deflection. Normally, first four states are sufficient to define the system dynamics. However, the fifth state is also defined for used in the performance index for controller design. Then the state equations become,

$$\dot{x}_1 = -\frac{f_2}{M} x_1 + \frac{f_1}{M} x_2 + \frac{f_2}{M} x_4 \quad (4-24)$$

$$\dot{x}_2 = x_1 - x_4 - \frac{Q_{in}}{A_p} \quad (4-25)$$

$$\dot{x}_3 = x_4 - \dot{z}_0 \quad (4-26)$$

$$\dot{x}_4 = \frac{f_2}{M_t} x_1 - \frac{f_1}{M_t} x_2 - \frac{k_t}{M_t} x_3 - \frac{f_2}{M_t} x_4 \quad (4-27)$$

$$\dot{x}_5 = x_1 - x_4 \quad (4-28)$$

For this active HP suspension system, linear state space model with state dependent coefficients become,

$$\begin{Bmatrix} \dot{x}_1 \\ \dot{x}_2 \\ \dot{x}_3 \\ \dot{x}_4 \\ \dot{x}_5 \end{Bmatrix} = \begin{bmatrix} -\frac{f_2}{M} & \frac{f_1}{M} & 0 & \frac{f_2}{M} & 0 \\ 1 & 0 & 0 & -1 & 0 \\ 0 & 0 & 0 & 1 & 0 \\ \frac{f_2}{M_t} & -\frac{f_1}{M_t} & -\frac{k_t}{M_t} & -\frac{f_2}{M_t} & 0 \\ 1 & 0 & 0 & -1 & 0 \end{bmatrix} \begin{Bmatrix} x_1 \\ x_2 \\ x_3 \\ x_4 \\ x_5 \end{Bmatrix} + \begin{Bmatrix} 0 \\ 0 \\ -1 \\ 0 \\ 0 \end{Bmatrix} w + \begin{Bmatrix} 0 \\ -\frac{1}{A_p} \\ 0 \\ 0 \\ 0 \end{Bmatrix} Q_{in} \quad (4-29)$$

When the road disturbance input is assumed as the filtered white noise, a new state equation can be defined as,

$$\dot{z}_0 = -\beta_r z_0 + w \quad (4-30)$$

where β_r is the constant which depends on the road type and w is the zero mean white noise. When a new state $x_6=z_0$ is also inserted into the equations of motions, and the state space equations are obtained as follows:

$$\dot{x}_1 = -\frac{f_2}{M} x_1 + \frac{f_1}{M} x_2 + \frac{f_2}{M} x_4 \quad (4-31)$$

$$\dot{x}_2 = x_1 - x_4 - \frac{Q_{in}}{A_p} \quad (4-32)$$

$$\dot{x}_3 = x_4 + \beta x_6 - w \quad (4-33)$$

$$\dot{x}_4 = \frac{f_2}{M_t} x_1 - \frac{f_1}{M_t} x_2 - \frac{k_t}{M_t} x_3 - \frac{f_2}{M_t} x_4 \quad (4-34)$$

$$\dot{x}_5 = x_1 - x_4 \quad (4-35)$$

$$\dot{x}_6 = -\beta x_6 + w \quad (4-36)$$

The state space equation with state dependent coefficients become,

$$\begin{Bmatrix} \dot{x}_1 \\ \dot{x}_2 \\ \dot{x}_3 \\ \dot{x}_4 \\ \dot{x}_5 \\ \dot{x}_6 \end{Bmatrix} = \begin{bmatrix} -\frac{f_2}{M} & \frac{f_1}{M} & 0 & \frac{f_2}{M} & 0 & 0 \\ 1 & 0 & 0 & -1 & 0 & 0 \\ 0 & 0 & 0 & 1 & 0 & \beta \\ \frac{f_2}{M_t} & -\frac{f_1}{M_t} & -\frac{k_t}{M_t} & -\frac{f_2}{M_t} & 0 & 0 \\ 1 & 0 & 0 & -1 & 0 & 0 \\ 0 & 0 & 0 & 0 & 0 & -\beta \end{bmatrix} \begin{Bmatrix} x_1 \\ x_2 \\ x_3 \\ x_4 \\ x_5 \\ x_6 \end{Bmatrix} + \begin{Bmatrix} 0 \\ 0 \\ -1 \\ 0 \\ 0 \\ 1 \end{Bmatrix} w + \begin{Bmatrix} 0 \\ -\frac{1}{A_p} \\ 0 \\ 0 \\ 0 \\ 0 \end{Bmatrix} Q_{in} \quad (4-37)$$

The suspension deflection is desired to be regulated or to be adjusted to user defined value at steady state, thus an integral state of the suspension deflection is also added as another state. Define new state x_7 as,

$$x_7 = \int (z_p - z_t) \quad (4-38)$$

Then the new state equation become,

$$\dot{x}_7 = z_p - z_t = x_5 \quad (4-39)$$

For this new system, the state space model with state dependent coefficients become,

$$\begin{Bmatrix} \dot{x}_1 \\ \dot{x}_2 \\ \dot{x}_3 \\ \dot{x}_4 \\ \dot{x}_5 \\ \dot{x}_6 \\ \dot{x}_7 \end{Bmatrix} = \begin{bmatrix} -\frac{f_2}{M} & \frac{f_1}{M} & 0 & \frac{f_2}{M} & 0 & 0 & 0 \\ 1 & 0 & 0 & -1 & 0 & 0 & 0 \\ 0 & 0 & 0 & 1 & 0 & \beta & 0 \\ \frac{f_2}{M_t} & -\frac{f_1}{M_t} & -\frac{k_t}{M_t} & -\frac{f_2}{M_t} & 0 & 0 & 0 \\ 1 & 0 & 0 & -1 & 0 & 0 & 0 \\ 0 & 0 & 0 & 0 & 0 & -\beta & 0 \\ 0 & 0 & 0 & 0 & 1 & 0 & 0 \end{bmatrix} \begin{Bmatrix} x_1 \\ x_2 \\ x_3 \\ x_4 \\ x_5 \\ x_6 \\ x_7 \end{Bmatrix} + \begin{Bmatrix} 0 \\ 0 \\ -1 \\ 0 \\ 0 \\ 1 \\ 0 \end{Bmatrix} w + \begin{Bmatrix} 0 \\ -\frac{1}{A_p} \\ 0 \\ 0 \\ 0 \\ 0 \\ 0 \end{Bmatrix} Q_{in} \quad (4-40)$$

When the road displacement input is taken as the integrated white noise, together with the integral control, the state space model becomes,

$$\begin{Bmatrix} \dot{x}_1 \\ \dot{x}_2 \\ \dot{x}_3 \\ \dot{x}_4 \\ \dot{x}_5 \\ \dot{x}_6 \end{Bmatrix} = \begin{bmatrix} -\frac{f_2}{M} & \frac{f_1}{M} & 0 & \frac{f_2}{M} & 0 & 0 \\ 1 & 0 & 0 & -1 & 0 & 0 \\ 0 & 0 & 0 & 1 & 0 & 0 \\ \frac{f_2}{M_t} & -\frac{f_1}{M_t} & -\frac{k_t}{M_t} & -\frac{f_2}{M_t} & 0 & 0 \\ 1 & 0 & 0 & -1 & 0 & 0 \\ 0 & 0 & 0 & 0 & 1 & 0 \end{bmatrix} \begin{Bmatrix} x_1 \\ x_2 \\ x_3 \\ x_4 \\ x_5 \\ x_6 \end{Bmatrix} + \begin{Bmatrix} 0 \\ 0 \\ -1 \\ 0 \\ 0 \\ 0 \end{Bmatrix} w + \begin{Bmatrix} 0 \\ -\frac{1}{A_p} \\ 0 \\ 0 \\ 0 \\ 0 \end{Bmatrix} Q_{in} \quad (4-41)$$

In all the models derived so far, the control input, which is the oil flow rate, is taken as unconstrained. As explained in reference [53], input saturation can also be inserted in the formulation and the controller design. By SDRE control input saturation can be easily modeled by defining the new state as,

$$x_8 = Q_{in} \quad (4-42)$$

State equation for the new state is,

$$\dot{x}_8 = u_1 \quad (4-43)$$

where u_1 is the new control input. Thus second state equation can be rewritten as,

$$\dot{x}_2 = x_1 - x_4 - \frac{\text{sat}(x_8)}{x_8 A_p} x_8 \quad (4-44)$$

where sat is the saturation function and can be defined as given in reference [53],

$$\text{sat}(Q_{in}) = \begin{cases} Q_{\max} & \text{if } \frac{Q_{in}}{Q_{\max}} \frac{\pi}{2} > \frac{\pi}{2} \\ Q_{\max} \sin\left(\frac{Q_{in}}{Q_{\max}} \frac{\pi}{2}\right) & \text{if } -\frac{\pi}{2} < \left(\frac{Q_{in}}{Q_{\max}} \frac{\pi}{2}\right) < \frac{\pi}{2} \\ -Q_{\max} & \text{if } \frac{Q_{in}}{Q_{\max}} \frac{\pi}{2} < -\frac{\pi}{2} \end{cases} \quad (4-45)$$

In Equation (4-44), since as x goes to zero, the limit goes to zero, the state equation is well behaved around the operating point. As explained also in reference [53], the input constraint and the derivative of input constraint can be implemented in the

SDRE formulation without much difficulty. Another saturation function which can be used in controller design is shown in Figure 4.4.

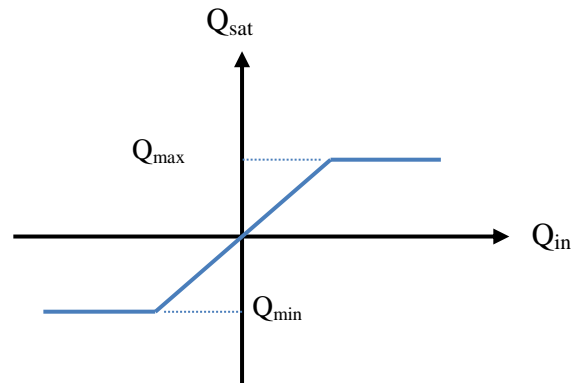


Figure 4.4: Saturation Function-Saturation of the Oil Flow Rate

4.2.3. Controller Design for Active HP Suspension System

After the linear state space models with state dependent coefficients are obtained for an active HP suspension system with different complexity levels, the SDRE control method is used to design the active controller. The aim of the active HP suspension system is to,

- ❖ improve the ride comfort by decreasing the vertical acceleration of the sprung mass,
- ❖ improve the road holding by decreasing the tire deflection,
- ❖ control the suspension packaging by decreasing the suspension deflection,
- ❖ adjust the vehicle attitude by driving the suspension deflection to zero, or by driving the suspension deflection to user specified suspension height value.

In most studies found in the literature, the first two performance requirements are studied. However, there is a conflict between the third and the first two performance criteria. As will be shown in the following section, when the active controller is designed only for ride comfort and road holding, suspension deflection performance is degraded at low frequencies. At steady state, suspension deflection stays at

nonzero values for certain types of road displacement inputs. In other words, there is a steady state error which is not desired in practice. To be able to overcome this problem, integral state of the suspension deflection is added in the controller design. The use of the integral state is also necessary to drive the suspension height to user specified reference values. In the following sections, two active controllers for the active HP suspension system are designed, with and without the integral state.

4.2.3.1. Active Controller without the Integral State

For this controller, the aim is to improve ride comfort, road holding, and control the suspension travel. The performance index to be minimized is given as

$$J(x) = \frac{1}{2} \int \{q_1 \ddot{z}_p^2 + q_2 \dot{z}_{pt}^2 + q_3 z_{t0}^2 + R Q_{in}^2\} dt \quad (4-46)$$

where q_i 's are the weighting parameters for the suspension performance variables, and R is the weighting parameter for the control input. The performance output is,

$$z_{per} = C_{per}(x)x \quad (4-47)$$

where z_{per} is the performance variables, $C_{per}(x)$ is the performance matrix given by,

$$C_{per}(x) = \begin{bmatrix} -\frac{f_2}{M} \sqrt{q_1} & \frac{f_1}{M} \sqrt{q_1} & 0 & \frac{f_2}{M} \sqrt{q_1} & 0 \\ 0 & 0 & 0 & 0 & \sqrt{q_2} \\ 0 & 0 & \sqrt{q_3} & 0 & 0 \end{bmatrix} \quad (4-48)$$

In order to examine the stability of the designed controller, Theorem 1 is used. Controllability and observability matrices are formed with symbolic parameters and variables. According to the Theorem 1, since the rank of the controllability and the observability matrices are five, the active HP suspension system is locally asymptotically stable.

4.2.3.2. Active Controller with the Integral State

In addition to the performance variables given in Equation (4-46), additional performance variables, integral of the suspension deflection and the suspension

deflection velocity, are added to the formulation. The aim of the integral controller is to improve the suspension deflection performance at steady state. When the integral controller is not used in the active suspension control, some disturbances may create nonzero suspension deflection which degrades the vehicle performance. When the integral of the suspension deflection is incorporated into controller design, the performance index becomes,

$$J(x) = \frac{1}{2} \int \left\{ q_1 \ddot{z}_p^2 + q_2 z_{pt}^2 + q_3 z_{t0}^2 + q_4 \left(\int z_{pt} \right)^2 + q_5 \dot{z}_{pt}^2 + R Q_{in}^2 \right\} dt \quad (4-49)$$

For this design, the performance output matrix is:

$$C_{per}(x) = \begin{bmatrix} -\frac{f_2}{M} \sqrt{q_1} & \frac{f_1}{M} \sqrt{q_1} & 0 & \frac{f_2}{M} \sqrt{q_1} & 0 & 0 \\ 0 & 0 & 0 & 0 & \sqrt{q_2} & 0 \\ 0 & 0 & \sqrt{q_3} & 0 & 0 & 0 \\ 0 & 0 & 0 & 0 & 0 & \sqrt{q_4} \\ \sqrt{q_5} & 0 & 0 & -\sqrt{q_5} & 0 & 0 \end{bmatrix} \quad (4-50)$$

To be able to set the suspension height to user defined suspension height value, r , the states x_5 and x_6 in Equation (4-23) and (4-38) can be redefined as,

$$x_5 = z_p - z_t - r \quad (4-51)$$

$$x_6 = \int (z_p - z_t - r) \quad (4-52)$$

Assuming that r is a nearly constant or slowly varying variable, the same state equations derived previously are used. For this case, the cost function to be minimized can be written as,

$$J(x) = \frac{1}{2} \int \left\{ q_1 \ddot{z}_p^2 + q_2 (z_{pt} - r)^2 + q_3 z_{t0}^2 + q_4 \left(\int (z_{pt} - r) \right)^2 + q_5 \dot{z}_{pt}^2 + R Q_{in}^2 \right\} dt \quad (4-53)$$

According to the Theorem 1, since the rank of the controllability and the observability matrices are both six, the active HP suspension is locally asymptotically stable.

4.2.3.3. Active Controller with the Adaptive Integral Controller

Even though, the active suspension is used to improve ride comfort and the vehicle attitude performance, there is a compromise for the ride comfort and vehicle attitude improvement. As will be shown in the following sections, when the active controller is used mainly for the ride comfort, the vehicle attitude performance requirement is not satisfied. Similarly, when the active controller is designed mainly for the vehicle attitude control, the ride comfort performance requirement is not satisfied. Therefore, a controller with a compromise performance for ride comfort and the vehicle attitude is obtained. One approach to simultaneous control of both targets is the use of an adaptive controller. Under normal road conditions, the active controller works mainly for the ride comfort performance. When the vehicle suspension height approaches some critical value, or when the suspension height comes to a set value and exceeds that value towards an upper threshold, the controller works mainly for the vehicle attitude control.

In the SDRE control, since the controller is renewed with the changing states, the weighting parameters can also be modified when the states change. In studies [62]-[63], SDRE control with state constraints are studied. State constraints can be used in the controller design in order to limit the value of the state to a specified value. When the state approaches the limiting value, weighting of the state increases, and thus the controller works to decrease that state mainly. Moreover, state constraints can be used to model the physical hard or bump stops and thus the nonlinear characteristics of the bump or hard stop can be incorporated in the controller design. Since the controllability and the observability matrices for the given domain of the adaptive weighting parameter are both six, active controller with the adaptive integral controller is locally asymptotically stable similar to the active controller with fixed integral controller.

4.2.4. Simulations

In this section, the performances of the designed controllers are to be examined by the time and frequency domain simulations. To get the frequency response functions, sinusoidal inputs at with different amplitudes and frequencies representing road

inputs are applied to the system model. At each frequency, the frequency response is obtained as the ratio of the rms of the performance variable to the rms of the road velocity input. For time domain simulations, random road inputs at different longitudinal velocities, ramp road displacement input, and body disturbance input in the form of a vertical body force, are used. The random road displacement input is used to examine ride comfort performance, and the ramp road displacement input and vertical body force input are used to examine the vehicle attitude performance. Finally, the reference suspension deflection input is used to examine the vehicle attitude performance in terms of suspension height adjustment.

4.2.4.1. Simulations with Active Controller without Integral Controller

Inputs with the same amplitude and frequency characteristics used in Chapter 3, are again used here to examine the performance of the active HP suspension system with respect to the passive counterpart in the frequency domain. Simulation results are shown in Figure 4.5 to Figure 4.7.

From the simulation results it is observed that the active controller considerably attenuates the sprung mass vertical acceleration and tire deflection around body bounce frequency. However, the active controller degrades the tire deflection response in the frequency range between body bounce to wheel hop frequency. For the suspension deflection, the active suspension has lower response around body bounce frequency. At lower frequencies, passive suspension has better performance and active suspension cannot improve suspension deflection performance. Therefore, in general active suspension improves performance variables particularly around the body bounce frequency. The required oil flow rate in the simulation is given in Figure 4.8.

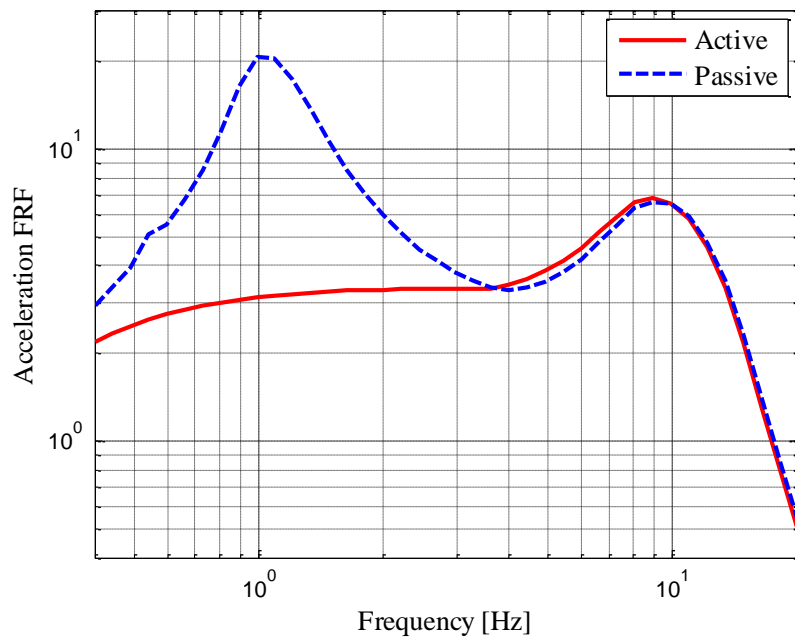


Figure 4.5: Acceleration FRF

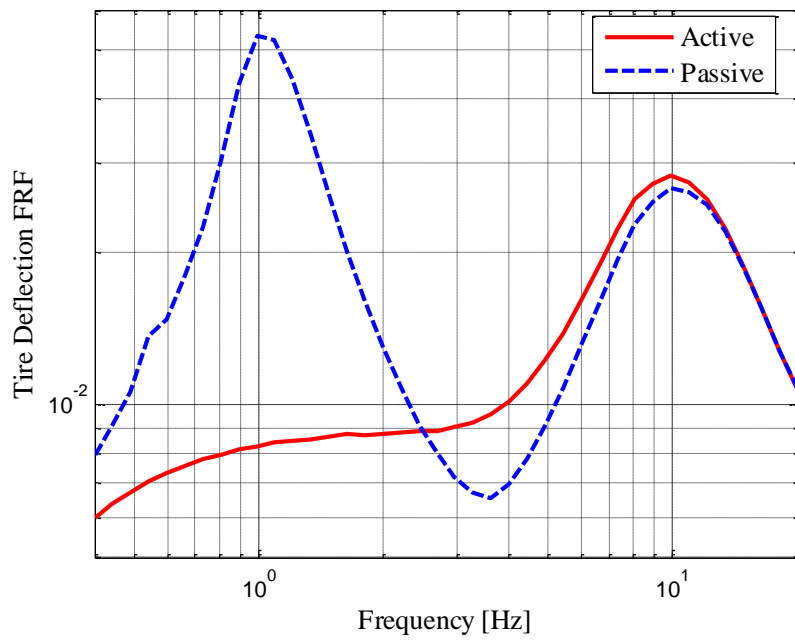


Figure 4.6: Tire Deflection FRF

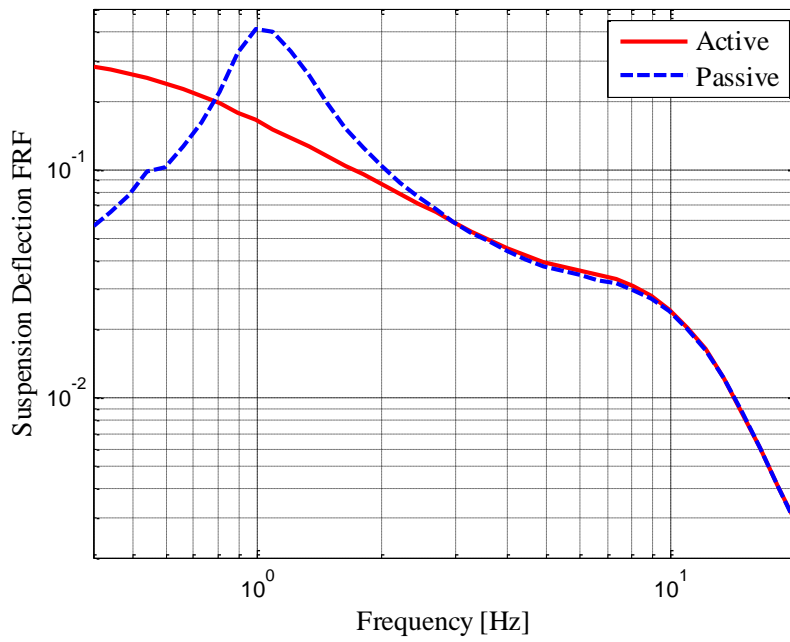


Figure 4.7: Suspension Deflection FRF

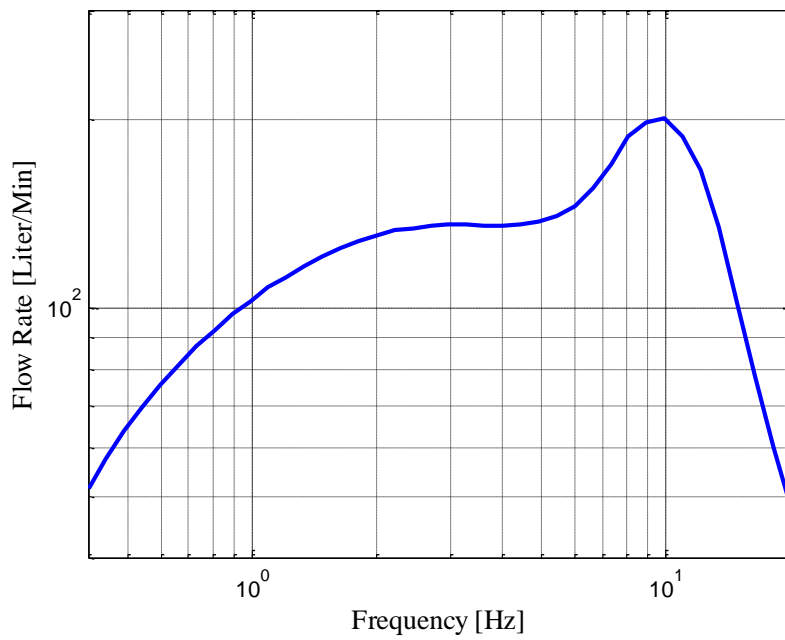


Figure 4.8: rms Value of the Oil Flow Rate

For the simulations with random road input at different longitudinal velocities, asphalt concrete on granular base random road inputs adopted from the study of Kılıç

[64] are used in this study. Power spectral densities of the random road displacement inputs are shown in Figure 4.9. Time history of the random road input at 50 kph longitudinal velocity is shown in Figure 4.10 and the simulation results for this input are shown in Figure 4.11 to Figure 4.14.

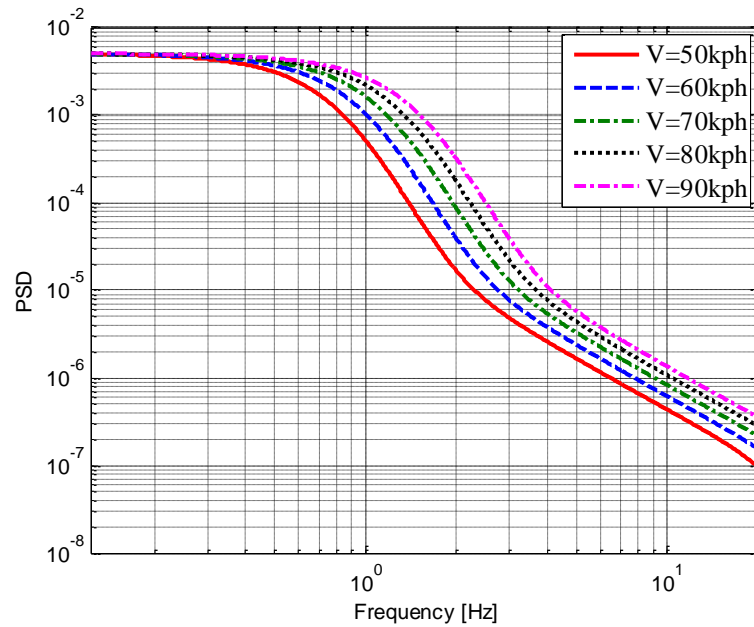


Figure 4.9: Power Spectral Densities of Random Road Displacement Input At Different Velocities

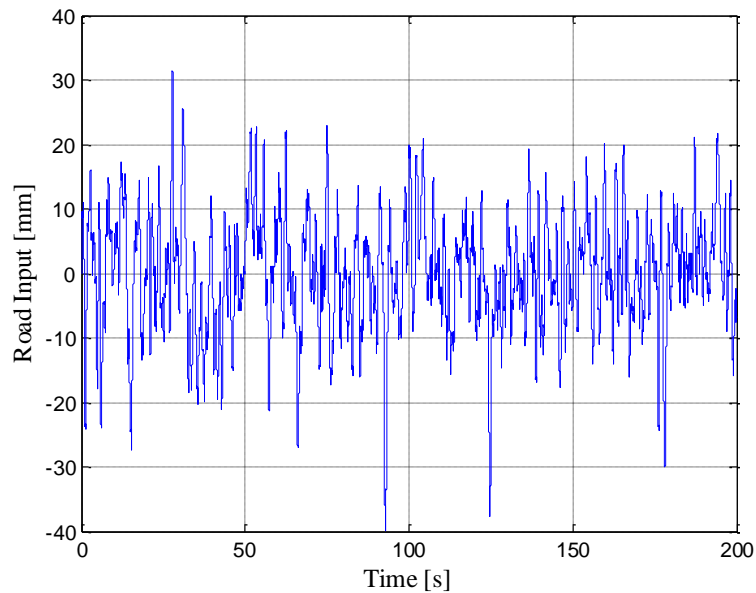


Figure 4.10: Random Road Input at 50 kph

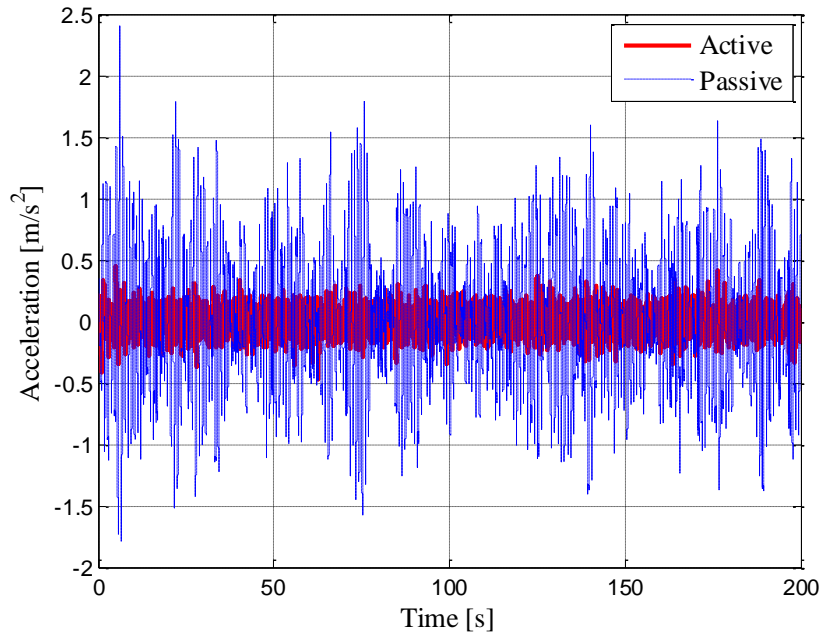


Figure 4.11: Acceleration Response

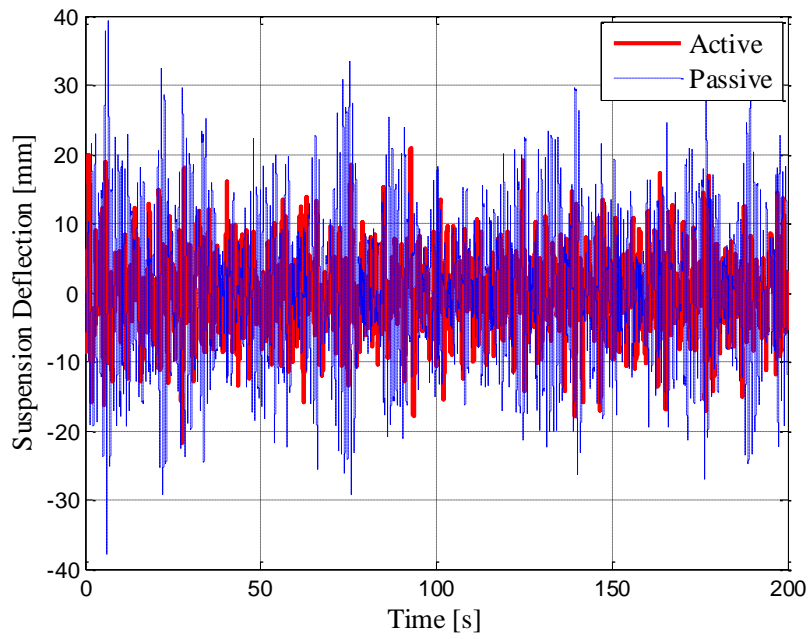


Figure 4.12: Suspension Deflection Response

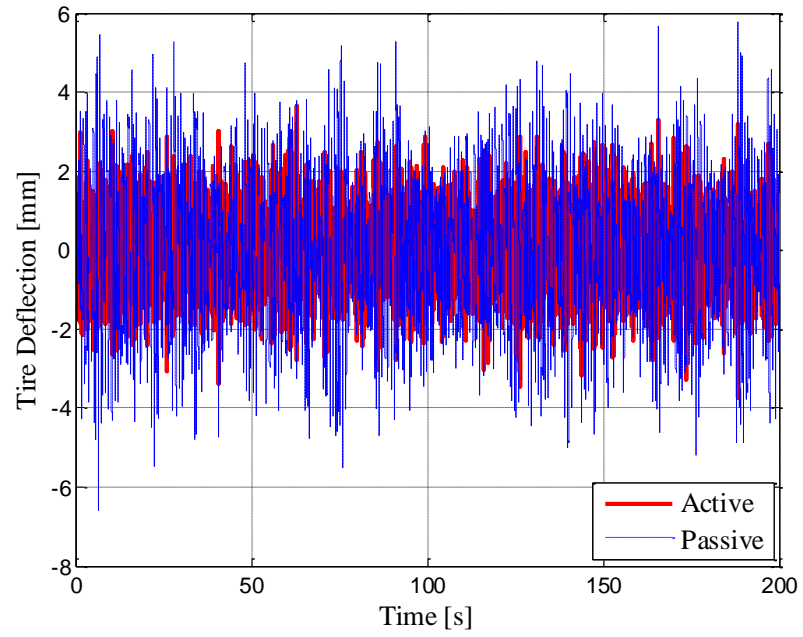


Figure 4.13: Tire Deflection Response

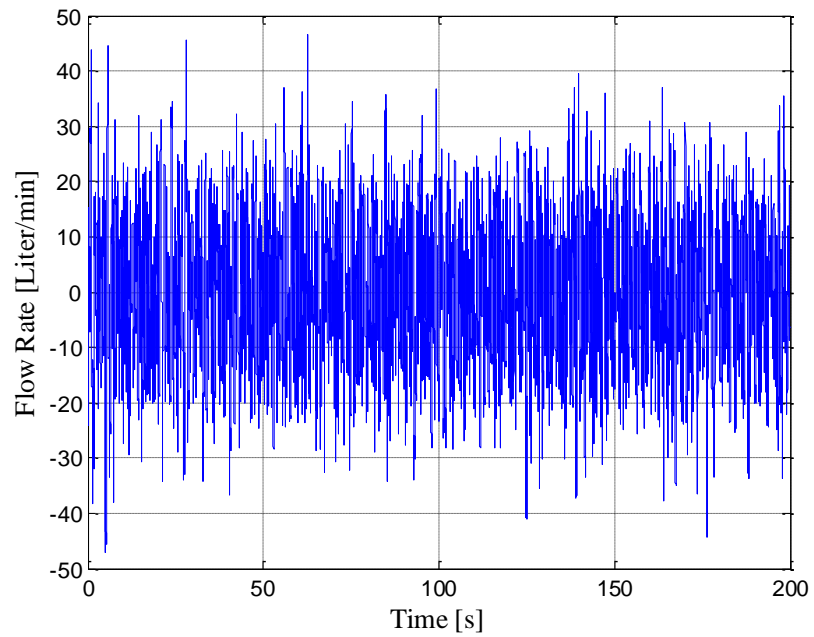


Figure 4.14: Oil Flow Rate

Comparisons of the active and the passive suspension are also made at various other longitudinal velocities. Table 4.1 shows the rms of the performance variables for the active and passive suspensions.

Table 4.1: rms Values of Performance Variables with the Active and Passive HP Suspensions

Long. Velocity [kph]	Acc.[m/s ²]		Tire Def.[mm]		Sus. Def.[mm]		Flow Rate [L/Min]	
	Act.	Pas.	Act.	Pas.	Act.	Pas.	Act.	Pas.
50	0.10	0.56	0.8	1.7	5.9	10.7	12.4	-
60	0.13	0.73	1.0	2.1	7.5	14.0	16.3	-
70	0.15	1.04	1.2	2.8	7.8	19.8	19.4	-
80	0.18	1.05	1.4	2.9	8.8	20.0	23.0	-
90	0.22	1.27	1.5	3.4	10.0	24.1	27.3	-

As Table 4.1 shows, the rms values of the active suspension are considerably lower than the rms values of the passive suspension. These performance improvements can be satisfied by reasonable amounts of oil flow rate. Moreover, as the longitudinal velocity increases, the amount of oil flow rate also increases.

4.2.4.2. Simulations of the Active System with the Integral Controller

After, the performance of the active system without the integral controller is examined in the previous section; the same steps have been followed to examine the performance of the active system with the integral controller. As can be seen from the simulation results, the active system without the integral controller, improves the ride comfort, road holding, and suspension packaging for the normal driving conditions on random road. However, for other road and body disturbance inputs, the active system without the integral controller cannot drive the suspension deflection to zero. Therefore, vehicle height changes with different road inputs. This may deteriorate vehicle handling, and cause unsafe vehicle driving. In previous studies, most active suspension systems do not include the integral controller. Moreover, for the active HP suspension system, in only one study [7], the vehicle attitude controller is added to the active system. In that study, separately designed vehicle attitude and the active controller are added to form a combined controller. At low frequencies, the vehicle attitude controller tries to improve suspension deflection performance, and at higher frequencies active controller works to improve ride comfort performance. In

this study, the active controller and the vehicle attitude controller are designed to control vehicle ride comfort and vehicle attitude simultaneously. Thus stability of the combined controller is guaranteed. By changing the weighting parameter in the performance index, relative performance of the vehicle attitude controller and the ride comfort controller can be adjusted.

There are six weighting coefficients used in the controller design. Three of these coefficients, q_2 , q_4 , and q_5 are directly associated with vehicle attitude control. When the values of these coefficients are increased the vehicle attitude performance is improved, however ride comfort performance is degraded. A sensitivity study is performed to obtain a sound understanding of the effects of these coefficients on ride comfort, attitude control, and the control input. The performance of the controller is evaluated by simulations in the frequency and the time domain. The effect of the vehicle attitude controller on ride comfort controller is also examined. The simulation results, for the effect of the controller weighting parameters q_2 , q_4 , and q_5 on the frequency response characteristics of the sprung mass acceleration, suspension deflection, and the tire deflections are given in Figure 4.15 to Figure 4.26.

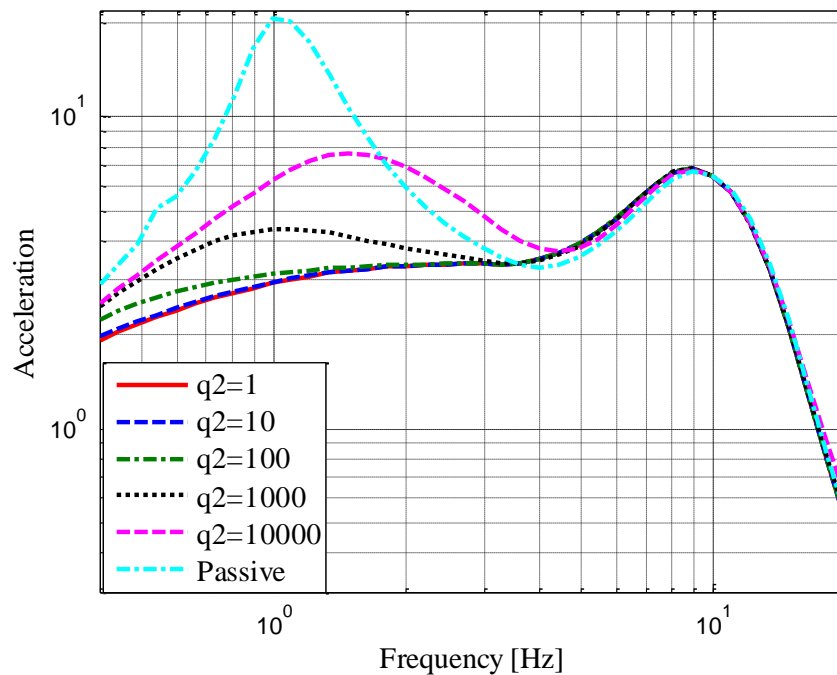


Figure 4.15: Acceleration FRF

Figure 4.15 shows that the best acceleration response is obtained for low values of q_2 . For these values the peak around the body bounce frequency tends to level off completely.

As Figure 4.16 illustrates, when the weighting of the suspension deflection is increased, suspension deflection response is lower and approach the passive suspension response at lower frequencies and thus steady state performance also increases. However, increasing q_2 causes deterioration in the ride comfort. This illustrates the compromise solution of the active controller for the ride comfort and suspension packaging performance. For tire deflection, it can be observed from Figure 4.17 that, increasing q_2 increases response amplitude around body bounce frequency, and decreases response amplitude after 3 Hz.

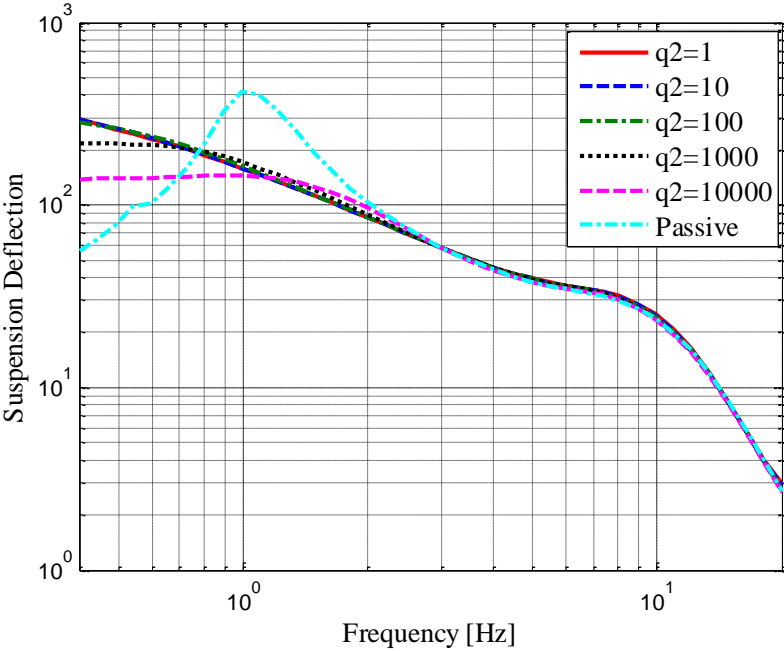


Figure 4.16: Suspension Deflection FRF

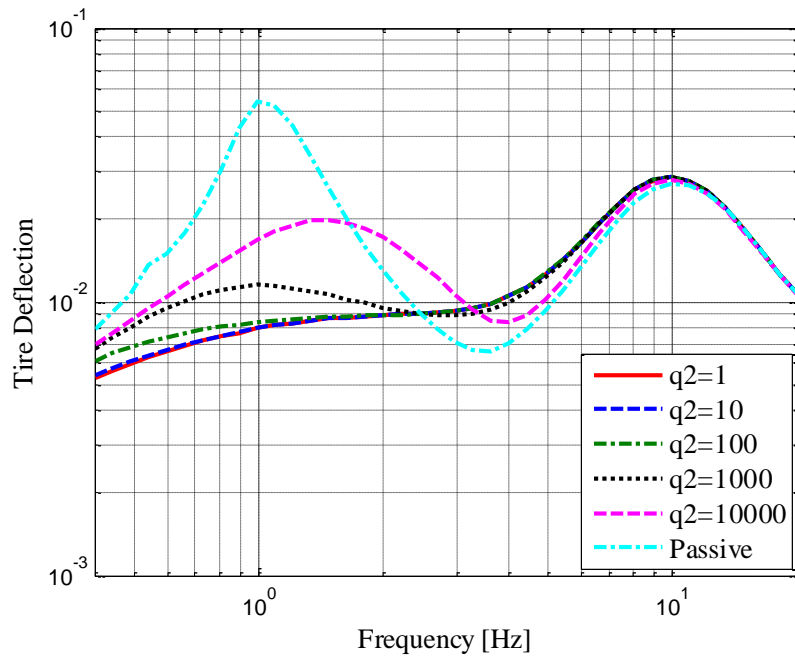


Figure 4.17: Tire Deflection FRF

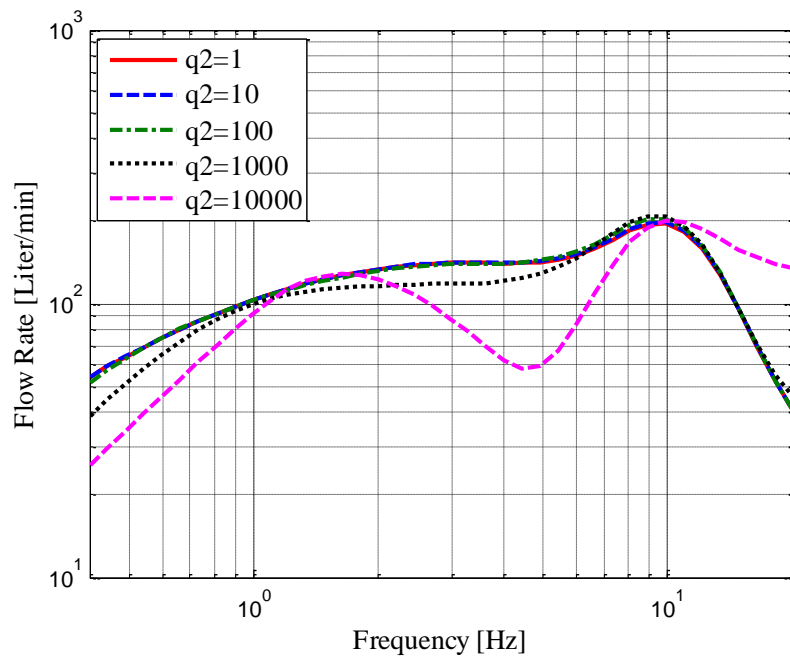


Figure 4.18: rms of the Oil Flow Rate

Figure 4.18 indicates that the required oil flow rate is reduced by increasing values of effect of q_2 , particularly at very high values. However, in this case, there is considerable need for larger flow rate at frequencies above the wheel hop frequency.

Weighting coefficient of the integral of suspension deflection, q_4 , has similar effects on the response variables as weighting coefficient q_2 , as shown in Figure 4.19 to Figure 4.22. When q_4 is increased, acceleration and tire deflection responses are raised around the body bounce frequency and the suspension deflection is reduced at frequencies lower than the body bounce frequency.

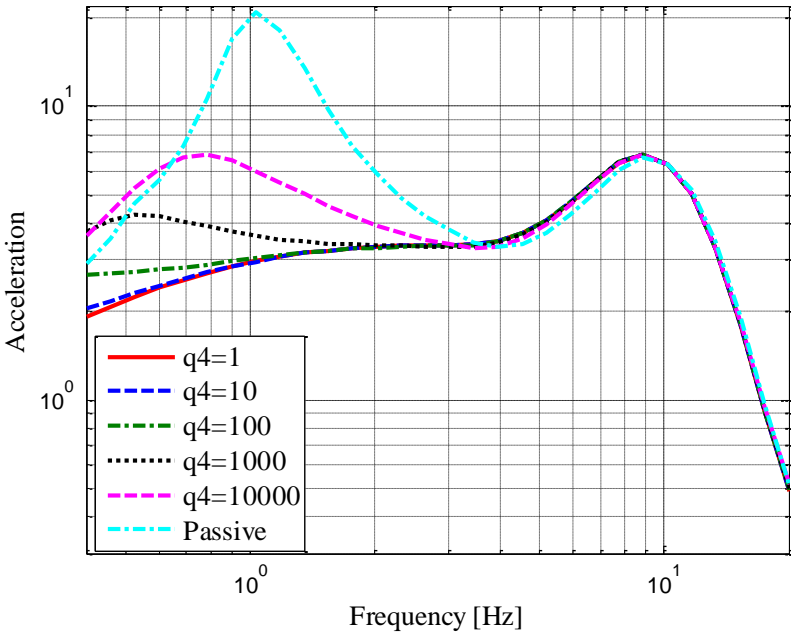


Figure 4.19: Acceleration FRF

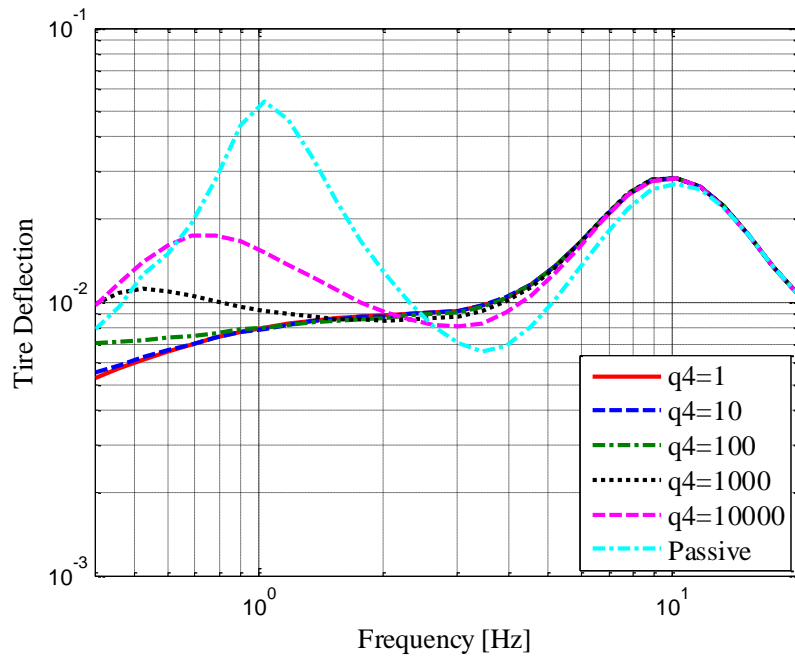


Figure 4.20: Tire Deflection FRF

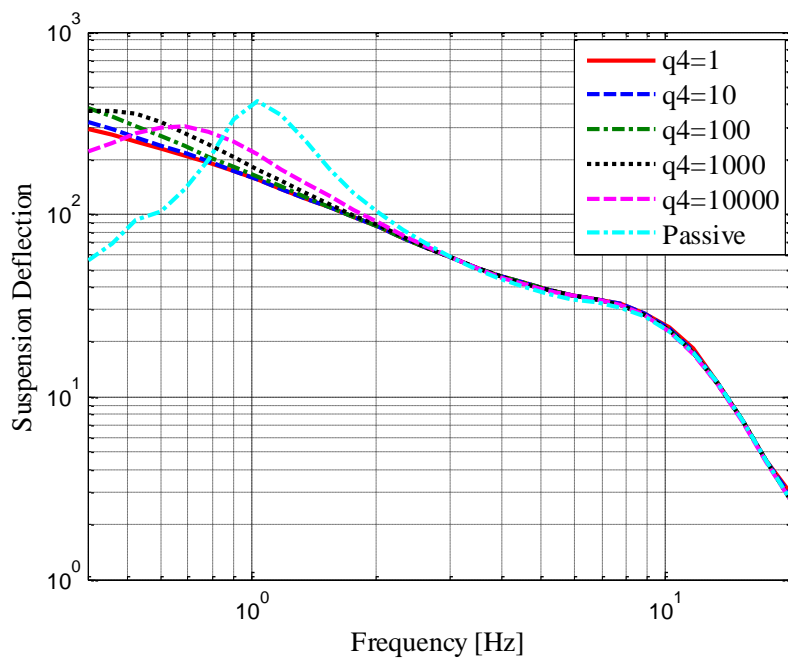


Figure 4.21: Suspension Deflection FRF

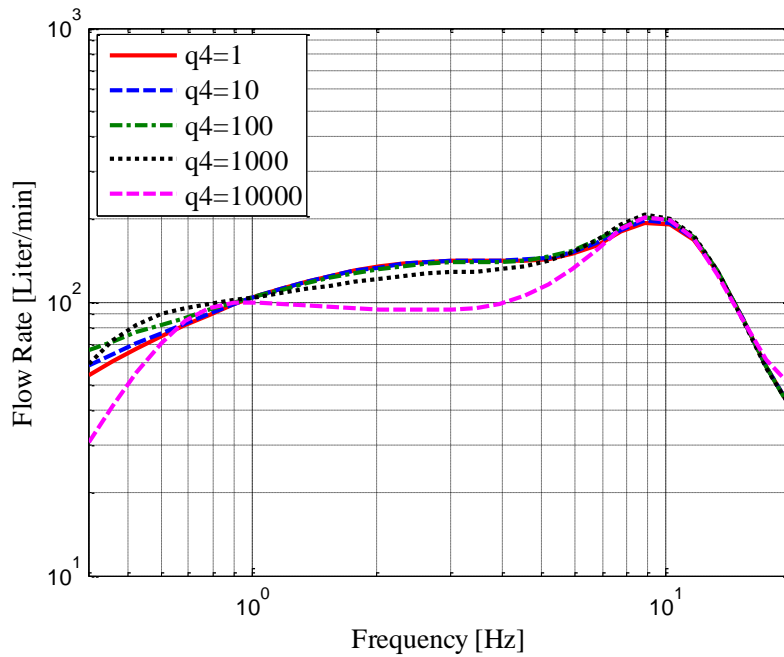


Figure 4.22: rms of the Oil Flow Rate

As Figure 4.18 and Figure 4.22 show, required oil flow rate is reduced as the values of the weighting coefficients q_2 and q_4 are increased. However, the high oil flow rate requirement above the wheel hop frequency in Figure 4.18, is not observed in Figure 4.22.

Effects of the weighting of the suspension deflection velocity, q_5 , on the response characteristics are somewhat different than the previous results as shown in Figure 4.23 to Figure 4.26. When q_5 is increased, acceleration also increases at mid frequencies and at frequencies higher than wheel hop frequency, and therefore ride comfort is worsened. However, tire deflection decreases around wheel hop frequency with increasing weighting coefficient q_5 . Moreover effects of the weighting coefficient q_5 on the response variables are more dominant than the effects of the response variables q_2 and q_4 . Oil flow rate requirement also increases considerably with increasing q_5 . Therefore in the controller design, the value of the weighting coefficient q_5 should be limited to maintain the level of ride comfort as well as to prevent excessive control effort.

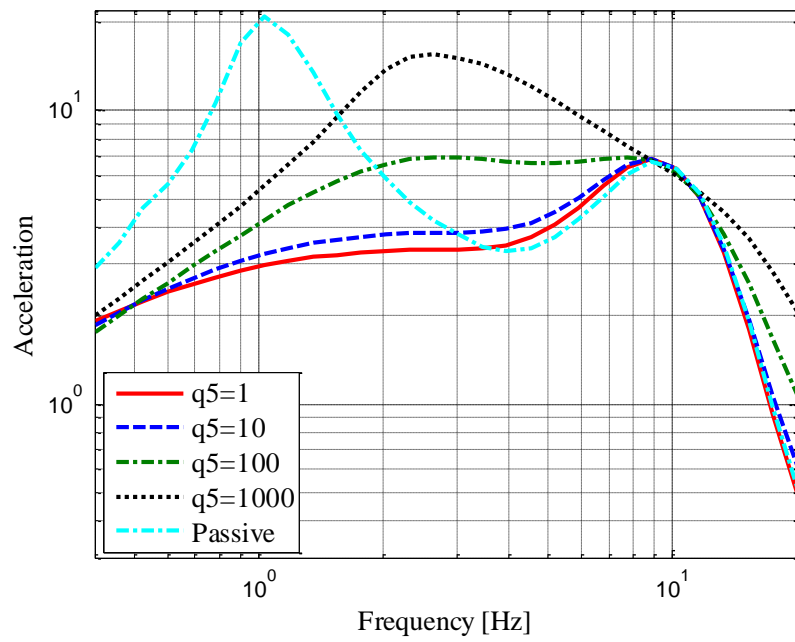


Figure 4.23: Acceleration FRF

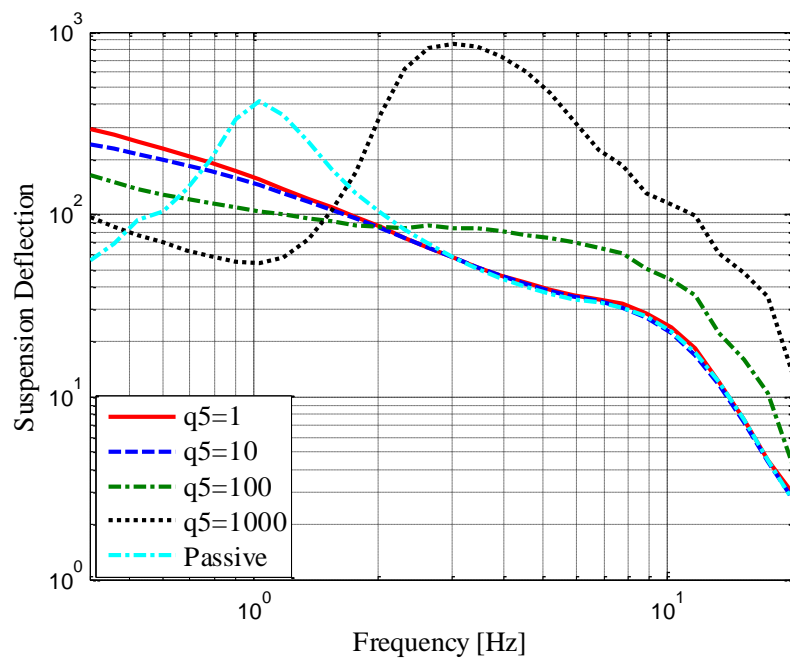


Figure 4.24: Suspension Deflection FRF

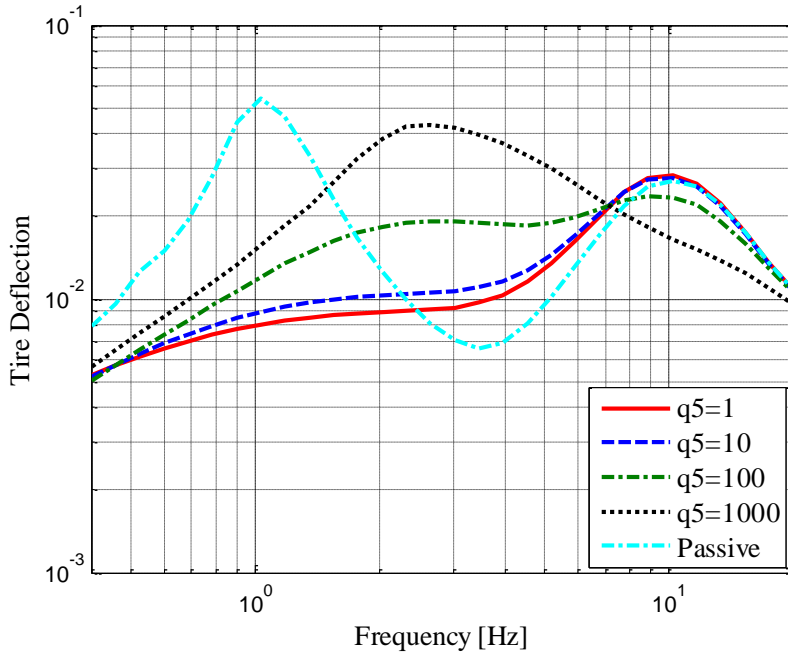


Figure 4.25: Tire Deflection FRF

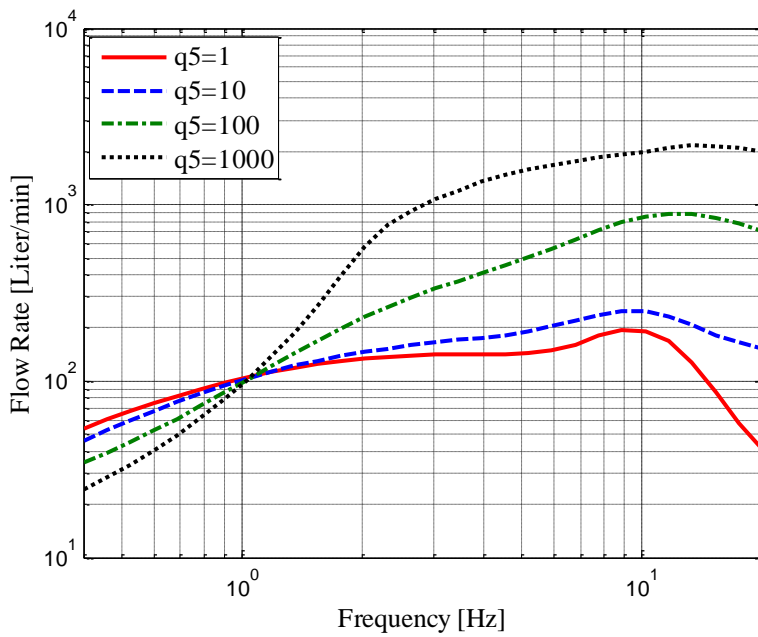


Figure 4.26: RMS of the Oil Flow Rate

After the performance of the active HP suspension system is examined in frequency domain, its performance will be examined in the time domain. Effect of the

weighting parameters on the rms values of the sprung mass acceleration, suspension deflection, and tire deflection are given in Figure 4.27 to Figure 4.30.

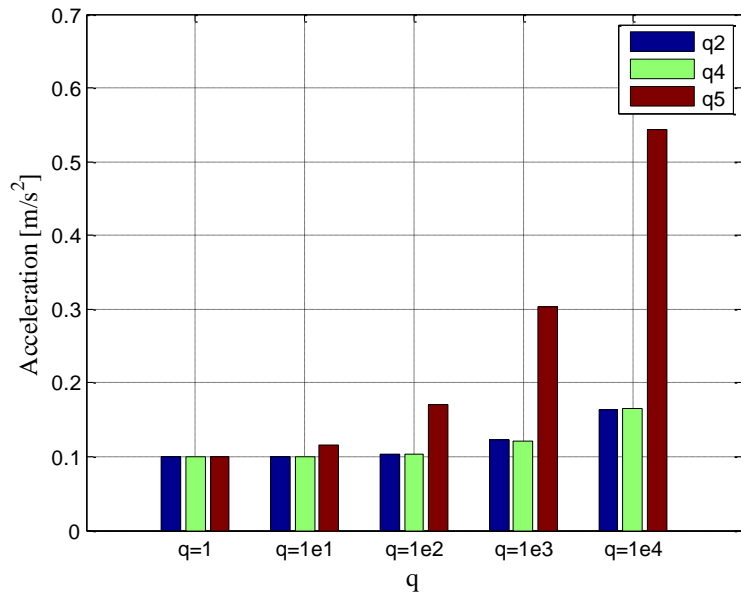


Figure 4.27: rms of the Acceleration

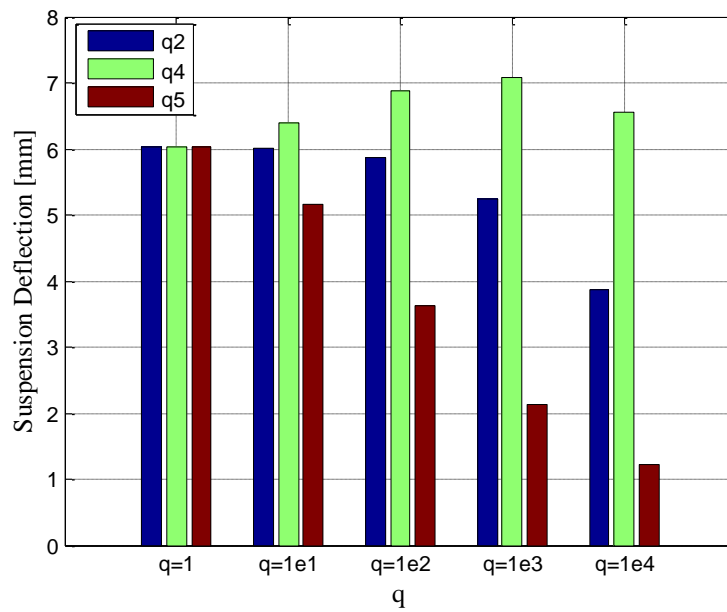


Figure 4.28: rms of the Suspension Deflection

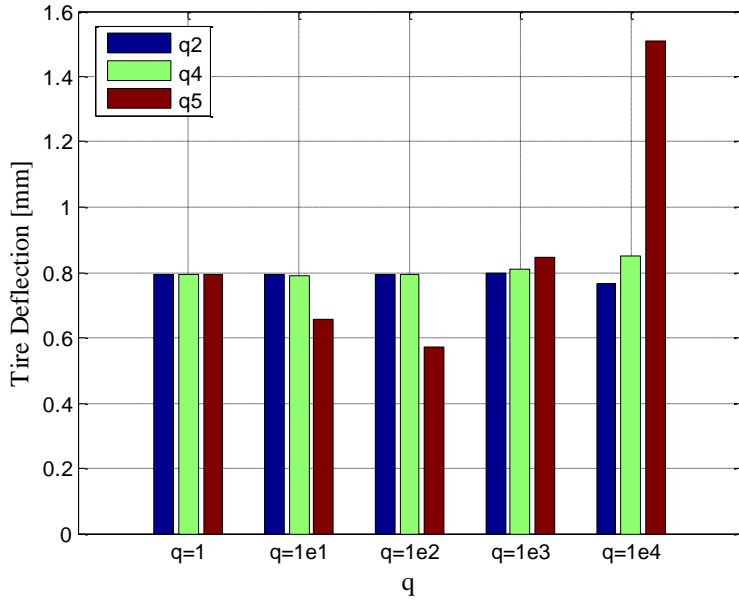


Figure 4.29: rms of the Tire Deflection

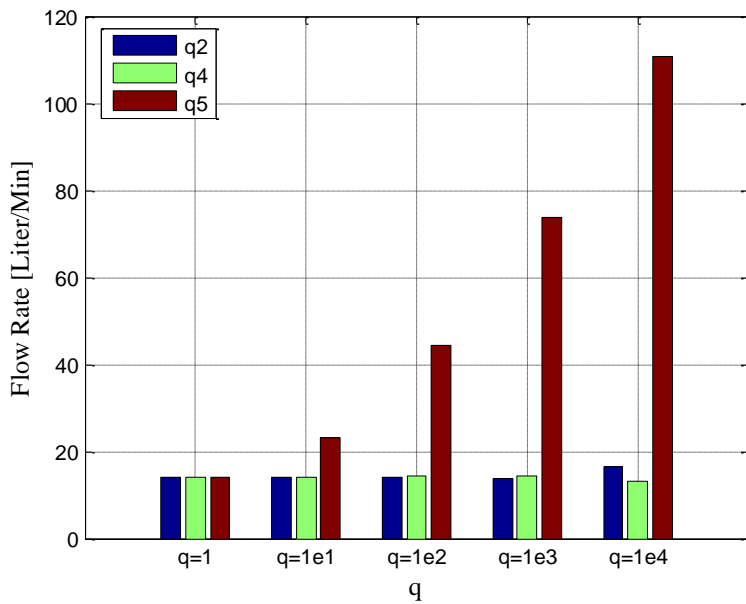


Figure 4.30: rms of the Flow Rate

As simulation result show, the effects of the weighting coefficient q_5 results on the rms value of the sprung mass acceleration and oil flow rate are very strong. To obtain a reasonable performance for ride comfort and the control input, weighting coefficient q_5 should be kept low for practical applications. On the other hand the

effects of the weighting coefficients q_2 and q_4 on the ride comfort performance are not as significant when compared with those of q_5 . Increasing the values of the weighting coefficients q_2 and q_4 decreases the ride comfort performance in almost the same level. However, an increase in the weighting coefficient q_4 does not have any influence on the oil flow rate, yet an increase in the weighting coefficient q_2 increases the required oil flow rate.

After the performance of the active controller has been investigated, now the attitude control performance of the active HP suspension system is examined. Active HP suspension system is simulated by the 7% ramp road starting at 2nd second. The effects of the controller parameters on the vehicle attitude performance are given in Figure 4.31 to Figure 4.35.

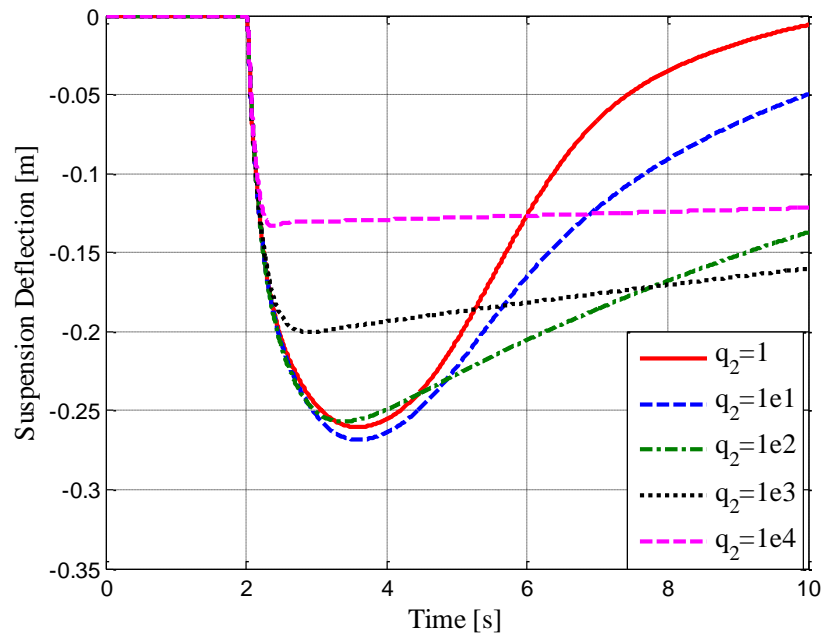


Figure 4.31: Suspension Deflection

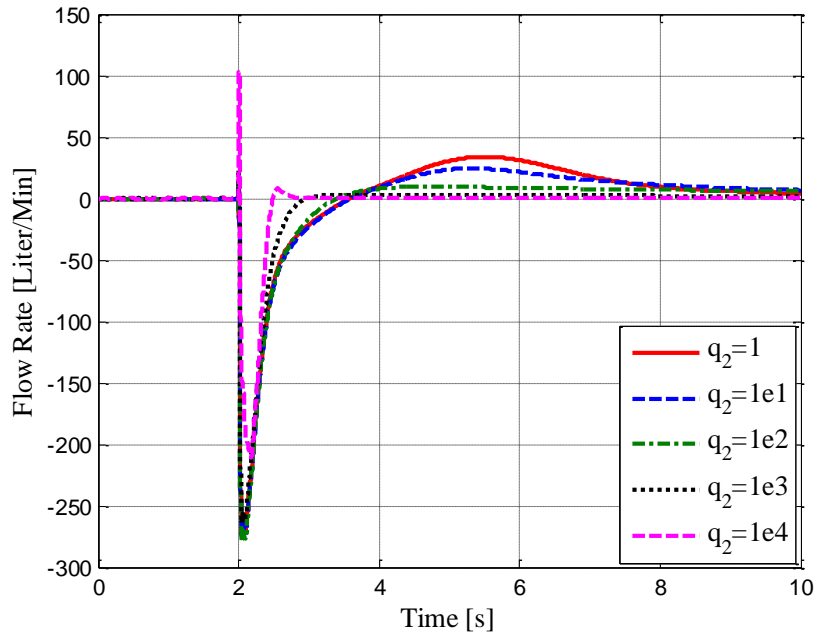


Figure 4.32: Oil Flow Rate

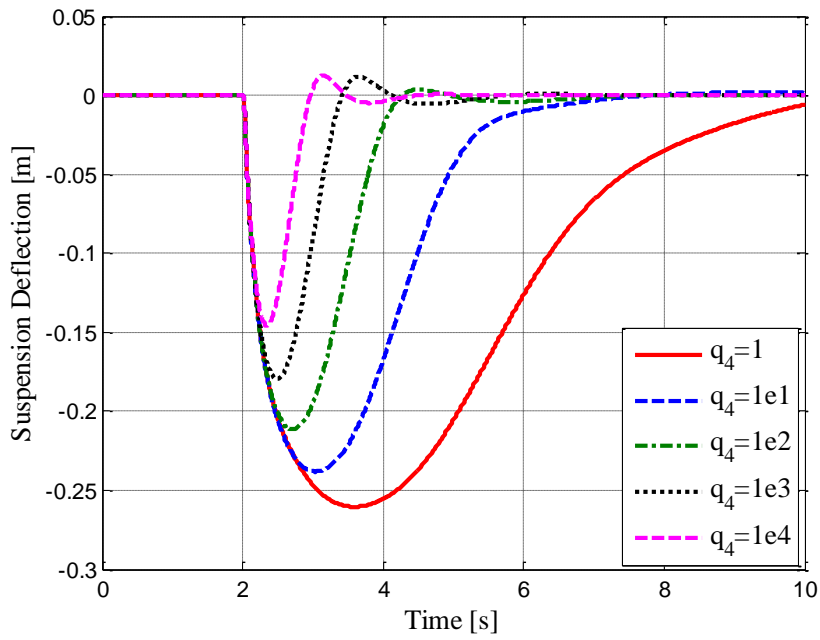


Figure 4.33: Suspension Deflection

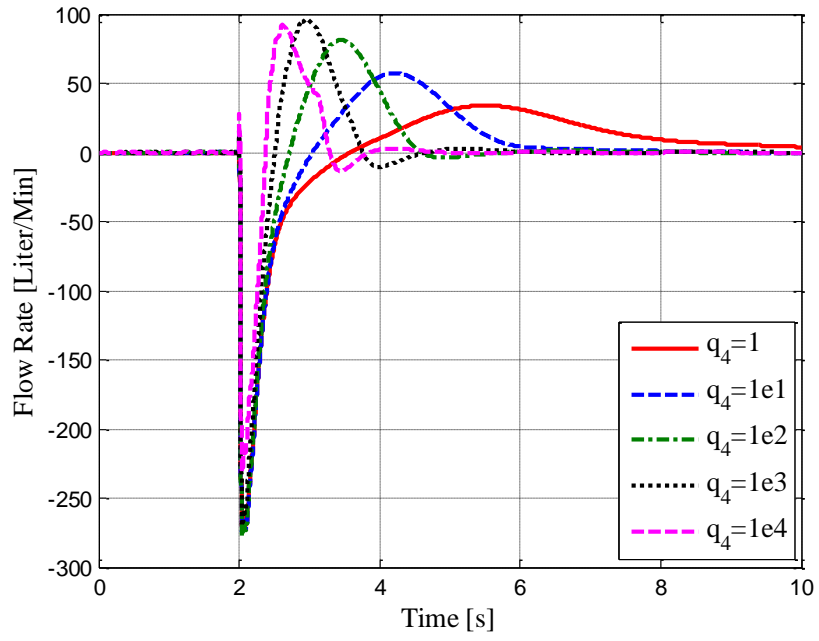


Figure 4.34: Oil Flow Rate

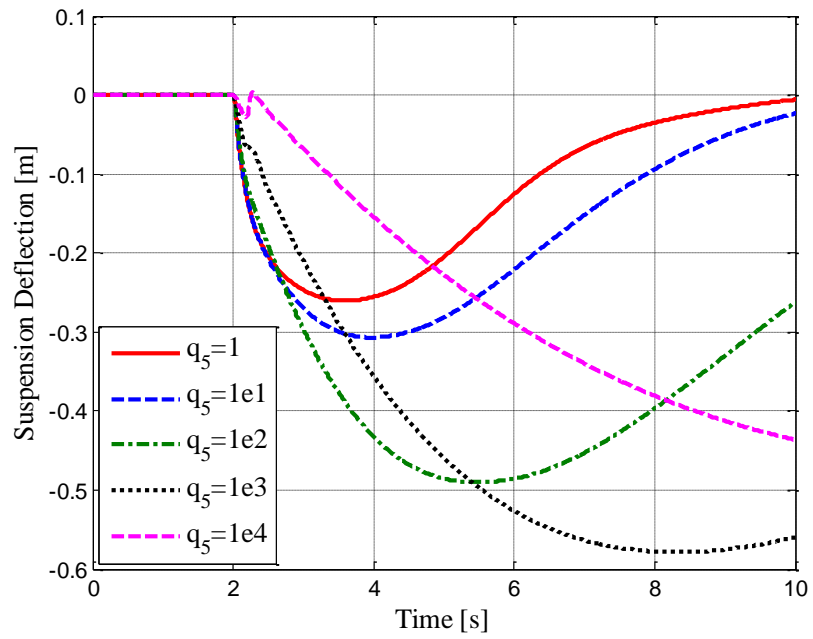


Figure 4.35: Suspension Deflection

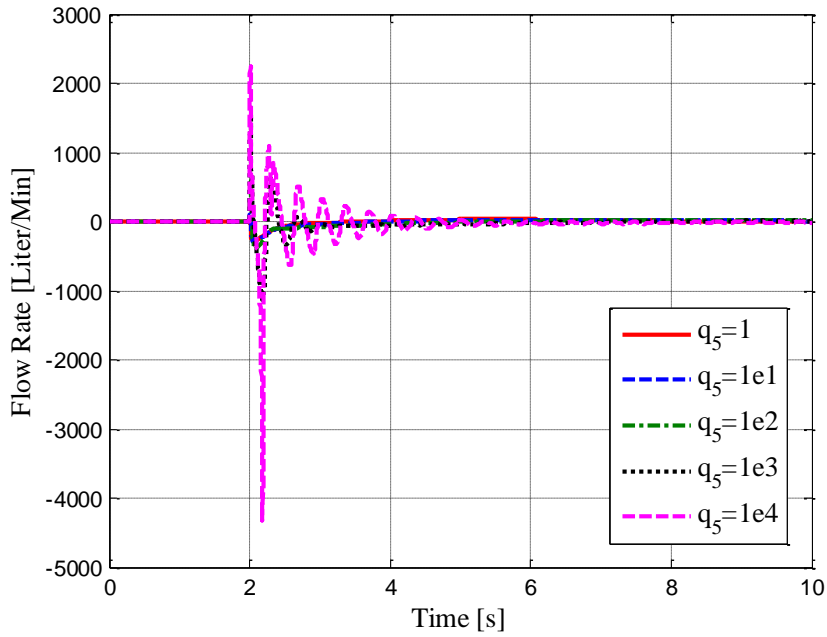


Figure 4.36: Oil Flow Rate

As can be seen from the simulation results, the weighting coefficient q_5 has a very strong negative effect on the suspension deflection. The oil flow rate also increases substantially with the increasing values of q_5 which requires a control input which is not practical in real applications. When q_2 increases the maximum value of the suspension deflection decreases. However, increasing the performance index q_2 alone degrades the performance of the steady state response. The best performance for decreasing the maximum value of the suspension deflection can be obtained by increasing the weighting coefficient q_4 . Further, the best steady state performance is obtained by increasing the value of the integral weighting coefficient. While these performance criteria are improved, the amount of the maximum oil flow rate does not change. This shows that the real time application of the vehicle attitude controller is practical. Therefore, the best way to decrease the maximum value of the suspension deflection may be to employ a higher value of q_4 .

After the performance of the active controller with respect to attitude control for ramp road inputs has been examined, now its attitude control performance is examined for the sprung mass vertical force input. Similar to previous case, the

effects of the controller weighting parameters on the vehicle attitude control performance were examined by the simulation. Simulation results are given Figure 4.37 to Figure 4.42.

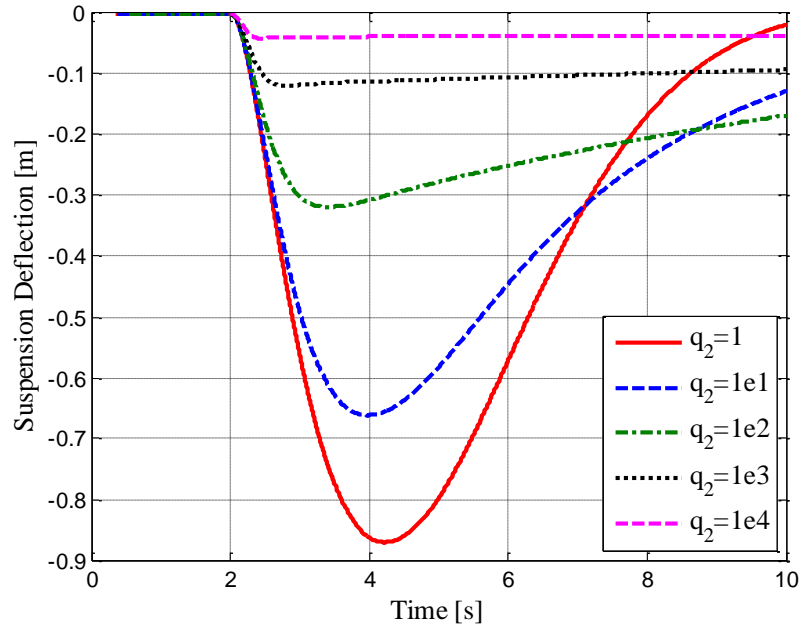


Figure 4.37: Suspension Deflection

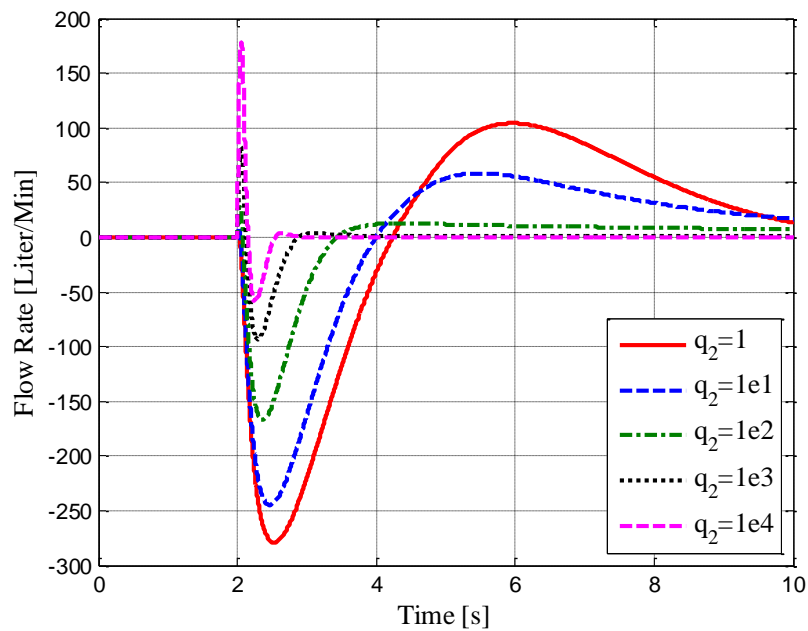


Figure 4.38: Oil Flow Rate

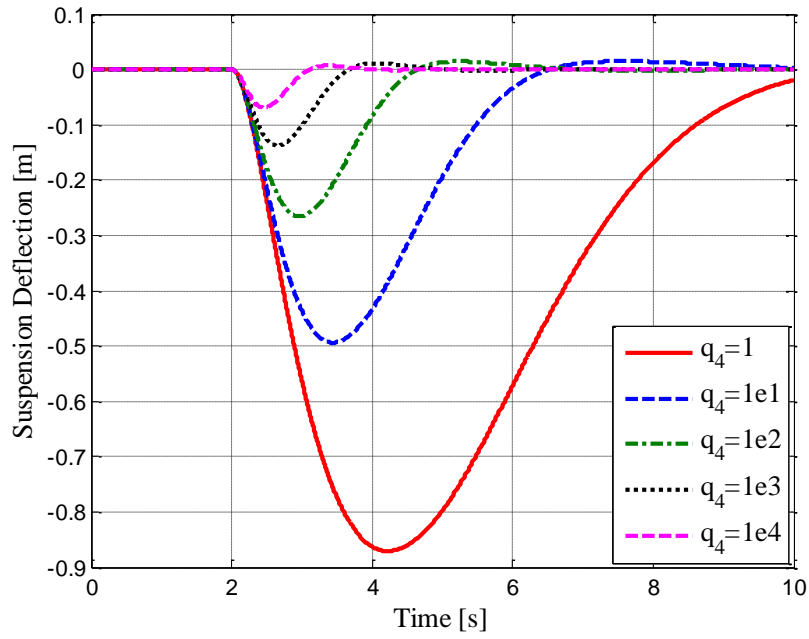


Figure 4.39: Suspension Deflection

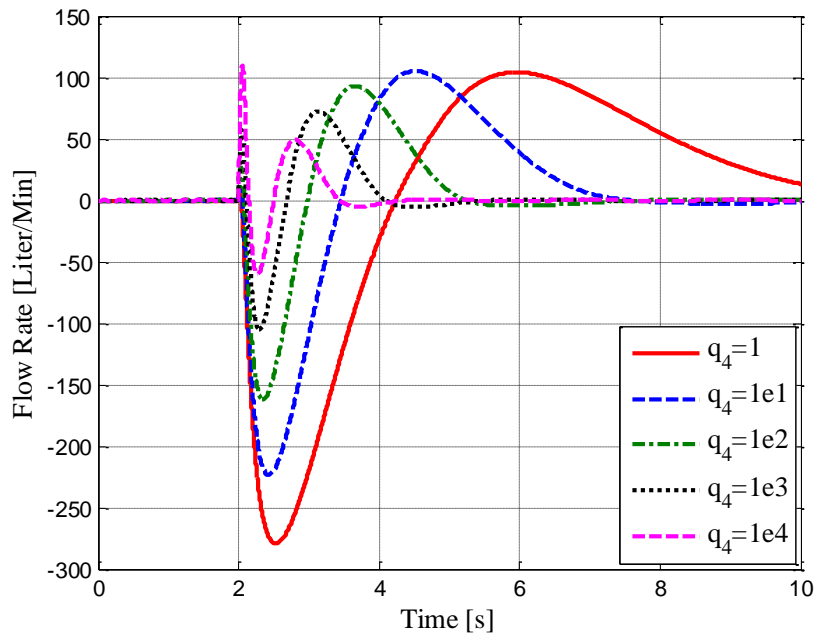


Figure 4.40: Oil Flow Rate

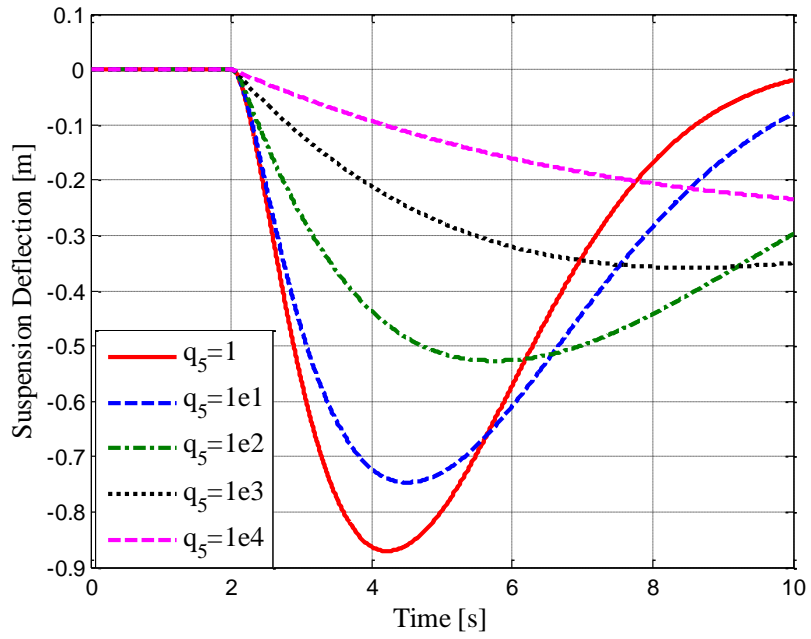


Figure 4.41: Suspension Deflection

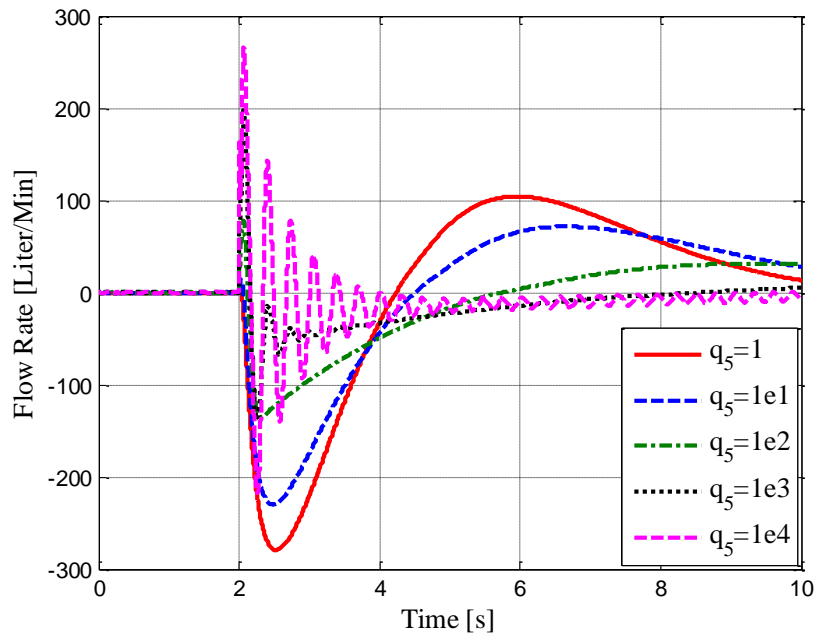


Figure 4.42: Oil Flow Rate

As can be seen from results, increasing the value of the weighing coefficient q_2 decreases the maximum value of the suspension deflection. Moreover, the oil flow

rate also decreases with it. However, when this weighting coefficient is increased, the steady state suspension deflection performance is degraded. This is due to the fact that when the weighting coefficient q_2 is increased while the weighting coefficient q_4 is kept constant, the weight of the integral controller is reduced in the control law. Figure 4.39 shows that when the weighting coefficient q_4 is increased, the maximum value of the suspension deflection is reduced. Moreover, for this performance improvement, the maximum value of the oil flow rate also decreases. Since the steady state performance is basically dictated by the integral controller and thus the weighting coefficient q_4 , increasing this coefficient increases the steady state performance substantially with respect to weighting coefficient q_2 . On the other hand when the weighting coefficient q_5 is increased, the maximum value of the suspension deflection decreases. However, the steady state performance of the suspension deflection again is degraded, since when the weighting coefficient q_5 increases, the effect of the weighting coefficient q_4 in the cost function decreases. Therefore, again increased values of the weighting coefficient q_4 give the best performance results.

One solution of getting improved performance of ride comfort and vehicle attitude simultaneously is using a weighting parameter somewhat between low and high values. By this way a compromise solution can be obtained. The other solution is the use of the adaptive controller which adapts to different controllers according to the response variables. According to the simulation results, three controllers with fixed parameter sets and one controller with the adaptive parameter set are designed. In the adaptive controller, the control weighting parameter q_4 is changed by the suspension deflection according to the Figure 4.43. Thus, when the vehicle travels on an asphalt road, ride comfort performance is important, and thus the integral weighting parameter should be low. However, when there is a ramp road or other body disturbance input, the priority of the controller switches to attitude control.

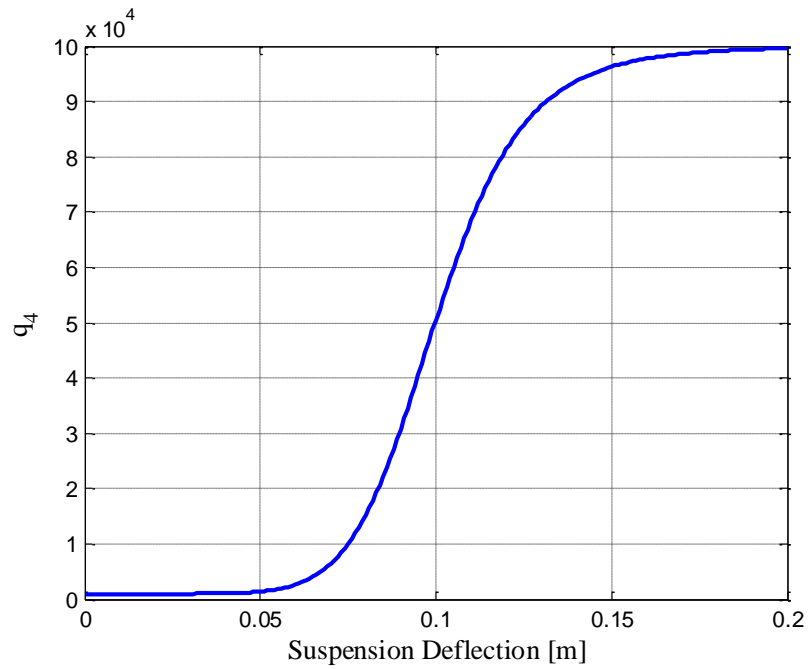


Figure 4.43: Change of Integral Controller Coefficient with Suspension Deflection

As Figure 4.43 shows, at low suspension deflection, integral weighting parameter is also low. However, at high suspension, integral weighting coefficient becomes also high. In order to compare the performance characteristics of the adaptive and fixed parameter controllers, four different controllers were designed. First controller is designed for the ride comfort performance, third controller is designed for the vehicle attitude controller, second controller is designed for the compromised ride comfort and the vehicle attitude, and the fourth controller was designed for the simultaneous ride comfort and vehicle attitude performance with adaptive switching. The weighting parameters of the four different controllers were given in Table 4.2.

Table 4.2: Weighting Coefficient Sets

	Set 1	Set 2	Set 3	Set 4
q₁	1.0	1.0	1.0	1.0
q₂	10	100	1000	10
q₃	1.0	1.0	1.0	1.0
q₄	1.0×10^3	1.0×10^4	1.0×10^5	$1.0 \times 10^3 - 1.0 \times 10^5$
q₅	1.0	10	10	1.0
R	1.0×10^5	1.0×10^5	1.0×10^5	1.0×10^5

First three sets are used as fixed weighting coefficients and the fourth set has the adaptive weighting. The weighting coefficient q_4 changes between 1.0×10^3 and 1.0×10^5 according to the magnitude of the suspension deflection. When the suspension deflection is low, the weighting coefficient q_4 is nearly equal to 1000. On the other hand when the suspension deflection is high, the weighting coefficient is adjusted to its maximum value which is 1.0×10^5 . First set of coefficients are mainly for the improved ride comfort and thus low values of the weighting coefficients q_2 , q_4 , and q_5 are used. The third set is mainly for the improved vehicle attitude control and thus larger values of weighting coefficients q_2 , q_4 , and q_5 are used.

Results from simulations with random road input at different longitudinal velocities are summarized in Table 4.3 to Table 4.7.

Table 4.3: rms Values for Random Road Simulations for 50 kph

	Passive	Set 1	Set 2	Set 3	Set 4
Vertical Acceleration rms [m/s²]	0.56	0.12	0.16	0.22	0.12
Suspension Deflection rms [mm]	10.7	7.1	5.8	4.6	7.1
Tire Deflection rms [mm]	1.7	0.8	0.7	0.8	0.8
Oil Flow Rate rms [L/min]	-	14.4	22.8	22.6	14.4

Table 4.4: rms Values for Random Road Simulations for 60 kph

	Passive	Set 1	Set 2	Set 3	Set 4
Vertical Acceleration rms [m/s²]	0.73	0.16	0.22	0.30	0.16
Suspension Deflection rms [mm]	13.9	9.0	7.7	6.2	9.0
Tire Deflection rms [mm]	2.1	1.0	0.9	1.00	1.0
Oil Flow Rate rms [L/min]	-	18.3	27.61	27.3	18.3

Table 4.5: rms Values for Random Road Simulations for 70 kph

	Passive	Set 1	Set 2	Set 3	Set 4
Vertical Acceleration rms [m/s²]	1.04	0.18	0.26	0.38	0.18
Suspension Deflection rms [mm]	19.81	9.2	8.4	7.6	9.2
Tire Deflection rms [mm]	2.8	1.1	1.1	1.3	1.1
Oil Flow Rate rms [L/min]	-	21.2	31.9	31.7	21.2

Table 4.6: rms Values for Random Road Simulations for 80 kph

	Passive	Set 1	Set 2	Set 3	Set 4
Vertical Acceleration rms [m/s²]	1.05	0.21	0.30	0.45	0.21
Suspension Deflection rms [mm]	20.0	10.3	9.7	8.7	10.3
Tire Deflection rms [mm]	2.9	1.3	1.2	1.5	1.3
Oil Flow Rate rms [L/min]	-	24.7	36.1	35.9	24.7

Table 4.7: rms Values for Random Road Simulations for 90 kph

	Passive	Set 1	Set 2	Set 3	Set 4
Vertical Acceleration rms [m/s²]	1.27	0.25	0.36	0.55	0.25
Suspension Deflection rms [mm]	24.1	11.7	11.00	10.3	11.7
Tire Deflection rms [mm]	3.4	1.4	1.4	1.7	1.4
Oil Flow Rate rms [L/min]	-	28.6	39.8	39.4	28.6

As can be seen from Table 4.3 to Table 4.7, the active suspension with first controller gives the best performance in terms of ride comfort. On the other hand, the active suspension with third controller gives the worst result with regard to ride comfort performance. Second controller provides a performance in between the third and the first controllers. In the case of the fourth controller, under normal road

conditions, suspension deflection is small and the adaptive weighting controller adjusts the weighting coefficient q_4 to low values. The resulting controller becomes similar to the first controller and thus it gives better performance with respect to ride comfort.

Simulation results for the ramp road displacement input are given in Figure 4.44 and Figure 4.45. As can be seen from Figure 4.44, the active suspension with the third controller minimizes the maximum value of the suspension deflection and gives the best results in terms of the vehicle attitude performance among all controllers. First controller gives the worst result with regard the suspension deflection performance. Second controller gives the compromise suspension deflection performance between first and third controllers. On the other hand since the amplitude of the suspension deflection is higher, at the beginning of the simulation, the weighting coefficients q_4 is adjusted to higher values and thus the fourth controller is adjusted for the vehicle attitude performance mainly. Therefore, the fourth controller gives better performance than the first and second controllers though not as good as the third controller.

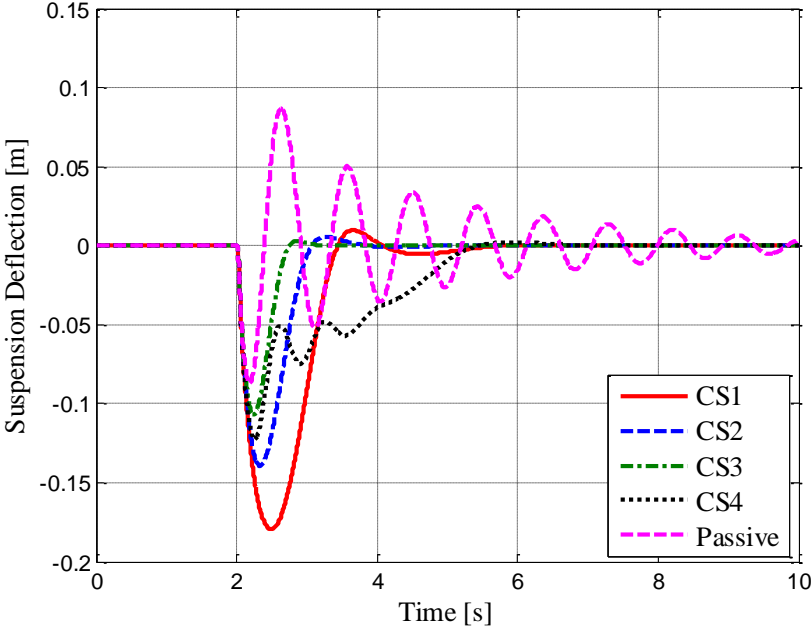


Figure 4.44: Suspension Deflection

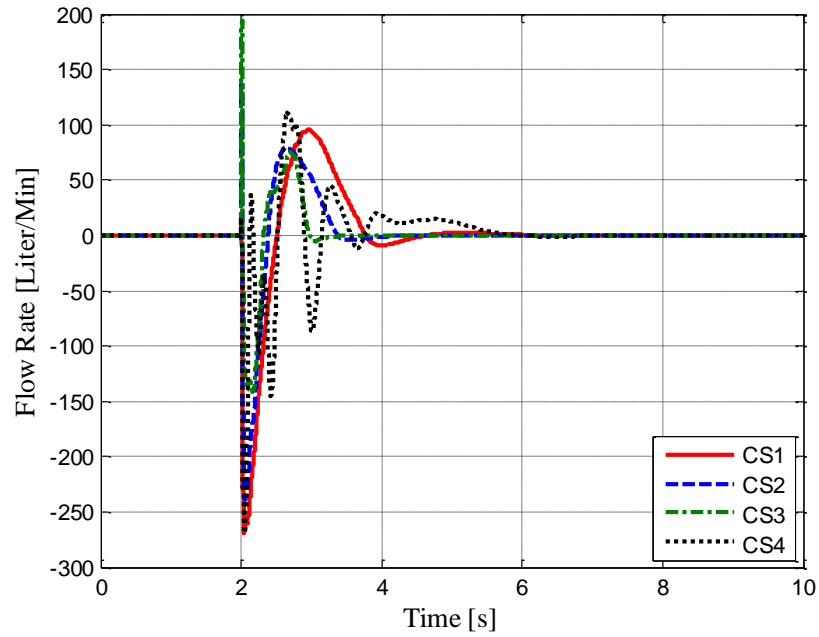


Figure 4.45: Oil Flow Rate

The attitude performance of the controllers is evaluated with simulations involving vertical body disturbance inputs. Simulation results are given in Figure 4.46 to Figure 4.47. As expected, the third controller provides the best suspension deflection results. First controller provides the worst performance and the second and the fourth controllers provide compromise results between the first and third controllers. When the amplitude of the disturbance input is larger, the performance of the adaptive controller becomes better since the weighting coefficient q_4 is adapted to higher values. This improves the applicability of the adaptive controller

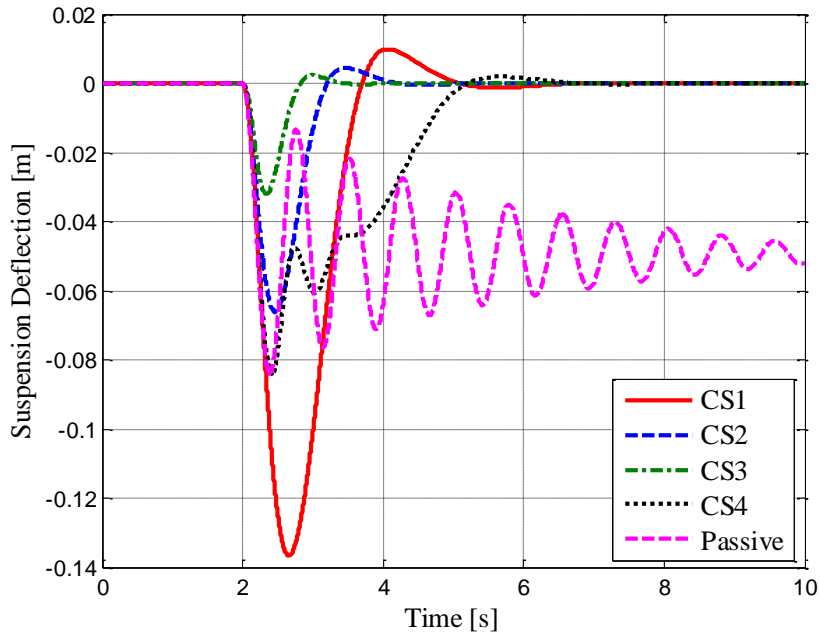


Figure 4.46: Suspension Deflection

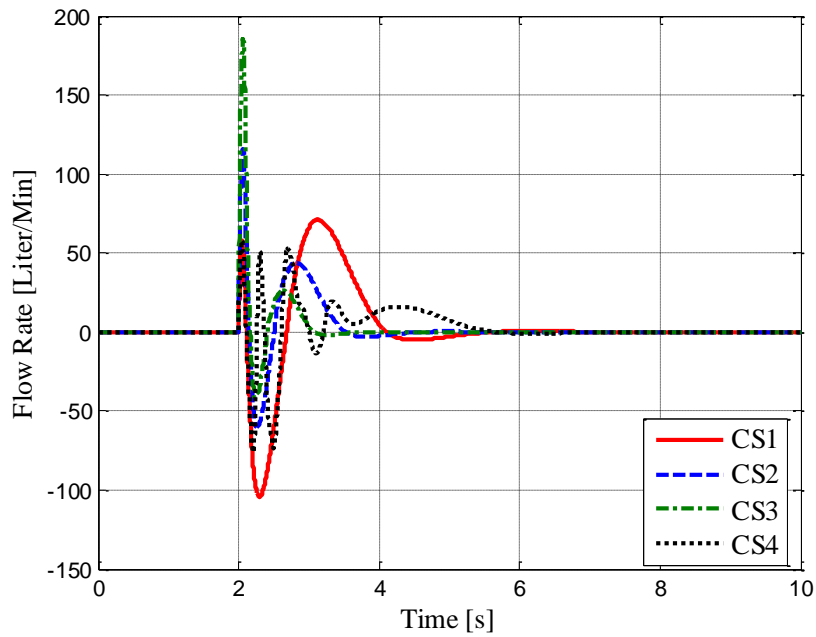


Figure 4.47: Oil Flow Rate

Another advantage of the HP suspension system is that suspension height can be adjusted by pumping oil into or removing oil from the suspension. Especially for the

off-road vehicles, military vehicles, sport utility vehicles, etc. which necessitate different driving conditions on different driving environments, adjustment of the suspension to the user defined reference suspension value is important. By this way, the vehicle body is lowered on a good road surface for better handling characteristic and vehicle longitudinal performance. On the contrary, in off-road environment, vehicle body may be lifted up. By this way, the mobility of the vehicle on the off-road environment is improved. Lowering and lifting of the vehicle body can be performed by the suspension height adjustment of the active HP suspension system. To examine the suspension height adjustment performance of the HP suspension system for the reference suspension height input given in Figure 4.48, simulations were performed and results are given in Figure 4.48 and Figure 4.49.

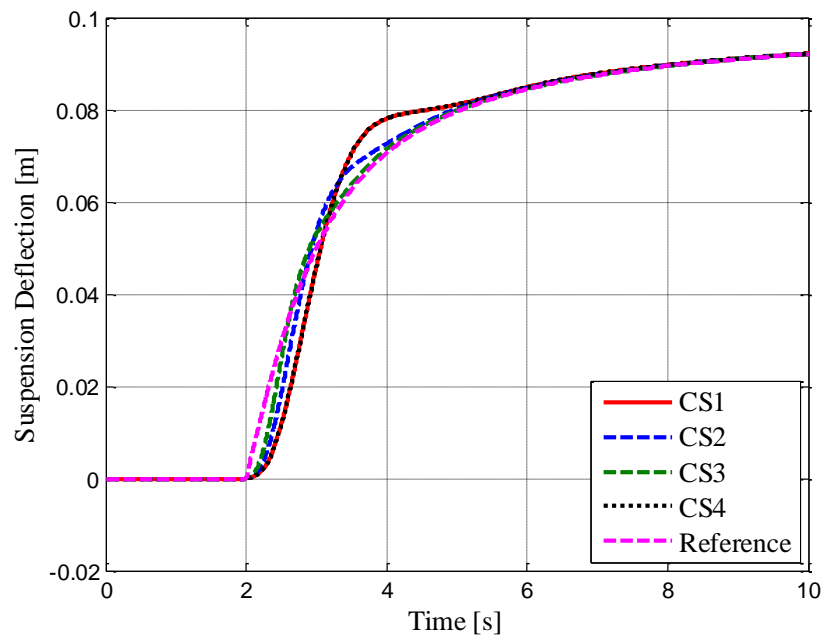


Figure 4.48: Suspension Deflection

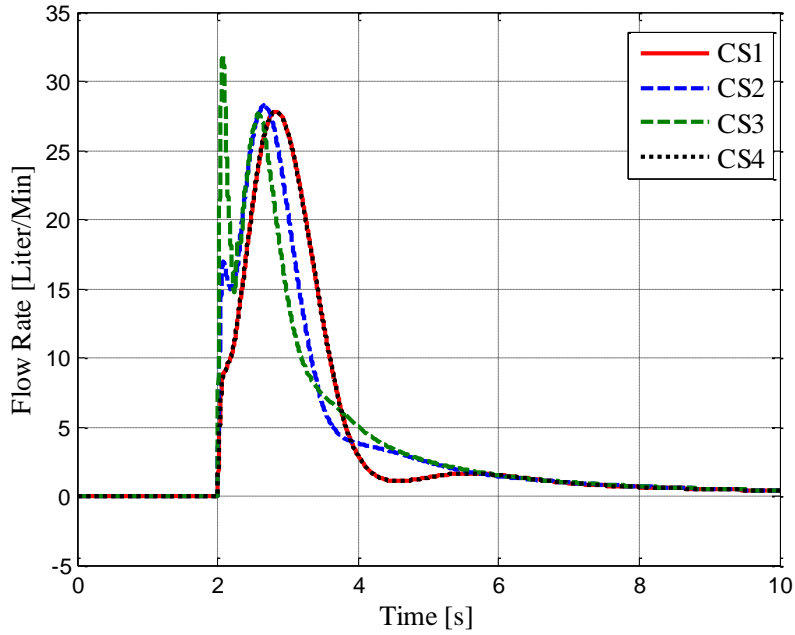


Figure 4.49: Oil Flow Rate

As Figure 4.48 illustrates, all controllers provide satisfactory performance for the vehicle suspension adjustment. The controllers are able to adjust the suspension deflection to reference inputs in a reasonable time

4.3. ACTIVE CONTROL OF ROLL PLANE HALF VEHICLE MODEL WITH THE HP SUSPENSION SYSTEM

In this section modeling and control of active half vehicle model with HP suspension system is to be studied. The half vehicle model can be used to examine the dynamics of the vehicle in roll and pitch motion. The first step is again the development of the roll plane half car model with the HP suspension systems. Then the state dependent linear model of the nonlinear half vehicle model will be derived. The aim of the controller is to attenuate the sprung mass acceleration, roll acceleration, left and right tire deflections, left and right suspension deflections, and to regulate the vehicle attitude or to adjust the suspension deflections to user desired height. The performance of the controller will be examined in the time domain. Performance of the vehicle attitude control will be examined by simulations using the vertical body force and roll plane moment disturbances. Height adjustment of the vehicle will be

performed against road and body force disturbance inputs. In the literature, nearly all of the active control studies are applied to the quarter car model and hence only the control of the vertical motion of the vehicle is considered. In some of these studies, vehicle attitude control is also considered. However, active control of the vehicle with HP suspension has not been fully studied for the half and full vehicle models, and the vehicle attitude control has not been applied to these higher order models.

In summary, in this chapter the following points will be elaborated.

- Active controller design for ride comfort
- Active controller design for handling
- Active controller design for vehicle body height adjustment
- Combined active controller

In the previous chapter, it was shown that the controller could not adjust the vehicle attitude at steady state. By combining an integral constraint on the suspension deflection, the vehicle attitude could be controlled. This situation is similar for the half vehicle model, and thus integral constraints will be imposed for the left and right suspensions in the design of the active controller for the half car model.

4.3.1.1. Modeling of Half Vehicle Roll Model with Active HP Suspension System

Sketch of the half vehicle roll model with an active HP suspension is shown in Figure 4.50.

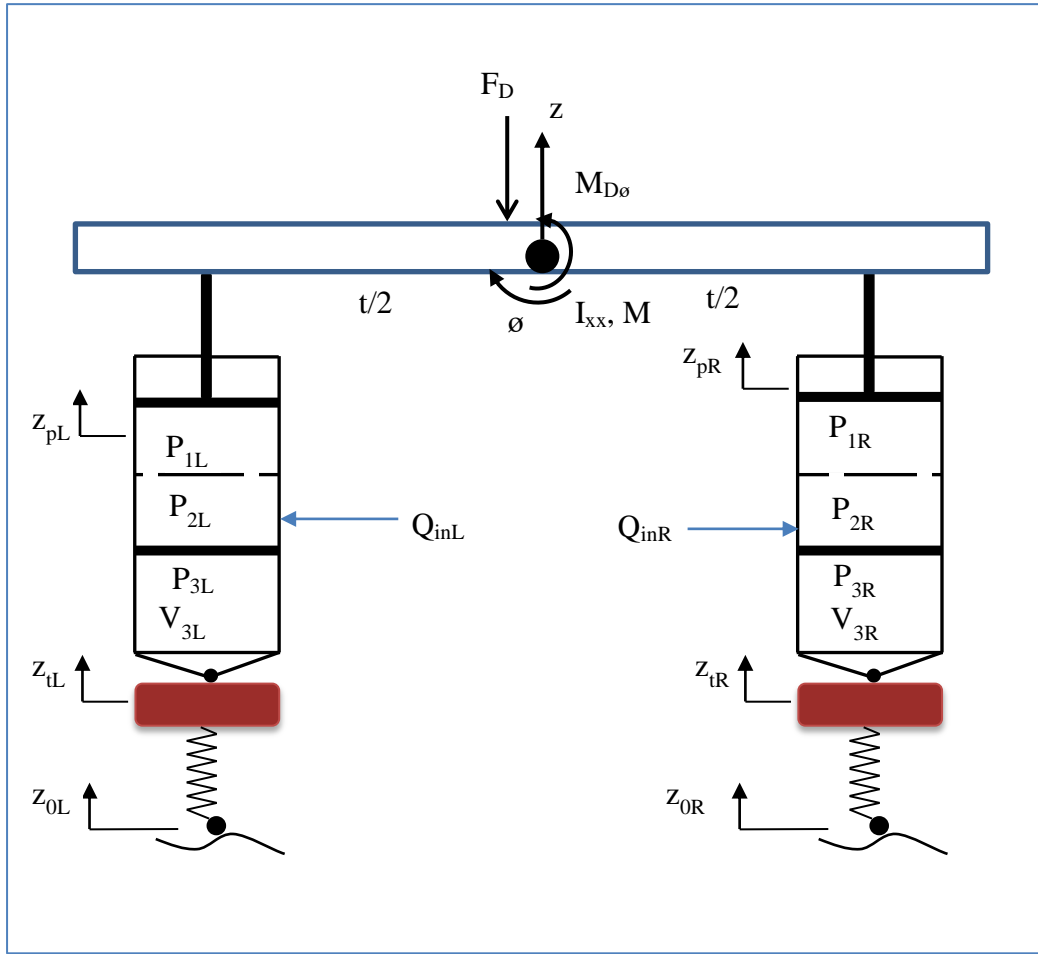


Figure 4.50. Half Vehicle Roll Model with Active HP Suspension System

The equation of motion for the suspension unit and the tire are the same with the equations developed for the quarter car model. In the derivation, “L” and “R” subscripts are used to define the left and right of the vehicle respectively, and the same variable and parameter notation in the previous chapter is used. Left piston force is given as,

$$F_L = \left[\begin{array}{l} \frac{P_{30L} V_{30L}^k}{[V_{30L} + A_p z_{fpL}]^k} - P_{Atm} - \frac{M_{fp} g + M_{fp} \ddot{z}_{fpL} + F_{fpL} + F_{fpHSL}}{A_p} \\ - \left[\frac{A_p \dot{z}_{ptL}}{A_v C_d} \right]^2 \frac{\rho}{2} \text{sign}(\dot{z}_{ptL}) \end{array} \right] A_p - F_{ptL} - F_{pHSL} \quad (4-54)$$

Right piston force is given as

$$F_R = \left[\begin{array}{c} \frac{P_{30R} V_{30R}^{\kappa}}{[V_{30R} + A_p z_{fpR}]^{\kappa}} - P_{Atm} - \frac{M_{fp} g + M_{fp} \ddot{z}_{fpR} + F_{fpR} + F_{fpHSR}}{A_p} \\ - \left[\frac{A_p \dot{z}_{ptR}}{A_v C_d} \right]^2 \frac{\rho}{2} \text{sign}(\dot{z}_{ptR}) \end{array} \right] A_p - F_{pR} - F_{pHSR} \quad (4-55)$$

In a similar way, equations of motion for the tires can be derived. To be able to derive a simpler model to be used in the controller design, some simplifications should be made. Assuming small angular displacements around equilibrium, the equation of motion for the vehicle body in vertical direction is,

$$F_L + F_R - Mg - F_D = M\ddot{z} \quad (4-56)$$

where F_D is the disturbance body force. The equation of motion of the body in roll direction is,

$$\frac{t}{2} F_L - \frac{t}{2} F_R - M_{D\phi} = I_{xx} \ddot{\phi} \quad (4-57)$$

where t is the track width, I_{xx} is the roll moment of inertia for half vehicle model, and $M_{D\phi}$ is the body disturbance moment in roll direction. From the kinematics, the relationships can be obtained as,

$$z_{pL} = z + \frac{t}{2} \phi \quad (4-58)$$

$$z_{pR} = z - \frac{t}{2} \phi \quad (4-59)$$

Moreover, assuming negligible floating piston dynamics and negligible friction forces, the front and rear piston forces become,

$$F_L = \left[\frac{P_{30L} V_{30L}^{\kappa}}{[V_{30L} + A_p z_{fpL}]^{\kappa}} - P_{Atm} - \frac{M_{fp} g}{A_p} - \left[\frac{A_p \dot{z}_{ptL}}{A_v C_d} \right]^2 \frac{\rho}{2} \text{sign}(\dot{z}_{ptL}) \right] A_p \quad (4-60)$$

$$F_R = \left[\frac{P_{30R} V_{30R}^{\kappa}}{[V_{30R} + A_p z_{fpR}]^{\kappa}} - P_{Atm} - \frac{M_{fp} g}{A_p} - \left[\frac{A_p \dot{z}_{ptR}}{A_v C_d} \right]^2 \frac{\rho}{2} \text{sign}(\dot{z}_{ptR}) \right] A_p \quad (4-61)$$

4.3.1.2. Static Analysis of the Suspension System

At static equilibrium left and right suspension forces become,

$$F_L = F_R = \frac{Mg}{2} \quad (4-62)$$

From these two equations, initial absolute gas pressures can be found as,

$$P_{30L} = P_{30R} = \frac{Mg}{2A_p} + \frac{M_{fp}g}{A_p} + P_{Atm} \quad (4-63)$$

Initial gas pressures are determined according to the static equilibrium analysis. The other important design step is the determination of the initial gas volumes which are specified according to the prespecified body bounce frequencies.

4.3.1.3. Stiffness Characteristics

Vertical Motion

Front and rear suspension forces are,

$$F_L = \frac{P_{30L} V_{30L}^{\kappa} A_p}{[V_{30L} + A_p z_{ptL}]^{\kappa}} - P_{Atm} A_p - M_{fp} g \quad (4-64)$$

$$F_R = \frac{P_{30R} V_{30R}^{\kappa} A_p}{[V_{30R} + A_p z_{ptR}]^{\kappa}} - P_{Atm} A_p - M_{fp} g \quad (4-65)$$

$$F = F_F + F_R = \frac{P_{30L} V_{30L}^{\kappa} A_p}{[V_{30L} + A_p z_{ptL}]^{\kappa}} + \frac{P_{30R} V_{30R}^{\kappa} A_p}{[V_{30R} + A_p z_{ptR}]^{\kappa}} - 2P_{Atm} A_p - 2M_{fp} g \quad (4-66)$$

Assuming that,

$$z_{pL} - z_{iL} = z_{pR} - z_{iR} = z_{pt} \quad (4-67)$$

and taking the derivative of the elastic force with the vertical displacements, the suspension stiffness can be found.

$$k = -\frac{dF}{dz_{pt}} = \frac{P_{30L} V_{30L}^{\kappa} \kappa A_p^2}{[V_{30L} + A_p z_{pt}]^{\kappa+1}} + \frac{P_{30R} V_{30R}^{\kappa} \kappa A_p^2}{[V_{30R} + A_p z_{pt}]^{\kappa+1}} \quad (4-68)$$

Roll Motion

The moment exerted by the elastic forces on the sprung mass about the mass center is,

$$M_\phi = \frac{t}{2}F_L - \frac{t}{2}F_R$$

$$M_\phi = \frac{t}{2} \left(\frac{P_{30L} V_{30L}^\kappa A_p}{\left[V_{30L} + A_p \left(z + \frac{t}{2} \phi - z_{tL} \right) \right]^\kappa} \right) - \frac{t}{2} \left(\frac{P_{30R} V_{30R}^\kappa A_p}{\left[V_{30R} + A_p \left(z - \frac{t}{2} \phi - z_{tR} \right) \right]^\kappa} \right) \quad (4-69)$$

Assuming $z_{tL}=z_{tR}=0$ and taking the derivative of the elastic moment with respect to roll angle ϕ ,

$$\frac{dM}{d\phi} = -\frac{t}{2} \left[\frac{P_{30L} V_{30L}^\kappa A_p \kappa \left(A_p \frac{dz}{d\phi} + A_p \frac{t}{2} \right)}{\left[V_{30L} + A_p \left(z + \frac{t}{2} \phi \right) \right]^{\kappa+1}} \right] + \frac{t}{2} \left[\frac{P_{30R} V_{30R}^\kappa A_p \kappa \left(A_p \frac{dz}{d\phi} - A_p \frac{t}{2} \right)}{\left[V_{30R} + A_p \left(z - \frac{t}{2} \phi \right) \right]^{\kappa+1}} \right] \quad (4-70)$$

where z and $\frac{dz}{d\phi}$ can be found from the static equilibrium equation in vertical direction as,

$$\frac{P_{30L} V_{30L}^\kappa A_p}{\left[V_{30L} + A_p \left(z + \frac{t}{2} \phi \right) \right]^\kappa} + \frac{P_{30R} V_{30R}^\kappa A_p}{\left[V_{30R} + A_p \left(z - \frac{t}{2} \phi \right) \right]^\kappa} - 2P_{Atm} A_p - 2M_{fp} g - Mg = 0 \quad (4-71)$$

$$-\frac{P_{30L} V_{30L}^\kappa A_p \kappa \left(\frac{dz}{d\phi} A_p + \frac{t}{2} A_p \right)}{\left[V_{30L} + A_p \left(z + \frac{t}{2} \phi \right) \right]^{\kappa+1}} - \frac{P_{30R} V_{30R}^\kappa A_p \kappa \left(\frac{dz}{d\phi} A_p - \frac{t}{2} A_p \right)}{\left[V_{30R} + A_p \left(z - \frac{t}{2} \phi \right) \right]^{\kappa+1}} = 0 \quad (4-72)$$

From the derived equation, the roll stiffness can be found as,

$$k_\phi = -\frac{dM}{d\phi} \quad (4-73)$$

An initial guess about the body bounce frequency and the roll frequency can be found from these stiffness values as at static equilibrium.

$$k_z = - \left. \frac{dF}{dz_{pt}} \right|_{z_{pt}=0, \phi=0} = \frac{P_{30L} \kappa A_p^2}{V_{30L}} + \frac{P_{30R} \kappa A_p^2}{V_{30R}} \quad (4-74)$$

In a similar, manner,

$$k_\phi = - \left. \frac{dM}{d\phi} \right|_{z_{pt}=0, \phi=0} \quad (4-75)$$

can be found. From these equations, the approximate natural frequencies can be found as,

$$\omega_{bb} \approx \sqrt{\frac{k_z}{M}} \quad (4-76)$$

$$\omega_{roll} \approx \sqrt{\frac{k_\phi}{I_{xx}}} \quad (4-77)$$

Note that in order to set the body bounce frequency to a design value initial gas volumes are used. In this case, the roll frequency is automatically set and cannot be tuned by changing suspension design parameters. The details of the calculation of the stiffness of half vehicle model are to be presented in Chapter 6.

4.3.1.4. State Space Representation of the Linearized Half Vehicle Model with the HP Suspensions

While deriving the state dependent linear state space model equation of the half vehicle roll model with the active HP suspension system, it is assumed that the friction forces and the floating piston dynamics are negligible as compared with the pressure and inertial forces. Let the dynamics left and right gas forces are represented as,

$$\begin{aligned}
F_{1L} &= \frac{P_{30L} V_{30L}^{\kappa} A_p}{\left[V_{30L} + A_p \left(z + \frac{t}{2} \dot{\phi} - z_{tL} \right) \right]^{\kappa}} - P_{\text{Atm}} A_p - M_{fp} g - \frac{Mg}{2} = \\
&= p_{1L} z_{fpL} + p_{2L} z_{fpL}^2 + p_{3L} z_{fpL}^3 + p_{4L} z_{fpL}^4 + p_{5L} z_{fpL}^5 + \\
&+ p_{6L} z_{fpL}^6 + p_{7L} z_{fpL}^7 + p_{8L} z_{fpL}^8 + p_{9L} z_{fpL}^9 = f_{1L} \left(z_{fpL} \right) z_{fpL}
\end{aligned} \tag{4-78}$$

$$\begin{aligned}
F_{1R} &= \frac{P_{30R} V_{30R}^{\kappa} A_p}{\left[V_{30R} + A_p \left(z - \frac{t}{2} \dot{\phi} - z_{tR} \right) \right]^{\kappa}} - P_{\text{Atm}} A_p - M_{fp} g - \frac{Mg}{2} = \\
&= p_{1R} z_{fpR} + p_{2R} z_{fpR}^2 + p_{3R} z_{fpR}^3 + p_{4R} z_{fpR}^4 + p_{5R} z_{fpR}^5 + \\
&+ p_{6R} z_{fpR}^6 + p_{7R} z_{fpR}^7 + p_{8R} z_{fpR}^8 + p_{9R} z_{fpR}^9 = f_{1R} \left(z_{fpR} \right) z_{fpR}
\end{aligned} \tag{4-79}$$

where

$$\begin{aligned}
f_{1L} \left(z_{fpL} \right) &= p_{1L} + p_{2L} z_{fpL} + p_{3L} z_{fpL}^2 + p_{4L} z_{fpL}^3 + p_{5L} z_{fpL}^4 + \\
&+ p_{6L} z_{fpL}^5 + p_{7L} z_{fpL}^6 + p_{8L} z_{fpL}^7 + p_{9L} z_{fpL}^8
\end{aligned} \tag{4-80}$$

$$\begin{aligned}
f_{1R} \left(z_{fpR} \right) &= p_{1R} + p_{2R} z_{fpR} + p_{3R} z_{fpR}^2 + p_{4R} z_{fpR}^3 + p_{5R} z_{fpR}^4 + \\
&+ p_{6R} z_{fpR}^5 + p_{7R} z_{fpR}^6 + p_{8R} z_{fpR}^7 + p_{9R} z_{fpR}^8
\end{aligned} \tag{4-81}$$

Similarly, state dependent orifice damping equation can be written as,

$$F_{2L} = A_p \left[\frac{A_p \left(\dot{z} + \frac{t}{2} \dot{\phi} - \dot{z}_{tL} \right)}{A_v C_d} \right]^2 \frac{\rho}{2} \text{sign} \left(\dot{z} + \frac{t}{2} \dot{\phi} - \dot{z}_{tL} \right) = f_{2L} \left(\dot{z}_{ptL} \right) \dot{z}_{ptL} \tag{4-82}$$

$$F_{2R} = A_p \left[\frac{A_p \left(\dot{z} - \frac{t}{2} \dot{\phi} - \dot{z}_{tR} \right)}{A_v C_d} \right]^2 \frac{\rho}{2} \text{sign} \left(\dot{z} - \frac{t}{2} \dot{\phi} - \dot{z}_{tR} \right) = f_{2R} \left(\dot{z}_{ptR} \right) \dot{z}_{ptR} \tag{4-83}$$

where,

$$f_{2L} \left(\dot{z}_{ptL} \right) = A_p \left[\frac{A_p}{A_v C_d} \right]^2 \frac{\rho}{2} \left(\dot{z} + \frac{t}{2} \dot{\phi} - \dot{z}_{tL} \right) \text{sign} \left(\dot{z} + \frac{t}{2} \dot{\phi} - \dot{z}_{tL} \right) \tag{4-84}$$

$$f_{2R}(\dot{z}_{ptR}) = A_p \left[\frac{A_p}{A_v C_d} \right]^2 \frac{\rho}{2} \left(\dot{z} - \frac{t}{2} \dot{\phi} - \dot{z}_{tR} \right) \text{sign} \left(\dot{z} - \frac{t}{2} \dot{\phi} - \dot{z}_{tR} \right) \quad (4-85)$$

Then the equations of motion become;

$$k_t (z_{0L} - z_{tL}) - f_{1L} z_{fptL} + f_{2L} \dot{z}_{ptL} = M_t \ddot{z}_{tL} \quad (4-86)$$

$$k_t (z_{0R} - z_{tR}) - f_{1R} z_{fptR} + f_{2R} \dot{z}_{ptR} = M_t \ddot{z}_{tR} \quad (4-87)$$

$$f_{1L} z_{fptL} - f_{2L} \dot{z}_{ptL} + f_{1R} z_{fptR} - f_{2R} \dot{z}_{ptR} - F_D = M \ddot{z} \quad (4-88)$$

$$\frac{t}{2} (f_{1L} z_{fptL} - f_{2L} \dot{z}_{ptL}) - \frac{t}{2} (f_{1R} z_{fptR} - f_{2R} \dot{z}_{ptR}) - M_{D\phi} = I_{xx} \ddot{\phi} \quad (4-89)$$

The relations between the floating piston velocity and the main piston velocity is,

$$\dot{z}_{fptL} = \dot{z}_{ptL} - \frac{Q_{inL}}{A_p} \quad (4-90)$$

$$\dot{z}_{fptR} = \dot{z}_{ptR} - \frac{Q_{inR}}{A_p} \quad (4-91)$$

Define state variables as,

$$x_1 = \dot{z} \quad (4-92)$$

$$x_2 = \dot{\phi} \quad (4-93)$$

$$x_3 = z_{fptL} = z + \frac{t}{2} \phi - z_{tL} - \frac{\int Q_{inL}}{A_p} \quad (4-94)$$

$$x_4 = z_{fptR} = z - \frac{t}{2} \phi - z_{tR} - \frac{\int Q_{inR}}{A_p} \quad (4-95)$$

$$x_5 = z_{pL} - z_{tL} = z + \frac{t}{2} \phi - z_{tL} \quad (4-96)$$

$$x_6 = z_{pR} - z_{tR} = z - \frac{t}{2} \phi - z_{tR} \quad (4-97)$$

$$x_7 = z_{tL} - z_{0L} \quad (4-98)$$

$$x_8 = z_{tR} - z_{0R} \quad (4-99)$$

$$x_9 = \dot{z}_{tL} \quad (4-100)$$

$$x_{10} = \dot{z}_{tR} \quad (4-101)$$

$$x_{11} = \int (z_{pL} - z_{tL}) = \int \left(z + \frac{t}{2} \phi - z_{tL} \right) \quad (4-102)$$

$$x_{12} = \int (z_{pR} - z_{tR}) = \int \left(z - \frac{t}{2} \phi - z_{tR} \right) \quad (4-103)$$

State equations can be written as,

$$\dot{x}_1 = \frac{1}{M} \left[f_{1L} x_3 - f_{2L} \left(x_1 + \frac{t}{2} x_2 - x_9 \right) + f_{1R} x_4 - f_{2R} \left(x_1 - \frac{t}{2} x_2 - x_{10} \right) - F_D \right] \quad (4-104)$$

$$\dot{x}_2 = \frac{1}{I_{xx}} \left\{ \begin{array}{l} \frac{t}{2} \left[f_{1L} x_3 - f_{2L} \left(x_1 + \frac{t}{2} x_2 - x_9 \right) \right] - \\ - \frac{t}{2} \left[f_{1R} x_4 - f_{2R} \left(x_1 - \frac{t}{2} x_2 - x_{10} \right) \right] - M_{D\phi} \end{array} \right\} \quad (4-105)$$

$$\dot{x}_3 = x_1 + \frac{t}{2} x_2 - x_9 - \frac{Q_{inL}}{A_p} \quad (4-106)$$

$$\dot{x}_4 = x_1 - \frac{t}{2} x_2 - x_{10} - \frac{Q_{inR}}{A_p} \quad (4-107)$$

$$\dot{x}_5 = x_1 + \frac{t}{2} x_2 - x_9 \quad (4-108)$$

$$\dot{x}_6 = x_1 - \frac{t}{2} x_2 - x_{10} \quad (4-109)$$

$$\dot{x}_7 = x_9 - \dot{z}_{0L} \quad (4-110)$$

$$\dot{x}_8 = x_{10} - \dot{z}_{0R} \quad (4-111)$$

$$\dot{x}_9 = \frac{1}{M_t} \left[-k_t x_7 - f_{1L} x_3 + f_{2L} \left(x_1 + \frac{t}{2} x_2 - x_9 \right) \right] \quad (4-112)$$

$$\dot{x}_{10} = \frac{1}{M_t} \left[-k_t x_8 - f_{1R} x_4 + f_{2R} \left(x_1 - \frac{t}{2} x_2 - x_{10} \right) \right] \quad (4-113)$$

$$\dot{x}_{11} = x_5 \quad (4-114)$$

$$\dot{x}_{12} = x_6 \quad (4-115)$$

Then the state dependent linear state space model of the half vehicle model with the HP suspension can be obtained from the state equations. The system and control input matrices are given in Appendix A.

HP suspension system and vehicle parameters for half vehicle model are given in Table 4.8.

Table 4.8: Suspension and Vehicle Parameters for Half Vehicle Model

Parameter	Symbol	Value
Sprung Mass	M [kg]	3300
Roll Moment of Inertia	I_{xx} [kgm ²]	1950
Distance between Roll Center and COG	h_{RC-COG} [m]	1.1
Track Width	t [m]	2
Left Suspension Initial Gas Volume	V_{30L} [m ³]	0.0019
Right Suspension Initial Gas Volume	V_{30R} [m ³]	0.0019
Left Suspension Orifice Opening	A_{vL} [m ²]	2e-4
Right Suspension Orifice Opening	A_{vR} [m ²]	2e-4
Left Suspension Piston Area	A_{pL} [m ²]	0.007
Right Suspension Piston Area	A_{pR} [m ²]	0.007

4.3.1.5. Design of an Active Controller for Half Vehicle Model with the Active HP Suspension System

Active controller for vehicle suspensions is designed primarily for vehicle ride comfort, vehicle attitude control, and handling control in mind. Vehicle ride comfort comprises reducing sprung mass acceleration, suspension deflection, and tire deflection. These three performance requirements for ride comfort are conflicting with each other. In the active control of the quarter car model, design of active controller for these performance variables is studied in detail. Moreover, another aim of the active controller is to satisfy the vehicle attitude control. In other words, the suspension deflection should be regulated around zero position or it should be

adjusted to a user specified reference value at steady state driving situation. In braking or acceleration, leveling of the vehicle in the pitch plane or in cornering leveling in the roll plane of the vehicle are other aims of the active controller. An active controller which comprises all these performances is considered here. For local controllers, the performance index to be minimized is written for the left and the right suspension separately as

$$J_L(x) = \frac{1}{2} \int \left\{ q_1 \ddot{z}_{ptL}^2 + q_2 z_{ptL}^2 + q_3 z_{t0L}^2 + q_4 \left(\int z_{ptL} \right)^2 + q_5 \dot{z}_{ptL}^2 + R_L Q_{inL}^2 \right\} dt \quad (4-116)$$

$$J_R(x) = \frac{1}{2} \int \left\{ q_1 \ddot{z}_{ptR}^2 + q_2 z_{ptR}^2 + q_3 z_{t0R}^2 + q_4 \left(\int z_{ptR} \right)^2 + q_5 \dot{z}_{ptR}^2 + R_R Q_{inR}^2 \right\} dt \quad (4-117)$$

In the global controller, the controller is designed using all the system knowledge and the control input is formed using all state variables in the system. The performance variables to be minimized are the vertical and roll acceleration of the sprung mass, left and right tire deflections, and the left and right suspension deflections. Therefore, the performance index to be minimized is,

$$J(x) = \frac{1}{2} \int \left\{ q_1 \ddot{z}^2 + q_2 \ddot{\phi}^2 + q_3 z_{ptL}^2 + q_3 z_{ptR}^2 + q_4 z_{t0L}^2 + q_4 z_{t0R}^2 + q_5 \left(\int z_{ptL} \right)^2 + \right. \\ \left. + q_5 \left(\int z_{ptR} \right)^2 + q_6 \dot{z}_{ptL}^2 + q_6 \dot{z}_{ptR}^2 + R_L Q_{inL}^2 + R_R Q_{inR}^2 \right\} dt \quad (4-118)$$

In the performance index, integral states for the left and the right tire deflections are used to adjust the left and the right suspension deflections and thus vehicle height and roll angle can be controlled especially at steady state. Firstly, the controller for vehicle ride comfort and the vehicle attitude control will be designed and then this controller will be adjusted for different purposes. The controller which is aimed to improve vehicle ride motion and to control the vehicle attitude should comprise states of common half vehicle model and the integral states of the left and right suspension deflections. When the active controller is designed only for ride comfort, suspension deflections at low frequencies and at steady state increases and cannot be regulated to zero position. To regulate the suspension deflection or to adjust the suspension deflections to reference user input value, integral constraints of the left and the right suspension deflections will be embedded into the cost function to be

minimized. In order to examine the stability of the designed controller, similar to previous controllers, Theorem 1 is used. However, since the order of the system matrix is large, calculating the rank of the symbolic controllability and observability matrices are difficult. For this reason, PBH rank test Theorem is used.

Theorem 2 [65]: Popov-Belevitc-Hautus (PBH) test for controllability, stabilizability, observability and detectability:

The pair (A, B) is stabilizable if and only if

$$\text{rank}[A - \lambda I \quad B] = n$$

for all eigenvalues λ of A with $\text{Re}\lambda \geq 0$.

The pair (A, B) is controllable if and only if

$$\text{rank}[A - \lambda I \quad B] = n$$

for every eigenvalue of A.

The pair (C, A) is detectable if and only if

$$\text{rank} \begin{bmatrix} A - \lambda I \\ C \end{bmatrix} = n$$

for all eigenvalues λ of A with $\text{Re}\lambda \geq 0$.

The pair (C, A) is observable if and only if

$$\text{rank} \begin{bmatrix} A - \lambda I \\ C \end{bmatrix} = n$$

for every eigenvalue A.

Stability of the active controller is evaluated in two ways: Firstly, rank of the symbolic controllability and the observability matrices are calculated. Secondly, matrices of the state dependent state space systems are evaluated at some state values in the operating range in the state domain.

Rank of the symbolic controllability and the observability matrices of the half vehicle model with active suspension system are both 12. Moreover, when the state

dependent matrices are evaluated at some state values in the operating domain of the states, it is observed that $\text{rank}[A - \lambda I \ B] = 12$ and $\text{rank} \begin{bmatrix} A - \lambda I \\ C \end{bmatrix} = 12$ for all eigenvalues of the A matrix. Therefore, the obtained active controller is locally asymptotically stable.

4.3.1.6. Simulations

4.3.1.6.1. Straight Line Driving: Random Road Displacement Input

In this section, the active HP suspension will be simulated with the same random road displacement input used in section 4.2.4.1 at different longitudinal velocities. Selected controller weighting parameters are given in Table 4.9.

Table 4.9: Controller Weighting Parameters

Weighting Parameter	Value
q_1	1
q_2	1
q_3	1
q_4	100
q_5	1
q_6	5e4
R_L	1e5
R_R	1e5

The rms values of the responses are given in Table 4.10 to Table 4.13.

Table 4.10. rms Values for Performance Variables for 60 kph

	\ddot{z} [m/s ²]	$\ddot{\phi}$ [rad/s ²]	z_{ptL} [mm]	z_{ptR} [mm]	z_{tOL} [mm]	z_{tOR} [mm]	Q_{inL} [L/Min]	Q_{inR} [L/Min]
Passive	0.61	0.57	13.4	13.1	1.9	1.9	-	-
Active	0.22	0.20	6.1	6.2	1.1	1.1	14.2	14.6

Table 4.11. rms Values for Performance Variables for 70 kph

	\ddot{z} [m/s ²]	$\ddot{\phi}$ [rad/s ²]	Z_{ptL} [mm]	Z_{ptR} [mm]	Z_{t0L} [mm]	Z_{t0R} [mm]	Q_{inL} [L/Min]	Q_{inR} [L/Min]
Passive	0.63	0.73	14.7	14.5	2.1	2.1	-	-
Active	0.26	0.29	7.7	8.0	1.3	1.3	18.1	17.4

Table 4.12. rms Values for Performance Variables for 80 kph

	\ddot{z} [m/s ²]	$\ddot{\phi}$ [rad/s ²]	Z_{ptL} [mm]	Z_{ptR} [mm]	Z_{t0L} [mm]	Z_{t0R} [mm]	Q_{inL} [L/Min]	Q_{inR} [L/Min]
Passive	0.82	0.87	18.4	18.6	2.5	2.5	-	-
Active	0.34	0.33	8.9	9.5	1.5	1.6	20.7	20.8

Table 4.13. rms Values for Performance Variables for 90 kph

	\ddot{z} [m/s ²]	$\ddot{\phi}$ [rad/s ²]	Z_{ptL} [mm]	Z_{ptR} [mm]	Z_{t0L} [mm]	Z_{t0R} [mm]	Q_{inL} [L/Min]	Q_{inR} [L/Min]
Passive	0.87	1.1	20.7	21.4	2.8	2.8	-	-
Active	0.38	0.38	10.3	10.2	1.7	1.7	23.2	23.0

As the simulation results show, the active suspension controller improves ride comfort by reducing the vertical and roll accelerations. For the performance improvement, moderate amounts of oil flow rates are required.

4.3.1.6.2. Steady State Cornering

After the ride comfort characteristics of the half vehicle model with active HP suspension systems has examined, the handling characteristics will be examined. For this purpose, simulations for steady state cornering and the double lane change maneuvers are to be performed. The input for the simulations is the disturbance moment induced by the lateral acceleration during maneuver. Lateral acceleration for the steady state cornering is taken from the well-known linear bicycle model and is given in Figure 4.51. Steady state cornering simulation is performed with a steering wheel input of 30 degree at 90 kph. The used vehicle model has an understeer characteristic with a steering wheel ratio of 18.

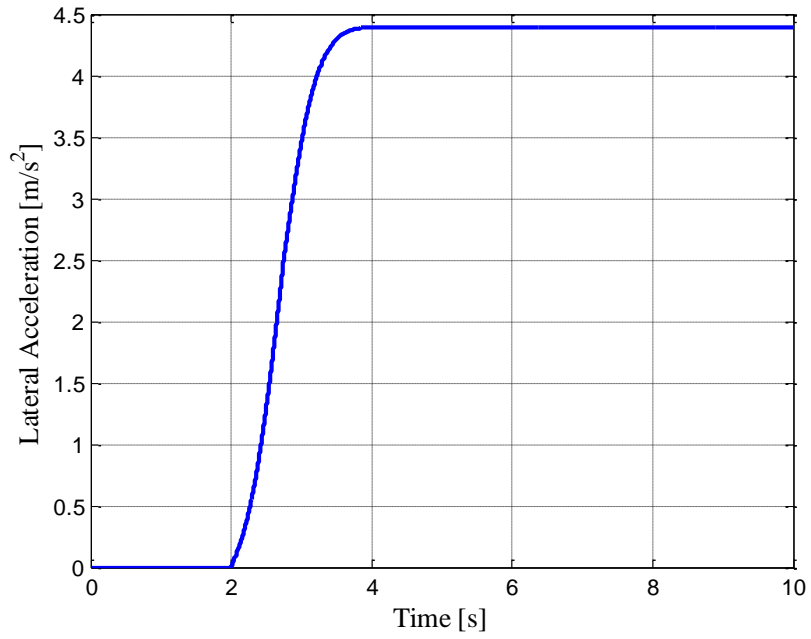


Figure 4.51: Lateral Acceleration

Simulation results are given in Figure 4.52 to Figure 4.58.

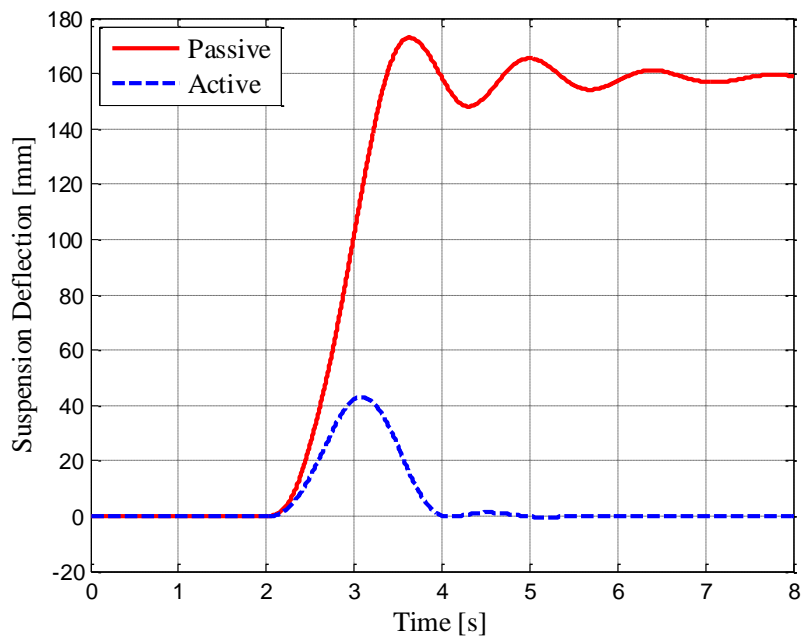


Figure 4.52: Left Suspension Deflection

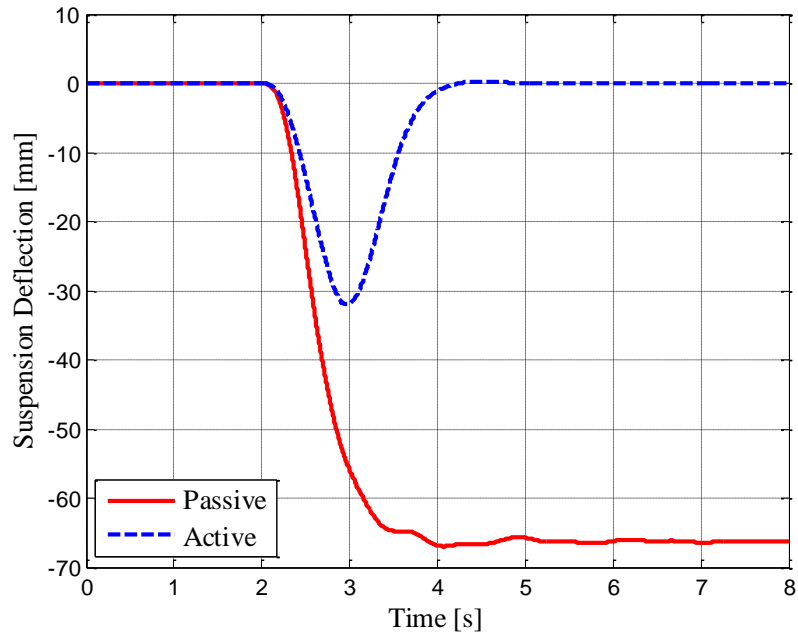


Figure 4.53: Right Suspension Deflection

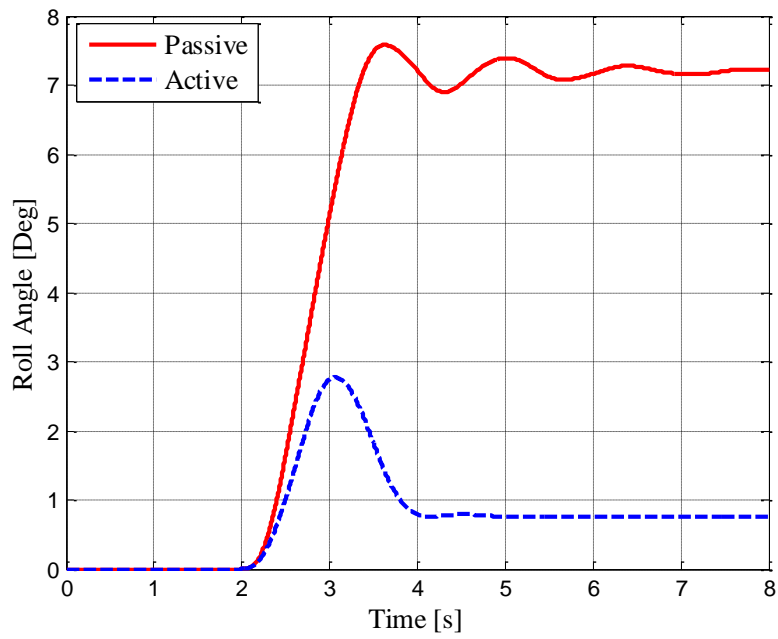


Figure 4.54: Roll Angle

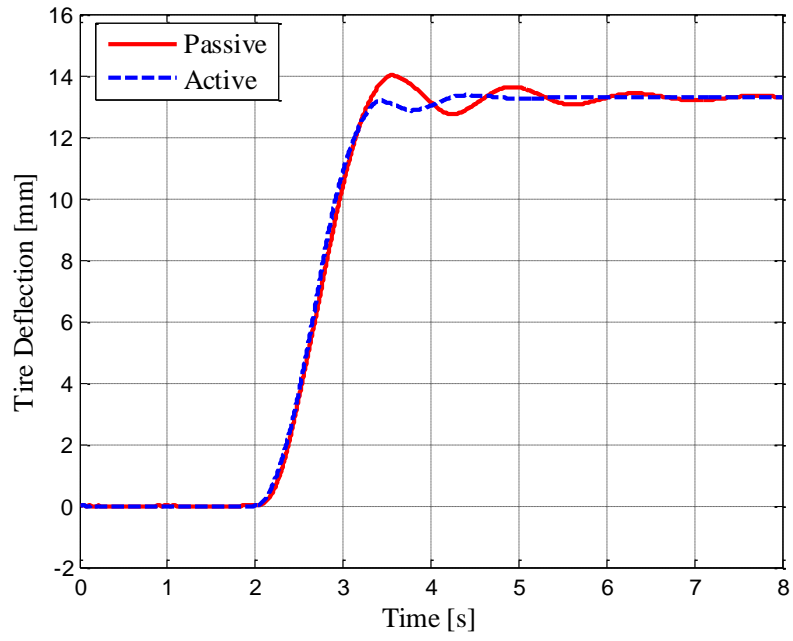


Figure 4.55: Left Tire Deflection

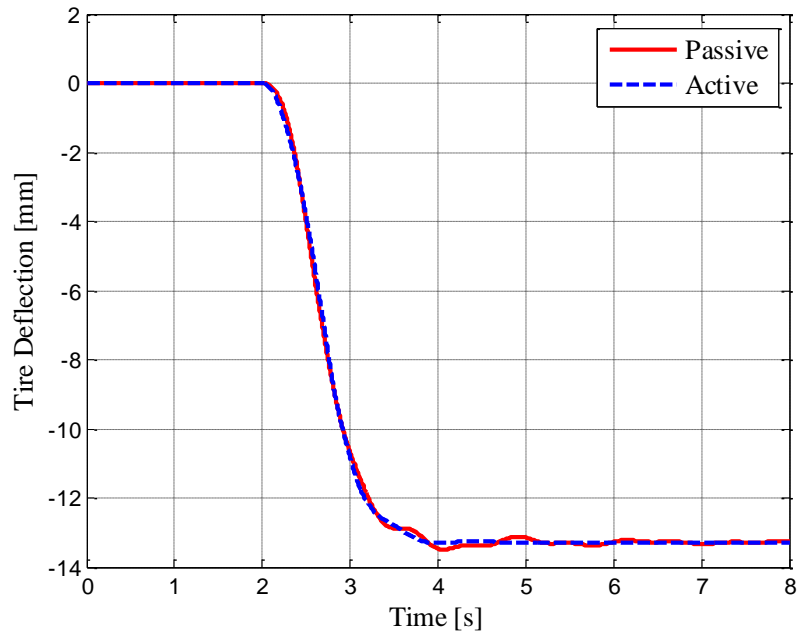


Figure 4.56: Right Tire Deflection

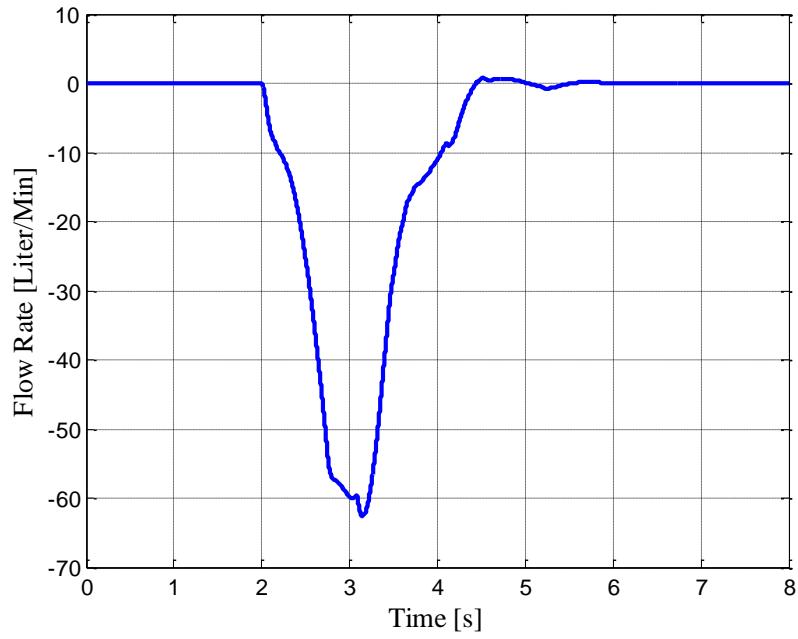


Figure 4.57: Left Suspension Flow Rate

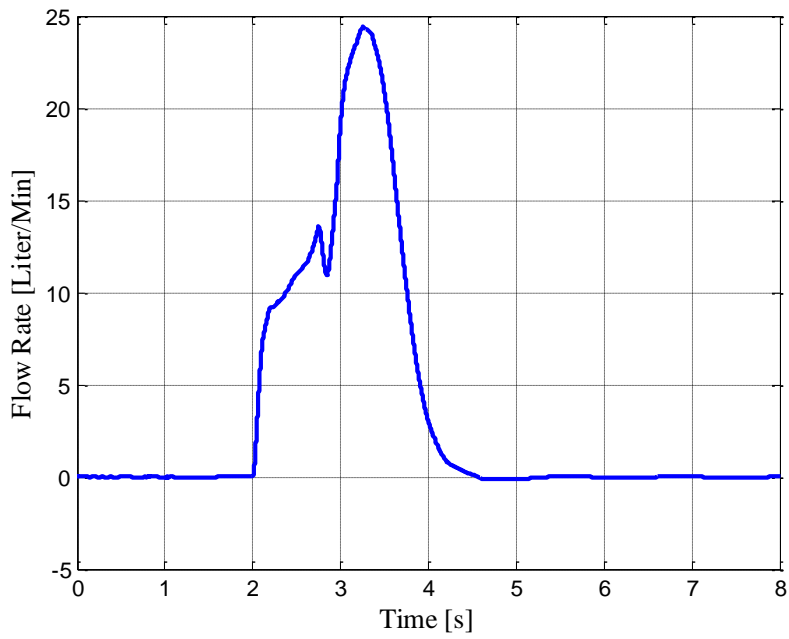


Figure 4.58: Right Suspension Flow Rate

As can be seen from Figure 4.54, the active suspension system has lower roll angle response than the passive suspension system. Active suspension system can drive the

suspension deflection and thus the roll angle to considerably small steady state values. Moreover, similar to the compromise solution between the vehicle attitude and ride comfort, there is also a compromise solution between ride comfort and vehicle handling. Increasing the values of the weighting coefficients for the suspension deflection improves the vehicle handling performance by reducing the roll angle. However, this diminishes the ride comfort performance by increasing the vertical and the roll accelerations.

4.3.1.6.3. Double Lane Change

The handling performance of the active controller in roll vehicle plane is examined by the double lane change maneuver as well. Similar to the previous case, the lateral acceleration response is taken from the simulation of the bicycle model. Lateral acceleration response for the double lane change maneuver at 90 kph is shown Figure 4.59.

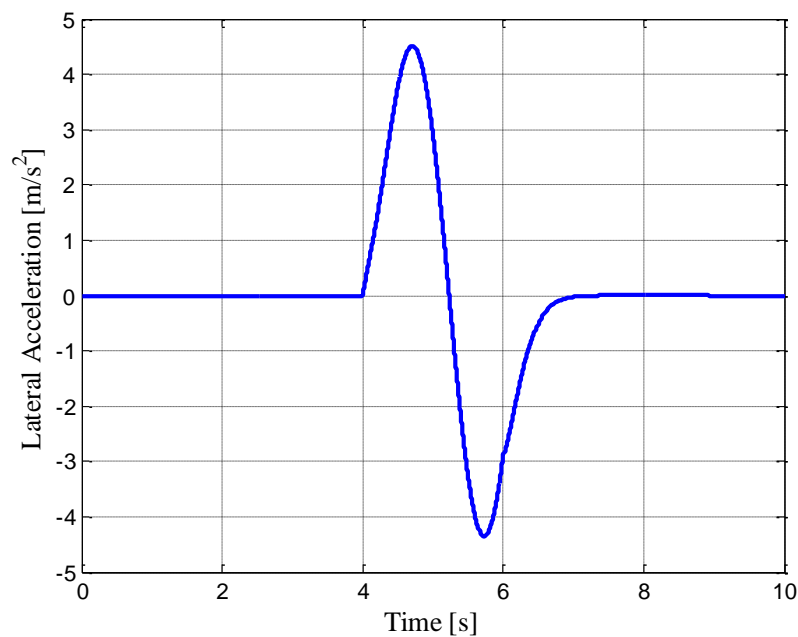


Figure 4.59: Lateral Acceleration

Simulation results are given in Figure 4.60 to Figure 4.66.

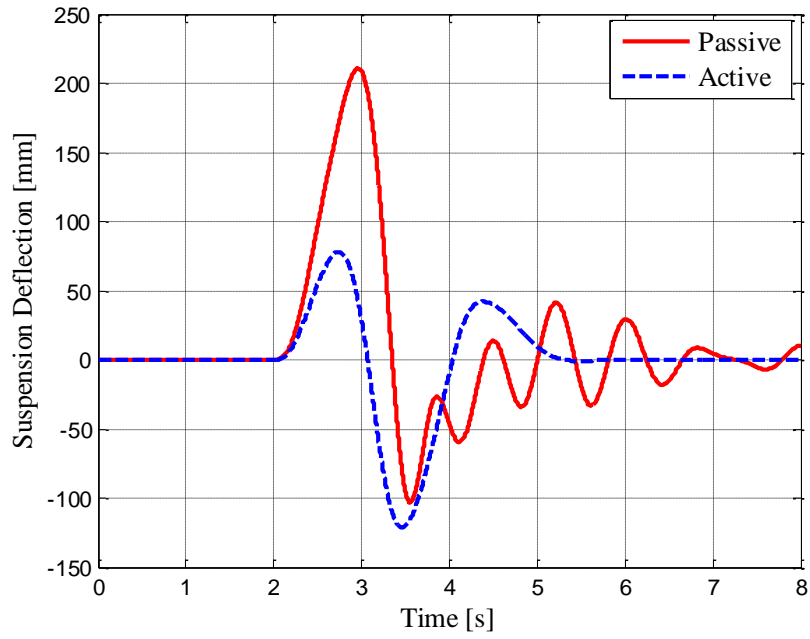


Figure 4.60: Left Suspension Deflection

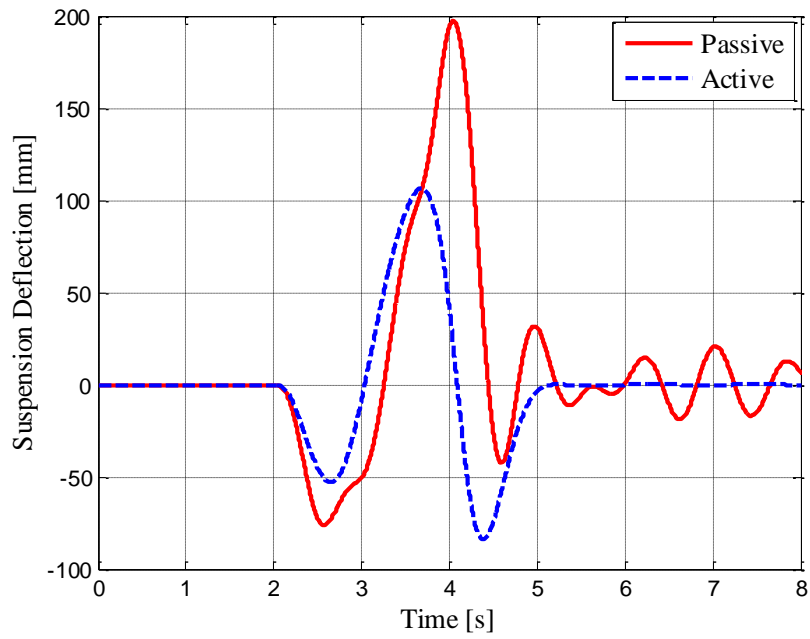


Figure 4.61: Right Suspension Deflection

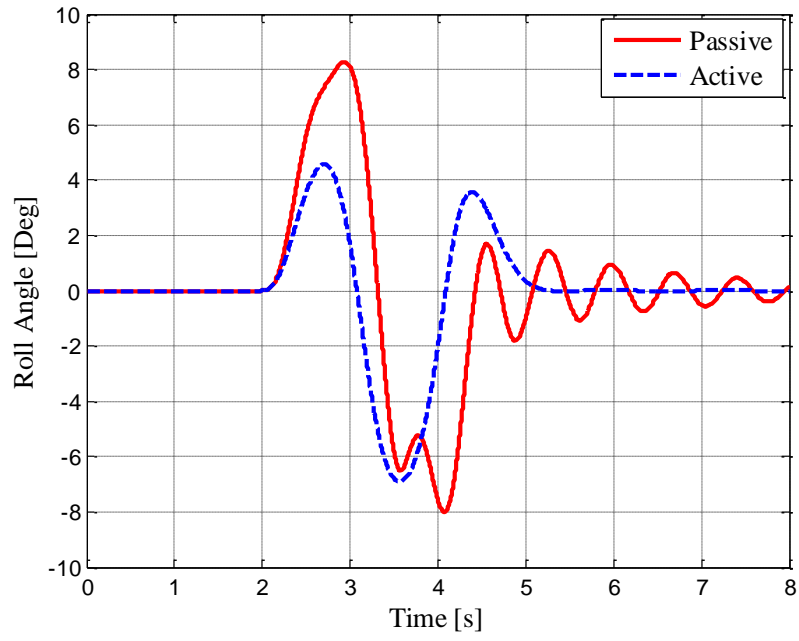


Figure 4.62: Roll Angle

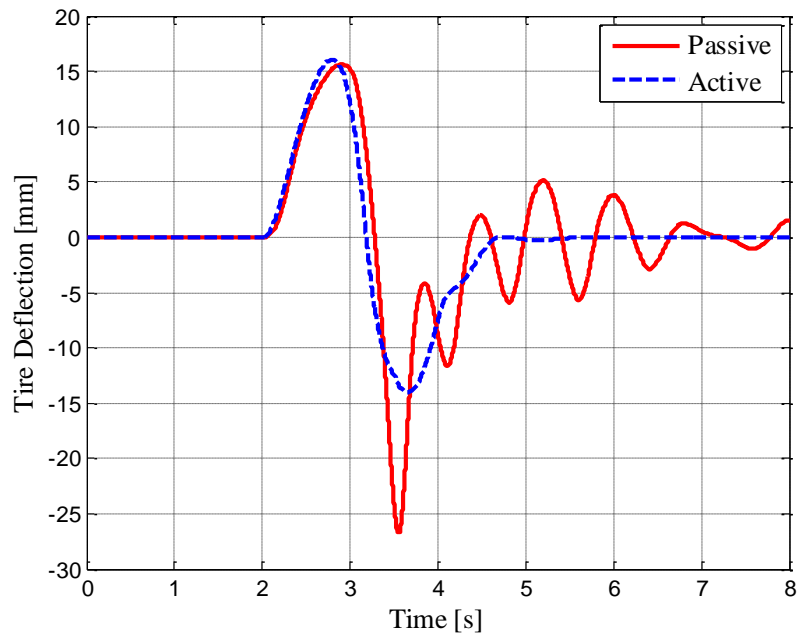


Figure 4.63: Left Tire Deflection

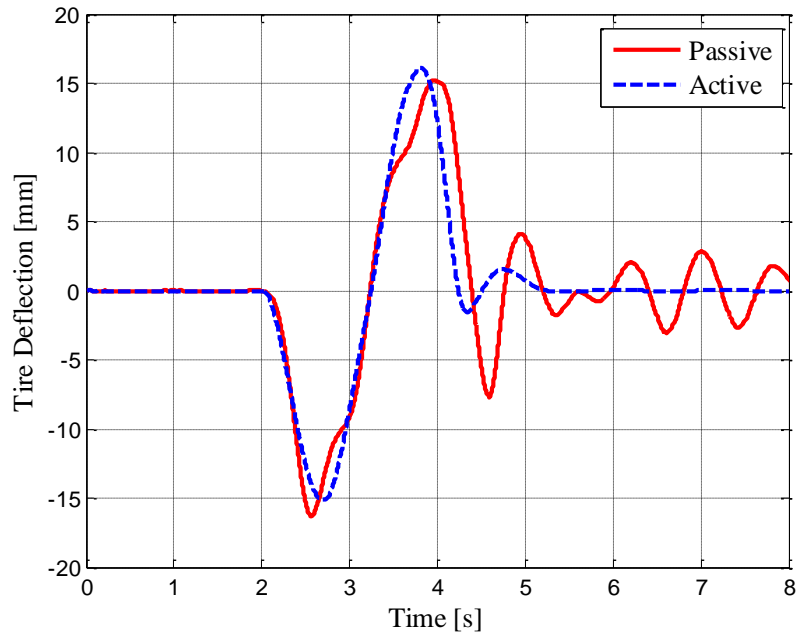


Figure 4.64: Right Tire Deflection

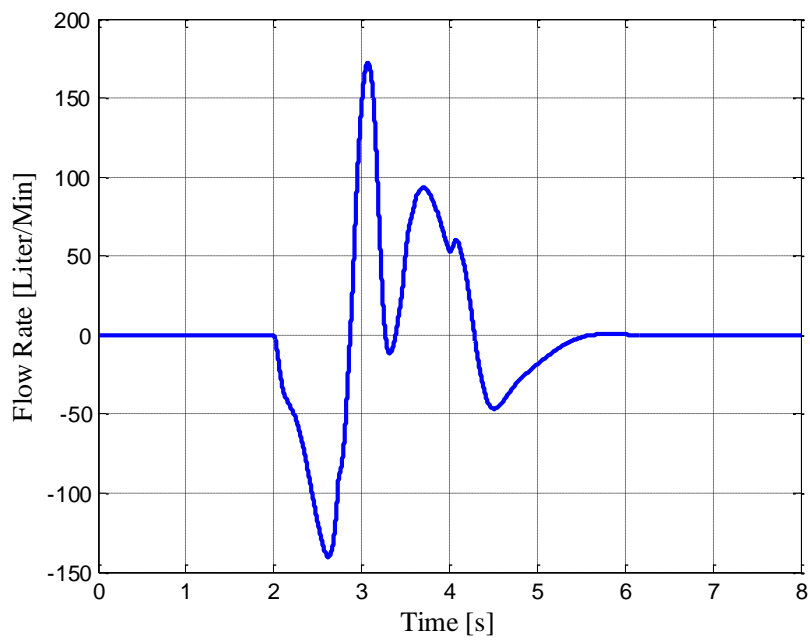


Figure 4.65: Left Suspension Flow Rate

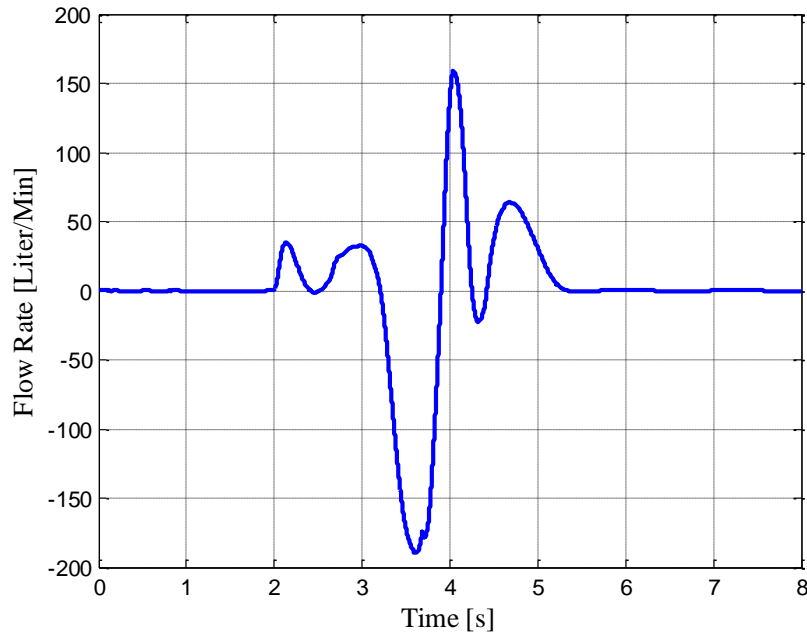


Figure 4.66: Right Suspension Flow Rate

As Figure 4.62 illustrates, the active suspension system has slightly better roll angle performance than the passive suspension system. However, since the double lane change maneuver is severe and highly transient, the weighting of the suspension deflections in the controller design may be increased to improve the vehicle handling further.

4.3.2. Conclusion

In this chapter, the performance of the active half vehicle model with HP suspension in roll plane is investigated. An active controller is designed to improve ride comfort, control the suspension deflection at steady state, and to improve vehicle handling.

In the next section, an active controller for the full vehicle model with HP suspension system is developed. Full vehicle model has seven degrees of freedom which comprises four tire degrees of freedom, and vertical, pitch, and the roll degrees of freedom of the vehicle body. One of the aims of the controller is to control the vertical, roll, and pitch dynamics of the vehicle. The other aim is to control the vehicle attitude at steady state against disturbances coming from the road and the vehicle body. Firstly, the active full vehicle model with HP suspension systems will

be developed and then the state dependent linear model of the developed nonlinear model will be obtained. After that, the controller will be designed and simulations will be performed both in time and frequency domain to examine the performance of the controller.

4.4. FULL VEHICLE MODEL WITH ACTIVE HP SUSPENSION SYSTEM

4.4.1. Modeling of the Full Vehicle Model with Active HP Suspension System

Schematic of the full vehicle model with active HP suspension system is shown in Figure 4.67. The equation of motion for the full vehicle model with the active suspension system can be derived in a similar way to the case of half vehicle model with the active suspension system. Thus, front left, front right, rear left and the rear right suspension forces can be written as,

$$F_{FL} = \left[\begin{array}{c} \frac{P_{30FL} V_{30FL}^{\kappa}}{[V_{30FL} + A_p z_{fpFL}]^{\kappa}} - P_{Atm} - \frac{M_{fp} g + M_{fp} \ddot{z}_{fpFL} + F_{fpFL} + F_{fpHSFL}}{A_p} \\ - \left[\frac{A_p \dot{z}_{ptFL}}{A_v C_d} \right]^2 \frac{\rho}{2} \text{sign}(\dot{z}_{ptFL}) \end{array} \right] A_p - \quad (4-119)$$

$$-F_{ptFL} - F_{pHSFL}$$

$$F_{FR} = \left[\begin{array}{c} \frac{P_{30FR} V_{30FR}^{\kappa}}{[V_{30FR} + A_p z_{fpFR}]^{\kappa}} - P_{Atm} - \frac{M_{fp} g + M_{fp} \ddot{z}_{fpFR} + F_{fpFR} + F_{fpHSFR}}{A_p} \\ - \left[\frac{A_p \dot{z}_{ptFR}}{A_v C_d} \right]^2 \frac{\rho}{2} \text{sign}(\dot{z}_{ptFR}) \end{array} \right] A_p - \quad (4-120)$$

$$-F_{ptFR} - F_{pHSFR}$$

$$F_{RL} = \left[\begin{array}{c} \frac{P_{30RL} V_{30RL}^{\kappa}}{[V_{30RL} + A_p z_{fpRL}]^{\kappa}} - P_{Atm} - \frac{M_{fp} g + M_{fp} \ddot{z}_{fpRL} + F_{fpRL} + F_{fpHSRL}}{A_p} \\ - \left[\frac{A_p \dot{z}_{ptRL}}{A_v C_d} \right]^2 \frac{\rho}{2} \text{sign}(\dot{z}_{ptRL}) \end{array} \right] A_p - \quad (4-121)$$

$$-F_{ptRL} - F_{pHSRL}$$

$$F_{RR} = \left[\begin{array}{c} \frac{P_{30RR} V_{30RR}^{\kappa}}{[V_{30RR} + A_p z_{fpRR}]^{\kappa}} - P_{Atm} - \frac{M_{fp} g + M_{fp} \ddot{z}_{fpRR} + F_{fpRR} + F_{fpHSRR}}{A_p} \\ - \left[\frac{A_p \dot{z}_{pRR}}{A_v C_d} \right]^2 \frac{\rho}{2} \text{sign}(\dot{z}_{pRR}) \end{array} \right] A_p - (4-122)$$

$$-F_{pRR} - F_{pHSRR}$$

where F_{FL} is the suspension force for front left suspension, F_{FR} is the suspension force for the front right suspension, F_{RL} is the suspension force for the rear left suspension, and the F_{RR} is the suspension force for the rear right suspension. Similarly the equation of motion for the front left tire, front right tire, rear left tire, and the rear right tire can be obtained.

The equation of motion for the vehicle in vertical direction (in +z direction) is,

$$F_{FL} + F_{FR} + F_{RL} + F_{RR} - Mg - F_d = M\ddot{z} \quad (4-123)$$

The equation of motion in roll direction (around +x direction) is,

$$F_{RL} \frac{t_r}{2} - F_{RR} \frac{t_r}{2} + F_{FL} \frac{t_f}{2} - F_{FR} \frac{t_f}{2} - M_{D\phi} = I_{xx} \ddot{\phi} \quad (4-124)$$

where t_f is the front track width, t_r is the rear track width, I_{xx} is the moment of inertia in roll direction, and ϕ is the roll angle. The equation of motion in pitch direction is,

$$F_{RL} b + F_{RR} b - F_{FL} a - F_{FR} a - M_{D\theta} = I_{yy} \ddot{\theta} \quad (4-125)$$

where a is the distance between front axle and center of gravity, b is the distance between rear axle and center of gravity, I_{yy} is the pitch moment of inertia, and θ is the pitch angle. Assuming small rotations around x and y axes, the following kinematical relationships for displacements can be written.

$$z_{pFL} = z + \frac{t_f}{2} \phi - a\theta \quad (4-126)$$

$$z_{pFR} = z - \frac{t_f}{2} \phi - a\theta \quad (4-127)$$

$$z_{pRL} = z + \frac{t_r}{2} \phi + b\theta \quad (4-128)$$

$$z_{pRR} = z - \frac{t_r}{2} \phi + b\theta \quad (4-129)$$

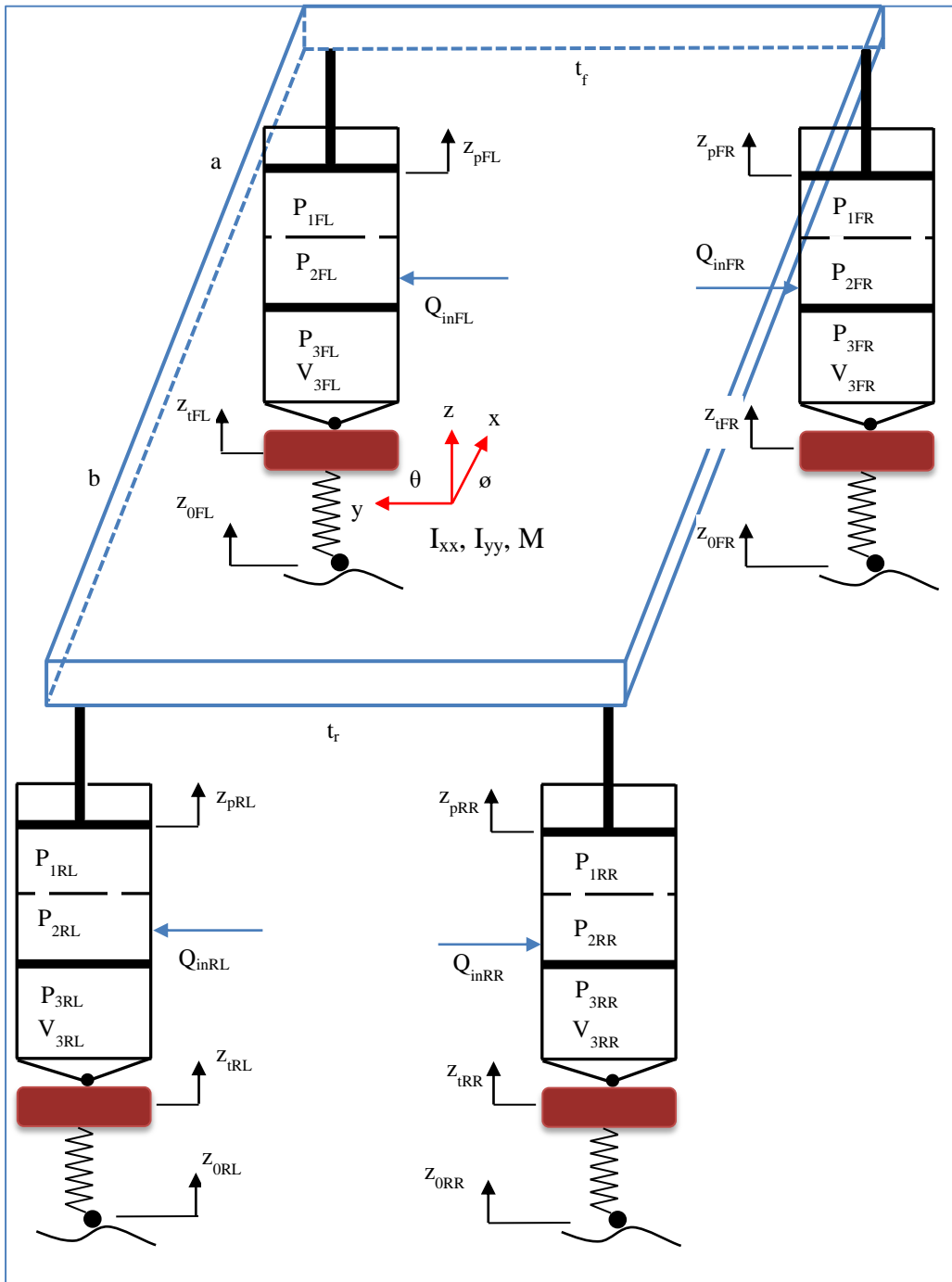


Figure 4.67. Full Vehicle Model with Active Suspension

4.4.2. Static Analysis of the Full Vehicle Model with HP Suspension System

In static condition, assuming left and right symmetry, the suspension forces become,

$$F_{FL} = F_{FR} = \frac{Mgb}{2(a+b)} \quad (4-130)$$

$$F_{RL} = F_{RR} = \frac{Mga}{2(a+b)} \quad (4-131)$$

Therefore, the absolute gas pressures at the static equilibrium become,

$$P_{30FL} = \frac{F_{FL} + M_{fp}g}{A_p} + P_{Atm} \quad (4-132)$$

$$P_{30FR} = \frac{F_{FR} + M_{fp}g}{A_p} + P_{Atm} \quad (4-133)$$

$$P_{30RL} = \frac{F_{RL} + M_{fp}g}{A_p} + P_{Atm} \quad (4-134)$$

$$P_{30RR} = \frac{F_{RR} + M_{fp}g}{A_p} + P_{Atm} \quad (4-135)$$

The gas forces can be expressed as,

$$F_{gasFL} = \frac{P_{30FL} V_{30FL}^{\kappa} A_p}{\left[V_{30FL} + A_p (z_{fpFL} - z_{tFL}) \right]^{\kappa}} - P_{Atm} A_p \quad (4-136)$$

$$F_{gasFR} = \frac{P_{30FR} V_{30FR}^{\kappa} A_p}{\left[V_{30FR} + A_p (z_{fpFR} - z_{tFR}) \right]^{\kappa}} - P_{Atm} A_p \quad (4-137)$$

$$F_{gasRL} = \frac{P_{30RL} V_{30RL}^{\kappa} A_p}{\left[V_{30RL} + A_p (z_{fpRL} - z_{tRL}) \right]^{\kappa}} - P_{Atm} A_p \quad (4-138)$$

$$F_{gasRR} = \frac{P_{30RR} V_{30RR}^{\kappa} A_p}{\left[V_{30RR} + A_p (z_{fpRR} - z_{tRR}) \right]^{\kappa}} - P_{Atm} A_p \quad (4-139)$$

4.4.3. Vertical Stiffness of the Full Vehicle Model

The total suspension force in vertical direction is,

$$F_z = F_{\text{gasFL}} + F_{\text{gasFR}} + F_{\text{gasRL}} + F_{\text{gasRR}} \quad (4-140)$$

Assume that all suspension deflections are equal to each other,

$$z_{\text{fpFL}} - z_{\text{tFL}} = z_{\text{pFL}} - z_{\text{tFL}} = z_{\text{ptFL}} = z_{\text{pt}} \quad (4-141)$$

$$z_{\text{fpFR}} - z_{\text{tFR}} = z_{\text{pFR}} - z_{\text{tFR}} = z_{\text{ptFR}} = z_{\text{pt}} \quad (4-142)$$

$$z_{\text{fpRL}} - z_{\text{tRL}} = z_{\text{pRL}} - z_{\text{tRL}} = z_{\text{ptRL}} = z_{\text{pt}} \quad (4-143)$$

$$z_{\text{fpRR}} - z_{\text{tRR}} = z_{\text{pRR}} - z_{\text{tRR}} = z_{\text{ptRR}} = z_{\text{pt}} \quad (4-144)$$

Then the vertical stiffness of the suspension is,

$$\begin{aligned} k = -\frac{dF_z}{dz_{\text{pt}}} &= \frac{\kappa P_{30FL} V_{30FL}^\kappa A_p^2}{[V_{30FL} + A_p z_{\text{pt}}]^{\kappa+1}} + \frac{\kappa P_{30FR} V_{30FR}^\kappa A_p^2}{[V_{30FR} + A_p z_{\text{pt}}]^{\kappa+1}} + \\ &+ \frac{\kappa P_{30RL} V_{30RL}^\kappa A_p^2}{[V_{30RL} + A_p z_{\text{pt}}]^{\kappa+1}} + \frac{\kappa P_{30RR} V_{30RR}^\kappa A_p^2}{[V_{30RR} + A_p z_{\text{pt}}]^{\kappa+1}} \end{aligned} \quad (4-145)$$

At static equilibrium, the suspension stiffness become,

$$k = -\frac{dF_z}{dz_{\text{pt}}} = \frac{\kappa P_{30FL} A_p^2}{V_{30FL}} + \frac{\kappa P_{30FR} A_p^2}{V_{30FR}} + \frac{\kappa P_{30RL} A_p^2}{V_{30RL}} + \frac{\kappa P_{30RR} A_p^2}{V_{30RR}} \quad (4-146)$$

4.4.4. Roll Stiffness of the Full Vehicle Model

Roll moment created by the suspension forces is,

$$M_\phi = \frac{t_f}{2} (F_{\text{gasFL}} - F_{\text{gasFR}}) + \frac{t_r}{2} (F_{\text{gasRL}} - F_{\text{gasRR}}) \quad (4-147)$$

Inserting the suspension forces obtained previously into Equation (4-147), an explicit equation for the roll moment can be obtained as,

$$\begin{aligned}
M_\phi = & \frac{t_f}{2} \left(\frac{\frac{P_{30FL} V_{30FL}^\kappa A_p}{\left[V_{30FL} + A_p \left(z + \frac{t_f}{2} \phi - a\theta - z_{tFL} \right) \right]^\kappa}}{\frac{P_{30FR} V_{30FR}^\kappa A_p}{\left[V_{30FR} + A_p \left(z - \frac{t_f}{2} \phi - a\theta - z_{tFR} \right) \right]^\kappa}} \right) + \\
& + \frac{t_r}{2} \left(\frac{\frac{P_{30RL} V_{30RL}^\kappa A_p}{\left[V_{30RL} + A_p \left(z + \frac{t_r}{2} \phi + b\theta - z_{tRL} \right) \right]^\kappa}}{\frac{P_{30RR} V_{30RR}^\kappa A_p}{\left[V_{30RR} + A_p \left(z - \frac{t_r}{2} \phi + b\theta - z_{tRR} \right) \right]^\kappa}} \right)
\end{aligned} \tag{4-148}$$

Assuming that the vertical displacement and the pitch angle are both zero, the only motion is the roll motion with the roll angle ϕ , roll moment becomes

$$\begin{aligned}
M_\phi = & \frac{t_f}{2} \left(\frac{\frac{P_{30FL} V_{30FL}^\kappa A_p}{\left[V_{30FL} + A_p \frac{t_f}{2} \phi \right]^\kappa}}{\frac{P_{30FR} V_{30FR}^\kappa A_p}{\left[V_{30FR} - A_p \frac{t_f}{2} \phi \right]^\kappa}} \right) + \\
& + \frac{t_r}{2} \left(\frac{\frac{P_{30RL} V_{30RL}^\kappa A_p}{\left[V_{30RL} + A_p \frac{t_r}{2} \phi \right]^\kappa}}{\frac{P_{30RR} V_{30RR}^\kappa A_p}{\left[V_{30RR} - A_p \frac{t_r}{2} \phi \right]^\kappa}} \right)
\end{aligned} \tag{4-149}$$

Then the roll stiffness can be derived as,

$$\begin{aligned}
k_\phi = & -\frac{dM_\phi}{d\phi} = \frac{t_f}{2} \left(\frac{\frac{\kappa \frac{t_f}{2} P_{30FL} V_{30FL}^\kappa A_p^2}{\left[V_{30FL} + A_p \frac{t_f}{2} \phi \right]^{\kappa+1}}}{\frac{\kappa \frac{t_f}{2} P_{30FR} V_{30FR}^\kappa A_p^2}{\left[V_{30FR} - A_p \frac{t_f}{2} \phi \right]^{\kappa+1}}} \right) + \\
& + \frac{t_r}{2} \left(\frac{\frac{\kappa \frac{t_r}{2} P_{30RL} V_{30RL}^\kappa A_p^2}{\left[V_{30RL} + A_p \frac{t_r}{2} \phi \right]^{\kappa+1}}}{\frac{\kappa \frac{t_r}{2} P_{30RR} V_{30RR}^\kappa A_p^2}{\left[V_{30RR} - A_p \frac{t_r}{2} \phi \right]^{\kappa+1}}} \right)
\end{aligned} \tag{4-150}$$

At static equilibrium the roll stiffness become,

$$k_{\phi} = -\frac{dM_{\phi}}{d\phi} = \frac{\kappa \frac{t_f^2}{4} P_{30FL} A_p^2}{V_{30FL}} + \frac{\kappa \frac{t_f^2}{4} P_{30FR} A_p^2}{V_{30FR}} + \frac{\kappa \frac{t_r^2}{4} P_{30RL} A_p^2}{V_{30RL}} + \frac{\kappa \frac{t_r^2}{4} P_{30RR} A_p^2}{V_{30RR}} \quad (4-151)$$

4.4.5. Pitch Stiffness of the Full Vehicle Model

Similarly the pitch moment created by the suspension forces is,

$$M_{\theta} = -a(F_{gasFL} + F_{gasFR}) + b(F_{gasRL} + F_{gasRR}) \quad (4-152)$$

When the suspension force expressions are inserted into Equation (4-152), the pitch moment becomes

$$M_{\theta} = -a \left(\frac{P_{30FL} V_{30FL}^{\kappa} A_p}{\left[V_{30FL} + A_p \left(z + \frac{t_f}{2} \phi - a\theta - z_{tFL} \right) \right]^{\kappa}} + \frac{P_{30FR} V_{30FR}^{\kappa} A_p}{\left[V_{30FR} + A_p \left(z - \frac{t_f}{2} \phi - a\theta - z_{tFR} \right) \right]^{\kappa}} \right) + b \left(\frac{P_{30RL} V_{30RL}^{\kappa} A_p}{\left[V_{30RL} + A_p \left(z + \frac{t_r}{2} \phi + b\theta - z_{tRL} \right) \right]^{\kappa}} + \frac{P_{30RR} V_{30RR}^{\kappa} A_p}{\left[V_{30RR} + A_p \left(z - \frac{t_r}{2} \phi + b\theta - z_{tRR} \right) \right]^{\kappa}} \right) \quad (4-153)$$

Assuming that the only motion is the pitch motion, then the pitch moment can be obtained as,

$$M_{\theta} = -a \left(\frac{P_{30FL} V_{30FL}^{\kappa} A_p}{\left[V_{30FL} - A_p a\theta \right]^{\kappa}} + \frac{P_{30FR} V_{30FR}^{\kappa} A_p}{\left[V_{30FR} - A_p a\theta \right]^{\kappa}} \right) + b \left(\frac{P_{30RL} V_{30RL}^{\kappa} A_p}{\left[V_{30RL} + A_p b\theta \right]^{\kappa}} + \frac{P_{30RR} V_{30RR}^{\kappa} A_p}{\left[V_{30RR} + A_p b\theta \right]^{\kappa}} \right) \quad (4-154)$$

Finally, the pitch stiffness is found as,

$$k_{\theta} = -\frac{dM_{\theta}}{d\theta} = \left(\frac{a^2 P_{30FL} V_{30FL}^{\kappa} A_p^2}{[V_{30FL} - A_p a\theta]^{\kappa+1}} + \frac{a^2 P_{30FR} V_{30FR}^{\kappa} A_p^2}{[V_{30FR} - A_p a\theta]^{\kappa+1}} \right) + \left(\frac{b^2 P_{30RL} V_{30RL}^{\kappa} A_p^2}{[V_{30RL} + A_p b\theta]^{\kappa+1}} + \frac{b^2 P_{30RR} V_{30RR}^{\kappa} A_p^2}{[V_{30RR} + A_p b\theta]^{\kappa+1}} \right) \quad (4-155)$$

At static condition, the pitch stiffness become,

$$k_{\theta} = \left(\frac{a^2 P_{30FL} A_p^2}{V_{30FL}} + \frac{a^2 P_{30FR} A_p^2}{V_{30FR}} \right) + \left(\frac{b^2 P_{30RL} A_p^2}{V_{30RL}} + \frac{b^2 P_{30RR} A_p^2}{V_{30RR}} \right) \quad (4-156)$$

Detailed examination of the stiffness and damping characteristics of the full vehicle model with HP suspension system is to be presented in Chapter 7.

4.4.6. State Dependent Linear Model of the Full Vehicle Model with the Active HP Suspension System

Now the state space model of the full vehicle with active HP suspension system is to be derived. Vehicle with four tires forms a statically indeterminate structure. For the sprung mass, three equilibrium equations in vertical, roll, and pitch directions can be written. Thus, in order to satisfy the equilibrium equations, three suspension forces are needed. Similar to the full vehicle model with four tires, depending on the initial suspension configurations, different solutions can be obtained. In the literature, studies of active suspension control of full vehicle model, four tire displacements and four suspension deflections are used as the states. However, as explained by Esmailzadeh and Fahimi [66], one of the tire deflections can be written in terms of the other states. By this way, 14 states are enough to define the complete full vehicle model with the HP suspension systems. The remaining states like suspension, integral of the suspension deflection, etc. are required to improve the vehicle performance in controller design. In summary, three states for the vertical, roll, and pitch velocities of the sprung mass, four states for the floating piston displacement, three states for tire deflections, four states for tire velocities, four states for suspension deflection, four states for the integral of the suspension deflections, four states for the double integral of the suspension deflections, and four states for the

road displacement inputs are used to define the full vehicle model with active HP suspension systems. If the fourth tire displacement is also used as the state, there can be problems in the solution of the SDRE. Moreover, in order to get controller which has reference trajectory control, road displacement inputs are also modeled and defined as states using the first order filter equations. In order for the controller to regulate the suspension deflections to zero values for ramp road inputs, second integral of the suspension deflections are used as the states. By this way, type of the system can be increased, and thus the controller has zero steady state responses for ramp input. Thus, the states are defined as

$$x_1 = \dot{z} \quad (4-157)$$

$$x_2 = \dot{\phi} \quad (4-158)$$

$$x_3 = \dot{\theta} \quad (4-159)$$

$$x_4 = z_{\text{fpFL}} = z_{\text{pFL}} - z_{\text{tFL}} \quad (4-160)$$

$$x_5 = z_{\text{fpFR}} = z_{\text{pFR}} - z_{\text{tFR}} \quad (4-161)$$

$$x_6 = z_{\text{fpRL}} = z_{\text{pRL}} - z_{\text{tRL}} \quad (4-162)$$

$$x_7 = z_{\text{fpRR}} = z_{\text{pRR}} - z_{\text{tRR}} \quad (4-163)$$

$$x_8 = z_{\text{ptFL}} = z_{\text{pFL}} - z_{\text{tFL}} \quad (4-164)$$

$$x_9 = z_{\text{ptFR}} = z_{\text{pFR}} - z_{\text{tFR}} \quad (4-165)$$

$$x_{10} = z_{\text{ptRL}} = z_{\text{pRL}} - z_{\text{tRL}} \quad (4-166)$$

$$x_{11} = z_{\text{ptRR}} = z_{\text{pRR}} - z_{\text{tRR}} \quad (4-167)$$

$$x_{12} = z_{\text{tFL}} \quad (4-168)$$

$$x_{13} = z_{\text{tFR}} \quad (4-169)$$

$$x_{14} = z_{\text{tRL}} \quad (4-170)$$

$$x_{15} = \dot{z}_{\text{tFL}} \quad (4-171)$$

$$x_{16} = \dot{z}_{\text{tFR}} \quad (4-172)$$

$$x_{17} = \dot{z}_{\text{tRL}} \quad (4-173)$$

$$x_{18} = \dot{z}_{\text{tRR}} \quad (4-174)$$

$$X_{19} = Z_{0FL} \quad (4-175)$$

$$X_{20} = Z_{0FR} \quad (4-176)$$

$$X_{21} = Z_{0RL} \quad (4-177)$$

$$X_{22} = Z_{0RR} \quad (4-178)$$

$$X_{23} = \int Z_{ptFL} \quad (4-179)$$

$$X_{24} = \int Z_{ptFR} \quad (4-180)$$

$$X_{25} = \int Z_{ptRL} \quad (4-181)$$

$$X_{26} = \int Z_{ptRR} \quad (4-182)$$

$$X_{27} = \iint Z_{ptFL} \quad (4-183)$$

$$X_{28} = \iint Z_{ptFR} \quad (4-184)$$

$$X_{29} = \iint Z_{ptRL} \quad (4-185)$$

$$X_{30} = \iint Z_{ptRR} \quad (4-186)$$

Assume that the floating piston dynamics and friction forces are negligible, then the equations of motions become,

$$F_{FL} = \left[\begin{array}{l} \frac{P_{30FL} V_{30FL}^{\kappa}}{\left[V_{30FL} + A_p (z_{fpFL} - z_{tFL}) \right]^{\kappa}} - P_{Atm} - \frac{M_{fp} g}{A_p} - \\ - \left[\frac{A_p \left(\dot{z} + \frac{t_f}{2} \dot{\phi} - a\dot{\theta} - \dot{z}_{tFL} \right)}{A_v C_d} \right]^2 \frac{\rho}{2} \text{sign} \left(\dot{z} + \frac{t_f}{2} \dot{\phi} - a\dot{\theta} - \dot{z}_{tFL} \right) \end{array} \right] A_p \quad (4-187)$$

$$F_{FR} = \left[\begin{array}{l} \frac{P_{30FR} V_{30FR}^{\kappa}}{\left[V_{30FR} + A_p (z_{fpFR} - z_{tFR}) \right]^{\kappa}} - P_{Atm} - \frac{M_{fp} g}{A_p} - \\ - \left[\frac{A_p \left(\dot{z} - \frac{t_f}{2} \dot{\phi} - a\dot{\theta} - \dot{z}_{tFR} \right)}{A_v C_d} \right]^2 \frac{\rho}{2} \text{sign} \left(\dot{z} - \frac{t_f}{2} \dot{\phi} - a\dot{\theta} - \dot{z}_{tFR} \right) \end{array} \right] A_p \quad (4-188)$$

$$F_{RL} = \left[\begin{array}{l} \left[\frac{P_{30RL} V_{30RL}^k}{V_{30RL} + A_p (z_{fpRL} - z_{tRL})} - P_{Atm} - \frac{M_{fp} g}{A_p} \right. \\ \left. - \frac{A_p \left(\dot{z} + \frac{t_r}{2} \dot{\phi} + b\dot{\theta} - \dot{z}_{tRL} \right)}{A_v C_d} \right]^2 \frac{\rho}{2} \text{sign} \left(\dot{z} + \frac{t_r}{2} \dot{\phi} + b\dot{\theta} - \dot{z}_{tRL} \right) \end{array} \right] A \quad (4-189)$$

$$F_{RR} = \left[\begin{array}{l} \left[\frac{P_{30RR} V_{30RR}^k}{V_{30RR} + A_p (z_{fpRR} - z_{tRR})} - P_{Atm} - \frac{M_{fp} g}{A_p} \right. \\ \left. - \frac{A_p \left(\dot{z} - \frac{t_r}{2} \dot{\phi} + b\dot{\theta} - \dot{z}_{tRR} \right)}{A_v C_d} \right]^2 \frac{\rho}{2} \text{sign} \left(\dot{z} - \frac{t_r}{2} \dot{\phi} + b\dot{\theta} - \dot{z}_{tRR} \right) \end{array} \right] A_p \quad (4-190)$$

Then, the state equations become,

$$\dot{x}_1 = \frac{1}{M} \left\{ \begin{array}{l} f_{1FL} x_4 + f_{1FR} x_5 + f_{1RL} x_6 + f_{1RR} x_7 - f_{2FL} \left(x_1 + \frac{t_f}{2} x_2 - ax_3 - x_{15} \right) - \\ - f_{2FR} \left(x_1 - \frac{t_f}{2} x_2 - ax_3 - x_{16} \right) - f_{2RL} \left(x_1 + \frac{t_r}{2} x_2 + bx_3 - x_{17} \right) - \\ - f_{2RR} \left(x_1 - \frac{t_r}{2} x_2 + bx_3 - x_{18} \right) \end{array} \right\} \quad (4-191)$$

$$\dot{x}_2 = \frac{1}{I_{xx}} \left\{ \begin{array}{l} \frac{t_f}{2} \left[\begin{array}{l} f_{1FL} x_4 - f_{2FL} \left(x_1 + \frac{t_f}{2} x_2 - ax_3 - x_{15} \right) - f_{1FR} x_5 + \\ + f_{2FR} \left(x_1 - \frac{t_f}{2} x_2 - ax_3 - x_{16} \right) \end{array} \right] + \\ + \frac{t_r}{2} \left[\begin{array}{l} f_{1RL} x_6 - f_{2RL} \left(x_1 + \frac{t_r}{2} x_2 + bx_3 - x_{17} \right) - f_{1RR} x_7 + \\ + f_{2RR} \left(x_1 - \frac{t_r}{2} x_2 + bx_3 - x_{18} \right) \end{array} \right] \end{array} \right\} \quad (4-192)$$

$$\dot{\mathbf{x}}_3 = \frac{1}{\mathbf{I}_{yy}} \left\{ \begin{array}{l} -\mathbf{a} \left[\begin{array}{l} \mathbf{f}_{1FL} \mathbf{x}_4 - \mathbf{f}_{2FL} \left(\mathbf{x}_1 + \frac{\mathbf{t}_f}{2} \mathbf{x}_2 - \mathbf{a} \mathbf{x}_3 - \mathbf{x}_{15} \right) + \mathbf{f}_{1FR} \mathbf{x}_5 - \\ - \mathbf{f}_{2FR} \left(\mathbf{x}_1 - \frac{\mathbf{t}_f}{2} \mathbf{x}_2 - \mathbf{a} \mathbf{x}_3 - \mathbf{x}_{16} \right) \end{array} \right] + \\ + \mathbf{b} \left[\begin{array}{l} \mathbf{f}_{1RL} \mathbf{x}_6 - \mathbf{f}_{2RL} \left(\mathbf{x}_1 + \frac{\mathbf{t}_r}{2} \mathbf{x}_2 + \mathbf{b} \mathbf{x}_3 - \mathbf{x}_{17} \right) + \mathbf{f}_{1RR} \mathbf{x}_7 - \\ - \mathbf{f}_{2RR} \left(\mathbf{x}_1 - \frac{\mathbf{t}_r}{2} \mathbf{x}_2 + \mathbf{b} \mathbf{x}_3 - \mathbf{x}_{18} \right) \end{array} \right] \end{array} \right\} \quad (4-193)$$

$$\dot{\mathbf{x}}_4 = \mathbf{x}_1 + \frac{\mathbf{t}_f}{2} \mathbf{x}_2 - \mathbf{a} \mathbf{x}_3 - \mathbf{x}_{15} - \frac{\mathbf{Q}_{inFL}}{\mathbf{A}_p} \quad (4-194)$$

$$\dot{\mathbf{x}}_5 = \mathbf{x}_1 - \frac{\mathbf{t}_f}{2} \mathbf{x}_2 - \mathbf{a} \mathbf{x}_3 - \mathbf{x}_{16} - \frac{\mathbf{Q}_{inFR}}{\mathbf{A}_p} \quad (4-195)$$

$$\dot{\mathbf{x}}_6 = \mathbf{x}_1 + \frac{\mathbf{t}_r}{2} \mathbf{x}_2 + \mathbf{b} \mathbf{x}_3 - \mathbf{x}_{17} - \frac{\mathbf{Q}_{inRL}}{\mathbf{A}_p} \quad (4-196)$$

$$\dot{\mathbf{x}}_7 = \mathbf{x}_1 - \frac{\mathbf{t}_r}{2} \mathbf{x}_2 + \mathbf{b} \mathbf{x}_3 - \mathbf{x}_{18} - \frac{\mathbf{Q}_{inRR}}{\mathbf{A}_p} \quad (4-197)$$

$$\dot{\mathbf{x}}_8 = \mathbf{x}_1 + \frac{\mathbf{t}_f}{2} \mathbf{x}_2 - \mathbf{a} \mathbf{x}_3 - \mathbf{x}_{15} \quad (4-198)$$

$$\dot{\mathbf{x}}_9 = \mathbf{x}_1 - \frac{\mathbf{t}_f}{2} \mathbf{x}_2 - \mathbf{a} \mathbf{x}_3 - \mathbf{x}_{16} \quad (4-199)$$

$$\dot{\mathbf{x}}_{10} = \mathbf{x}_1 + \frac{\mathbf{t}_r}{2} \mathbf{x}_2 + \mathbf{b} \mathbf{x}_3 - \mathbf{x}_{17} \quad (4-200)$$

$$\dot{\mathbf{x}}_{11} = \mathbf{x}_1 - \frac{\mathbf{t}_r}{2} \mathbf{x}_2 + \mathbf{b} \mathbf{x}_3 - \mathbf{x}_{18} \quad (4-201)$$

$$\dot{\mathbf{x}}_{12} = \mathbf{x}_{15} \quad (4-202)$$

$$\dot{\mathbf{x}}_{13} = \mathbf{x}_{16} \quad (4-203)$$

$$\dot{\mathbf{x}}_{14} = \mathbf{x}_{17} \quad (4-204)$$

$$\dot{\mathbf{x}}_{15} = -\frac{1}{\mathbf{M}_t} \left\{ \mathbf{k}_t (\mathbf{x}_{12} - \mathbf{x}_{19}) + \mathbf{f}_{1FL} \mathbf{x}_4 - \mathbf{f}_{2FL} \left(\mathbf{x}_1 + \frac{\mathbf{t}_f}{2} \mathbf{x}_2 - \mathbf{a} \mathbf{x}_3 - \mathbf{x}_{15} \right) \right\} \quad (4-205)$$

$$\dot{\mathbf{x}}_{16} = -\frac{1}{\mathbf{M}_t} \left\{ \mathbf{k}_t (\mathbf{x}_{13} - \mathbf{x}_{20}) + \mathbf{f}_{1FR} \mathbf{x}_5 - \mathbf{f}_{2FR} \left(\mathbf{x}_1 - \frac{\mathbf{t}_f}{2} \mathbf{x}_2 - \mathbf{a} \mathbf{x}_3 - \mathbf{x}_{16} \right) \right\} \quad (4-206)$$

$$\dot{x}_{17} = -\frac{1}{M_t} \left\{ k_t (x_{14} - x_{21}) + f_{1RL} x_6 - f_{2RL} \left(x_1 + \frac{t_r}{2} x_2 + b x_3 - x_{17} \right) \right\} \quad (4-207)$$

$$\dot{x}_{18} = -\frac{1}{M_t} \left\{ k_t \left(x_{10} - x_{11} + x_{14} - x_{22} - \frac{t_r}{t_f} (x_8 - x_9 + x_{12} - x_{13}) \right) + \right. \\ \left. + f_{1RR} x_7 - f_{2RR} \left(x_1 - \frac{t_r}{2} x_2 + b x_3 - x_{18} \right) \right\} \quad (4-208)$$

$$\dot{x}_{19} = -R_v x_{19} + w_{FL} \quad (4-209)$$

$$\dot{x}_{20} = -R_v x_{20} + w_{FR} \quad (4-210)$$

$$\dot{x}_{21} = -R_v x_{21} + w_{RL} \quad (4-211)$$

$$\dot{x}_{22} = -R_v x_{22} + w_{RR} \quad (4-212)$$

$$\dot{x}_{23} = x_8 \quad (4-213)$$

$$\dot{x}_{24} = x_9 \quad (4-214)$$

$$\dot{x}_{25} = x_{10} \quad (4-215)$$

$$\dot{x}_{26} = x_{11} \quad (4-216)$$

$$\dot{x}_{27} = x_{23} \quad (4-217)$$

$$\dot{x}_{28} = x_{24} \quad (4-218)$$

$$\dot{x}_{29} = x_{25} \quad (4-219)$$

$$\dot{x}_{30} = x_{26} \quad (4-220)$$

HP suspension system and vehicle parameters for full vehicle model are given in Table 4.14.

Table 4.14: Suspension and Vehicle Parameters for Full Vehicle Model

Parameter	Symbol	Value
Sprung Mass	M [kg]	6000
Roll Moment of Inertia	I_{xx} [kgm ²]	3545
Pitch Moment of Inertia	I_{yy} [kgm ²]	13376
Distance Between Front Axle and COG	a [m]	1.815
Distance Between Rear Axle and COG	b [m]	1.485
Distance between Front	$h_{RC-COGL}$ [m]	1.1

Roll Center and COG		
Distance between Rear Roll Center and COG	$h_{RC-COGR}$ [m]	1.1
Front Track Width	t_f [m]	2
Rear Track Width	t_r [m]	2
Front Left Suspension Initial Gas Volume	V_{30FL} [m ³]	0.0019
Front Right Suspension Initial Gas Volume	V_{30FR} [m ³]	0.0019
Rear Left Suspension Initial Gas Volume	V_{30RL} [m ³]	0.0019
Rear Right Suspension Initial Gas Volume	V_{30RR} [m ³]	0.0019
Front Left Suspension Orifice Opening	A_{vFL} [m ²]	2e-4
Front Right Suspension Orifice Opening	A_{vFR} [m ²]	2e-4
Rear Left Suspension Orifice Opening	A_{vRL} [m ²]	2e-4
Rear Right Suspension Orifice Opening	A_{vRR} [m ²]	2e-4
Front Left Suspension Piston Area	A_{pFL} [m ²]	0.007
Front Right Suspension Piston Area	A_{pFR} [m ²]	0.007
Rear Left Suspension Piston Area	A_{pRL} [m ²]	0.007
Rear Right Suspension Piston Area	A_{pRR} [m ²]	0.007

4.4.7. Design of the Controller for the Full Vehicle Model with Active HP Suspensions

The aim of the controller is to improve vehicle ride comfort, to control the vehicle attitude or the suspension deflections, and to improve the vehicle handling. The performance index to be minimized is,

$$\mathbf{J} = \frac{1}{2} \int_0^{\infty} \left\{ \begin{aligned}
& q_1 \ddot{z}^2 + q_2 \ddot{\phi}^2 + q_3 \ddot{\theta}^2 + q_4 z_{ptFL}^2 + q_4 z_{ptFR}^2 + q_4 z_{ptRL}^2 + q_4 z_{ptRR}^2 + \\
& + q_5 z_{t0FL}^2 + q_5 z_{t0FR}^2 + q_5 z_{t0RL}^2 + q_5 z_{t0RR}^2 + q_6 \left[\int (z_{ptFL} - z_{ptFLref}) \right]^2 + \\
& + q_6 \left[\int (z_{ptFR} - z_{ptFRref}) \right]^2 + q_6 \left[\int (z_{ptRL} - z_{ptRLref}) \right]^2 + \\
& + q_6 \left[\int (z_{ptRR} - z_{ptRRref}) \right]^2 + q_7 \left[\int \int (z_{ptFL} - z_{ptFLref}) \right]^2 + \\
& + q_7 \left[\int \int (z_{ptFR} - z_{ptFRref}) \right]^2 + q_7 \left[\int \int (z_{ptRL} - z_{ptRLref}) \right]^2 + \\
& + q_7 \left[\int \int (z_{ptRR} - z_{ptRRref}) \right]^2 + q_8 \dot{z}_{ptFL}^2 + q_8 \dot{z}_{ptFR}^2 + q_8 \dot{z}_{ptRL}^2 + q_8 \dot{z}_{ptRR}^2 + \\
& + R_{FL} Q_{inFL}^2 + R_{FR} Q_{inFR}^2 + R_{RL} Q_{inRL}^2 + R_{RR} Q_{inRR}^2
\end{aligned} \right\} dt \quad (4-221)$$

In the performance index, weighting coefficients q_1 , q_2 , and q_3 are used to penalize the vertical, roll and pitch accelerations, respectively. Weighting coefficients q_4 and q_5 are used to decrease the suspension deflections, and tire deflections respectively. In order to improve the steady state performance of the vehicle, integrals of the suspension deflections are included in the performance index by the weighting parameters q_6 and q_7 . Moreover, suspension deflection velocity is weighted by the weighting parameter q_8 in order to increase the specific performances. Finally, in order to get a realistic amount of oil flow rate for real applications, control input which is the oil flow rate is penalized by the weighting coefficients R_{ij} 's in the performance index.

Stability of the active controller can be evaluated like the stability of the active controller for the half vehicle model. However, calculating the rank of the symbolic controllability and the observability matrices are time consuming for active controller for the full vehicle model. Thus, the stability of the active controller is examined according to Theorem 2. Similarly, state space matrices are evaluated at state values in the operating range of the state domain. $\text{rank}[A - \lambda I \quad B] = 30$ for all

eigenvalues λ of A with $\text{Re}\lambda \geq 0$. Moreover, $\text{rank} \begin{bmatrix} A - \lambda I \\ C \end{bmatrix} = 30$ for all eigenvalues λ

of A with $\text{Re}\lambda \geq 0$. Thus, the pair (A, B) and (A, C) are stabilizable and detectable in the linear sense, then the active controller is locally asymptotically stable. When the state space model of the active controller is examined, it is observed that, four states

which are the road displacement inputs, are uncontrollable but stable states. Thus system is stabilizable but not controllable.

4.4.8. Simulations

The performance of the controller will be examined in the time domain. The ride comfort characteristics of the full vehicle model with active and passive suspensions are going to be examined and compared to each other by simulations with random road input. Then, handling characteristics of the full vehicle model with active and passive HP suspension systems are going to be examined by a braking in cornering maneuver. Controller weighting parameters are given in Table 4.15.

Table 4.15: Controller Weighting Parameters

Weighting Parameter	Value
q_1	1e-4
q_2	1e-4
q_3	1e-4
q_4	100
q_5	1e4
q_6	1e4
q_7	10
q_8	1
R_{FL}	1e5
R_{FR}	1e5
R_{RL}	1e5
R_{RR}	1e5

4.4.8.1. Simulation with Random Road Displacement Input

Random road displacement inputs same as those used in section 4.2.4.1 at different vehicle longitudinal speeds are used to simulate the full vehicle model with active suspension. The rms values of the responses are listed in Table 4.16 to Table 4.19.

Table 4.16: rms Values of Responses for the Active and Passive Suspensions at V=60 kph

	Active	Passive
Vertical Acceleration [m/s^2]	0.13	0.46
Roll Acceleration [rad/s^2]	0.15	0.27
Pitch Acceleration [rad/s^2]	0.08	0.23
Front Left Sus. Def. [mm]	5.3	8.2

Front Right Sus. Def. [mm]	5.0	8.9
Rear Left Sus. Def. [mm]	4.0	12.7
Rear Right Sus. Def. [mm]	4.1	13.1
Front Left Tire Def. [mm]	1.0	1.4
Front Right Tire Def. [mm]	1.0	1.5
Rear Left Tire Def. [mm]	1.1	2.1
Rear Right Tire Def. [mm]	1.0	2.1
Front Left Flow Rate [Liter/min]	17.2	-
Front Right Flow Rate [Liter/min]	17.0	-
Rear Left Flow Rate [Liter/min]	18.4	-
Rear Right Flow Rate [Liter/min]	18.3	-

Table 4.17: rms Values of Responses for the Active and Passive Suspensions at V=70 kph

	Active	Passive
Vertical Acceleration [m/s^2]	0.16	0.44
Roll Acceleration [rad/s^2]	0.23	0.58
Pitch Acceleration [rad/s^2]	0.09	0.23
Front Left Sus. Def. [mm]	6.5	11.4
Front Right Sus. Def. [mm]	6.9	11.3
Rear Left Sus. Def. [mm]	5.0	13.4
Rear Right Sus. Def. [mm]	4.8	13.1
Front Left Tire Def. [mm]	1.2	1.8
Front Right Tire Def. [mm]	1.2	1.8
Rear Left Tire Def. [mm]	1.2	2.2
Rear Right Tire Def. [mm]	1.2	2.2
Front Left Flow Rate [Liter/min]	19.1	-
Front Right Flow Rate [Liter/min]	18.9	-
Rear Left Flow Rate [Liter/min]	21.9	-
Rear Right Flow Rate [Liter/min]	21.6	-

Table 4.18: rms Values of Responses for the Active and Passive Suspensions at V=80 kph

	Active	Passive
Vertical Acceleration [m/s^2]	0.21	0.66
Roll Acceleration [rad/s^2]	0.28	0.78
Pitch Acceleration [rad/s^2]	0.12	0.3
Front Left Sus. Def. [mm]	7.5	14.9
Front Right Sus. Def. [mm]	8.0	14.7
Rear Left Sus. Def. [mm]	6.2	19.5
Rear Right Sus. Def. [mm]	6.4	18.7
Front Left Tire Def. [mm]	1.4	2.2
Front Right Tire Def. [mm]	1.4	2.1
Rear Left Tire Def. [mm]	1.4	3.1

Rear Right Tire Def. [mm]	1.4	3.0
Front Left Flow Rate [Liter/min]	21.9	-
Front Right Flow Rate [Liter/min]	21.9	-
Rear Left Flow Rate [Liter/min]	25.1	-
Rear Right Flow Rate [Liter/min]	25.2	-

Table 4.19: rms Values of Responses for the Active and Passive Suspensions at V=90 kph

	Active	Passive
Vertical Acceleration [m/s^2]	0.25	0.63
Roll Acceleration [rad/s^2]	0.34	0.87
Pitch Acceleration [rad/s^2]	0.13	0.27
Front Left Sus. Def. [mm]	8.6	15.6
Front Right Sus. Def. [mm]	8.8	16.3
Rear Left Sus. Def. [mm]	7.1	18.4
Rear Right Sus. Def. [mm]	7.1	17.8
Front Left Tire Def. [mm]	1.5	2.3
Front Right Tire Def. [mm]	1.5	2.3
Rear Left Tire Def. [mm]	1.6	3.0
Rear Right Tire Def. [mm]	1.6	2.9
Front Left Flow Rate [Liter/min]	24.0	-
Front Right Flow Rate [Liter/min]	24.3	-
Rear Left Flow Rate [Liter/min]	27.8	-
Rear Right Flow Rate [Liter/min]	27.4	-

The active suspension controller is designed mainly to improve ride comfort. As can be seen from the rms values of the responses, all vertical, roll, and the pitch accelerations are improved by the active suspension control. With the active suspension control, both suspension deflections and the tire deflection responses are also improved. To get these suspension improvements, the required oil flow rate is feasible.

4.4.8.2. Braking In Cornering Simulation

For handling analysis, braking in cornering test is performed. In this test scenario, a braking force is applied while the vehicle is in steady state turning motion. In the passive suspension, there will be a steady state roll angle due to the disturbance moment created by the steering input and braking force, respectively. However, in

the active suspension, roll and pitch angle deflections will be lowered due to the action of the active suspension control. The lateral and longitudinal accelerations used in the simulation are taken from the full vehicle model derived in Chapter 7 and are given in Figure 4.68 and Figure 4.69. Braking in cornering simulation is performed with a 40 degree steering wheel input at 90 kph. Simulation results are given in Figure 4.70 to Figure 4.83.

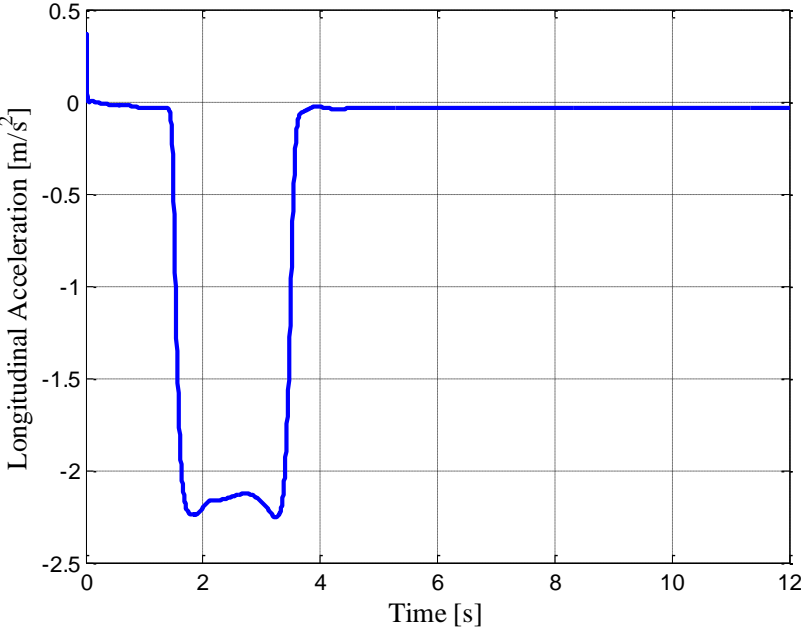


Figure 4.68: Longitudinal Acceleration

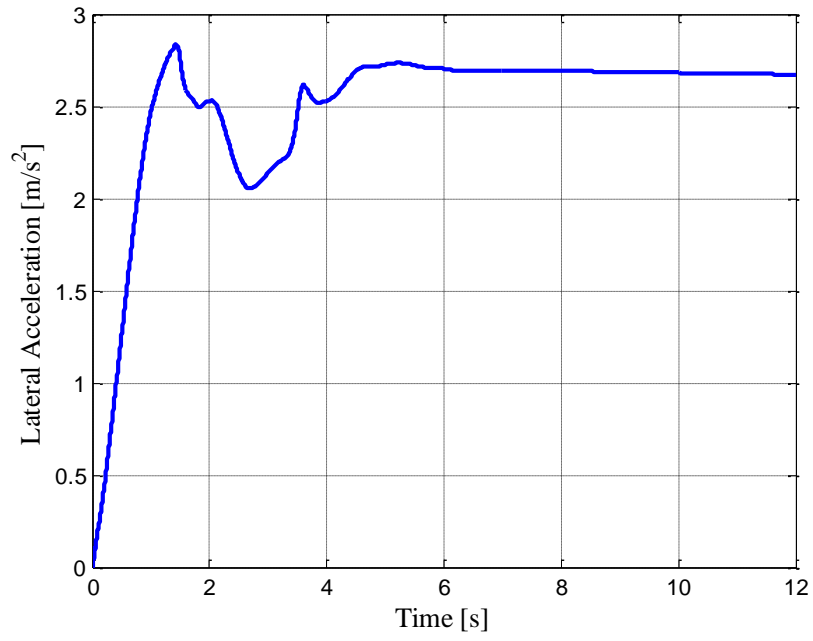


Figure 4.69: Lateral Acceleration

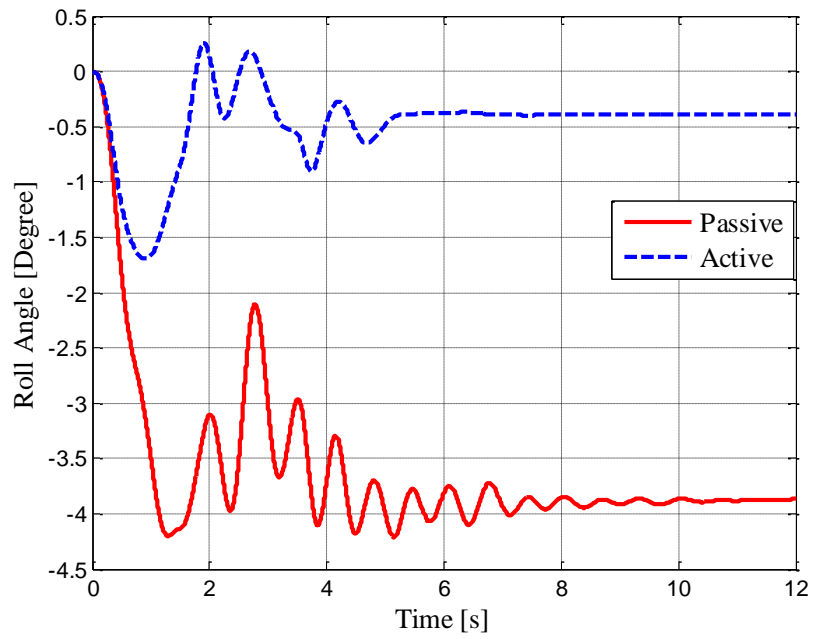


Figure 4.70: Roll Angle

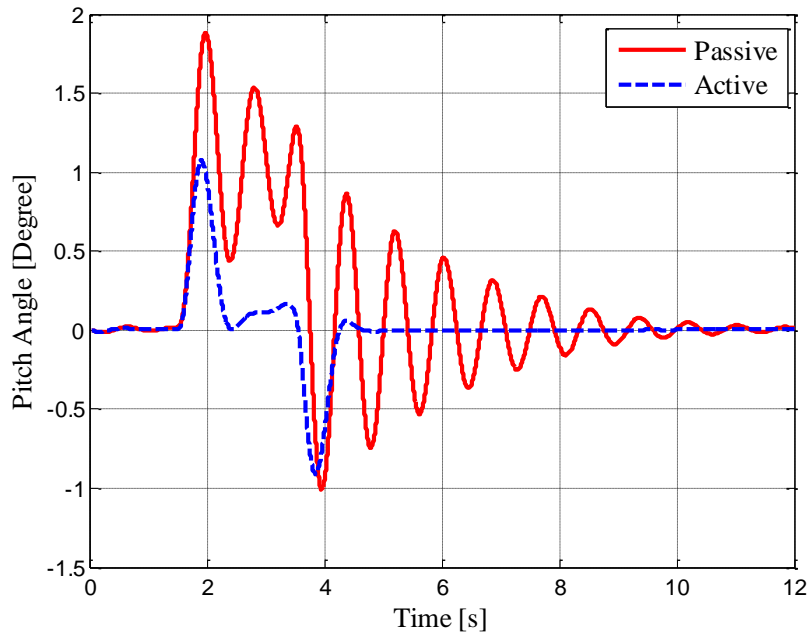


Figure 4.71: Pitch Angle

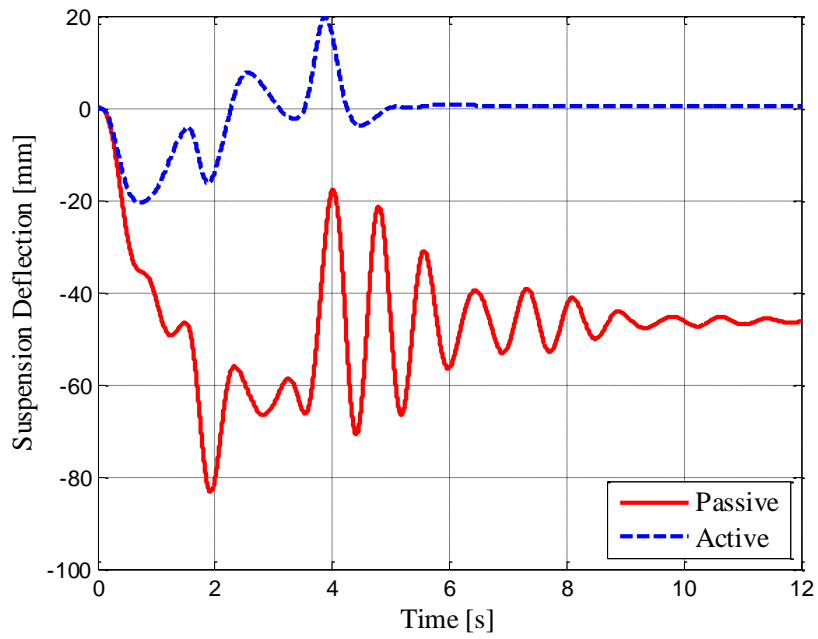


Figure 4.72: Front Left Suspension Deflection

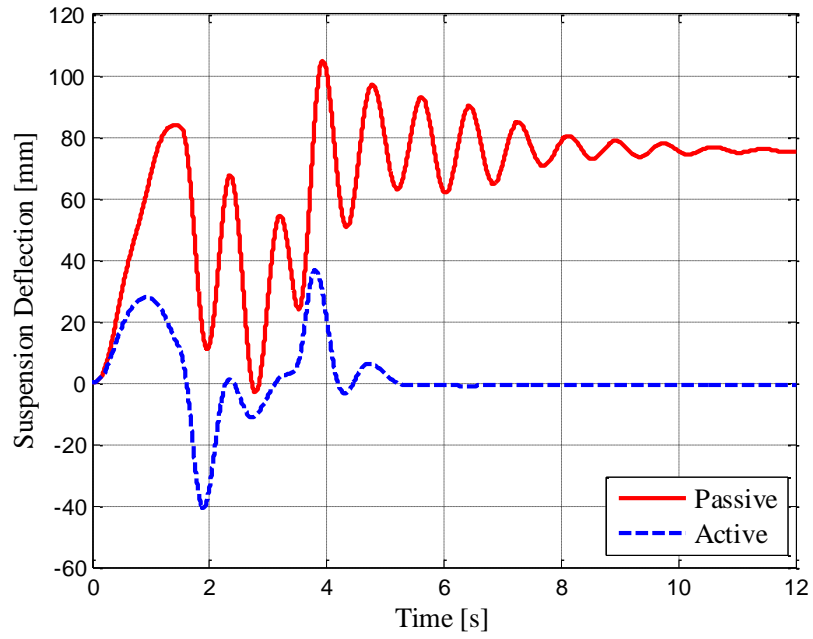


Figure 4.73: Front Right Suspension Deflection

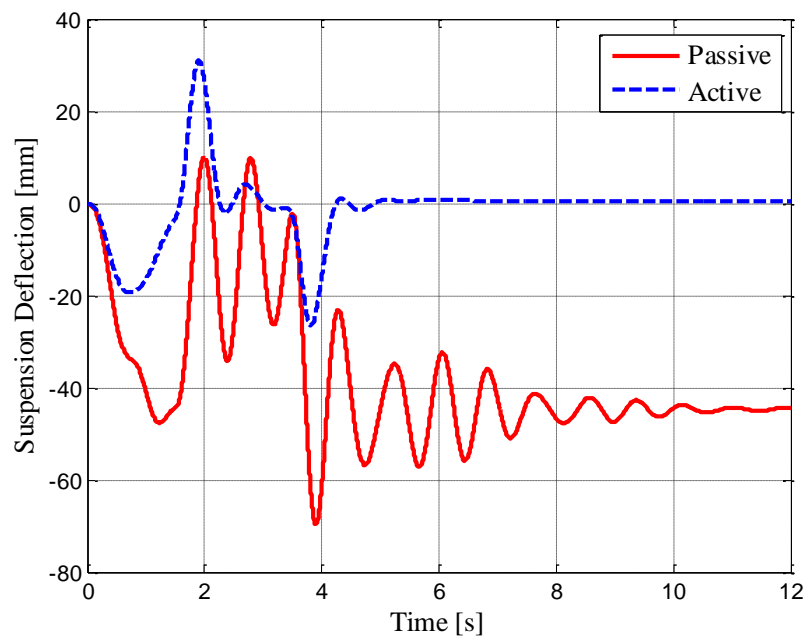


Figure 4.74: Rear Left Suspension Deflection

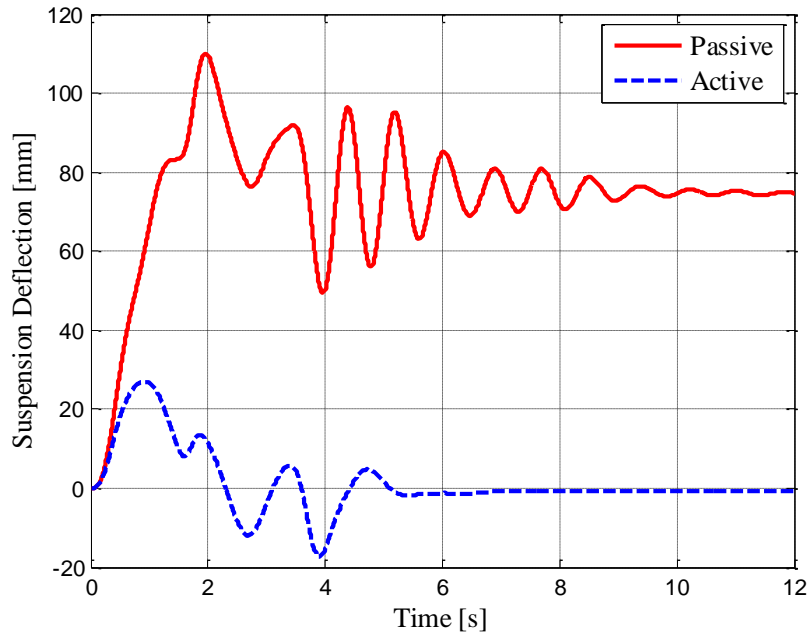


Figure 4.75: Rear Right Suspension Deflection

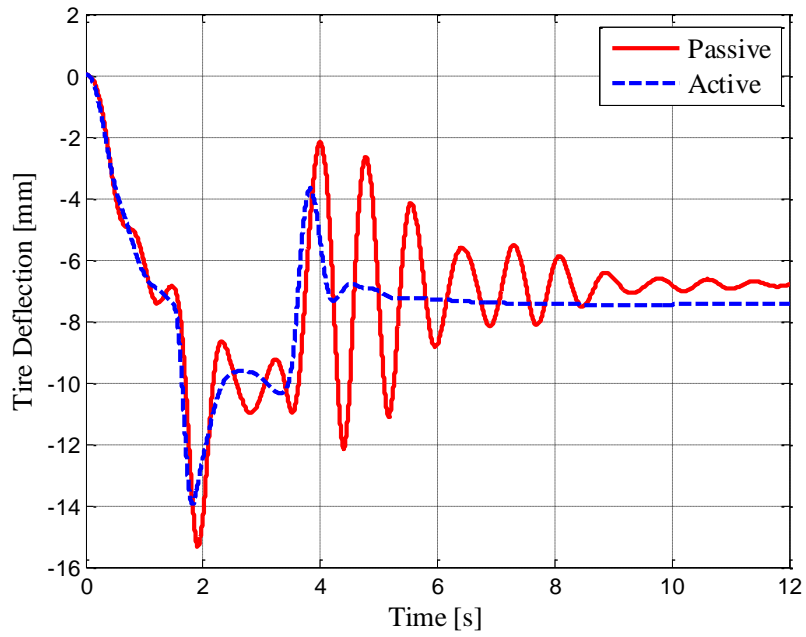


Figure 4.76: Front Left Tire Deflection

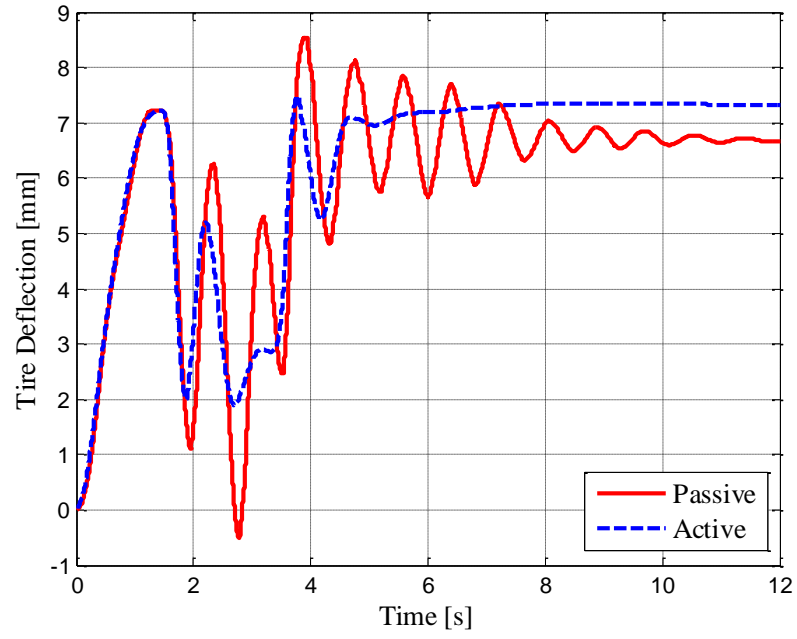


Figure 4.77: Front Right Tire Deflection

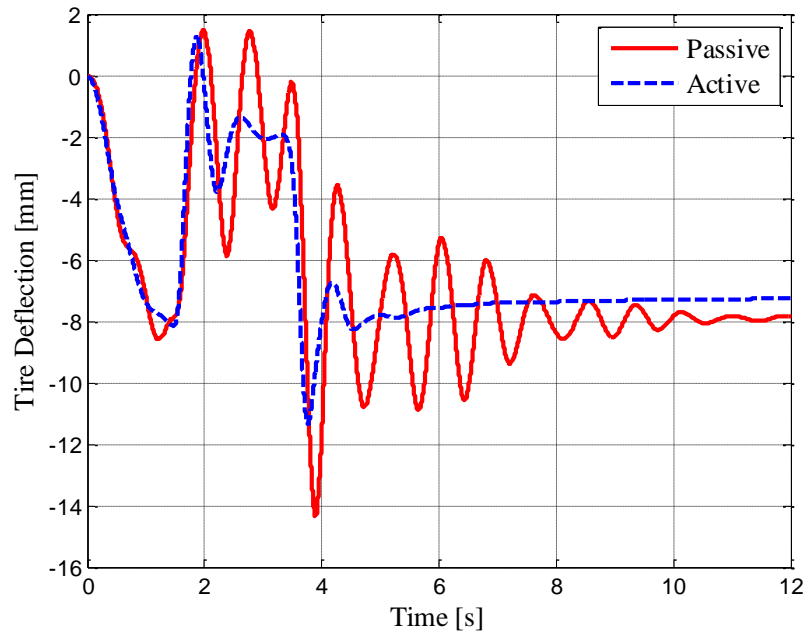


Figure 4.78: Rear Left Tire Deflection

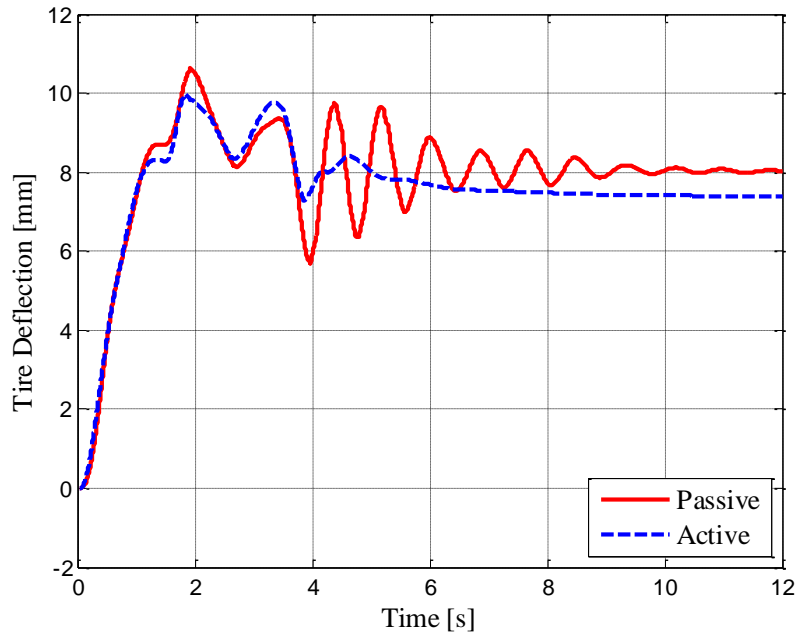


Figure 4.79: Rear Right Tire Deflection

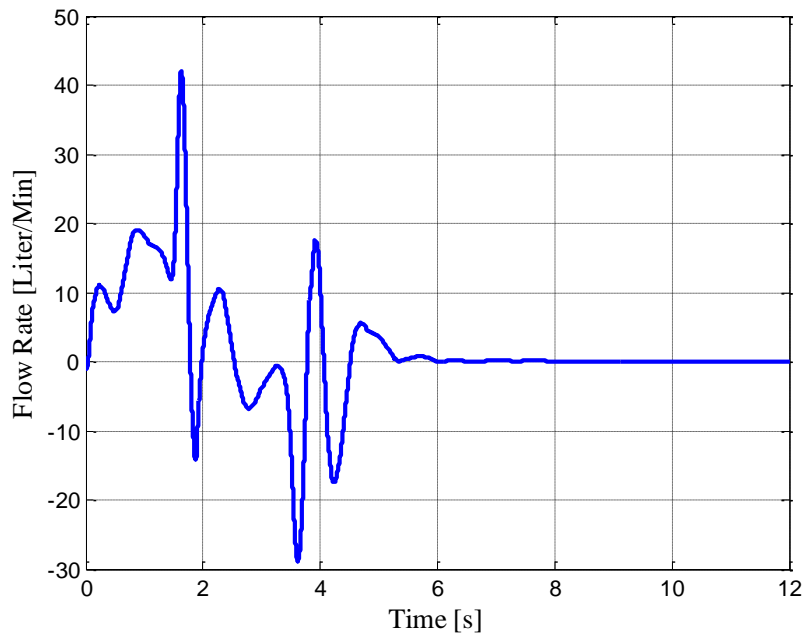


Figure 4.80: Front Left Flow Rate

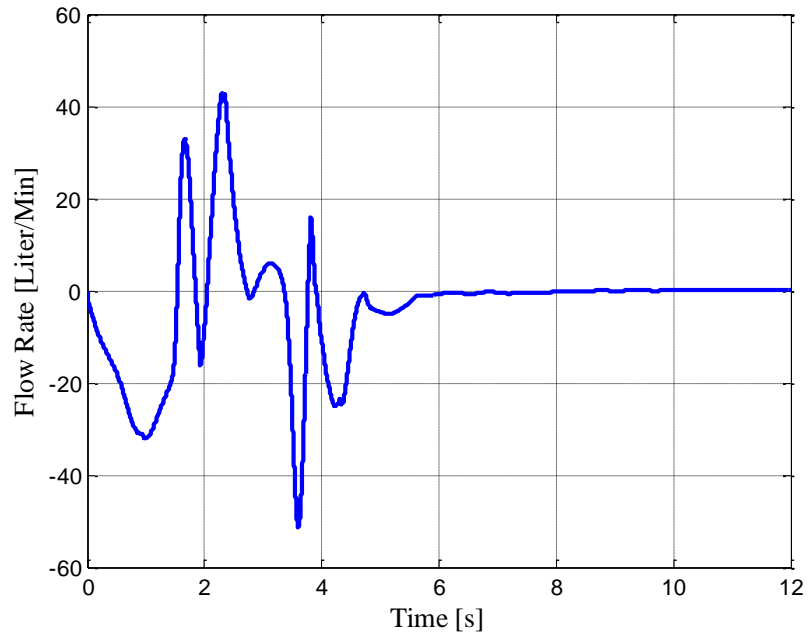


Figure 4.81: Front Right Flow Rate

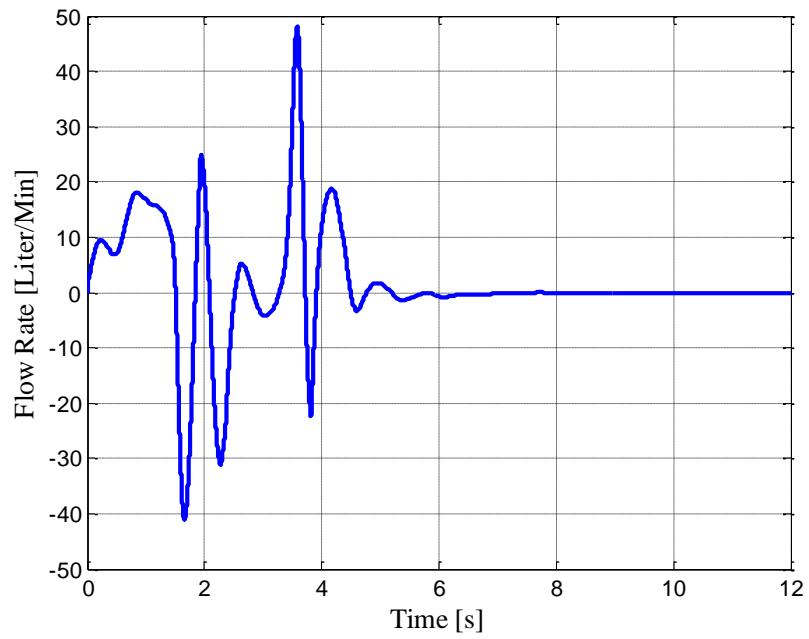


Figure 4.82: Rear Left Flow Rate

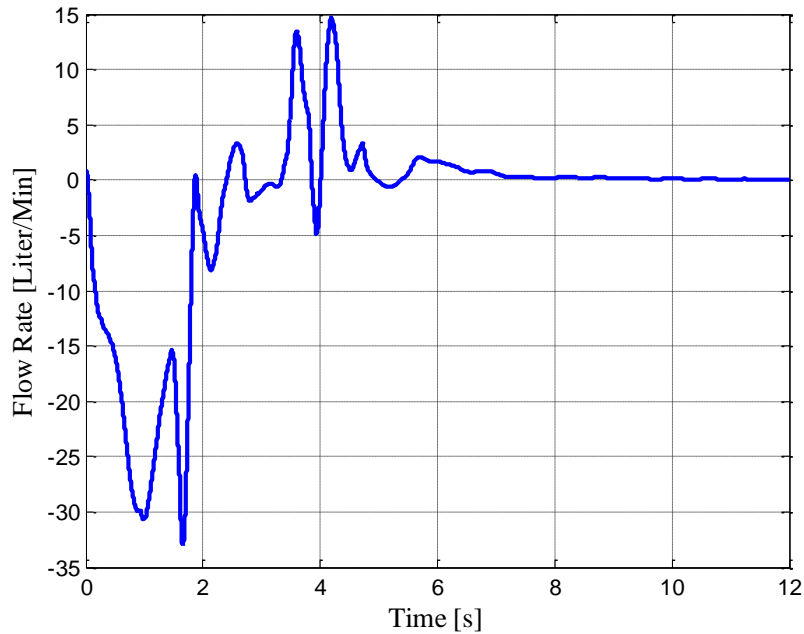


Figure 4.83: Rear Right Flow Rate

As simulation results show, the active suspension has better roll and pitch performance as compared with the passive suspension. Active controller decreases the roll angle considerably and thus handling performance of the vehicle is improved considerably. Moreover, the pitch angle is reduced by the active controller and thus braking-acceleration performance of the vehicle is improved. In the simulations, some oscillations are observed in the case of the passive suspension system. Since the orifice damper has little damping at low suspension velocities, the vibrations induced by the disturbances cannot be damped out with the passive suspensions. On the contrary, active controller has damped out those oscillations completely. Thus, the use of the orifice damping in the passive suspension system is not adequate.

4.5. CONCLUSION

In this chapter, modeling and design of an active HP suspension system have been investigated. An active HP suspension system is designed for a quarter car model. The aim of the controller is to decrease sprung mass acceleration to improve ride comfort, and to reduce the suspension deflection to improve vehicle attitude control. The active controller is designed for only ride comfort first, and then for combined

ride comfort and vehicle attitude control. A detailed sensitivity study is performed to examine the effect of the controller weighting parameters on the vehicle performance characteristics. Performances of the controllers are examined by the time and frequency domain simulations. According to results:

- ❖ SDRE formulation can be successfully adapted to model and control the active HP suspension system.
- ❖ By expressing nonlinear gas model and orifice equations as linear stiffness and damping equations using direct parameterization method, a convenient form of the model is obtained.
- ❖ General active HP controllers with different complexity and order can be designed with the SDRE control method.
- ❖ Saturation of the oil flow rate, modeling of the physical hard bound can be appropriately modeled and incorporated into SDRE control design.
- ❖ Active HP suspension system designed for only ride comfort cannot control the vehicle attitude and there is going to be a steady state error for certain types of road inputs.
- ❖ In order to design the HP suspension system for both ride comfort and vehicle attitude control, the use of the integral state and constraint in the formulation is a must.
- ❖ According to the sensitivity study, suspension deflection integral weighting parameter has the most prominent effect on the performance of the vehicle attitude control.
- ❖ Only a compromise solution for the ride comfort and vehicle attitude control can be achieved.
- ❖ By increasing the integral of the suspension deflection weighting parameter, vehicle attitude performance is improved, yet vehicle ride comfort performance is degraded.
- ❖ In order to improve the performance of the active controller for ride comfort and vehicle attitude control, adaptive active suspension controller can be designed by using the state constraint.

- ❖ By tuning the suspension deflection integral weighting parameter according to the suspension deflection, both ride comfort and vehicle attitude performances can be improved.
- ❖ At low suspension deflection, controller is tuned for ride comfort and at high suspension deflection; controller is tuned for vehicle attitude control.
- ❖ The designed active suspension controller can be further applied to the half vehicle model with active HP suspension system.
- ❖ When the integral of the suspension deflection weighting is increased, vehicle handling performance is increased.
- ❖ Simulation results show that active suspension control can improve ride comfort and vehicle handling simultaneously. Vehicle attitude control can be satisfied with the active suspension controller.
- ❖ Active suspension controller designed for the full vehicle model is used to improve ride comfort, vehicle handling, and braking/acceleration performance of the vehicle.
- ❖ For the derivation of the state dependent model of the full vehicle model with active HP suspension system, one of the tire displacements is written in terms of the other state variables. This removes over-constraint states in the problem formulation and prevents possible problem of the solution of the Riccati equation.

CHAPTER 5

INTERCONNECTED HP SUSPENSION SYSTEMS

In Chapter 4, vehicles with individual active HP suspension systems have been studied. In this chapter, another important application of HP suspension system, interconnection of HP suspension systems, is studied. Interconnection in mechanical suspension systems can be performed with mechanical linkages, as in the case of anti-roll bar. One of the advantages of the fluid power systems with respect to the mechanical systems is that pressurized fluid can be transferred easily between different circuit elements. In a similar situation, the pressurized hydraulic oil can be transferred among different suspension units by simply addition of the hydraulic conductors, such as hoses and fittings. As will be illustrated in the following chapters, by interconnecting individual HP suspension systems in different configurations, handling and the ride comfort characteristics of the vehicle may be improved considerably with respect to unconnected HP suspension systems.

5.1. INTRODUCTION

An example of vehicle with three axles is shown in Figure 5.1 and the schematic of the vehicle in pitch direction is shown in Figure 5.2. F_F , F_M , and F_R are the suspension forces of the three suspension units. The main idea behind using the multiple axles in a vehicle is to decrease the axle load which is restricted by the regulations, improve the mobility of the vehicle as in the case of military vehicles, and to protect the vehicle components by distributing the load evenly on axles. For a vehicle with the HP suspension system, individual HP suspension units may be

interconnected. These interconnections change the stiffness and damping characteristics of the vehicle considerably. For a vehicle with two axles, the interconnections in the pitch and roll planes are simpler. However, for a full vehicle model as explained in the study of the Cao [19], connections are more complex and there are a number of possibilities. Similarly, there are many different possible HP interconnections in a vehicle with multi-axles. When the HP suspensions are interconnected to each other, some pressure variables are equated and the suspension force characteristics change. Thus, the interconnections will be classified firstly in terms of the independent suspension forces in static condition. This analysis gives an insight into the feasibility of different possible interconnections. Otherwise, for a vehicle with three and more axles, feasible interconnections cannot be seen easily without a mathematical classification of the interconnections on some basis.



Figure 5.1: A Military Vehicle with Three-Axles [67]

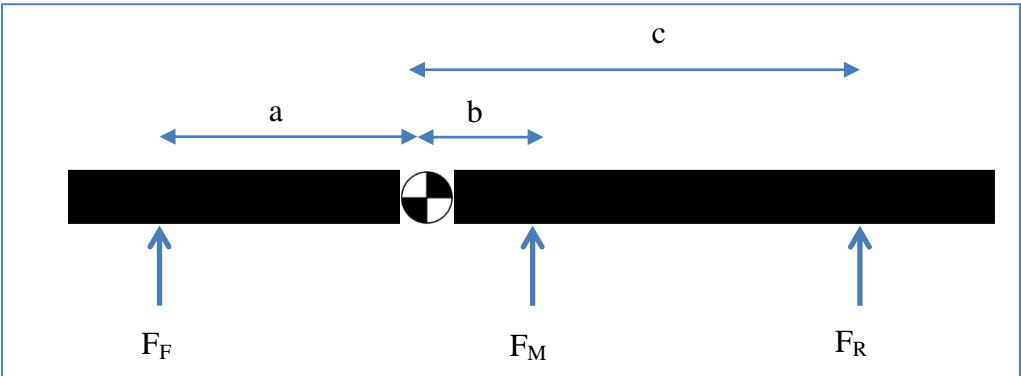


Figure 5.2: Pitch Plane Vehicle Model

After possible configurations are found, these configurations will be analyzed statically in terms of pitch stiffness and pitch damping characteristics. One of the possible interconnections for a three axle vehicle is illustrated in Figure 5.3.

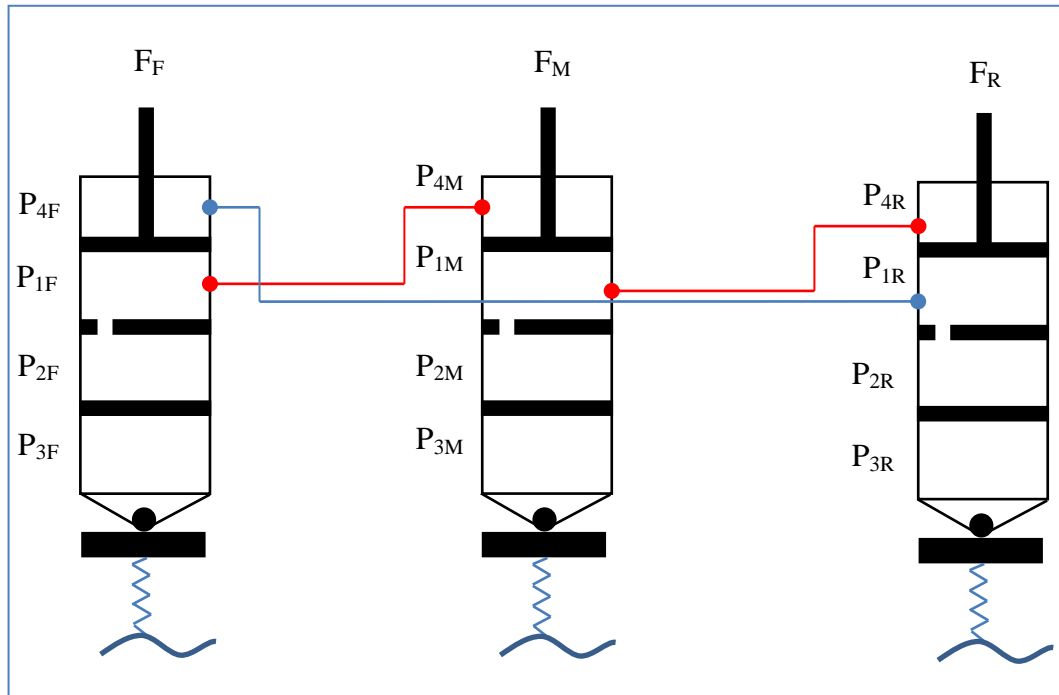


Figure 5.3: One Possible Interconnection Configuration in the Pitch Plane

5.2. SOLVABILITY OF THE SUSPENSION FORCES AND THE SUSPENSION PRESSURES

Since at static equilibrium two independent equilibrium equations are written and since the suspension forces and the pressures are linear in these equations, existence/uniqueness of the solutions for linear systems is going to be examined.

Theorem 3 [68]: A linear system with m equations and n unknowns,

$$[A]_{m \times n} \{x\}_{n \times 1} = \{b\}_{m \times 1}$$

is

- ❖ Inconsistent if $\text{rank}[A] < r = \text{rank}[A \ b]$
- ❖ Consistent if $\text{rank}[A] = r = \text{rank}[A \ b]$

Consistent system has,

- A unique solution if and only if $\text{rank}[A]=r=n$
- An $(n-r)$ parameter family of infinite solutions if and only if $\text{rank}[A]=r<n$.

Therefore, the feasibility of the interconnection is to be determined in the view of the Theorem 2.

5.3. EXAMINATION OF THE POSSIBLE HP INTERCONNECTIONS FOR A VEHICLE WITH THREE AXLES

In this part, possible classifications are going to be determined in terms of the solvability of the static equilibrium equations. Since a vehicle with three axles in a pitch plane is a statically indeterminate system, the suspension forces cannot be found uniquely in the static case from the static equilibrium equations. Initial configuration of the system changes the values of the suspension forces in static equilibrium. In the pitch plane of the vehicle, two independent static equilibrium equations can be written in the vertical and pitch direction since pitch plane model of the vehicle has two degrees of freedom. These equations are,

$$F_F + F_M + F_R = Mg \quad (5-1)$$

$$aF_F - bF_M - cF_R = 0 \quad (5-2)$$

where suspension forces are

$$F_F = P_{1F}A_p - P_{4F}A_{pr} \quad (5-3)$$

$$F_M = P_{1M}A_p - P_{4M}A_{pr} \quad (5-4)$$

$$F_R = P_{1R}A_p - P_{4R}A_{pr} \quad (5-5)$$

In the unconnected case, P_{1F} , P_{1M} , P_{1R} , P_{4F} , P_{4M} , P_{4R} are six independent pressure variables if all the HP suspension units has double gas chambers. When the suspensions are interconnected to each other, these pressure variables are equated to each other in the static case and thus the number of independent pressure variables decreases. Different possible interconnections should be found based on the relations among these pressure variables. Since there are two equilibrium equations, at least two independent suspension forces are necessary. Therefore, interconnections which

result in only one independent suspension force forms an infeasible configuration. One of the examples of infeasible configuration is illustrated in Figure 5.4. This configuration satisfies the equilibrium equations only for a special case where $a=c$, and $b=0$.

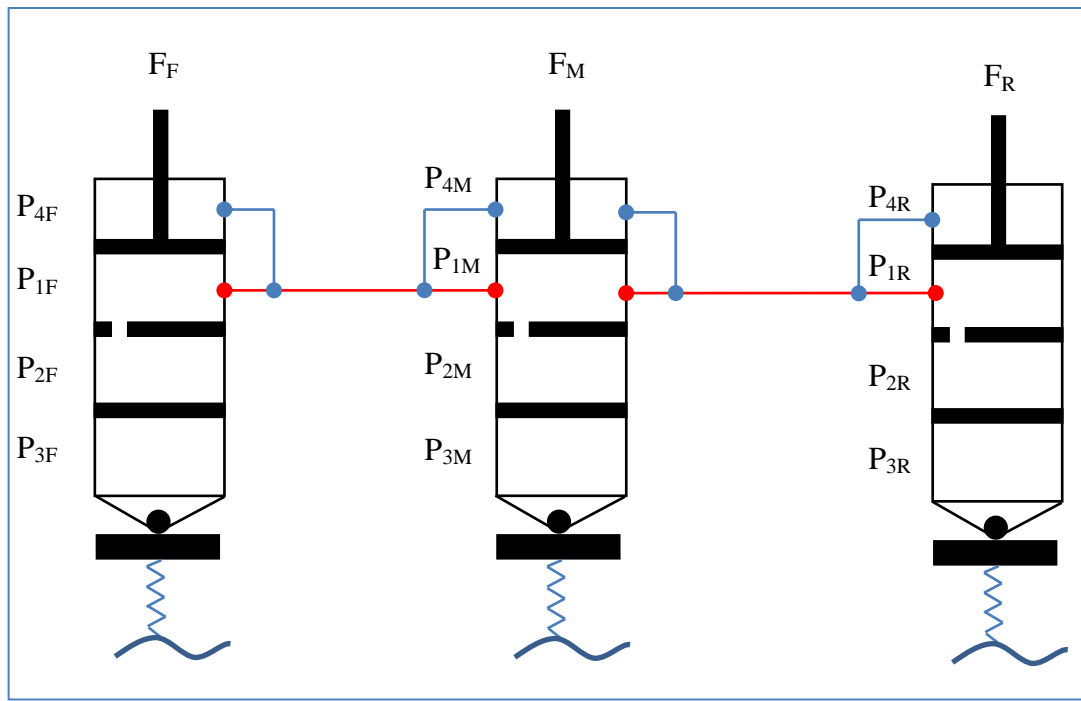


Figure 5.4: Unfeasible Interconnection Configurations

The degree of freedom of the interconnections can be defined on the bases of the independent suspension forces. Degrees of freedom can also be defined in terms of the independent pressure variables. However, the solution of the static equilibrium equations are directly related with the suspension forces, rather than the pressure variables. Thus, the number of the independent suspension forces is defined as the number of the degree of freedom of the interconnections. An interconnection should have at least two degrees of freedom to form feasible interconnections. Suspension forces for interconnections with two degree of freedom have a unique solution. For the interconnections which have more than two degrees of freedom, there are an infinite number of solutions. The definition of feasibility defined above has a sense in mathematical point of view. In physical point of view, an interconnection should be also physically feasible such that the pressures and the suspension forces turn out

to be positive variables. Therefore, the necessary but not sufficient condition is that an interconnection should have at least two degrees of freedom. In the unconnected suspension configurations, depending on the suspension type (double-sided cylinder or single sided cylinder), there are three to six independent pressure variables, and an unconnected suspension configuration has three degrees of freedom. If only one of the three suspensions is double-sided type, there are four independent pressure variables. In this case, the unconnected suspension configuration has still three degrees of freedom. If only one of the three suspension units is single-sided type, there are five independent pressure variables.

5.3.1. One Degree of Freedom Interconnections

When the interconnections are performed in such a way that all suspension forces are equal to each other, the obtained interconnection has one degree of freedom. Since there are two equilibrium equations, static equilibrium equations are inconsistent and there is no solution and thus configuration is infeasible.

5.3.2. Two Degrees of Freedom Interconnections

In two degrees of freedom interconnection, there are two independent suspension forces. In general (other than the specific case), these two independent suspension forces can be solved from the static equilibrium equations. According to the type of the suspension units used, there are different interconnections. An example of two degrees of freedom interconnections are given in Figure 5.5.

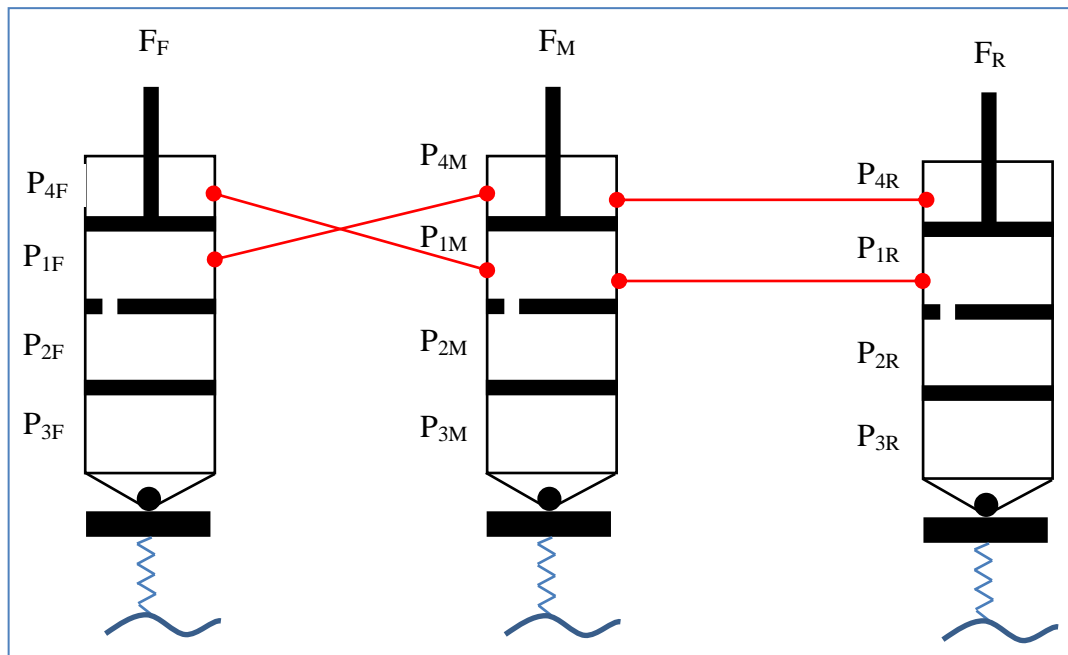


Figure 5.5: Two Degrees of Interconnections

5.3.3. Three Degrees of Freedom Interconnections

In three degrees of freedom interconnections, there are three independent suspension forces. In general, since there are only two equilibrium equations, there is no unique solution of the pressure values at static equilibrium, and thus there are an infinite number of solutions. To be able to determine the values of the suspension force in static case, one suspension force is set to a value and from that value the remaining suspension forces are obtained. Three degrees of freedom interconnections have the advantage of one free suspension force. This property gives the flexibility of selecting the design parameters. Example of three degrees of freedom interconnection is given in Figure 5.6.

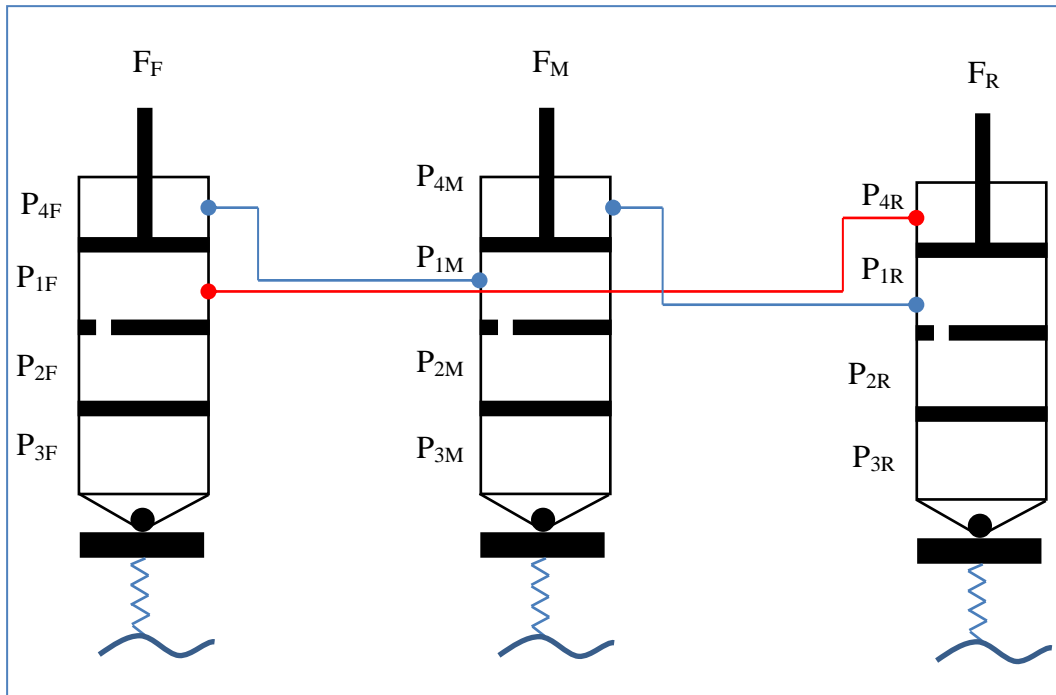


Figure 5.6: Three Degrees of freedom Interconnection

After the suspension forces are determined from the static analysis, the pressure forces are determined from Equations (5-3), (5-4), and (5-5). Similar to the suspension forces, when the number of the independent pressure variables is higher than 3, there is an infinite number of solutions.

5.4. CONCLUSION

In general, the results found here can be summarized (except for specific cases) as follows according to the Theorem 3.

$n = \text{Number of Degrees of Freedom} = \text{Number of Independent Suspension Forces}$

- ❖ If $n=1$: Inconsistent set of equations: There is no solution, system does not reach static equilibrium.
- ❖ If $n=2$: Consistent set of equations: There is a unique solution to the suspension forces.
- ❖ If $n=3$: Consistent set of equations: There is a one parameter family of solutions. (Infinite number of solutions).

After the suspension forces are found, whether they are physical or not must be checked. In a similar manner, the pressure variables should be physical for proper interconnection. In summary, for an interconnection to be proper:

- 1) The equilibrium equations should be consistent,
- 2) The suspension forces should be positive,
- 3) The pressure variables should be positive.

Consistency of the equation can be also examined according to the Theorem 3 directly, when the Equations (5-1) and (5-2) are combined by the Equations (5-3), (5-4), and (5-5).

Interconnected HP suspension systems have different uses in vehicles. One of these is the improvement of the handling and braking/traction performances. Another use of the interconnected HP suspension system is the distribution or equalization of the suspension force among different axle groups. In order to increase the handling and braking/acceleration performance of the so called “X” type of interconnection is used. However, in order to equalize the suspension forces, parallel interconnection is used. In X type interconnections, piston side of front (left) suspension unit is connected to the rod side of the rear (right) suspension unit, and the rod side of the front (left) suspension unit is connected to piston side of the rear (right) suspension unit. In parallel interconnections, piston and rod side of a suspension unit are connected to piston and rod side of another suspension unit, respectively.

CHAPTER 6

ANALYSIS AND DESIGN OF A PITCH INTERCONNECTED HP SUSPENSION SYSTEM FOR THREE-AXLE VEHICLES

6.1. INTRODUCTION

In this chapter, interconnected HP suspension systems for a three-axle vehicle for the pitch plane are studied. It was shown in the literature that, when there are connections between the piston side of the front suspension and the rod side of the rear suspension, and rod side of the front suspension and the piston side of the rear suspension; the pitch stiffness of the interconnected suspension increases with respect to pitch stiffness of the unconnected suspension systems. This characteristic of the interconnected suspension system is useful in improving the performance of the vehicle with respect to braking/acceleration performance, and to other special vehicle characteristics like firing stability and mobility in military vehicles. When the vertical stiffness and the damping characteristics of the interconnected and the unconnected suspension systems are equated to each other, the pitch stiffness and the pitch damping of the interconnected suspension are higher than those of the unconnected suspension system. Higher pitch stiffness and damping improves the vehicle performance against certain disturbances coming to vehicle bodies. Therefore, vehicles with interconnected suspension system have improved performances against disturbances coming from braking/accelerating and firing

shocks of the vehicle with firing ability. For improved braking/accelerating performances and the firing performance of the vehicle, low pitch angles and oscillations are desired. In the following parts these response characteristics are examined in a more detailed way.

For a vehicle with two axles X interconnection is straightforward. The stiffness and the damping characteristics of the vehicle with X type interconnected HP suspension system were studied in the literature [19], [69]. However, for large and heavy vehicles, more than two axles are required. The main reasons for using more than two axles are the improvement of the mobility of the vehicle and reduction of the axle loads. For a vehicle with three axles, there may be different interconnected configurations. A vehicle with three axles forms a statically indeterminate problem and axle loads can be found from the coupled solutions of the static equilibrium equations and the suspension deflections. When the stiffness of the suspension units is changed, the static suspension forces also change. Therefore there may be an infinite number of solutions. When the HP suspension units are interconnected to each other, static suspension pressures are related to each other and therefore suspension characteristics and in turn the static suspension forces change.

In this chapter, for a vehicle with three axles, possible interconnections will be examined. Possible interconnections include full interconnected suspension, semi-interconnected suspension, and unconnected suspension. Full interconnection can be defined as an interconnection such that piston side and rod side of each suspension units are interconnected at least one times. Similarly, semi-interconnection can be defined such that at least one piston or rod side of the suspension unit is not connected to other piston or rod side of the suspension units. Finally unconnected configurations can be defined such that all piston or rod side of the suspension units are unconnected. In this chapter two full interconnected configurations, three semi-interconnected suspension configurations and one unconnected suspension configurations are examined. First, a mathematical model of nine degree of freedom vehicle model is derived. Then the suspension forces for different suspension configurations are going to be derived. After the model of the vehicle with different

suspension configurations are obtained, vertical stiffness and damping and pitch stiffness and damping characteristics are going to be obtained. The suspension configurations are compared in terms of

- ❖ Leveling performance against the disturbances coming from the vehicle body,
- ❖ Pitch stiffness
- ❖ Pitch damping

Then simulations are performed to further examine the performance of the vehicle with different suspension configurations. To be able to make a realizable comparison of the stiffness and the damping of the different suspension configurations, vertical stiffness and the damping of the suspensions are equated to each other. To equate the vertical stiffness of different suspension configurations, initial gas volumes are adjusted and to equate the vertical damping of the configurations damping valve parameters are set accordingly.

In this study, the initial suspension parameters are selected such that the three suspension forces are equal to each other as much as possible. This constitutes an optimization problem. A Lagrange Multiplier optimization method is used to find the optimum suspension forces which are as close as possible to each other. After all parameters of the suspension configurations are determined, simulations are performed to examine the performances of the suspensions for ride comfort, braking/accelerating performance, and firing mobility. For ride comfort simulations, random road inputs and road bump inputs are used. For random road simulations root mean square values of the responses are calculated and for bump road simulations maximum and the minimum values of the responses are observed. For handling performance, simulations with braking input at wheels are performed. For firing performance, a simulation with a firing shock is performed. For both simulations maximum overshoot values are obtained to grade the suspension configurations. A suspension metric is determined to specify the suspension configurations for specified use of purposes.

6.2. DEVELOPMENT OF A THREE-AXLE VEHICLE MODEL IN PITCH PLANE

In this part a pitch plane model of a three-axle vehicle is to be developed. The schematic of the vehicle model is shown in Figure 6.1. For the simulation of the designed suspension configurations, a nine degree of freedoms vehicle model is formed. The vehicle model consists of longitudinal, vertical, and pitch degrees of freedom of the sprung mass, vertical degrees of freedoms of three equivalent tires, and rotational degrees of freedom for the three equivalent tires.

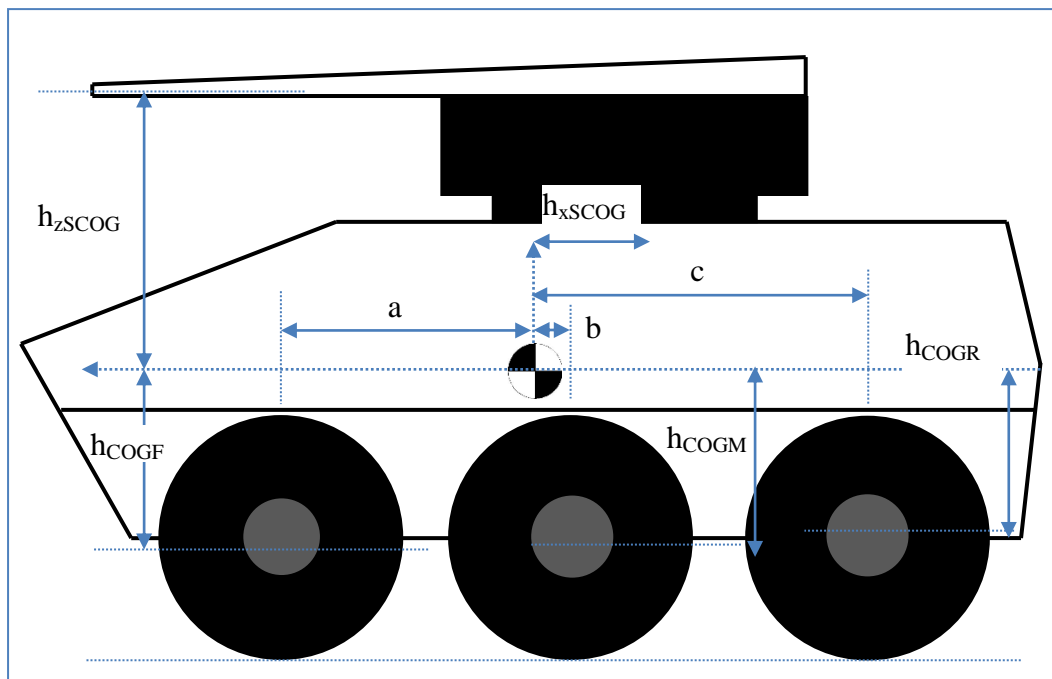


Figure 6.1: Pitch Plane Model of a Three-Axle Vehicle

The interaction of the tires with the road surface is modeled using the Magic Formula tire model. By this way, braking, traction, fire shock input, and road inputs can be used in the simulation. Free body diagrams of the tires and the vehicle sprung mass is shown in Figure 6.2. Definition of the variables and parameters used in the formulations are given in Table 6.1 and Table 6.2, respectively. In the variable and parameter definitions “i” stands for the “F”, “M”, and “R” which refer to front, middle, and rear, respectively.

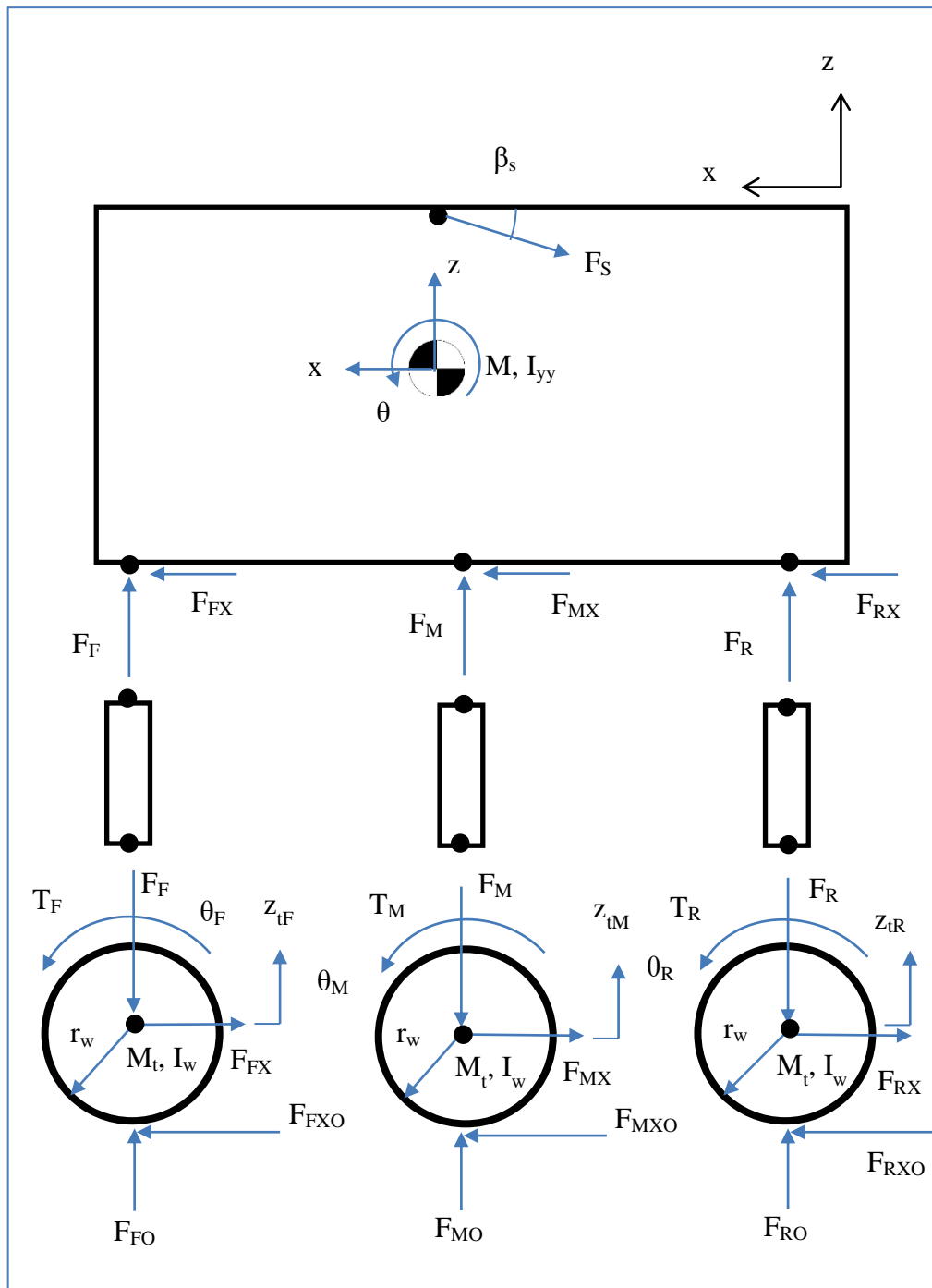


Figure 6.2: Free Body Diagram of the Tires and the Vehicle Sprung Mass

Equation of Motion of the Tires:

Equations of motion for the front, intermediate and the rear tires are written as,

$$F_{FO} - F_F = M\ddot{z}_{tF} \quad (6-1)$$

$$F_{FXO} - F_{FX} = M_t \ddot{x}_{tF} \quad (6-2)$$

$$T_F - F_{FXO} r_{tF} = I_{tyy} \ddot{\theta}_{tF} \quad (6-3)$$

$$F_{MO} - F_M = M_t \ddot{z}_{tM} \quad (6-4)$$

$$F_{MXO} - F_{MX} = M_t \ddot{x}_{tM} \quad (6-5)$$

$$T_M - F_{MXO} r_{tM} = I_{tyy} \ddot{\theta}_{tM} \quad (6-6)$$

$$F_{RO} - F_R = M_t \ddot{z}_{tR} \quad (6-7)$$

$$F_{RXO} - F_{RX} = M_t \ddot{x}_{tR} \quad (6-8)$$

$$T_R - F_{RXO} r_{tR} = I_{tyy} \ddot{\theta}_{tR} \quad (6-9)$$

Equation of motion for the sprung mass can be written as,

$$F_{FX} + F_{MX} + F_{RX} - F_S \cos(\beta) = M \ddot{x}_S \quad (6-10)$$

$$F_F + F_M + F_R - Mg - F_S \sin(\beta) - F_D = M \ddot{z} \quad (6-11)$$

$$-aF_F + bF_M + cF_R - M_s - h_{COGF} F_{FX} - h_{COGF} F_{MX} - h_{COGF} F_{RX} = I_{yy} \ddot{\theta} \quad (6-12)$$

Assuming small displacements, kinematical relationships can be written as,

$$z_{pF} = z - a\theta \quad (6-13)$$

$$z_{pM} = z + b\theta \quad (6-14)$$

$$z_{pR} = z + c\theta \quad (6-15)$$

where z_{pF} , z_{pM} , and z_{pR} are the front, intermediate, and the rear piston displacements respectively.

Table 6.1: Definition of variable

Definition	Symbol
Sprung Mass and Tire Longitudinal Displacement	x
Longitudinal Velocity	u
Tire Rotation	θ_i
Braking or Traction Force Between Tire and the Road	F_{iXO}
Vertical Reaction Force Between Tire and Road	F_{iO}
Longitudinal Slip	S
Longitudinal Force Acting on the Wheel Center of Tire	F_{iX}
Vertical Suspension Force on Tire	F_i
Braking or Traction Torque Acting on the Wheel	T_i
Missile Shock Force	F_S
Moment of Missile Shock Force	M_S

Table 6.2: Definition of Parameters

Definition	Symbol
Vertical Distance between Missile Launcher Centerline and COG	h_{zSCOG}
Horizontal Distance between Missile Launcher Mounting and COG	h_{xSCOG}
Vertical Distance between the Wheel Center and COG	h_{COGi}
Firing Angle	β_s
Longitudinal Distance between the Front Axle and COG	a
Longitudinal Distance between the Middle Axle and COG	b
Longitudinal Distance between the Rear Axle and COG	c
Loaded Tire Radius of tire	r_{ti}
Mass Moment of Inertia of Tire about y Axis	I_{tyy}
Pitch Moment of Inertia of Sprung Mass	I_{yy}
Magic Formula Tire Model Parameter	C, B, D, E, S_x, S_y
Magic Formula Tire Model Parameter	$b's$

Longitudinal Slips

In the braking situation, longitudinal slips can be found for each tire as,

$$S_F = \frac{-r_{tF}\dot{\theta}_F + u}{u} \quad (6-16)$$

$$S_M = \frac{-r_{tM}\dot{\theta}_M + u}{u} \quad (6-17)$$

$$S_R = \frac{-r_{tR}\dot{\theta}_R + u}{u} \quad (6-18)$$

Tire Model

Longitudinal tire forces between the ground and the tire contact can be found from the Magic Formula Tire Model. For longitudinal tire forces, Magic Formula tire model can be written as [70], [71], [72]:

$$C = b_0 \quad (6-19)$$

$$D = b_1 F_z^2 + b_2 F_z \quad (6-20)$$

$$B = \frac{(b_3 F_z^2 + b_4 F_z) e^{(-b_5 F_z)}}{CD} \quad (6-21)$$

$$E = b_6 F_z^2 + b_7 F_z + b_8 \quad (6-22)$$

$$S_h = b_9 F_z + b_0 \quad (6-23)$$

$$S_v = 0 \quad (6-24)$$

$$X_s = s + S_h \quad (6-25)$$

$$F_x = D \sin \left\{ C \tan^{-1} \left[BX_s - E \left[BX_s - \tan^{-1} (BX_s) \right] \right] \right\} + S_v \quad (6-26)$$

A longitudinal force characteristic of the Magic Formula tire model for different vertical tire load is shown in Figure 6.3. As Figure 6.3 shows, when the vertical load is increased, longitudinal traction/braking force also increases.

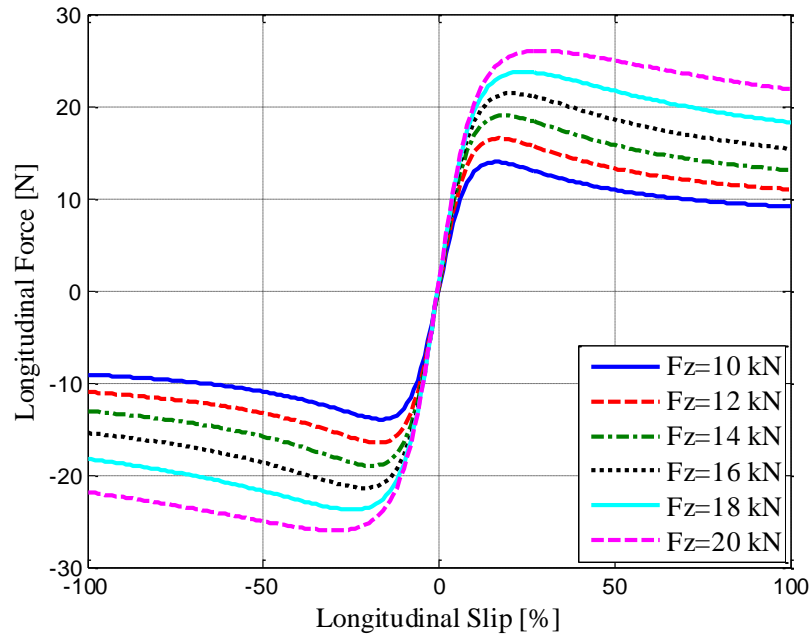


Figure 6.3: Magic Formula Tire Characteristics

6.3. MODELING OF A PITCH INTERCONNECTED HP SUSPENSION SYSTEM FOR A THREE AXLE VEHICLE

In previous part, a general formulation of the vehicle model and the tire model were derived. The suspension forces used in the general formulation is to be derived in this chapter. Firstly different suspension configurations are determined and then their mathematical models are derived. Then stiffness and damping characteristics of the interconnected and the unconnected suspension configurations are calculated. A comparison is to be made about the stiffness and the damping characteristics. Vehicle parameters are given in Table 6.3.

Table 6.3: Vehicle Parameters

Parameters	Symbol	Value
Vehicle Mass	M [kg]	4500
Pitch Moment of Inertia	I_{yy} [kgm ²]	9484
Tire Mass Moment of Inertia about y Axis	I_{tyy} [kgm ²]	18.75
Front Axle to Center of Gravity Distance	a [m]	2
Middle Axle to Center of Gravity Distance	b [m]	0.3
Rear Axle to Center of Gravity Distance	c [m]	2
Tire Radius at Static Equilibrium	r_t [m]	0.5
Vertical Distance Between the Wheel Center and COG At Static Equilibrium for Front, Middle, and Rear Axles	h_{COGij} [m]	1.1
Vertical Distance Between Missile Launcher Centerline and COG	h_{zSCOG} [m]	1.5
Horizontal Distance Between Missile Launcher Mounting and COG	h_{xSCOG} [m]	0

6.3.1. Possible Interconnected Suspension Layout

For a vehicle with three axles there are different possible interconnections as already explained in Chapter 5. Among these interconnections, the ones which are suitable for increasing the pitch stiffness are shown in Figure 6.4 to Figure 6.8. In each suspension unit there may be two independent pressure variables in static conditions. In the first two arrangements, both volumes of each suspension units are interconnected to volumes of other suspension units in X arrangements. In the remaining three arrangements only two suspension units are interconnected to each other in X arrangements. The unconnected suspension configuration is also included to provide the reference suspension characteristics. Therefore, in total six suspension configurations are modeled and compared to each other in terms of pitch stiffness and pitch damping characteristics. In this chapter, while forming the interconnections, the following rules are followed:

- ❖ There is only one port for each volume of each suspension units.
- ❖ The port of one suspension unit is connected to the port of the other suspension units in X arrangement.

When all volumes of the suspension units are interconnected to each other, the interconnection is defined as full-interconnection. When only two suspension units

are interconnected, the interconnection is defined as semi-interconnection. In this study, two full interconnections and three semi-interconnections are formed.

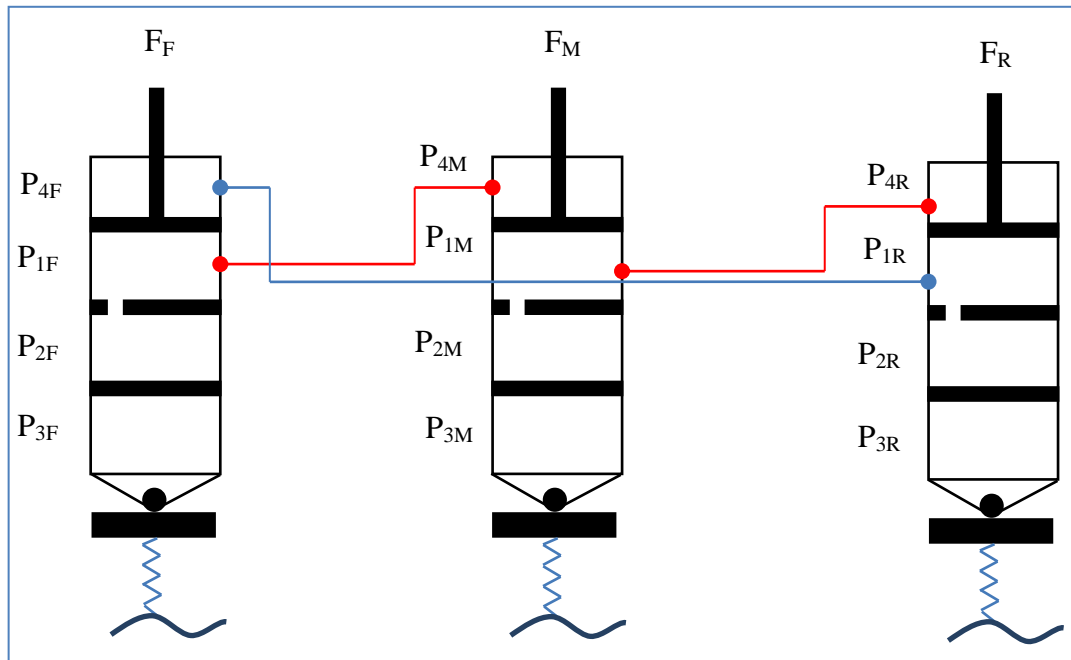


Figure 6.4: First Possible Full Interconnection

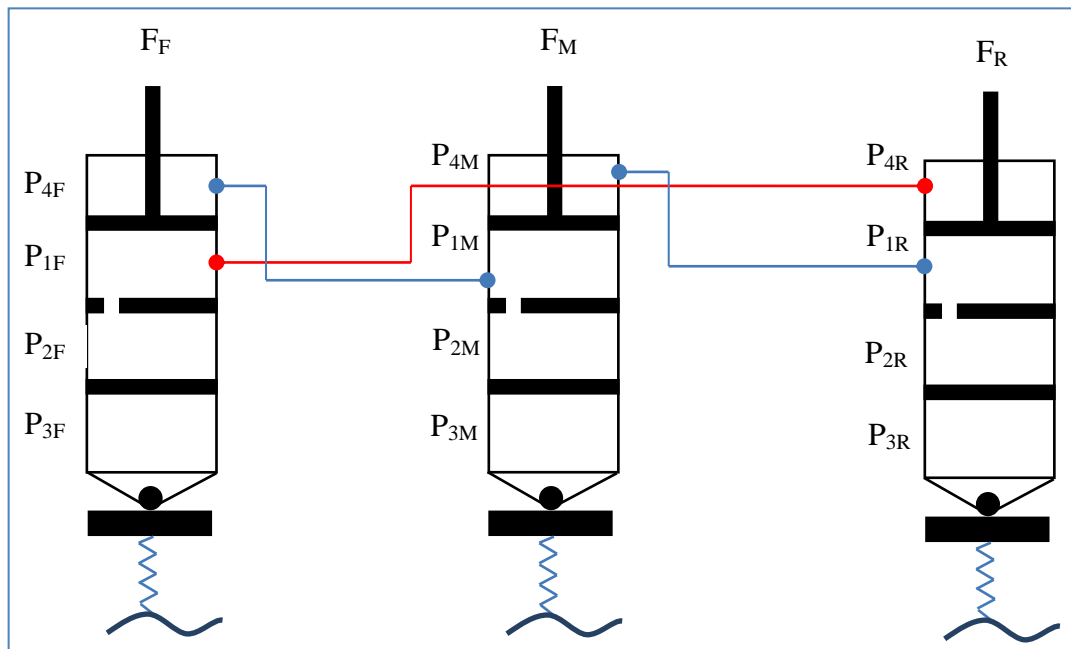


Figure 6.5: Second Possible Full Interconnection

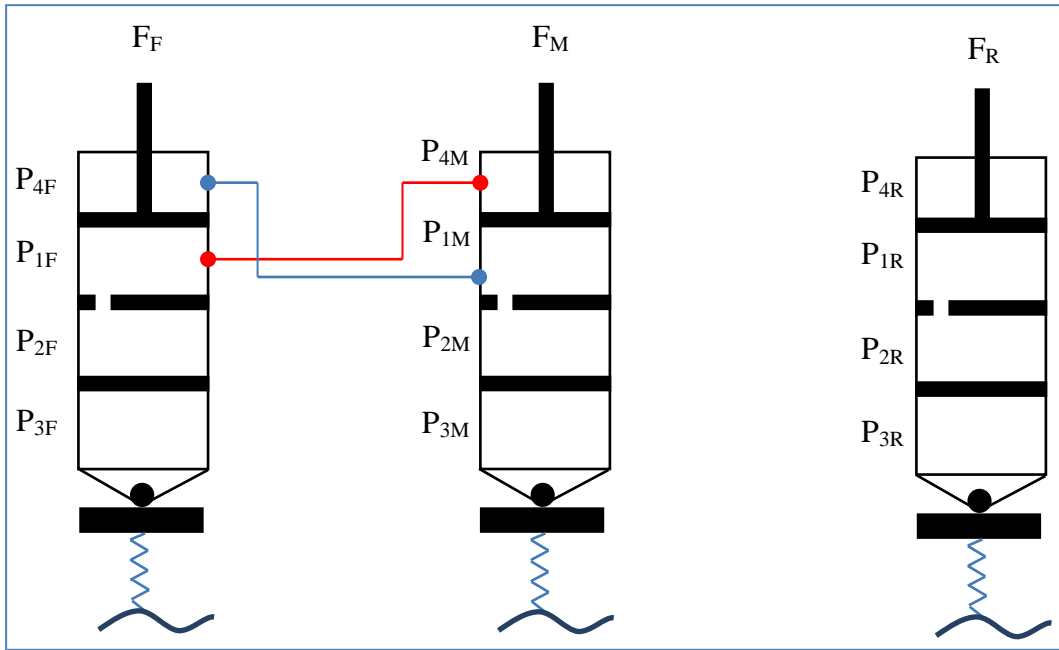


Figure 6.6: First Possible Semi-Interconnection

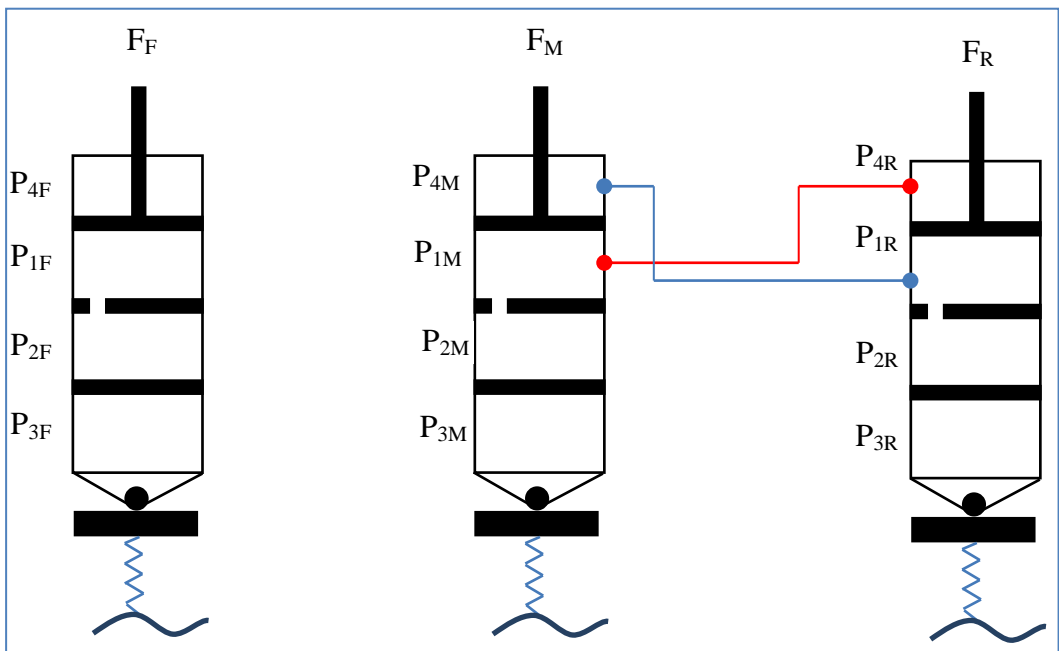


Figure 6.7: Second Possible Semi-Interconnection

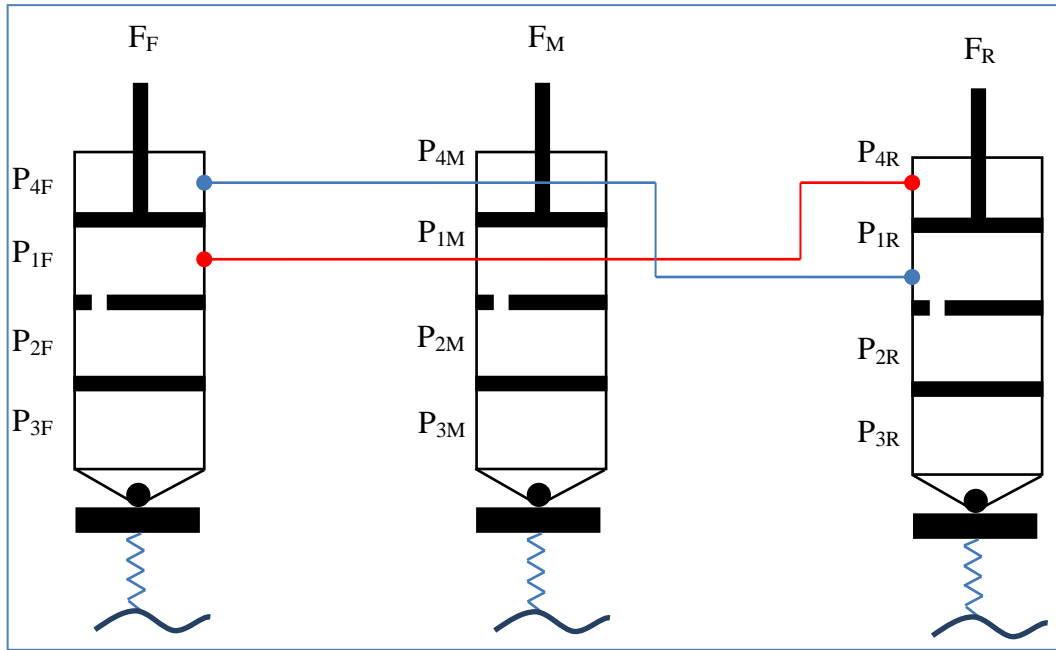


Figure 6.8: Third Possible Semi-Interconnection

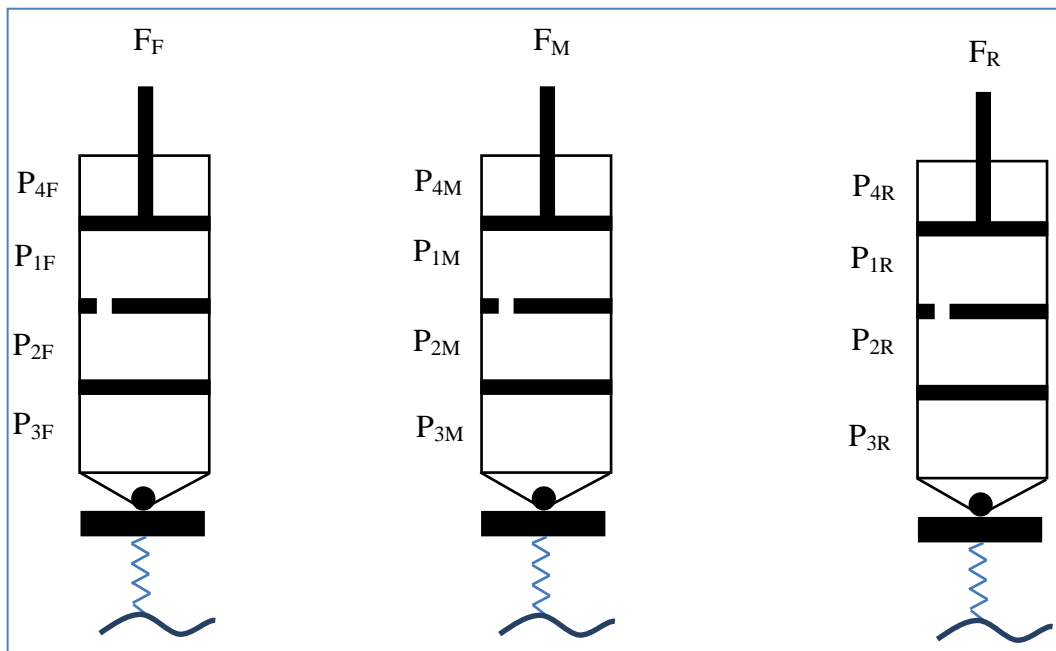


Figure 6.9: Unconnected Suspension Configuration

In chapter 5, the degree of freedom of the interconnection is defined as the number of the independent suspension forces. Therefore, the degrees of freedom of the selected configurations are all three and all configurations are feasible.

6.3.2. Mathematical Modeling of the Pitch Interconnected HP Suspension Systems

In this section, the equations of motion of the selected suspension configurations are going to be derived. After the governing equations are derived, stiffness and damping characteristics of the interconnected and the unconnected HP suspension configurations are to be obtained. The definitions of the parameters and variables used in the derivation are listed in Table 6.4 and Table 6.5.

Table 6.4: Definition of Parameters

Definition of Parameters	Symbol
Initial Gas Volume In the Third Volume	V_{30i}
Initial Gas Pressure in the Third Volume	P_{30i}
Resistance Of The Hydraulic Hose Between The Fourth Volume Of The Front Suspension And The First Volume Of The Rear Suspension	R_{4F1R}
Resistance Of The Hydraulic Hose Between The Fourth Volume Of The Middle Suspension And The First Volume Of The Front Suspension	R_{4M1F}
Resistance Of The Hydraulic Hose Between The Fourth Volume Of The Rear Suspension And The First Volume Of The Middle Suspension	R_{4R1M}
Diameter of the Hose Connecting Fourth Oil Volume of Front Suspension and First Oil Volume of Rear Suspension Units	D_{4F1R}
Diameter of the Hose Connecting Fourth Oil Volume of Middle Suspension and First Oil Volume of Front Suspension Units	D_{4M1F}
Diameter of the Hose Connecting Fourth Oil Volume of Rear Suspension and First Oil Volume of Middle Suspension Units	D_{4R1M}
Length of the Hose Connecting Fourth Oil Volume of Front Suspension and First Oil Volume of Rear Suspension Units	L_{4F1R}
Length of the Hose Connecting Fourth Oil Volume of Middle Suspension and First Oil Volume of Front Suspension Units	L_{4M1F}
Length of the Hose Connecting Fourth Oil Volume of Rear Suspension and First Oil Volume of Middle Suspension Units	L_{4R1M}
Oil Viscosity	μ

Table 6.5: Definition of Variables Used in Derivation

Definition of Variables	Symbol
Absolute Gas Pressure in the Third Volume	P_{3i}
Oil Pressure in the First Volume	P_{1i}
Oil Pressure in the Second Volume	P_{2i}
Oil Pressure in the Fourth Volume	P_{4i}
Oil Flow Rate between the Second and First Oil Volumes	Q_{2i1i}
Oil Flow Rate between the Fourth Volume of the Front Suspension and the First Volume of the Rear Suspension	Q_{4F1R}
Oil Flow Rate between the Fourth Volume of the Middle Suspension and the First Volume of the Front Suspension	Q_{4M1F}
Oil Flow Rate Between the Fourth Volume of the Rear Suspension and the First Volume of the Middle Suspension	Q_{4R1M}
Floating Piston Displacement	Z_{fpi}
Piston Displacement	Z_{pi}

For brevity, modeling of the first interconnected HP suspension system only is derived here. Models of the other interconnected HP suspension system can be derived similarly.

6.3.2.1. Modeling of the First Suspension Configuration

Oil continuity equations for the first volume of the front, intermediate, and the rear suspensions can be written as,

$$Q_{2F1F} + A_{pr} (\dot{z}_{pM} - \dot{z}_{tM}) = A_p (\dot{z}_{pF} - \dot{z}_{tF}) \quad (6-27)$$

$$Q_{2M1M} + A_{pr} (\dot{z}_{pR} - \dot{z}_{tR}) = A_p (\dot{z}_{pM} - \dot{z}_{tM}) \quad (6-28)$$

$$Q_{2R1R} + A_{pr} (\dot{z}_{pF} - \dot{z}_{tF}) = A_p (\dot{z}_{pR} - \dot{z}_{tR}) \quad (6-29)$$

From the oil continuity equations for the second volumes of the front, intermediate and the rear suspension units, floating piston displacements can be written as,

$$z_{fpF} = z_{pF} - \frac{A_{pr}}{A_p} (z_{pM} - z_{tM}) \quad (6-30)$$

$$z_{fpM} = z_{pM} - \frac{A_{pr}}{A_p} (z_{pR} - z_{tR}) \quad (6-31)$$

$$z_{ipR} = z_{pR} - \frac{A_{pr}}{A_p} (z_{pF} - z_{tF}) \quad (6-32)$$

Oil flow equations through the hydraulic hose can be written assuming laminar flow,

$$Q_{4F1R} = A_{pr} (\dot{z}_{pF} - \dot{z}_{tF}) = R_{4F1R} (P_{4F} - P_{1R}) \quad (6-33)$$

$$Q_{4M1F} = A_{pr} (\dot{z}_{pM} - \dot{z}_{tM}) = R_{4M1F} (P_{4M} - P_{1F}) \quad (6-34)$$

$$Q_{4R1M} = A_{pr} (\dot{z}_{pR} - \dot{z}_{tR}) = R_{4R1M} (P_{4R} - P_{1M}) \quad (6-35)$$

From these equations, oil pressures in fourth oil volumes can be written as,

$$P_{4F} = P_{1R} + \frac{A_{pr} (\dot{z}_{pF} - \dot{z}_{tF})}{R_{4F1R}} \quad (6-36)$$

$$P_{4M} = P_{1F} + \frac{A_{pr} (\dot{z}_{pM} - \dot{z}_{tM})}{R_{4M1F}} \quad (6-37)$$

$$P_{4R} = P_{1M} + \frac{A_{pr} (\dot{z}_{pR} - \dot{z}_{tR})}{R_{4R1M}} \quad (6-38)$$

Hose lose factors, R_{4F1R} , R_{4M1F} , and R_{4R1M} can be found as,

$$R_{4F1R} = \frac{\pi D_{4F1R}^4}{128 \mu L_{4F1R}} \quad (6-39)$$

$$R_{4M1F} = \frac{\pi D_{4M1F}^4}{128 \mu L_{4M1F}} \quad (6-40)$$

$$R_{4R1M} = \frac{\pi D_{4R1M}^4}{128 \mu L_{4R1M}} \quad (6-41)$$

Front, intermediate, and the rear suspension forces can be written as,

$$F_F = P_{1F} A_p - P_{4F} A_{pr} \quad (6-42)$$

$$F_M = P_{1M} A_p - P_{4M} A_{pr} \quad (6-43)$$

$$F_R = P_{1R} A_p - P_{4R} A_{pr} \quad (6-44)$$

After the suspension forces are found, the static analysis which is required to find the suspension forces and pressures at initial static equilibrium is performed. To be able to find the suspension forces, in addition to static equilibrium equations, suspension deflection relations should also be written. For a vehicle with two axles, the suspension forces can be directly found from the static equilibrium equations. Whatever the initial pressures in the suspension, the final pressures can be determined when the vehicle reaches static equilibrium. However, for a vehicle with three axles, the parameters of the suspension units before they are mounted on the vehicle are important. Those parameters affect the suspension forces and displacements after they are mounted on the vehicle and the vehicle reaches static equilibrium.

Static analysis for multi-axle vehicles is rather complex as compared with the static analysis of two-axle vehicle. Therefore, while performing static analysis, a procedure starting from the simplest one to more complex one is followed.

6.3.2.1.1. The Suspension Forces, Gas Pressures and Volumes, Suspension and Tire Deflections after the Vehicle Reaches Static Equilibrium

In this section, for a given suspension, tire and the vehicle parameters, the suspension and tire deflections and parameters are going to be determined when the vehicle reaches static equilibrium. In other words given the values of the suspension parameters before they are mounted on vehicle, the values of the suspension parameters after the vehicle reaches static equilibrium are sought.

6.3.2.1.2. The Optimum Initial Suspension Parameters Which Yield Equal Suspension Forces as Much as Possible

In this section, the initial suspension parameters are found in order to find the optimal suspension force characteristics at static equilibrium. The optimization problems become:

$$\text{Argmin}_{\substack{P_{3IF}, P_{3IM}, P_{3IR} \\ L_{SF}, L_{SM}, L_{SR} \\ L_{TF}, L_{TM}, L_{TR}}} \left\{ (F_F - F_M)^2 + (F_F - F_R)^2 + (F_M - F_R)^2 \right\}$$

subject to static equilibrium equations.

However, this optimization problem is difficult, since the optimization includes the solving equilibrium equation derived in previous chapter. To be able to simplify the optimization process, some conditions on the optimization can be inserted. For example, after the optimization, the followings are desired: $z=0$, $\theta=0$. By this way, the optimization structure can be changed.

6.3.2.1.3. Finding the Optimum Suspension Force Characteristics First and then Finding the Initial Suspension Parameters

Now the optimum suspension force characteristics are to be found after the vehicle reaches static equilibrium. From this knowledge the optimum initial suspension parameters are going to be found. Suspension forces at static conditions are given by:

$$F_F = P_{30F}A_p - P_{Atm}A_p - M_{fp}g - P_{30R}A_{pr} + P_{Atm}A_{pr} + \frac{M_{fp}gA_{pr}}{A_p} \quad (6-45)$$

$$F_M = P_{30M}A_p - P_{Atm}A_p - M_{fp}g - P_{30F}A_{pr} + P_{Atm}A_{pr} + \frac{M_{fp}gA_{pr}}{A_p} \quad (6-46)$$

$$F_R = P_{30R}A_p - P_{Atm}A_p - M_{fp}g - P_{30M}A_{pr} + P_{Atm}A_{pr} + \frac{M_{fp}gA_{pr}}{A_p} \quad (6-47)$$

At static equilibrium, the following equations can be written.

$$F_F + F_M + F_R = Mg \quad (6-48)$$

$$-aF_F + bF_M + cF_R = 0 \quad (6-49)$$

There are two equations and three independent suspension forces. Therefore, one suspension force can be set freely, and then two remaining suspension force values can be found. Here the aim is to make the suspension forces as close as possible to each other. Therefore, the optimization problems become:

Minimize

$$(F_F - F_R)^2 + (F_F - F_M)^2 + (F_M - F_R)^2$$

subject to Equations (6-48) and (6-49).

This optimization problem can be solved by using the Lagrange Multiplier Optimization Method. Thus, the equality constraints, the static equilibrium equations, can be used in the optimization easily. Optimal suspension forces can be found as:

$$F_{\text{Foptimal}} = \frac{\text{Mg}(b^2 + ab + ac + c^2)}{2(a^2 + b^2 + c^2 + ab + ac - bc)} \quad (6-50)$$

$$F_{\text{Moptimal}} = \frac{\text{Mg}(a^2 + ab - bc + c^2)}{2(a^2 + b^2 + c^2 + ab + ac - bc)} \quad (6-51)$$

$$F_{\text{Roptimal}} = \frac{\text{Mg}(a^2 + ac - bc + b^2)}{2(a^2 + b^2 + c^2 + ab + ac - bc)} \quad (6-52)$$

After that, the initial suspension parameters are found such that at the equilibrium these suspension forces are attained.

6.3.2.2. Stiffness Characteristics

The front, intermediate, and rear suspension forces are written as,

$$F_{\text{F}} = \frac{P_{30\text{F}} V_{30\text{F}}^{\text{K}} A_{\text{p}}}{\left[V_{30\text{F}} + A_{\text{p}} \left(z_{\text{pF}} - z_{\text{tF}} - \frac{A_{\text{pr}}}{A_{\text{p}}} (z_{\text{pM}} - z_{\text{tM}}) \right) \right]^{\text{K}}} - \frac{P_{30\text{R}} V_{30\text{R}}^{\text{K}} A_{\text{pr}}}{\left[V_{30\text{R}} + A_{\text{p}} \left(z_{\text{pR}} - z_{\text{tR}} - \frac{A_{\text{pr}}}{A_{\text{p}}} (z_{\text{pF}} - z_{\text{tF}}) \right) \right]^{\text{K}}} \quad (6-53)$$

$$F_{\text{M}} = \frac{P_{30\text{M}} V_{30\text{M}}^{\text{K}} A_{\text{p}}}{\left[V_{30\text{M}} + A_{\text{p}} \left(z_{\text{pM}} - z_{\text{tM}} - \frac{A_{\text{pr}}}{A_{\text{p}}} (z_{\text{pR}} - z_{\text{tR}}) \right) \right]^{\text{K}}} - \frac{P_{30\text{F}} V_{30\text{F}}^{\text{K}} A_{\text{pr}}}{\left[V_{30\text{F}} + A_{\text{p}} \left(z_{\text{pF}} - z_{\text{tF}} - \frac{A_{\text{pr}}}{A_{\text{p}}} (z_{\text{pM}} - z_{\text{tM}}) \right) \right]^{\text{K}}} \quad (6-54)$$

$$F_R = \frac{P_{30R} V_{30R}^\kappa A_p}{\left[V_{30R} + A_p \left(z_{pR} - z_{tR} - \frac{A_{pr}}{A_p} (z_{pF} - z_{tF}) \right) \right]^\kappa} - \frac{P_{30M} V_{30M}^\kappa A_{pr}}{\left[V_{30M} + A_p \left(z_{pM} - z_{tM} - \frac{A_{pr}}{A_p} (z_{pR} - z_{tR}) \right) \right]^\kappa} \quad (6-55)$$

Let us use the abbreviation as, $z_{pF} - z_{tF} = z_{ptF}$, $z_{pM} - z_{tM} = z_{ptM}$, $z_{pR} - z_{tR} = z_{ptR}$. To be able to find the vertical stiffness of the suspension, it is assumed that,

$$z_{ptF} = z_{ptM} = z_{ptR} = z \quad (6-56)$$

Then the vertical stiffness can be found as,

$$k = - \frac{d(F_F + F_M + F_R)}{dz} \quad (6-57)$$

$$k = \frac{P_{30F} V_{30F}^\kappa A_r^2 \kappa}{[V_{30F} + A_r z]^{\kappa+1}} + \frac{P_{30M} V_{30M}^\kappa A_r^2 \kappa}{[V_{30M} + A_r z]^{\kappa+1}} + \frac{P_{30R} V_{30R}^\kappa A_r^2 \kappa}{[V_{30R} + A_r z]^{\kappa+1}} \quad (6-58)$$

At static equilibrium, the vertical stiffness can be found as,

$$k = \frac{P_{30F} A_r^2 \kappa}{V_{30F}} + \frac{P_{30M} A_r^2 \kappa}{V_{30M}} + \frac{P_{30R} A_r^2 \kappa}{V_{30R}} \quad (6-59)$$

As explained in the reference [19], pitch stiffness can be found from,

$$k_\theta = - \frac{dM_\theta}{d\theta} \quad (6-60)$$

where M is the pitch moment

$$M_\theta = -aF_F + bF_M + cF_R \quad (6-61)$$

M_θ can be expressed as:

$$\begin{aligned}
M_{\theta} = & -a \left\{ \frac{P_{30F} V_{30F}^{\kappa} A_p}{\left[V_{30F} + A_p \left(z_{ptF} - \frac{A_{pr}}{A_p} z_{ptM} \right) \right]^{\kappa}} - \frac{P_{30R} V_{30R}^{\kappa} A_{pr}}{\left[V_{30R} + A_p \left(z_{ptR} - \frac{A_{pr}}{A_p} z_{ptF} \right) \right]^{\kappa}} \right\} + \\
& +b \left\{ \frac{P_{30M} V_{30M}^{\kappa} A_p}{\left[V_{30M} + A_p \left(z_{ptM} - \frac{A_{pr}}{A_p} z_{ptR} \right) \right]^{\kappa}} - \frac{P_{30F} V_{30F}^{\kappa} A_{pr}}{\left[V_{30F} + A_p \left(z_{ptF} - \frac{A_{pr}}{A_p} z_{ptM} \right) \right]^{\kappa}} \right\} + \\
& +c \left\{ \frac{P_{30R} V_{30R}^{\kappa} A_p}{\left[V_{30R} + A_p \left(z_{ptR} - \frac{A_{pr}}{A_p} z_{ptF} \right) \right]^{\kappa}} - \frac{P_{30M} V_{30M}^{\kappa} A_{pr}}{\left[V_{30M} + A_p \left(z_{ptM} - \frac{A_{pr}}{A_p} z_{ptR} \right) \right]^{\kappa}} \right\} \quad (6-62)
\end{aligned}$$

Inserting the kinematic relations derived before into the moment equation, and assuming that tire displacements are zero $z_{tF}=z_{tM}=z_{tR}=0$, pitch moment can be found as,

$$\begin{aligned}
& \left. \begin{aligned}
& \frac{-P_{30F} V_{30F}^{\kappa} A_p \left[A_r \frac{dz}{d\theta} - (aA_p + bA_{pr}) \right] \kappa}{\left[V_{30F} + A_r z - (aA_p + bA_{pr}) \theta \right]^{\kappa+1}} + \\
& \frac{P_{30R} V_{30R}^{\kappa} A_{pr} \left[A_r \frac{dz}{d\theta} + (cA_p + aA_{pr}) \right] \kappa}{\left[V_{30R} + A_r z + (cA_p + aA_{pr}) \theta \right]^{\kappa+1}}
\end{aligned} \right\} - \\
& \left. \begin{aligned}
& \frac{-P_{30M} V_{30M}^{\kappa} A_p \left[A_r \frac{dz}{d\theta} + (bA_p - cA_{pr}) \right] \kappa}{\left[V_{30M} + A_r z + (bA_p - cA_{pr}) \theta \right]^{\kappa+1}} + \\
& \frac{P_{30F} V_{30F}^{\kappa} A_{pr} \left[A_r \frac{dz}{d\theta} - (aA_p + bA_{pr}) \right] \kappa}{\left[V_{30F} + A_r z - (aA_p + bA_{pr}) \theta \right]^{\kappa+1}}
\end{aligned} \right\} - \\
& \left. \begin{aligned}
& \frac{-P_{30R} V_{30R}^{\kappa} A_p \left[A_r \frac{dz}{d\theta} + (cA_p + aA_{pr}) \right] \kappa}{\left[V_{30R} + A_r z + (cA_p + aA_{pr}) \theta \right]^{\kappa+1}} + \\
& \frac{P_{30M} V_{30M}^{\kappa} A_{pr} \left[A_r \frac{dz}{d\theta} + (bA_p - cA_{pr}) \right] \kappa}{\left[V_{30M} + A_r z + (bA_p - cA_{pr}) \theta \right]^{\kappa+1}}
\end{aligned} \right\} - \tag{6-63}
\end{aligned}$$

In this equation $\frac{dz}{d\theta}$ can be found from the static equilibrium equation in vertical direction. Static equilibrium equation is,

$$F_F + F_M + F_R - Mg = 0 \tag{6-64}$$

Taking derivative of this equation with respect to vertical and pitch displacement,

$$\frac{\partial F_F}{\partial z} \partial z + \frac{\partial F_M}{\partial z} \partial z + \frac{\partial F_R}{\partial z} \partial z + \frac{\partial F_F}{\partial \theta} \partial \theta + \frac{\partial F_M}{\partial \theta} \partial \theta + \frac{\partial F_R}{\partial \theta} \partial \theta = 0 \tag{6-65}$$

From these equations $\frac{dz}{d\theta}$ can be found. Moreover for a given θ , z can be found from the static equilibrium equations. To simplify the analysis, vertical displacement can be fixed at zero value and thus the only variable is the pitch displacement.

6.3.2.3. Damping Characteristics

The front, intermediate, and rear suspension forces are given as:

$$\begin{aligned}
 F_F = & -A_p \left[\frac{A_p (\dot{z}_{pF} - \dot{z}_{tF}) - A_{pr} (\dot{z}_{pM} - \dot{z}_{tM})}{A_v C_D} \right]^2 \frac{\rho}{2} \text{sign} \left[\begin{array}{c} A_p (\dot{z}_{pF} - \dot{z}_{tF}) - \\ -A_{pr} (\dot{z}_{pM} - \dot{z}_{tM}) \end{array} \right] + \\
 & + A_{pr} \left[\frac{A_p (\dot{z}_{pR} - \dot{z}_{tR}) - A_{pr} (\dot{z}_{pF} - \dot{z}_{tF})}{A_v C_D} \right]^2 \frac{\rho}{2} \text{sign} \left[\begin{array}{c} A_p (\dot{z}_{pR} - \dot{z}_{tR}) - \\ -A_{pr} (\dot{z}_{pF} - \dot{z}_{tF}) \end{array} \right] - \\
 & - \frac{A_{pr}^2 (\dot{z}_{pF} - \dot{z}_{tF})}{R_{4FIR}}
 \end{aligned} \tag{6-66}$$

$$\begin{aligned}
 F_M = & -A_p \left[\frac{A_p (\dot{z}_{pM} - \dot{z}_{tM}) - A_{pr} (\dot{z}_{pR} - \dot{z}_{tR})}{A_v C_D} \right]^2 \frac{\rho}{2} \text{sign} \left[\begin{array}{c} A_p (\dot{z}_{pM} - \dot{z}_{tM}) - \\ -A_{pr} (\dot{z}_{pR} - \dot{z}_{tR}) \end{array} \right] + \\
 & + A_{pr} \left[\frac{A_p (\dot{z}_{pF} - \dot{z}_{tF}) - A_{pr} (\dot{z}_{pM} - \dot{z}_{tM})}{A_v C_D} \right]^2 \frac{\rho}{2} \text{sign} \left[\begin{array}{c} A_p (\dot{z}_{pF} - \dot{z}_{tF}) - \\ -A_{pr} (\dot{z}_{pM} - \dot{z}_{tM}) \end{array} \right] - \\
 & - \frac{A_{pr}^2 (\dot{z}_{pM} - \dot{z}_{tM})}{R_{4MIF}}
 \end{aligned} \tag{6-67}$$

$$\begin{aligned}
 F_R = & -A_p \left[\frac{A_p (\dot{z}_{pR} - \dot{z}_{tR}) - A_{pr} (\dot{z}_{pF} - \dot{z}_{tF})}{A_v C_D} \right]^2 \frac{\rho}{2} \text{sign} \left[\begin{array}{c} A_p (\dot{z}_{pR} - \dot{z}_{tR}) - \\ -A_{pr} (\dot{z}_{pF} - \dot{z}_{tF}) \end{array} \right] + \\
 & + A_{pr} \left[\frac{A_p (\dot{z}_{pM} - \dot{z}_{tM}) - A_{pr} (\dot{z}_{pR} - \dot{z}_{tR})}{A_v C_D} \right]^2 \frac{\rho}{2} \text{sign} \left[\begin{array}{c} A_p (\dot{z}_{pM} - \dot{z}_{tM}) - \\ -A_{pr} (\dot{z}_{pR} - \dot{z}_{tR}) \end{array} \right] - \\
 & - \frac{A_{pr}^2 (\dot{z}_{pR} - \dot{z}_{tR})}{R_{4RIM}}
 \end{aligned} \tag{6-68}$$

Assume that all suspension relative velocities are equal to each other. Then

$$\dot{z}_{pF} - \dot{z}_{tF} = \dot{z}_{pF} = \dot{z}_{pM} - \dot{z}_{tM} = \dot{z}_{pM} = \dot{z}_{pR} - \dot{z}_{tR} = \dot{z}_{pR} = \dot{z} \tag{6-69}$$

The vertical damping force can be found as,

$$F_F = -A_r \left[\frac{A_r \dot{z}}{A_v C_D} \right]^2 \frac{\rho}{2} \text{sign}(\dot{z}) - \frac{A_{pr}^2 \dot{z}}{R_{4FIR}} \tag{6-70}$$

$$F_M = -A_r \left[\frac{A_r \dot{z}}{A_v C_D} \right]^2 \frac{\rho}{2} \text{sign}(\dot{z}) - \frac{A_{pr}^2 \dot{z}}{R_{4M1F}} \quad (6-71)$$

$$F_R = -A_r \left[\frac{A_r \dot{z}}{A_v C_D} \right]^2 \frac{\rho}{2} \text{sign}(\dot{z}) - \frac{A_{pr}^2 \dot{z}}{R_{4R1M}} \quad (6-72)$$

The total damping force is,

$$F_{Damp} = -3A_r \left[\frac{A_r \dot{z}}{A_v C_D} \right]^2 \frac{\rho}{2} \text{sign}(\dot{z}) - \frac{A_{pr}^2 \dot{z}}{R_{4F1R}} - \frac{A_{pr}^2 \dot{z}}{R_{4M1F}} - \frac{A_{pr}^2 \dot{z}}{R_{4R1M}} \quad (6-73)$$

Assume that $\dot{z} = 0$ and $\dot{z}_{iF} = \dot{z}_{iM} = \dot{z}_{iR} = 0$, the pitch damping moment can be found as,

$$M_{Damp} = -aF_F + bF_M + cF_R \quad (6-74)$$

$$M_{Damp} = -a \left\{ \begin{aligned} & A_p \left[\frac{A_p a \dot{\theta} + A_{pr} b \dot{\theta}}{A_v C_D} \right]^2 \frac{\rho}{2} \text{sign}(\dot{\theta}) + \\ & + A_{pr} \left[\frac{A_p c \dot{\theta} + A_{pr} a \dot{\theta}}{A_v C_D} \right]^2 \frac{\rho}{2} \text{sign}(\dot{\theta}) + \frac{A_{pr}^2 a \dot{\theta}}{R_{4F1R}} \end{aligned} \right\} +$$

$$+b \left\{ \begin{aligned} & -A_p \left[\frac{A_p b \dot{\theta} - A_{pr} c \dot{\theta}}{A_v C_D} \right]^2 \frac{\rho}{2} \text{sign}[A_p b \dot{\theta} - A_{pr} c \dot{\theta}] - \\ & -A_{pr} \left[\frac{A_p a \dot{\theta} + A_{pr} b \dot{\theta}}{A_v C_D} \right]^2 \frac{\rho}{2} \text{sign}(\dot{\theta}) - \frac{A_{pr}^2 b \dot{\theta}}{R_{4M1F}} \end{aligned} \right\} +$$

$$+c \left\{ \begin{aligned} & -A_p \left[\frac{A_p c \dot{\theta} + A_{pr} a \dot{\theta}}{A_v C_D} \right]^2 \frac{\rho}{2} \text{sign}(\dot{\theta}) + \\ & + A_{pr} \left[\frac{A_p b \dot{\theta} - A_{pr} c \dot{\theta}}{A_v C_D} \right]^2 \frac{\rho}{2} \text{sign}[A_p b \dot{\theta} - A_{pr} c \dot{\theta}] - \frac{A_{pr}^2 c \dot{\theta}}{R_{4R1M}} \end{aligned} \right\} \quad (6-75)$$

Suspension parameters are given in Table 6.6.

Table 6.6: Suspension Parameters

Parameters	Symbol	Value
Piston Area for Front, Middle, and Rear Suspension	A_p [m ²]	0.007
Oil Dynamic Viscosity	μ [mPa.s]	82
Hose Diameter	D [mm]	25

Other suspension parameters are given in the following parts depending on the type and strength of the interconnections.

6.4. A GENERAL FORMULA FOR THE PITCH INTERCONNECTED HP SUSPENSION SYSTEM FOR THE THREE AXLE VEHICLES

After the models of the different interconnected HP suspension configurations are derived, general formulas for the suspension forces of the full interconnection and the semi-interconnections are going to be developed. These general formulas are valid for the following cases:

- ❖ Fourth oil volume of the any suspension unit and the first oil volume of the one of the remaining suspension units are connected to each other, also called X arrangement.
- ❖ Each oil volume is connected only once.

When the first volume of the i^{th} suspension unit is connected to the fourth volume of the j^{th} suspension unit, and when the fourth oil volume of the i^{th} suspension unit is connected to the first oil volume of the k^{th} suspension unit, the suspension force can be found by,

$$\begin{aligned}
F_i = & \frac{P_{30i} V_{30i}^\kappa A_p}{\left[V_{30i} + A_p \left(z_{pi} - z_{ti} - \frac{A_{pr}^*}{A_p} (z_{pj} - z_{tj}) \right) \right]^\kappa} - \\
& - P_{Atm} A_p - M_{fp} (g + \ddot{z}_{fpi}) - \\
& - A_p \left[\frac{A_p (\dot{z}_{pi} - \dot{z}_{ti}) - A_{pr}^* (\dot{z}_{pj} - \dot{z}_{tj})}{A_v C_D} \right]^2 \frac{\rho}{2} \text{sign} \left[\begin{array}{l} A_p (\dot{z}_{pi} - \dot{z}_{ti}) - \\ - A_{pr}^* (\dot{z}_{pj} - \dot{z}_{tj}) \end{array} \right] - \\
& - \frac{P_{30k} V_{30k}^\kappa A_{pr}^+}{\left[V_{30k} + A_p \left(z_{pk} - z_{tk} - \frac{A_{pr}^+}{A_p} (z_{pi} - z_{ti}) \right) \right]^\kappa} + P_{Atm} A_{pr}^+ + \\
& + \frac{M_{fp} (g + \ddot{z}_{fpk}) A_{pr}^+}{A_p} + \\
& + A_{pr}^+ \left[\frac{A_p (\dot{z}_{pk} - \dot{z}_{tk}) - A_{pr}^+ (\dot{z}_{pi} - \dot{z}_{ti})}{A_v C_D} \right]^2 \frac{\rho}{2} \text{sign} \left[\begin{array}{l} A_p (\dot{z}_{pk} - \dot{z}_{tk}) - \\ - A_{pr}^+ (\dot{z}_{pi} - \dot{z}_{ti}) \end{array} \right] - \\
& - \frac{A_{pr}^{+2} (\dot{z}_{pi} - \dot{z}_{ti})}{R_{4ilk}}
\end{aligned} \tag{6-76}$$

where i, j, and k represent F, M, and R. A_{pr}^* and A_{pr}^+ can be found as,

$$A_{pr}^* = \begin{cases} A_{pr} & \text{if 1}^{st} \text{ oil volume of } i^{th} \text{ suspension unit is connected} \\ 0 & \text{if 1}^{st} \text{ oil volume of } i^{th} \text{ suspension unit is unconnected} \end{cases}$$

$$A_{pr}^+ = \begin{cases} A_{pr} & \text{if 4}^{th} \text{ oil volume of } i^{th} \text{ suspension unit is connected} \\ 0 & \text{if 4}^{th} \text{ oil volume of } i^{th} \text{ suspension unit is unconnected} \end{cases}$$

6.4.1. Stiffness Properties

Assuming that $z_{pi}-z_{ti}=z_{pj}-z_{tj}=z_{pk}-z_{tk}=z_{pt}$, and assuming that the first and fourth oil volumes of i^{th} suspension unit is interconnected as specified above, vertical stiffness of i^{th} unit can be found as,

$$k_i = - \frac{\partial F_i}{\partial z_{pt}} = \frac{P_{30i} V_{30i}^\kappa A_p A_r \kappa}{\left[V_{30i} + A_r z_{pt} \right]^{\kappa+1}} - \frac{P_{30k} V_{30k}^\kappa A_{pr} A_r \kappa}{\left[V_{30k} + A_r z_{pt} \right]^{\kappa+1}} \tag{6-77}$$

For the pitch stiffness, the layout of the configuration is important, so here a general formula is not given.

6.4.2. Damping Properties

Assuming that $\dot{z}_{pi} - \dot{z}_{ti} = \dot{z}_{pj} - \dot{z}_{tj} = \dot{z}_{pk} - \dot{z}_{tk} = \dot{z}_{pt}$, and assuming that the first and fourth oil volumes of i^{th} suspension unit is interconnected as specified above, the damping force of i^{th} unit in vertical direction can be found as

$$\begin{aligned}
 F_{\text{dampi}} = & -A_p \left[\frac{A_p (\dot{z}_{pi} - \dot{z}_{ti}) - A_{pr} (\dot{z}_{pj} - \dot{z}_{tj})}{A_v C_D} \right]^2 \frac{\rho}{2} \text{sign} \left[\begin{array}{c} A_p (\dot{z}_{pi} - \dot{z}_{ti}) - \\ -A_{pr} (\dot{z}_{pj} - \dot{z}_{tj}) \end{array} \right] + \\
 & + A_{pr} \left[\frac{A_p (\dot{z}_{pk} - \dot{z}_{tk}) - A_{pr} (\dot{z}_{pi} - \dot{z}_{ti})}{A_v C_D} \right]^2 \frac{\rho}{2} \text{sign} \left[\begin{array}{c} A_p (\dot{z}_{pk} - \dot{z}_{tk}) - \\ -A_{pr} (\dot{z}_{pi} - \dot{z}_{ti}) \end{array} \right] - \\
 & - \frac{A_{pr}^2 (\dot{z}_{pi} - \dot{z}_{ti})}{R_{4i1k}}
 \end{aligned} \tag{6-78}$$

Similarly for the pitch damping, the layout of the interconnection is important and thus a general formula for the pitch damping is not given.

6.5. COMPARISON OF THE STIFFNESS PROPERTIES OF THE DIFFERENT INTERCONNECTED SUSPENSION CONFIGURATIONS

After the mathematical model of different suspension configurations are derived, their dynamic properties will be compared to each other. When the same suspension geometry, vehicle, and suspension parameters are used for all suspension configurations, completely different suspensions are obtained. To be able to make a reasonable comparison between different suspension configurations, some of their properties are equated to each other. In this study, vertical stiffness values at static equilibrium are equated to each other by changing the suspension dimensions, when the pitch properties are to be compared. Initial gas volumes of the suspension units are optimized in order to have an equal vertical stiffness for different suspension configurations. Therefore, optimization problem becomes,

$$\underset{x}{\text{Arg min}} (k_{zi} - k_{z6})$$

where $x : \{V_{30i}\}$ is the parameter set to be optimized and k_{zi} is the vertical stiffness of i^{th} suspension configuration. While comparing the stiffness properties of the suspension configurations, two different piston rod areas are used. These are $A_r=0.6A_p$ and $A_r=0.8A_p$.

Case 1: $A_r=0.6A_p$

The properties of the different suspension configurations are given in Table 6.7.

Table 6.7: Suspension Parameters

Parameters	Symbol	Suspension Configurations					
		1 st	2 nd	3 rd	4 th	5 th	6 th
Piston Area	A_p [m ²]	0.007	0.007	0.007	0.007	0.007	0.007
Initial Gas Volume	V_{30F} [m ³]	0.0011	0.0011	0.0012	0.0019	0.0012	0.0019
Initial Gas Volume	V_{30M} [m ³]	0.0011	0.0011	0.0012	0.0012	0.0019	0.0019
Initial Gas Volume	V_{30R} [m ³]	0.0011	0.0011	0.0019	0.0012	0.0012	0.0019
First Sus Initial Gas Pressure	P_{30F} [bar]	37.2	37.5	38.0	23.7	37.3	23.7
Intermediate Sus. Initial Gas Pressure	P_{30M} [bar]	36.4	35.5	36.7	35.2	21.9	21.9
Rear Sus. Initial Gas Pressure	P_{30R} [bar]	34.7	35.2	20.6	34.2	35.1	20.6
First Sus. Force	F_F [N]	15875	15875	15875	15875	15875	15875
Intermediate Sus. Force	F_M [N]	14614	14614	14614	14614	14614	14614
Rear Sus. Force	F_R [N]	13683	13683	13683	13683	13683	13683

Vertical stiffness characteristics of the different interconnected suspension configurations are given in Figure 6.10. As can be seen from Figure 6.10, all suspension configurations have practically equal vertical stiffness characteristics. After the vertical stiffness characteristics of all suspension configurations have been equalized, now the pitch stiffness characteristics which given in Figure 6.11 are examined.

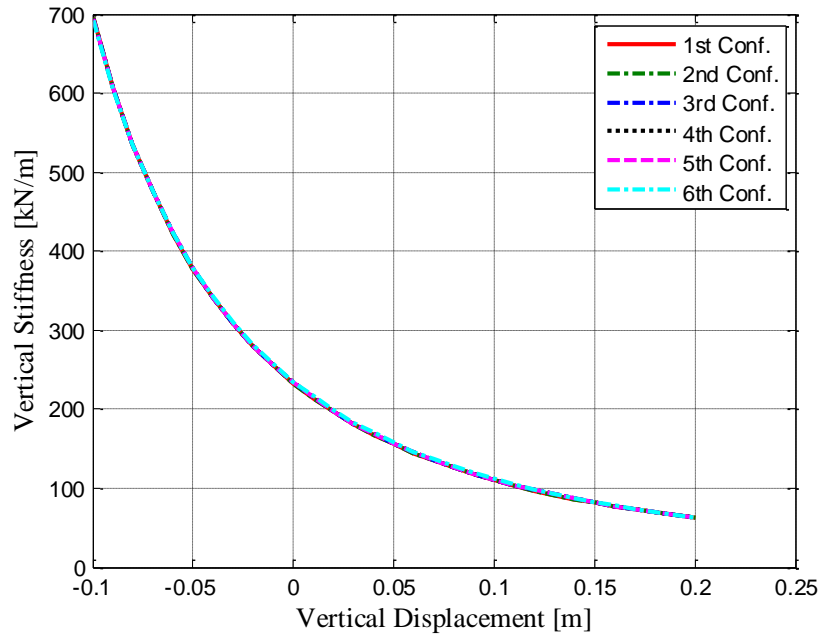


Figure 6.10: Vertical Stiffness of Different Suspension Configurations

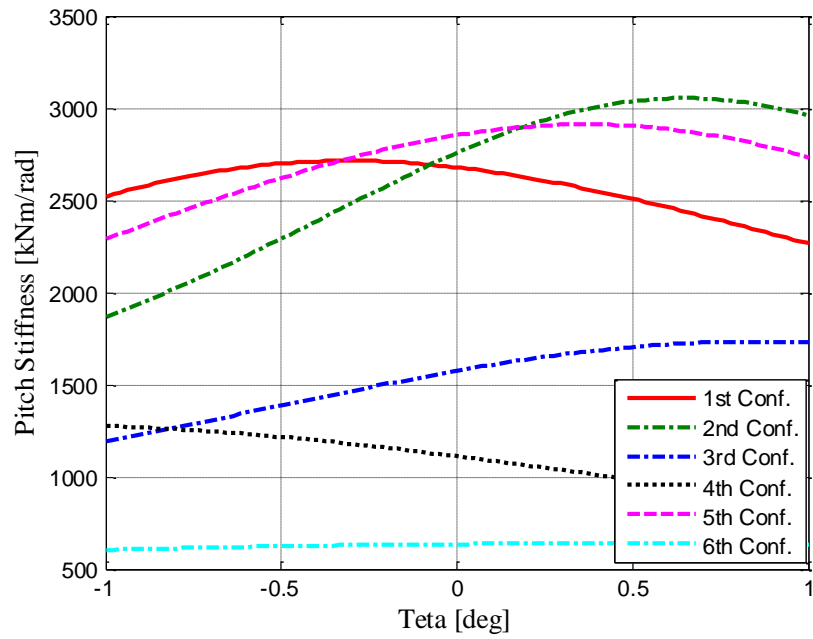


Figure 6.11: Pitch Stiffness of Different Suspension Configurations for $A_t=0.6A_p$

As Figure 6.11, illustrates, first, second and fifth suspension configurations have the highest pitch stiffness characteristics. Sixth interconnected HP suspension

configuration has the lowest pitch stiffness among all suspension configurations. The semi-interconnected HP suspension configurations which are third and fourth have lower pitch stiffness with respect to first, second and fifth, and higher pitch stiffness as compared with the sixth suspension configuration.

Case 2: $A_r=0.8A_p$

The properties of the different suspension configurations are given in Table 6.8.

Table 6.8: Suspension Parameters

Parameters	Symbol	Value					
		1 st	2 nd	3 rd	4 th	5 th	6 th
Piston Area	A_p [m ²]	0.007	0.007	0.007	0.007	0.007	0.007
Initial Gas Volume	V_{30F} [m ³]	0.0015	0.0015	0.0015	0.0019	0.0015	0.0019
Initial Gas Volume	V_{30M} [m ³]	0.0015	0.0015	0.0015	0.0015	0.0019	0.0019
Initial Gas Volume	V_{30R} [m ³]	0.0015	0.0015	0.0019	0.0015	0.0015	0.0019
First Sus. Initial Gas Pressure	P_{30F} [bar]	28.7	28.9	29.0	23.7	28.7	23.7
Intermediate Sus. Initial Gas Pressure	P_{30M} [bar]	27.4	26.9	27.5	26.8	21.9	21.9
Rear Sus. Initial Gas Pressure	P_{30R} [bar]	25.8	26.1	20.6	25.7	26.1	20.6
First Sus. Force	F_F [N]	15875	15875	15875	15875	15875	15875
Intermediate Sus. Force	F_M [N]	14614	14614	14614	14614	14614	14614
Rear Sus. Force	F_R [N]	13683	13683	13683	13683	13683	13683

The vertical and pitch stiffness of the different suspension configurations are given in Figure 6.12 and Figure 6.13, respectively. As Figure 6.12 shows, vertical stiffness characteristics of all suspension configurations are the same. When the ratio of the rod to piston area, also called the strength of the interconnection, is increased, there is a trend for all suspensions to get close to unconnected suspension configurations in terms of the stiffness characteristics as can be seen from Figure 6.11 and Figure 6.13.

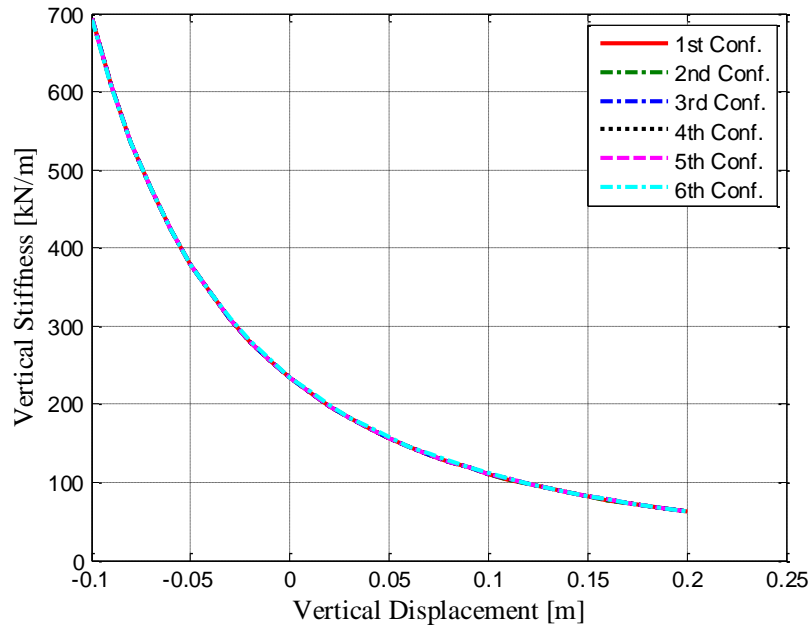


Figure 6.12: Vertical Stiffness of Different Suspension Configurations

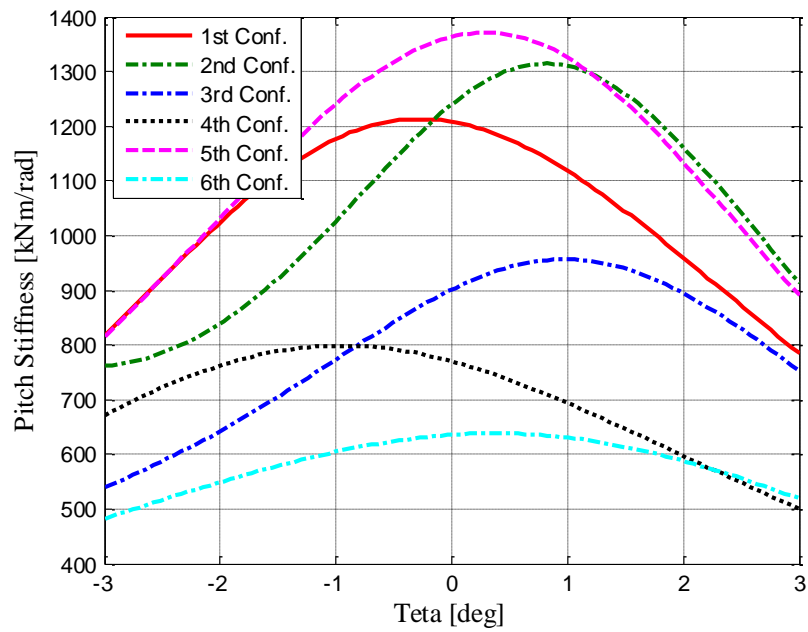


Figure 6.13: Pitch Stiffness of Different Suspension Configurations for $A_f=0.8A_p$

In summary as Figure 6.11 and Figure 6.13 shows, the fifth suspension configuration in which front and the rear suspension units are interconnected to the each other has

the maximum pitch stiffness. Since front and the rear suspension units are connected to each other, maximum amount of the oil is displaced by the pitch angle from front to rear and rear to front suspension. Moreover, first and second suspension configurations which are full interconnections have also high pitch stiffness. This is due to the fact that a high amount of oil is displaced between suspension units. However, third and fourth semi-interconnections have lower pitch stiffness as compared with the other interconnections. This is due to the fact that, the interconnections are either between front and intermediate suspensions, or intermediate and rear suspensions. Thus the amount of oil displaced between suspensions is not as much as in other interconnections. When the interconnection is made only between the intermediate and front, or intermediate and rear suspension units, the pitch stiffness is not high since the piston displacement is related with the distances between the suspension units and the center of gravity (COG). The distance between the intermediate suspension unit and the COG is small resulting in lower amount of oil displaced among suspensions. When the interconnection is made through the front and intermediate, or between intermediate and rear suspension units, asymmetric suspension pitch stiffness are obtained.

6.6. COMPARISON OF THE DAMPING PROPERTIES OF DIFFERENT SUSPENSION CONFIGURATIONS

Now the damping characteristics of the derived suspension configurations are going to be compared. First, the suspension damping forces in the pure vertical direction are equalized to each other by changing the valve parameters. Then the pitch damping moments are examined. Comparisons are made for two cases of the piston rod areas which are $A_r=0.6A_p$ and $A_r=0.8A_p$. When the vertical suspension forces are equated to each other, the sixth suspension configuration which has unconnected front, intermediate, and rear suspension units is taken as the reference configuration. The vertical damping forces of the other suspension configurations are equated to the vertical damping force of the sixth suspension configurations by optimization as,

$$\text{Arg min}_x (F_{\text{Damp}i} - F_{\text{Damp}6})$$

where $x : \{A_{\text{valve}}, A_{\text{max pos}}, A_{\text{max neg}}, \Delta P_{\text{max pos}}, \Delta P_{\text{max neg}}\}$ is the parameter set to be optimized and $F_{\text{Damp}i}$ is the vertical damping force for i^{th} suspension configurations.

Case 1: $A_r=0.6A_p$

Vertical damping forces and the pitch damping moments of the derived suspension configurations are given in Figure 6.14 and Figure 6.15.

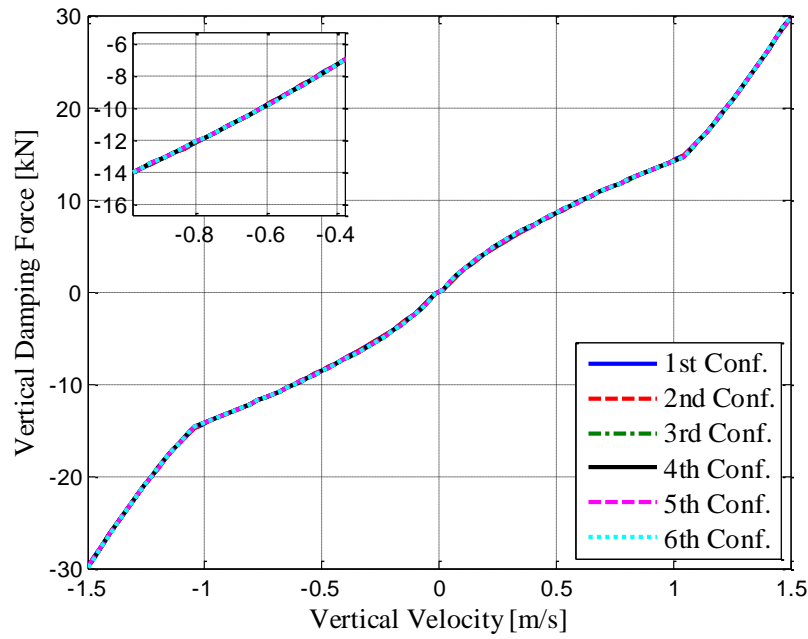


Figure 6.14: Vertical Damping Force for Suspension Configurations

As can be understood from Figure 6.14, all suspension configurations have nearly equivalent vertical damping characteristics.

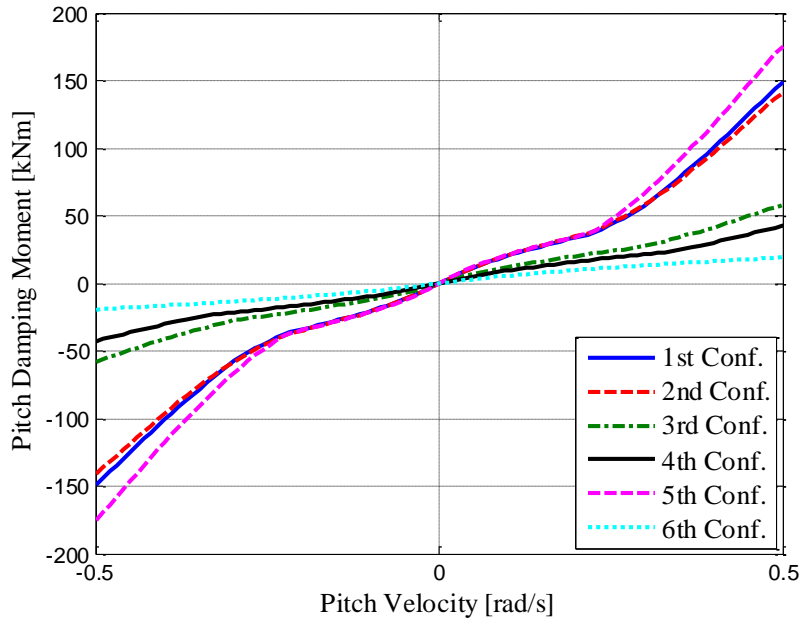


Figure 6.15: Pitch Damping Moment for Interconnected Suspension Configurations

Case 1: $A_r=0.8A_p$

Vertical damping forces and the pitch damping moments of the derived suspension configurations are given in Figure 6.16 and Figure 6.17.

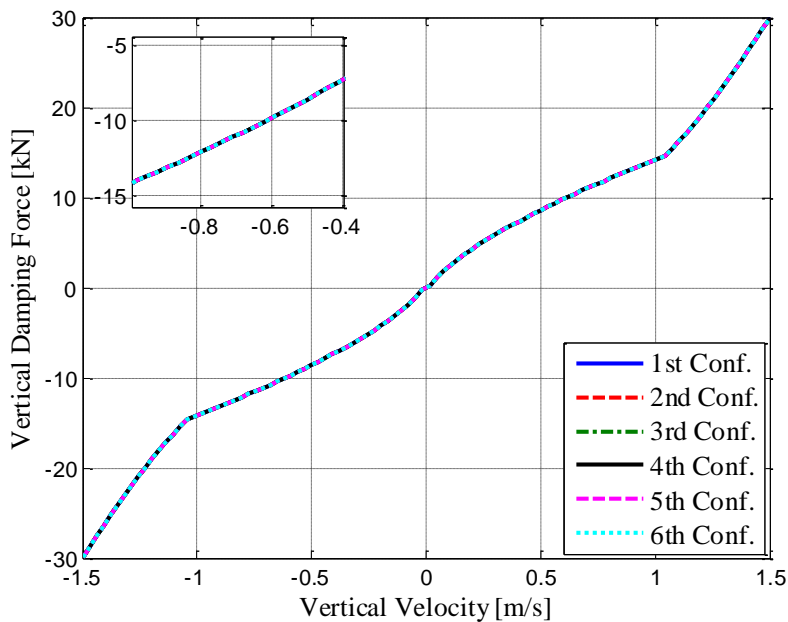


Figure 6.16: Vertical Damping Force for Suspension Configurations

As Figure 6.16 illustrates, all suspension configurations have equivalent vertical damping characteristics.

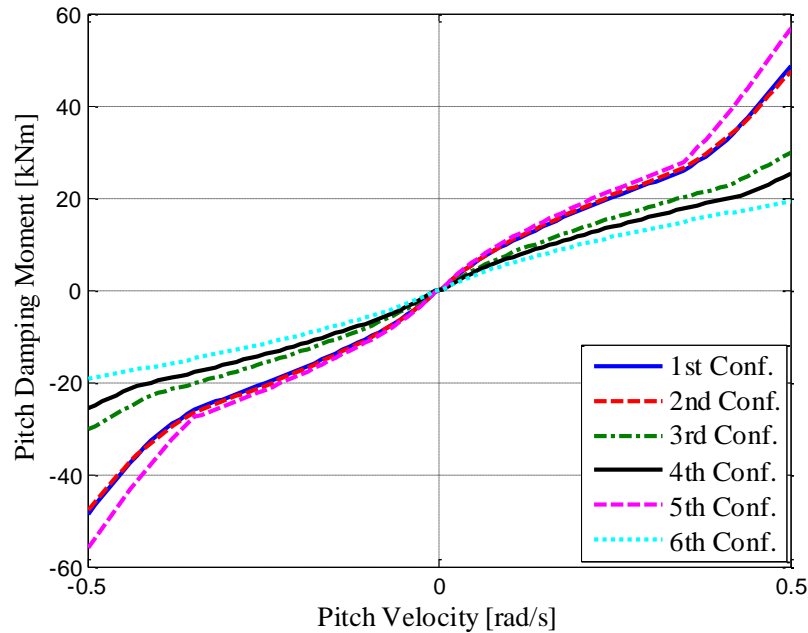


Figure 6.17: Pitch Damping Moment for Suspension Configurations

As can be seen from Figure 6.15 and Figure 6.17, when the suspension configurations have equivalent vertical damping force, the fifth suspension configuration has the highest pitch damping moment. The first and second interconnection configurations have also high pitch damping. Finally, the unconnected suspension configuration has the lowest pitch damping moment as compared to other suspension configurations. As the strength of the interconnection increases, the difference between the pitch damping characteristics of different suspension configurations increases. On the other hand when the strength of the interconnection decreases, suspension pitch damping gets close to each other.

6.7. LOAD-LEVELING, STATIC DEFLECTION, AND SUSPENSION FORCE CHARACTERISTICS

After the stiffness and the damping characteristics of the different suspension configurations are examined, the load leveling and static deflection characteristics of the obtained suspension configurations are going to be examined. When the vehicle

is subjected to a vertical load or when the mass of the vehicle is increased, a new static equilibrium is obtained and suspension forces change. For the suspensions, it is desired to have as small as possible vertical and pitch deflections and it is desired to have nearly equivalent suspension forces with the original case.

When there is an increase in mass ΔM of the vehicle at a distance ΔL from the center of gravity, vehicle reaches static equilibrium at a new vertical and pitch position. Comparisons are made with $A_r=0.6A_p$ and $A_r=0.8A_p$ rod piston areas.

Now the simulations are performed with the obtained suspension configurations. The results are given in Table 6.9 to Table 6.12.

The disturbance mass is 2000 kg and it is placed ± 0.6 m from the center of gravity.

Table 6.9: Static Equilibrium for $A_r=0.6A_p$, $\Delta L=0.6$ m and $\Delta M=2000$ kg

	Displacement		Suspension Forces [kN]		
	Vertical [m]	Pitch [Degree]	Front	Intermediate	Rear
1st Con.	-0.062	-0.13	19.9	21.4	22.6
2nd Con.	-0.062	-0.14	19.9	21.4	22.6
3rd Con.	-0.062	-0.24	18.7	24.2	20.9
4th Con.	-0.07	-0.10	19.8	21.5	22.5
5th Con.	-0.062	-0.11	19.9	21.2	22.6
6th Con.	-0.062	-0.60	19.9	21.3	22.6

Table 6.10: Static Equilibriums for $A_r=0.8A_p$, $\Delta L=0.6$ m and $\Delta M=2000$ kg

	Displacement		Suspension Forces [kN]		
	Vertical [m]	Pitch [Degree]	Front	Intermediate	Rear
1st Con.	-0.062	-0.30	19.9	21.3	22.6
2nd Con.	-0.062	-0.30	19.9	21.4	22.6
3rd Con.	-0.062	-0.42	19.3	22.7	21.8
4th Con.	-0.066	-0.32	20.1	21.0	22.8
5th Con.	-0.062	-0.26	19.9	21.2	22.6
6th Con.	-0.062	-0.60	19.9	21.3	22.6

Table 6.11: Static Equilibrium for $A_r=0.6A_p$, $\Delta L=-0.6m$ and $\Delta M=2000kg$

	Displacement		Suspension Forces [kN]		
	Vertical [m]	Pitch [Degree]	Front	Intermediate	Rear
1st Con.	-0.062	0.14	26.1	20.7	17.1
2nd Con.	-0.062	0.13	26.0	20.7	17.0
3rd Con.	-0.062	0.23	27.3	17.8	18.7
4th Con.	-0.073	0.60	23.1	27.5	13.1
5th Con.	-0.062	0.11	25.9	21.1	16.8
6th Con.	-0.062	0.59	26.1	20.5	17.2

Table 6.12: Static Equilibriums for $A_r=0.8A_p$, $\Delta L=-0.6m$ and $\Delta M=2000kg$

	Displacement		Suspension Forces [kN]		
	Vertical.[m]	Pitch [Degree]	Front	Intermediate	Rear
1st Con.	-0.062	0.31	26.1	20.6	17.1
2nd Con.	-0.062	0.29	26.1	20.6	17.1
3rd Con.	-0.062	0.40	26.7	19.1	18.0
4th Con.	-0.067	0.67	25.2	22.7	15.9
5th Con.	-0.062	0.26	26.0	20.9	17.0
6th Con.	-0.062	0.59	26.1	20.5	17.2

As can be seen from Table 6.9 to Table 6.12, the first, second, and the fifth suspension configurations have the lowest pitch deflections due to extra mass. The fourth and the sixth (unconnected) HP suspension configuration has the highest pitch deflection due to their low pitch stiffness characteristics. Therefore, from these results, it can be said that, interconnected suspension configurations increase the load leveling performance of the vehicle.

6.8. SIMULATIONS

In this part simulations are performed in order to examine the characteristics of the suspension configurations considered so far. With the simulation results, performances of the suspensions are evaluated. Firstly, the simulations are to be performed for improved ride comfort characteristics. Random road inputs and the bump road inputs are used as the disturbance inputs at the simulations. HP suspension will be simulated with the same random road displacement input used in section 4.2.4.1 at different longitudinal speeds. The rms values of the performance parameters are

calculated and tabulated. The bump road input is formed at 25 kph longitudinal vehicle velocity.

6.8.1. Simulations with Random Road

Case 1: $A_r=0.6A_p$

Simulation results are given in Table 6.13 to Table 6.16.

Table 6.13: Random Road Simulations for V=60kph

	1 st	2 nd	3 rd	4 th	5 th	6 th
Ver. Acc. [m/s²]	0.27	0.27	0.27	0.27	0.27	0.28
Pitch. Acc. [rad/s²]	0.23	0.23	0.21	0.18	0.24	0.15
Front Tire Disp [mm]	1.3	1.3	1.3	1.0	1.2	1.0
Intermediate Tire Disp [mm]	1.0	1.0	1.3	0.8	1.0	0.9
Rear Tire Disp [mm]	1.3	1.3	1.1	1.3	1.4	1.0
Front Sus. Disp [mm]	4.1	4.1	3.6	4.3	4.1	5.2
Intermediate Sus. Disp [mm]	4.3	4.3	3.8	4.8	4.2	4.4
Rear Sus. Disp [mm]	4.8	4.8	5.4	5.5	4.6	5.5

Table 6.14: Random Road Simulations for V=70kph

	1 st	2 nd	3 rd	4 th	5 th	6 th
Ver. Acc. [m/s²]	0.36	0.36	0.36	0.35	0.36	0.36
Pitch. Acc. [rad/s²]	0.33	0.34	0.28	0.23	0.35	0.18
Front Tire Disp [mm]	1.7	1.7	1.7	1.2	1.6	1.3
Intermediate Tire Disp [mm]	1.3	1.3	1.7	1.1	1.2	1.1
Rear Tire Disp [mm]	1.8	1.8	1.5	1.7	1.9	1.3
Front Sus. Disp [mm]	5.3	5.3	4.9	5.3	5.2	6.4
Intermediate Sus. Disp [mm]	5.7	5.6	5.1	6.3	5.6	5.8
Rear Sus. Disp [mm]	6.2	6.2	6.8	7.2	5.9	6.9

Table 6.15: Random Road Simulations for V=80kph

	1 st	2 nd	3 rd	4 th	5 th	6 th
Ver. Acc. [m/s²]	0.44	0.44	0.45	0.42	0.44	0.45
Pitch. Acc. [rad/s²]	0.43	0.43	0.33	0.28	0.45	0.21
Front Tire Disp [mm]	2.1	2.1	1.9	1.4	2.0	1.5
Intermediate Tire Disp [mm]	1.6	1.6	2.0	1.3	1.5	1.4
Rear Tire Disp [mm]	2.2	2.2	1.8	2.0	2.4	1.5
Front Sus. Disp [mm]	6.3	6.3	6.0	6.1	6.2	7.6
Intermediate Sus. Disp [mm]	6.9	6.9	6.4	7.7	7.0	7.1
Rear Sus. Disp [mm]	7.6	7.5	8.3	8.9	7.2	8.2

Table 6.16: Random Road Simulations for V=90kph

	1 st	2 nd	3 rd	4 th	5 th	6 th
Ver. Acc. [m/s²]	0.58	0.58	0.59	0.55	0.59	0.59
Pitch. Acc. [rad/s²]	0.56	0.57	0.42	0.36	0.60	0.25
Front Tire Disp [mm]	2.7	2.7	2.4	1.8	2.6	1.9
Intermediate Tire Disp [mm]	2.1	2.0	2.5	1.7	2.0	1.7
Rear Tire Disp [mm]	2.9	2.9	2.3	2.6	3.2	1.9
Front Sus. Disp [mm]	8.3	8.4	8.1	7.9	8.3	10.0
Intermediate Sus. Disp [mm]	9.3	9.3	8.7	10.3	9.4	9.4
Rear Sus. Disp [mm]	10.2	10.1	10.9	11.8	9.7	10.6

As Table 6.13 to Table 6.16 illustrate, vertical accelerations of the suspension configurations are almost equal to each other. This is due to equal vertical damping and stiffness characteristics of the suspension configurations. The first, second, and fifth suspension configurations have the highest pitch acceleration due their higher pitch stiffness. The sixth suspension configuration has the lowest pitch acceleration due to its low pitch stiffness and damping characteristics.

Case 1: $A_r=0.8A_p$

Simulation results with the random road input for $A_r=0.8A_p$ are given in Table 6.17 to Table 6.20.

Table 6.17: Random Road Simulations for V=60kph

	1 st	2 nd	3 rd	4 th	5 th	6 th
Ver. Acc. [m/s²]	0.27	0.27	0.28	0.27	0.27	0.28
Pitch. Acc. [rad/s²]	0.19	0.19	1.7	0.16	0.19	0.15
Front Tire Disp [mm]	1.0	1.0	1.1	1.0	1.0	1.0
Intermediate Tire Disp [mm]	0.9	0.9	1.0	0.8	0.9	0.9
Rear Tire Disp [mm]	1.2	1.2	1.1	1.1	1.2	1.0
Front Sus. Disp [mm]	4.0	4.0	4.2	4.7	4.1	5.2
Intermediate Sus. Disp [mm]	4.3	4.3	4.1	4.5	4.4	4.4
Rear Sus. Disp [mm]	5.2	5.2	5.5	5.5	5.1	5.5

Table 6.18: Random Road Simulations for V=70kph

	1 st	2 nd	3 rd	4 th	5 th	6 th
Ver. Acc. [m/s²]	0.36	0.36	0.36	0.35	0.36	0.36
Pitch. Acc. [rad/s²]	0.24	0.24	0.21	0.20	0.26	0.18
Front Tire Disp [mm]	1.3	1.3	1.4	1.2	1.3	1.3
Intermediate Tire Disp [mm]	1.2	1.2	1.3	1.1	1.2	1.1
Rear Tire Disp [mm]	1.5	1.5	1.4	1.4	1.6	1.3
Front Sus. Disp [mm]	5.1	5.1	5.4	5.8	5.1	6.4
Intermediate Sus. Disp [mm]	5.7	5.7	5.5	6.0	5.8	5.8
Rear Sus. Disp [mm]	6.7	6.6	6.9	7.0	6.5	6.9

Table 6.19: Random Road Simulations for V=80kph

	1 st	2 nd	3 rd	4 th	5 th	6 th
Ver. Acc. [m/s²]	0.44	0.44	0.45	0.43	0.44	0.45
Pitch. Acc. [rad/s²]	0.30	0.30	0.25	0.24	0.32	0.21
Front Tire Disp [mm]	1.5	1.6	1.6	1.5	1.5	1.5
Intermediate Tire Disp [mm]	1.5	1.5	1.6	1.3	1.4	1.4
Rear Tire Disp [mm]	1.9	1.9	1.6	1.7	2.0	1.5
Front Sus. Disp [mm]	6.1	6.1	6.5	6.8	6.1	7.6
Intermediate Sus. Disp [mm]	7.0	7.0	6.8	7.3	7.1	7.1
Rear Sus. Disp [mm]	8.2	8.2	8.4	8.6	8.0	8.2

Table 6.20: Random Road Simulations for V=90kph

	1 st	2 nd	3 rd	4 th	5 th	6 th
Ver. Acc. [m/s²]	0.58	0.58	0.59	0.57	0.58	0.59
Pitch. Acc. [rad/s²]	0.38	0.38	0.31	0.29	0.41	0.25
Front Tire Disp [mm]	2.0	2.0	2.0	1.8	1.9	1.9
Intermediate Tire Disp [mm]	1.9	1.9	2.0	1.7	1.9	1.7
Rear Tire Disp [mm]	2.4	2.4	2.1	2.1	2.5	1.9
Front Sus. Disp [mm]	8.0	8.1	8.7	8.8	8.0	10.0
Intermediate Sus. Disp [mm]	9.4	9.4	9.1	9.7	9.5	9.4
Rear Sus. Disp [mm]	10.9	10.8	10.9	11.2	10.7	10.6

Similar results can be obtained as in the previous case, as can be seen from Table 6.17 to Table 6.20. As a result, the first, second, and the fifth suspension configurations which have the higher pitch stiffness and the damping characteristics

have the lowest ride comfort characteristics among suspension configurations considered.

6.8.2. Simulation with Bump Input

Now the performance of the interconnected and the unconnected HP suspension systems will be examined with the bump road simulations. The input used in the simulation is given in Figure 6.18.

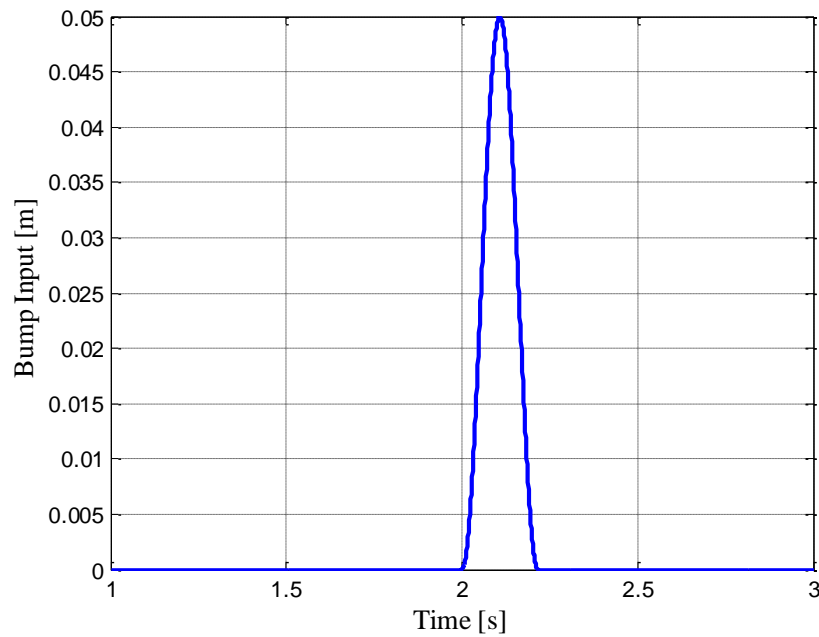


Figure 6.18: Ramp Input

Firstly the simulations will be performed for $A_r=0.6A_p$ and then for $A_r=0.8A_p$.

Case 1: $A_r=0.6A_p$

Simulation results are given in Figure 6.19 to Figure 6.27.

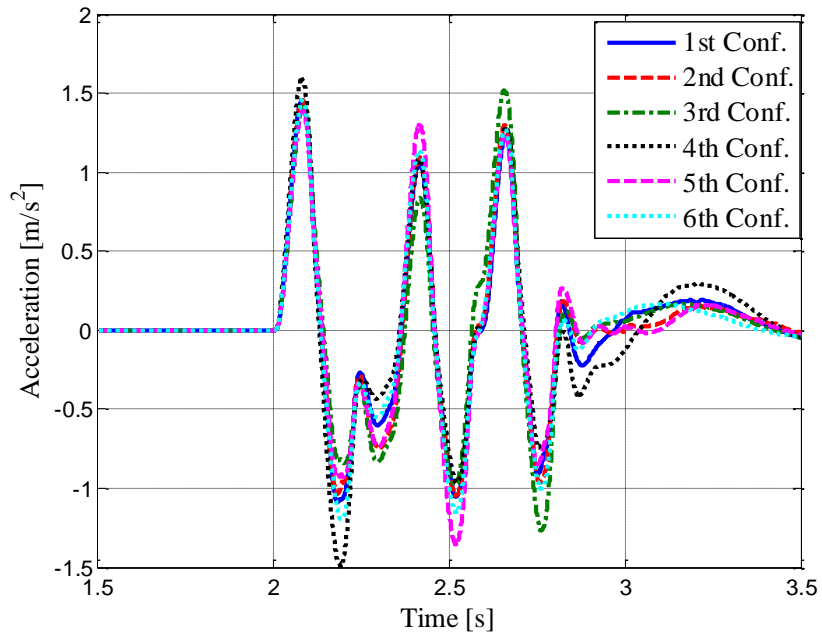


Figure 6.19: Sprung Mass Vertical Acceleration

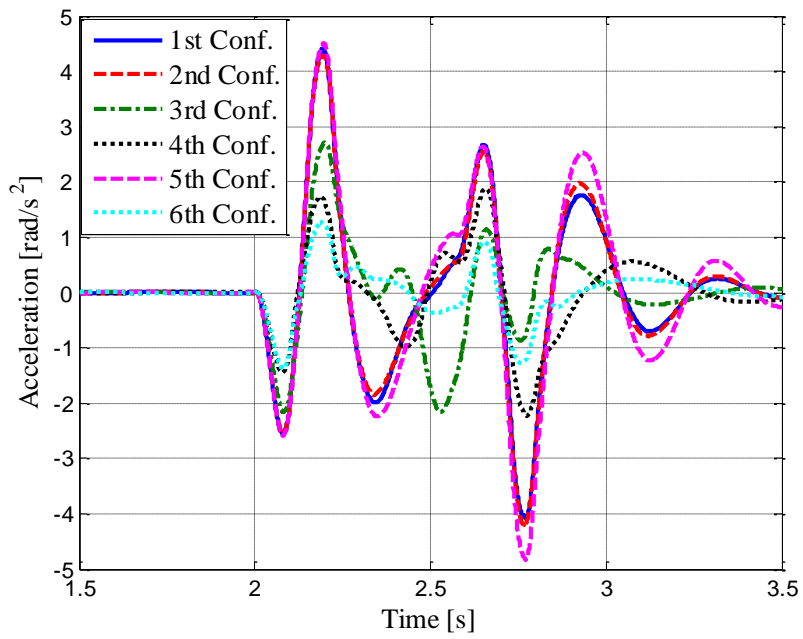


Figure 6.20: Pitch Acceleration

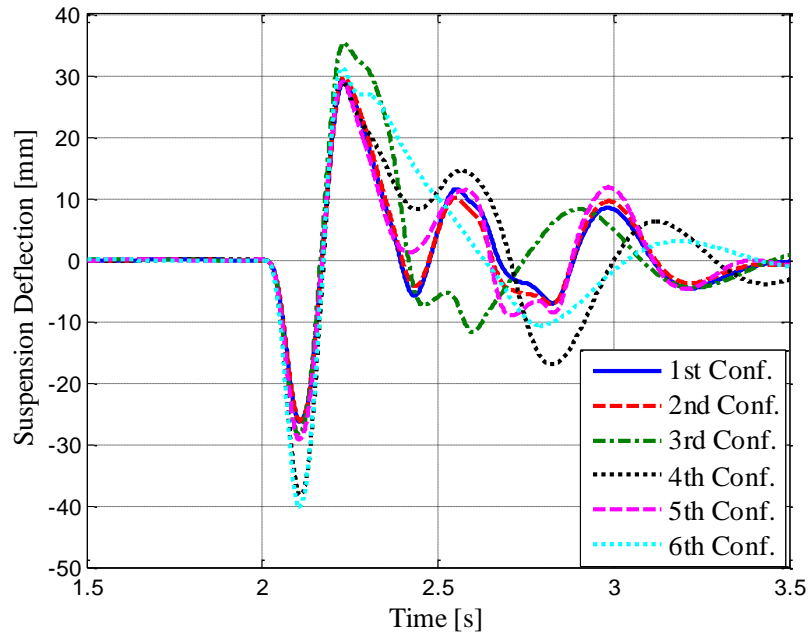


Figure 6.21: Front Suspension Deflection

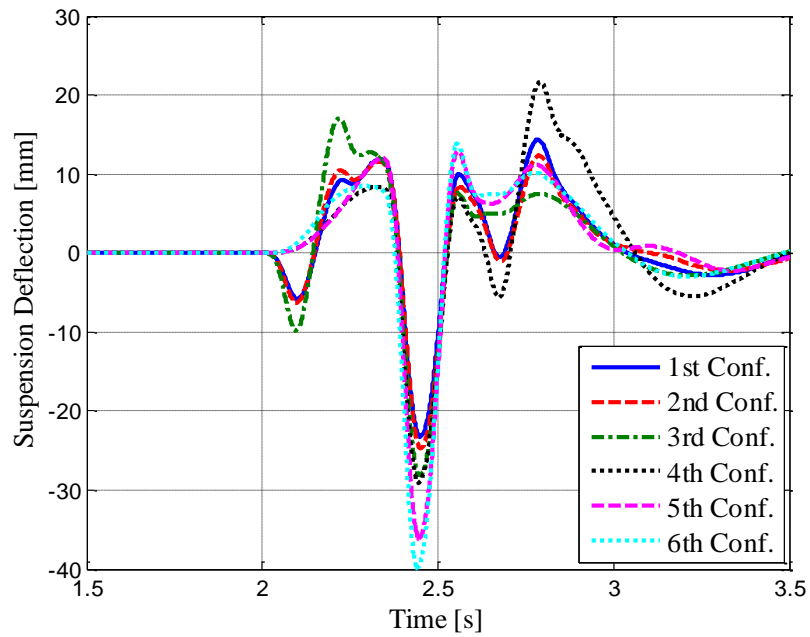


Figure 6.22: Intermediate Suspension Deflection

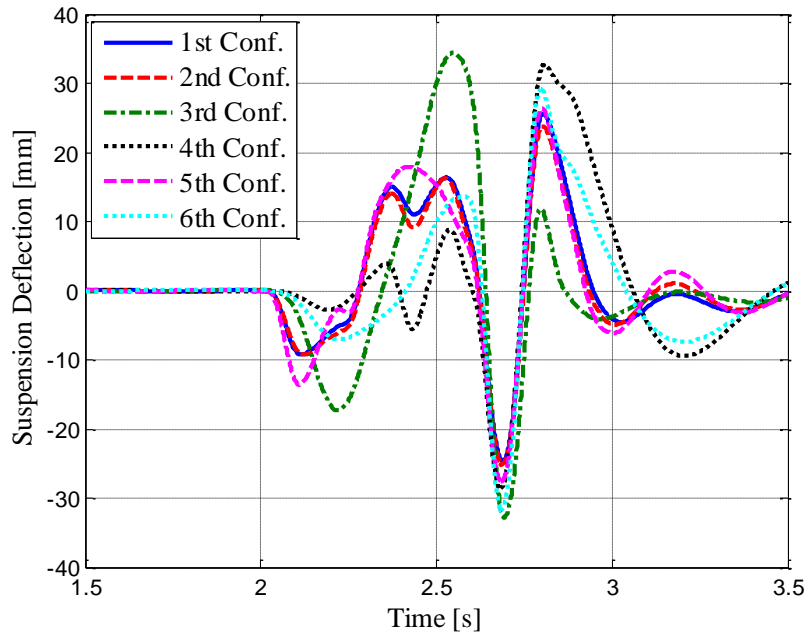


Figure 6.23: Rear Suspension Deflection

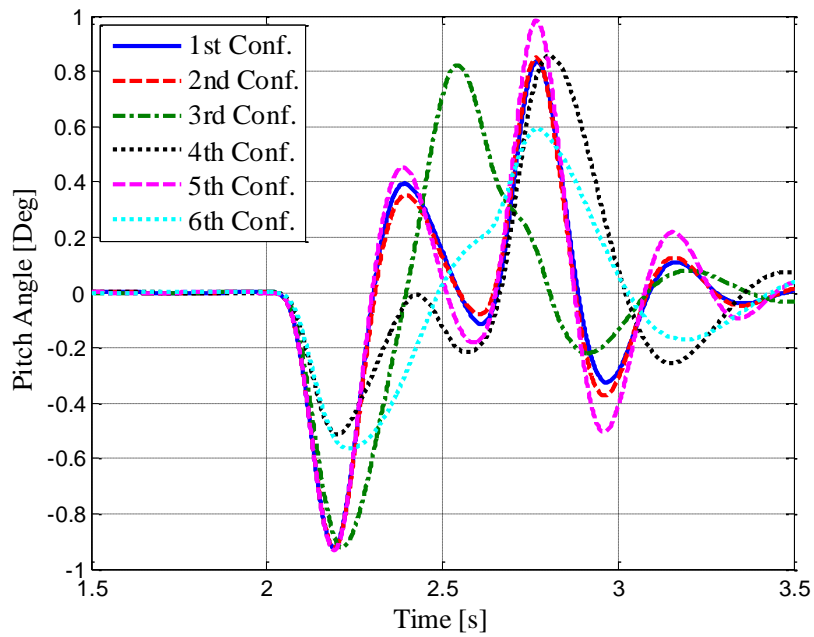


Figure 6.24: Pitch Angle

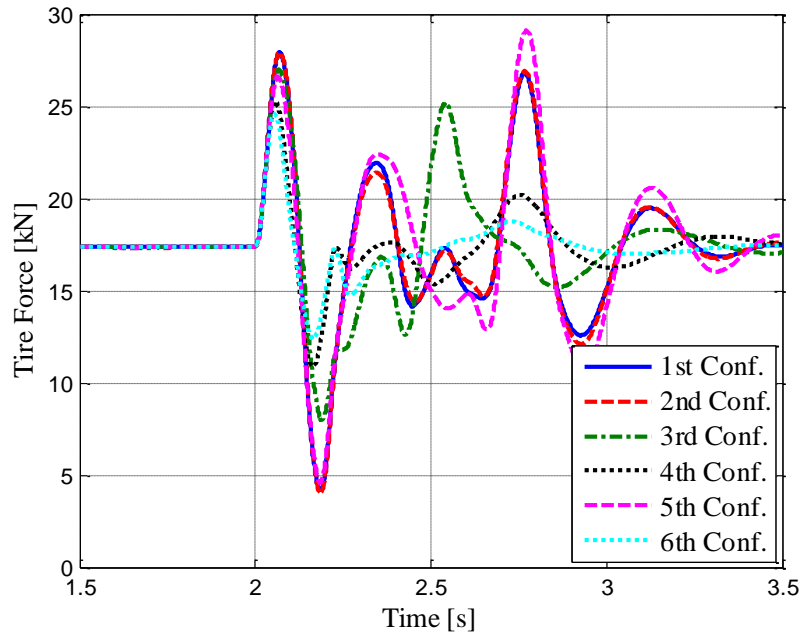


Figure 6.25: Front Tire Force

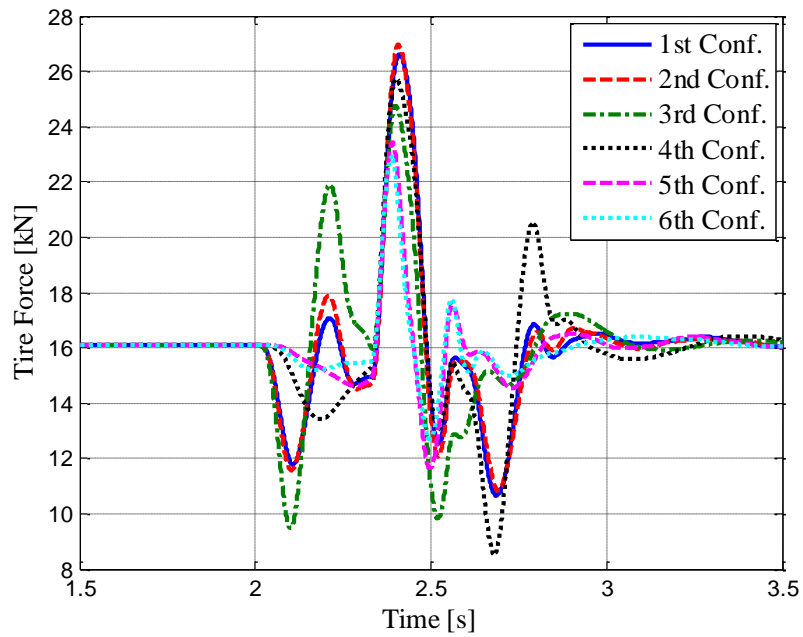


Figure 6.26: Intermediate Tire Force

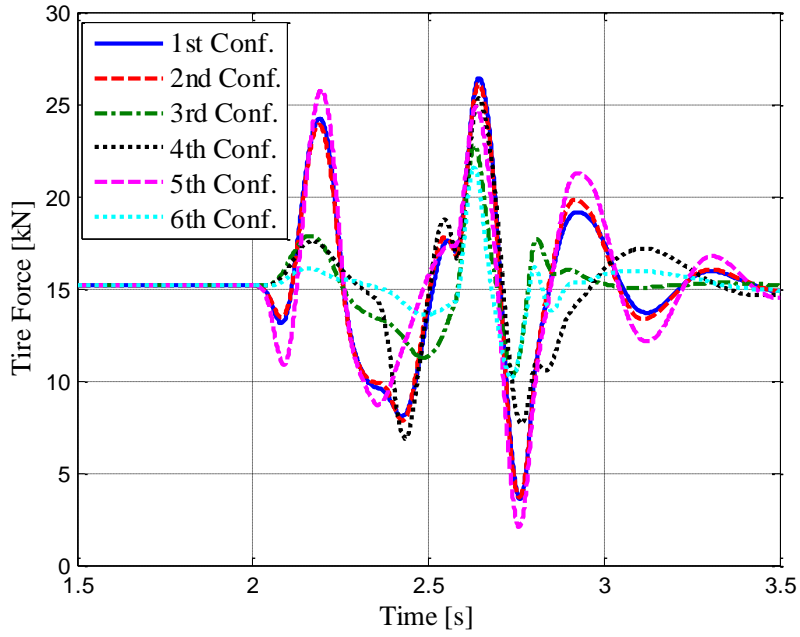


Figure 6.27: Rear Tire Force

Maximum and the minimum values of the response variables are given in Table 6.21 and Table 6.22.

Table 6.21: Maximum Values of the Performance Variables

	1 st	2 nd	3 rd	4 th	5 th	6 th
Ver. Acc. [m/s²]	1.5	1.5	1.5	1.6	1.4	1.5
Pitch. Acc. [rad/s²]	4.4	4.3	2.7	1.9	4.5	1.3
Pitch Angle [deg]	0.8	0.9	0.8	0.9	1.0	0.6
Front Tire Disp [mm]	22.0	22.2	15.6	10.8	21.2	8.2
Intermediate Tire Disp [mm]	9.1	8.8	11.0	12.6	7.4	5.6
Rear Tire Disp [mm]	19.3	19.2	8.0	13.8	21.8	8.4
Front Sus. Disp [mm]	28.7	29.5	35.3	29.0	29.1	31.2
Intermediate Sus. Disp [mm]	14.4	12.3	17.1	21.7	12.9	13.8
Rear Sus. Disp [mm]	25.6	23.8	34.4	32.7	26.5	29.2

Table 6.22: Minimum Values of the Performance Variables

	1 st	2 nd	3 rd	4 th	5 th	6 th
Ver. Acc. [m/s²]	-1.1	-1.0	-1.3	-1.5	-1.4	-1.2
Pitch. Acc. [rad/s²]	-4.1	-4.2	-2.2	-2.2	-4.8	-1.4
Pitch Angle [deg]	-0.9	-0.9	-0.9	-0.5	-0.9	-0.6
Front Tire Disp [mm]	-17.6	-17.7	-16.1	-13.2	-19.6	-12.1
Intermediate Tire Disp[mm]	-17.5	-18.1	-14.4	-16.1	-12.2	-11.4
Rear Tire Disp [mm]	-18.8	-18.3	-12.7	-16.9	-17.6	-10.6
Front Sus. Disp [mm]	-26.3	-26.2	-28.5	-38.3	-29.3	-40.2
Intermediate Sus. Disp[mm]	-23.2	-24.7	-28.1	-29.1	-36.1	-39.9
Rear Sus. Disp [mm]	-24.7	-25.1	-32.8	-28.6	-27.6	-31.8

As can be seen from Table 6.21 and Table 6.22, all suspension configurations have closely equal positive vertical accelerations. Moreover, there are some differences between the negative vertical accelerations of the suspension configurations, yet these differences are small. For pitch accelerations, the first, second, and fifth suspension configurations have the highest values due to their high pitch stiffness and damping characteristics. Moreover, unconnected suspension configuration which has the lowest pitch stiffness and damping among all suspension configurations has the lowest pitch acceleration. The third and fourth suspension configurations have the pitch acceleration responses in between the first, second, and fifth and sixth suspension configurations due to their medium pitch stiffness and damping characteristic. As a result, with regard to ride comfort, the sixth suspension configuration has the best performance, and the first, second, and the fifth suspension configurations have the worst results. The remaining suspension configurations have somewhat compromise performance between these two groups of configurations.

Case 1: $A_r=0.8A_p$

Simulation results are given in Figure 6.28 to Figure 6.36.

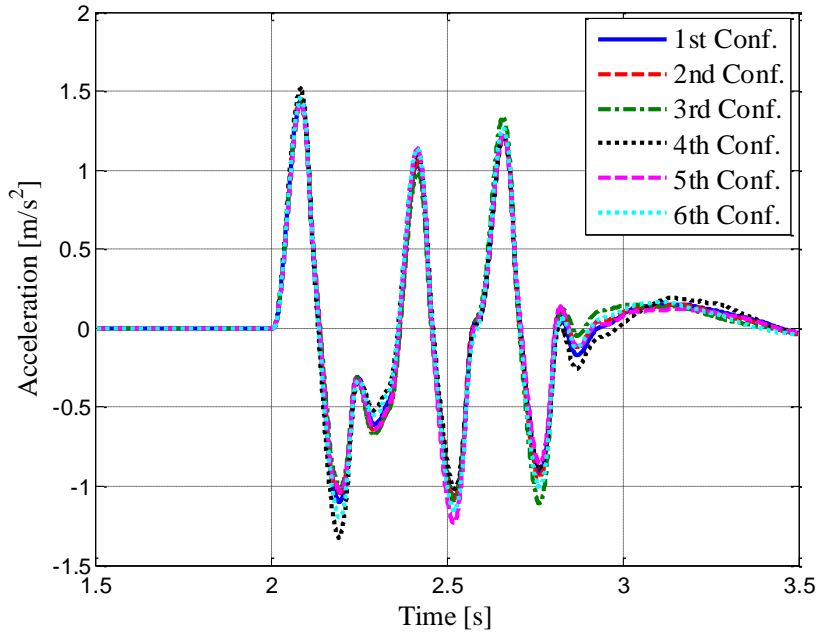


Figure 6.28: Sprung Mass Vertical Acceleration

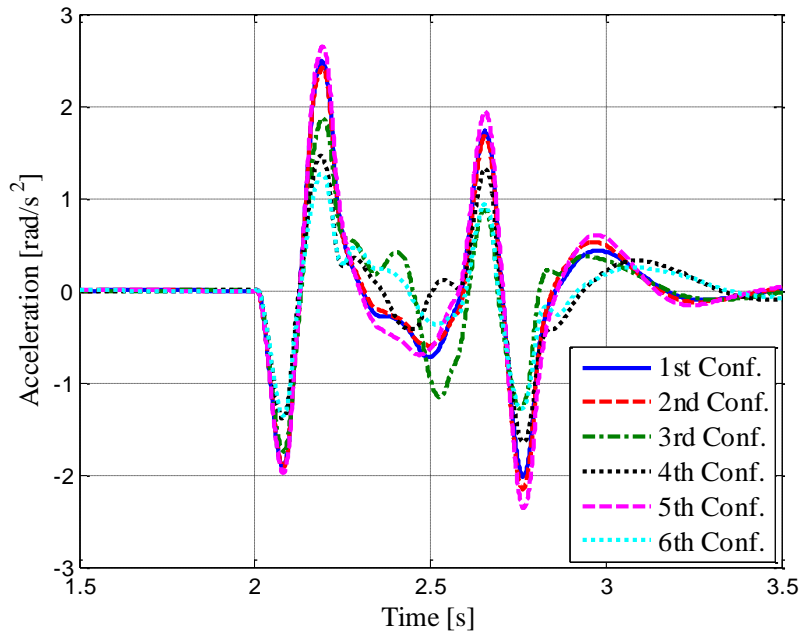


Figure 6.29: Pitch Acceleration

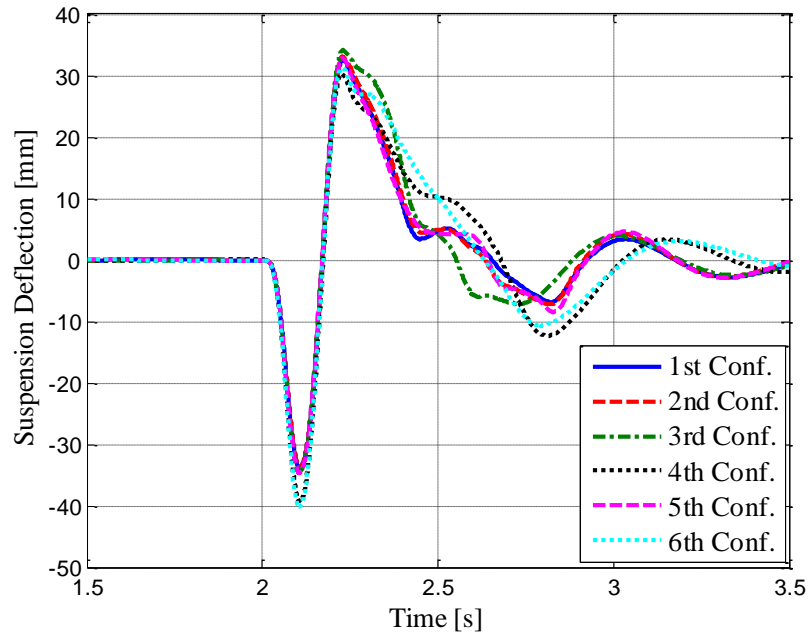


Figure 6.30: Front Suspension Deflection

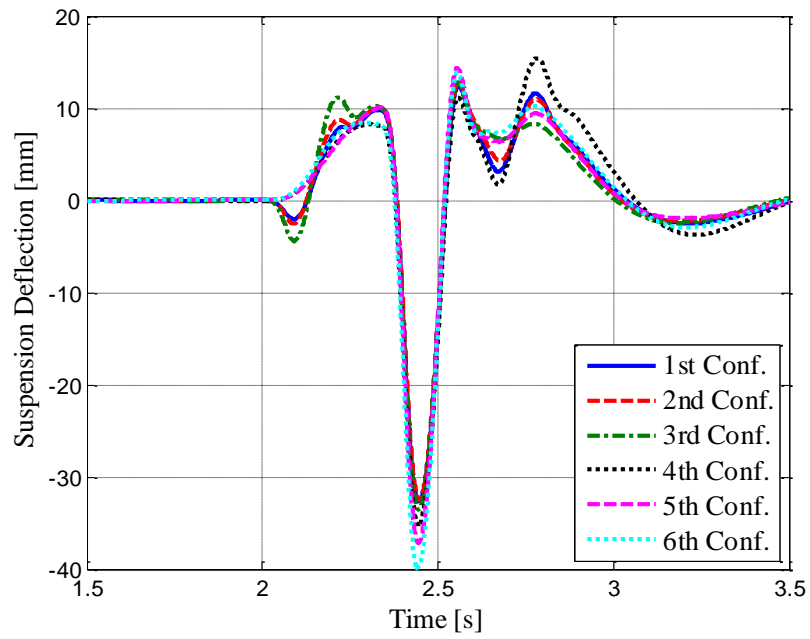


Figure 6.31: Intermediate Suspension Deflection

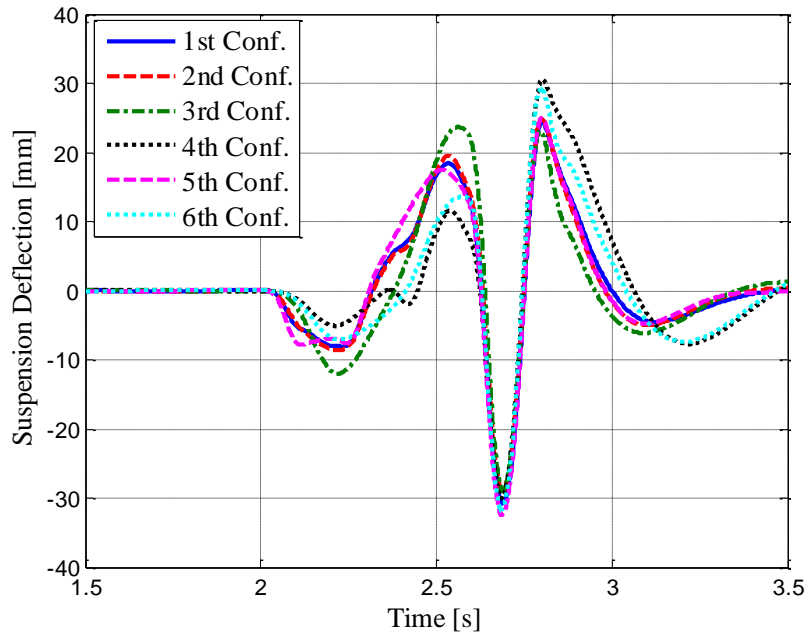


Figure 6.32: Rear Suspension Deflection

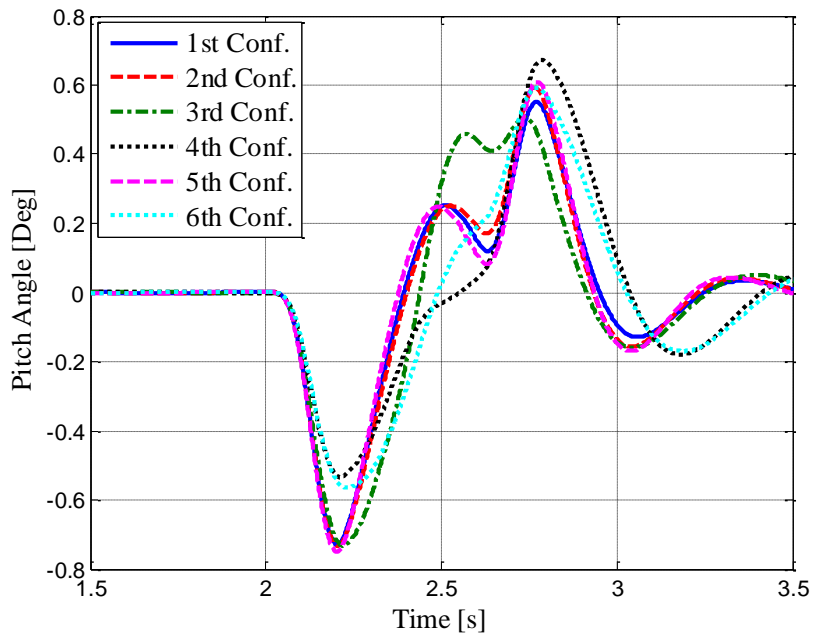


Figure 6.33: Pitch Angle Response

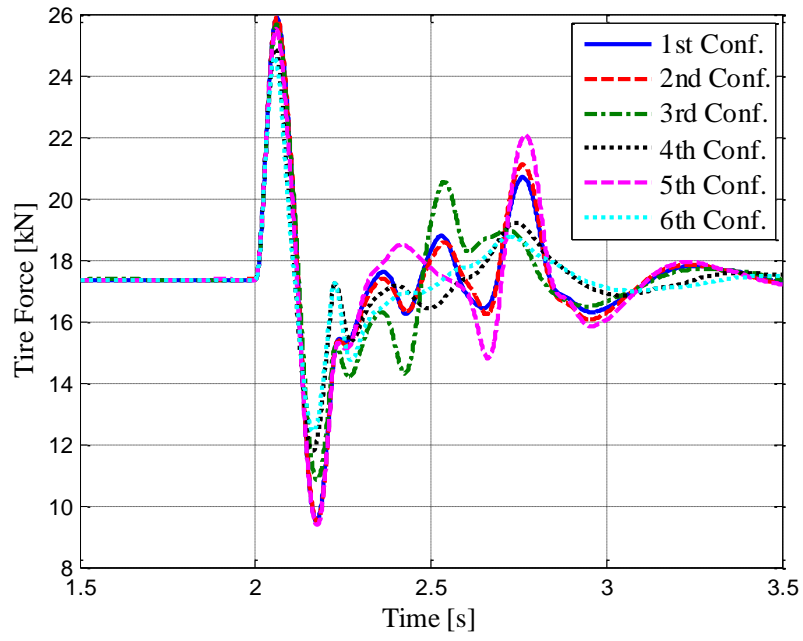


Figure 6.34: Front Tire Force

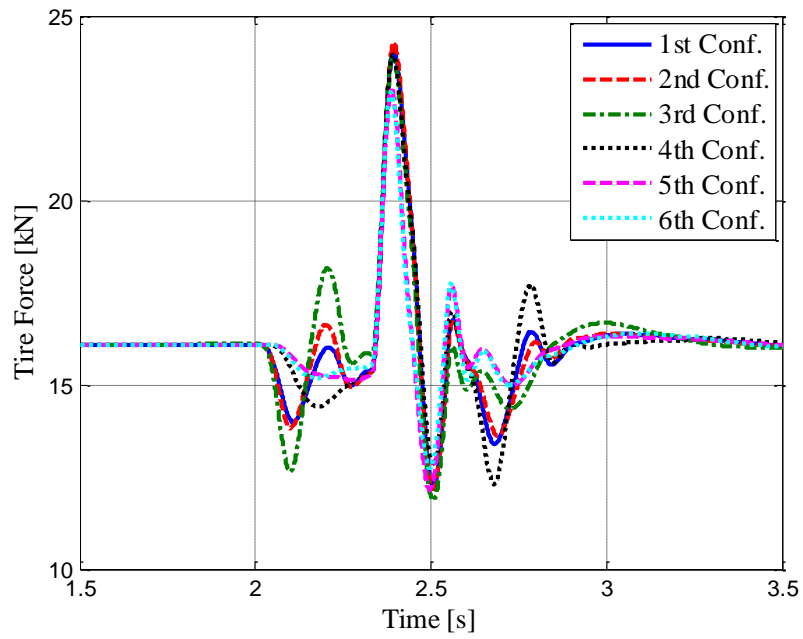


Figure 6.35: Intermediate Tire Force

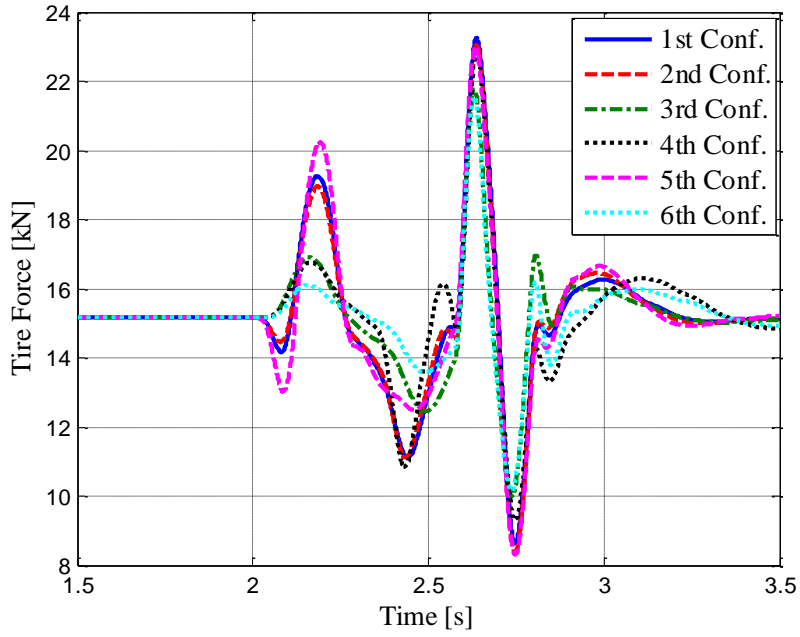


Figure 6.36: Rear Tire Force

Maximum and minimum values of the responses are given in Table 6.23 and Table 6.24.

Table 6.23: Maximum Values of the Performance Variables

	1 st	2 nd	3 rd	4 th	5 th	6 th
Ver. Acc. [m/s²]	1.4	1.5	1.4	1.5	1.4	1.5
Pitch. Acc. [rad/s²]	2.5	2.4	1.9	1.5	2.6	1.3
Pitch Angle [deg]	0.6	0.6	0.5	0.7	0.6	0.6
Front Tire Disp [mm]	13.1	13.1	10.9	9.3	13.3	8.2
Intermediate Tire Disp [mm]	6.4	6.6	7.1	6.3	6.6	5.6
Rear Tire Disp [mm]	10.9	11.3	8.6	9.8	11.5	8.4
Front Sus. Disp [mm]	32.5	33.1	34.2	30.2	32.8	31.2
Intermediate Sus. Disp [mm]	12.4	12.8	12.7	15.4	14.4	13.8
Rear Sus. Disp [mm]	24.3	24.9	23.7	30.5	24.8	29.2

Table 6.24: Minimum Values of the Performance Variables

	1 st	2 nd	3 rd	4 th	5 th	6 th
Ver. Acc. [m/s²]	-1.1	-1.1	-1.1	-1.3	-1.2	-1.2
Pitch. Acc. [rad/s²]	-2.0	-2.2	-1.8	-1.6	-2.4	-1.4
Pitch Angle [deg]	-0.7	-0.7	-0.7	-0.5	-0.8	-0.6
Front Tire Disp [mm]	-14.2	-14.2	-13.8	-12.5	-13.6	-12.1
Intermediate Tire Disp [mm]	-13.3	-13.6	-13.0	-13.1	-11.5	-11.4
Rear Tire Disp [mm]	-13.5	-13.2	-11.0	-12.8	-13.1	-10.6
Front Sus. Disp [mm]	-33.9	-33.7	-34.5	-39.3	-34.6	-40.2
Intermediate Sus. Disp [mm]	-32.7	-32.5	-33.5	-35.3	-37.2	-39.9
Rear Sus. Disp [mm]	-30.8	-29.1	-28.9	-30.0	-32.4	-31.8

As can be seen from in Table 6.23 and Table 6.24, the sixth suspension configuration has the lowest pitch acceleration response. Pitch accelerations of the first, second, and the fifth suspension configurations have higher than the other suspension configurations. Moreover, since the piston rod area is set to a higher value, the difference between the response variables get smaller as compared with the previous case. Therefore, similar to the previous observations, unconnected suspension configuration has the best ride comfort performance.

6.8.3. Simulations with Body Disturbance Inputs

Now performance of the vehicle with respect to the disturbances coming from the vehicle body is to be examined. First braking performance and then the firing shock performance of the vehicle are examined with simulations.

6.8.3.1. Simulation with Braking Input

To be able to examine the performance of the different suspension configurations, simulations with various braking scenarios were performed. The braking torque model was adapted from the study of Cao [19] shown in Figure 6.37.

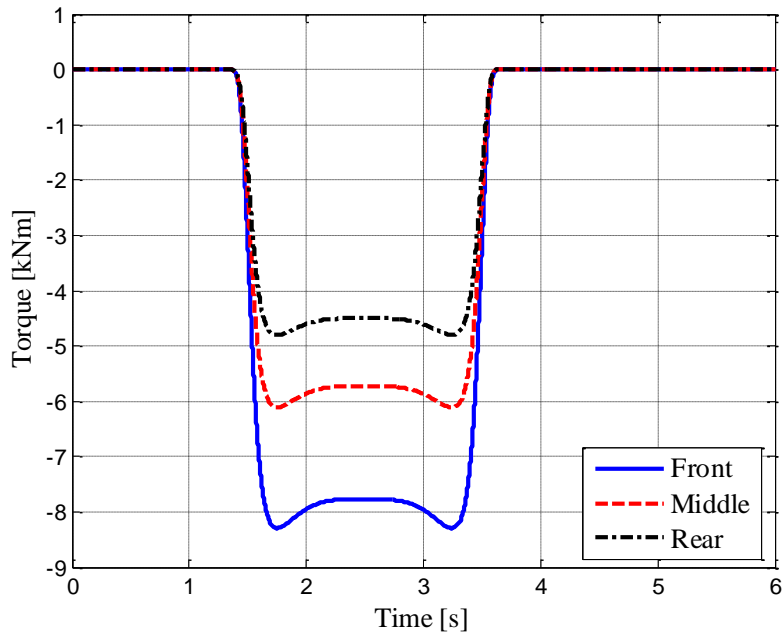


Figure 6.37: Brake Torque Input

Case 1: $A_r=0.6A_p$

Simulation results are given in Figure 6.38 to Figure 6.44.

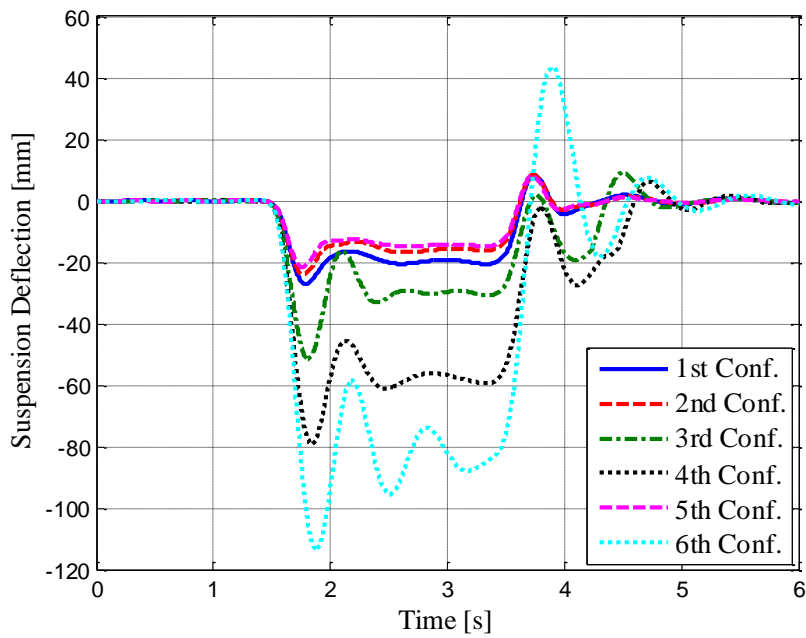


Figure 6.38: Front Suspension Deflection

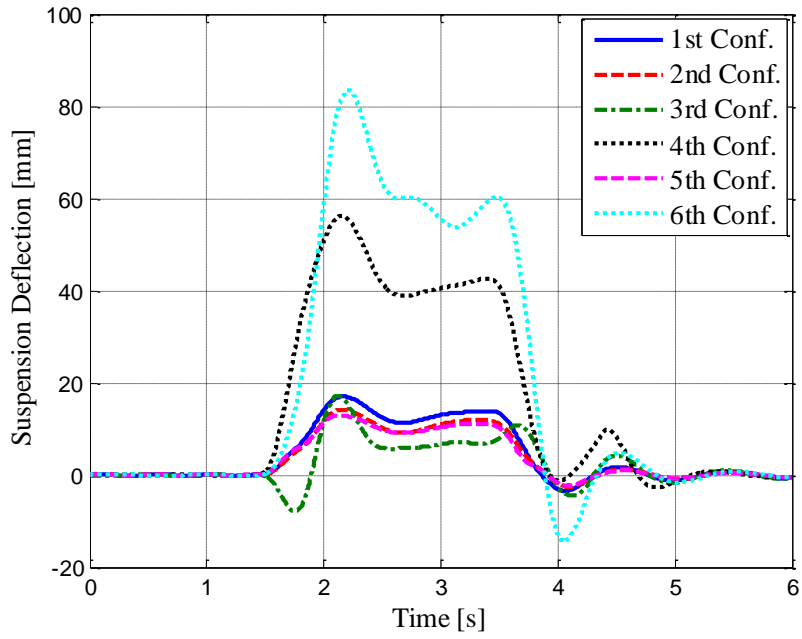


Figure 6.39: Intermediate Suspension Deflection

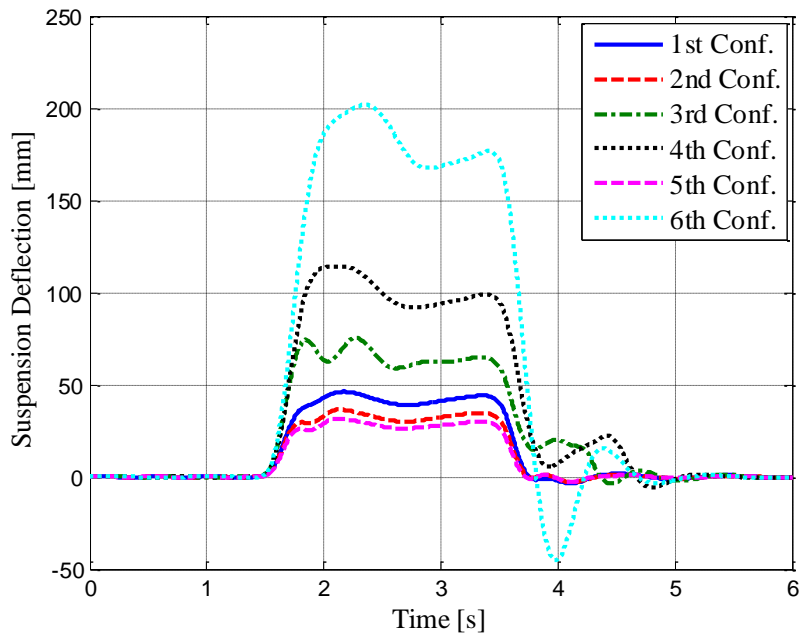


Figure 6.40: Rear Suspension Deflection

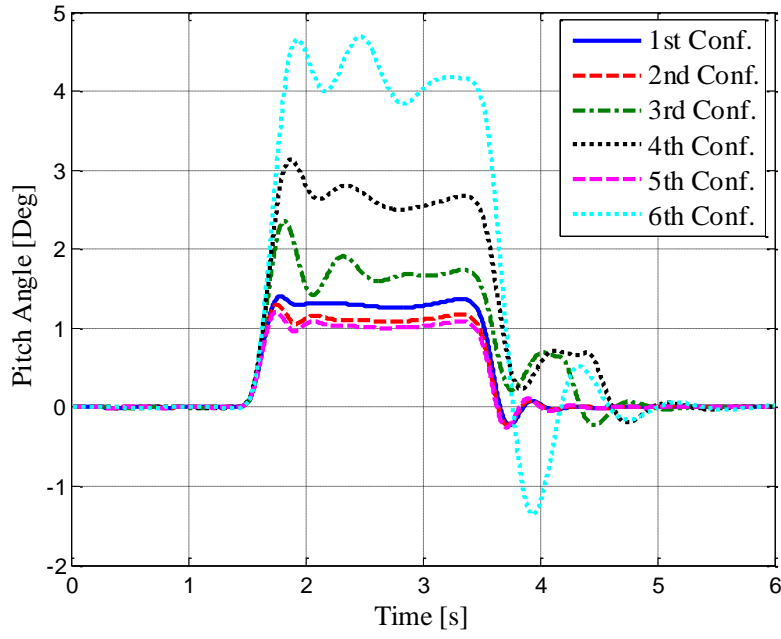


Figure 6.41: Pitch Angle

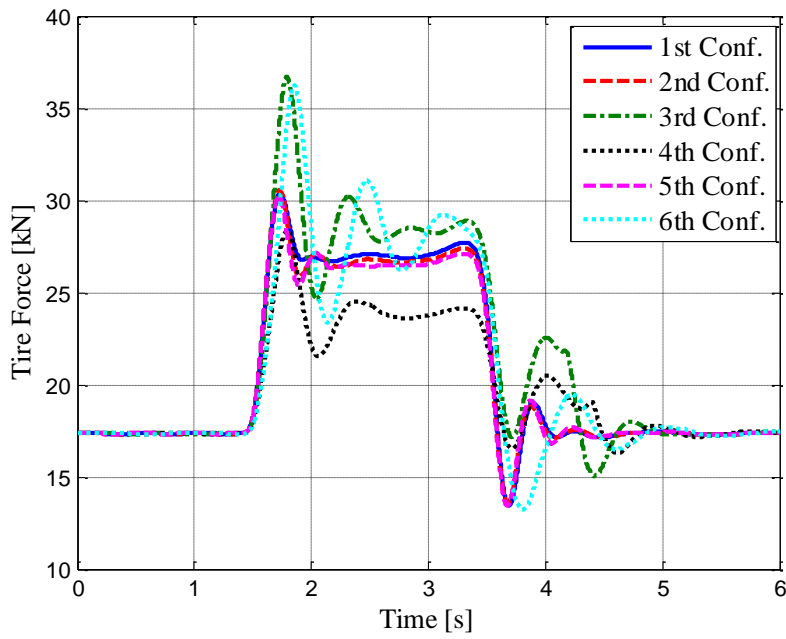


Figure 6.42: Front Tire Force

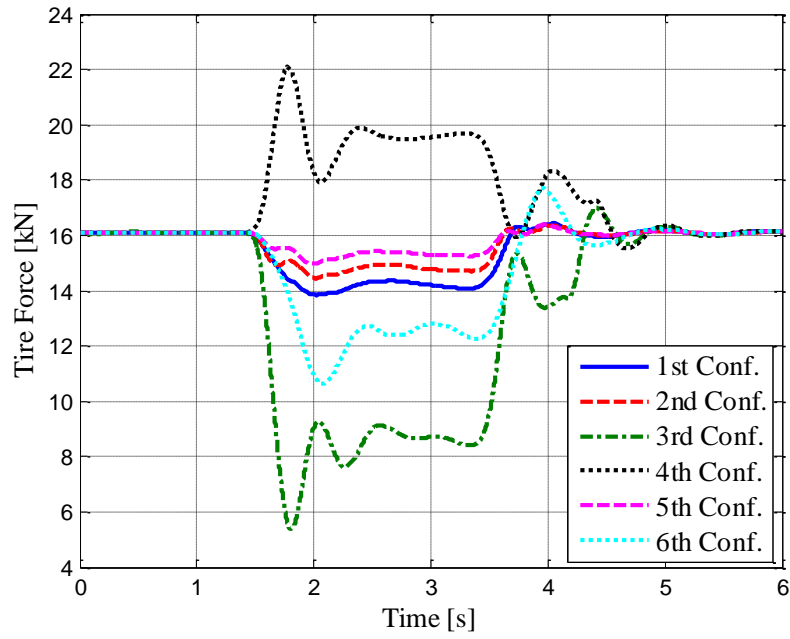


Figure 6.43: Intermediate Tire Force

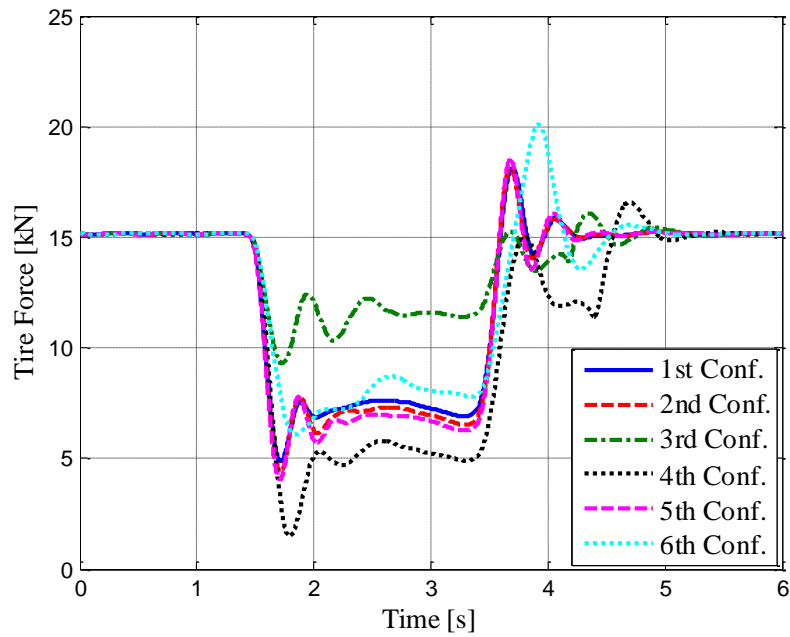


Figure 6.44: Rear Tire Force

As can be seen from the pitch angle response, the first, second, and the fifth suspension configurations have the lowest pitch angle response as compared with

responses of the other suspension configurations. The response of the third suspension configuration has lower pitch angle response than the response of the fourth suspension configuration. This situation can also be seen from the pitch stiffness analysis of the suspension configurations. The sixth suspension configuration which is the unconnected suspension configuration has the worst pitch angle response and thus it has the worst braking performance among the given suspension configurations.

Case 2: $A_r=0.8A_p$

Simulation results are given in Figure 6.45 to Figure 6.51.

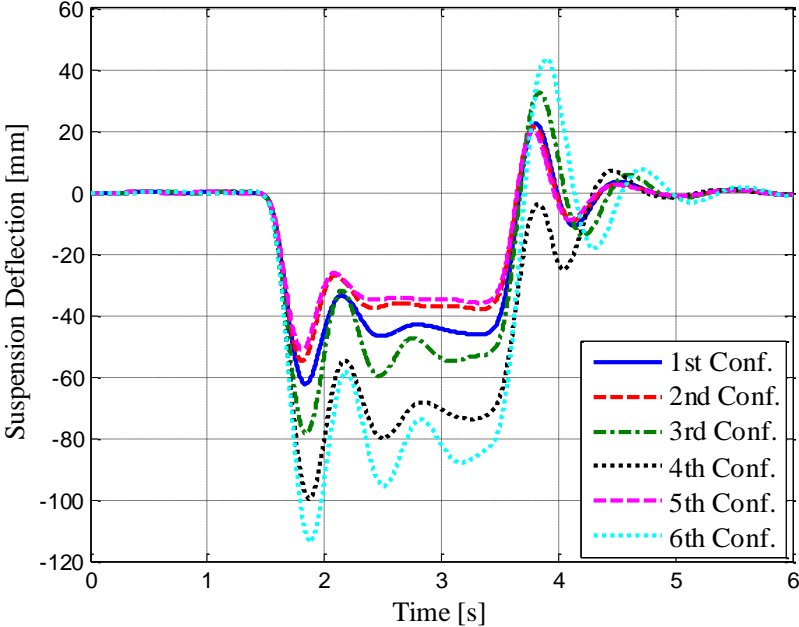


Figure 6.45: Front Suspension Deflection

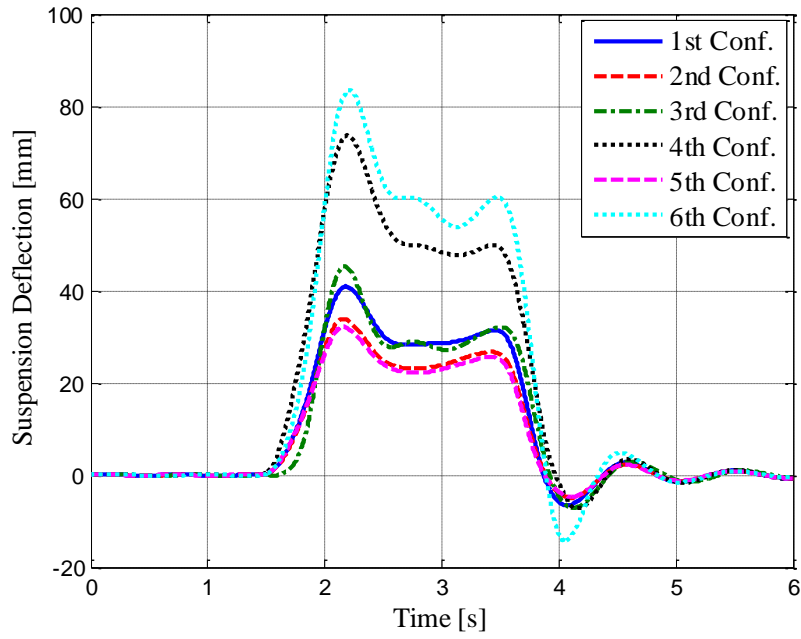


Figure 6.46: Intermediate Suspension Deflection

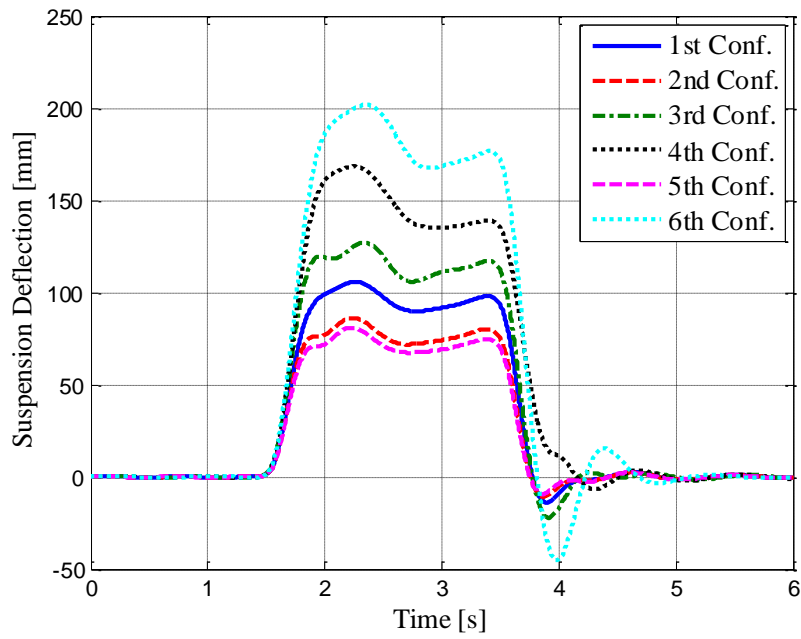


Figure 6.47: Rear Suspension Deflection

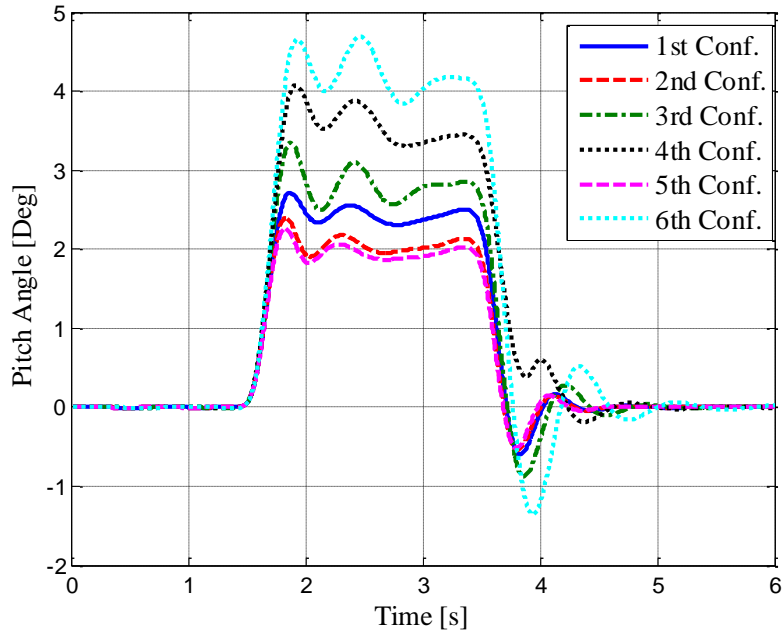


Figure 6.48: Pitch Angle

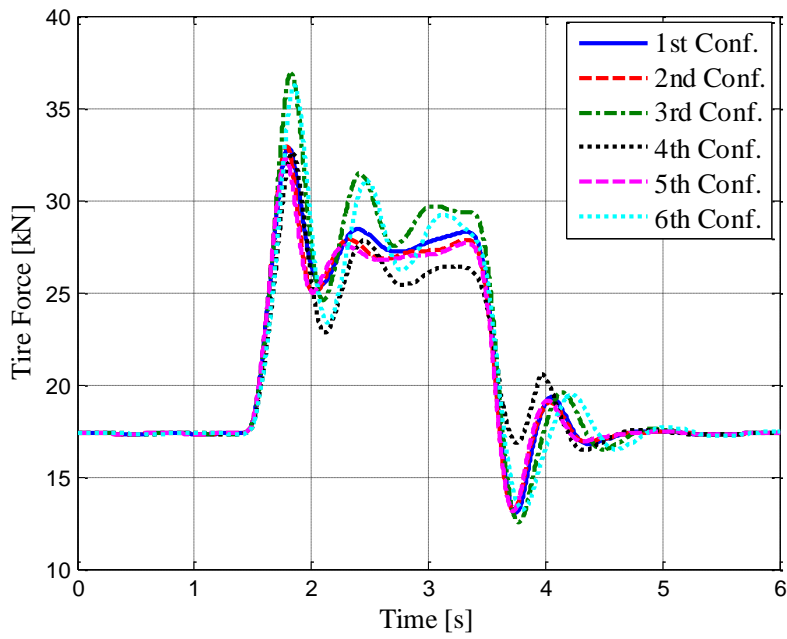


Figure 6.49: Front Tire Force

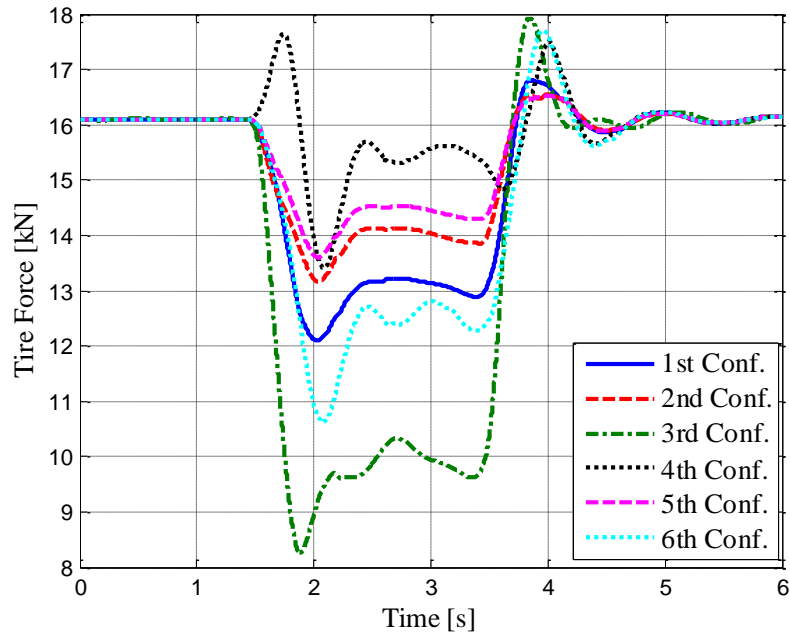


Figure 6.50: Intermediate Tire Force

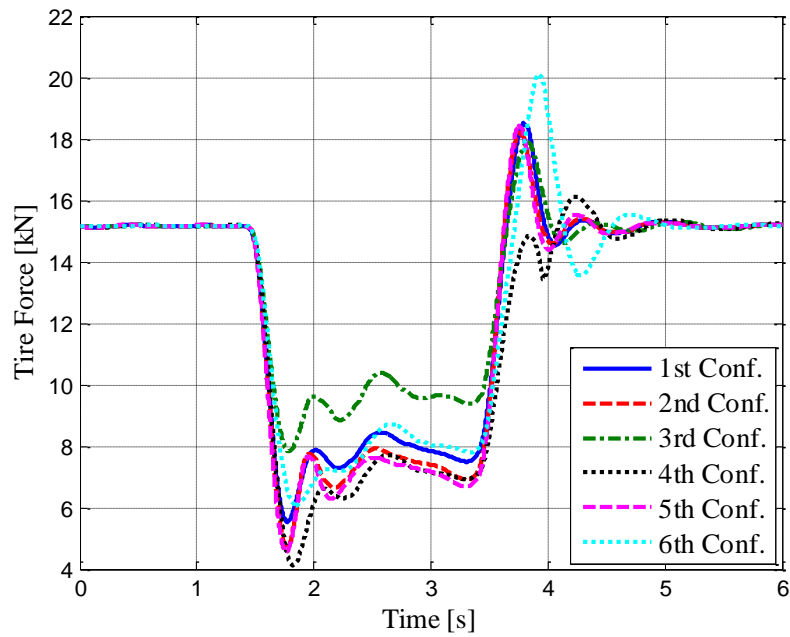


Figure 6.51: Rear Tire Force

As can be seen from Figure 6.48, there are considerable differences between the pitch angle responses of the first, second, and the fifth and sixth configurations.

Accordingly, the first, second, and the fifth suspension configurations have the best braking performance, and the sixth suspension configuration has the worst braking performance. Maximum values of the pitch angle are given in Table 6.25.

Table 6.25: Maximum Values of the Performance Variables

	Pitch Angle [Deg]	
	$A_r=0.6A_p$	$A_r=0.8A_p$
1 st	1.4	2.7
2 nd	1.3	2.4
3 rd	2.4	3.3
4 th	3.1	4.1
5 th	1.2	2.3
6 th	4.7	4.7

6.8.3.2. Simulation with Firing Shock Input

The final simulation is performed with the firing shock input as shown in Figure 6.52.

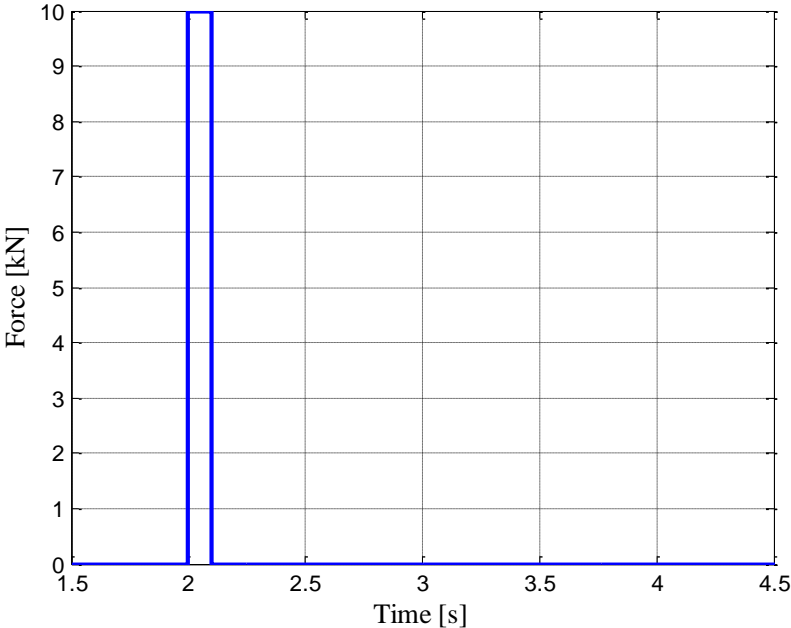


Figure 6.52: Firing Shock Input

Case 1: $A_r=0.6A_p$

Simulation results are shown in Figure 6.53 to Figure 6.59.

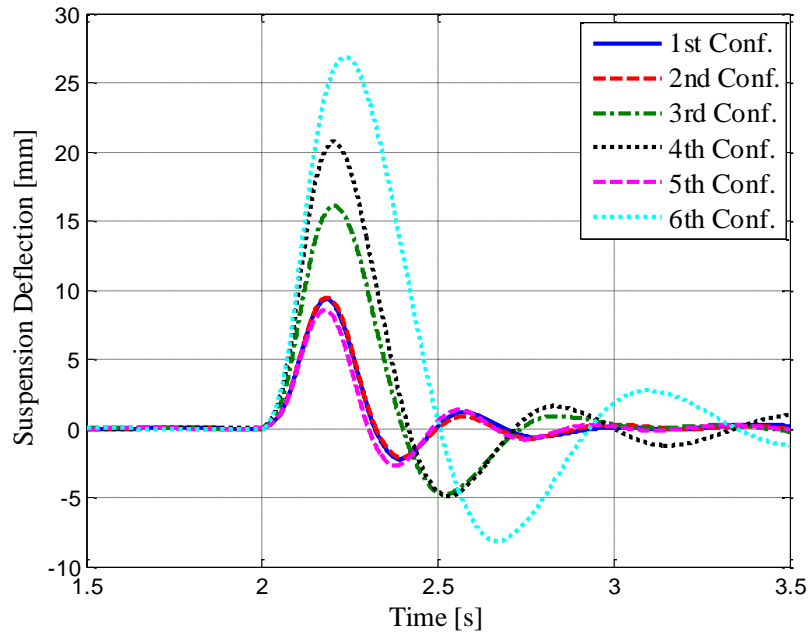


Figure 6.53: Front Suspension Deflection

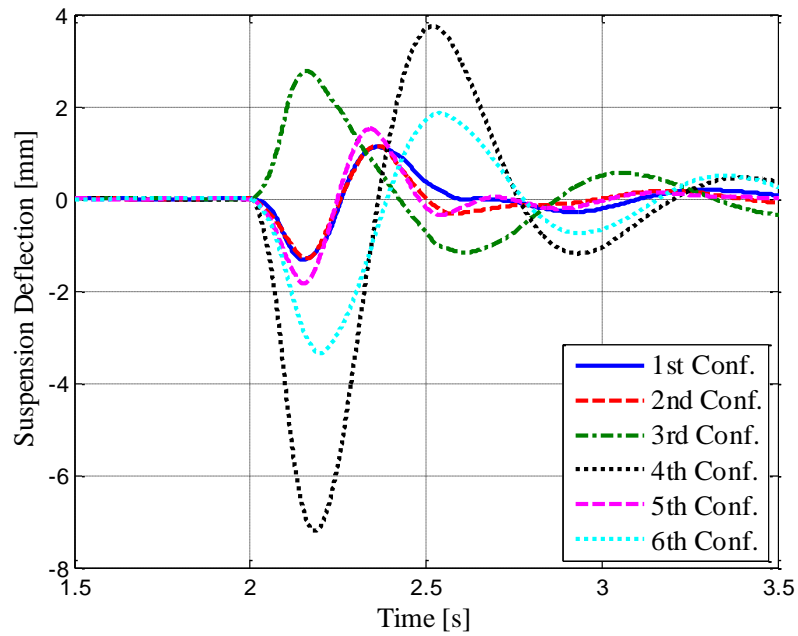


Figure 6.54: Intermediate Suspension Deflection

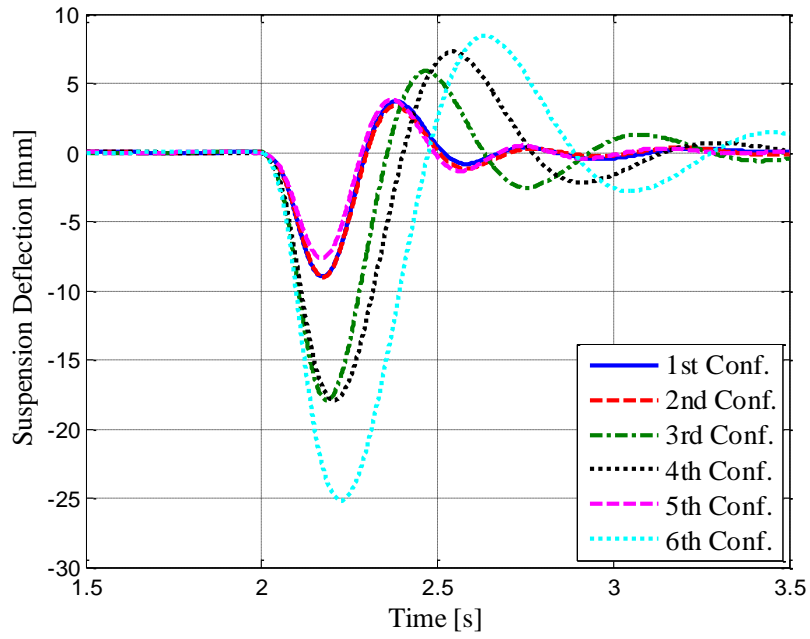


Figure 6.55: Rear Suspension Deflection

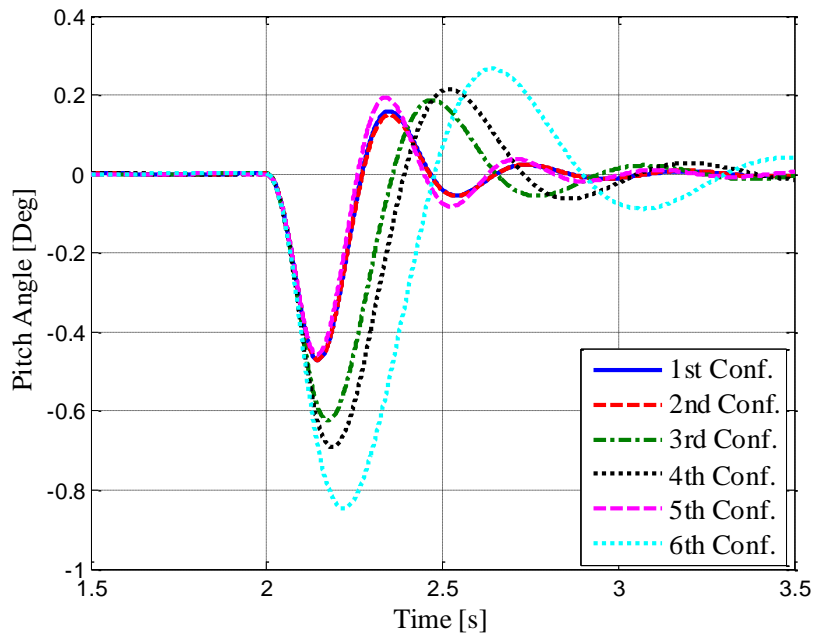


Figure 6.56: Pitch Angle Response

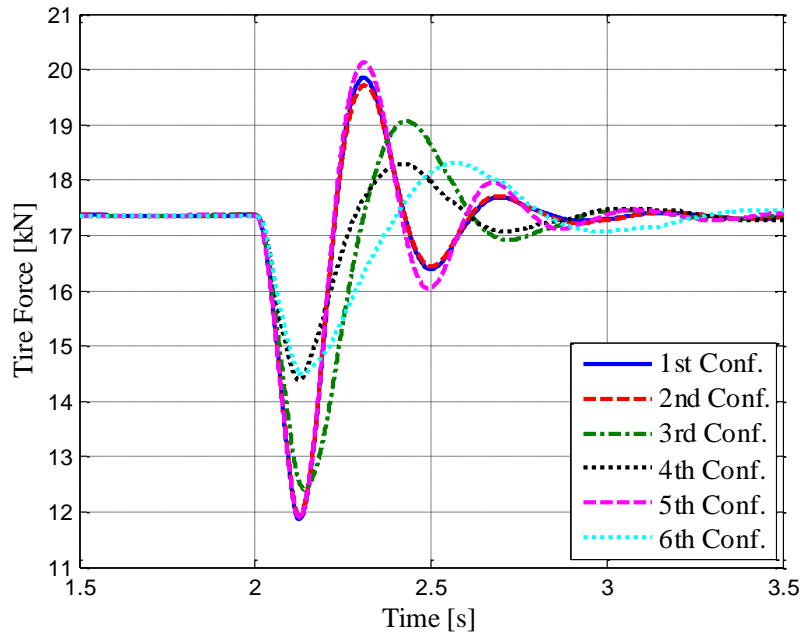


Figure 6.57: Front Tire Force

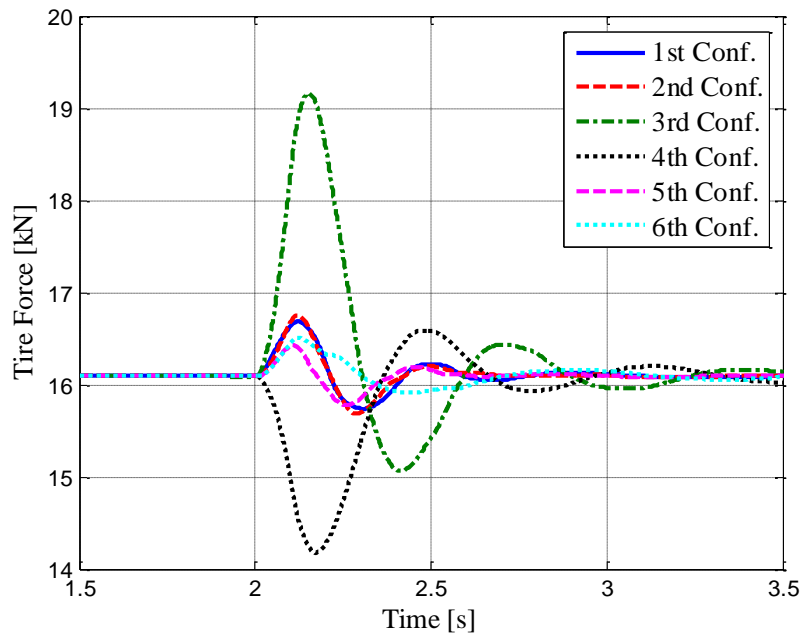


Figure 6.58: Intermediate Tire Force

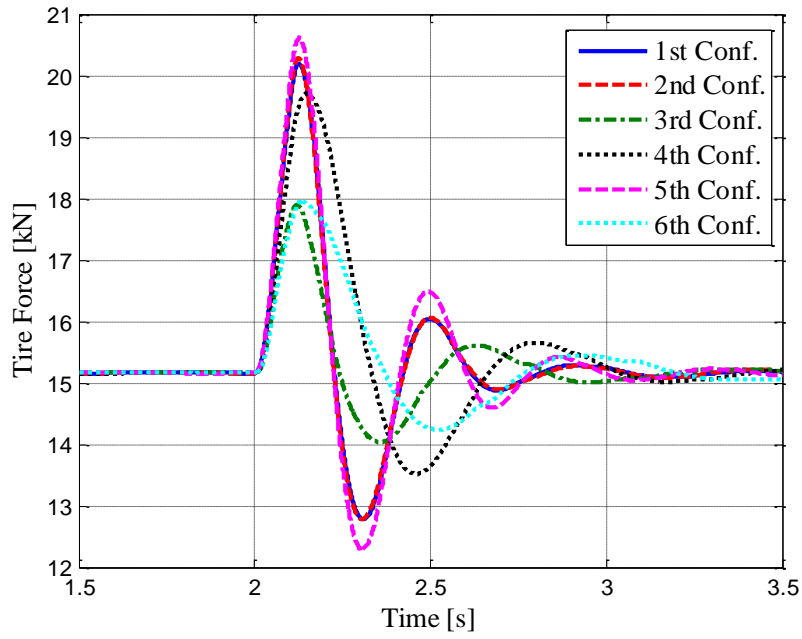


Figure 6.59: Rear Tire Force

As can be seen from the pitch angle response, the first, second, and fifth suspension configurations have the lowest pitch angle response as well as lowest suspension deflection together with quickest settling times, and thus they have the best performance against the firing shock.

Case 2: $A_r=0.8A_p$

For second case, the simulation results are given in Figure 6.60 to Figure 6.66.

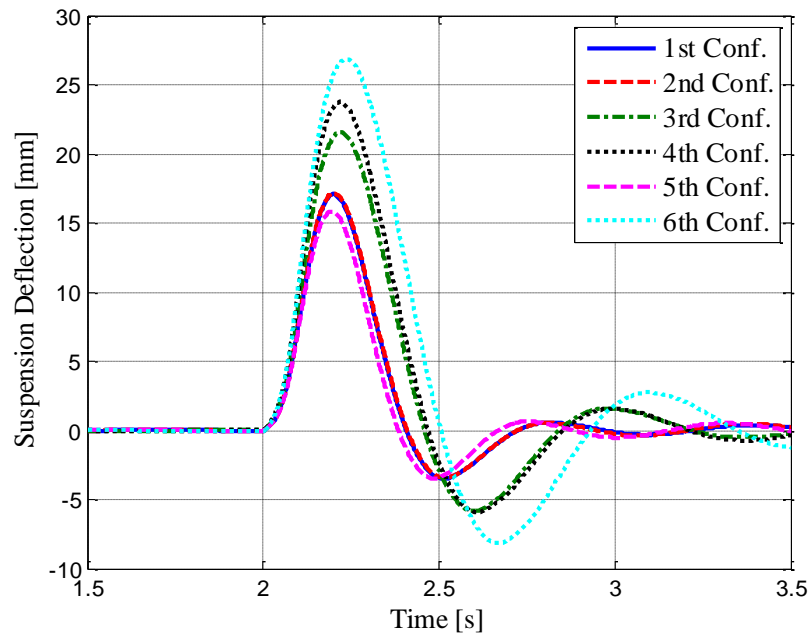


Figure 6.60: Front Suspension Deflection

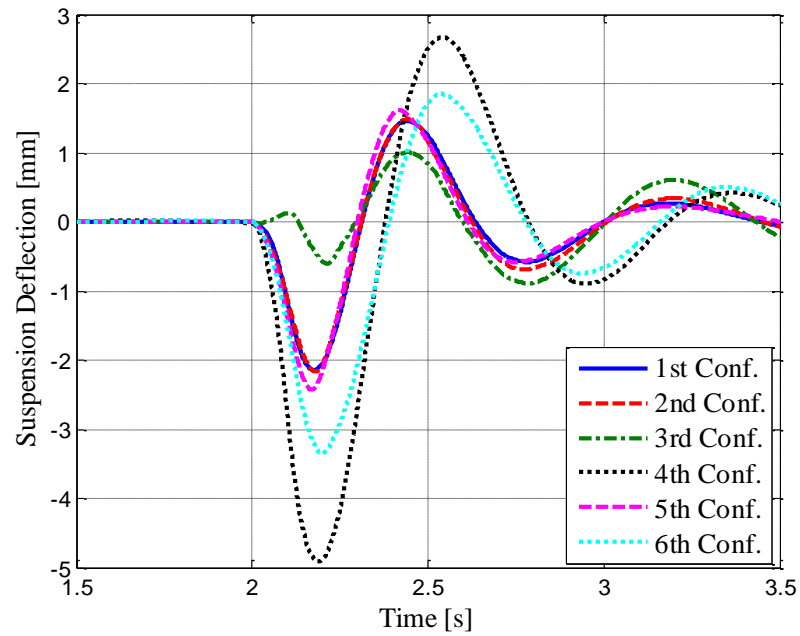


Figure 6.61: Intermediate Suspension Deflection

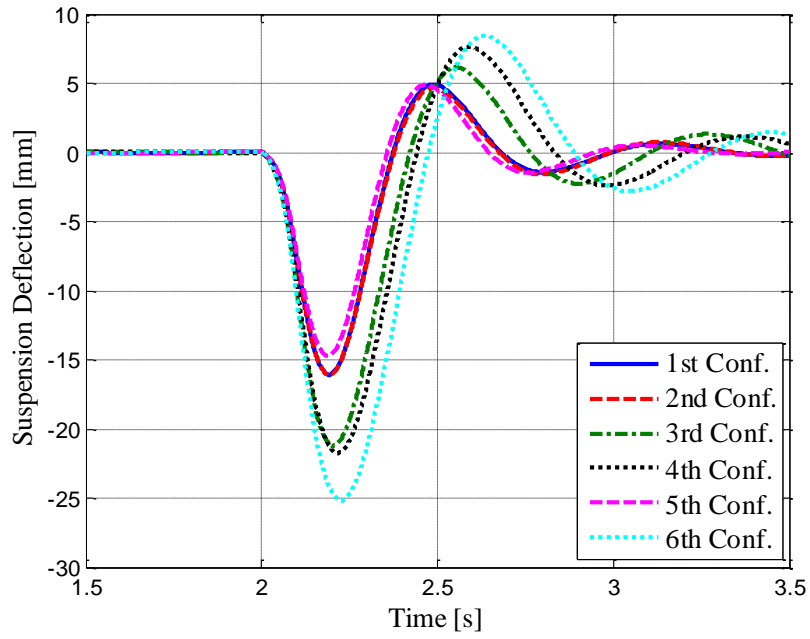


Figure 6.62: Rear Suspension Deflection

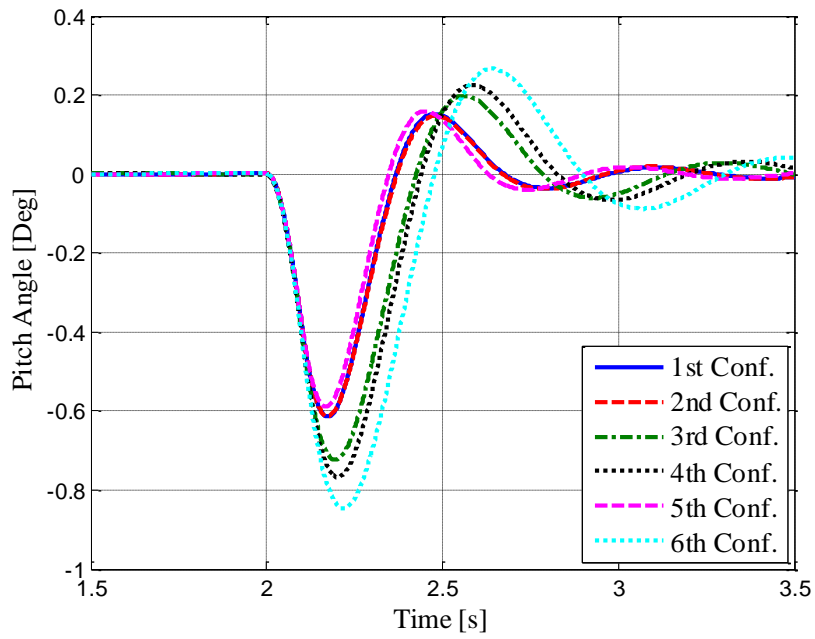


Figure 6.63: Pitch Angle Response

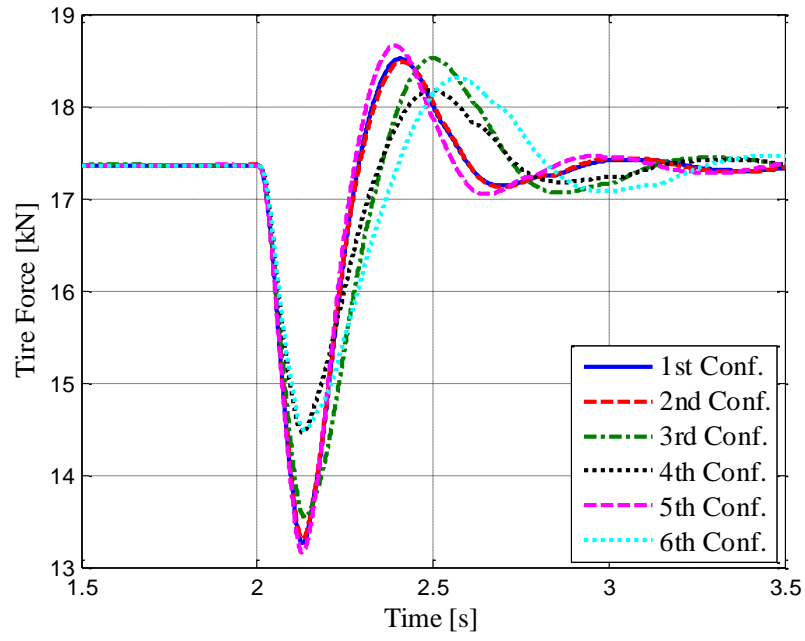


Figure 6.64: Front Tire Force

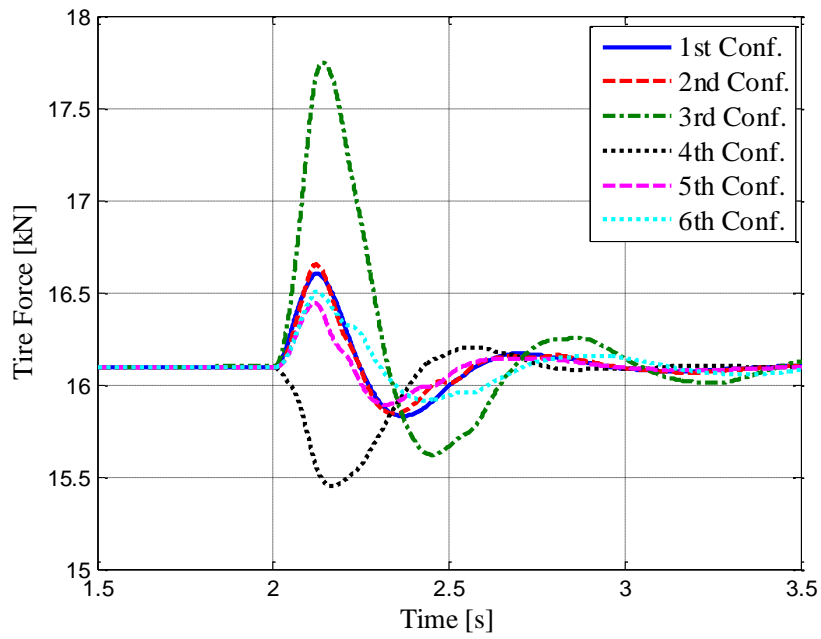


Figure 6.65: Intermediate Tire Force

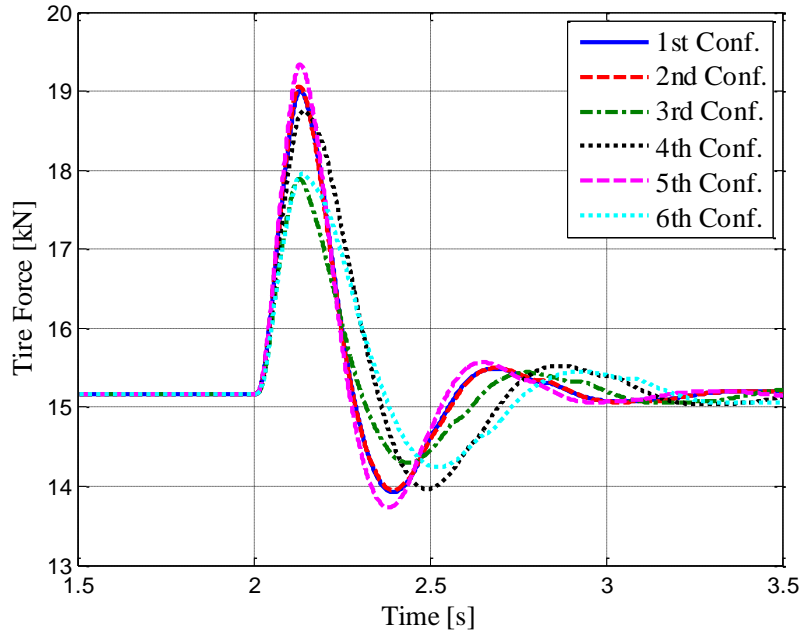


Figure 6.66: Rear Tire Force

Minimum values of the pitch angles are summarized in Table 6.26.

Table 6.26: Minimum Values of the Performance Variables

	Pitch Angle [Deg]	
	$A_r=0.6A_p$	$A_r=0.8A_p$
1 st	-0.5	-0.6
2 nd	-0.5	-0.6
3 rd	-0.6	-0.7
4 th	-0.7	-0.8
5 th	-0.5	-0.6
6 th	-0.8	-0.8

Even though there is not much difference between the minimum values of the pitch angle responses as can be seen from Table 6.26, when the magnitude of the shock moment acting on the sprung mass increases, the difference between the minimum values of the pitch angle response also increases. Therefore, the capacity of the interconnected HP suspension system can be exploited more.

6.9. COMPARISON OF SUSPENSION CONFIGURATIONS

In this section, the suspension configurations analyzed so far are going to be compared in terms of different performance considerations; ride comfort, braking/acceleration performance, and firing shock performance. The suspension metrics used for this purpose can be defined as,

$$M = \frac{\left(w_{RCPV} \frac{\ddot{z}_{RMS}}{\ddot{z}_{RMS_{6th}}} + w_{RCPV} \frac{\ddot{\theta}_{RMS}}{\ddot{\theta}_{RMS_{6th}}} + w_{SPV} \frac{\ddot{z}}{\ddot{z}_{6th}} + w_{SPP} \frac{\ddot{\theta}}{\ddot{\theta}_{6th}} + w_{FSP} \frac{\theta_{MAX}}{\theta_{MAX_{6th}}} + w_{BP} \frac{\theta_{MAX}}{\theta_{MAX_{6th}}} \right)}{w_{RCPV} + w_{RCPV} + w_{SPV} + w_{SPP} + w_{FSP} + w_{BP}} 100$$

where w_{RCPV} is the weighting factor of vertical acceleration for ride comfort, w_{RCPV} is the weighting factor for the pitch acceleration of the ride comfort, w_{SPV} is the weighting factor for the maximum and minimum values of the vertical acceleration for the bump road input, w_{SPP} is the weighting factor for the maximum and the minimum values of the pitch acceleration for bump road input, w_{FSP} is the weighting factor for maximum pitch angle for firing shock performance, w_{BP} is the weighting factor for the pitch angle for the braking input, \ddot{z}_{RMS} is the rms of the vertical acceleration of the sprung mass, $\ddot{\theta}_{RMS}$ is the rms of the pitch acceleration, \ddot{z} is the vertical acceleration, $\ddot{\theta}$ is the pitch acceleration, and θ_{MAX} is the maximum values of the pitch angle. The weighting factors are given in Table 6.27.

The suspension metrics calculated for vehicle with improved ride comfort and for improved pitch performances are shown in Table 6.28.

Table 6.27: Weighting Factors Used For a Military Vehicles

	w_{RCPV}	w_{RCPV}	w_{SPV}	w_{SPP}	w_{FSP}	w_{BP}
Ride Comfort	10	10	10	10	1	1
Pitch	1	1	1	1	10	10

Table 6.28: Calculated Suspension Metrics for Military Vehicles

Suspension Conf.	Ride Comfort		Handling	
	Suspension Metric (Ar=0.8Ap)	Suspension Metric (Ar=0.6Ap)	Suspension Metric (Ar=0.8Ap)	Suspension Metric (Ar=0.6Ap)
1 st	131	183	78	70
2 nd	130	182	75	69
3 rd	114	140	85	77
4 th	106	120	96	84
5 th	135	188	75	69
6 th	100	100	100	100

For a military vehicle with firing capability, the first, second, and the fourth suspension gives the best results for both piston rod areas as can be seen from Table 6.28. However, for a vehicle designed mainly for ride comfort, unconnected suspension configurations give the best performance. However, in real road vehicles, suspension should always be designed for best ride comfort with necessary driving road safety. For this reason, pitch angle and roll angle should always be limited for specific maneuvers. In Chapter 8 and 9, when the full vehicle model is examined in terms of the ride comfort and driving safety performances, the role of the interconnected suspension system will be better understood.

6.10. PARAMETER SENSITIVITY ANALYSIS

In order to see the effect of the suspension parameters on the vehicle performance, a detailed sensitivity analysis is performed. With the sensitivity analysis, variation of the stiffness, damping, and vehicle responses with the suspension design parameters are examined.

6.10.1. Change of the Vertical Stiffness with the Piston Area, Rod Area, and Initial Gas Volume

Change of the vertical stiffness of the vehicle with the piston area, initial gas volumes, and the piston rod area are shown in Figure 6.67, Figure 6.68, and Figure 6.69.

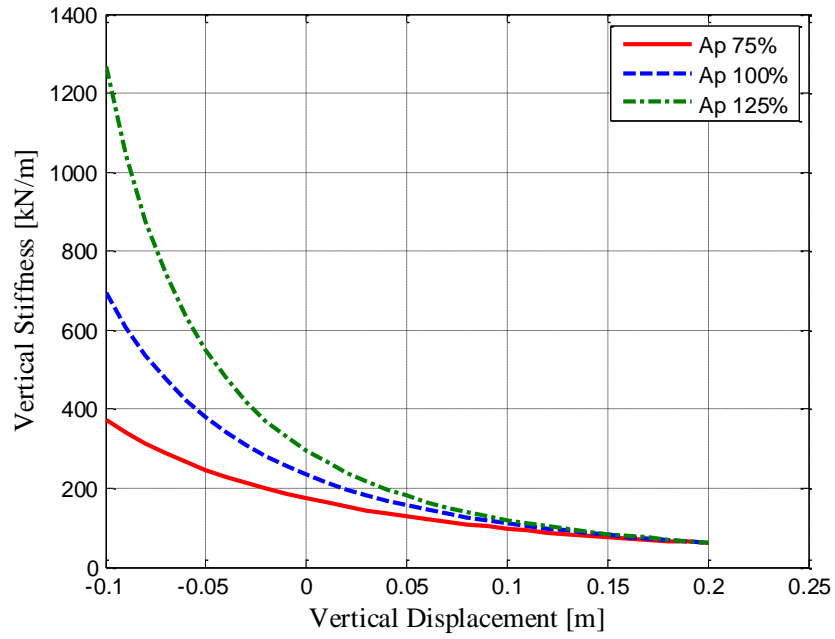


Figure 6.67: Change of the Vertical Stiffness with the Piston Area

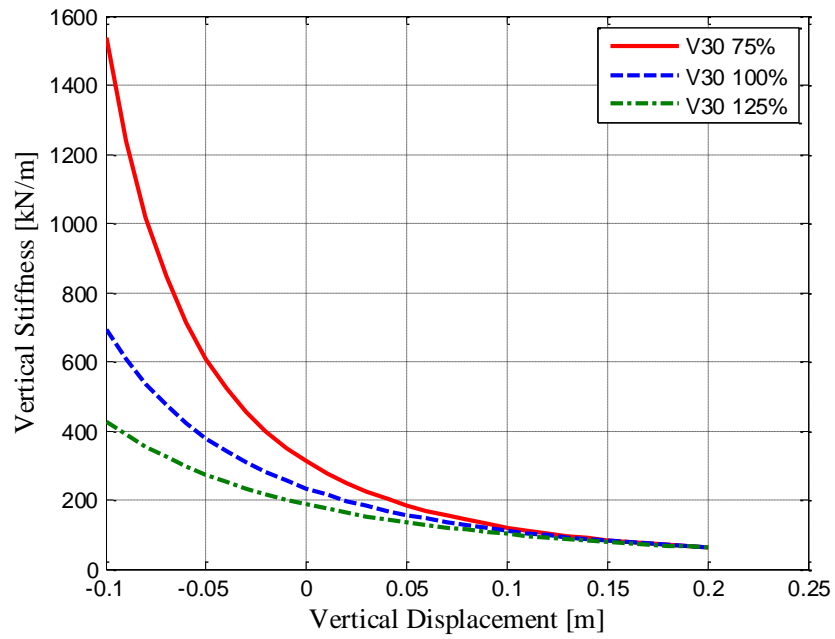


Figure 6.68: Change of the Vertical Stiffness with the Initial Gas Volume

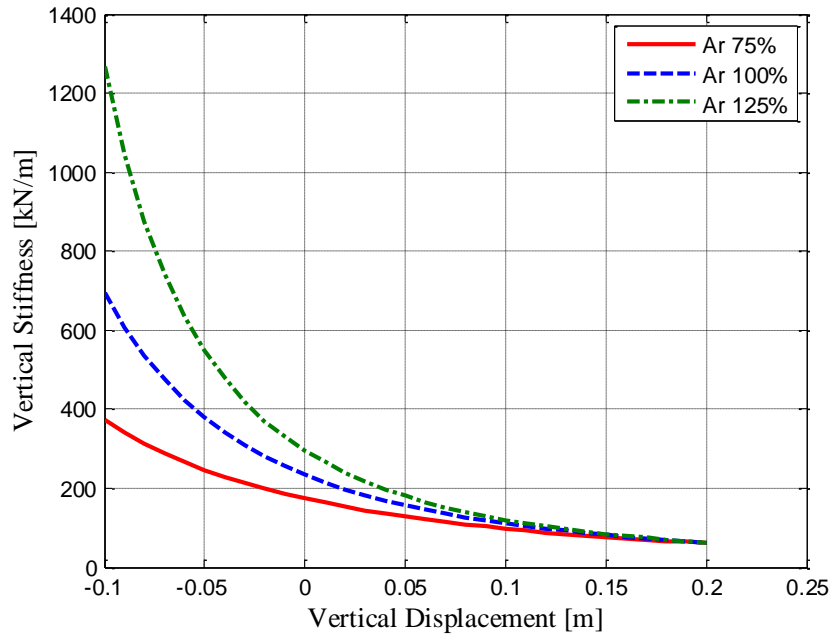


Figure 6.69: Change of the Vertical Stiffness with the Rod Area

The results obtained in Figure 6.67, Figure 6.68 are similar to the results obtained in Chapter 3. On the other hand, as can be seen from Figure 6.69, when the piston rod area is decreased, while keeping all other parameters the same, the vertical stiffness of the suspension decreased. As stated before, the suspension unit force depends on the pressure force between the piston side and the rod side. When the piston rod area is decreased, the suspension force also decreases. Thus the effective piston area decreases which results in decreased vertical suspension force. On the contrary, when the piston rod area increases, vertical suspension stiffness also increases

6.10.2. Change of the Pitch Stiffness with the Piston Area, Rod Area, and Initial Gas Volume

Change of the pitch stiffness with the piston area, initial gas volumes, and the piston rod area are given in Figure 6.70, Figure 6.71, and Figure 6.72, respectively. When the initial gas volumes are decreased, the suspension stiffness increases and thus pitches stiffness also increases. Moreover, increasing piston area increases suspension stiffness which results in increased pitch stiffness. When piston area is

increased, as can be seen from Figure 6.72, pitch stiffness decreases due to the characteristics of the interconnected HP suspension systems

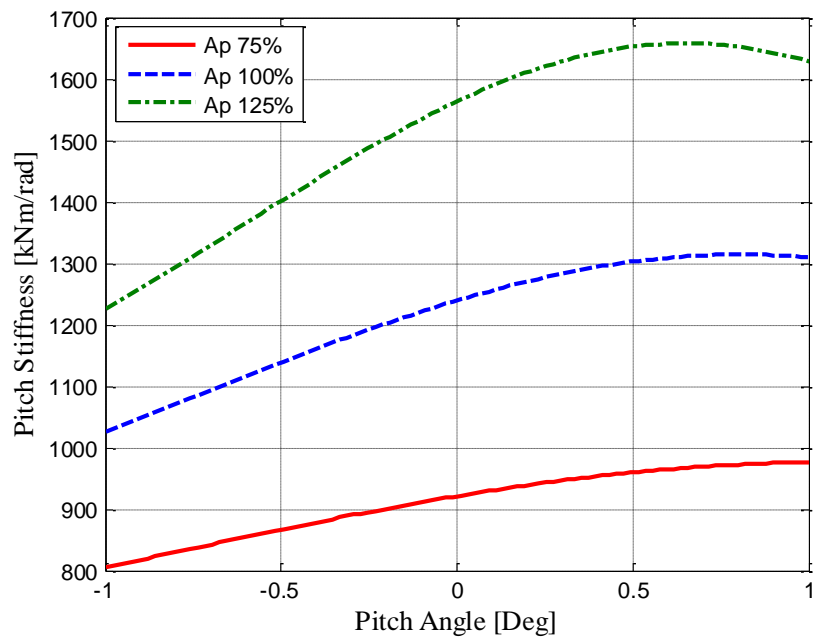


Figure 6.70: Change of the Pitch Stiffness with the Piston Area

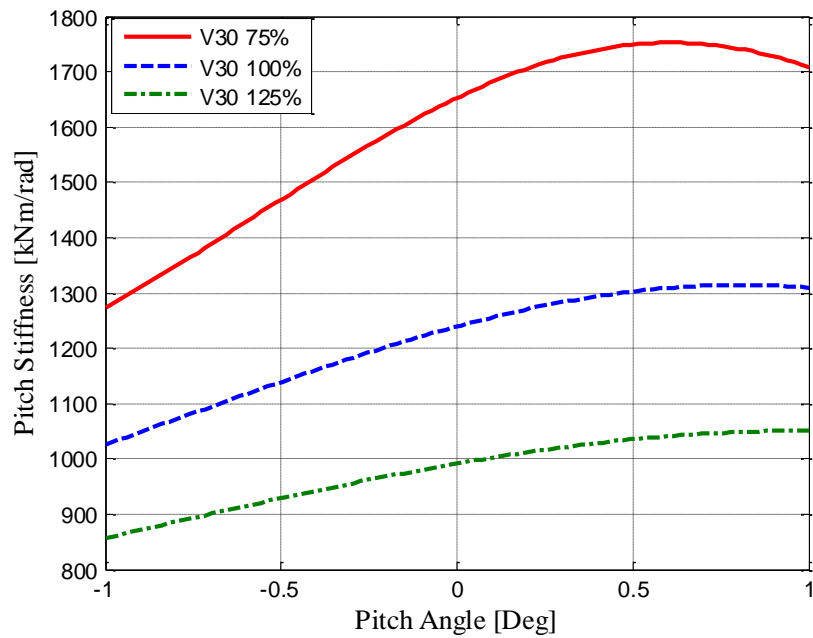


Figure 6.71: Change of the Pitch Stiffness with the Piston Area

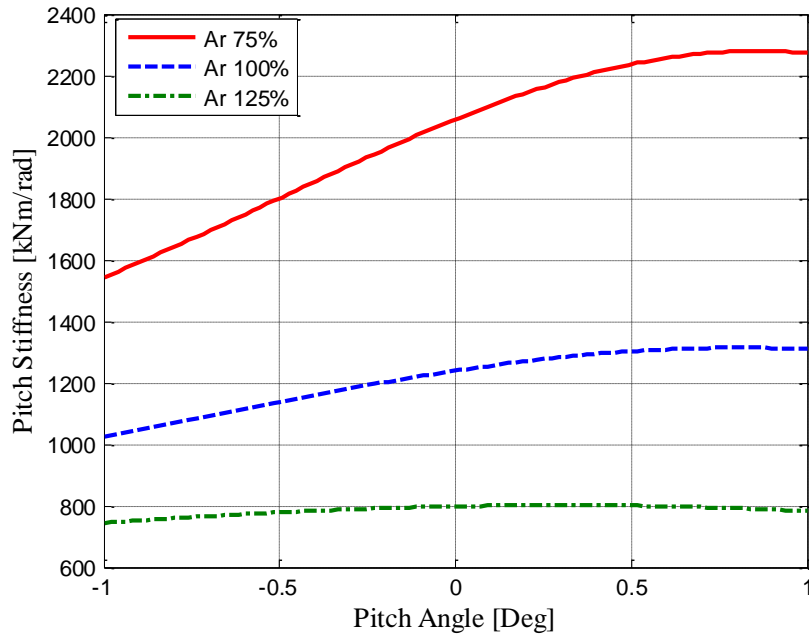


Figure 6.72: Change of the Pitch Stiffness with the Piston Rod Area

6.10.3. Change of the Vertical Damping with the Piston Area, Rod Area, and Damper Valve Parameters

After the change of the stiffness characteristics of interconnected suspension system with the suspension design parameters are investigated, now the change of the damping characteristics with piston area, rod area and the damping valve parameters are examined. Figure 6.73 to Figure 6.75 show the changes of the vertical damping force with the piston area, rod area, and the maximum valve openings. Results observed from Figure 6.73 and Figure 6.75 are similar to results found in Chapter 3. As Figure 6.74 illustrates, decreasing rod area results in a decrease in effective piston area which in turns decreases vertical damping force.

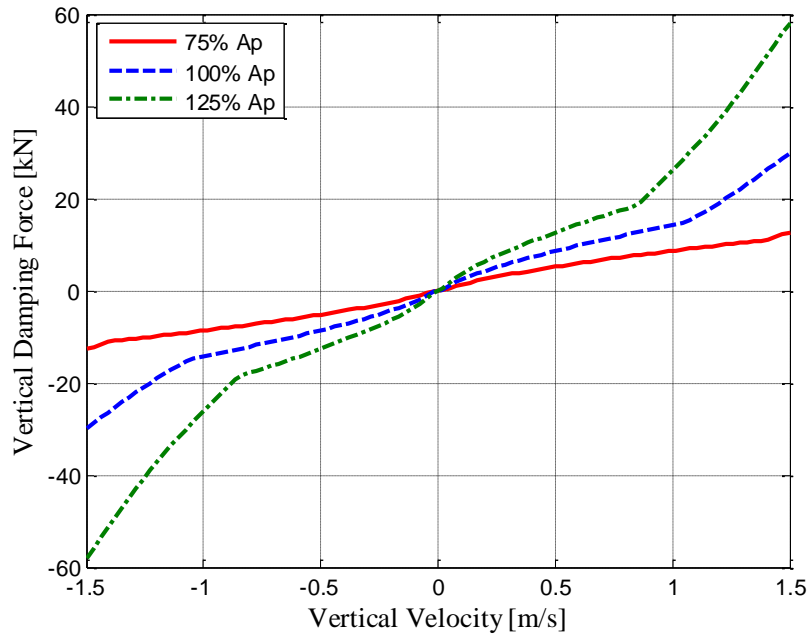


Figure 6.73: Change of the Vertical Damping Force with the Piston Area

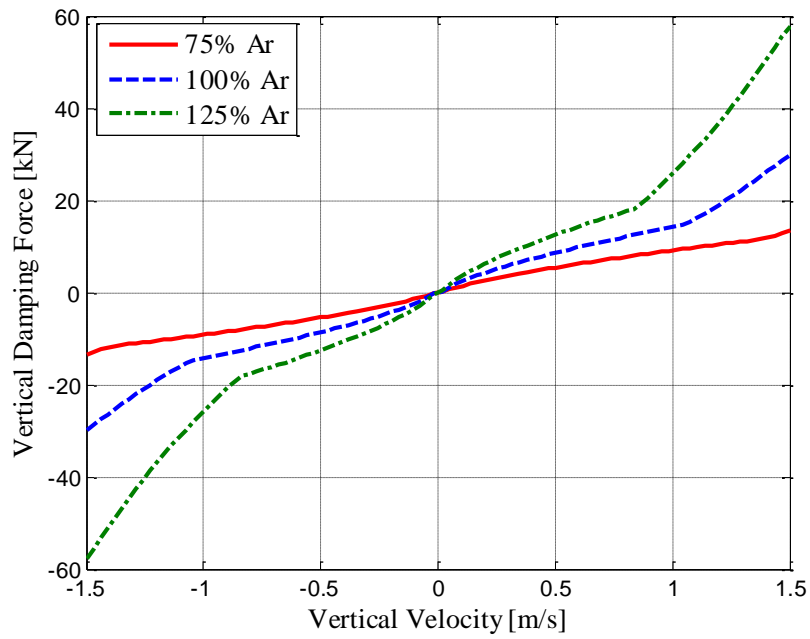


Figure 6.74: Change of the Vertical Damping Force with the Piston Area

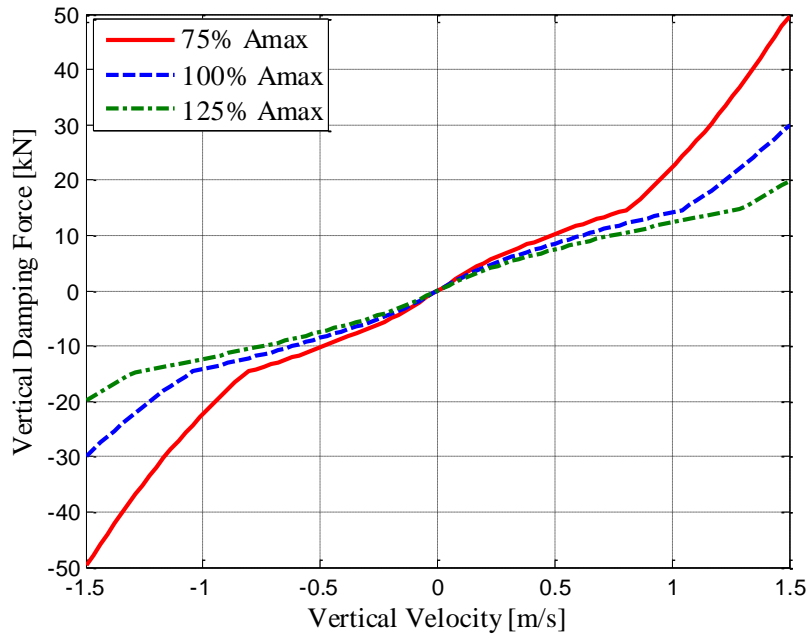


Figure 6.75: Change of the Vertical Damping Force with the Maximum Valve Opening

6.10.4. Change of the Pitch Damping with the Piston Area, Rod Area, and Damper Valve Parameters

Change of the pitch damping moment with the piston area, rod area, and the maximum valve openings are given in Figure 6.76, Figure 6.77, and Figure 6.78.

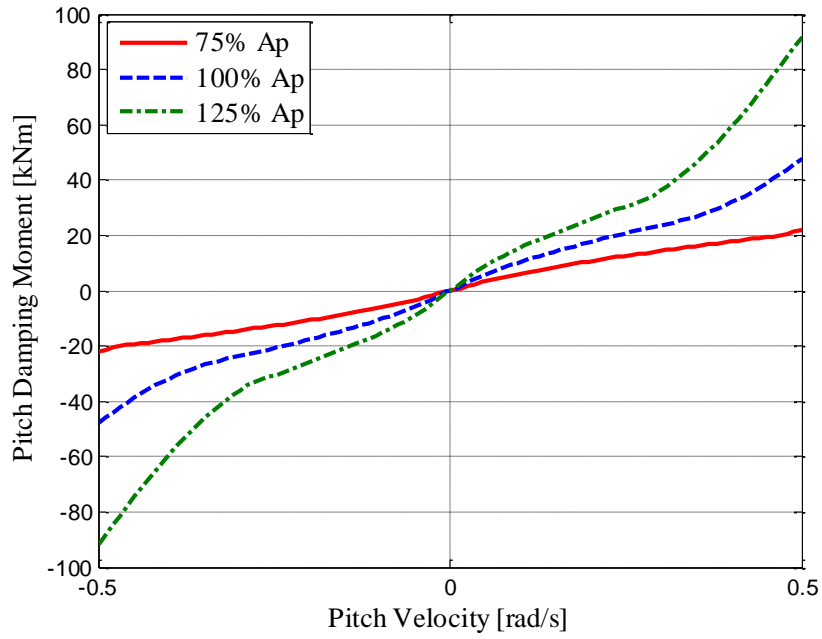


Figure 6.76: Change of the Pitch Damping Moment with the Piston Area

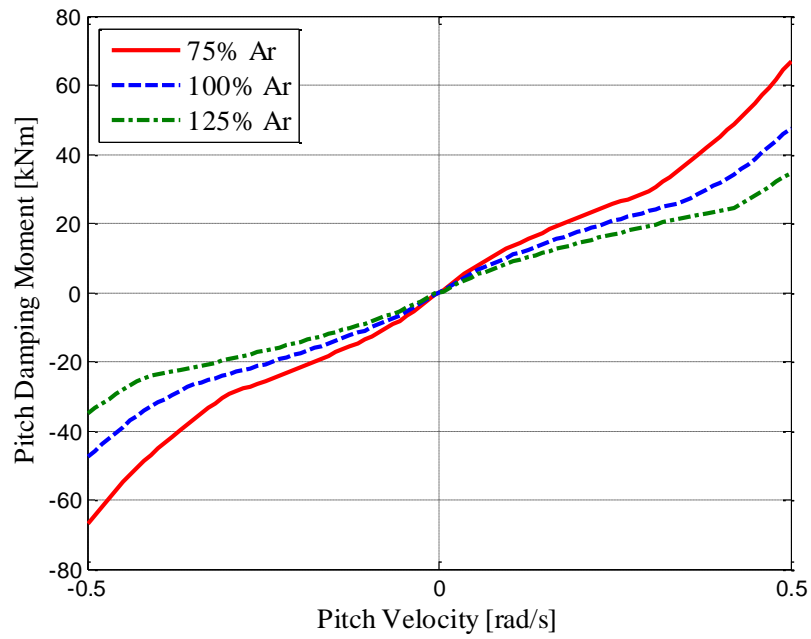


Figure 6.77: Change of the Pitch Damping Moment with the Piston Rod Area

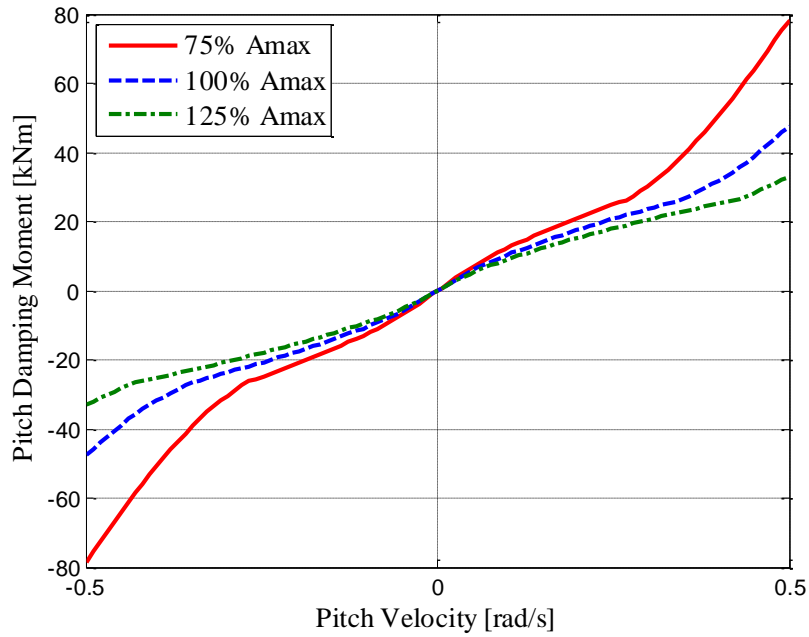


Figure 6.78: Change of the Pitch Damping Moment with the Maximum Valve Opening

As can be seen from Figure 6.76, when the piston area increases, pitch damping also increases. Moreover, when the rod area is decreased, the strength of the interconnection increases and the interconnected HP suspension system provides higher pitch damping moment. After the effect of suspension design parameters on stiffness and damping characteristics of the interconnected HP suspension system are examined, now the change of the performance variables with the suspension design parameters are studied. The results obtained can also be directly observed from the parameters sensitivity analysis performed in this part. However, to make the sensitivity analysis results performed so far clear, the results are to be given.

6.10.5. Braking Simulation

❖ Sensitivity w.r.t. Piston Area

Change of the braking simulation results with the piston area are shown in Figure 6.79 to Figure 6.85. Since the effect of the parameters on the physical response variables are directly seen rather than indirectly as in the case of stiffness and damping, this sensitivity study gives an easy interpretation. As can be seen from

Figure 6.82, when the piston area increases, suspension stiffness, and thus pitch stiffness increases. Increased pitch stiffness results in a decreased pitch angle response in braking simulation.

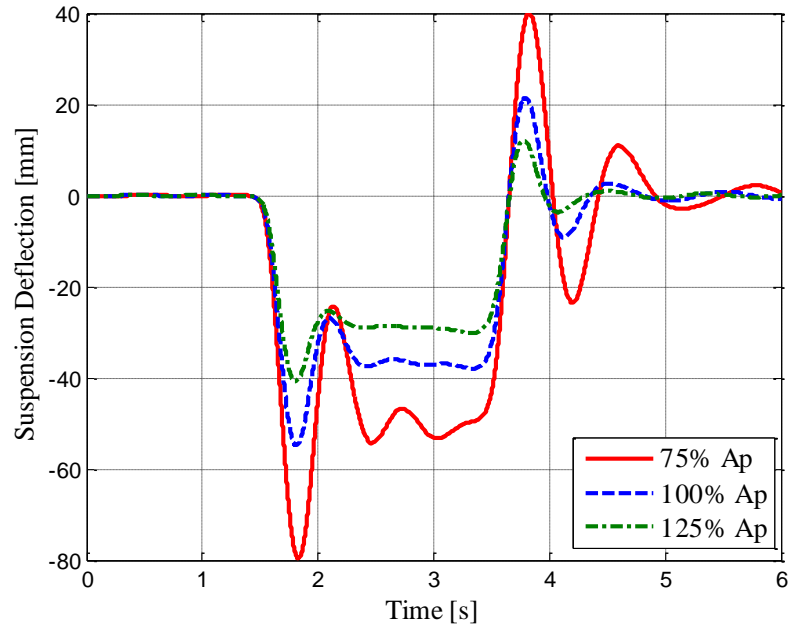


Figure 6.79: Change of Front Suspension Deflection with Piston Area

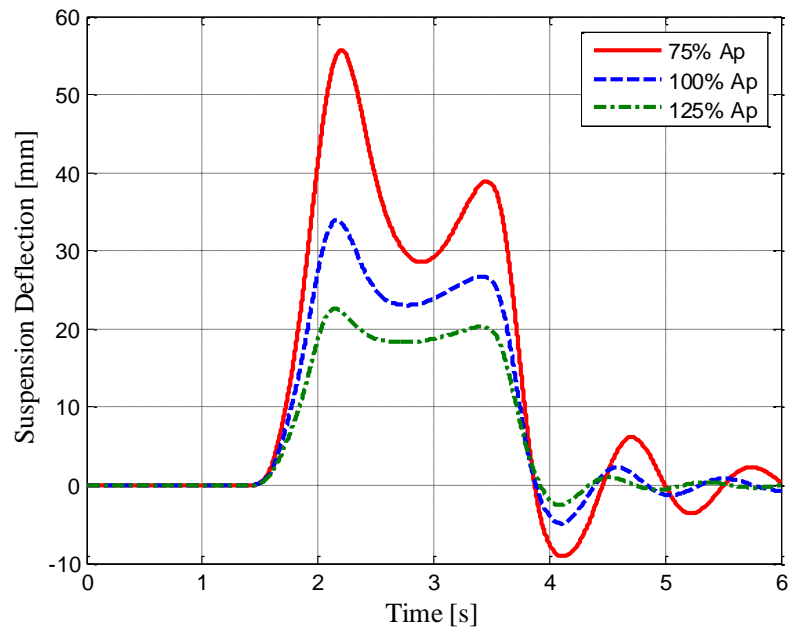


Figure 6.80: Change of Intermediate Suspension Deflection with Piston Area

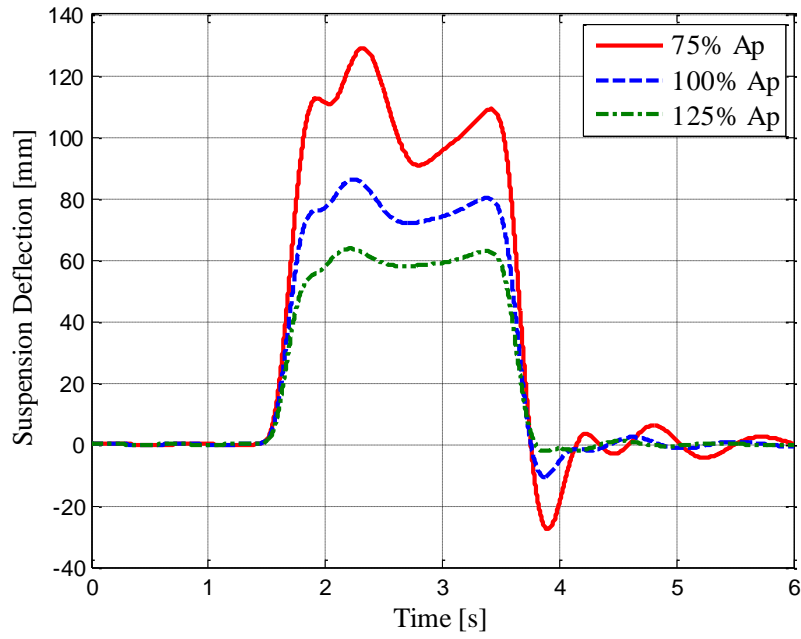


Figure 6.81: Change of Rear Suspension Deflection with Piston Area

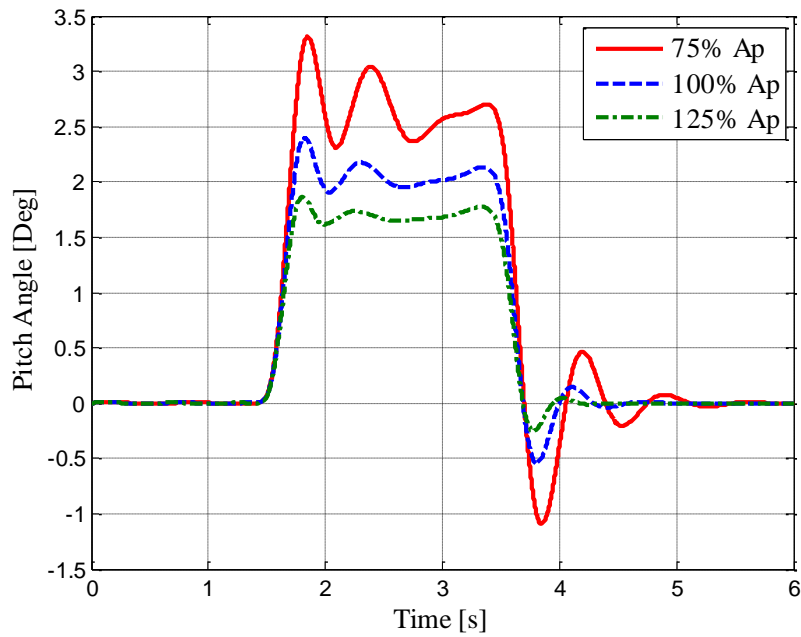


Figure 6.82: Change of Pitch Angle with Piston Area

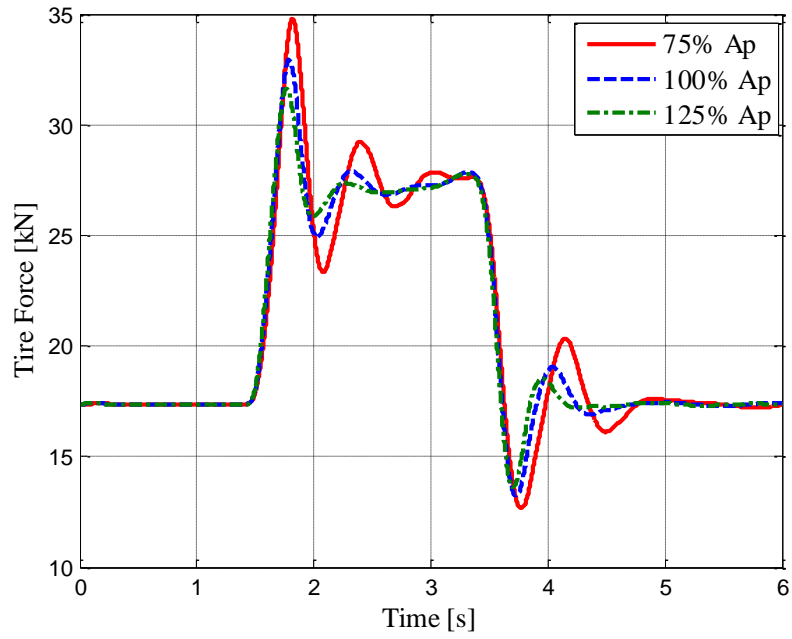


Figure 6.83: Change of Front Tire Force with Piston Area

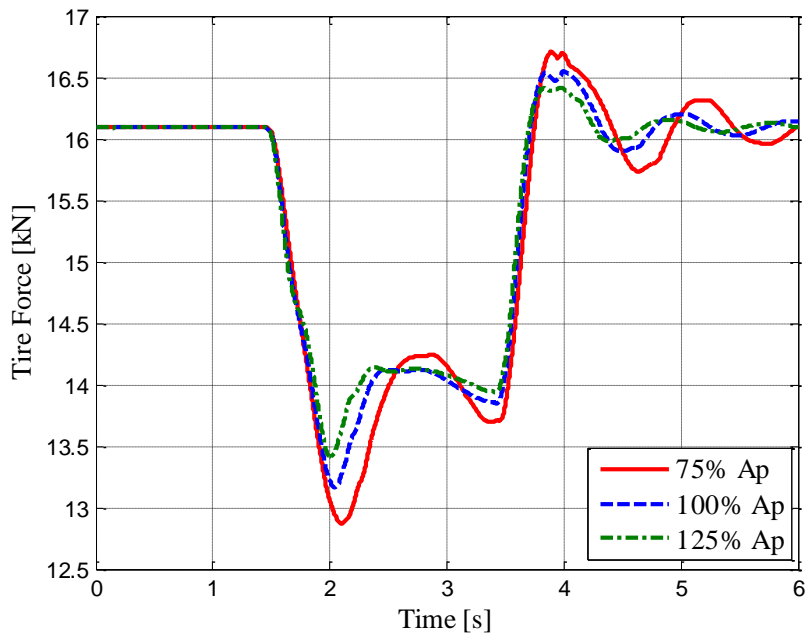


Figure 6.84: Change of Intermediate Tire Force with Piston Area

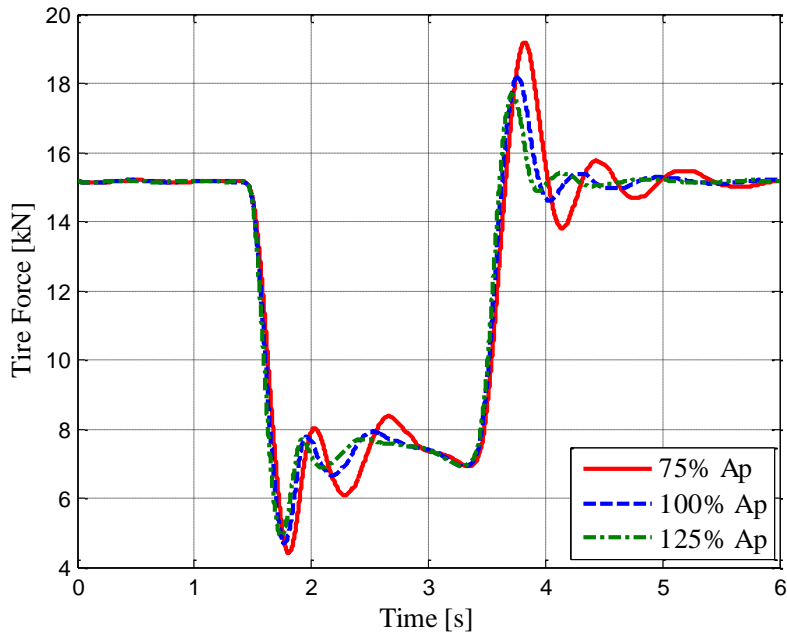


Figure 6.85: Change of Rear Tire Force with Piston Area

❖ **Sensitivity w.r.t. Piston Rod Area**

Change of the braking simulation results with the piston rod area are given in Figure 6.86 to Figure 6.92. As Figure 6.89 shows, when the piston rod area is decreased, the strength of the interconnection and thus the pitch stiffness increases. Increased pitch stiffness results in a decreased pitch angle response.

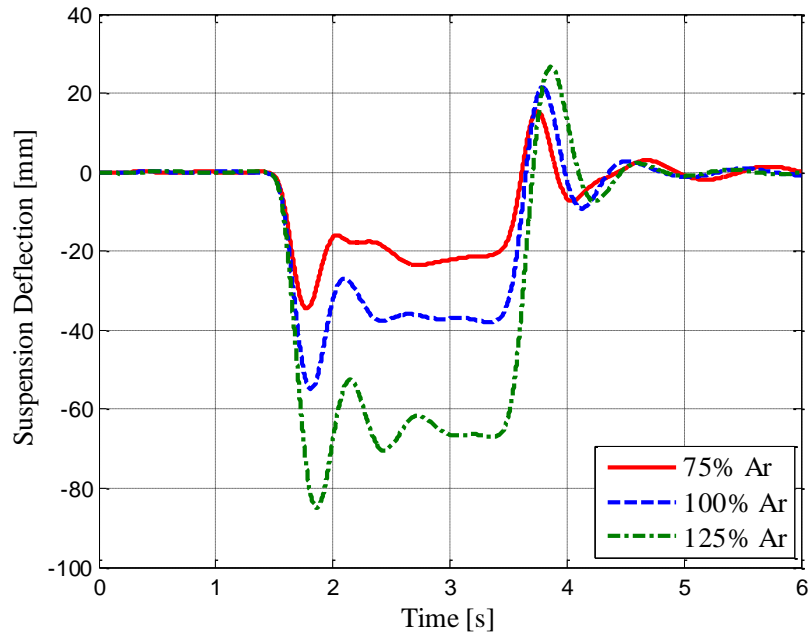


Figure 6.86: Change of Front Suspension Deflection with Piston Area

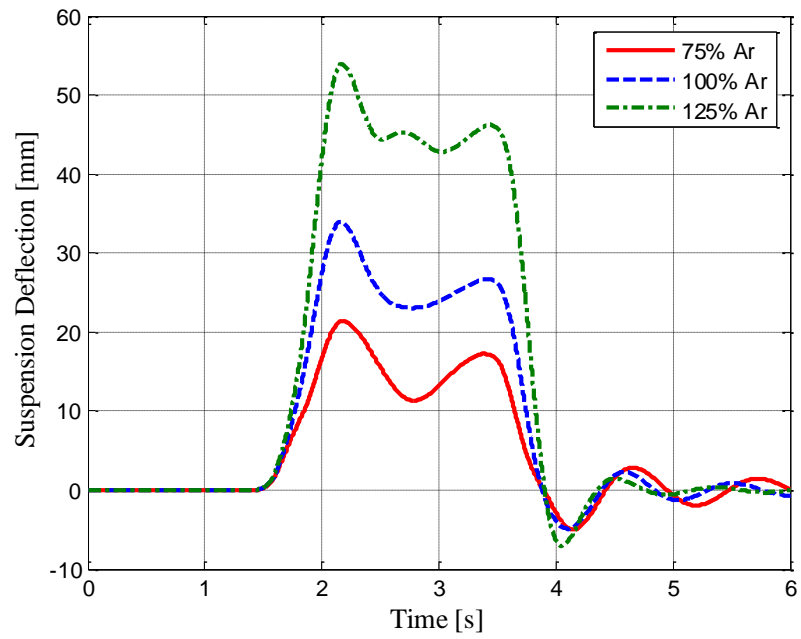


Figure 6.87: Change of Intermediate Suspension Deflection with Piston Area

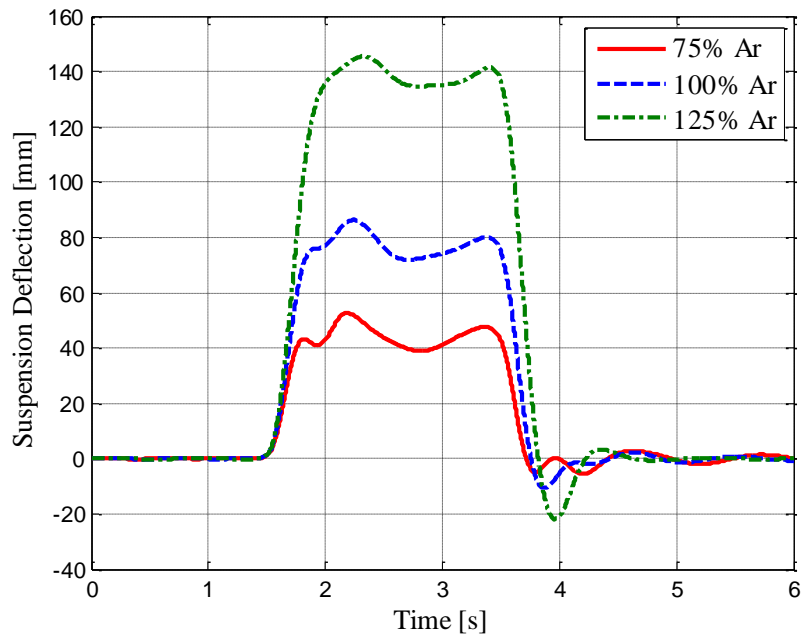


Figure 6.88: Change of Rear Suspension Deflection with Piston Area

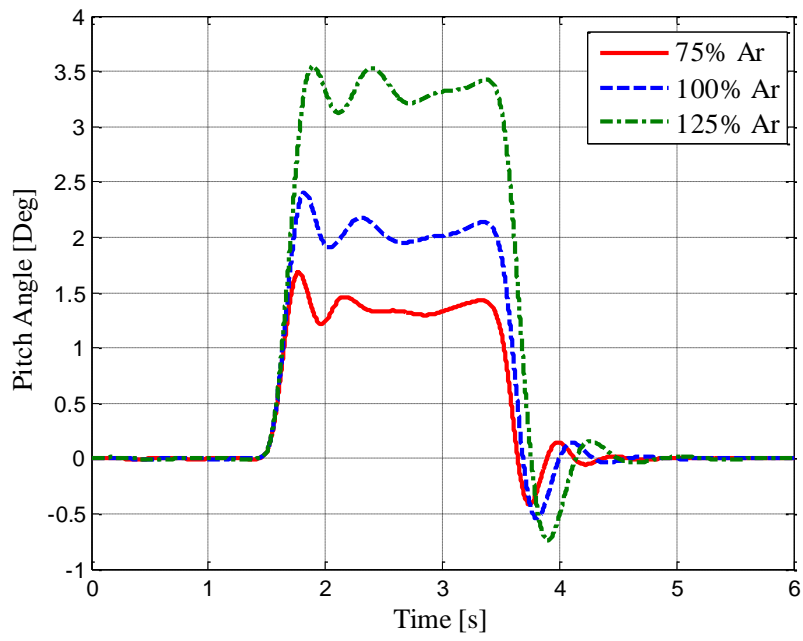


Figure 6.89: Change of Pitch Angle with Piston Area

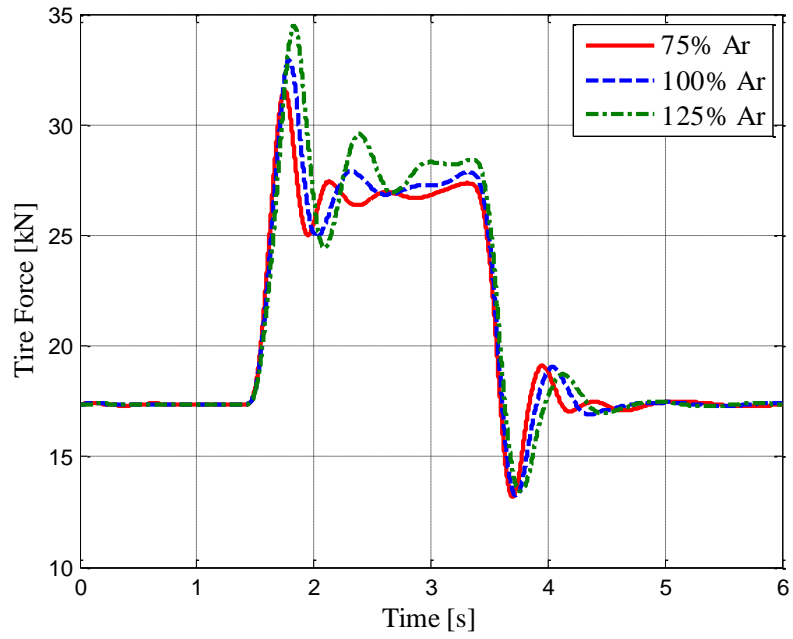


Figure 6.90: Change of Front Tire Force with Piston Area

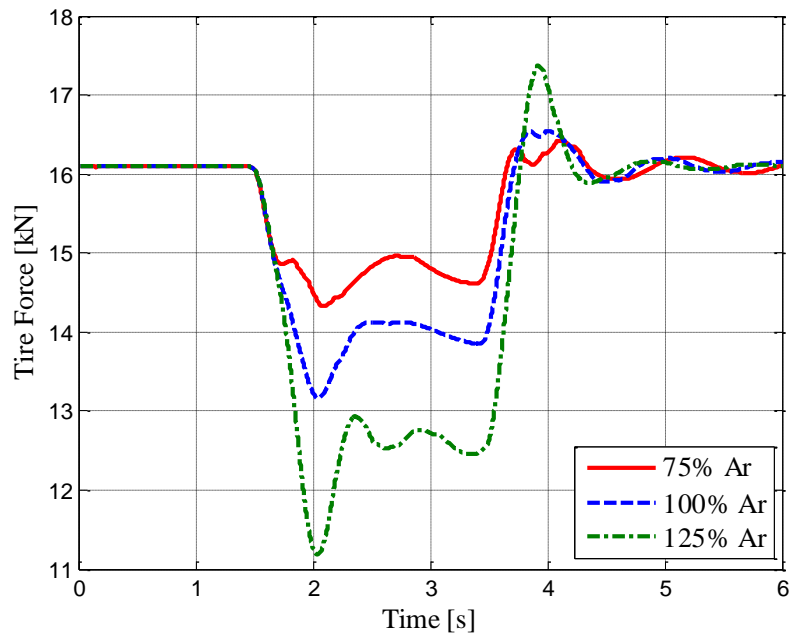


Figure 6.91: Change of Intermediate Tire Force with Piston Area

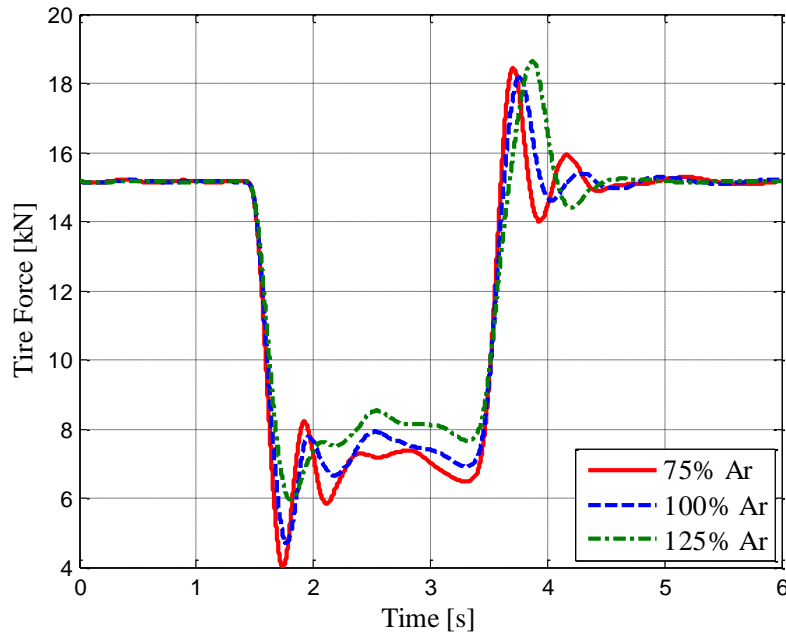


Figure 6.92: Change of Rear Tire Force with Piston Area

❖ **Sensitivity w.r.t. Initial Gas Volume**

Change of the braking simulation results with the initial gas volumes are given in Figure 6.93 to Figure 6.99. As can be seen from Figure 6.96, when the initial gas volume is decreased, suspension stiffness and thus vertical stiffness increases. Increased pitch stiffness decreases the pitch angle response for the braking simulation.

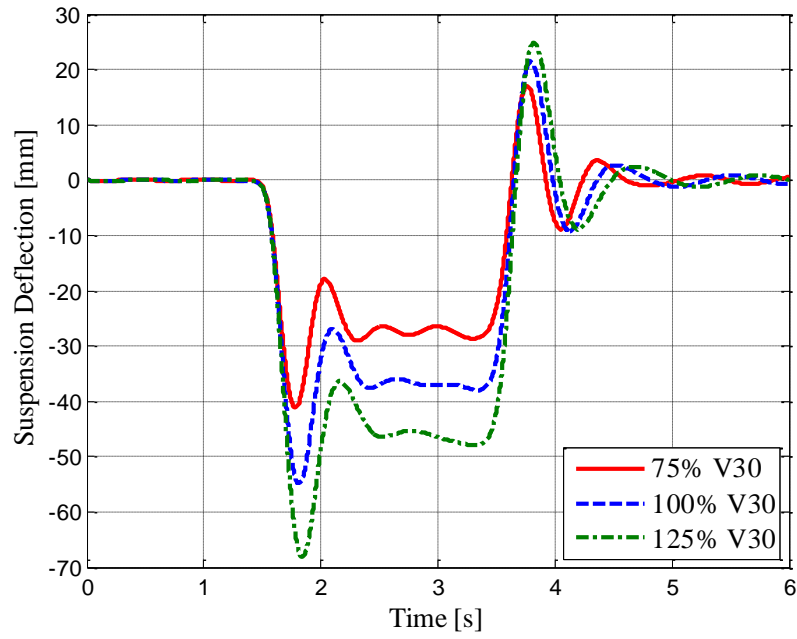


Figure 6.93: Change of Front Suspension Deflection with Initial Gas Volume

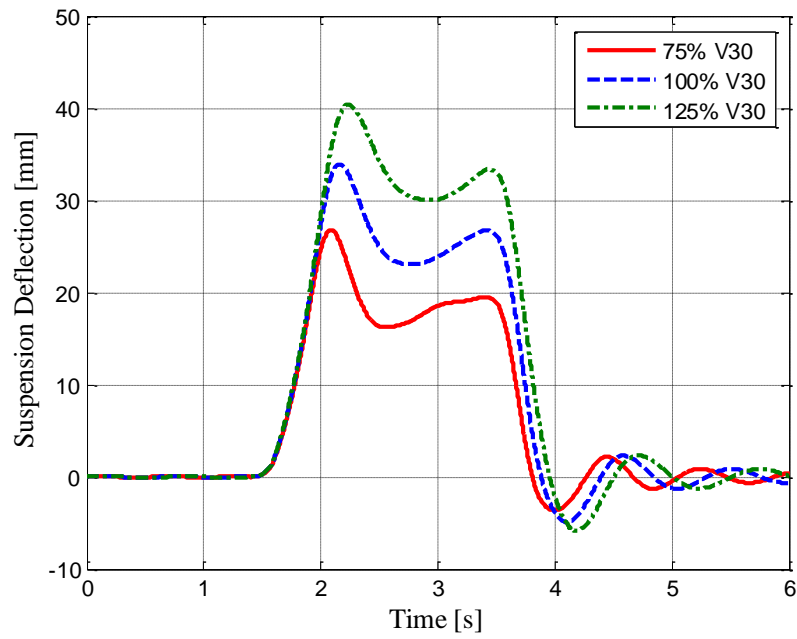


Figure 6.94: Change of Intermediate Suspension Deflection with Initial Gas Volume

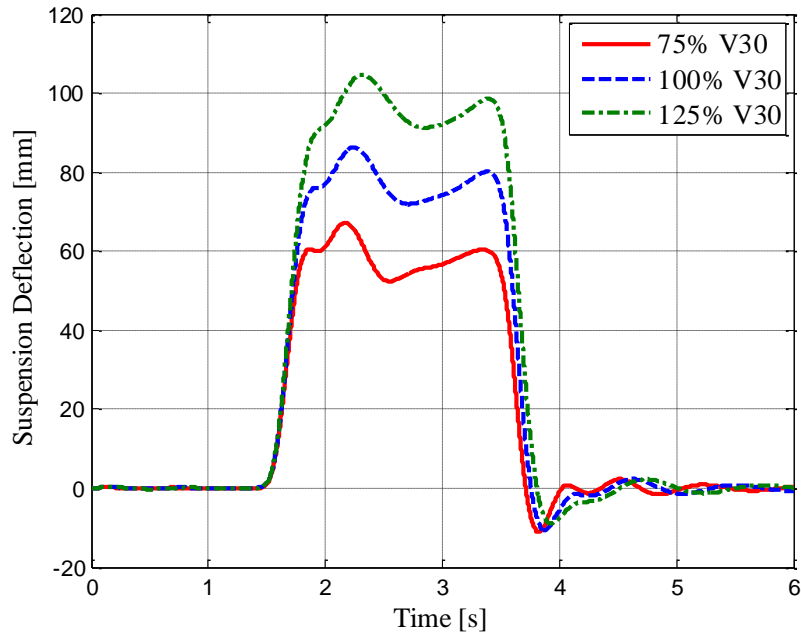


Figure 6.95: Change of Rear Suspension Deflection with Initial Gas Volume

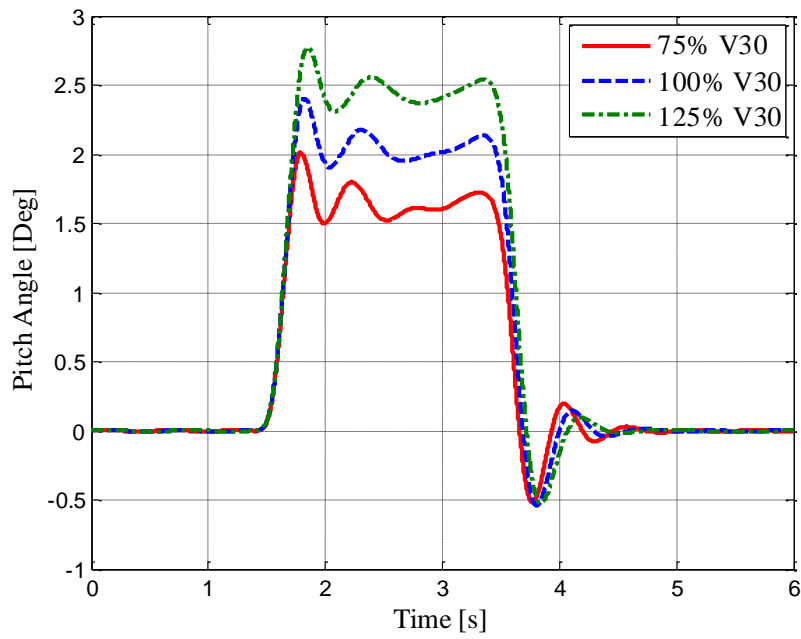


Figure 6.96: Change of Pitch Angle with Initial Gas Volume

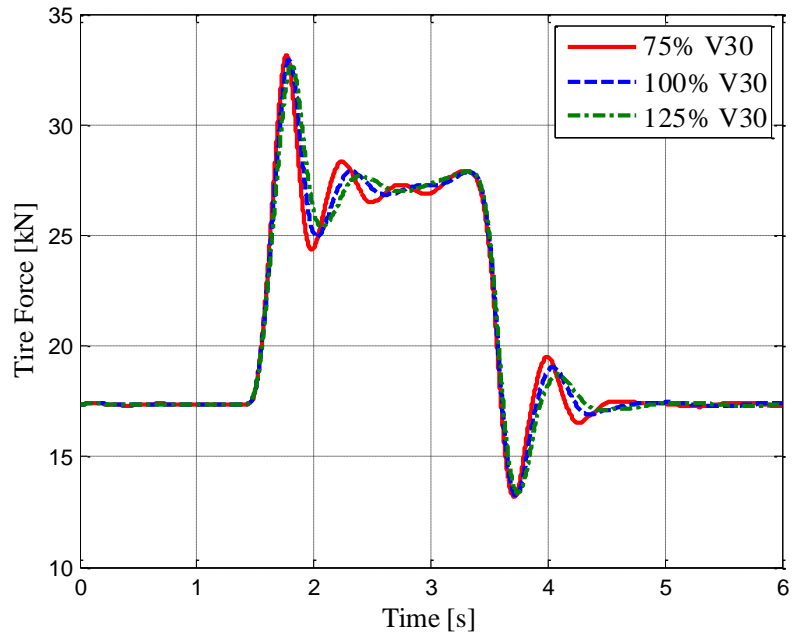


Figure 6.97: Change of Front Tire Force with Initial Gas Volume

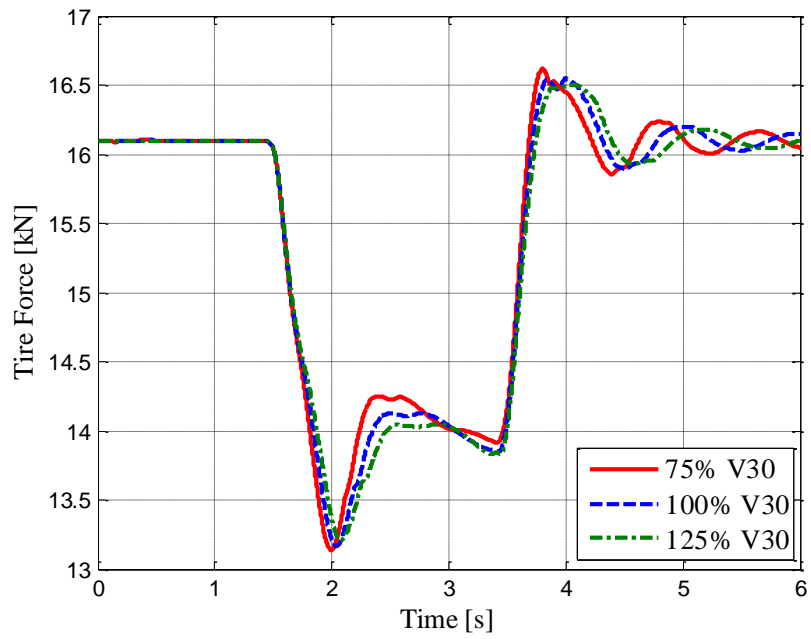


Figure 6.98: Change of Intermediate Tire Force with Initial Gas Volume

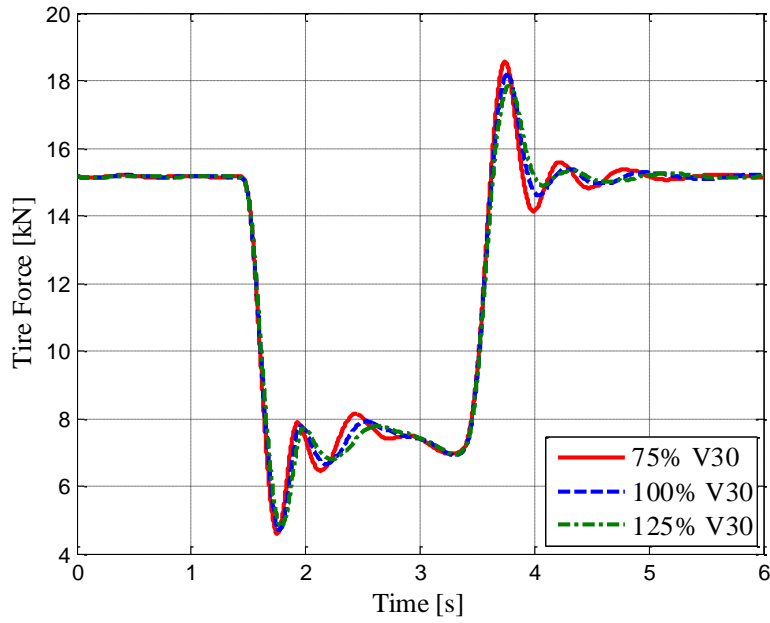


Figure 6.99: Change of Rear Tire Force with Initial Gas Volume

❖ **Sensitivity w.r.t. Valve Opening**

Change of the braking simulation results with the maximum valve opening are given in Figure 6.100 to Figure 6.106.

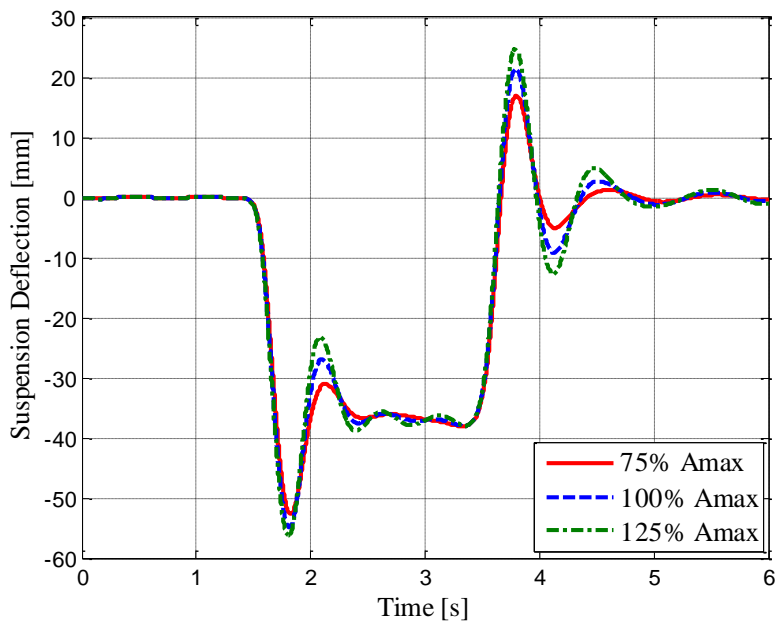


Figure 6.100: Change of Front Suspension Deflection with Valve Opening

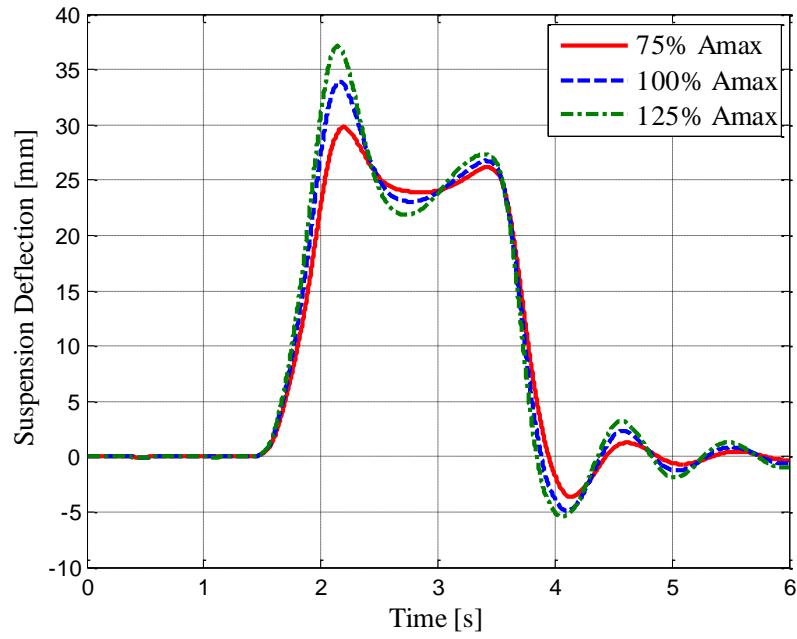


Figure 6.101: Change of Intermediate Suspension Deflection with Valve Opening

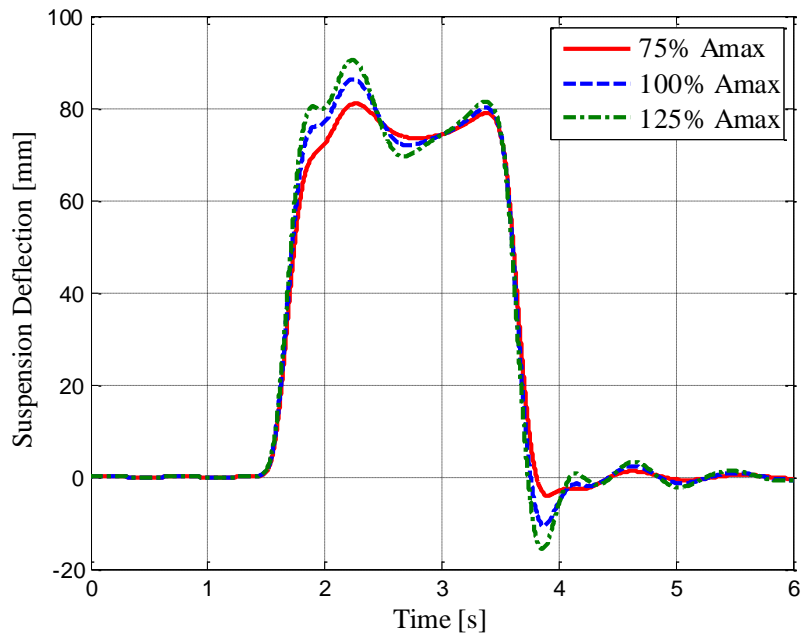


Figure 6.102: Change of Rear Suspension Deflection with Valve Opening

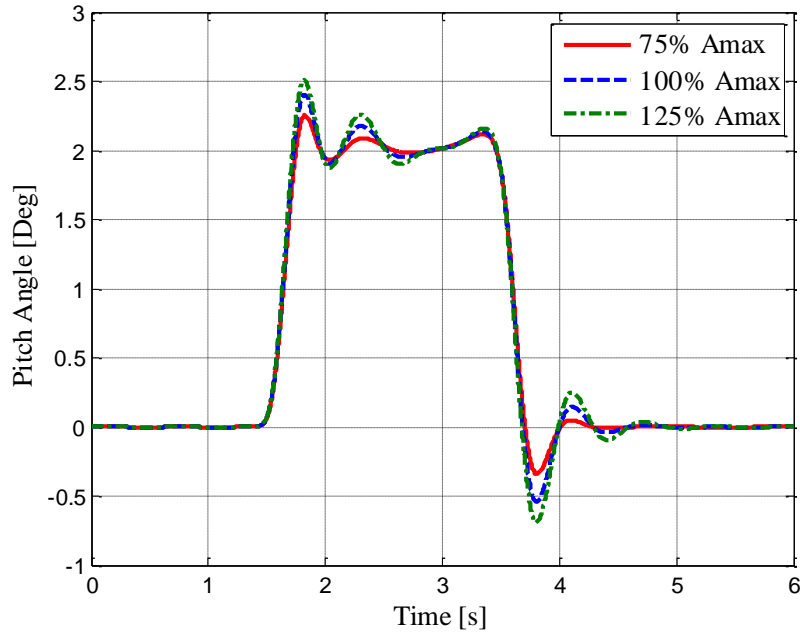


Figure 6.103: Change of Pitch Angle with Valve Opening

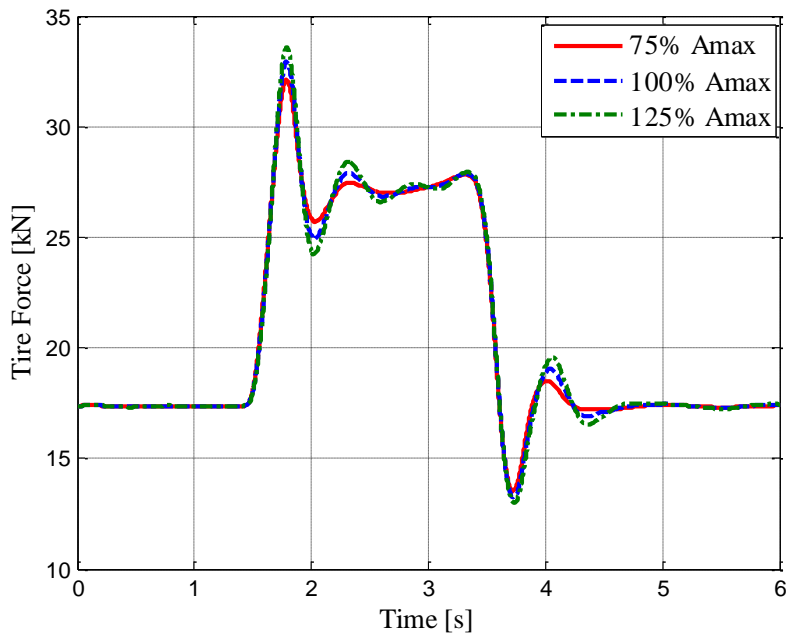


Figure 6.104: Change of Front Tire Force with Valve Opening

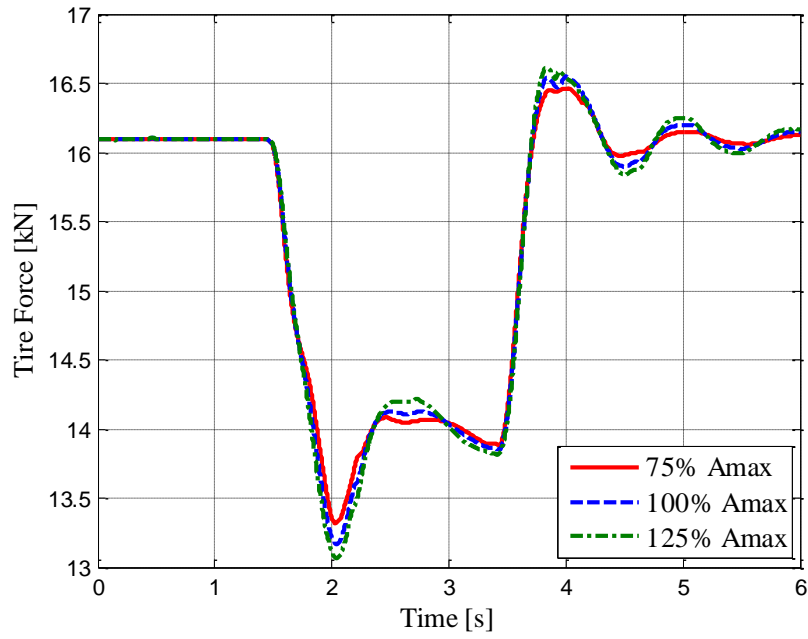


Figure 6.105: Change of Intermediate Tire Force with Valve Opening

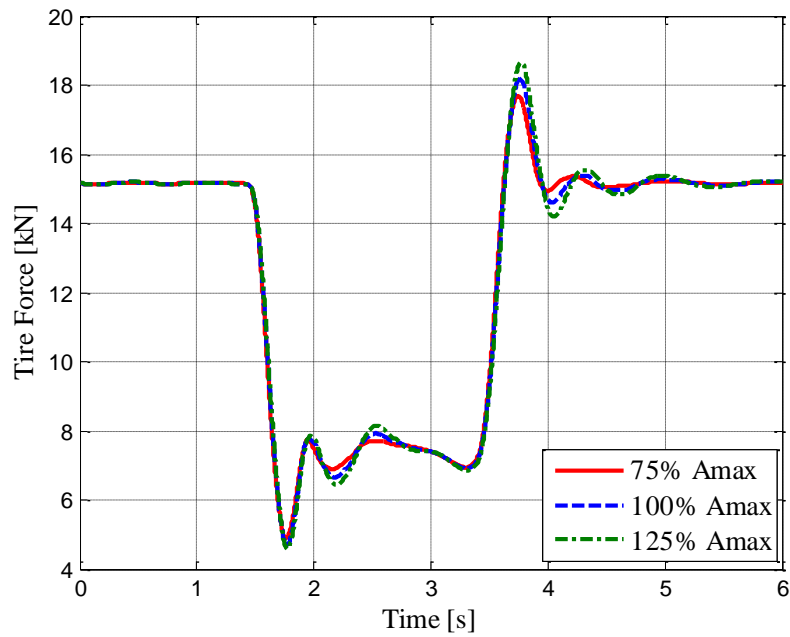


Figure 6.106: Change of Rear Tire Force with Valve Opening

As Figure 6.103 shows, as the valve opening is decreased, suspension damping and thus pitch damping is increased. Thus increased pitch damping decreases the pitch

angle. However, since the suspension damping has important effect on the suspension dynamics mostly on the high frequencies, suspension damping has little effect on the pitch angle of braking maneuver which is close to steady state maneuver. All results observed from Figure 6.79 to Figure 6.106 are related to vertical and pitch stiffness and damping which studied in detail. Since effects of the suspension design parameters on simulation results are observed, a tough understanding can be obtained on parametric study.

6.10.6. Random Road Simulation

After the parametric study with the braking performance is performed, now the parametric study with respect to ride comfort is to be performed Random road displacement inputs same as those used in section 4.2.4.1 at different longitudinal speeds are used in simulations. Change of the rms values of the vertical and pitch accelerations with respect to suspension design parameters are given in Table 6.29 to Table 6.32.

❖ Sensitivity w.r.t. Piston Area

Table 6.29: Vertical and Pitch Acceleration rms for Different Piston Areas

	100 %	75 %	125 %
Vertical Acceleration rms [m/s^2]	0.58	0.57	0.60
Pitch Acceleration rms [rad/s^2]	0.38	0.33	0.44

❖ Sensitivity w.r.t. Piston Rod Area

Table 6.30: Vertical and Pitch Acceleration rms for Different Piston Rod Areas

	Unconnected	$A_r=0.8A_p$	$A_r=0.6A_p$
Vertical Acceleration rms [m/s^2]	0.61	0.58	0.56
Pitch Acceleration rms [rad/s^2]	0.29	0.38	0.51

❖ Sensitivity w.r.t. Initial Gas Volume

Table 6.31: Vertical and Pitch Acceleration rms for Different Initial Gas Volumes

	100 %	75 %	125 %
Vertical Acceleration rms [m/s^2]	0.58	0.70	0.50
Pitch Acceleration rms [rad/s^2]	0.38	0.44	0.35

❖ **Sensitivity w.r.t. Maximum Valve Openings**

Table 6.32: Vertical and Pitch Acceleration rms for Different Maximum Valve Openings

	100 %	75 %	125 %
Vertical Acceleration rms [m/s^2]	0.58	0.55	0.62
Pitch Acceleration rms [rad/s^2]	0.38	0.40	0.38

Again, the effect of the suspension design variables on the rms values of the vertical and pitch accelerations can be interpreted in terms of the change in the stiffness and damping characteristics. When the piston area is decreased, suspension stiffness and damping also decrease and thus vertical acceleration and pitch acceleration decreases. This improves the ride comfort performance of the vehicle. However, piston rod area has somewhat different effect on the vertical and pitch stiffness and damping characteristics of the interconnected HP suspension system. When the piston rod area is decreased, suspension vertical stiffness and damping also decrease. On the contrary, when the suspension piston rod area is decreased, pitch stiffness and damping increases. Therefore, decreased vertical stiffness and damping results in decreased vertical acceleration. However, increased pitch stiffness and damping result in increased pitch acceleration. As regard to initial gas volume, increasing initial gas volume increase suspension vertical and pitch stiffness. Thus, vertical and pitch accelerations also increase and ride comfort is decreased. Finally, when the valve opening is decreased, suspension damping increases. Depending on the frequency content of the road displacement inputs, vertical and pitch accelerations may increase or decrease. In our case, increased suspension damping decreases vertical accelerations slightly, and nearly has no effect on the pitch acceleration.

6.11. CONCLUSION

In this chapter, analysis of the pitch interconnected HP suspension systems for a three-axle vehicle has been carried out. As the first step, a nine degree of freedom vehicle model for a three axle vehicle is derived. Then, full and semi-interconnected HP suspension configurations were enumerated. Stiffness and damping characteristics of these interconnected suspensions are formed and compared to each

other. A detailed parameter sensitivity analysis was performed in order to examine the effects of the suspension design parameters on the stiffness and the damping characteristics. Then, simulations are performed to examine the vehicle ride comfort, braking/acceleration, and fire shock performances. According to the results obtained, a suspension metric is formed to classify the interconnections quantitatively in terms of ride comfort and pitch performance. After that, a specific interconnection was selected for further sensitivity analysis. In this sensitivity analysis, effects of the suspension design parameters on the suspension performance variables were inspected directly. The results are summarized below:

- ❖ For a vehicle with three axles, different full and semi-interconnected HP suspension configurations can be obtained.
- ❖ When an unconnected HP suspension configuration is converted into an interconnected HP suspension configuration, completely different suspension characteristics are obtained in terms of the vertical and pitch stiffness and damping properties.
- ❖ In order to compare the stiffness and the damping characteristics of the interconnected HP suspension configurations, some of their properties should be equalized and other characteristics should be compared.
- ❖ In this study, vertical stiffness and the damping characteristics of different interconnected HP suspension configurations are equated to each other by a mathematical optimization approach.
- ❖ In order to have suspension configurations with equal vertical stiffness, there are two methods. First method is to equate the vertical stiffness of the suspensions at static equilibrium. By this way, analytical expressions can be obtained for the suspension parameters resulting in equal stiffness. However, the stiffness of the HP suspension systems changes with the changing suspension displacement. Second method of obtaining equivalent suspension stiffness is to equate the stiffness characteristics for a range of vertical suspension displacement. Then, for a range of suspension displacement, equivalent suspension stiffness characteristics are obtained. However, instead

of analytical expressions, numerical values of the suspension parameters are obtained by optimization. In this study, the second approach is used.

- ❖ In order to obtain equivalent suspension damping characteristics for different suspension configurations, damping force of suspension are equated to each other for a range of suspension velocities by mathematical optimization, like the second method of getting equivalent suspension stiffness.
- ❖ Pitch stiffness and damping characteristics of the interconnected HP suspension configurations which have equivalent vertical stiffness and damping characteristics are compared to each other. A suspension configuration which has connection between front and rear suspension units has highest pitch stiffness and damping. This is due to the amount of the fluid displaced among suspension configurations with the vehicle motion.
- ❖ Suspension configurations have the highest pitch stiffness at zero pitch angle. When the pitch angle increases, pitch stiffness decreases.
- ❖ Fully interconnected HP suspension configurations have the highest pitch stiffness and damping characteristics than come the semi-interconnected and unconnected HP suspension configurations.
- ❖ According to the sensitivity study, when the piston area is increased, vertical and pitch stiffness and damping also increase.
- ❖ When the initial gas volume is increased vertical and pitch stiffness decrease.
- ❖ When the piston rod area is decreased, vertical stiffness and damping decrease, however, pitch stiffness and damping increase.
- ❖ Suspension configurations having equivalent vertical stiffness and damping characteristics have approximately the same vertical accelerations.
- ❖ Interconnected HP suspension configurations decrease the pitch angle of the vehicle in braking and firing simulations as compared with the unconnected HP suspension configurations.
- ❖ According to the simulation results, interconnected HP suspension systems have higher pitch performance and lower ride comfort performance.

Therefore, in an unconnected HP suspension system, the only way of increasing pitch stiffness and the damping is to increase the vertical suspension stiffness and

damping, respectively. However, in an interconnected HP suspension system, pitch stiffness and damping can be increased both by increasing the vertical stiffness and damping and by decreasing the piston area. Therefore, interconnected HP suspension system for the improved pitch performance of the vehicle has a promising solution by more flexible design parameters.

CHAPTER 7

ANALYSIS AND DESIGN OF THE FULL INTERCONNECTED HP SUSPENSION SYSTEM FOR THREE-AXLE VEHICLES

In the previous chapter, interconnected HP suspension systems were examined for a three-axle vehicle in the pitch plane. It has been shown that, with specific interconnections, the pitch stiffness and damping characteristics of the vehicle can be increased considerably. While increasing pitch stiffness and the damping, almost equal vertical stiffness and the damping characteristics can be obtained for the unconnected and the interconnected HP suspension systems. In this chapter, design and analysis of the interconnected HP suspension systems for a three-axle full vehicle model are performed.

7.1. INTRODUCTION

Interconnections between suspensions are sought to improve both the pitch and the roll stiffness of the vehicle. For this reason, different interconnections are enumerated and their characteristics are examined. Pitch and roll stiffness and damping and warp moment characteristics are compared to each other. To be able to determine the appropriate suspension type, a quantitative analysis is performed. According to the results, groups of interconnected suspension type are selected for further performance examination. To determine the effects of the suspension parameters on the stiffness and the damping characteristics of the HP suspension

system, a detailed sensitivity analysis is performed. From the results, the selection of the design parameters and their importance on the vehicle performance are evaluated. In order to make a complete performance evaluation, a full vehicle model with interconnected HP suspension system is derived. Simulations are performed to examine the performance of the full vehicle model with the interconnected HP suspension system. Simulations are performed with random road displacement inputs at different longitudinal velocities to examine the ride comfort characteristics of the designed suspensions. Then, a simulation with braking in cornering input is performed to determine the handling performance of the vehicle. For vehicles with firing performance, the performance of the interconnected suspension system for firing and mobility performance are examined by the simulations. For these reason 9 dof and 18 dof full vehicle models are derived. 9 dof full vehicle model is used for the derivation of the stiffness and damping characteristics, and the 18 dof full vehicle model is used for the ride comfort, handling, and the mobility performance evaluations.

7.2. FULL VEHICLE MODEL

The parameters and the variables used in the derivation of the full vehicle models are presented in Table 7.1. In variable definition “ij” stands for front left, front right, intermediate left, intermediate right, rear left, and rear right.

Table 7.1: Variable Definition

Variable	Definition
F_{ij}	Suspension Force
F_{ijX}	Reaction Force between Suspension and Sprung Mass in x Direction
F_{ijY}	Reaction Force between Suspension and Sprung Mass in y Direction
M_{ij}	Reaction Moment between Tire and Sprung Mass in z Direction
F_{ijXO}	Traction or Braking Force on Tire
F_{ijYO}	Cornering Force on Tire
F_{ijO}	Reaction Force Between Ground and Tire in z Direction
F_{ijRC}	Vertical Force on Tire due to Jacking Moment
z_{pij}	Piston Displacement
θ_{ij}	Tire Rotational Displacement
T_{ij}	Tire Traction or Braking Torque
δ_{ij}	Steering Input at Tires
u	Longitudinal Velocity in Ground Plane
v	Lateral Velocity in Ground Plane
r	Yaw Velocity
Ψ	Yaw Angle
a_{Gx}	Sprung Mass Acceleration in x Direction
a_{Gy}	Sprung Mass Acceleration in y Direction
a_{Gz}	Sprung Mass Acceleration in z Direction
α_{Gx}	Sprung Mass Angular Acceleration in x Direction
α_{Gy}	Sprung Mass Angular Acceleration in y Direction
α_{Gz}	Sprung Mass Angular Acceleration in z Direction
ω_{Gx}	Sprung Mass Angular Velocity in x Direction
ω_{Gy}	Sprung Mass Angular Velocity in y Direction
ω_{Gz}	Sprung Mass Angular Velocity in z Direction
F_x	Forces on Sprung Mass in x Direction
F_y	Forces on Sprung Mass in y Direction
F_z	Forces on Sprung Mass in z Direction
a_{txij}	Acceleration of Tire in x Direction
a_{tyij}	Acceleration of Tire in y Direction
a_{tzij}	Acceleration of Tire in z Direction
α_{tzij}	Tire Angular Acceleration in z Direction
α_{tyij}	Tire Angular Acceleration in y Direction
F_{tRCij}	Reaction Force on Tire Due to Suspension Jacking
α_{ij}	Slip Angle
S_{ij}	Longitudinal Slip
F_D	Disturbance Moment in Vertical Direction
M_θ	Disturbance Moment in Pitch Direction
M_ϕ	Disturbance Moment in Roll Direction

7.2.1. Modeling of the Nine Degree of Freedom Full Vehicle Model

In this section, the model of the vehicle with three axles is going to be derived. The model has nine degrees of freedom. The sprung mass has three degrees of freedom in the roll, pitch, and vertical directions, and the tires have six degrees of freedom in the vertical directions. The schematic of the full vehicle model with three axles is shown in Figure 7.1.

The equation of motion for the sprung mass in the vertical, roll, and pitch directions can be written as,

$$F_{FL} + F_{FR} + F_{ML} + F_{MR} + F_{RL} + F_{RR} - F_D = M_s \ddot{z} \quad (7-1)$$

$$-a(F_{FL} + F_{FR}) + b(F_{ML} + F_{MR}) + c(F_{RL} + F_{RR}) - M_{D\theta} = I_{yy} \ddot{\theta} \quad (7-2)$$

$$\frac{t_f}{2}(F_{FL} - F_{FR}) + \frac{t_m}{2}(F_{ML} - F_{MR}) + \frac{t_r}{2}(F_{RL} - F_{RR}) - M_{D\phi} = I_{xx} \ddot{\phi} \quad (7-3)$$

Assuming small displacement, suspension piston displacement and velocities can be expressed as follows:

$$z_{pFL} = z - a\theta + \frac{t_f}{2}\phi \quad (7-4)$$

$$z_{pFR} = z - a\theta - \frac{t_f}{2}\phi \quad (7-5)$$

$$z_{pML} = z + b\theta + \frac{t_m}{2}\phi \quad (7-6)$$

$$z_{pMR} = z + b\theta - \frac{t_m}{2}\phi \quad (7-7)$$

$$z_{pRL} = z + c\theta + \frac{t_r}{2}\phi \quad (7-8)$$

$$z_{pRR} = z + c\theta - \frac{t_r}{2}\phi \quad (7-9)$$

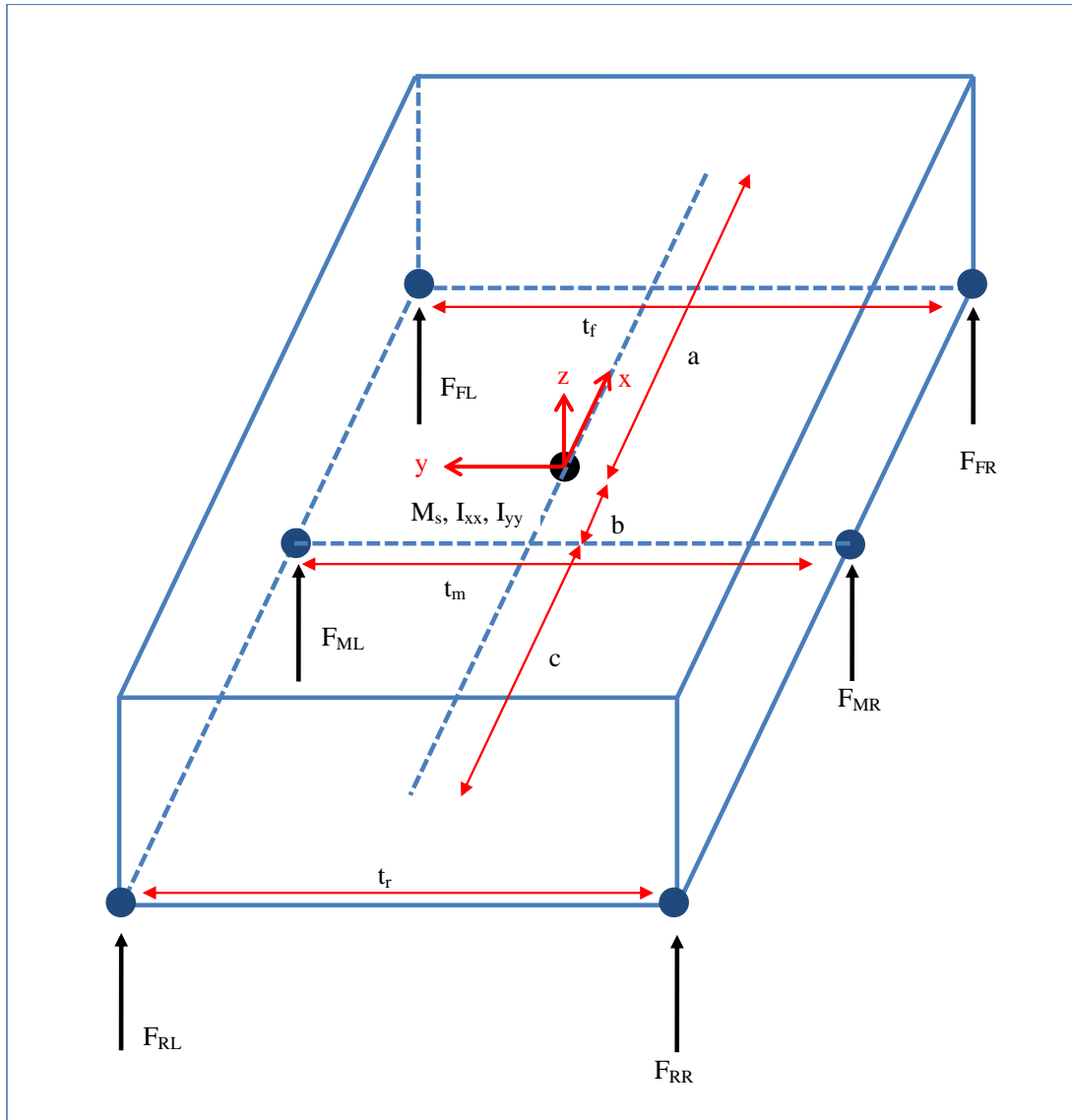


Figure 7.1: Nine Degree of Freedom Full Vehicle Model

7.3. MODELING OF THE EIGHTEEN DEGREE OF FREEDOM FULL VEHICLE MODEL

The vehicle ride model derived in the previous part includes the vertical, roll, and pitch motions of the sprung mass and the vertical motions of the tires. Road displacement inputs at the tires and the roll, pitch and vertical body disturbance moments and forces are the inputs to the ride model. Roll and pitch body disturbance moments can be calculated from the lateral and longitudinal accelerations obtained from the simulations of the complete vehicle models or from simple vehicle handling

models like bicycle model. Body disturbance moments can be used in the vehicle ride model in the simulations for the vehicle inertial forces due to cornering and braking-traction. By this way vehicle ride model can be used for ride and handling studies. In vehicle ride model, tire braking-tractive and steering inputs cannot be used. Another approach for the simulation of the vehicle ride and the handling dynamic is the use of the more accurate and complex vehicle models. In this model both handling inputs which are steering, braking, and tractive inputs, and the ride inputs which are the road displacement inputs can be used directly. Therefore, in this part full vehicle model which consists of vehicle ride, handling, and tire dynamics are derived. Full vehicle model with three axles has 18 degrees of freedom which are three displacements, and three rotations of sprung mass and the vertical displacements and rotations for each tire.

In the literature, there are different full vehicle models which comprise vehicle ride, handling, and tire models of different complexity [73]-[78]. In these studies 14 degrees of freedom vehicle models are derived with different assumptions. Modeling of the suspension linkage kinematics in low order vehicle models is a difficult and complex issue. For this reason different modeling concepts for the suspension kinematics are studied. Roll center approach is one of the most commonly used methods of representing the effects of the suspension kinematics on the sprung mass. However, using roll center approach has some limitations. In severe maneuvers, when the suspension moves, roll center also moves and thus constant roll center cannot be used. Moreover, for a vehicle with three or more axles, the use of the roll center approach is difficult as explained in the reference [78]. While the suspension kinematic is modeled, one of the important considerations is the suspension jacking forces [73], [77]. As explained in the reference [77], modeling of suspension jacking force is necessary for accurate vehicle modeling. In the study of Huh et al. [79], handling and the driving characteristics of a three-axle-vehicle is studied and an 18 dof full vehicle model is developed to be used in the simulations.

In this study, a full vehicle model with three-axes is modeled. Interconnected HP suspension system is used in the derived model. The derived model consists of the degrees of freedom of,

- ❖ 6 dof of Sprung Mass (Roll, Pitch, Yaw, Vertical, Lateral, and Longitudinal)
- ❖ 12 dof of 6 Tires (Vertical, and Rotational for each tire)

While deriving the equation of motions Newton-Euler method is used. For tires, a Magic Formula tire model which gives combined lateral and longitudinal force characteristics is selected. The schematic of the full vehicle model with three axes is shown in Figure 7.2 and the free body diagrams of the tires are shown in Figure 7.3.

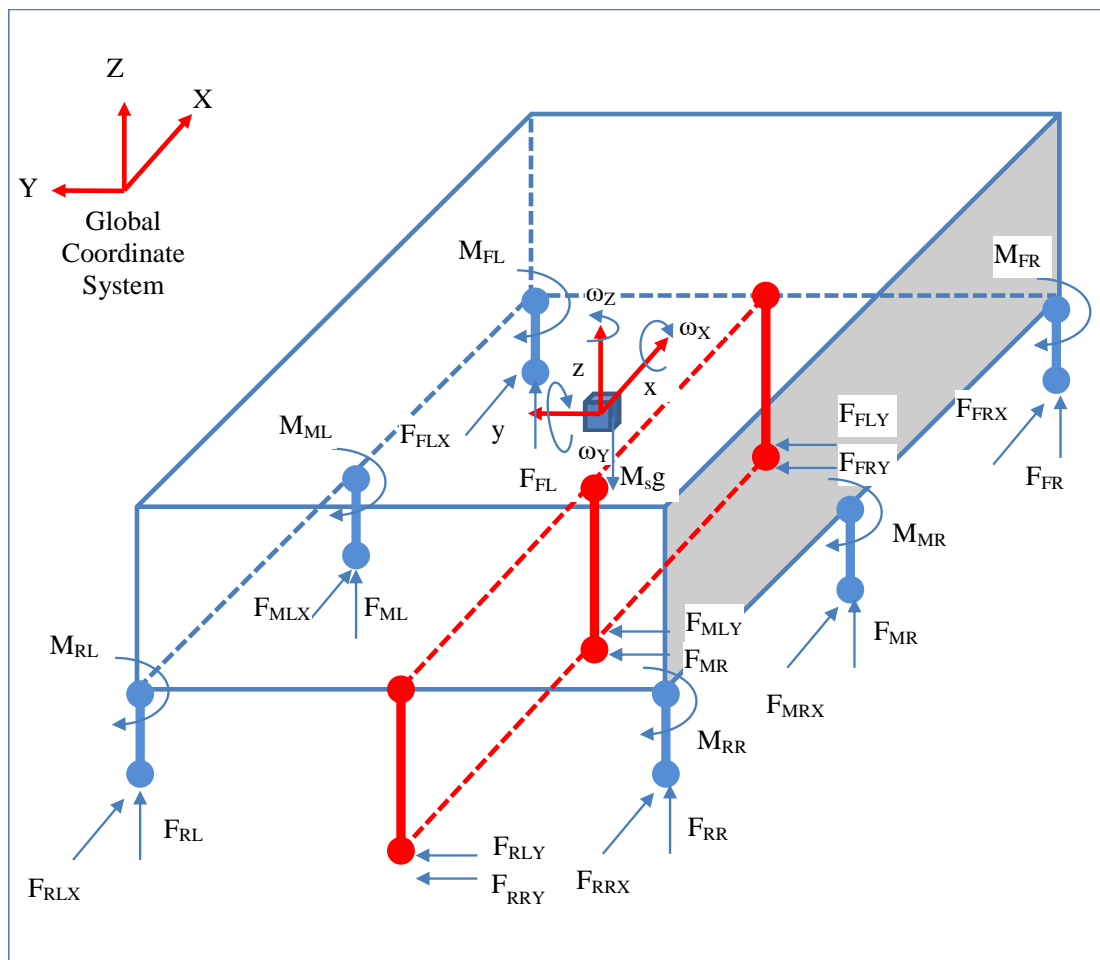


Figure 7.2: Full Vehicle Model - Sprung Mass Free Body Diagram

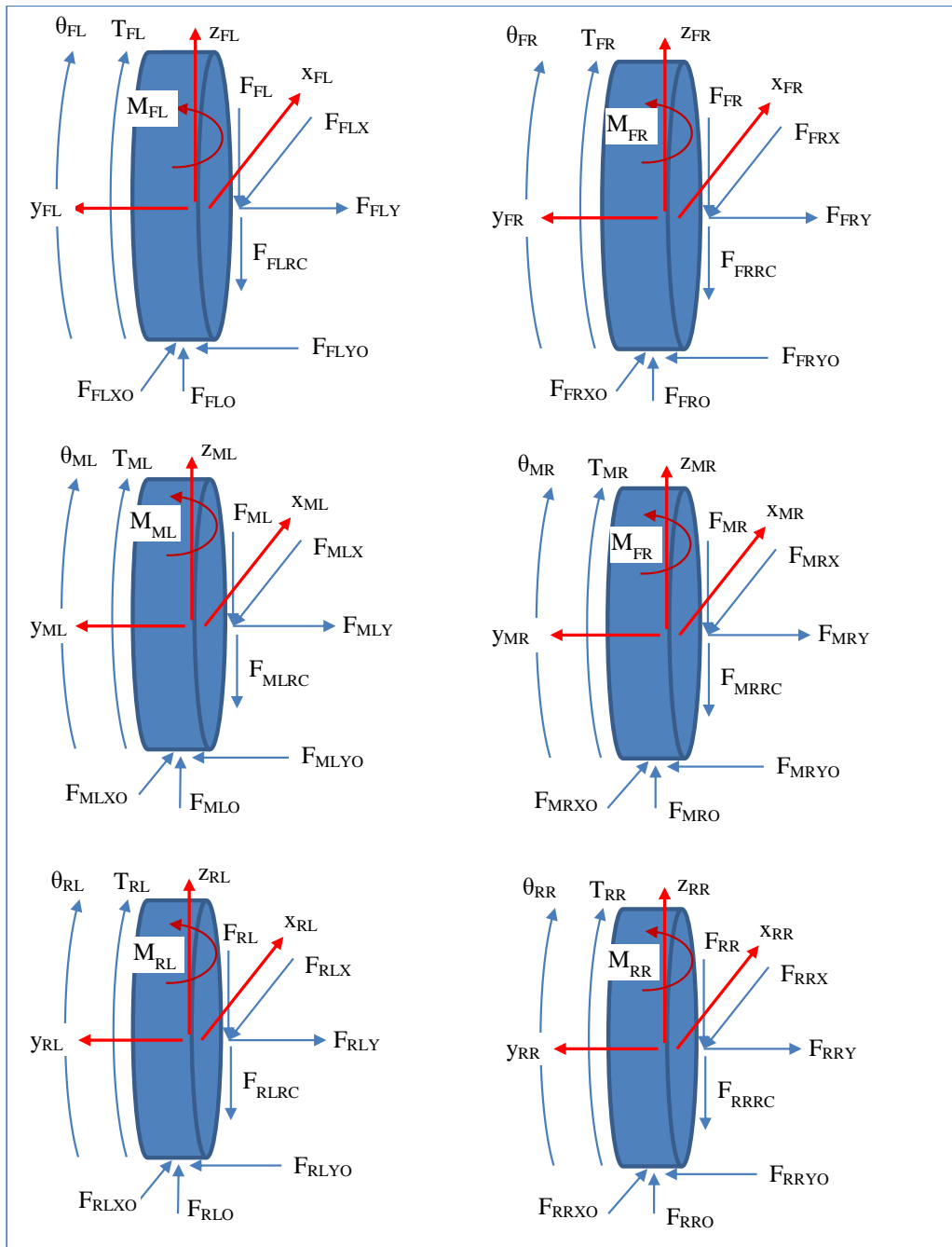


Figure 7.3: Free body Diagrams of Tires

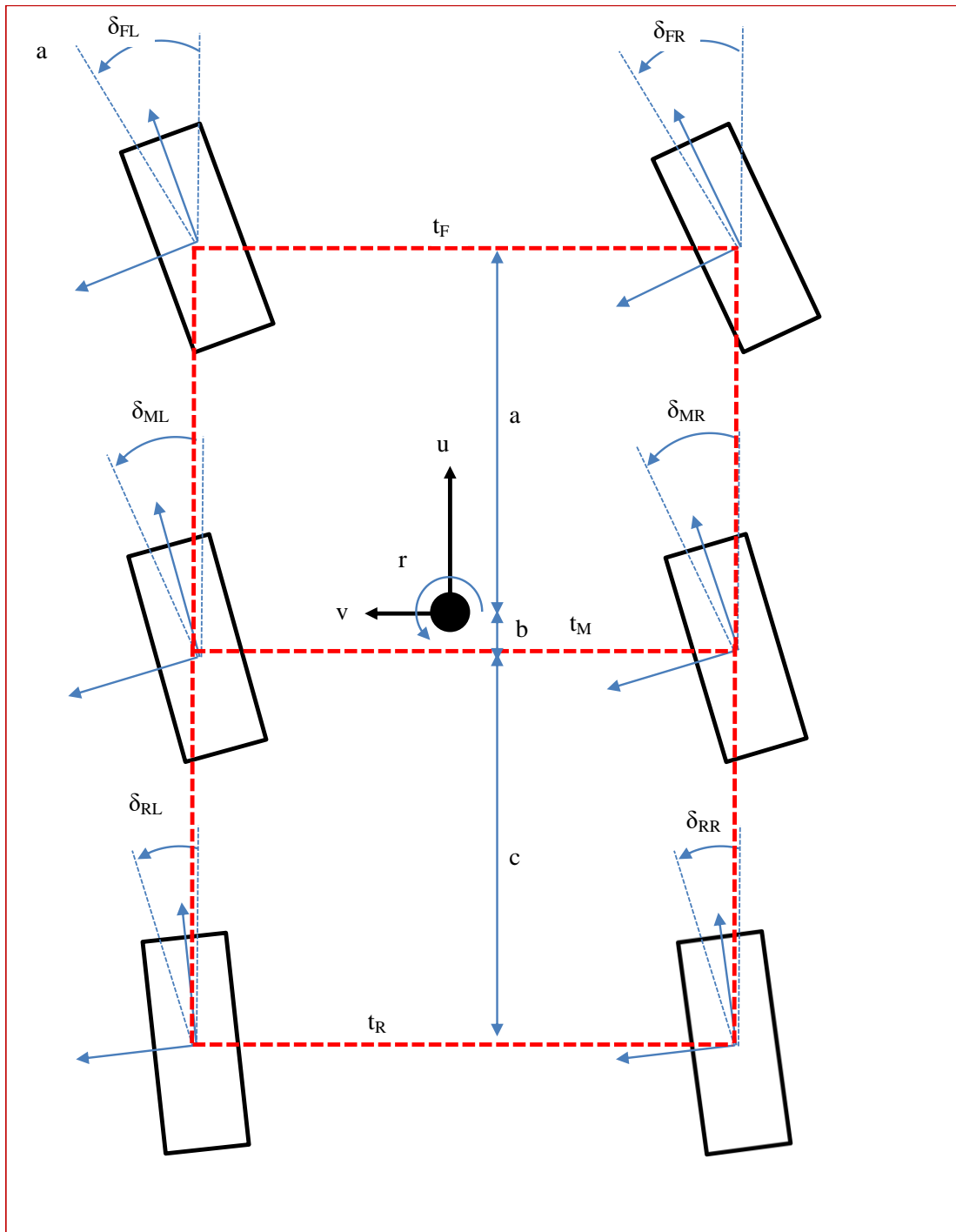


Figure 7.4: Slip Angle Definitions

Roll center approach can be applied to a vehicle with two axles easily. However, as stated in the study of Guiggiani [78], for a three axle vehicle it is difficult to adapt. While deriving the equations of motion, it is assumed the lateral forces are applied to

the sprung mass around roll center points which are fixed on ground. In pitch motions, the longitudinal forces are assumed to be applied at wheel-hub center. The rotational motion of the sprung mass and tire is defined by the Ψ , θ , and ϕ angles which are the yaw, pitch, and roll angles respectively. Yaw angle, Ψ , defines the motion of the tires and the sprung mass on the ground plane. $x^1y^1z^1$ is the frame obtained when the initial frame is rotated about Z axis of XYZ frame by angle yaw angle Ψ ,

$$\begin{Bmatrix} x^1 \\ y^1 \\ z^1 \end{Bmatrix} = \begin{bmatrix} \cos \Psi & \sin \Psi & 0 \\ -\sin \Psi & \cos \Psi & 0 \\ 0 & 0 & 1 \end{bmatrix} \begin{Bmatrix} X \\ Y \\ Z \end{Bmatrix} \Rightarrow \begin{Bmatrix} x^1 \\ y^1 \\ z^1 \end{Bmatrix} = \mathbf{R}_1 \begin{Bmatrix} X \\ Y \\ Z \end{Bmatrix} \quad (7-10)$$

Then the $x^1y^1z^1$ frame is rotated about the y^1 axis by pitch angle θ and the $x^2y^2z^2$ coordinate frame is obtained.

$$\begin{Bmatrix} x^2 \\ y^2 \\ z^2 \end{Bmatrix} = \begin{bmatrix} \cos \theta & 0 & -\sin \theta \\ 0 & 1 & 0 \\ \sin \theta & 0 & \cos \theta \end{bmatrix} \begin{Bmatrix} x^1 \\ y^1 \\ z^1 \end{Bmatrix} \Rightarrow \begin{Bmatrix} x^2 \\ y^2 \\ z^2 \end{Bmatrix} = \mathbf{R}_2 \begin{Bmatrix} x^1 \\ y^1 \\ z^1 \end{Bmatrix} \quad (7-11)$$

Then the $x^2y^2z^2$ frame is rotated about the x^2 axis by roll angle ϕ and the xyz coordinate frame is obtained.

$$\begin{Bmatrix} x \\ y \\ z \end{Bmatrix} = \begin{bmatrix} 1 & 0 & 0 \\ 0 & \cos \phi & \sin \phi \\ 0 & -\sin \phi & \cos \phi \end{bmatrix} \begin{Bmatrix} x^2 \\ y^2 \\ z^2 \end{Bmatrix} \Rightarrow \begin{Bmatrix} x \\ y \\ z \end{Bmatrix} = \mathbf{R}_3 \begin{Bmatrix} x^2 \\ y^2 \\ z^2 \end{Bmatrix} \quad (7-12)$$

While writing the kinematic constraint between tires and the sprung mass, it is assumed that tires move on the ground plane. Then the sprung mass has three relative motions with respect to tires which are roll, pitch, and the vertical movement. The Newton- Euler equations for sprung mass can be written as,

$$\begin{Bmatrix} \sum F_x \\ \sum F_y \\ \sum F_z \end{Bmatrix} = \mathbf{M}_s \begin{Bmatrix} a_{Gx} \\ a_{Gy} \\ a_{Gz} \end{Bmatrix} \quad (7-13)$$

$$\begin{Bmatrix} \sum M_x \\ \sum M_y \\ \sum M_z \end{Bmatrix} = [I] \begin{Bmatrix} \alpha_x \\ \alpha_y \\ \alpha_z \end{Bmatrix} + \begin{bmatrix} 0 & -\omega_z & \omega_y \\ \omega_z & 0 & -\omega_x \\ -\omega_y & \omega_x & 0 \end{bmatrix} [I] \begin{Bmatrix} \omega_x \\ \omega_y \\ \omega_z \end{Bmatrix} \quad (7-14)$$

If the xyz frames are the principal axes, the Euler equations become,

$$\sum M_x = I_{xx} \alpha_x - (I_{yy} - I_{zz}) \omega_y \omega_z \quad (7-15)$$

$$\sum M_y = I_{yy} \alpha_y - (I_{zz} - I_{xx}) \omega_x \omega_z \quad (7-16)$$

$$\sum M_z = I_{zz} \alpha_z - (I_{xx} - I_{yy}) \omega_x \omega_y \quad (7-17)$$

Assuming that, tires are always perpendicular to the ground, the equations of motion for each tire can be written as,

$$\begin{Bmatrix} \sum F_{tx} \\ \sum F_{ty} \\ \sum F_{tz} \end{Bmatrix} = M_s \begin{Bmatrix} a_{tGx} \\ a_{tGy} \\ a_{tGz} \end{Bmatrix} \quad (7-18)$$

$$\sum M_{ty} = I_{tyy} \alpha_{ty} \quad (7-19)$$

$$\sum M_{tz} = I_{tzz} \alpha_{tz} \quad (7-20)$$

For the front left tire:

$$F_{FLXO} - F_{FLX} = M_t a_{tGxFL} \quad (7-21)$$

$$F_{FLYO} - F_{FLY} = M_t a_{tGyFL} \quad (7-22)$$

$$F_{FLO} - F_{FL} + F_{FLRC} = M_t a_{tGzFL} \quad (7-23)$$

$$T_{FL} - F_{FLXO} r_{tFL} = I_{tyy} \alpha_{tyFL} \quad (7-24)$$

$$M_{FL} = I_{tzz} \alpha_{tzFL} \quad (7-25)$$

Similar Equations can be written for the remaining tires.

Slip angles for the tires as shown in Figure 7.4 are defined as,

$$\alpha_{FL} = \delta_{FL} - \tan^{-1} \left(\frac{v + ar}{u - r \frac{t_f}{2}} \right) \quad (7-26)$$

$$\alpha_{FR} = \delta_{FR} - \tan^{-1} \left(\frac{v + ar}{u + r \frac{t_f}{2}} \right) \quad (7-27)$$

$$\alpha_{ML} = \delta_{ML} - \tan^{-1} \left(\frac{v - br}{u - r \frac{t_m}{2}} \right) \quad (7-28)$$

$$\alpha_{MR} = \delta_{MR} - \tan^{-1} \left(\frac{v - br}{u + r \frac{t_m}{2}} \right) \quad (7-29)$$

$$\alpha_{RL} = \delta_{RL} - \tan^{-1} \left(\frac{v - cr}{u - r \frac{t_r}{2}} \right) \quad (7-30)$$

$$\alpha_{RR} = \delta_{RR} - \tan^{-1} \left(\frac{v - cr}{u + r \frac{t_r}{2}} \right) \quad (7-31)$$

In these equations, u and v are the corresponding velocities in the moving reference frame fixed to the center of gravity of the sprung mass.

In the braking situation, longitudinal slips can be found for each tire as,

$$S_{FL} = \frac{-r_{iFL} \dot{\theta}_{FL} + u_{FL}}{u_{FL}} \quad (7-32)$$

$$S_{FR} = \frac{-r_{iFR} \dot{\theta}_{FR} + u_{FR}}{u_{FR}} \quad (7-33)$$

$$S_{ML} = \frac{-r_{iML} \dot{\theta}_{ML} + u_{ML}}{u_{ML}} \quad (7-34)$$

$$S_{MR} = \frac{-r_{iMR} \dot{\theta}_{MR} + u_{MR}}{u_{MR}} \quad (7-35)$$

$$S_{RL} = \frac{-r_{iRL} \dot{\theta}_{RL} + u_{RL}}{u_{RL}} \quad (7-36)$$

$$S_{RR} = \frac{-r_{iRR} \dot{\theta}_{RR} + u_{RR}}{u_{RR}} \quad (7-37)$$

For the interaction of the tires and the ground, the Magic Formula tire model is the most commonly used tire model. It has different versions with varying complexity. For pure lateral and longitudinal forces, Magic Formula can be directly used. However for combined lateral and longitudinal force characteristics, use of the Magic Formula requires extra parameters. The Magic Formula Tire model used in this study is adapted from the references [70], [71], [72]. Lateral force F_y can be defined as:

$$C = a_0 \quad (7-38)$$

$$D = a_1 F_z^2 + a_2 F_z \quad (7-39)$$

$$B = \frac{a_3 \sin \left(2 \tan^{-1} \left(\frac{F_z}{a_4} \right) \right) (1 - a_5 |\gamma|)}{CD} \quad (7-40)$$

$$E = a_6 F_z + a_7 \quad (7-41)$$

$$S_h = a_9 F_z + a_{10} + a_8 \gamma \quad (7-42)$$

$$S_v = a_{11} F_z \gamma + a_{12} F_z + a_{13} \quad (7-43)$$

$$X_\alpha = \alpha + S_h \quad (7-44)$$

$$F_y = D \sin \left\{ C \tan^{-1} \left[BX_\alpha - E \left[BX_\alpha - \tan^{-1} (BX_\alpha) \right] \right] \right\} + S_v \quad (7-45)$$

Magic Formula tire model for longitudinal forces is given in Chapter 6.

The tire forces F_y and F_x are pure lateral and pure longitudinal tire forces respectively. For the combined case, these tire forces can be found as,

$$\alpha_* = \frac{\alpha}{\alpha_{\max}} \quad (7-46)$$

$$s_* = \frac{s}{s_{\max}} \quad (7-47)$$

$$\sigma_* = \sqrt{\alpha_*^2 + s_*^2} \quad (7-48)$$

$$F_{y*} = \frac{\alpha_*}{\sigma_*} F_y \quad (7-49)$$

$$F_{x*} = \frac{s_*}{\sigma_*} F_x \quad (7-50)$$

Definitions of the parameters and the variables used in the Magic Formula tire model are given in Table 7.2.

Table 7.2: Definition Parameters/Variables for Magic Formula Tire Model

Definition of Parameter/Variable	Symbol
Slip Angle	α
Longitudinal Slip	s
Pure Lateral Tire Force	F_y
Pure Longitudinal Tire Force	F_x
Lateral Tire Force in Combined Case	F_{y*}
Longitudinal Tire Force in Combined Case	F_{x*}
Vertical Tire Force	F_z
Ratio of Slip Angle to Slip Angle at which Maximum Lateral Force Occurs	α_*
Ratio of Longitudinal Slip to Longitudinal Slip at which Maximum Longitudinal Force Occurs	s_*
Magic Formula Tire Model Parameters	a's and b's
Magic Formula Tire Model Parameters	B,C,D,E,S _h ,S _v

Cornering force vs slip angle characteristics for different vertical tire load is shown in Figure 7.5.

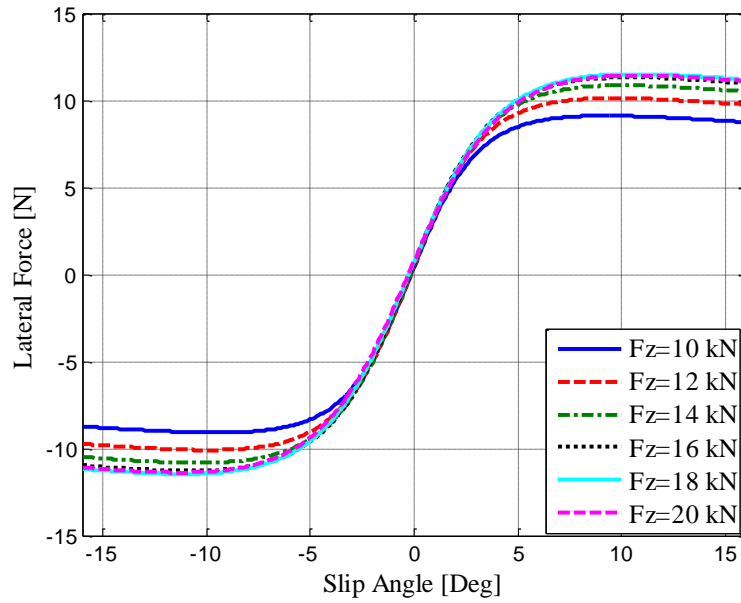


Figure 7.5: Cornering Force vs Slip Angle Characteristics for Different Vertical Tire Load at zero Longitudinal Slip

Longitudinal force vs longitudinal slip characteristics for different vertical tire load is shown in Figure 7.6.

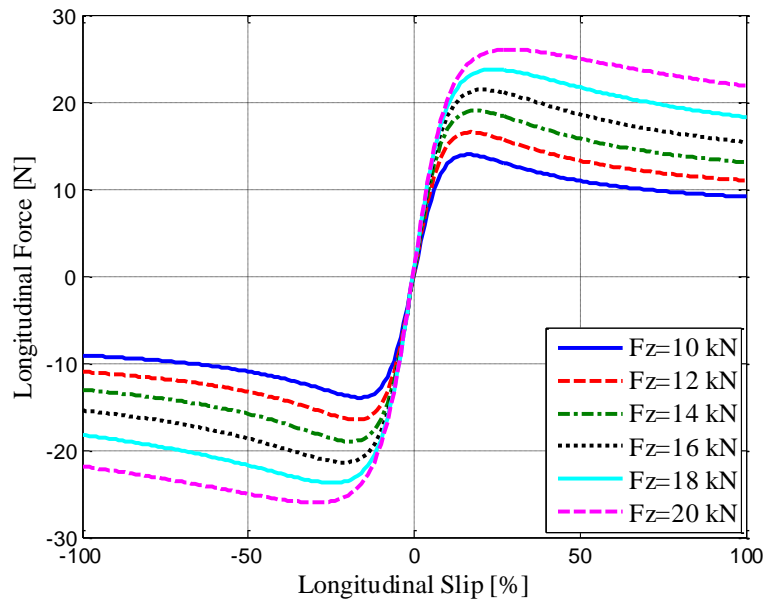


Figure 7.6: Longitudinal Force vs Longitudinal Slip Characteristics for Different Vertical Tire Load at Zero Slip Angle

Variation of the cornering force with longitudinal slip and slip angle is shown in Figure 7.7 and change of the longitudinal force with longitudinal slip and slip angle is shown in Figure 7.8.

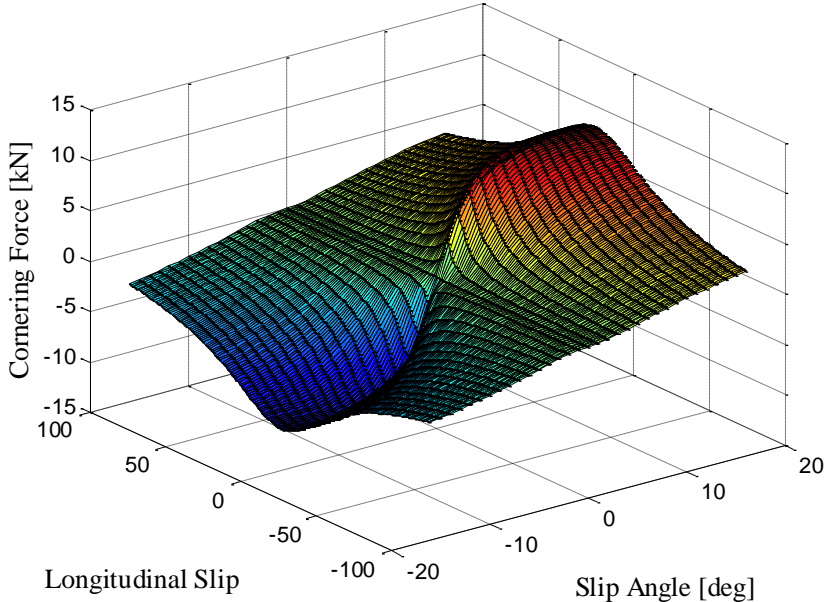


Figure 7.7: Change of Cornering Force with Slip Angle and Longitudinal Slip

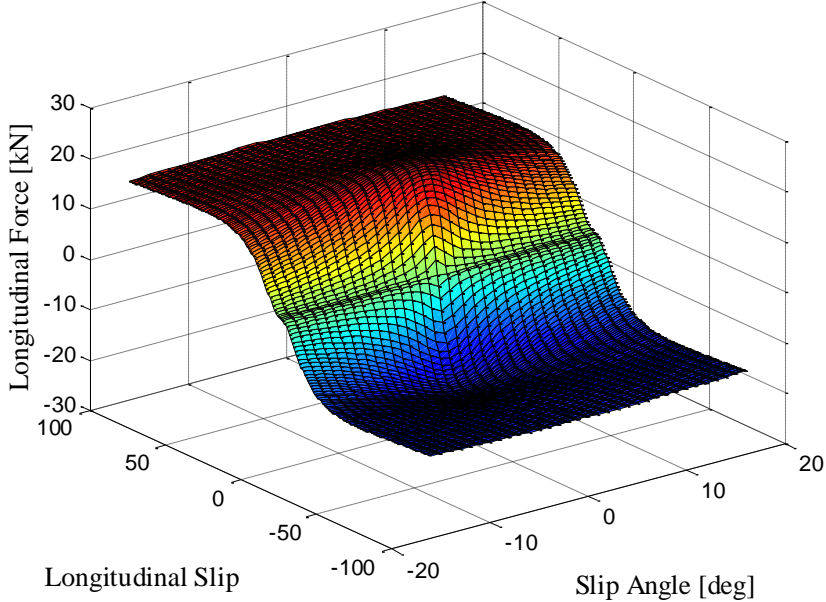


Figure 7.8: Change of Longitudinal Force with Slip Angle and Longitudinal Slip

Vehicle parameters are given in Table 7.3.

Table 7.3: Vehicle Parameters

Parameters	Symbol	Value
Vehicle Mass	M [kg]	9000
Roll Moment of Inertia	I_{xx} [kgm^2]	5318
Pitch Moment of Inertia	I_{yy} [kgm^2]	18968
Yaw Moment of Inertia	I_{zz} [kgm^2]	20910
Tire Mass Moment of Inertia about z Axis	I_{tzz} [kgm^2]	9.4
Front Axle to Center of Gravity Distance	a [m]	2
Middle Axle to Center of Gravity Distance	b [m]	0.3
Rear Axle to Center of Gravity Distance	c [m]	2
Distance Between Roll Center and Center of Gravity At Static Equilibrium for Front, Middle, and Rear Axles	h_{RC-COG} [m]	1.1
Vertical Distance Between Missile Launcher Centerline and COG	h_{zSCOG} [m]	1.5
Horizontal Distance Between Missile Launcher Mounting and COG	h_{xSCOG} [m]	0
Vertical Distance Between the Wheel Center and COG At Static Equilibrium for Front, Middle, and Rear Axles	h_{COGij} [m]	1.1
Firing Elevation Angle	β_s [deg]	10
Firing Azimuth Angle	λ_s [deg]	20

7.3.1. Interconnected Suspension Layouts

In Chapter 6, different interconnected suspension configurations were examined for the three axle vehicle in pitch plane. Among these interconnections, two full interconnections and one semi-interconnection result in higher pitch stiffness. The aim of the interconnected HP suspension system for the full vehicle model is to increase the roll and pitch performance of the vehicle by increasing the roll and pitch stiffness and damping without affecting the bounce properties. Therefore, X type interconnected HP suspension system should be used both in roll and pitch plane of the full vehicle model.

For a vehicle with three axles, there are six suspension units. These suspension units can be interconnected in different configurations. However, finding the proper configuration is an important task for the performance improvement of the full vehicle model. Therefore, both an indirect approach and the direct approaches can be

used to find the initial suspension configurations which will yield performance improvements.

In the indirect approach, all schematically different suspension configurations are enumerated. Then these suspension configurations are tested to satisfy some criteria to result in feasible suspension configurations. Then the performance of these suspension configurations are examined by simulations and the best suspension configuration is found. This method takes somewhat longer to find the proper suspension.

In the direct approach, the type of the suspension configuration which improves the performance is initially known. Then the candidate configurations are specified and those which satisfy the performance requirements are determined. They are examined by the simulations. Since the some basic knowledge about the suspension configuration which improves the pitch and roll performance of the vehicle is known a priori, this method is used determine the proper suspension configurations.

7.3.1.1. Solvability of the Suspension Forces and the Suspension Pressures

In this section, the existence and uniqueness of the solutions of the suspension forces and the suspension pressures are going to be examined. Since at static equilibrium three independent equilibrium equations are written, and since the suspension forces and the pressures are linear in these equations, existence/uniqueness theorem for linear systems can be used. To be able to solve the static equilibrium equation for a full vehicle model, three equilibrium equations in the vertical, pitch, and the roll directions should be satisfied. Further, a vehicle with more than three tires forms a statically indeterminate system since; the number of the independent suspension forces is higher than the number of equations. Therefore for a full vehicle model to reach static equilibrium at least three independent suspension forces are required. The interconnected suspension configurations are evaluated according to this condition at a first glance. This condition is necessary but not sufficient condition to get a feasible interconnection. Static equilibrium equations are;

$$\sum F_z = F_{FL} + F_{FR} + F_{ML} + F_{MR} + F_{RL} + F_{RR} = Mg \quad (7-51)$$

$$\sum M_{\phi} = \frac{t_f}{2}(F_{FL} - F_{FR}) + \frac{t_m}{2}(F_{ML} - F_{MR}) + \frac{t_r}{2}(F_{RL} - F_{RR}) = 0 \quad (7-52)$$

$$\sum M_0 = -a(F_{FL} + F_{FR}) + b(F_{ML} + F_{MR}) + c(F_{RL} + F_{RR}) = 0 \quad (7-53)$$

The first condition is used to select the proposed suspension configurations at the first stage. Then all pressure variables and the suspension forces should be positive to get a feasible suspension interconnection. When these conditions are satisfied, the performance of the interconnection is open for evaluation.

Now the existence and the uniqueness conditions of the solutions of the suspension forces and the suspension pressures at the static equilibrium are to be examined in terms of the Theorem 3. In matrix form, the static equilibrium equations can be written as,

$$\begin{bmatrix} 1 & 1 & 1 & 1 & 1 & 1 \\ \frac{t_f}{2} & -\frac{t_f}{2} & \frac{t_m}{2} & -\frac{t_m}{2} & \frac{t_r}{2} & -\frac{t_r}{2} \\ -a & -a & b & b & c & c \end{bmatrix} \begin{Bmatrix} F_{FL} \\ F_{FR} \\ F_{ML} \\ F_{MR} \\ F_{RL} \\ F_{RR} \end{Bmatrix} = \begin{Bmatrix} Mg \\ 0 \\ 0 \end{Bmatrix} \quad (7-54)$$

Similarly, the oil pressure can be calculated from,

$$\begin{bmatrix} A_p & 0 & 0 & 0 & 0 & 0 \\ 0 & A_p & 0 & 0 & 0 & 0 \\ 0 & 0 & A_p & 0 & 0 & 0 \\ 0 & 0 & 0 & A_p & 0 & 0 \\ 0 & 0 & 0 & 0 & A_p & 0 \\ 0 & 0 & 0 & 0 & 0 & A_p \\ -A_{pr} & 0 & 0 & 0 & 0 & 0 \\ 0 & -A_{pr} & 0 & 0 & 0 & 0 \\ 0 & 0 & -A_{pr} & 0 & 0 & 0 \\ 0 & 0 & 0 & -A_{pr} & 0 & 0 \\ 0 & 0 & 0 & 0 & -A_{pr} & 0 \\ 0 & 0 & 0 & 0 & 0 & -A_{pr} \end{bmatrix}^T \begin{Bmatrix} P_{1FL} \\ P_{1FR} \\ P_{1ML} \\ P_{1MR} \\ P_{1RL} \\ P_{1RR} \\ P_{4FL} \\ P_{4FR} \\ P_{4ML} \\ P_{4MR} \\ P_{4RL} \\ P_{4RR} \end{Bmatrix} = \begin{Bmatrix} F_{FL} \\ F_{FR} \\ F_{ML} \\ F_{MR} \\ F_{RL} \\ F_{RR} \end{Bmatrix} \quad (7-55)$$

In combined form, these equations will be

$$\begin{bmatrix}
 A_p & \frac{A_p t_f}{2} & -aA_p \\
 A_p & \frac{-A_p t_f}{2} & -aA_p \\
 A_p & \frac{A_p t_m}{2} & bA_p \\
 A_p & \frac{-A_p t_m}{2} & bA_p \\
 A_p & \frac{A_p t_r}{2} & cA_p \\
 A_p & \frac{-A_p t_r}{2} & cA_p \\
 -A_{pr} & \frac{-A_{pr} t_f}{2} & aA_{pr} \\
 -A_{pr} & \frac{A_{pr} t_f}{2} & aA_{pr} \\
 -A_{pr} & \frac{-A_{pr} t_m}{2} & -bA_{pr} \\
 -A_{pr} & \frac{A_{pr} t_m}{2} & -bA_{pr} \\
 -A_{pr} & \frac{-A_{pr} t_r}{2} & -cA_{pr} \\
 -A_{pr} & \frac{A_{pr} t_r}{2} & -cA_{pr}
 \end{bmatrix}^T
 \begin{Bmatrix}
 P_{1FL} \\
 P_{1FR} \\
 P_{1ML} \\
 P_{1MR} \\
 P_{1RL} \\
 P_{1RR} \\
 P_{4FL} \\
 P_{4FR} \\
 P_{4ML} \\
 P_{4MR} \\
 P_{4RL} \\
 P_{4RR}
 \end{Bmatrix}
 =
 \begin{Bmatrix}
 Mg \\
 0 \\
 0
 \end{Bmatrix}
 \tag{7-56}$$

Therefore, the equations given above should be examined in terms of consistency to obtain a solution. When there are only two independent suspension forces or pressures, the equation system becomes an inconsistent system and thus there is no solution. The interconnected suspension configurations for the full vehicle model can be classified according to its mathematical solvability (its mathematical degrees of freedom) and the number of ports of pressure chambers as fully interconnected, semi-interconnected, and unconnected. After the consistency of the solution is guaranteed, the uniqueness of the solutions can be examined. If there is no unique

solution at the initial condition, the vehicle may stay at static equilibrium at different conditions depending on the initial suspension parameters.

If the suspension forces and the initial pressures are set in such a way that the static equilibrium equations are not satisfied, the vehicle reaches static equilibrium equations at other force and pressures values. These values are determined from the combined solutions of the static equilibrium equations and the suspension parameters which determine the stiffness and the deflection characteristics of the suspension. Therefore, according to the above explanations, there are two approaches which are used to calculate the suspension forces and pressures at the static equilibrium:

- ❖ Set the independent initial pressures and the initial parameters of each suspension unit and calculate the pressures and suspension forces when the vehicle reaches static equilibrium. This method requires the solution of coupled static equilibrium equation and the suspension deflection equations together with the tire deflection equations.
- ❖ Set the suspension forces and the independent initial pressures to their design values such that the vehicle stays at static equilibrium equations with the desired parameters.

The suspension design parameters can be set by using the both approaches. In first approach, an optimization study should be performed to calculate the optimum suspension initial parameters in order to satisfy the user objective at the static equilibrium. In the second approach, the objective at the static equilibrium conditions is defined, and the suspension initial parameters are calculated by solving the linear equations directly. In this study, second method is used to calculate the design suspension forces and design initial pressures.

Among the infinitely many suspension forces which satisfy the static equilibrium equations, the ones which are closest to each other are taken as the initial design suspension forces, as previously explained in Chapter 6. After the suspension forces are set to known design values, suspension pressures at static equilibrium can be calculated directly.

7.3.1.2. Mathematical Degree of Freedom of Interconnected HP Suspension Systems

The mathematical degree of freedom of the interconnected suspension configurations was defined as the number of the independent suspension forces. According to the mathematical degrees of freedom, the feasibility of the suspension configuration can be determined. To get a feasible suspension configuration, the degrees of freedom should be at least three. For three degrees of freedom suspension configurations, the resulting interconnection is statically determinate and the pressure variables and thus the suspension forces can be found from the static equilibrium equations. When the degree of freedom of the interconnections is higher than three, both static equilibrium equations and the suspension deflection equations are to be used to find the pressure variables and the suspension forces at static equilibrium. This provides flexibility to the suspension designer to determine the pressure variables and the suspension forces.

7.3.1.3. Type of the Interconnected HP Suspension System

When the first and the fourth chambers of each suspension unit are connected at least once, the resulting suspension configuration is called a fully interconnected HP suspension system. When one of the chambers of the suspension units is not connected, the resulting suspension configuration is called as semi-interconnection. When none of the chamber is connected, the resulting suspension configuration is called as the unconnected suspension. Unconnected HP suspension system for the full vehicle model is shown in Figure 7.21. As can be seen from Figure 7.16, the interconnected suspension configuration is used only to improve the pitch performance of the vehicle. This suspension configuration was examined in Chapter 6 in detail. There are many possible interconnections for the full vehicle model. With a systematic method as in Chapter 5, all of these interconnections can be found. However, to increase the performance of the vehicle in roll and pitch directions, specific interconnections among these should be found.

7.3.1.4. Determination of the Full Interconnections

As a first approach to improve the roll and the pitch performance of the vehicle, X coupling among the longitudinal and the lateral directions should be performed. For example, the first pressure chamber of the front left suspension unit should be interconnected to the fourth suspension unit of the intermediate right or rear right suspension unit. Moreover, each pressure chamber is connected only one time to other pressure chambers. Then four different interconnections can be identified. These interconnections are;

P1FL-P4MR-----P1ML-P4RR-----P1RL-P4FR-----P1FR-P4ML-----P1MR-P4RL-----
P1RR-P4FL

P1FL-P4RR-----P1ML-P4FR-----P1RL-P4MR-----P1FR-P4ML-----P1MR-P4RL-----
P1RR-P4FL

P1FL-P4MR-----P1ML-P4RR-----P1RL-P4FR-----P1FR-P4RL-----P1MR-P4FL-----
P1RR-P4ML

P1FL-P4RR-----P1ML-P4FR-----P1RL-P4MR-----P1FR-P4RL-----P1MR-P4FL-----
P1RR-P4ML

These interconnections are shown in Figure 7.9 to Figure 7.12. The first and the fourth interconnected HP suspension systems have a symmetric structure with respect to the pitch axis. The interconnection configurations studied in Chapter 6 were extended for the full vehicle model to improve the roll and the pitch performances. There are also other full interconnections which can be obtained by the extension of the pitch interconnections to the full vehicle model. Figure 7.13 shows an interconnection with front and rear suspensions interconnected by X coupling in roll and pitch directions, and the intermediate suspensions interconnected by X coupling in the roll plane. This interconnection can be also generalized to other axles as illustrated in Figure 7.14 and Figure 7.15. The interconnections shown so far contain both pitch and roll connections. There are also full interconnections which only contain either roll or pitch connections. These are given in Figure 7.15 and Figure 7.16.

7.3.1.5. Determination of the Semi-interconnections

To be able to make a comparison among fully interconnected, unconnected, and semi-interconnected HP suspension systems, semi interconnection configurations are also modeled and shown in Figure 7.18 to Figure 7.21. There are other semi-interconnections in which only the suspension units on one axis are interconnected. For brevity these are not explained in detail. The interconnected HP suspension systems used in Chapter 6 (3th, 4th, and 5th) can be adapted to the full vehicle model and semi-interconnections may be formed. These also are not explained in detail here.

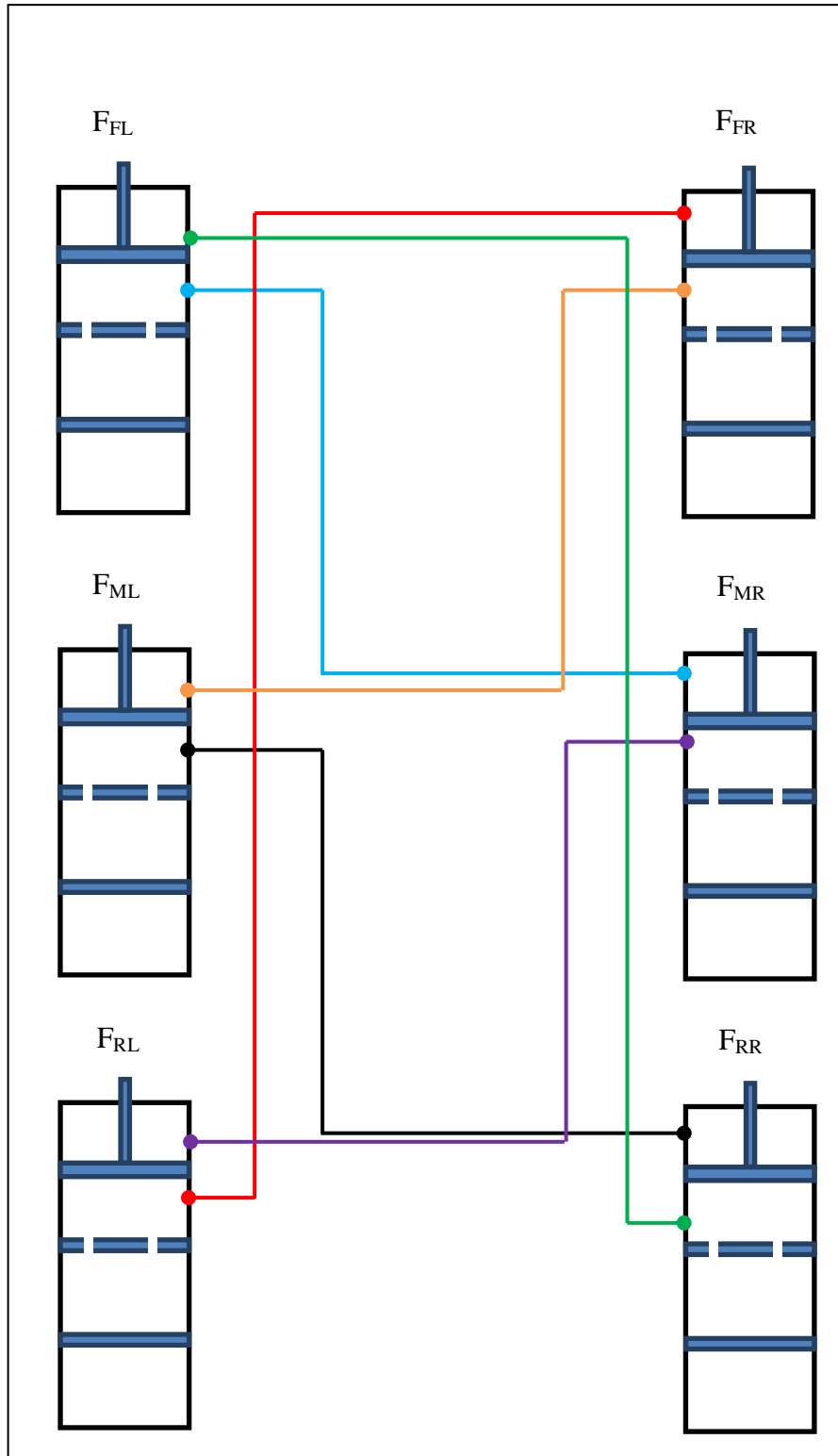


Figure 7.9: First Interconnected HP Suspension System for a Three Axle Vehicle

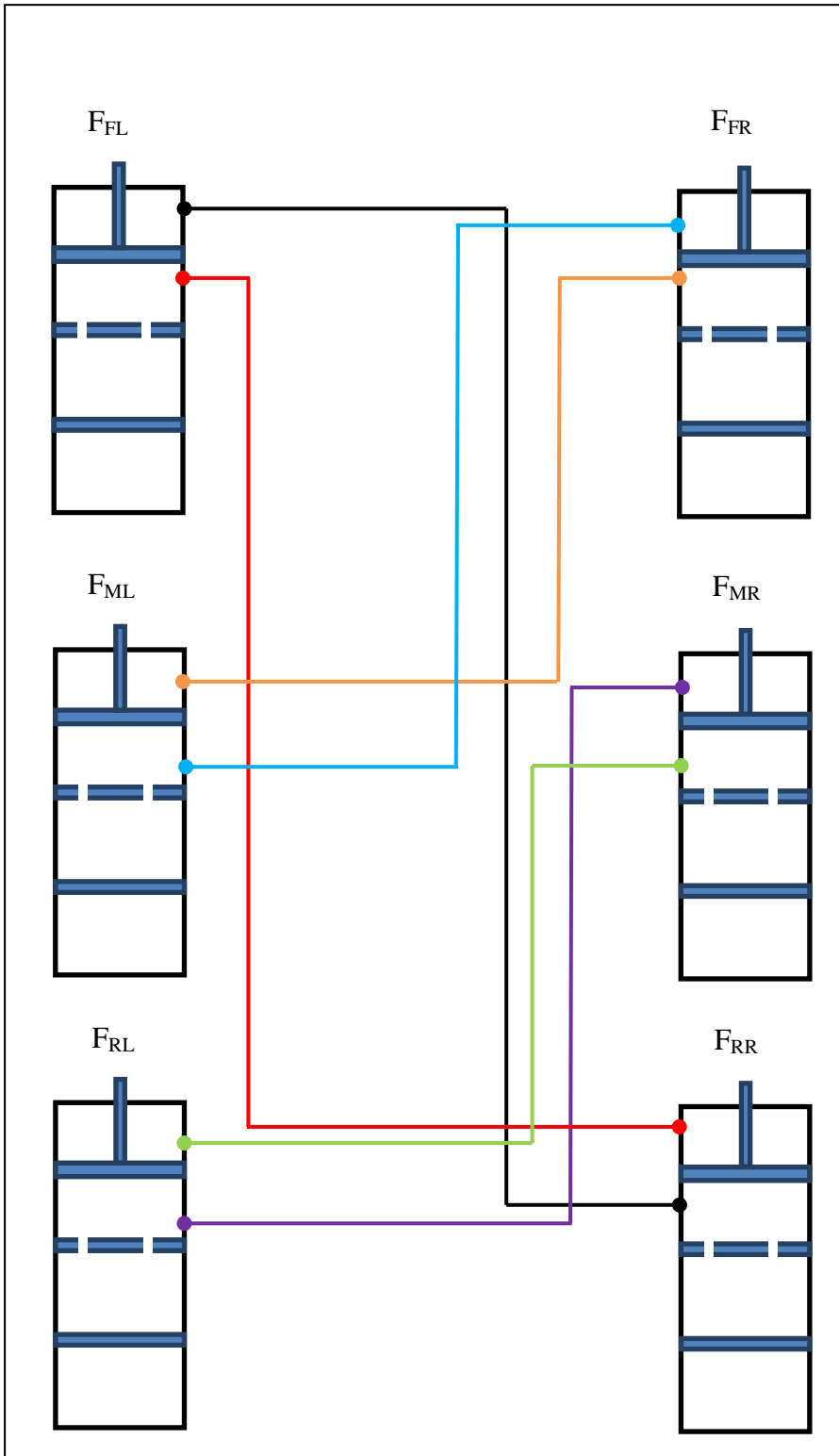


Figure 7.10: Second Interconnected HP Suspension System for a Three Axle Vehicle

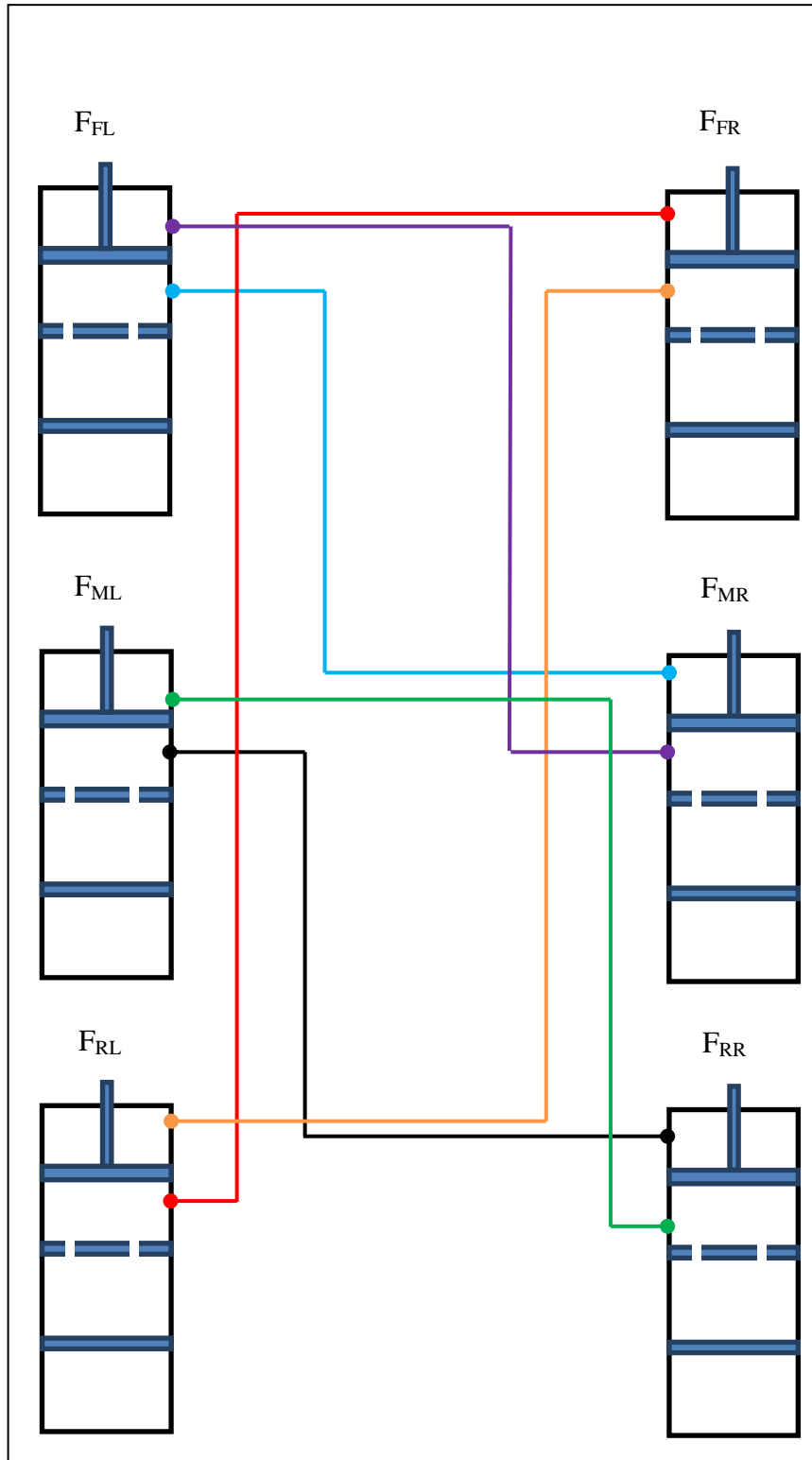


Figure 7.11: Third Interconnected HP Suspension System for a Three Axle Vehicle

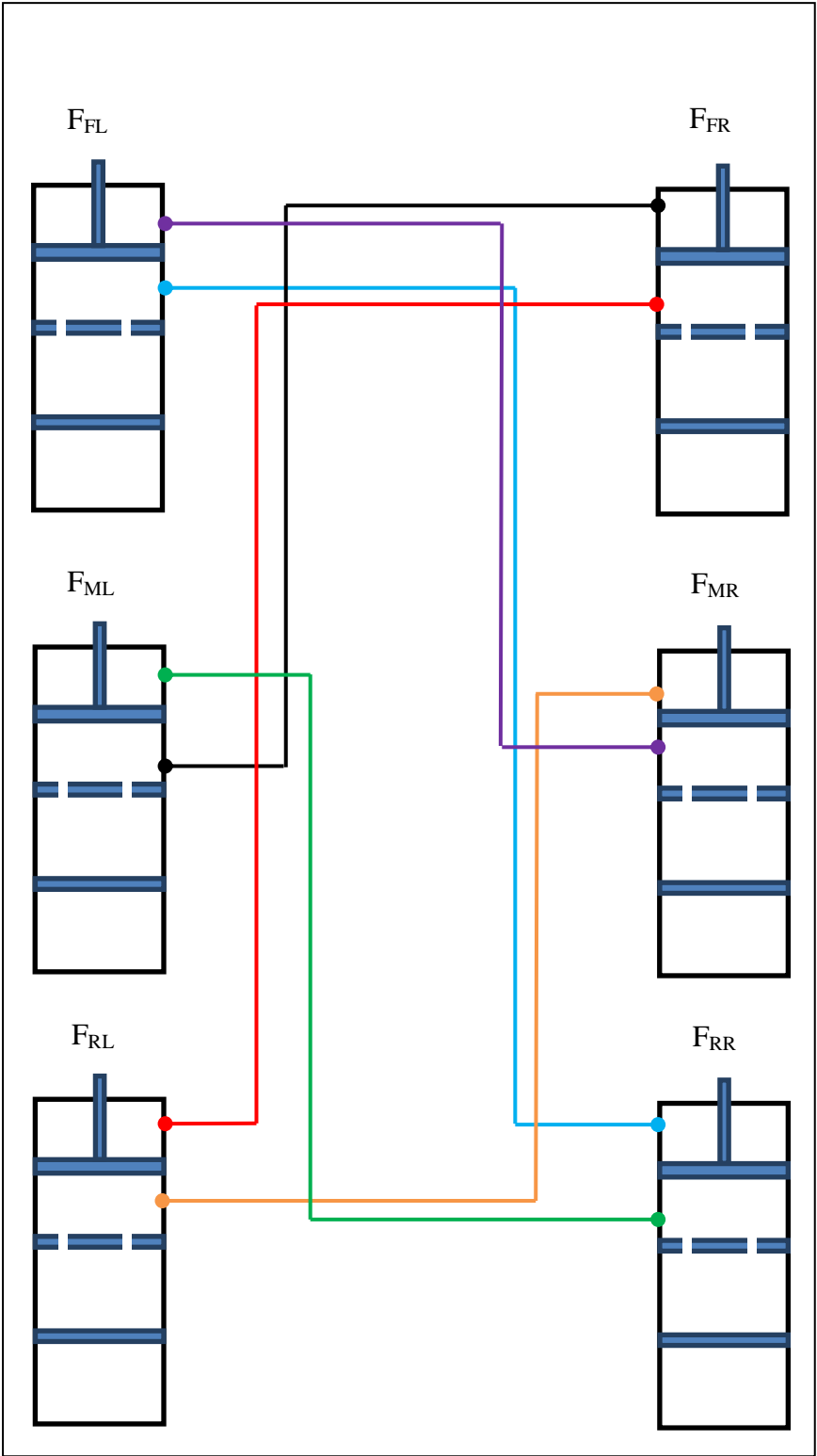


Figure 7.12: Fourth Interconnected HP Suspension System for a Three Axle Vehicle

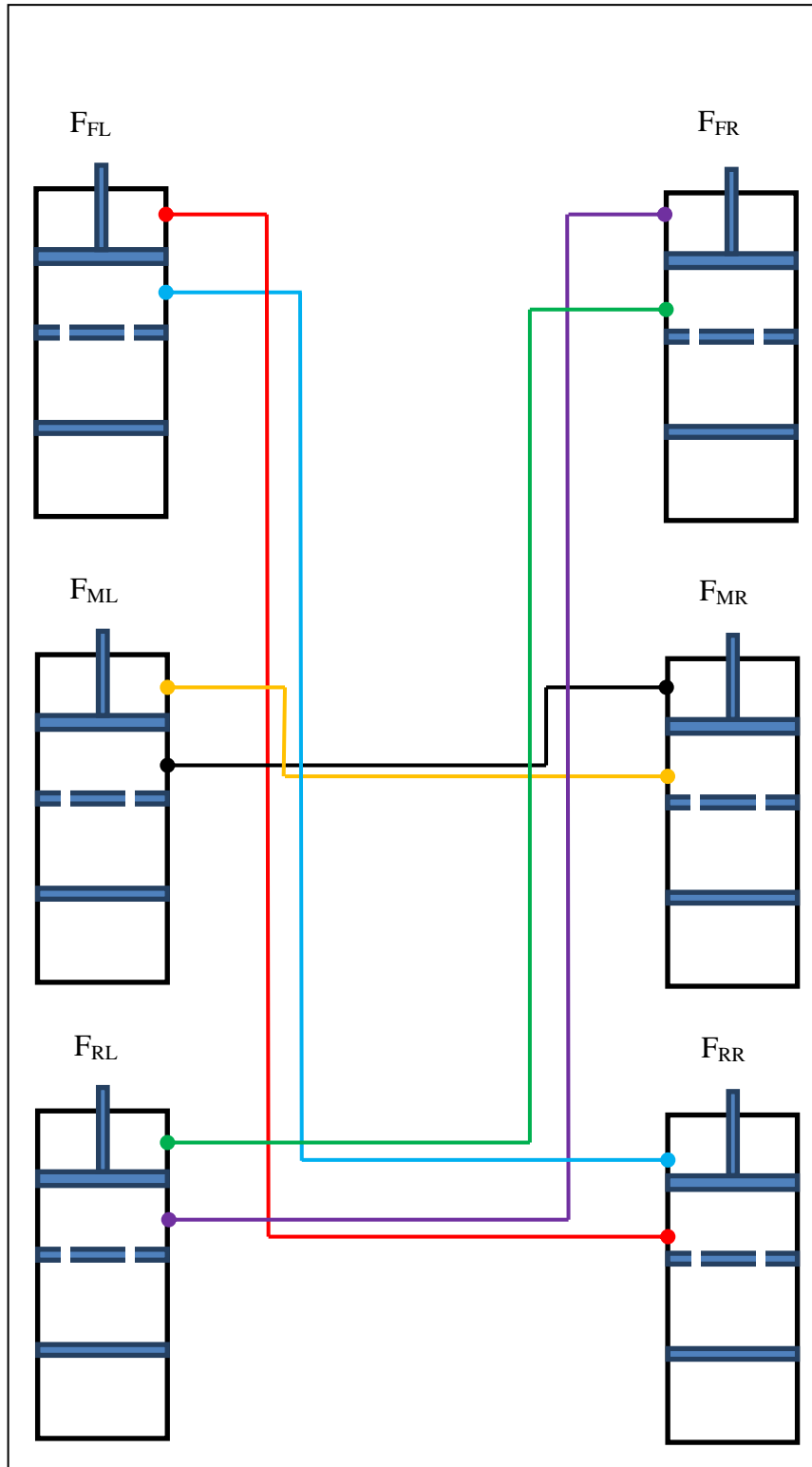


Figure 7.13: Fifth Interconnected HP Suspension System for a Three Axle Vehicle

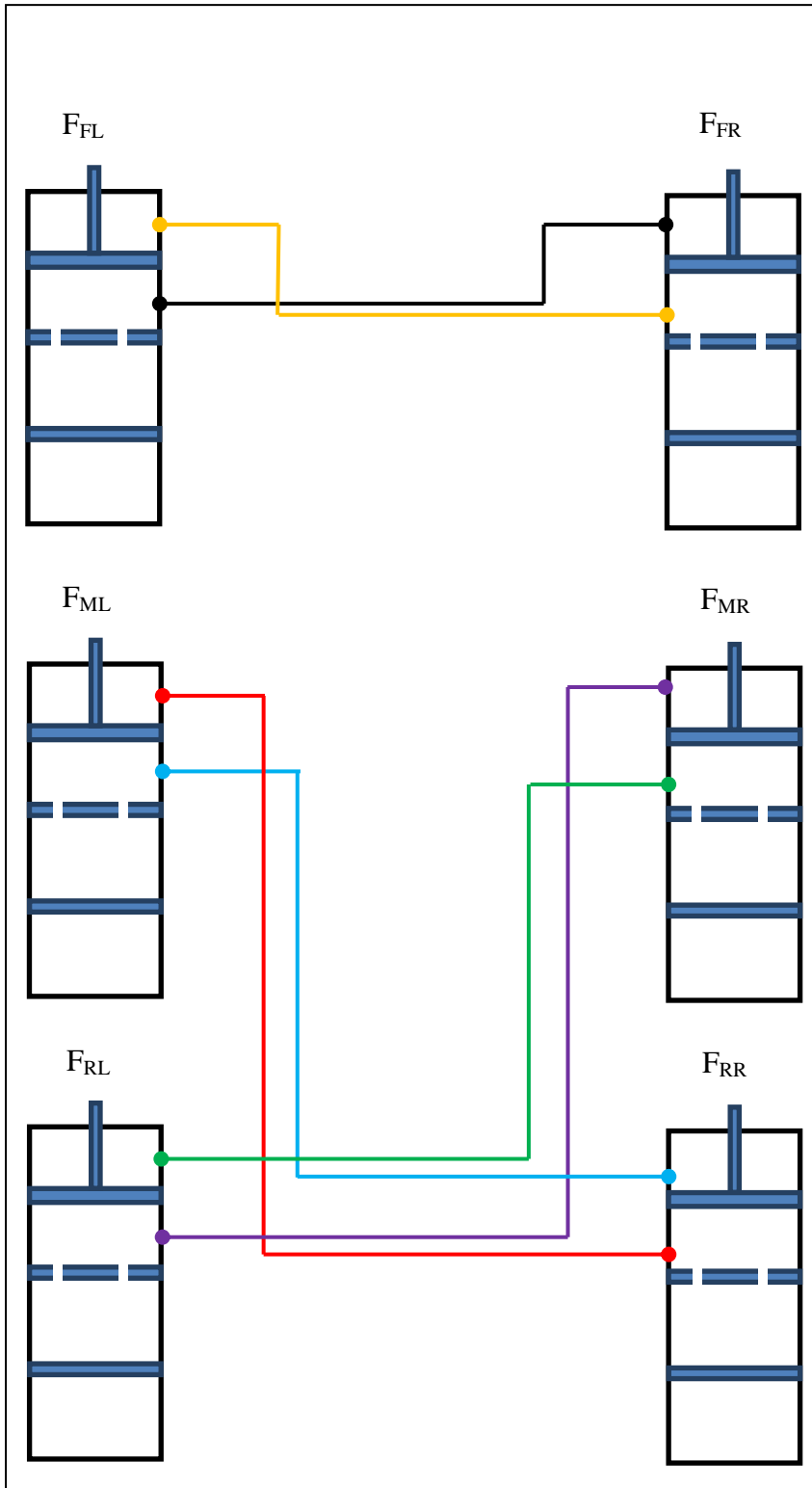


Figure 7.14: Sixth Interconnected HP Suspension System for a Three Axle Vehicle

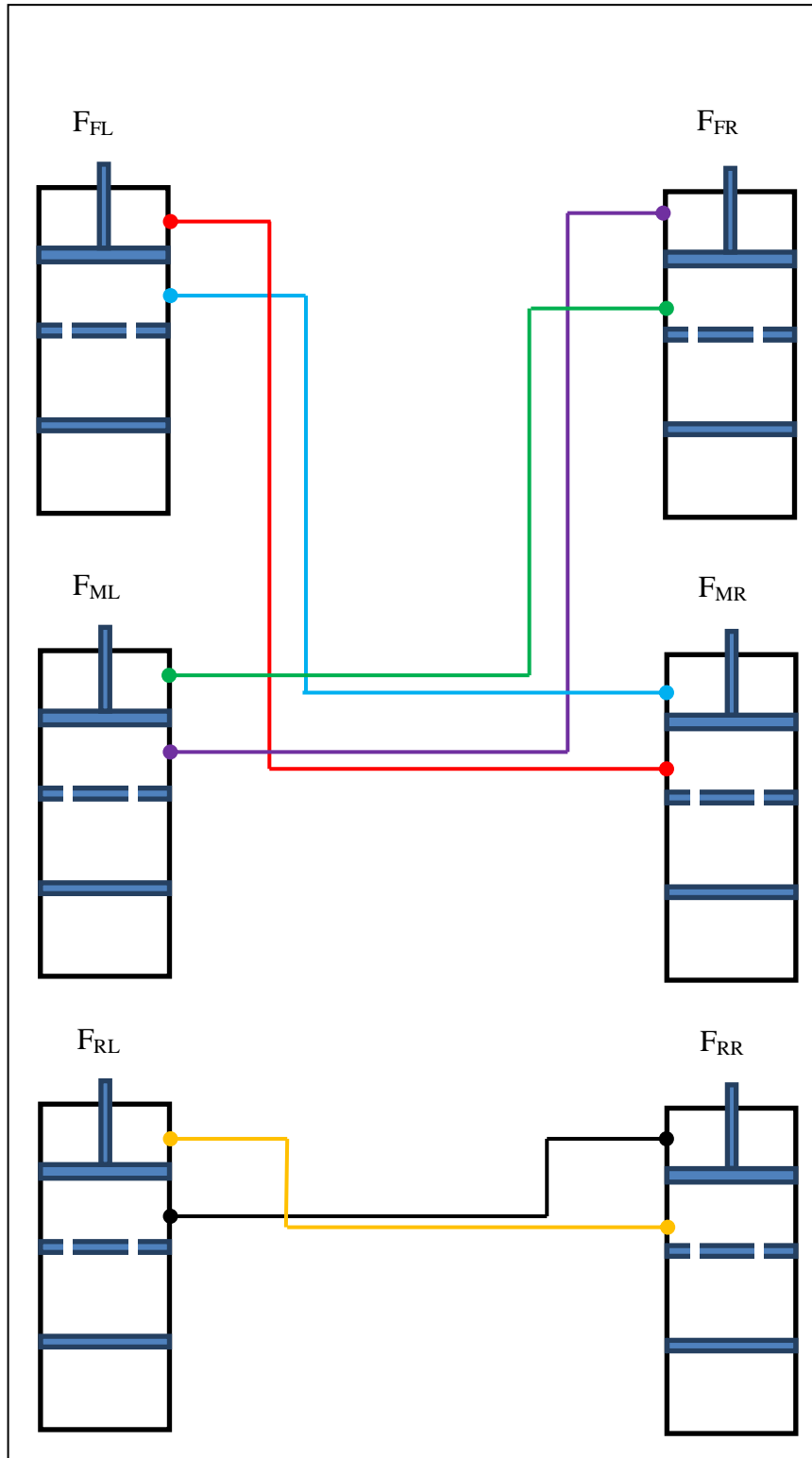


Figure 7.15: Seventh Interconnected HP Suspension System for a Three Axle Vehicle

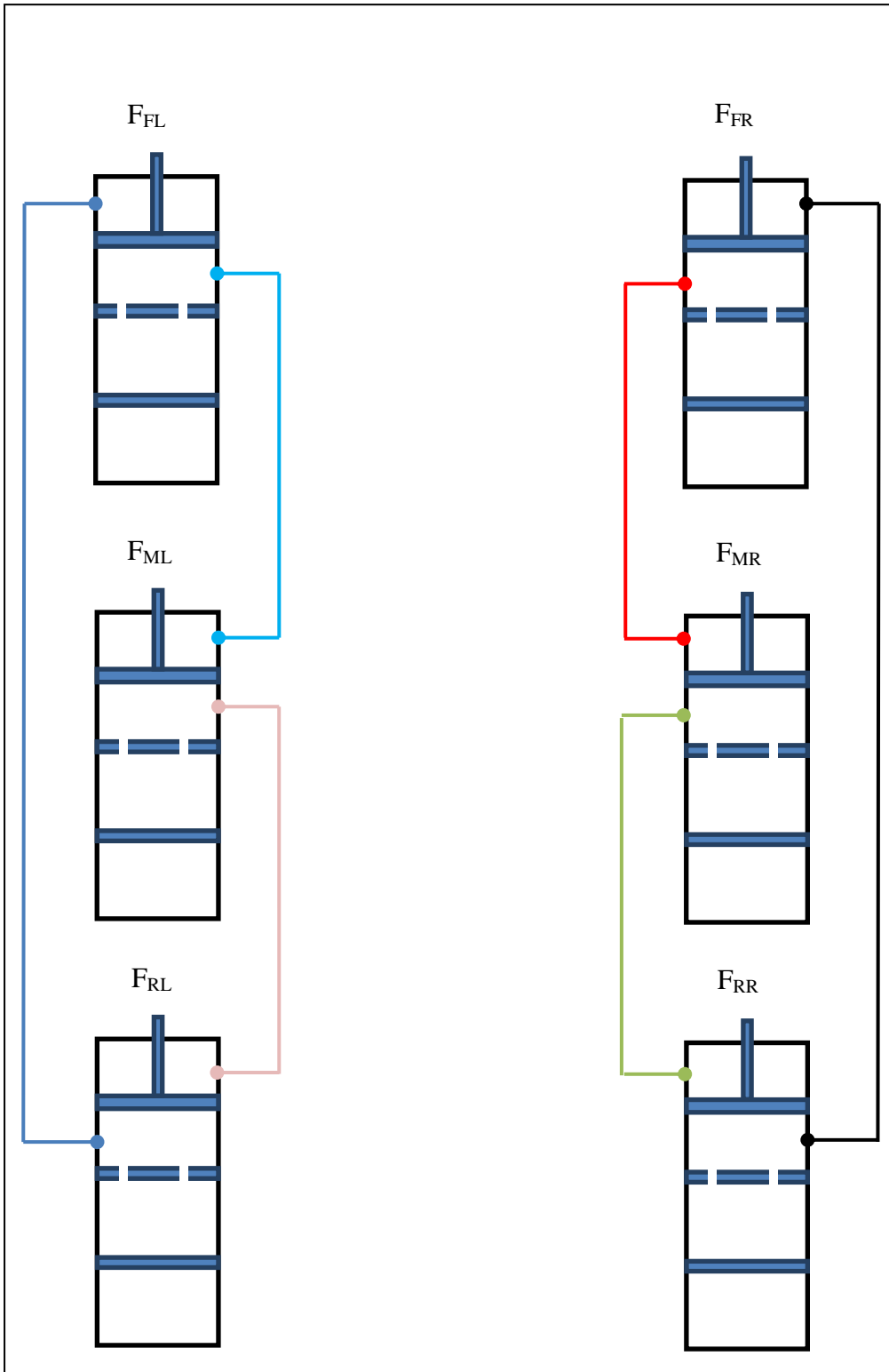


Figure 7.16: Eighth Interconnected HP Suspension System for a Three Axle Vehicle

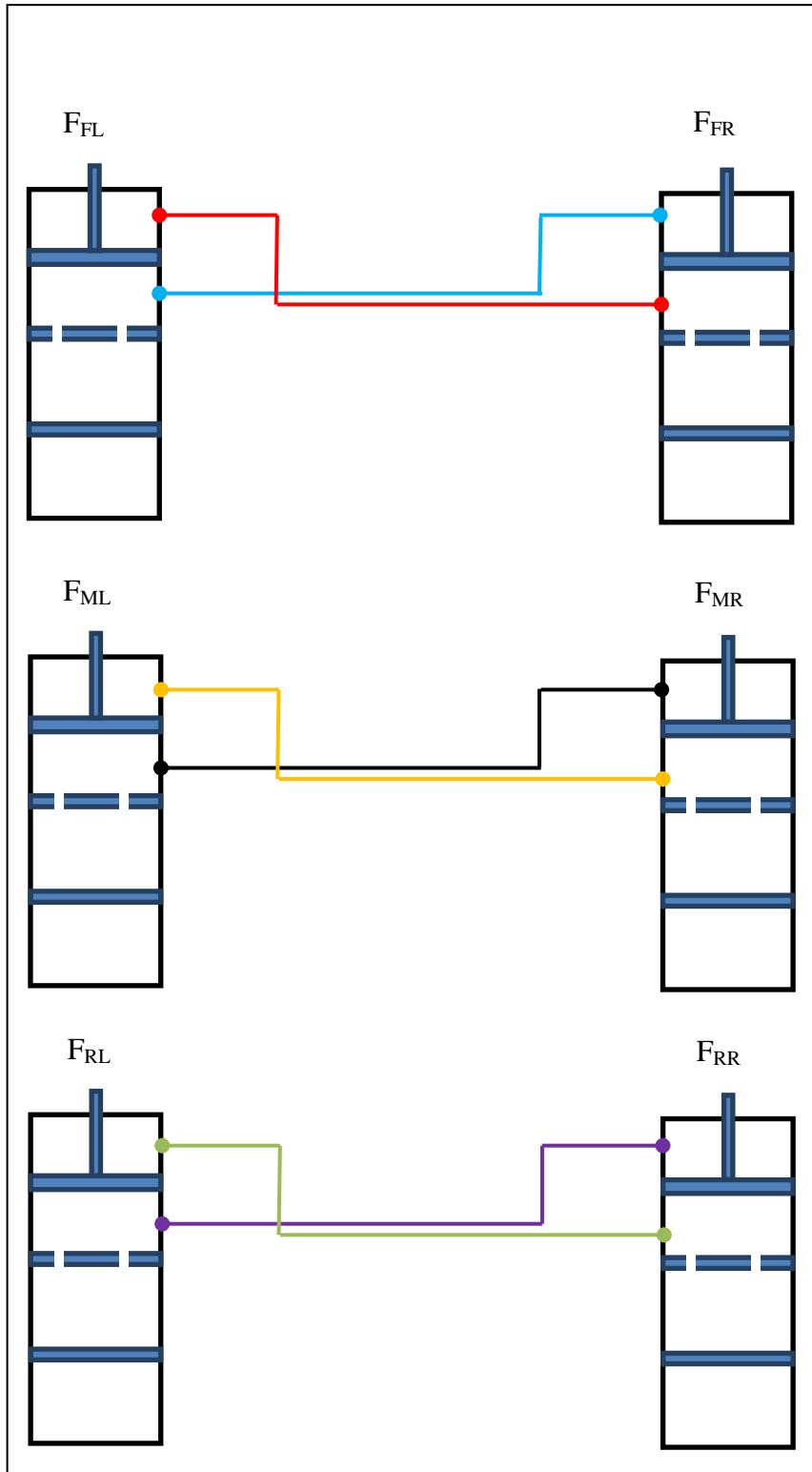


Figure 7.17: Ninth Interconnected HP Suspension System for a Three Axle Vehicle

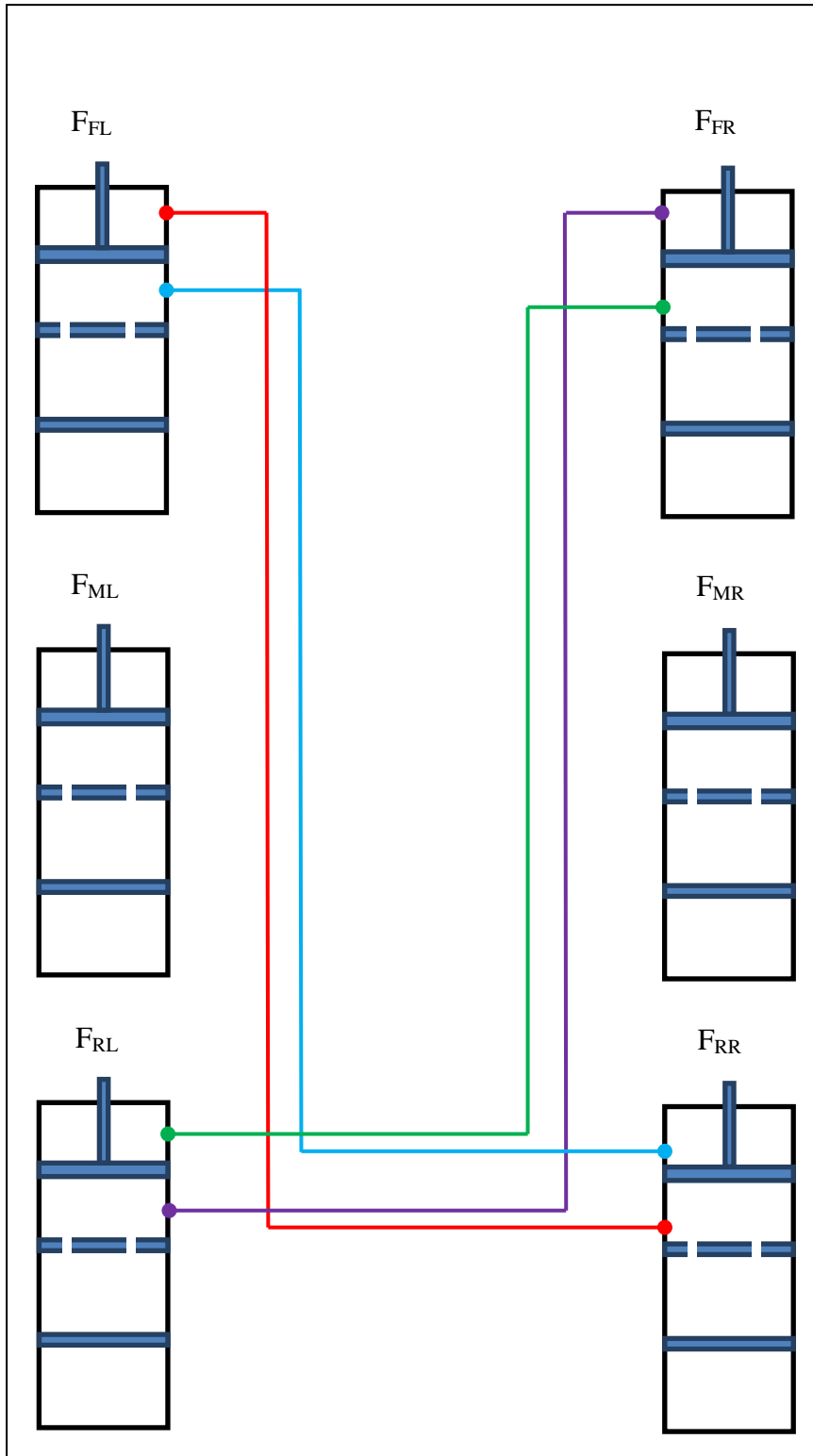


Figure 7.18: Tenth Interconnected HP Suspension System for a Three Axle Vehicle

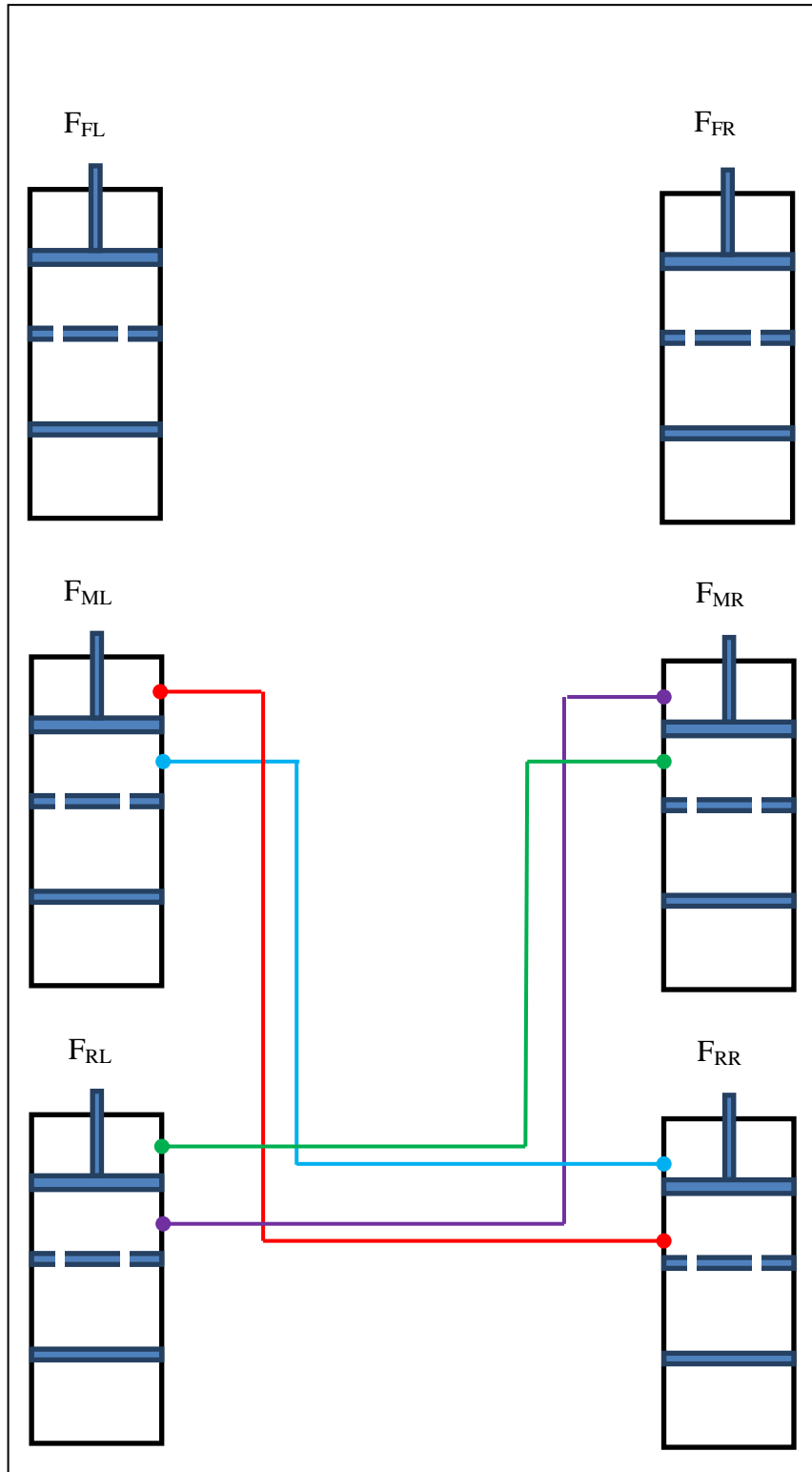


Figure 7.19: Eleventh Interconnected HP Suspension System for a Three Axle Vehicle

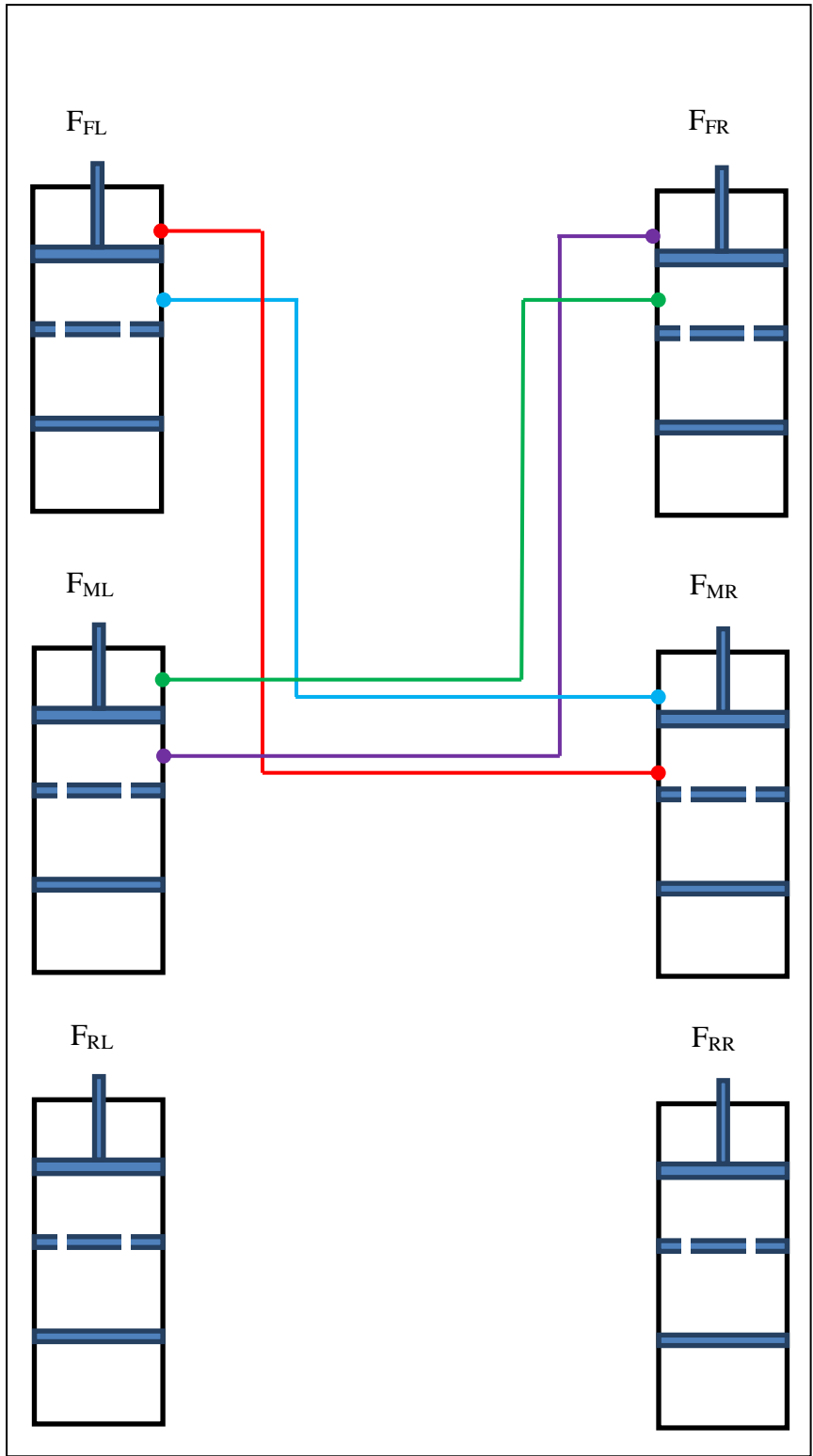


Figure 7.20: Twelfth Interconnected HP Suspension System for a Three Axle Vehicle

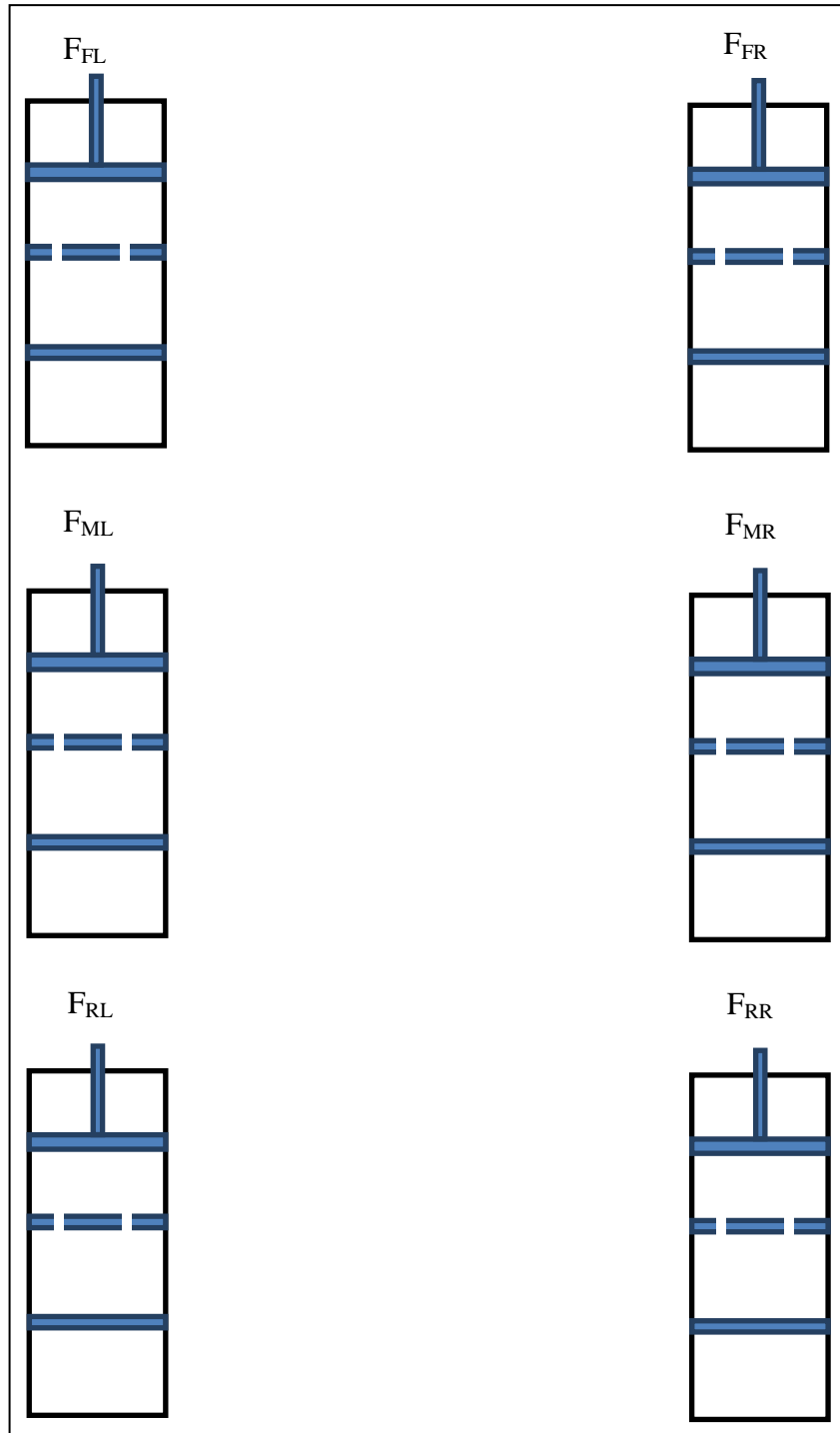


Figure 7.21: Thirteenth HP Suspension System for a Three Axle Vehicle-
Unconnected HP Suspension Configuration

Among the configurations given above, the existence and uniqueness of solutions of the static equilibrium equations and pressure equations are going to be given for the first configuration only.

In the first interconnection configuration, the suspension system improves both the pitch and the roll motions of the vehicle. To be able to go further with this configuration, the first condition of the feasible interconnected suspension is analyzed. For this configuration suspension forces become,

$$F_{FL} = P_{IFL}A_p - P_{IRR}A_{pr} \quad (7-57)$$

$$F_{FR} = P_{IFR}A_p - P_{IRL}A_{pr} \quad (7-58)$$

$$F_{ML} = P_{IML}A_p - P_{IFR}A_{pr} \quad (7-59)$$

$$F_{MR} = P_{IMR}A_p - P_{IFL}A_{pr} \quad (7-60)$$

$$F_{RL} = P_{IRL}A_p - P_{IMR}A_{pr} \quad (7-61)$$

$$F_{RR} = P_{IRR}A_p - P_{IML}A_{pr} \quad (7-62)$$

There are six independent pressure variables which are P_{IFL} , P_{IFR} , P_{IML} , P_{IMR} , P_{IRL} , P_{IRR} , and there are six independent suspension forces resulting in a six degree of freedom interconnection.

Since

$$\begin{aligned} & \text{rank} \left\{ \begin{bmatrix} 1 & 1 & 1 & 1 & 1 & 1 \\ \frac{t_f}{2} & -\frac{t_f}{2} & \frac{t_m}{2} & -\frac{t_m}{2} & \frac{t_r}{2} & -\frac{t_r}{2} \\ -a & -a & b & b & c & c \end{bmatrix} \right\} = \\ & = \text{rank} \begin{bmatrix} 1 & 1 & 1 & 1 & 1 & 1 & Mg \\ \frac{t_f}{2} & -\frac{t_f}{2} & \frac{t_m}{2} & -\frac{t_m}{2} & \frac{t_r}{2} & -\frac{t_r}{2} & 0 \\ -a & -a & b & b & c & c & 0 \end{bmatrix} = 3 \end{aligned} \quad (7-63)$$

the system of equations is consistent. Since $n=6 > \text{rank}=3$, there are 3 parameter families of infinite solutions. Further since,

$$\begin{aligned}
& \text{rank} \left\{ \begin{bmatrix} A_p & 0 & 0 & 0 & 0 & -A_{pr} \\ 0 & A_p & 0 & 0 & -A_{pr} & 0 \\ 0 & -A_{pr} & A_p & 0 & 0 & 0 \\ -A_{pr} & 0 & 0 & A_p & 0 & 0 \\ 0 & 0 & 0 & -A_{pr} & A_p & 0 \\ 0 & 0 & -A_{pr} & 0 & 0 & A_p \end{bmatrix} \right\} = 6 \\
& \text{rank} \left\{ \begin{bmatrix} A_p & 0 & 0 & 0 & 0 & -A_{pr} & F_{FL} \\ 0 & A_p & 0 & 0 & -A_{pr} & 0 & F_{FR} \\ 0 & -A_{pr} & A_p & 0 & 0 & 0 & F_{ML} \\ -A_{pr} & 0 & 0 & A_p & 0 & 0 & F_{MR} \\ 0 & 0 & 0 & -A_{pr} & A_p & 0 & F_{RL} \\ 0 & 0 & -A_{pr} & 0 & 0 & A_p & F_{RR} \end{bmatrix} \right\} = 6 \tag{7-64}
\end{aligned}$$

the system of equations is consistent. Since $\text{rank}=6=n=6$, the pressure variables have unique values. The other suspension configurations can be analyzed with regard to Theorem 3. There are many other interconnections which include full and semi-interconnections. Some of these interconnections are feasible and some of them are infeasible. As in Chapter 6, different combinations of the interconnections can be derived and then can be examined as to whether they are feasible or not. An infeasible suspension configuration is shown in Figure 7.22. Since there are only two independent forces, it forms an infeasible interconnection.

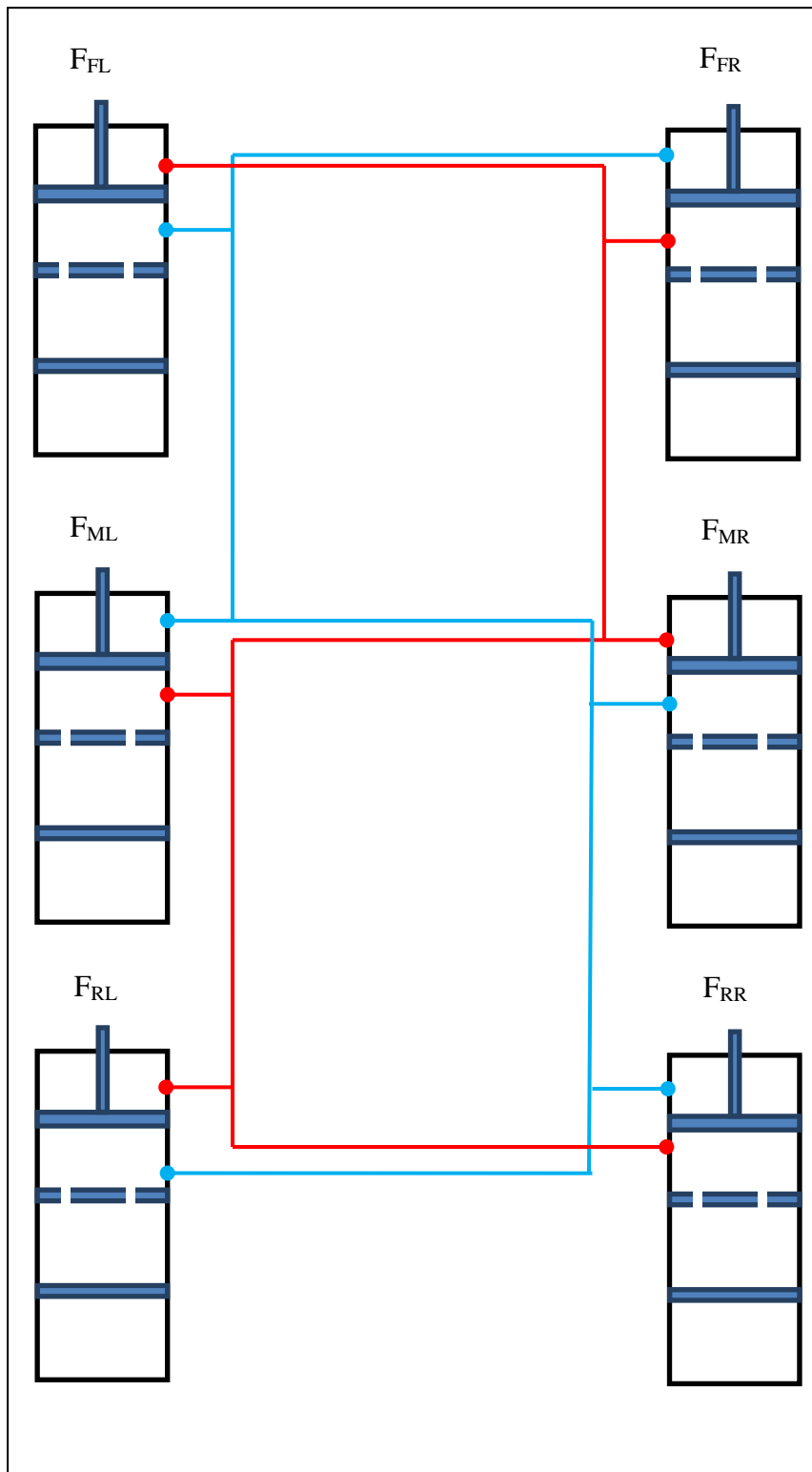


Figure 7.22: Infeasible Interconnected HP Suspension System for a Three Axle Vehicle

Interconnected HP suspension configurations presented above have six dofs.

7.4. MODELING OF THE INTERCONNECTED HP SUSPENSION SYSTEM FOR THE FULL VEHICLE MODEL WITH THREE AXLES

In chapter 6, a general formula is given for the suspension forces. By adapting that formula, the suspension forces for the specified suspension configurations can be found easily. After the suspension forces are found, the stiffness and the damping properties of the interconnected HP suspension configurations are found. Similar to the method in the study of Cao [19], the stiffness and the damping properties of the interconnected suspension system can be found. Assuming that wheel hub displacements are fixed, by rotating the sprung mass about the roll and the pitch axes while keeping the vertical displacement of the sprung mass fixed, stiffness and damping characteristic can be found. In Chapter 6, the pitch stiffness is calculated by rotating the sprung mass about the pitch axis. However, the vertical displacement is found by satisfying the equilibrium equations and the vertical displacement is found by solving the equilibrium equations. Similarly, the roll and the pitch damping are found by rotating the sprung mass around pitch axis and the roll axis at constant velocities assuming that the wheel hub velocities are zero. Therefore, the stiffness characteristics can be found by:

$$k = -\frac{dF}{dz} \quad (7-65)$$

$$F = F_{FL} + F_{FR} + F_{ML} + F_{MR} + F_{RL} + F_{RR} \quad (7-66)$$

$$k_{\theta} = -\frac{dM_{\theta}}{d\theta} \quad (7-67)$$

$$M_{\theta} = -a(F_{FL} + F_{FR}) + b(F_{ML} + F_{MR}) + c(F_{RL} + F_{RR}) \quad (7-68)$$

$$k_{\phi} = -\frac{dM_{\phi}}{d\phi} \quad (7-69)$$

$$M_{\phi} = \frac{t_r}{2}(F_{FL} - F_{FR}) + \frac{t_m}{2}(F_{ML} - F_{MR}) + \frac{t_r}{2}(F_{RL} - F_{RR}) \quad (7-70)$$

While calculating the vertical stiffness and vertical damping, it is assumed that the pitch and roll angles and velocities are zero. Therefore, all piston relative displacements are equal to each other and all piston relative velocities are equal to each other. Thus,

$$Z_{ptFL} = Z_{ptFR} = Z_{ptML} = Z_{ptMR} = Z_{ptRL} = Z_{ptRR} = Z_{pt} \quad (7-71)$$

$$\dot{Z}_{ptFL} = \dot{Z}_{ptFR} = \dot{Z}_{ptML} = \dot{Z}_{ptMR} = \dot{Z}_{ptRL} = \dot{Z}_{ptRR} = \dot{Z}_{pt} \quad (7-72)$$

In following sections, the stiffness and the damping characteristics of the first suspension configuration are derived. The derivations for other configurations can be performed similarly.

7.4.1. 1st Interconnected Suspension Configuration

In this part, the model of the interconnected HP suspension system for a full vehicle model with three axles is to be derived. The suspension force of each suspension units is obtained. Suspension forces of the front left, front right, intermediate left, intermediate right, rear left, and rear right suspension units can be found from the derived equation.

7.4.1.1. Static Analysis

At static equilibrium, the suspension forces can be found by Equations (7-57)-(7-62). Since the number of the unknown suspension forces is higher than the number equilibrium equations, there are an infinite number of solutions. For a vehicle with two axles, assuming left and right symmetry, the forces of the front and rear suspension units can be found uniquely from the static equilibrium equations whatever the initial conditions of the suspension. However, for a vehicle with more than 2 axles, when the initial suspension parameters change, the suspension forces at static equilibrium also change. Therefore, the initial suspension parameters should be tuned in order to get desired suspension characteristics at static equilibrium. This is one of main differences between two and multi-axles vehicle (three and more axles). Similar to Chapter 6, the suspension forces at static equilibrium are tuned such that they are as close as to each other for the sharing of the vehicle weight equivalently. Therefore, equivalent suspension forces can be found by mathematical optimization.

$$\arg \min_{i,j=FL,FR,ML,MR,RL,RR} \sum (F_{i0} - F_{j0})^2$$

subject to static equilibrium equations. Assuming left and right symmetry of the vehicle optimum suspension forces are found as,

$$F_{FL0} = F_{FR0} = \frac{Mg(b^2 + ab + c^2 + ac)}{4(a^2 + ab + ac + b^2 - bc + c^2)} \quad (7-73)$$

$$F_{ML0} = F_{MR0} = \frac{Mg(a^2 + ab + c^2 - bc)}{4(a^2 + ab + ac + b^2 - bc + c^2)} \quad (7-74)$$

$$F_{RL0} = F_{RR0} = \frac{Mg(a^2 + ac + b^2 - bc)}{4(a^2 + ab + ac + b^2 - bc + c^2)} \quad (7-75)$$

From these equations initial pressure variables can be found.

7.4.1.2. Stiffness Characteristics

Elastic components of the suspension forces are,

$$F_{FL} = \frac{P_{30FL} V_{30FL}^k A_p}{\left[V_{30FL} + A_p \left(z_{pFL} - z_{tFL} - \frac{A_{pr}}{A_p} (z_{pMR} - z_{tMR}) \right) \right]^k} - \frac{P_{30RR} V_{30RR}^k A_{pr}}{\left[V_{30RR} + A_p \left(z_{pRR} - z_{tRR} - \frac{A_{pr}}{A_p} (z_{pFL} - z_{tFL}) \right) \right]^k} \quad (7-76)$$

$$F_{FR} = \frac{P_{30FR} V_{30FR}^k A_p}{\left[V_{30FR} + A_p \left(z_{pFR} - z_{tFR} - \frac{A_{pr}}{A_p} (z_{pML} - z_{tML}) \right) \right]^k} - \frac{P_{30RL} V_{30RL}^k A_{pr}}{\left[V_{30RL} + A_p \left(z_{pRL} - z_{tRL} - \frac{A_{pr}}{A_p} (z_{pFR} - z_{tFR}) \right) \right]^k} \quad (7-77)$$

$$F_{ML} = \frac{P_{30ML} V_{30ML}^K A_p}{\left[V_{30ML} + A_p \left(z_{pML} - z_{tML} - \frac{A_{pr}}{A_p} (z_{pRR} - z_{tRR}) \right) \right]^K} - \frac{P_{30FR} V_{30FR}^K A_{pr}}{\left[V_{30FR} + A_p \left(z_{pFR} - z_{tFR} - \frac{A_{pr}}{A_p} (z_{pML} - z_{tML}) \right) \right]^K} \quad (7-78)$$

$$F_{MR} = \frac{P_{30MR} V_{30MR}^K A_p}{\left[V_{30MR} + A_p \left(z_{pMR} - z_{tMR} - \frac{A_{pr}}{A_p} (z_{pRL} - z_{tRL}) \right) \right]^K} - \frac{P_{30FL} V_{30FL}^K A_{pr}}{\left[V_{30FL} + A_p \left(z_{pFL} - z_{tFL} - \frac{A_{pr}}{A_p} (z_{pMR} - z_{tMR}) \right) \right]^K} \quad (7-79)$$

$$F_{RL} = \frac{P_{30RL} V_{30RL}^K A_p}{\left[V_{30RL} + A_p \left(z_{pRL} - z_{tRL} - \frac{A_{pr}}{A_p} (z_{pFR} - z_{tFR}) \right) \right]^K} - \frac{P_{30MR} V_{30MR}^K A_{pr}}{\left[V_{30MR} + A_p \left(z_{pMR} - z_{tMR} - \frac{A_{pr}}{A_p} (z_{pRL} - z_{tRL}) \right) \right]^K} \quad (7-80)$$

$$F_{RR} = \frac{P_{30RR} V_{30RR}^K A_p}{\left[V_{30RR} + A_p \left(z_{pRR} - z_{tRR} - \frac{A_{pr}}{A_p} (z_{pFL} - z_{tFL}) \right) \right]^K} - \frac{P_{30ML} V_{30ML}^K A_{pr}}{\left[V_{30ML} + A_p \left(z_{pML} - z_{tML} - \frac{A_{pr}}{A_p} (z_{pRR} - z_{tRR}) \right) \right]^K} \quad (7-81)$$

Assuming that all suspension relative displacements are equal to each other, then the vertical stiffness can be found as:

$$\begin{aligned}
k = & \frac{P_{30FL} V_{30FL}^\kappa A_r^2 \kappa}{[V_{30FL} + A_r z_{pt}]^{\kappa+1}} + \frac{P_{30FR} V_{30FR}^\kappa A_r^2 \kappa}{[V_{30FR} + A_r z_{pt}]^{\kappa+1}} + \frac{P_{30ML} V_{30ML}^\kappa A_r^2 \kappa}{[V_{30ML} + A_r z_{pt}]^{\kappa+1}} + \\
& + \frac{P_{30MR} V_{30MR}^\kappa A_r^2 \kappa}{[V_{30MR} + A_r z_{pt}]^{\kappa+1}} + \frac{P_{30RL} V_{30RL}^\kappa A_r^2 \kappa}{[V_{30RL} + A_r z_{pt}]^{\kappa+1}} + \frac{P_{30RR} V_{30RR}^\kappa A_r^2 \kappa}{[V_{30RR} + A_r z_{pt}]^{\kappa+1}}
\end{aligned} \tag{7-82}$$

At static equilibrium, the vertical stiffness becomes,

$$\begin{aligned}
k_z = & \frac{P_{30FL} A_r^2 \kappa}{V_{30FL}} + \frac{P_{30FR} A_r^2 \kappa}{V_{30FR}} + \frac{P_{30ML} A_r^2 \kappa}{V_{30ML}} + \\
& + \frac{P_{30MR} A_r^2 \kappa}{V_{30MR}} + \frac{P_{30RL} A_r^2 \kappa}{V_{30RL}} + \frac{P_{30RR} A_r^2 \kappa}{V_{30RR}}
\end{aligned} \tag{7-83}$$

Assuming that piston displacements, wheel hub displacements, and pitch rotation are zero, roll stiffness can be found.

$$\begin{aligned}
& \left. \begin{aligned}
& \frac{\mathbf{P}_{30FL} \mathbf{V}_{30FL}^\kappa \mathbf{A}_p \left(\frac{t_f}{2} \mathbf{A}_p + \frac{t_m}{2} \mathbf{A}_{pr} \right) \boldsymbol{\kappa}}{\left[\mathbf{V}_{30FL} + \left(\phi \frac{t_f}{2} \mathbf{A}_p + \phi \frac{t_m}{2} \mathbf{A}_{pr} \right) \right]^{\kappa+1}} + \frac{\mathbf{P}_{30RR} \mathbf{V}_{30RR}^\kappa \mathbf{A}_{pr} \left(\frac{t_r}{2} \mathbf{A}_p + \frac{t_f}{2} \mathbf{A}_{pr} \right) \boldsymbol{\kappa}}{\left[\mathbf{V}_{30RR} + \left(-\phi \frac{t_r}{2} \mathbf{A}_p - \phi \frac{t_f}{2} \mathbf{A}_{pr} \right) \right]^{\kappa+1}} + \\
& + \frac{\mathbf{P}_{30FR} \mathbf{V}_{30FR}^\kappa \mathbf{A}_p \left(\frac{t_f}{2} \mathbf{A}_p + \frac{t_m}{2} \mathbf{A}_{pr} \right) \boldsymbol{\kappa}}{\left[\mathbf{V}_{30FR} + \left(-\phi \frac{t_f}{2} \mathbf{A}_p - \phi \frac{t_m}{2} \mathbf{A}_{pr} \right) \right]^{\kappa+1}} + \frac{\mathbf{P}_{30RL} \mathbf{V}_{30RL}^\kappa \mathbf{A}_{pr} \left(\frac{t_r}{2} \mathbf{A}_p + \frac{t_f}{2} \mathbf{A}_{pr} \right) \boldsymbol{\kappa}}{\left[\mathbf{V}_{30RL} + \left(\phi \frac{t_r}{2} \mathbf{A}_p + \phi \frac{t_f}{2} \mathbf{A}_{pr} \right) \right]^{\kappa+1}}
\end{aligned} \right\} + \\
& + \frac{t_m}{2} \left. \begin{aligned}
& \frac{\mathbf{P}_{30ML} \mathbf{V}_{30ML}^\kappa \mathbf{A}_p \left(\frac{t_m}{2} \mathbf{A}_p + \frac{t_r}{2} \mathbf{A}_{pr} \right) \boldsymbol{\kappa}}{\left[\mathbf{V}_{30ML} + \left(\phi \frac{t_m}{2} \mathbf{A}_p + \phi \frac{t_r}{2} \mathbf{A}_{pr} \right) \right]^{\kappa+1}} + \frac{\mathbf{P}_{30FR} \mathbf{V}_{30FR}^\kappa \mathbf{A}_{pr} \left(\frac{t_f}{2} \mathbf{A}_p + \frac{t_m}{2} \mathbf{A}_{pr} \right) \boldsymbol{\kappa}}{\left[\mathbf{V}_{30FR} + \left(-\phi \frac{t_f}{2} \mathbf{A}_p - \phi \frac{t_m}{2} \mathbf{A}_{pr} \right) \right]^{\kappa+1}} + \\
& + \frac{\mathbf{P}_{30MR} \mathbf{V}_{30MR}^\kappa \mathbf{A}_p \left(\frac{t_m}{2} \mathbf{A}_p + \frac{t_r}{2} \mathbf{A}_{pr} \right) \boldsymbol{\kappa}}{\left[\mathbf{V}_{30MR} + \left(-\phi \frac{t_m}{2} \mathbf{A}_p - \phi \frac{t_r}{2} \mathbf{A}_{pr} \right) \right]^{\kappa+1}} + \frac{\mathbf{P}_{30FL} \mathbf{V}_{30FL}^\kappa \mathbf{A}_{pr} \left(\frac{t_f}{2} \mathbf{A}_p + \frac{t_m}{2} \mathbf{A}_{pr} \right) \boldsymbol{\kappa}}{\left[\mathbf{V}_{30FL} + \left(\phi \frac{t_f}{2} \mathbf{A}_p + \phi \frac{t_m}{2} \mathbf{A}_{pr} \right) \right]^{\kappa+1}}
\end{aligned} \right\} \\
& + \frac{t_r}{2} \left. \begin{aligned}
& \frac{\mathbf{P}_{30RL} \mathbf{V}_{30RL}^\kappa \mathbf{A}_p \left(\frac{t_r}{2} \mathbf{A}_p + \frac{t_f}{2} \mathbf{A}_{pr} \right) \boldsymbol{\kappa}}{\left[\mathbf{V}_{30RL} + \left(\phi \frac{t_r}{2} \mathbf{A}_p + \phi \frac{t_f}{2} \mathbf{A}_{pr} \right) \right]^{\kappa+1}} + \frac{\mathbf{P}_{30MR} \mathbf{V}_{30MR}^\kappa \mathbf{A}_{pr} \left(\frac{t_m}{2} \mathbf{A}_p + \frac{t_r}{2} \mathbf{A}_{pr} \right) \boldsymbol{\kappa}}{\left[\mathbf{V}_{30MR} + \left(-\phi \frac{t_m}{2} \mathbf{A}_p - \phi \frac{t_r}{2} \mathbf{A}_{pr} \right) \right]^{\kappa+1}} + \\
& + \frac{\mathbf{P}_{30RR} \mathbf{V}_{30RR}^\kappa \mathbf{A}_p \left(\frac{t_r}{2} \mathbf{A}_p + \frac{t_f}{2} \mathbf{A}_{pr} \right) \boldsymbol{\kappa}}{\left[\mathbf{V}_{30RR} + \left(-\phi \frac{t_r}{2} \mathbf{A}_p - \phi \frac{t_f}{2} \mathbf{A}_{pr} \right) \right]^{\kappa+1}} + \frac{\mathbf{P}_{30ML} \mathbf{V}_{30ML}^\kappa \mathbf{A}_{pr} \left(\frac{t_m}{2} \mathbf{A}_p + \frac{t_r}{2} \mathbf{A}_{pr} \right) \boldsymbol{\kappa}}{\left[\mathbf{V}_{30ML} + \left(\phi \frac{t_m}{2} \mathbf{A}_p + \phi \frac{t_r}{2} \mathbf{A}_{pr} \right) \right]^{\kappa+1}}
\end{aligned} \right\} \quad (7-84)
\end{aligned}$$

Similarly, assuming that piston displacements, wheel hub displacements, and roll rotation are zero, pitch stiffness can be found.

$$\begin{aligned}
k_\theta = & \left. \begin{aligned} & \frac{P_{30FL} V_{30FL}^\kappa A_p (aA_p + A_{pr} b) \kappa}{[V_{30FL} + (-aA_p \theta - A_{pr} b \theta)]^{\kappa+1}} + \frac{P_{30RR} V_{30RR}^\kappa A_{pr} (cA_p + A_{pr} a) \kappa}{[V_{30RR} + (cA_p \theta + A_{pr} a \theta)]^{\kappa+1}} + \\ & + \frac{P_{30FR} V_{30FR}^\kappa A_p (aA_p + A_{pr} b) \kappa}{[V_{30FR} + (-aA_p \theta - A_{pr} b \theta)]^{\kappa+1}} + \frac{P_{30RL} V_{30RL}^\kappa A_{pr} (cA_p + A_{pr} a) \kappa}{[V_{30RL} + (cA_p \theta + A_{pr} a \theta)]^{\kappa+1}} \end{aligned} \right\} + \\
& + b \left. \begin{aligned} & \frac{P_{30ML} V_{30ML}^\kappa A_p (bA_p - A_{pr} c) \kappa}{[V_{30ML} + (bA_p \theta - A_{pr} c \theta)]^{\kappa+1}} + \frac{P_{30FR} V_{30FR}^\kappa A_{pr} (aA_p + A_{pr} b) \kappa}{[V_{30FR} + (-aA_p \theta - A_{pr} b \theta)]^{\kappa+1}} + \\ & + \frac{P_{30MR} V_{30MR}^\kappa A_p (bA_p - A_{pr} c) \kappa}{[V_{30MR} + (bA_p \theta - A_{pr} c \theta)]^{\kappa+1}} + \frac{P_{30FL} V_{30FL}^\kappa A_{pr} (aA_p + A_{pr} b) \kappa}{[V_{30FL} + (-aA_p \theta - A_{pr} b \theta)]^{\kappa+1}} \end{aligned} \right\} + \\
& + c \left. \begin{aligned} & \frac{P_{30RL} V_{30RL}^\kappa A_p (cA_p + A_{pr} a) \kappa}{[V_{30RL} + (cA_p \theta + A_{pr} a \theta)]^{\kappa+1}} - \frac{P_{30MR} V_{30MR}^\kappa A_{pr} (bA_p - A_{pr} c) \kappa}{[V_{30MR} + (bA_p \theta - A_{pr} c \theta)]^{\kappa+1}} + \\ & + \frac{P_{30RR} V_{30RR}^\kappa A_{pr} (cA_p + A_{pr} a) \kappa}{[V_{30RR} + (cA_p \theta + A_{pr} a \theta)]^{\kappa+1}} - \frac{P_{30ML} V_{30ML}^\kappa A_p (bA_p - A_{pr} c) \kappa}{[V_{30ML} + (bA_p \theta - A_{pr} c \theta)]^{\kappa+1}} \end{aligned} \right\} \quad (7-85)
\end{aligned}$$

7.4.1.3. Damping Properties

Damping component of the suspension forces are,

$$\begin{aligned}
F_{FL} = & A_p \left[\frac{A_p (\dot{z}_{pFL} - \dot{z}_{tFL}) - A_{pr} (\dot{z}_{pMR} - \dot{z}_{tMR})}{A_v C_D} \right]^2 \frac{\rho}{2} \text{sign} \left[\begin{array}{l} A_p (\dot{z}_{pFL} - \dot{z}_{tFL}) - \\ -A_{pr} (\dot{z}_{pMR} - \dot{z}_{tMR}) \end{array} \right] - \\
& - A_{pr} \left[\frac{A_p (\dot{z}_{pRR} - \dot{z}_{tRR}) - A_{pr} (\dot{z}_{pFL} - \dot{z}_{tFL})}{A_v C_D} \right]^2 \frac{\rho}{2} \text{sign} \left[\begin{array}{l} A_p (\dot{z}_{pRR} - \dot{z}_{tRR}) - \\ -A_{pr} (\dot{z}_{pFL} - \dot{z}_{tFL}) \end{array} \right] + \quad (7-86) \\
& + \frac{A_{pr}^2 (\dot{z}_{pFL} - \dot{z}_{tFL})}{R_{4FL1RR}}
\end{aligned}$$

$$\begin{aligned}
F_{FR} = & A_p \left[\frac{A_p (\dot{z}_{pFR} - \dot{z}_{tFR}) - A_{pr} (\dot{z}_{pML} - \dot{z}_{tML})}{A_v C_D} \right]^2 \frac{\rho}{2} \text{sign} \left[\begin{array}{c} A_p (\dot{z}_{pFR} - \dot{z}_{tFR}) - \\ -A_{pr} (\dot{z}_{pML} - \dot{z}_{tML}) \end{array} \right] - \\
& -A_{pr} \left[\frac{A_p (\dot{z}_{pRL} - \dot{z}_{tRL}) - A_{pr} (\dot{z}_{pFR} - \dot{z}_{tFR})}{A_v C_D} \right]^2 \frac{\rho}{2} \text{sign} \left[\begin{array}{c} A_p (\dot{z}_{pRL} - \dot{z}_{tRL}) - \\ -A_{pr} (\dot{z}_{pFR} - \dot{z}_{tFR}) \end{array} \right] + \quad (7-87) \\
& + \frac{A_{pr}^2 (\dot{z}_{pFR} - \dot{z}_{tFR})}{R_{4FR1RL}}
\end{aligned}$$

$$\begin{aligned}
F_{ML} = & A_p \left[\frac{A_p (\dot{z}_{pML} - \dot{z}_{tML}) - A_{pr} (\dot{z}_{pRR} - \dot{z}_{tRR})}{A_v C_D} \right]^2 \frac{\rho}{2} \text{sign} \left[\begin{array}{c} A_p (\dot{z}_{pML} - \dot{z}_{tML}) - \\ -A_{pr} (\dot{z}_{pRR} - \dot{z}_{tRR}) \end{array} \right] - \\
& -A_{pr} \left[\frac{A_p (\dot{z}_{pFR} - \dot{z}_{tFR}) - A_{pr} (\dot{z}_{pML} - \dot{z}_{tML})}{A_v C_D} \right]^2 \frac{\rho}{2} \text{sign} \left[\begin{array}{c} A_p (\dot{z}_{pFR} - \dot{z}_{tFR}) - \\ -A_{pr} (\dot{z}_{pML} - \dot{z}_{tML}) \end{array} \right] + \quad (7-88) \\
& + \frac{A_{pr}^2 (\dot{z}_{pML} - \dot{z}_{tML})}{R_{4ML1FR}}
\end{aligned}$$

$$\begin{aligned}
F_{MR} = & A_p \left[\frac{A_p (\dot{z}_{pMR} - \dot{z}_{tMR}) - A_{pr} (\dot{z}_{pRL} - \dot{z}_{tRL})}{A_v C_D} \right]^2 \frac{\rho}{2} \text{sign} \left[\begin{array}{c} A_p (\dot{z}_{pMR} - \dot{z}_{tMR}) - \\ -A_{pr} (\dot{z}_{pRL} - \dot{z}_{tRL}) \end{array} \right] - \\
& -A_{pr} \left[\frac{A_p (\dot{z}_{pFL} - \dot{z}_{tFL}) - A_{pr} (\dot{z}_{pMR} - \dot{z}_{tMR})}{A_v C_D} \right]^2 \frac{\rho}{2} \text{sign} \left[\begin{array}{c} A_p (\dot{z}_{pFL} - \dot{z}_{tFL}) - \\ -A_{pr} (\dot{z}_{pMR} - \dot{z}_{tMR}) \end{array} \right] + \quad (7-89) \\
& + \frac{A_{pr}^2 (\dot{z}_{pMR} - \dot{z}_{tMR})}{R_{4MR1FL}}
\end{aligned}$$

$$\begin{aligned}
F_{RL} = & A_p \left[\frac{A_p (\dot{z}_{pRL} - \dot{z}_{tRL}) - A_{pr} (\dot{z}_{pFR} - \dot{z}_{tFR})}{A_v C_D} \right]^2 \frac{\rho}{2} \text{sign} \left[\begin{array}{c} A_p (\dot{z}_{pRL} - \dot{z}_{tRL}) - \\ -A_{pr} (\dot{z}_{pFR} - \dot{z}_{tFR}) \end{array} \right] - \\
& -A_{pr} \left[\frac{A_p (\dot{z}_{pMR} - \dot{z}_{tMR}) - A_{pr} (\dot{z}_{pRL} - \dot{z}_{tRL})}{A_v C_D} \right]^2 \frac{\rho}{2} \text{sign} \left[\begin{array}{c} A_p (\dot{z}_{pMR} - \dot{z}_{tMR}) - \\ -A_{pr} (\dot{z}_{pRL} - \dot{z}_{tRL}) \end{array} \right] + \quad (7-90) \\
& + \frac{A_{pr}^2 (\dot{z}_{pRL} - \dot{z}_{tRL})}{R_{4RL1MR}}
\end{aligned}$$

$$\begin{aligned}
F_{RR} = & A_p \left[\frac{A_p (\dot{z}_{pRR} - \dot{z}_{tRR}) - A_{pr} (\dot{z}_{pFL} - \dot{z}_{tFL})}{A_v C_D} \right]^2 \frac{\rho}{2} \text{sign} \left[\begin{array}{c} A_p (\dot{z}_{pRR} - \dot{z}_{tRR}) - \\ -A_{pr} (\dot{z}_{pFL} - \dot{z}_{tFL}) \end{array} \right] - \\
& -A_{pr} \left[\frac{A_p (\dot{z}_{pML} - \dot{z}_{tML}) - A_{pr} (\dot{z}_{pRR} - \dot{z}_{tRR})}{A_v C_D} \right]^2 \frac{\rho}{2} \text{sign} \left[\begin{array}{c} A_p (\dot{z}_{pML} - \dot{z}_{tML}) - \\ -A_{pr} (\dot{z}_{pRR} - \dot{z}_{tRR}) \end{array} \right] + \quad (7-91) \\
& + \frac{A_{pr}^2 (\dot{z}_{pRR} - \dot{z}_{tRR})}{R_{4RR1ML}}
\end{aligned}$$

Assuming all suspension relative velocities are equal to each other, vertical damping force is expressed as:

$$F_D = F_{FLD} + F_{FRD} + F_{MLD} + F_{MRD} + F_{RLD} + F_{RRD} \quad (7-92)$$

$$\begin{aligned}
F_D = & 6A_r \left[\frac{A_r \dot{z}_{pt}}{A_v C_D} \right]^2 \frac{\rho}{2} \text{sign}(\dot{z}_{pt}) + \frac{A_{pr}^2 \dot{z}_{pt}}{R_{4FL1RR}} + \frac{A_{pr}^2 \dot{z}_{pt}}{R_{4FR1RL}} + \\
& + \frac{A_{pr}^2 \dot{z}_{pt}}{R_{4ML1FR}} + \frac{A_{pr}^2 \dot{z}_{pt}}{R_{4MR1FL}} + \frac{A_{pr}^2 \dot{z}_{pt}}{R_{4RL1MR}} + \frac{A_{pr}^2 \dot{z}_{pt}}{R_{4RR1ML}} \quad (7-93)
\end{aligned}$$

Assuming that, piston velocities, wheel hub velocities, and pitch velocity are zero, damping moment in roll direction is given by the expression:

$$M_\phi = \frac{t_f}{2} (F_{FL} - F_{FR}) + \frac{t_m}{2} (F_{ML} - F_{MR}) + \frac{t_r}{2} (F_{RL} - F_{RR}) \quad (7-94)$$

where F_{FL} , F_{FR} , F_{ML} , F_{MR} , F_{RL} , and F_{RR} can be obtained from Equations (7-76) to (7-81).

$$\begin{aligned}
M_\phi = & \frac{t_f}{2} \left(\begin{aligned} & 2A_p \left[\frac{A_p \frac{t_f}{2} \dot{\phi} + A_{pr} \frac{t_m}{2} \dot{\phi}}{A_v C_D} \right]^2 \frac{\rho}{2} \text{sign}[\dot{\phi}] + \\ & + 2A_{pr} \left[\frac{A_p \frac{t_r}{2} \dot{\phi} + A_{pr} \frac{t_f}{2} \dot{\phi}}{A_v C_D} \right]^2 \frac{\rho}{2} \text{sign}[\dot{\phi}] + \frac{A_{pr}^2 \frac{t_f}{2} \dot{\phi}}{R_{4FL1RR}} + \frac{A_{pr}^2 \frac{t_f}{2} \dot{\phi}}{R_{4FR1RL}} \end{aligned} \right) + \\
& + \frac{t_m}{2} \left(\begin{aligned} & 2A_p \left[\frac{A_p \frac{t_m}{2} \dot{\phi} + A_{pr} \frac{t_r}{2} \dot{\phi}}{A_v C_D} \right]^2 \frac{\rho}{2} \text{sign}[\dot{\phi}] + \\ & + 2A_{pr} \left[\frac{A_p \frac{t_f}{2} \dot{\phi} + A_{pr} \frac{t_m}{2} \dot{\phi}}{A_v C_D} \right]^2 \frac{\rho}{2} \text{sign}[\dot{\phi}] + \frac{A_{pr}^2 \frac{t_m}{2} \dot{\phi}}{R_{4ML1FR}} + \frac{A_{pr}^2 \frac{t_m}{2} \dot{\phi}}{R_{4MR1FL}} \end{aligned} \right) + \\
& + \frac{t_r}{2} \left(\begin{aligned} & 2A_p \left[\frac{A_p \frac{t_r}{2} \dot{\phi} + A_{pr} \frac{t_f}{2} \dot{\phi}}{A_v C_D} \right]^2 \frac{\rho}{2} \text{sign}[\dot{\phi}] + \\ & + 2A_{pr} \left[\frac{A_p \frac{t_m}{2} \dot{\phi} + A_{pr} \frac{t_r}{2} \dot{\phi}}{A_v C_D} \right]^2 \frac{\rho}{2} \text{sign}[\dot{\phi}] + \frac{A_{pr}^2 \frac{t_r}{2} \dot{\phi}}{R_{4RL1MR}} + \frac{A_{pr}^2 \frac{t_r}{2} \dot{\phi}}{R_{4RR1ML}} \end{aligned} \right) \quad (7-95)
\end{aligned}$$

Similarly, assuming that, piston velocities, wheel hub velocities, and roll velocity are zero, damping moment in pitch direction is given by the expression:

$$M_\theta = -a(F_{FL} + F_{FR}) + b(F_{ML} + F_{MR}) + c(F_{RL} + F_{RR}) \quad (7-96)$$

$$\begin{aligned}
\mathbf{M}_\theta = & \mathbf{a} \left(\begin{aligned} & 2A_p \left[\frac{A_p a \dot{\theta} + A_{pr} b \dot{\theta}}{A_v C_D} \right]^2 \frac{\rho}{2} \text{sign}[\dot{\theta}] + \\ & + 2A_{pr} \left[\frac{A_p c \dot{\theta} + A_{pr} a \dot{\theta}}{A_v C_D} \right]^2 \frac{\rho}{2} \text{sign}[\dot{\theta}] + \frac{A_{pr}^2 a \dot{\theta}}{R_{4FL1RR}} + \frac{A_{pr}^2 a \dot{\theta}}{R_{4FR1RL}} \end{aligned} \right) + \\
& \mathbf{b} \left(\begin{aligned} & 2A_p \left[\frac{A_p b \dot{\theta} - A_{pr} c \dot{\theta}}{A_v C_D} \right]^2 \frac{\rho}{2} \text{sign}[A_p b \dot{\theta} - A_{pr} c \dot{\theta}] + \\ & + 2A_{pr} \left[\frac{A_p a \dot{\theta} + A_{pr} b \dot{\theta}}{A_v C_D} \right]^2 \frac{\rho}{2} \text{sign}[\dot{\theta}] + \frac{A_{pr}^2 b \dot{\theta}}{R_{4ML1FR}} + \frac{A_{pr}^2 b \dot{\theta}}{R_{4MR1FL}} \end{aligned} \right) + \\
& \mathbf{c} \left(\begin{aligned} & 2A_p \left[\frac{A_p c \dot{\theta} + A_{pr} a \dot{\theta}}{A_v C_D} \right]^2 \frac{\rho}{2} \text{sign}[\dot{\theta}] - \\ & - 2A_{pr} \left[\frac{A_p b \dot{\theta} - A_{pr} c \dot{\theta}}{A_v C_D} \right]^2 \frac{\rho}{2} \text{sign}[A_p b \dot{\theta} - A_{pr} c \dot{\theta}] + \\ & + \frac{A_{pr}^2 c \dot{\theta}}{R_{4RL1MR}} + \frac{A_{pr}^2 c \dot{\theta}}{R_{4RR1ML}} \end{aligned} \right) \quad (7-97)
\end{aligned}$$

7.4.1.4. Warp Moment

For a vehicle with two axles, warp stiffness and warp moment are defined in the literature. However, for a vehicle with three and more axles there is no exact definition in the literature. For this reason, the warp moment is calculated with the assumptions:

$$Z_{pFL} = -Z_{pFR} = -Z \quad (7-98)$$

$$Z_{pRL} = -Z_{pRR} = Z \quad (7-99)$$

$$Z_{pML} = \frac{a + b - c}{a + b + c} Z \quad (7-100)$$

$$Z_{pMR} = -\frac{a + b - c}{a + b + c} Z \quad (7-101)$$

Assuming wheel hub displacements are zero, warp moment can be calculated as

$$M_{\text{warp}} = \frac{t_f}{2}(F_{\text{FL}} - F_{\text{FR}}) + \frac{t_m}{2}(F_{\text{MR}} - F_{\text{ML}}) + \frac{t_r}{2}(F_{\text{RR}} - F_{\text{RL}}) \quad (7-102)$$

7.5. COMPARISON OF STIFFNESS PROPERTIES OF THE INTERCONNECTED HP SUSPENSION SYSTEM

When unconnected suspension configurations are converted into interconnected suspension configurations, the new suspension configurations have completely different stiffness and damping properties. To be able to compare the stiffness properties of the interconnected HP suspension systems in a proper manner, vertical stiffness of all suspension configurations are equated to each other. The same procedure followed in Chapter 6 is followed here as well.

Comparisons of the interconnected suspension configurations are again performed for different rod areas, $A_r=0.8A_p$ and $A_r=0.6A_p$ in order to see the effect of the interconnections.

7.5.1. Case 1: $A_r=0.6A_p$

Before, calculating the vertical stiffness of the interconnected HP suspension system, the initial gas pressures and the initial gas volumes should be determined. Therefore, static analysis should be performed. These volumes can be determined according to the body bounce frequency requirement. For this case, the initial oil pressures at static equilibrium are summarized in Table 7.4 and the initial gas volumes which result in equivalent vertical stiffness are summarized in Table 7.5.

Table 7.4: Initial Oil Pressure at Static Equilibrium for Different Interconnected Configurations

Suspension Configuration	Pressure [bar]					
	P _{30FL}	P _{30FR}	P _{30ML}	P _{30MR}	P _{30RL}	P _{30RR}
1 st	37.2	37.2	36.4	36.4	34.7	34.7
4 th	37.5	37.5	35.5	35.5	35.2	35.2
5 th	37.3	37.3	35.8	35.8	35.1	35.1
6 th	38.8	38.8	35.2	35.2	34.2	34.2
7 th	38.0	38.0	36.7	36.7	33.6	33.6
8 th	37.2	37.2	36.4	36.4	34.7	34.7
9 th	38.8	38.8	35.8	35.8	33.6	33.6
10 th	37.3	37.3	21.9	21.9	35.1	35.1
11 th	23.7	23.7	35.2	35.2	34.2	34.2
12 th	38.0	38.0	36.7	36.7	20.6	20.6
13 th	23.7	23.7	21.9	21.9	20.6	20.6

Unconnected suspension configurations (13th) with the given pressures and the interconnected suspension configurations with the given pressures have the same vertical suspension force characteristics. As can be seen from the Table 7.4, since in the interconnected suspension configurations, the effective static load area is smaller relative to the effective road area of unconnected suspension configurations; the initial pressures of the interconnected suspension configurations are higher than the initial pressure of the unconnected suspension configuration.

Table 7.5: Gas Volumes of Front, Intermediate, and Rear Suspension Volumes

Suspension Configuration	Volume [L]		
	V _{30F}	V _{30M}	V _{30R}
1 st	1.1	1.1	1.1
4 th	1.1	1.1	1.1
5 th	1.1	1.1	1.1
6 th	1.1	1.1	1.1
7 th	1.1	1.1	1.1
8 th	1.1	1.1	1.1
9 th	1.1	1.1	1.1
10 th	1.2	1.9	1.2
11 th	1.9	1.2	1.2
12 th	1.2	1.2	1.9
13 th	1.9	1.9	1.9

As Table 7.5 shows, to be able to get the same vertical stiffness characteristics of the interconnected and the unconnected suspension configurations, different gas volumes at static equilibrium are needed. Moreover, since interconnected suspension configurations have smaller effective piston area, they also have smaller gas volume for the similar vertical suspension stiffness of the unconnected suspension configurations as expected.

Equivalent vertical stiffness characteristics of the suspension configurations are given Figure 7.23 and roll and pitch stiffness characteristics for different interconnection configurations are given in Figure 7.24 and Figure 7.25.

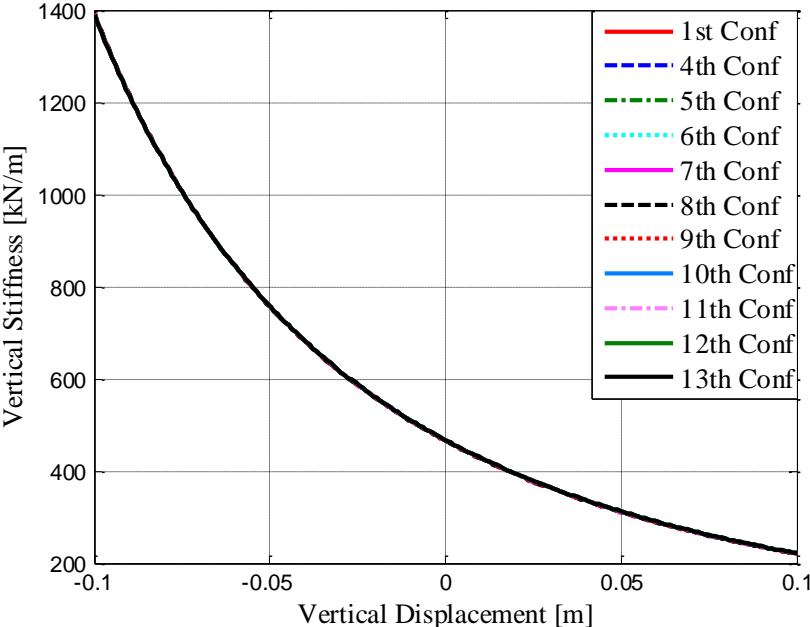


Figure 7.23: Vertical Stiffness of Different Interconnections

As can be seen from Figure 7.23, after the optimization study, all suspension configurations have the same vertical stiffness characteristics for equivalent remaining suspension parameters.

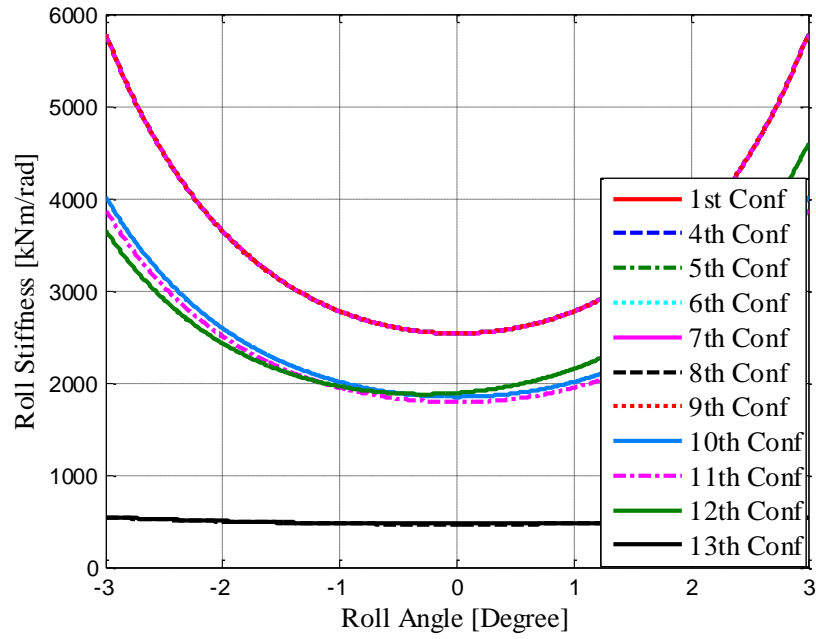


Figure 7.24: Roll Stiffness of Different Interconnections

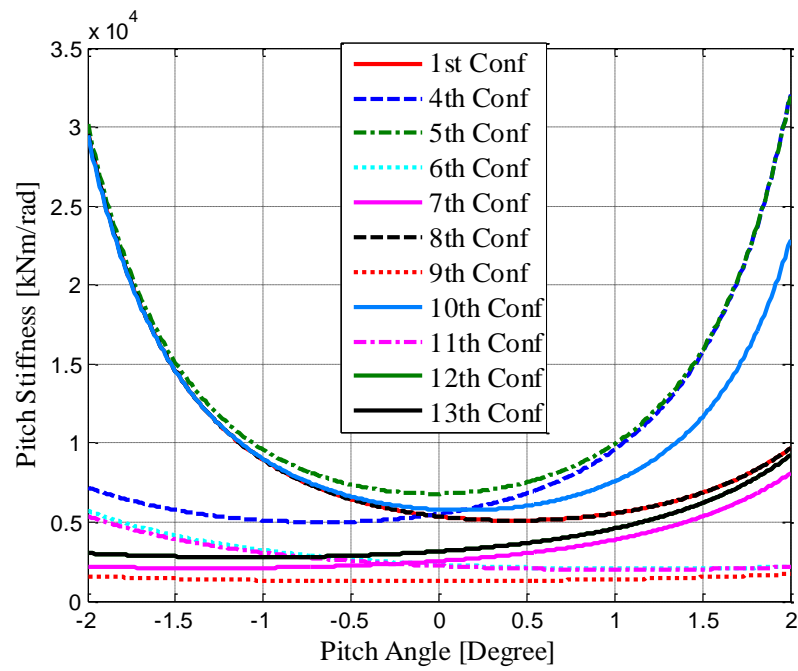


Figure 7.25: Pitch Stiffness of Different Interconnections

Figure 7.24 and Figure 7.25 show the stiffness and the damping characteristics qualitatively. In order to compare the roll and the pitch stiffness in a quantitative

manner, integral of the roll and the pitch stiffness values for the specified deflection sets are calculated. The results are given in Figure 7.26 and Figure 7.27.

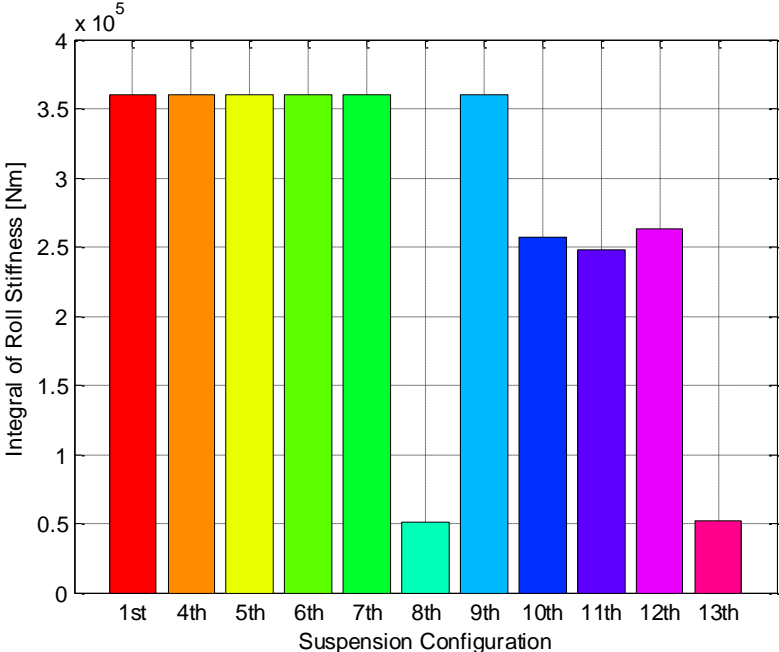


Figure 7.26: Integral of Roll Stiffness

From Figure 7.26, it can be seen that, 1st, 4th, 5th, 6th, 7th, and 9th interconnected HP suspension configurations have the similar roll stiffness characteristics. This is due to the fact that these suspension configurations are fully interconnected in the roll direction. However, the 8th and 13th interconnections have minimum roll stiffness since they are either interconnected purely on pitch plane or unconnected. In other words, they are not connected in the roll plane. The remaining interconnections, 10th, 11th, and 12th, have roll stiffness characteristics between these two groups of suspensions since they are semi-interconnected in the roll plane.

Figure 7.27 shows the comparison of the pitch stiffness characteristics of the different interconnections. 5th suspension configuration has the highest pitch stiffness characteristics. This is due to the nature of the pitch stiffness interconnection which is placed between the first and fourth oil volumes of the front and the rear suspension. Thus, the amount of oil displaced is maximum. Moreover, the 1st, 4th, and 10th configurations have also high pitch stiffness characteristics. The 9th and 13th

interconnected suspension configurations have the lowest pitch stiffness, since the 9th suspension configuration is purely interconnected in the roll plane and it does not have an interconnection in the pitch plane. The 13th suspension configuration is an unconnected and thus it does not have a pitch interconnection and has also very low pitch stiffness. The remaining interconnections have semi-interconnected pitch connections and thus they have pitch stiffness values between the unconnected and fully pitch interconnected configurations.

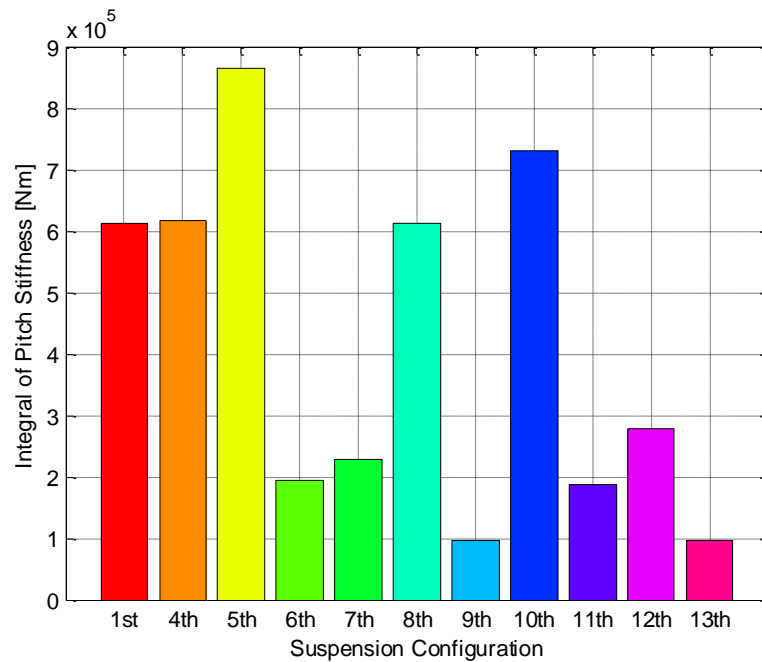


Figure 7.27: Integral of Pitch Stiffness

The roll and the pitch stiffness values at zero roll and pitch deflections are summarized in Table 7.6. These stiffness values are normalized with respect to the stiffness values of the unconnected suspension configuration.

Table 7.6: Roll and Pitch Stiffness Characteristics of Different Interconnections

Suspension Conf.	Roll Stiffness [kNm/rad]	Pitch Stiffness [kNm/rad]	Roll Stiffness [%]	Pitch Stiffness [%]
1st	2537	5359	540	421
4th	2537	5517	540	434
5th	2537	6803	540	535
6th	2537	2313	540	182
7th	2537	2532	540	199
8th	466	5359	100	421
9th	2537	1261	540	100
10th	1848	5785	393	455
11th	1791	2225	381	175
12th	1891	3150	402	248
13th	470	1272	100	100

As can be understood from Table 7.6, the first, second, third, and tenth suspension configurations have both high pitch and roll stiffness values. Since the eighth suspension configuration has only pitch interconnection, it has lower roll stiffness and high pitch stiffness. Similarly, the ninth suspension configuration has only roll interconnection, and thus it has higher roll stiffness and low pitch stiffness,

7.5.2. Case 2: $A_r=0.8A_p$

Similarly interconnections with $A_r=0.8A_p$ have been analyzed. The ratio of the rod area to piston area is important suspension parameter of the interconnected suspension configuration and it represents the strength of the interconnections. When this ratio is decreased, the interconnection becomes more prominent and when it is increased, the interconnection becomes weak and the suspension configuration begins to get closer to the unconnected suspension. Again to be able to make a reasonable comparison between different suspension configurations, vertical stiffness and the damping characteristics of the different suspension configurations have been equalized. The calculated initial gas pressures and initial gas volumes are summarized in Table 7.7 and Table 7.8, respectively.

Table 7.7: Initial Oil Pressure at Static Equilibrium for Different Interconnected Configurations

Suspension Configuration	Pressure [bar]					
	P _{30FL}	P _{30FR}	P _{30ML}	P _{30MR}	P _{30RL}	P _{30RR}
1 st	28.7	28.7	27.4	27.4	25.8	25.8
4 th	28.9	28.9	26.9	26.9	26.1	26.1
5 th	28.7	28.7	27.1	27.1	26.1	26.1
6 th	29.4	29.4	26.8	26.8	25.7	25.7
7 th	29.0	29.0	27.5	27.5	25.4	25.4
8 th	28.7	28.7	27.4	27.4	25.8	25.8
9 th	29.4	29.4	27.1	27.1	25.4	25.4
10 th	28.7	28.7	21.9	21.9	26.1	26.1
11 th	23.7	23.7	26.8	26.8	25.7	25.7
12 th	29.0	29.0	27.5	27.5	20.6	20.6
13 th	23.7	23.7	21.9	21.9	20.6	20.6

Table 7.8: Gas Volumes of Front, Intermediate, and Rear Suspension Volumes

Suspension Configuration	Volume [L]		
	V _{30F}	V _{30M}	V _{30R}
1 st	1.5	1.5	1.5
4 th	1.5	1.5	1.5
5 th	1.5	1.5	1.5
6 th	1.5	1.5	1.5
7 th	1.5	1.5	1.5
8 th	1.5	1.5	1.5
9 th	1.5	1.5	1.5
10 th	1.5	1.9	1.5
11 th	1.9	1.5	1.5
12 th	1.5	1.5	1.9
13 th	1.9	1.9	1.9

With the obtained initial gas volumes, vertical stiffness characteristics are obtained. Vertical stiffness characteristics of different interconnected suspension configurations are given Figure 7.28. As can be seen from Figure 7.28, vertical stiffness characteristics of the different suspension configurations are equivalent to each other. Therefore pitch and the roll stiffness can be compared. Roll and pitch

stiffness of different interconnection configurations are given in Figure 7.29 and Figure 7.30, respectively.

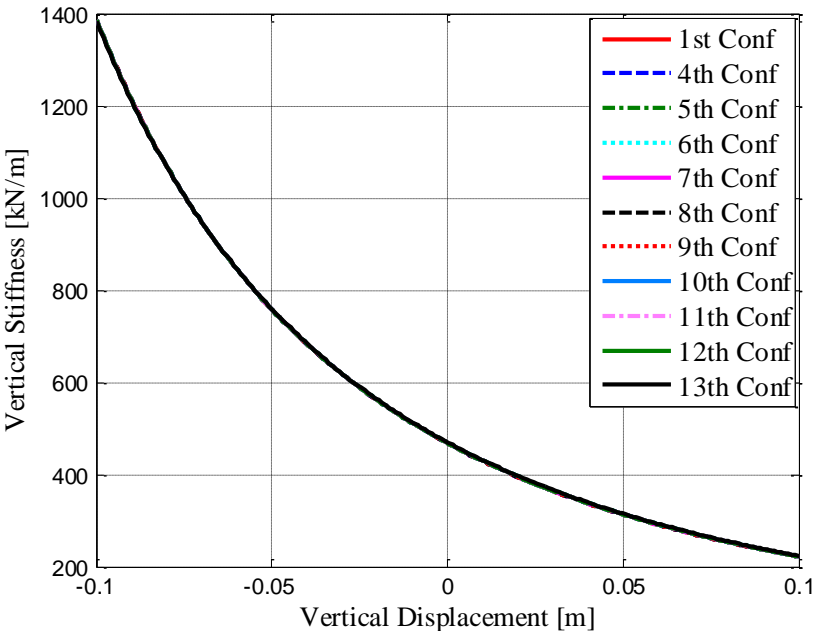


Figure 7.28: Vertical Stiffness of Different Interconnections

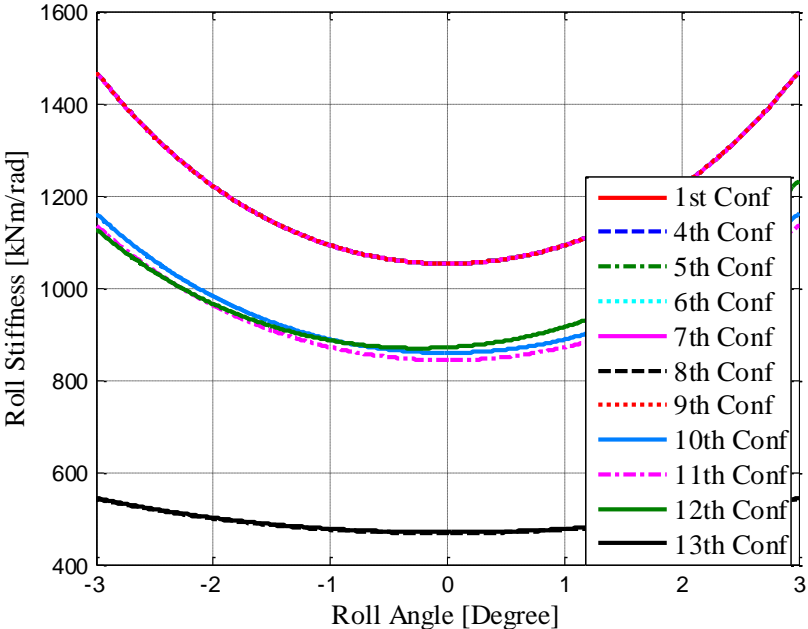


Figure 7.29: Roll Stiffness of Different Interconnections

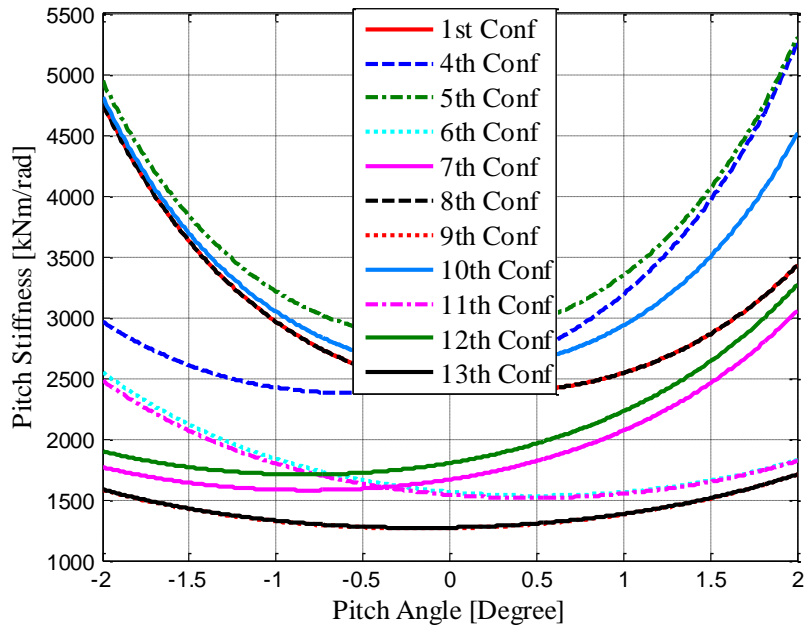


Figure 7.30: Pitch Stiffness of Different Interconnections

To be able to compare the roll and pitch stiffness quantitatively, the area under the integral of the roll and the pitch stiffness values are calculated. The calculated values are shown in Figure 7.31 and Figure 7.32.

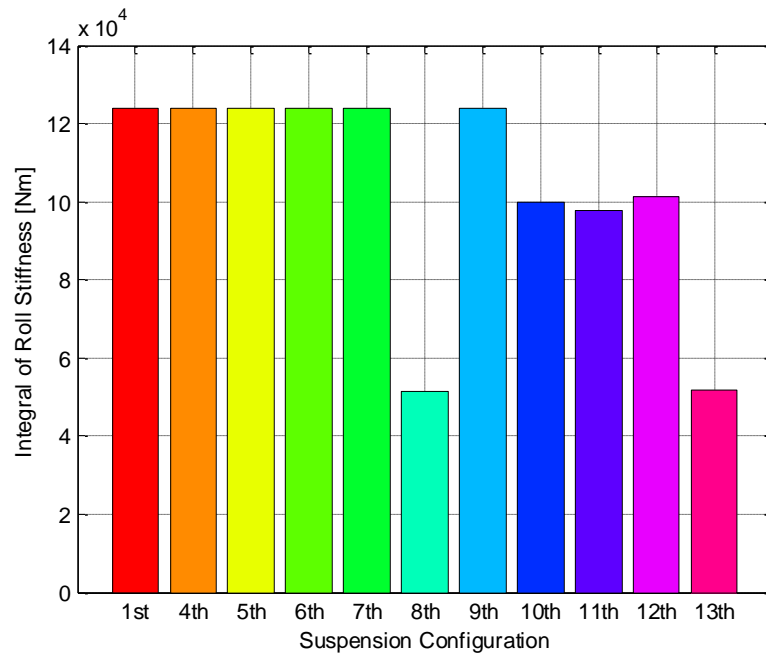


Figure 7.31: Integral of Roll Stiffness

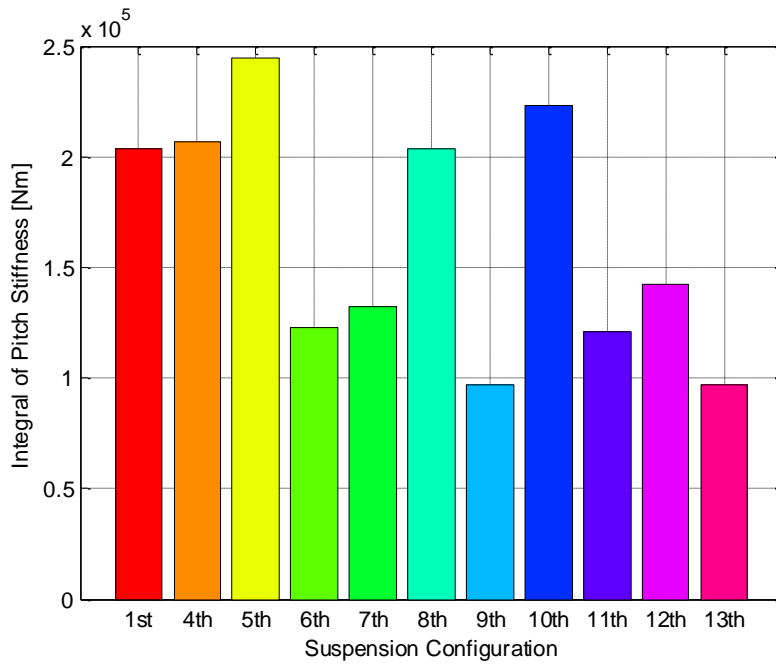


Figure 7.32: Integral of Pitch Stiffness

According to Figure 7.31 and Figure 7.32, the results are similar to the case with interconnections for $A_r=0.6A_p$. The roll and pitch stiffness values at static equilibrium are summarized in Table 7.9.

Table 7.9: Roll and Pitch Stiffness Characteristics of Different Interconnections

Suspension Conf.	Roll Stiffness [kNm/rad]	Pitch Stiffness [kNm/rad]	Roll Stiffness [%]	Pitch Stiffness [%]
1st	1053	2416	224	190
4th	1053	2480	224	195
5th	1053	2832	224	223
6th	1053	1564	224	123
7th	1053	1667	224	131
8th	468	2416	100	190
9th	1053	1266	224	100
10th	859	2582	183	203
11th	843	1540	179	121
12th	871	1802	185	142
13th	470	1272	100	100

As can be seen from Table 7.9, interconnections for $A_r=0.8A_p$ have lower roll and pitch stiffness as compared with the interconnections for $A_r=0.6A_p$. In other words, the magnitudes of the roll and the pitch stiffness decreased to less than half of those of the interconnections for $A_r=0.6A_p$.

7.6. COMPARISON OF DAMPING PROPERTIES OF THE INTERCONNECTED HP SUSPENSION SYSTEM

In order to compare the damping characteristics of the interconnected suspension configurations in a proper manner, the approach explained in Chapter 6 is again used. First, suspensions with equal damping characteristics in vertical direction are obtained, and then the pitch and roll damping characteristics are formed and compared. In order to get equivalent vertical damping characteristics, damping valve parameters are optimized.

7.6.1. Case 1: $A_r=0.6A_p$

The vertical damping force of different suspension configurations are given in Figure 7.33 and roll and pitch damping moments are given in Figure 7.34 and Figure 7.35, respectively.

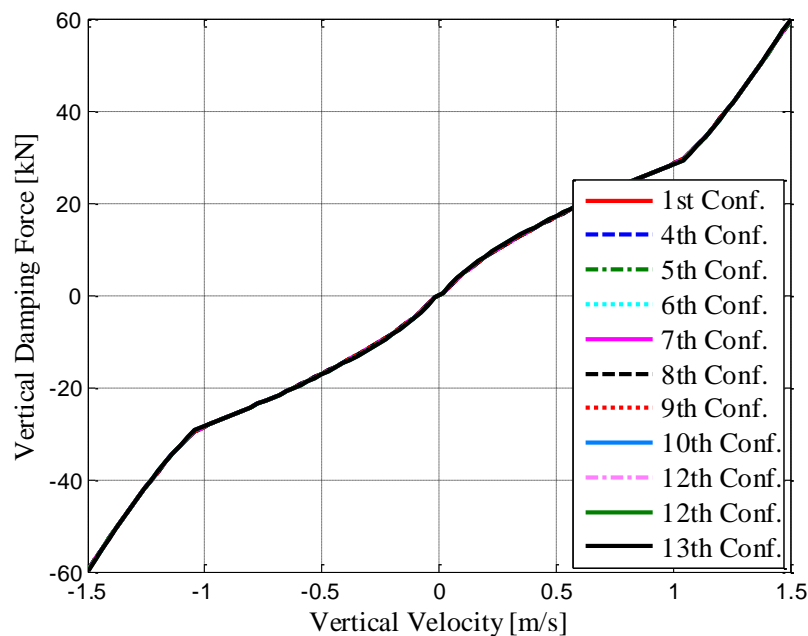


Figure 7.33: Vertical Damping of Different Interconnections

As can be seen from Figure 7.33, all suspension configurations have almost identical vertical damping characteristics.

As can be seen from Figure 7.34 and Figure 7.35, some of the interconnected HP suspension systems have similar roll and pitch damping performances and some of them have different roll and pitch damping performances. To be able to compare the different suspension configurations in terms of roll and pitch damping in a quantitative manner, the area under the curves are calculated. Figure 7.36 and Figure 7.37 show the values of the integral of the roll and pitch interconnections.

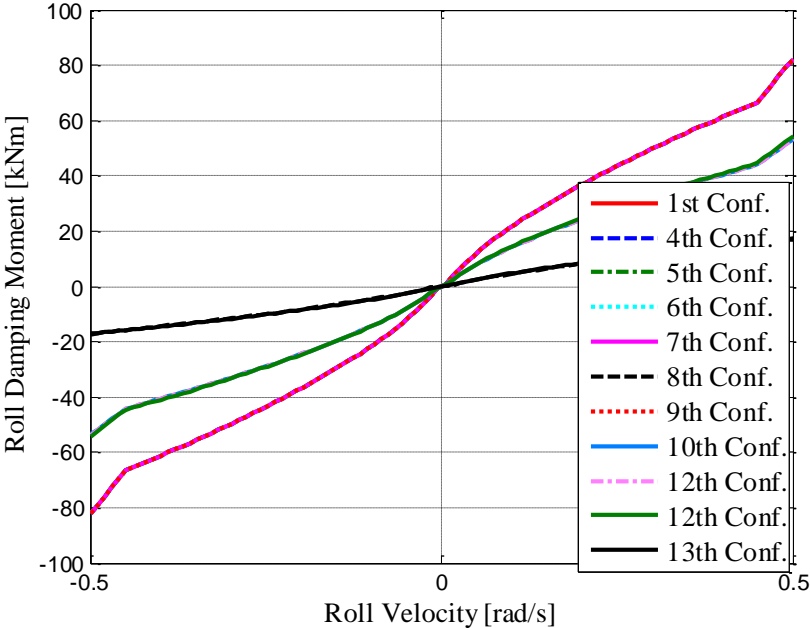


Figure 7.34: Roll Damping of Different Interconnections

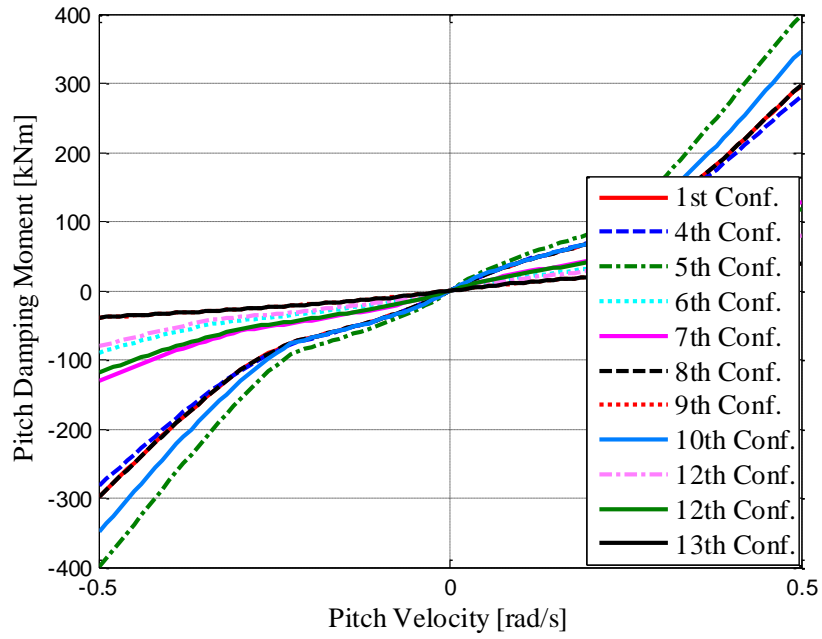


Figure 7.35: Pitch Damping of Different Interconnections

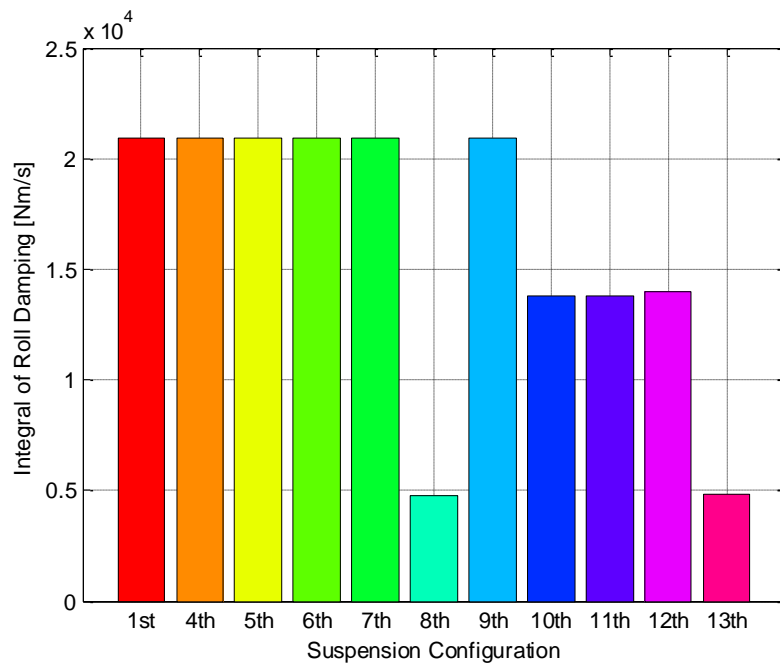


Figure 7.36: Integral of Roll Damping of Different Interconnections

As can be seen from Figure 7.36, the first, fourth, fifth, sixth, seventh, and ninth suspension configurations which are fully interconnected in roll plane have the

highest roll damping. Since the eighth and thirteenth suspension configurations are unconnected in roll plane, they have lower roll damping. The tenth, eleventh, and twelfth suspension configurations have semi-interconnection in roll plane and thus they have higher roll damping as compared to unconnected suspension configurations in roll plane and they have lower roll damping as compared to fully interconnected suspension configurations.

As Figure 7.37 illustrates, the first, fourth, fifth, eighth, and tenth interconnections have the higher pitch damping. Unconnected suspension configurations in the pitch plane which are the ninth and thirteenth have lower pitch damping. The remaining suspension configurations have pitch damping between the fully interconnected and the unconnected interconnections.

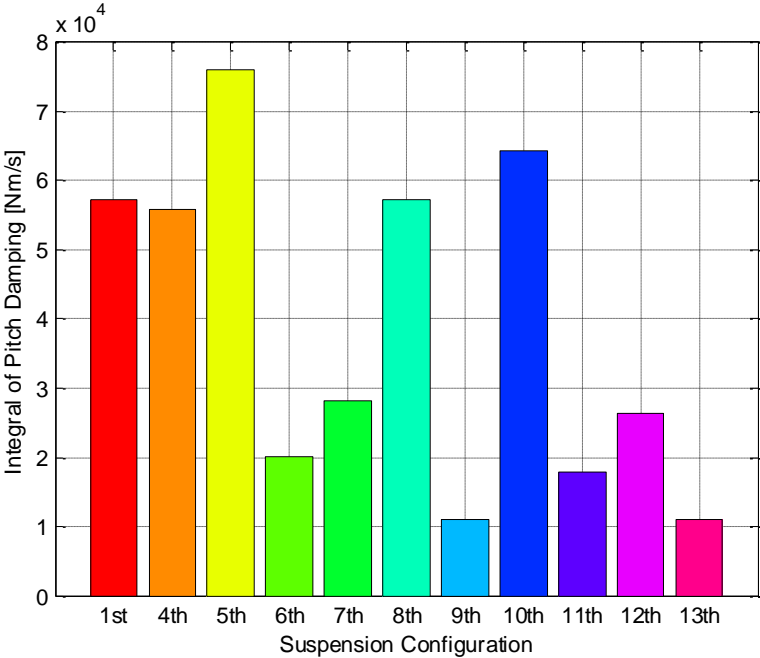


Figure 7.37: Integral of Pitch Damping of Different Interconnections

The normalized values of the integral of the roll and pitch damping with respect to the unconnected suspension configuration (13th) are summarized in Table 7.10.

Table 7.10: Integral of Roll and Pitch Damping of Different Interconnections

Suspension Conf.	Int Roll Damping	Int Pitch Damping	Roll Damping [%]	Pitch Damping [%]
1st	2.0925e+04	5.7195e+04	434	518
4th	2.0925e+04	5.5938e+04	434	506
5th	2.0925e+04	7.6055e+04	434	689
6th	2.0925e+04	2.0156e+04	434	182
7th	2.0925e+04	2.8165e+04	434	255
8th	4.7601e+03	5.7309e+04	99	519
9th	2.0925e+04	1.1032e+04	434	100
10th	1.3799e+04	6.4354e+04	286	583
11th	1.3804e+04	1.7883e+04	286	162
12th	1.3973e+04	2.6409e+04	290	239
13th	4.8175e+03	1.1045e+04	100	100

7.6.2. Case 2: $A_r=0.8 A_p$

The vertical damping force of different suspension configurations are given in Figure 7.38 and roll and pitch damping moments are given in Figure 7.39 and Figure 7.40, respectively. As Figure 7.38 illustrates, all interconnected suspension configurations have equivalent vertical damping characteristics.

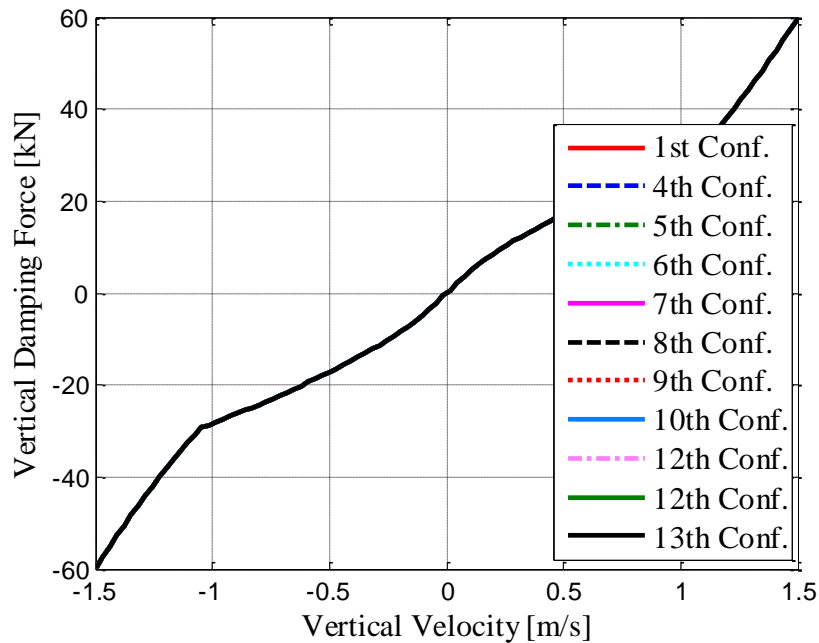


Figure 7.38: Vertical Damping of Different Interconnections

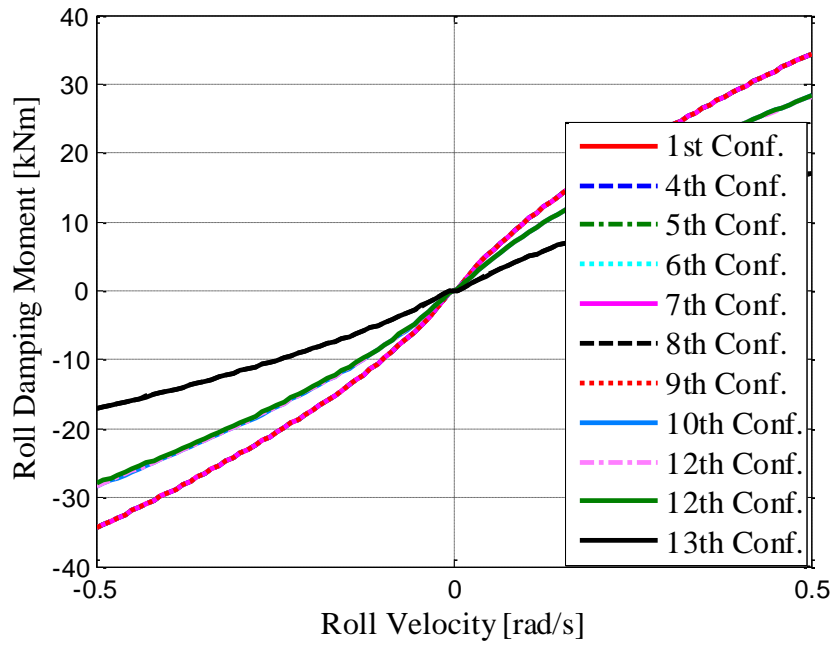


Figure 7.39: Roll Damping of Different Interconnections

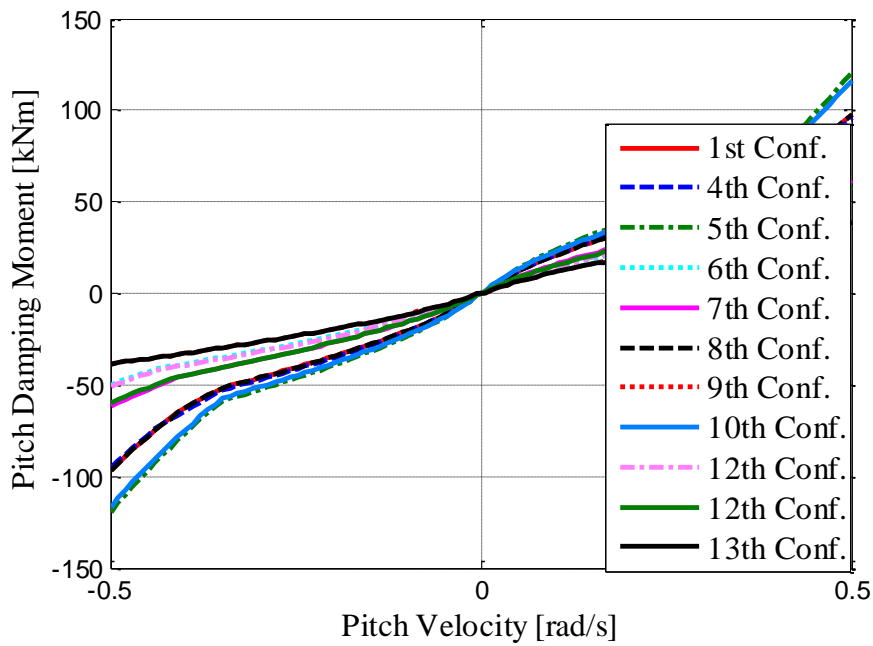


Figure 7.40: Pitch Damping of Different Interconnections

In order to compare suspensions quantitatively, the integral of the roll and pitch damping are calculated. These integral values are given in Figure 7.41 and Figure

7.42. Since the strength of the interconnection is reduced, the roll and pitch damping are lower as compared with the roll and pitch damping of the suspension configurations for $A_r=0.6A_p$.

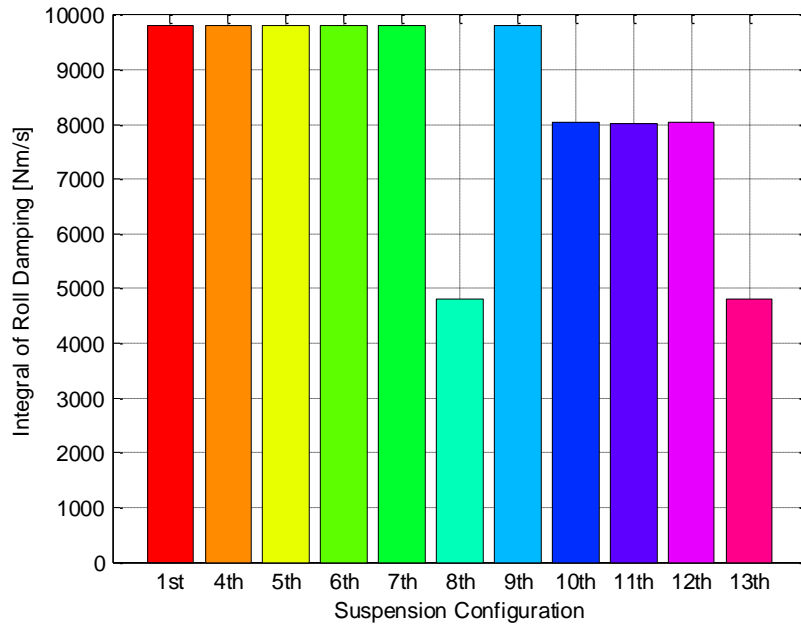


Figure 7.41: Integral of Roll Damping of Different Interconnections

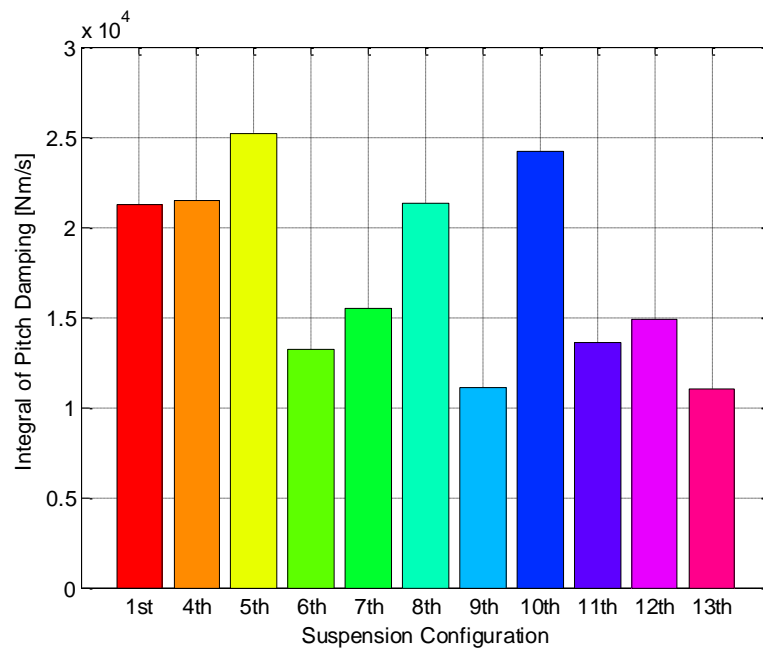


Figure 7.42: Integral of Pitch Damping of Different Interconnections

The normalized integral values are summarized also in Table 7.11.

Table 7.11: Integral of Roll and Pitch Damping Characteristics of Different Interconnections

Suspension Conf.	$A_r=0.8A_p$			
	Int. Roll Damping	Int Pitch Damping	Roll Damping [%]	Pitch Damping [%]
1st	9.8208e+03	2.1285e+04	204	193
4th	9.8208e+03	2.1514e+04	204	195
5th	9.8208e+03	2.5163e+04	204	228
6th	9.8208e+03	1.3255e+04	204	120
7th	9.8208e+03	1.5526e+04	204	141
8th	4.8177e+03	2.1314e+04	100	193
9th	9.8208e+03	1.1079e+04	204	100
10th	8.0411e+03	2.4238e+04	167	219
11th	8.0220e+03	1.3568e+04	167	123
12th	8.0341e+03	1.4856e+04	167	135
13th	4.8175e+03	1.1045e+04	100	100

In summary, there are two important tuning approaches for the interconnected suspensions. One of them is the type of the suspension configurations and the other is the ratio of the rod area to piston area. By changing the type of the interconnection, different suspension characteristics can be obtained both in the roll and pitch directions. These characteristics change with the connection type (full interconnection or semi-interconnection) and connection direction (pitch plane, roll plane, full). In all interconnections when the ratio of the rod area to piston area is reduced, the stiffness and the damping characteristics of the suspension configurations increase. While designing the suspension, these two design features can be observed.

7.7. COMPARISON OF WARP MOMENT CHARACTERISTICS OF THE INTERCONNECTED HP SUSPENSION SYSTEM

In this section warp moment characteristics are compared. Comparisons are performed first for $A_r=0.6A_p$ and then $A_r=0.8A_p$.

7.7.1. Case 1: $A_r=0.6A_p$

Warp moment for different suspension configurations are given in Figure 7.43.

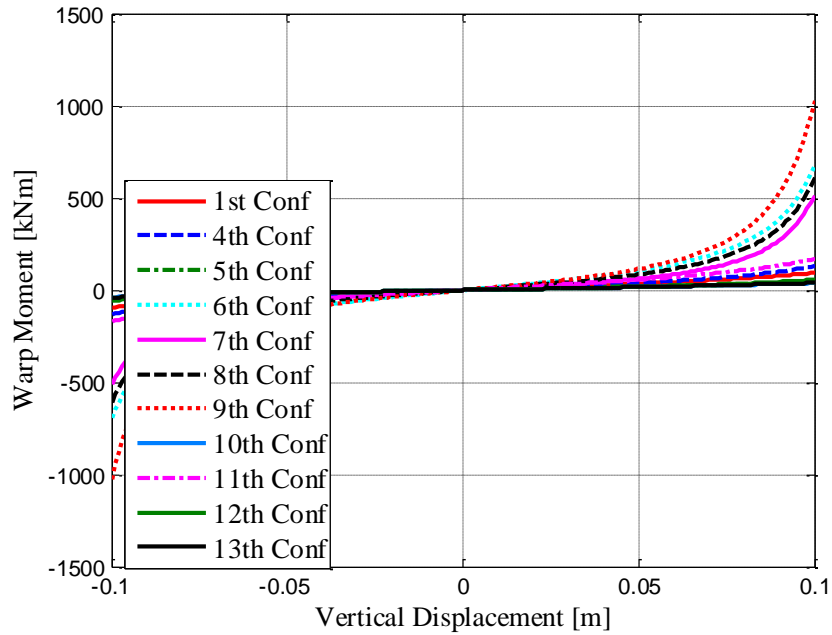


Figure 7.43: Warp Moment of Different Interconnections

Integral values are summarized in Table 7.12.

Table 7.12: Integral of Warp Moment for Different Interconnections

Suspension Conf.	Int Warp Moment	Int Warp Moment [%]
1st	3.9192e+03	220
4th	4.6721e+03	262
5th	2.0111e+03	113
6th	1.5620e+04	876
7th	1.0393e+04	583
8th	1.3385e+04	751
9th	1.9854e+04	1114
10th	1.7659e+03	99
11th	6.4739e+03	363
12th	2.1213e+03	119
13th	1.7830e+03	100

As can be seen from Table 7.12, the fifth, tenth, twelfth, and thirteenth suspension configurations have lower warp moment. However, the sixth and ninth suspension configurations have very high warp moment as compared to other configurations.

7.7.2. Case 2: $A_r=0.8A_p$

Warp moment for different suspension configurations are given in Figure 7.44.

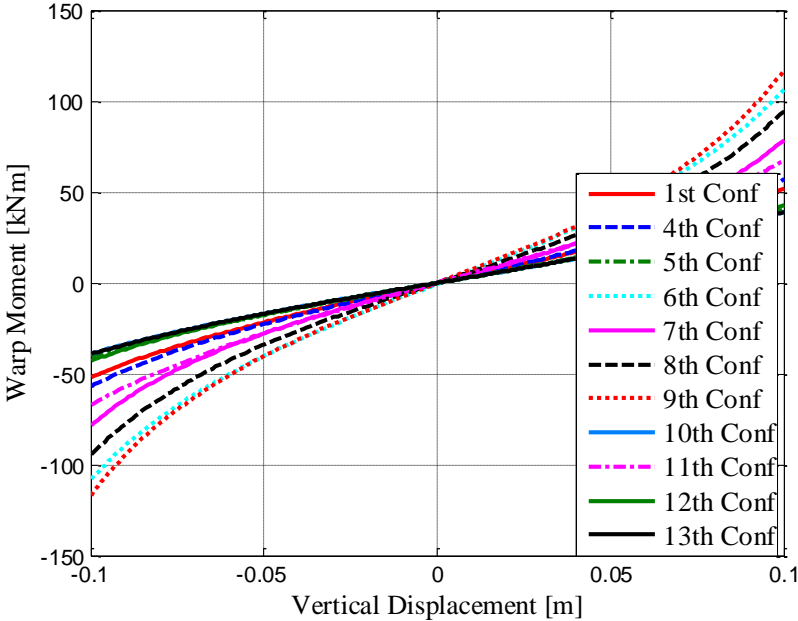


Figure 7.44: Warp Moment of Different Interconnections

The integral values are summarized also in Table 7.13.

Table 7.13: Integral of Warp Moment for Different Interconnections

Suspension Conf.	Int Warp Moment	Int Warp Moment [%]
1st	2.3025e+03	129
4th	2.4492e+03	137
5th	1.8448e+03	103
6th	4.3377e+03	243
7th	3.1314e+03	176
8th	3.8049e+03	213
9th	4.5857e+03	257
10th	1.7745e+03	100
11th	2.9574e+03	166
12th	1.8628e+03	104
13th	1.7830e+03	100

Suspension configurations have somewhat closer warp moment characteristics to each other for the interconnection for $A_r=0.8A_p$, as compared for the suspension configurations for $A_r=0.6A_p$, due to strength of the interconnections.

7.8. COMPARING THE SUSPENSION CONFIGURATIONS FOR ROLL AND PITCH PERFORMANCE

The stiffness and damping characteristics of different interconnections are compared to each other for two different values of the rod to piston area, now they are compared in the view of the combined characteristics. For this reason, a metric for performance of the vehicle is determined. The calculations are to be performed with $A_r=0.8A_p$ and the suspension metric is calculated according to,

$$SM = \frac{w_{PS} \frac{k_{PS}}{k_{PS13th}} + w_{RS} \frac{k_{RS}}{k_{RS13th}} - w_{WM} \frac{k_{WM}}{k_{WM13th}}}{w_{PS} + w_{RS} - w_{WM}} \quad (7-103)$$

where SM is the suspension metric, w_{PS} is the pitch stiffness weighting factor, k_{PS} is the pitch stiffness, w_{RS} is the roll stiffness weighting factor, k_{RS} is the roll stiffness, w_{WM} is the warp moment weighting factor, k_{WM} is the warp moment integral. The applicability of this suspension metric can also be evaluated after the time domain simulations. The SM for different suspension configurations are given in Table 7.14 for the weighting factors, $w_{PS}=0.4$; $w_{RS}=1$, $w_{WM}=0.2$ and for $w_{PS}=0.4$; $w_{RS}=2$, $w_{WM}=0.2$.

Table 7.14: Suspension Metrics of Different Interconnected Configurations

Suspension Conf.	Normalized Values			SM1	SM2
	Pitch Stiffness	Roll Stiffness	Warp Moment		
1 st	190	224	129	228	226
4 th	195	224	137	229	227
5 th	223	224	103	244	235
6 th	123	224	243	187	204
7 th	131	224	176	201	212
8 th	190	100	213	111	106
9 th	100	224	257	177	198
10 th	203	183	100	203	194
11 th	121	179	166	162	170
12 th	142	185	104	184	185
13 th	100	100	100	100	100

While selecting the vehicle suspension weighting metrics, mainly roll and pitch performances are considered. It is known that the handling performance of the vehicle is directly related with the roll angle and thus roll stiffness of the vehicle. Similarly, the braking-traction and the firing performance of the vehicles are related to the pitch stiffness and thus the pitch angle responses. However, since handling is more important for safe driving, in both situations its parameters are high. According to the results, all suspension configurations except, eighth and thirteenth have high suspension metrics.

7.9. SENSITIVITY STUDY: EFFECT OF THE SUSPENSION PARAMETERS ON THE STIFFNESS AND DAMPING CHARACTERISTICS OF THE INTERCONNECTED SUSPENSION SYSTEMS

After the stiffness and the damping characteristic of the interconnected HP suspension system are derived, a sensitivity study is to be performed. With the sensitivity study, effect of the suspension parameters on the stiffness and the damping characteristics are to be examined. The examined suspension parameters are A_p , A_r , V_{30} , A_{maxpos} , A_{maxneg} . To be able to obtain the sensitivity plots, the related parameters are perturbed by 25 % about its nominal value. Sensitivity study is to be performed with the first suspension configurations only.

7.9.1. Stiffness Sensitivity Study

In this part, changes of the vertical, roll, and the pitch stiffness with the suspension parameters which are initial gas pressures, piston area, and the rod area are to be examined.

7.9.1.1. Effect of Piston Area

Changes of the vertical, roll, and the pitch stiffness with piston area are shown in Figure 7.45, Figure 7.46, and Figure 7.47, respectively for $A_r=0.6A_p$. The parameters of the first interconnected suspension configurations derived in previous parts are used to get the nominal stiffness values. Then the piston area is perturbed to 25% lower and upper values from the nominal values and the stiffness are computed.

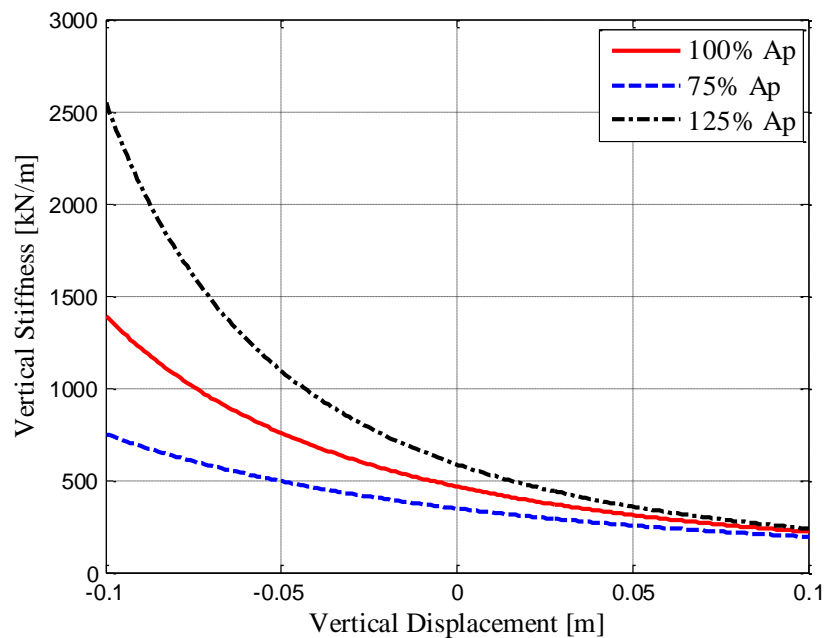


Figure 7.45: Change of the Vertical Stiffness with Piston Area for $A_r=0.6A_p$

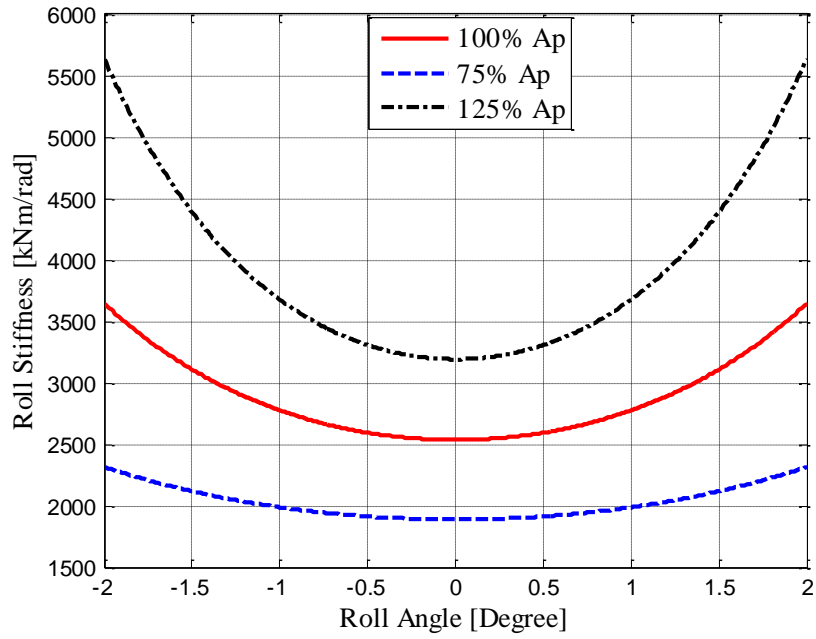


Figure 7.46: Change of the Roll Stiffness with Piston Area for $A_r=0.6A_p$

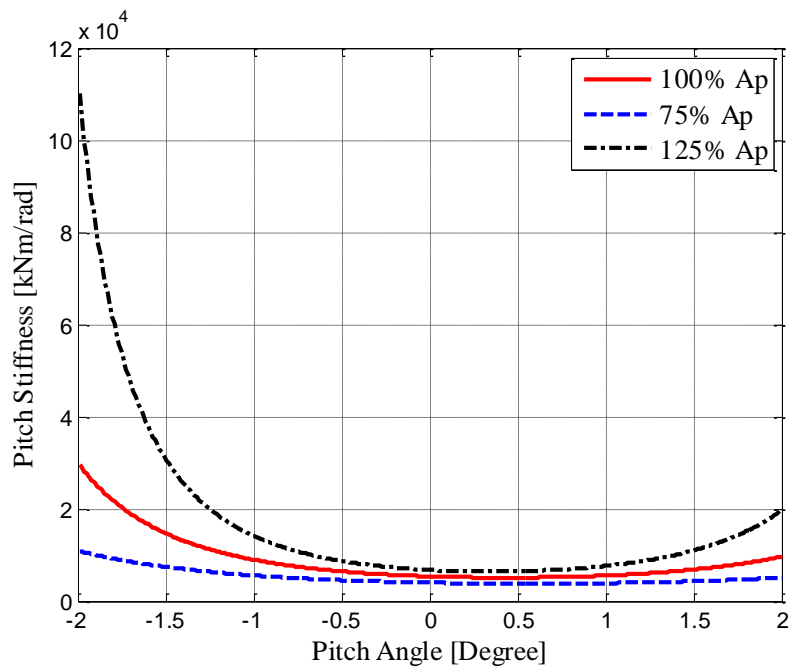


Figure 7.47: Change of the Pitch Stiffness with Piston Area for $A_r=0.6A_p$

As Figure 7.45 to Figure 7.47 shows, when the piston area is increased, vertical, roll, and the pitch stiffness increases.

7.9.1.2. Effect of Initial Gas Volume

Now the changes of the stiffness with the initial gas volumes are obtained. The results are given in Figure 7.48 to Figure 7.50.

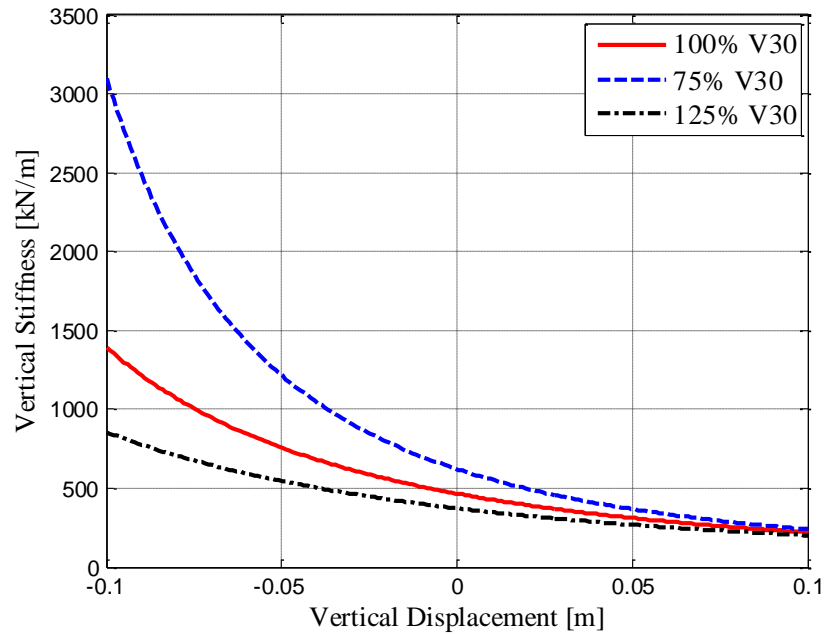


Figure 7.48: Change of the Vertical Stiffness with Initial Gas Volume for $A_r=0.6A_p$

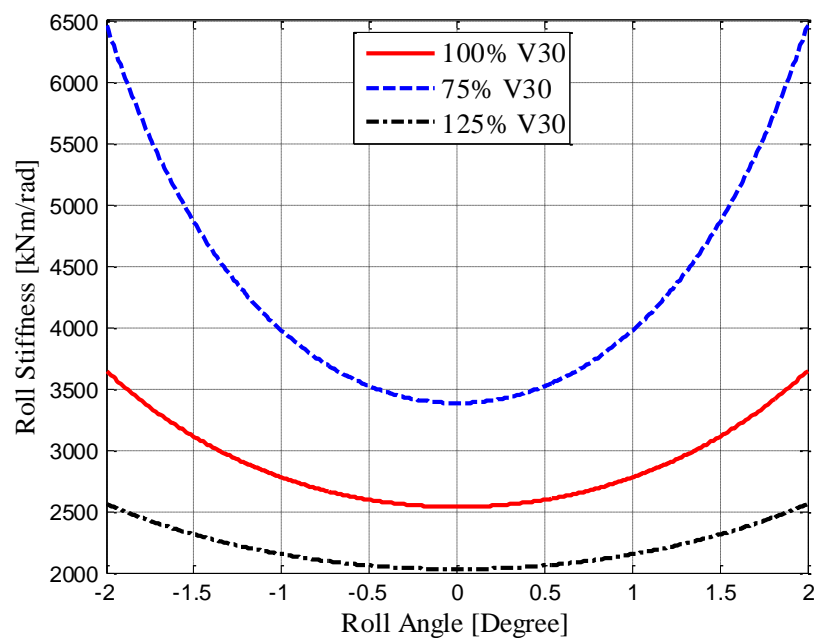


Figure 7.49: Change of the Roll Stiffness with Initial Gas Volume for $A_r=0.6A_p$

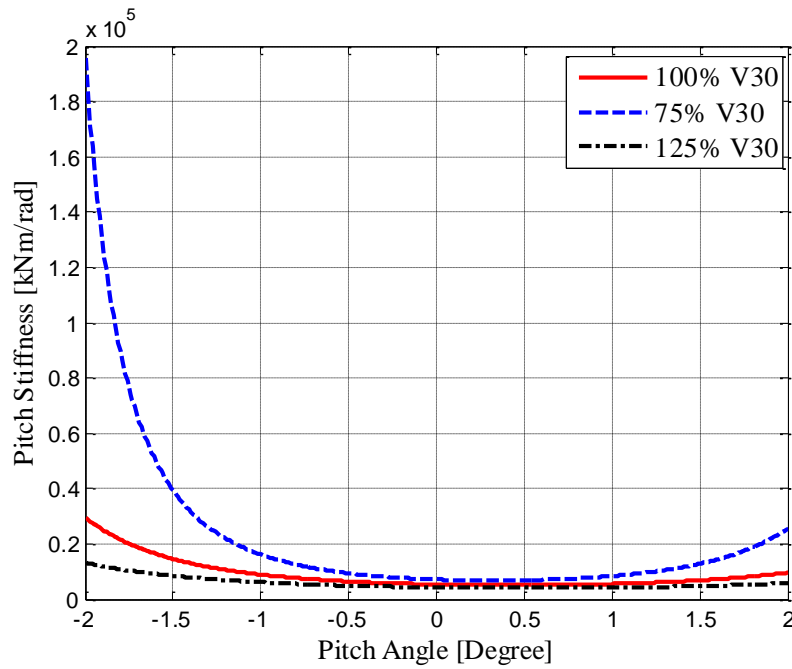


Figure 7.50: Change of the Pitch Stiffness with Initial Gas Volume for $A_r=0.6A_p$

As can be seen from Figure 7.48 to Figure 7.50, when the initial gas volumes of the suspension configuration are decreased, vertical, roll, and the pitch stiffness increases and when the initial gas volumes are increased, vertical, roll, and the pitch stiffness decrease.

7.9.1.3. Effect of Piston Rod Area

While calculating the sensitivities of the vertical, roll, and the pitch stiffness with the piston rod area, parameters of the unconnected suspension configuration are used as the nominal parameter set. Then the piston rod area is lowered to $0.8A_p$ and $0.6A_p$ to see the effect of the interconnection on the stiffness characteristics. When the unconnected suspension configuration is connected to get the first suspension configurations with the same nominal parameters, stiffness values change and completely different suspension characteristics are obtained. Results are given in Figure 7.51 to Figure 7.53.

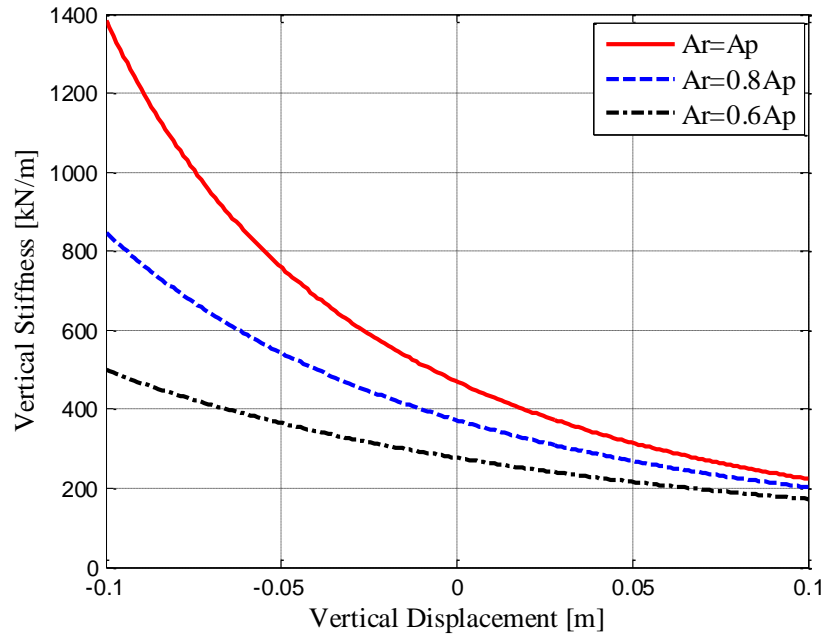


Figure 7.51: Change of the Vertical Stiffness with Rod Area

In previous parts, it was stated that when the unconnected suspension configurations are converted into interconnected suspension configurations, completely different suspension characteristics are obtained. Figure 7.51 shows that unconnected suspension configurations have the highest vertical stiffness when all parameters are kept constant. When the unconnected suspension configuration is changed into interconnected suspension configuration, vertical stiffness of the suspension decreases. This is due to fact that, in the interconnected suspension configurations, the effective piston area is lower as compared with the effective piston area of the unconnected suspension configurations. Therefore, similar result is obtained as given in Figure 7.45. Moreover when the strength of the interconnection is increased, the vertical suspension stiffness further decreases. The reason for getting lower initial gas volumes for the interconnected suspension configurations with respect to unconnected HP suspension configuration in order to equalize the vertical stiffness of unconnected and interconnected suspension configurations is the effective piston area. In order to get rid of the stiffness decrease due to decreasing effective piston area, initial gas volumes are decreased and stiffness increases. In final situation, vertical stiffness remains the same. However, the interconnection results in higher

roll and pitch stiffness as can be seen from Figure 7.52 and Figure 7.53. In other words, interconnected suspension results in lower vertical stiffness. This results in pitch and roll stiffness decrement. However, it is explained before that interconnection increases roll and pitch stiffness. Thus the overall effect is rises of the roll and pitch stiffness.

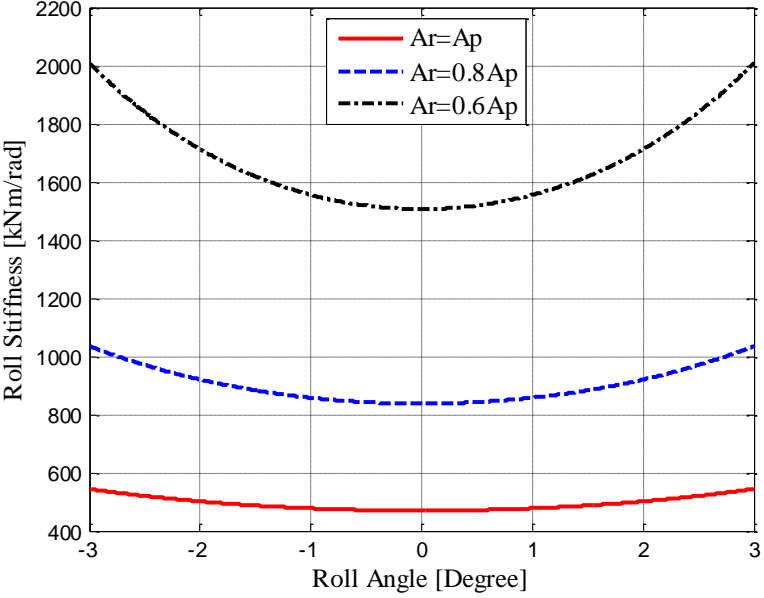


Figure 7.52: Change of the Roll Stiffness with Rod Area

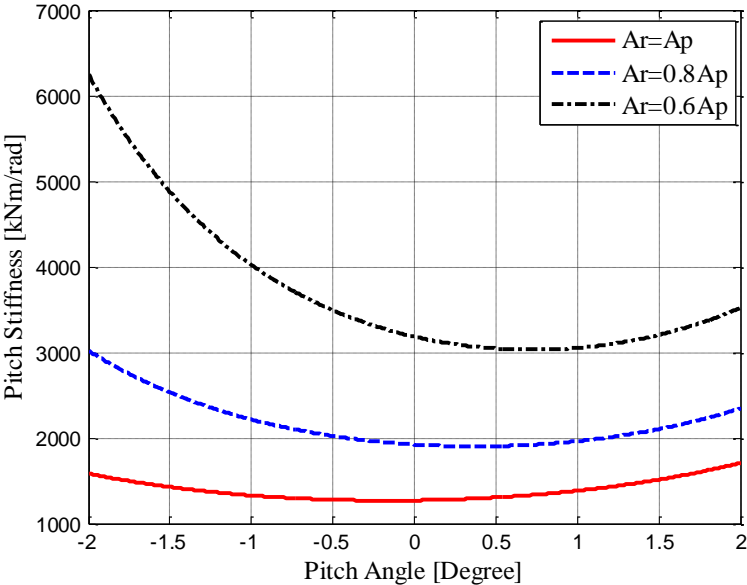


Figure 7.53: Change of the Pitch Stiffness with Rod Area

7.9.2. Damping Sensitivity Study

Now the changes of the vertical, roll, and the pitch damping of the interconnected suspension configurations with the maximum valve opening, piston area, and the rod area are to be found. For the sensitivity study with the maximum valve opening and the piston area, the nominal parameters of the first interconnection suspension configurations are used. However, for the sensitivity study with the rod area, parameters of the unconnected suspension configurations are used to see the effect of the interconnection on the damping characteristics of the suspension.

7.9.2.1. Effect of Maximum Valve Opening

Change of the damping characteristics with the maximum valve openings are shown in Figure 7.54 to Figure 7.56.

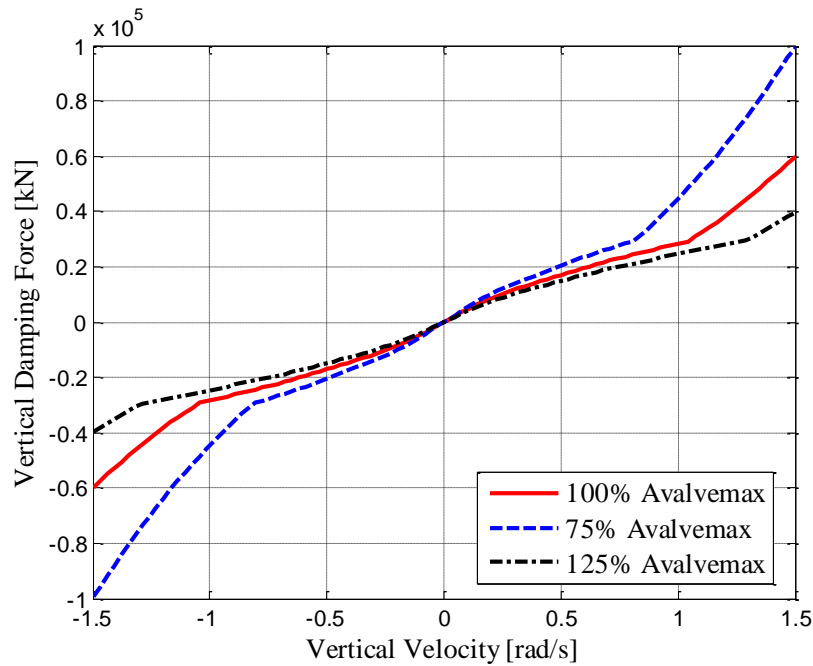


Figure 7.54: Change of the Vertical Damping with Maximum Valve Opening

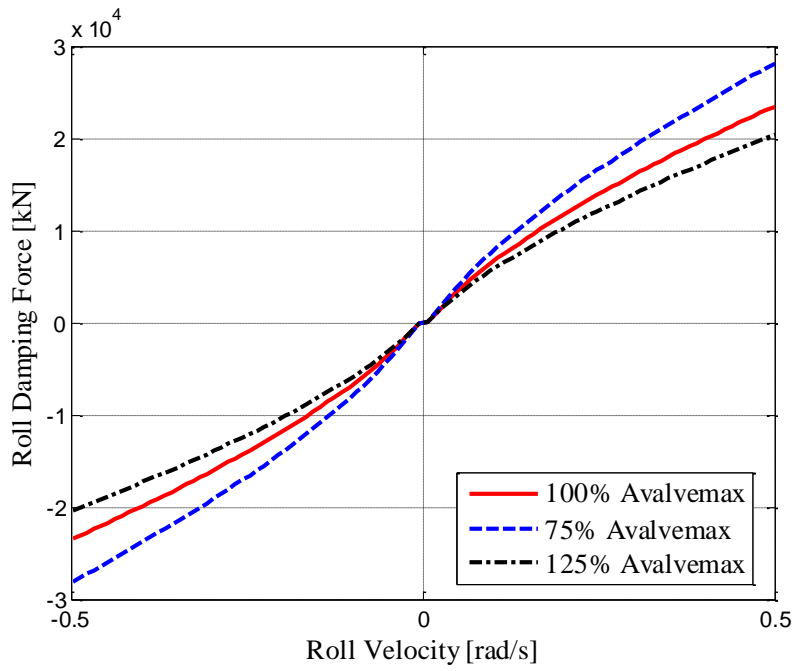


Figure 7.55: Change of the Roll Damping with Maximum Valve Opening

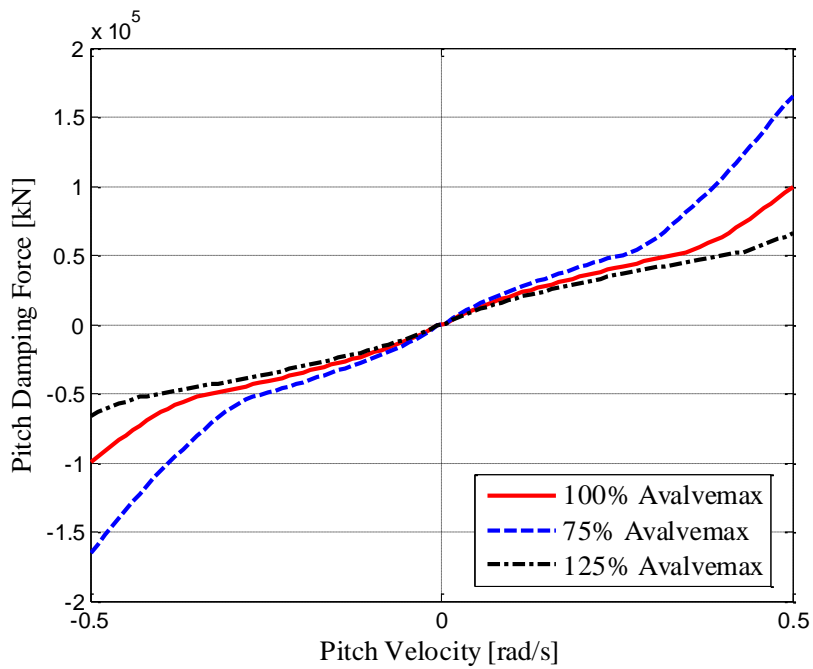


Figure 7.56: Change of the Pitch Damping with Maximum Valve Opening

As Figure 7.54 to Figure 7.56 illustrate, when the maximum valve opening is decreased, vertical, roll, and pitch damping increase.

7.9.2.2. Effect of Piston Area

Change of the damping characteristic with the piston area is shown in Figure 7.57 to Figure 7.59.

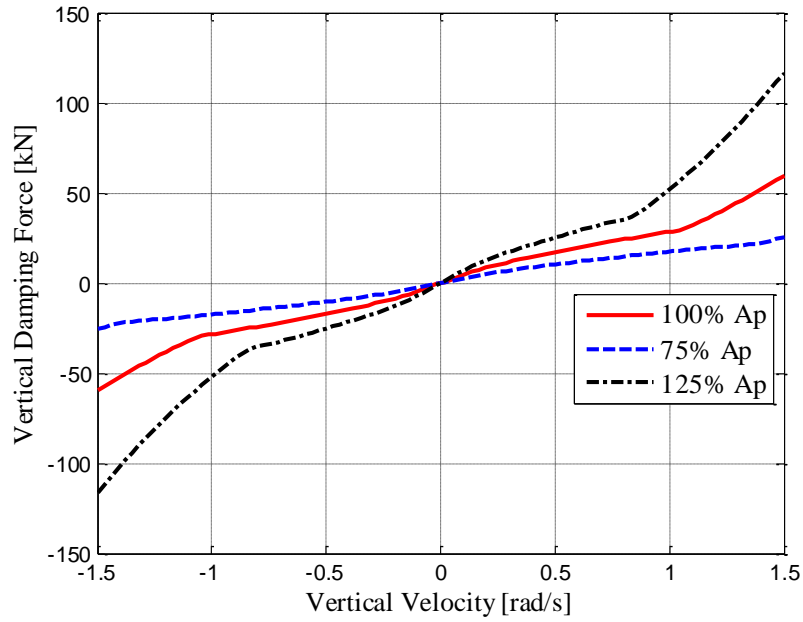


Figure 7.57: Change of the Vertical Damping with Piston Area

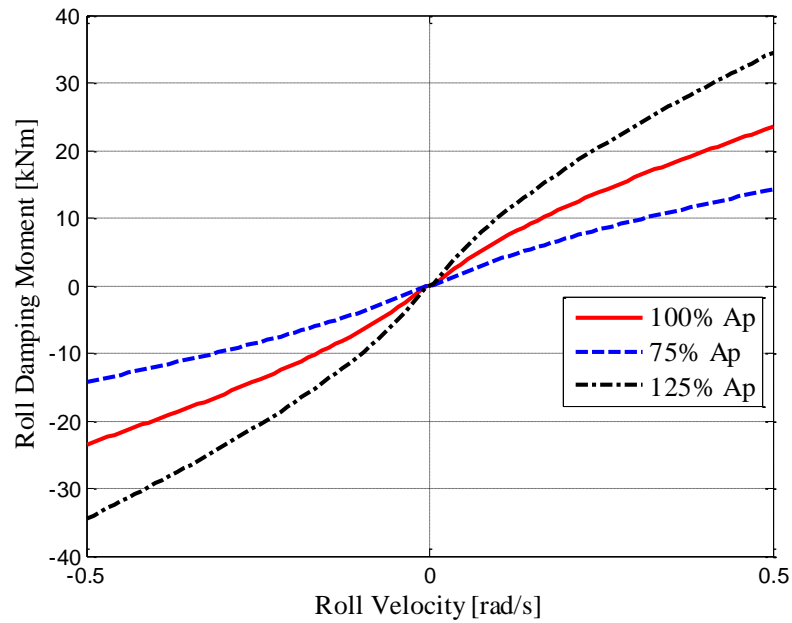


Figure 7.58: Change of the Roll Damping with Piston Area

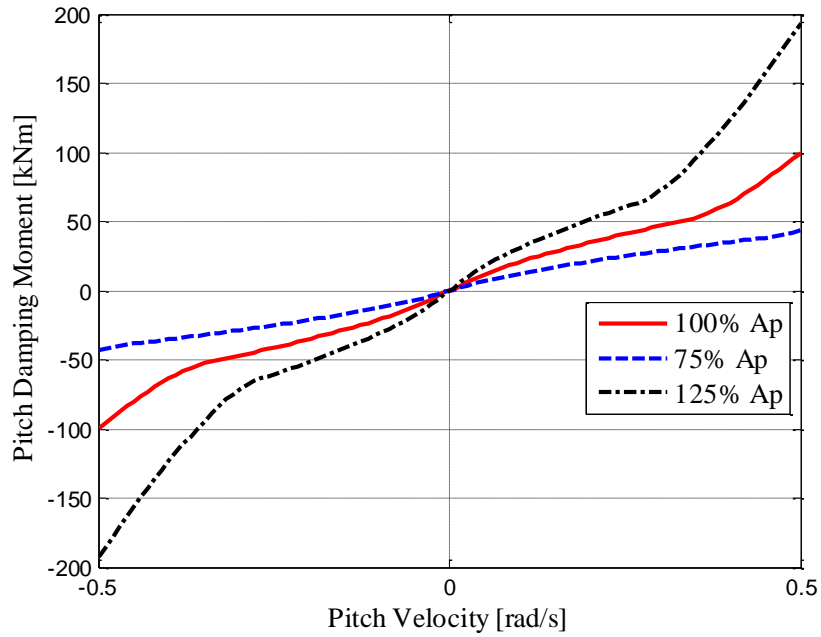


Figure 7.59: Change of the Pitch Damping with Piston Area

When the piston area increases, the amount of the oil passing through the orifice also increases which results in increased damping force and moment.

7.9.2.3. Effect of Rod Area

Change of the damping characteristics with the rod area are shown in Figure 7.60 to Figure 7.62. While calculating the damping characteristics, nominal parameters of the unconnected HP suspension system are used. Then the rod area is lowered to $A_r=0.8A_p$ and $A_r=0.6 A_p$ to examine the effect of the interconnection on the damping characteristics.

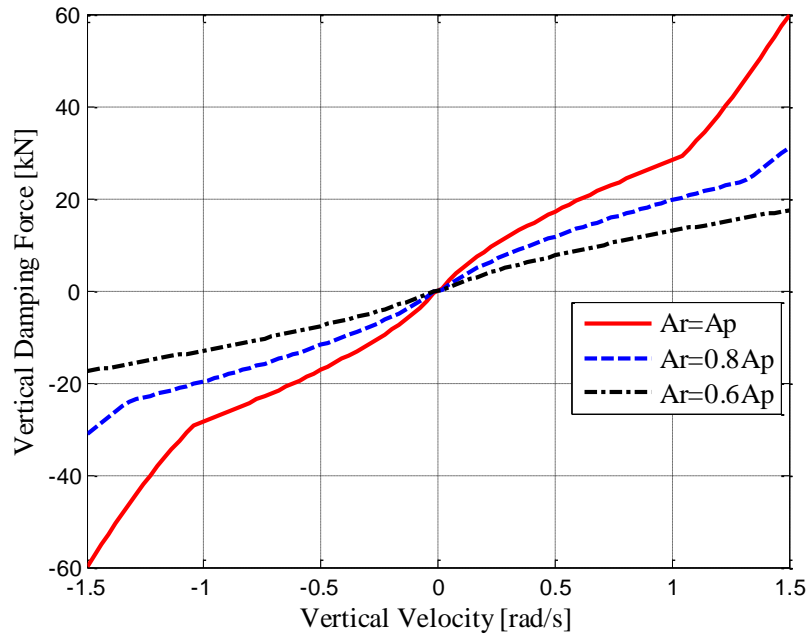


Figure 7.60: Change of the Vertical Damping with Rod Area

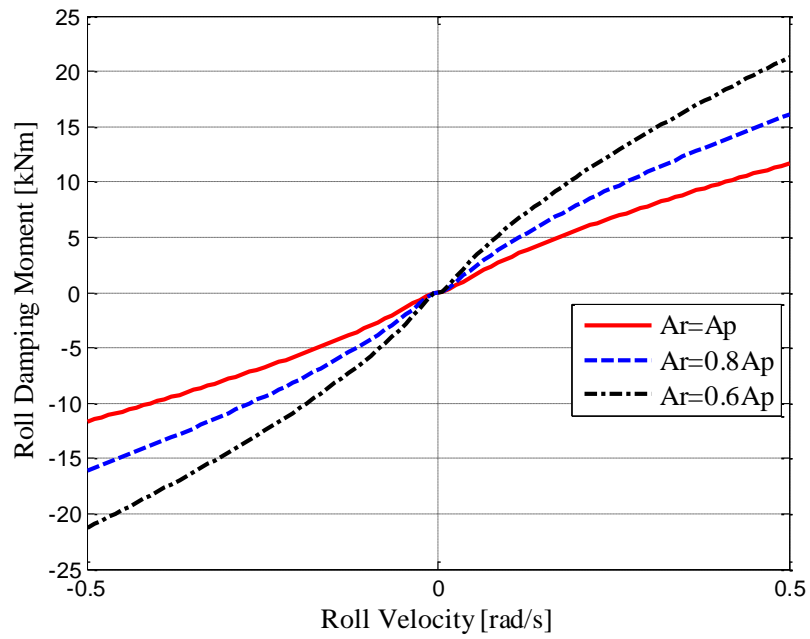


Figure 7.61: Change of the Roll Damping with Rod Area

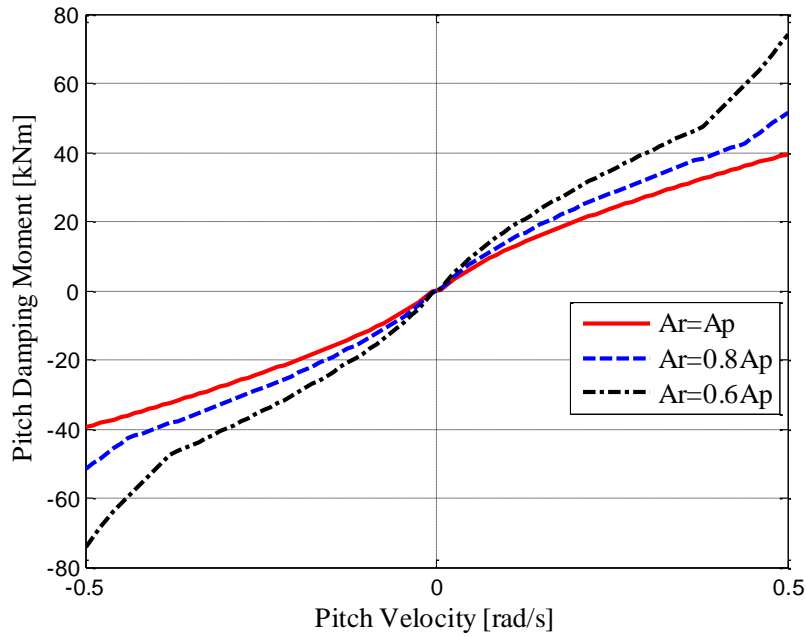


Figure 7.62: Change of the Pitch Damping with Rod Area

As Figure 7.60 illustrates, when the suspension configuration is changed from unconnected to interconnected, effective piston area decreases. A decrease in effective piston area causes a decrease in vertical damping force as can be seen Figure 7.57. However, interconnected suspension configuration results in an increase in roll and pitch damping moments; the overall effect is the increase in roll and pitch damping. In other words, a decrease in effective piston area due to interconnection results in a decrement in roll and pitch damping. However, the interconnection itself causes roll and pitch damping to increase. The overall effect is the increase of roll and pitch damping.

7.10. SIMULATIONS

In this part, the performances of the suspension configurations are evaluated with simulations. First ride comfort characteristics, and then the handling performance of the vehicle with three axles are examined.

7.10.1. Ride Comfort Simulations

In this part, the ride comfort performance of a vehicle with three axles is going to be evaluated with random road displacement inputs same as those used in section 4.2.4.1 at different vehicle longitudinal speed. rms values of the responses are given in Table 7.15 to Table 7.18.

Table 7.15: rms Values for Random Road Simulation at 60 kph Longitudinal Velocity

	$A_r=0.6A_p$	$A_r=0.8A_p$	Unconnected
Vertical Acceleration [m/s²]	0.21	0.21	0.22
Pitch Acceleration [rad/s²]	0.18	0.14	0.12
Roll Acceleration [rad/s²]	0.26	0.25	0.26

Table 7.16: rms Values for Random Road Simulation at 70 kph Longitudinal Velocity

	$A_r=0.6A_p$	$A_r=0.8A_p$	Unconnected
Vertical Acceleration [m/s²]	0.25	0.25	0.28
Pitch Acceleration [rad/s²]	0.26	0.19	0.16
Roll Acceleration [rad/s²]	0.40	0.41	0.45

Table 7.17: rms Values for Random Road Simulation at 80 kph Longitudinal Velocity

	$A_r=0.6A_p$	$A_r=0.8A_p$	Unconnected
Vertical Acceleration [m/s²]	0.35	0.36	0.38
Pitch Acceleration [rad/s²]	0.37	0.28	0.20
Roll Acceleration [rad/s²]	0.63	0.59	0.54

Table 7.18: rms Values for Random Road Simulation at 90 kph Longitudinal Velocity

	$A_r=0.6A_p$	$A_r=0.8A_p$	Unconnected
Vertical Acceleration [m/s²]	0.41	0.42	0.44
Pitch Acceleration [rad/s²]	0.54	0.32	0.22
Roll Acceleration [rad/s²]	0.98	0.79	0.63

As can be seen from Table 7.15 to Table 7.18, the vertical accelerations of the interconnected and the unconnected suspensions are close to each other. This is due

to the fact that the interconnected and the unconnected suspension configurations have equivalent vertical stiffness and damping characteristics. However, since interconnected HP suspension configurations have higher pitch and roll stiffness and damping, the roll and pitch accelerations of the interconnected HP suspension system are higher than those of the unconnected suspension. In conclusion, the interconnected suspension systems have the same vertical ride comfort performance with the unconnected suspension systems, yet they have slightly degraded ride comfort performances in roll and pitch directions.

7.10.2. Vehicle Handling Simulation

Since, the interconnected HP suspension system is fully modeled both in the roll and pitch planes, the simulations exciting both roll and pitch dynamics of vehicle is necessary. Braking in turn simulations are performed to evaluate the handling properties of the interconnected HP suspension system. As proposed in the study of Cao [19], braking force is to be applied in proportion to the static tire load. Only front wheels are steered in cornering. The braking torques and the steering inputs are shown in Figure 7.63 and Figure 7.64, respectively.

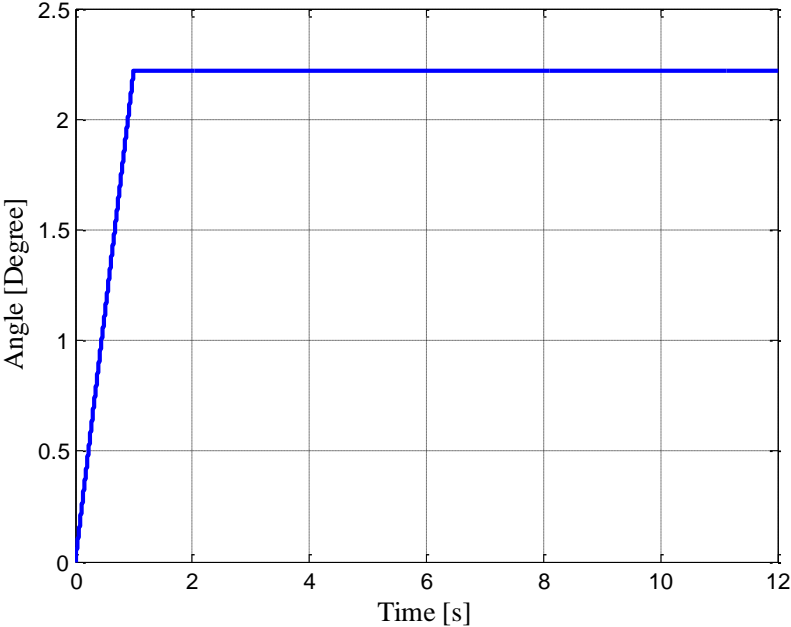


Figure 7.63: Steering Input

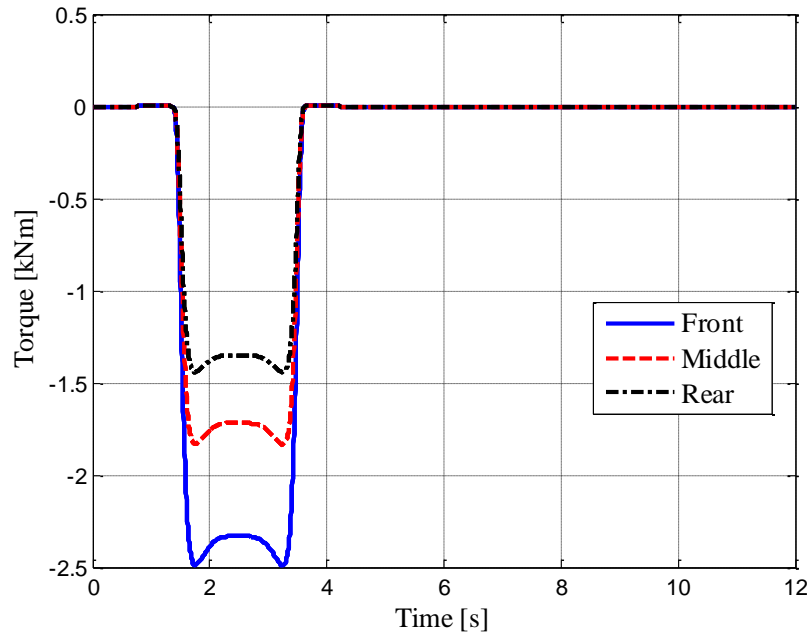


Figure 7.64: Braking Input

One of the important considerations while determining the tire parameter for the vehicle is the stability concern. If the tire cornering stiffness and the vehicle parameters are not selected appropriately, unstable vehicle behavior can be observed. This prevents the evaluation of the vehicle handling performance. For a vehicle with two axles, handling stability has been well studied in literature. There are some studies which examine the vehicle handling for three axle vehicles [80]-[81]. According to these studies, cornering stiffness values can be selected for a stable vehicle. After that, simulations are performed. Simulation results are given in Figure 7.65 to Figure 7.73.

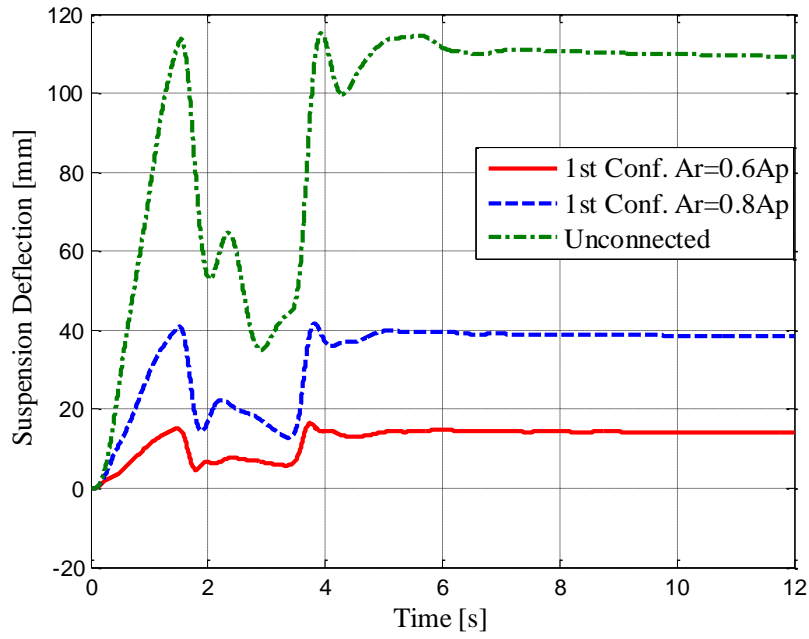


Figure 7.65: Front Left Suspension Deflection

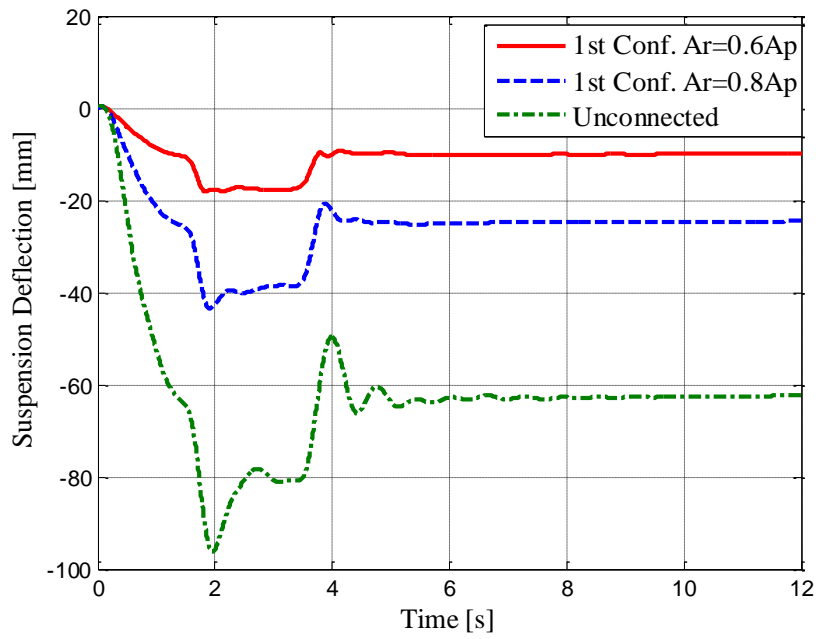


Figure 7.66: Front Right Suspension Deflection

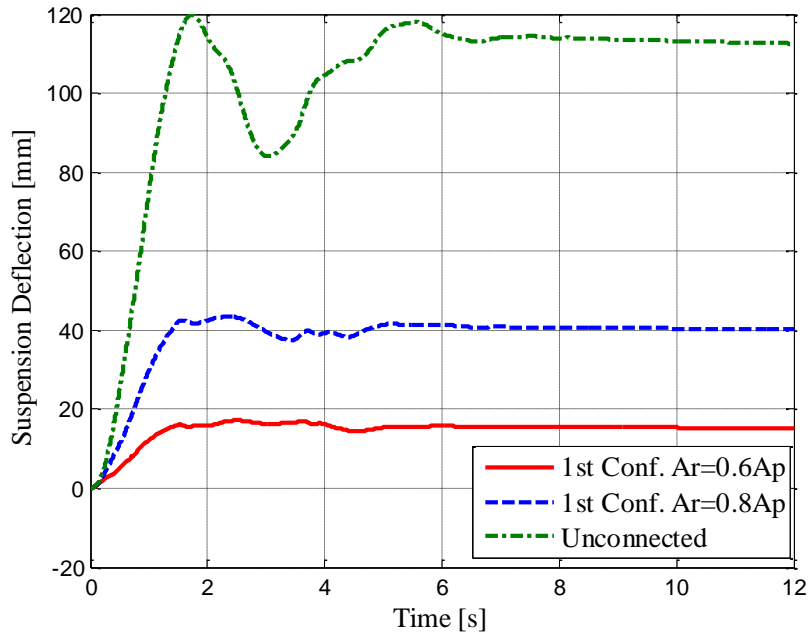


Figure 7.67: Intermediate Left Suspension Deflection

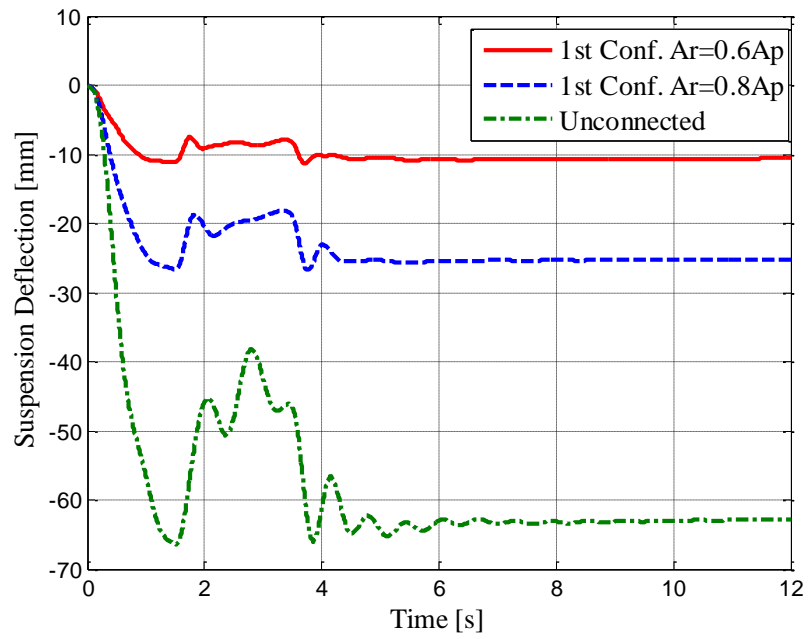


Figure 7.68: Intermediate Right Suspension Deflection

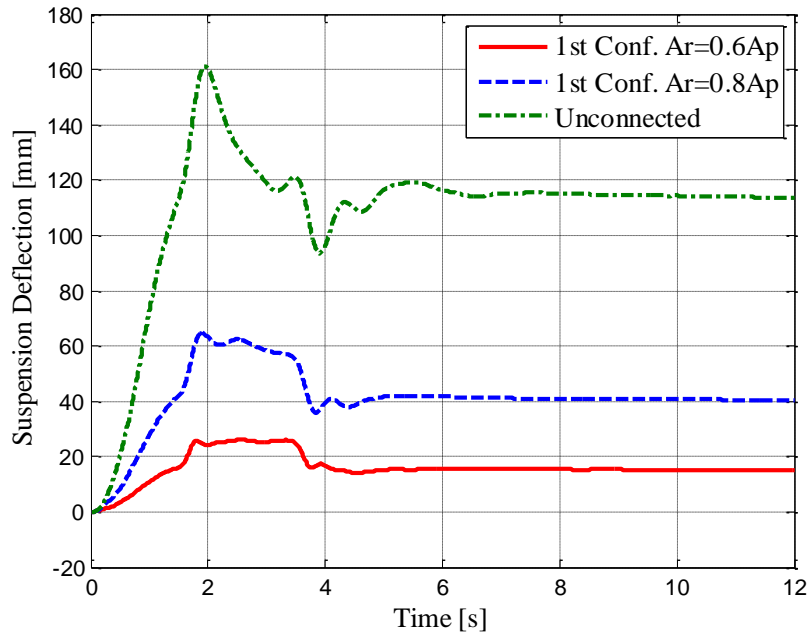


Figure 7.69: Rear Left Suspension Deflection

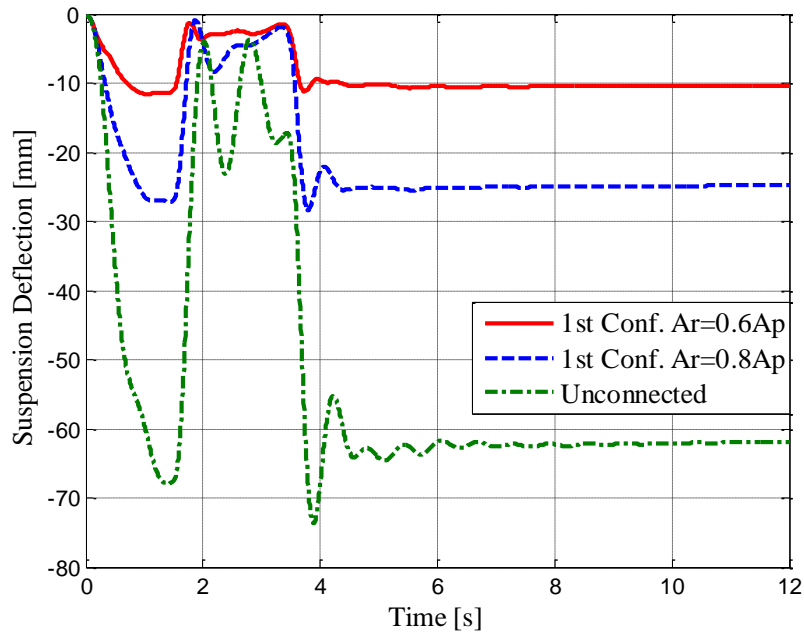


Figure 7.70: Rear Right Suspension Deflection

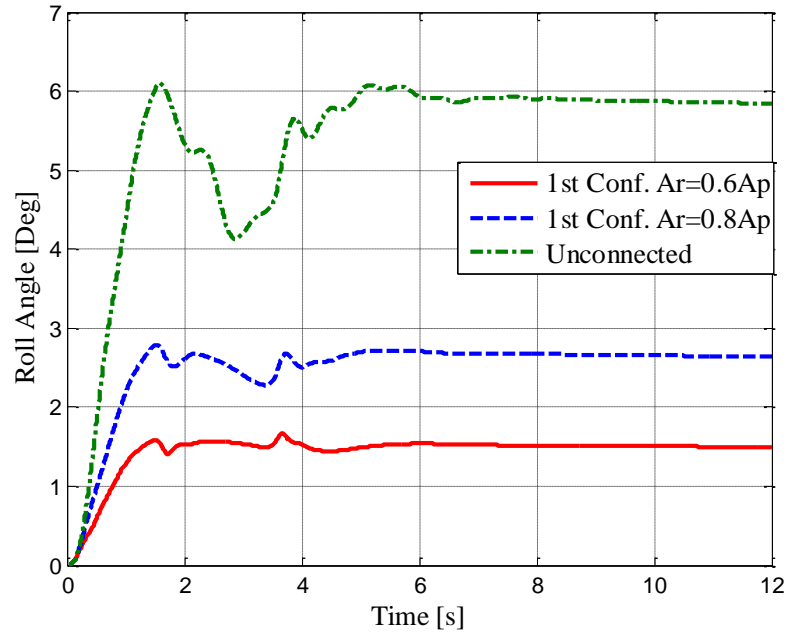


Figure 7.71: Roll Angle

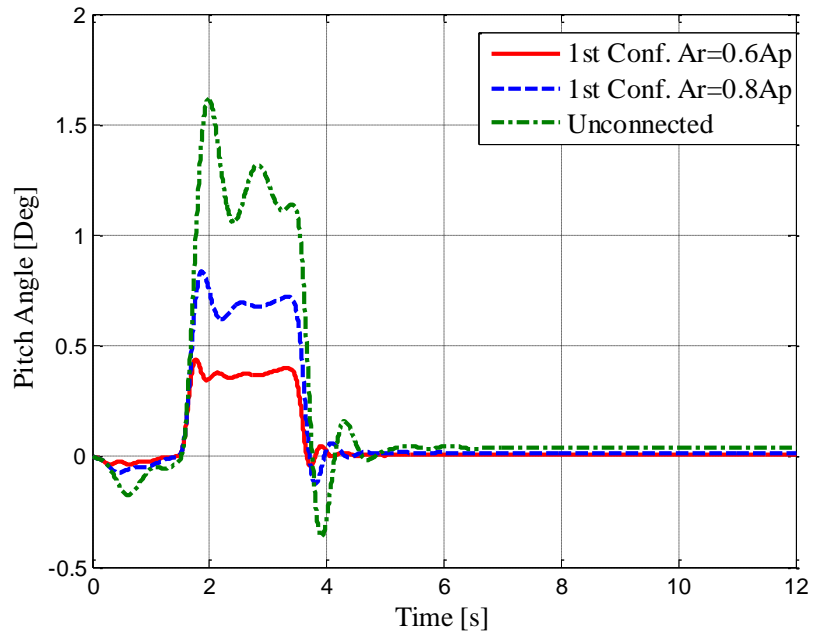


Figure 7.72: Pitch Angle

As can be seen from Figure 7.71, vehicle with the unconnected HP suspension system has the highest roll angle and the vehicle with interconnected HP suspension

system has the lower roll angle response. When the strength of the interconnection is increased, roll angle decreases further. The interconnected HP suspension system also improves the vehicle pitch performance by decreasing the pitch angle as can be seen from Figure 7.72.

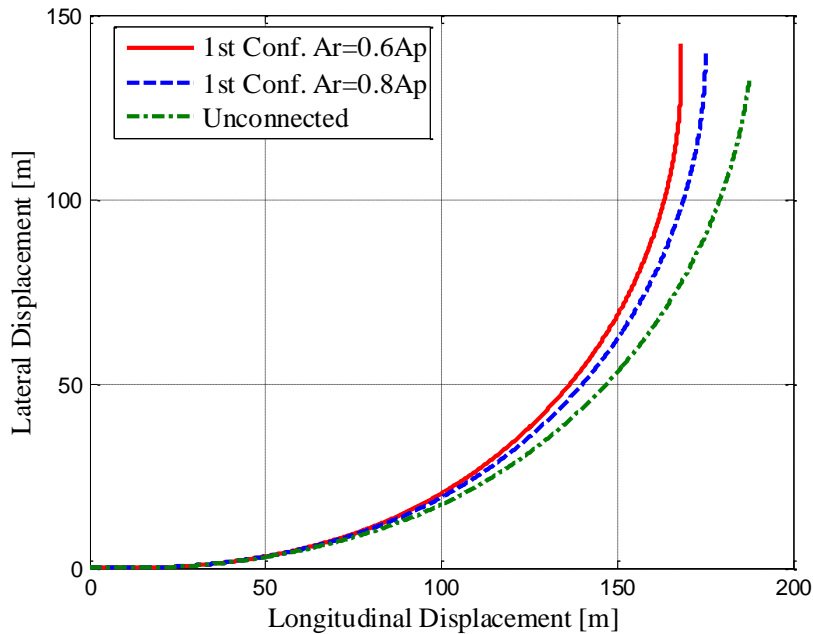


Figure 7.73: Trajectory of the Vehicle

Finally, the effect of the interconnected suspension on vehicle handling is examined by the vehicle path. Figure 7.73 shows the longitudinal and lateral displacement of the vehicle. As can be seen from Figure 7.73, vehicle with the interconnected HP suspension system follows a trajectory with a higher curvature on the road. In other words, the vehicle with the interconnected HP suspension system curves more rapidly than the vehicle with unconnected suspension configurations.

7.10.3. Firing Shock Simulation

Finally, the firing performance of the vehicle with fully interconnected HP suspension system is to be examined. Firing performance of vehicles is related to the roll and pitch angle caused by the firing shock and also the settling time of the roll and pitch angles. In order to fire more bullets during unit time period, vehicle should reach the steady state conditions in minimum time. The simulation is performed with

the firing shock force given in Figure 7.74. The elevation angle of the gun is 20 degrees and the azimuth angle of the gun is 30 degrees. Simulation results are given in Figure 7.75 to Figure 7.82. As can be seen from the simulation results, maximum values and the settling time of the vehicle with the interconnected HP suspension system is better with respect to settling time and maximum values of the vehicle with the unconnected HP suspension system.

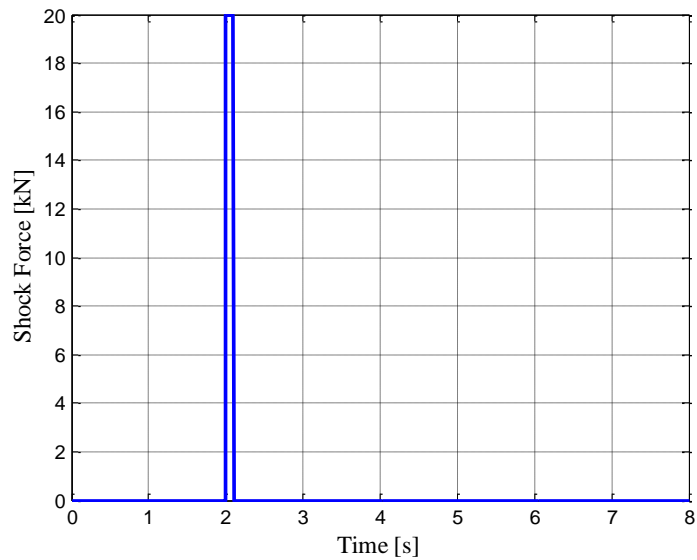


Figure 7.74: Firing Shock Force

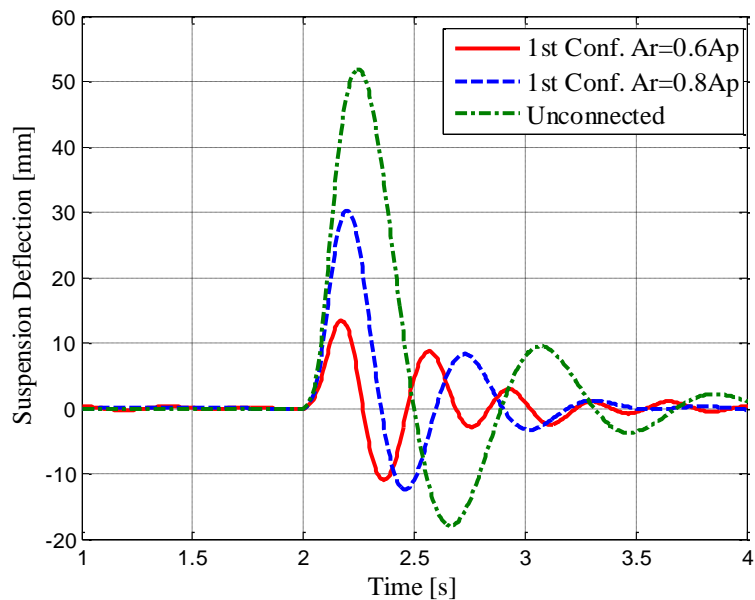


Figure 7.75: Front Left Suspension Deflection

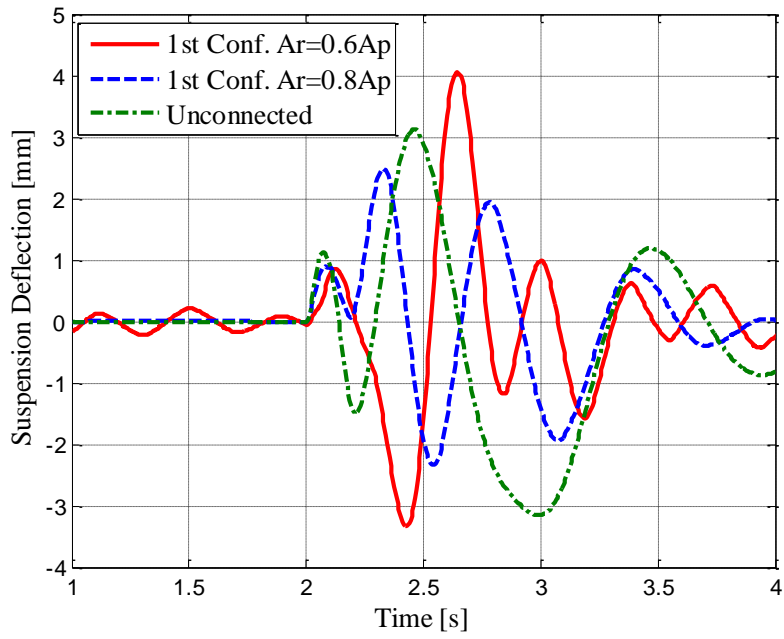


Figure 7.76: Front Right Suspension Deflection

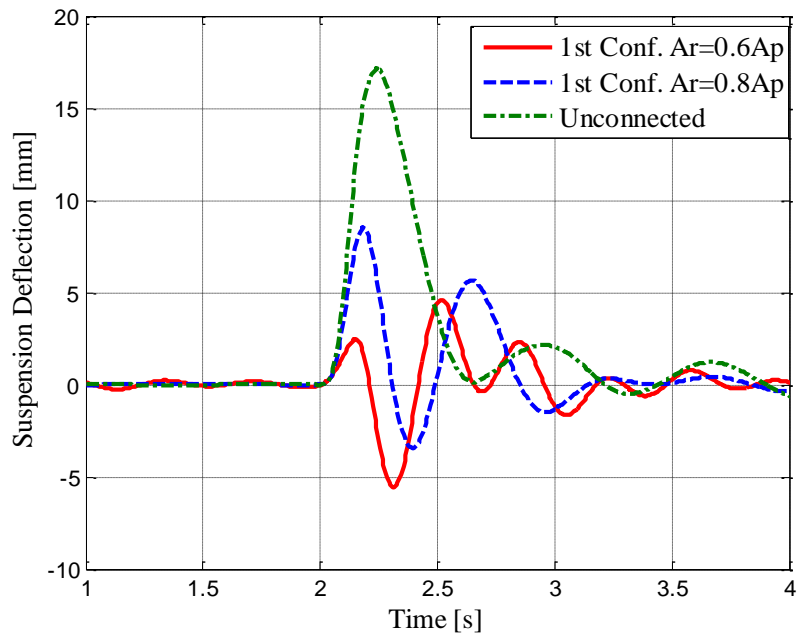


Figure 7.77: Intermediate Left Suspension Deflection

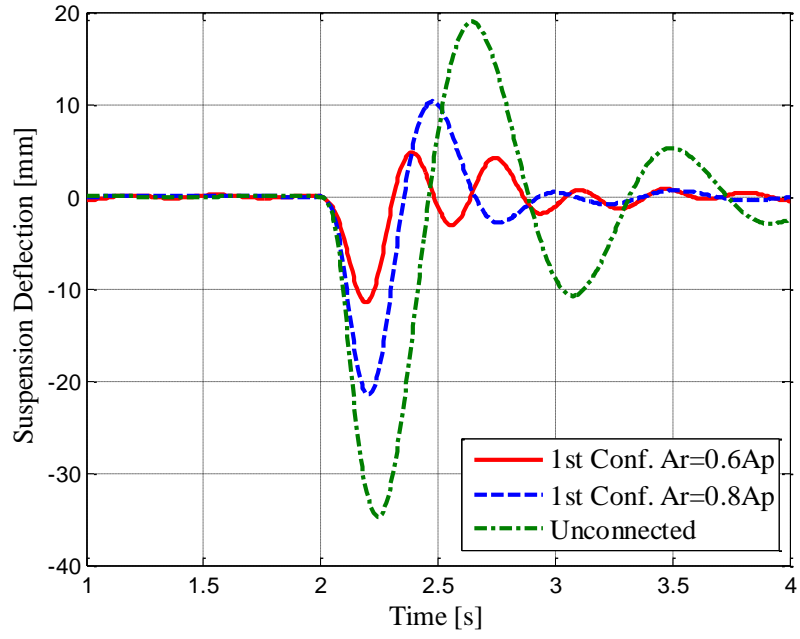


Figure 7.78: Intermediate Right Suspension Deflection

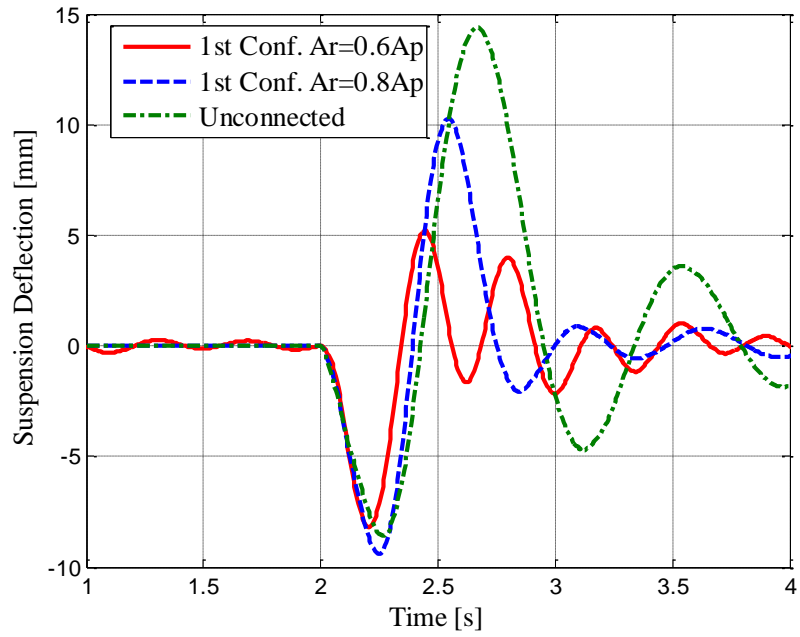


Figure 7.79: Rear Left Suspension Deflection

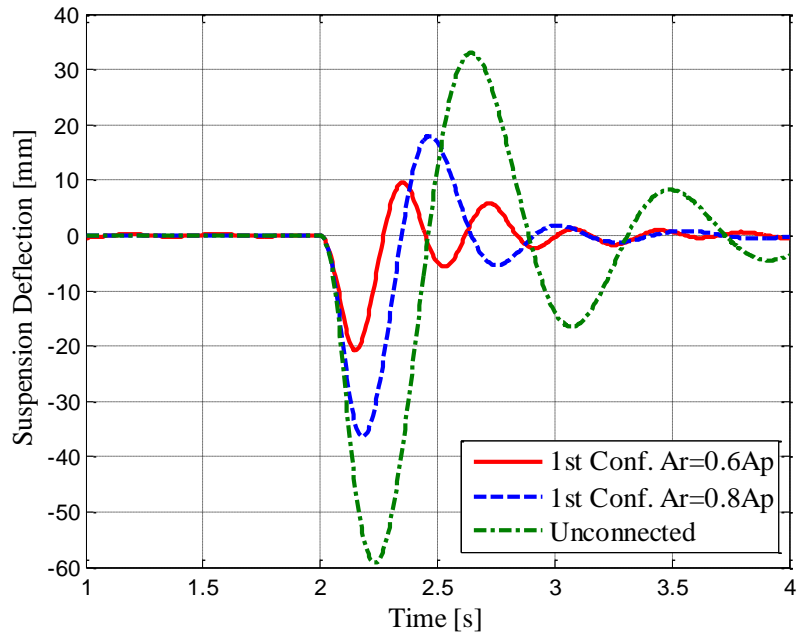


Figure 7.80: Rear Right Suspension Deflection

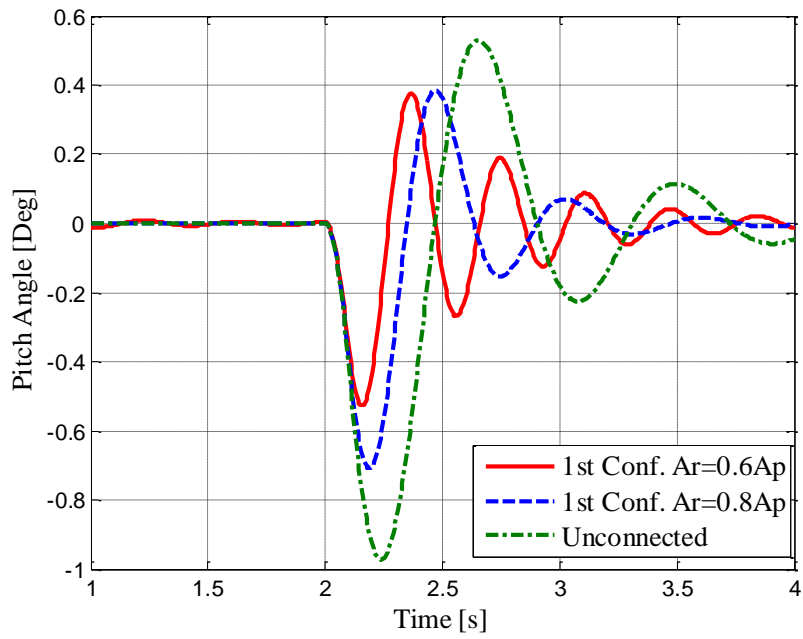


Figure 7.81: Pitch Angle

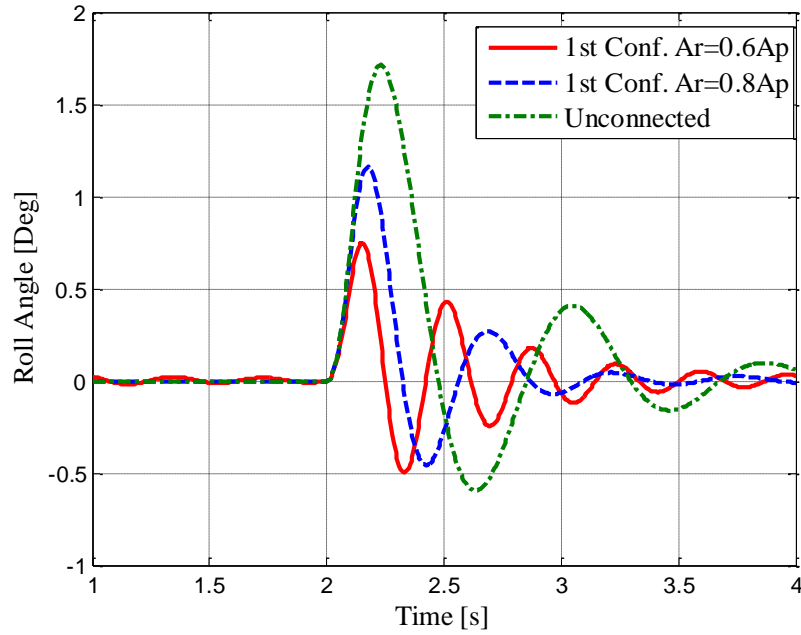


Figure 7.82: Roll Angle

7.11. CONCLUSION

In this chapter the design and analysis of the full vehicle model with different interconnected HP suspension systems have been studied. The interconnected HP suspension system constitutes roll, pitch, and roll and pitch interconnection with different configurations. To be able to make a reasonable comparison among the interconnected HP suspension system, the vertical stiffness and damping characteristics have been equalized by optimizing the initial gas volumes and damping valve parameters. Then the stiffness and damping characteristics of the interconnected HP suspension system have been compared in the vertical, roll, and pitch directions. According to the results, when the suspension is fully interconnected in coupled roll and pitch directions, the roll and pitch characteristic values are increased. When it is semi-interconnected in coupled roll and pitch directions, a somewhat lower roll and pitch stiffness and damping characteristics have been obtained with respect to fully interconnected HP suspension system. However, fully interconnected HP suspension system in either roll or in pitch directions have high stiffness and damping only in the roll or pitch directions. The stiffness and damping

characteristics of the pure roll or pure pitch interconnections are similar to stiffness and damping characteristics of the unconnected suspension. After the stiffness and damping characteristics of the HP suspension system have been examined a detailed sensitivity analysis have been performed. Change of the vertical, roll, and pitch stiffness and damping characteristics with respect to suspension design parameters which are initial gas volumes, piston area, rod area, and damping valve parameters have been studied. In sensitivity study, the nominal parameters of the first interconnected HP suspension system have been used. According to the result, when the initial gas volumes are reduced, vertical, roll, and pitch stiffness increases. Moreover, when the piston area increases, stiffness characteristics of the suspension increase. Finally, the effect of the piston rod area which resembles the strength of the interconnection has been investigated. When the unconnected suspension configurations are converted into interconnected suspension configurations, vertical stiffness decreases, however the roll and pitch stiffness increase. This result is important characteristic of the interconnected HP suspension system and will be used in the optimization studies. After the stiffness sensitivity analysis has been completed, damping sensitivity analysis has been performed. As expected, when the valve opening areas are decreased, vertical, roll, and pitch damping increases. Also an increase in piston area increases the damping characteristics. Finally, when the rod area is increased vertical damping decreases yet roll and pitch damping increases. After sensitivity study, the performance of the vehicle with fully interconnected HP suspension system has been examined by the simulations. For this reason a 18 dof full vehicle model with combined lateral and longitudinal Magic Formula tire model is derived. To examine the ride comfort performance, simulations with random road displacement input at different longitudinal velocities have been performed. According to the results, interconnection does not affect vertical ride comfort, yet it results in a slight roll and pitch ride comfort degradation. Handling performance of the interconnected HP suspension system has been examined by braking in cornering maneuver simulations. The results show that the interconnected HP suspension system reduces the roll angle considerably. The firing shock performance of the HP suspension system has also been examined by the firing shock simulation. The

results show that the vehicle with the interconnected HP suspension system comes to steady state in shorter time and with lower maximum response values.

As a conclusion, for a multi-axle vehicle, considerable performance improvement can be obtained by fully roll and pitch coupled HP suspension systems by properly tuning the design parameters of the suspension.

CHAPTER 8

DESIGN OF THE PITCH INTERCONNECTED HP SUSPENSION SYSTEM FOR MULTI-AXLE VEHICLE

In this chapter, the roll and pitch interconnection for multi-axle vehicles is going to be examined. For a vehicle with four and more axles, there are many different multi-axle interconnections. These interconnections are explained according to the results of the previous chapter. Then a guideline for the design of the interconnected HP suspension system for multi-axle vehicles is presented.

8.1. INTRODUCTION

For a vehicle with three axles, the possible interconnections were classified as full interconnections and semi-interconnections. In full interconnections, first and fourth volumes of each suspension units are connected to each other. In semi-interconnections first and fourth oil volumes of only two suspension units are interconnected to each other. According to the results obtained, full and semi-interconnections result in suspension configurations which have the highest pitch stiffness. However, for a vehicle with four and more axles, there are many more possible interconnections which may improve roll and pitch performance of the vehicle. These interconnections can be enumerated as done in the previous chapters. Again X coupled interconnections between different axles of the vehicle can be tried in coupled roll and pitch plane of the vehicle. As shown in the previous chapters, in general fully interconnected HP suspension system improves the roll and/or pitch

performances in the plane of connection (or connections). In Chapter 7, it was shown that a full interconnection purely in the roll plane improves the performance of the vehicle only in the vehicle roll plane. However, in the pitch plane, its performance is exactly the same as the performance of the unconnected suspension. Similarly, a fully interconnected HP suspension system in the pure pitch plane of the vehicle improves the pitch performance, yet it has low performance in the roll plane, identical to the roll performance of the unconnected HP suspension system. Moreover, in the roll plane, closely equivalent roll stiffness and the damping characteristics are obtained according to the type of the interconnections which are unconnected, semi-interconnected, and full-interconnected. In other words, all fully interconnected HP suspension systems in the roll plane have similar dynamic characteristic and all semi-interconnected HP suspension systems have similar dynamic characteristics. However, in the pitch plane of the vehicle, according to the type of the interconnections both for the full or semi-interconnections different characteristics can be obtained. After the type of the interconnection is determined, selection of the suspension design parameters is made. A general guideline for the design of the interconnected HP suspension system for a multi-axle vehicle is proposed in the following sections.

8.2. INTERCONNECTED HP SUSPENSION SYSTEM FOR A MULTI-AXLE VEHICLE

For a vehicle with three axles possible interconnections in pitch, roll, and coupled pitch and roll plane of the vehicle have been enumerated in Chapter 7. From the results of Chapter 7, the generalization of the interconnection for multi-axle vehicles can be made.

According to the Chapter 7 results:

- ❖ When different suspension units of the interconnected suspension system have similar parameters, the roll plane properties of the interconnected HP suspension system strongly depends on the type of the interconnected suspension system which may be fully interconnected, semi-interconnected and unconnected suspension. Therefore, in order to increase or reduce the roll

stiffness or roll damping characteristics, one or more interconnection in the roll plane can be added or removed.

- ❖ The pitch plane characteristics of the interconnected HP suspension system depend strongly on the configurations of the interconnection. However, in general, fully interconnected HP suspension systems consisting of pitch interconnections of all suspension units have higher pitch stiffness and damping. When the distance between the suspension units at which the pitch interconnection is performed increases, pitch stiffness and damping also increases. This is because the amount of the oil pumped between interconnected suspensions units due to the motion of the vehicle is proportional to the distance between them. For this reason, as shown in Chapter 6 and 7, when the front and rear suspension units are interconnected to each other, pitch stiffness and the damping is high.

To illustrate, the interconnected suspension configurations shown in Figure 8.1 and Figure 8.2 have similar pitch characteristics, yet they have different roll characteristics. Interconnected suspension configurations shown in Figure 8.1 have full roll interconnections which are of the pure X type. This means that, the fourth oil volume of a suspension unit is interconnected to the first oil volume of the opposite suspension unit in the roll plane, and the first oil volume of the same suspension unit is interconnected to the fourth oil volume of the opposite suspension unit in the roll plane.

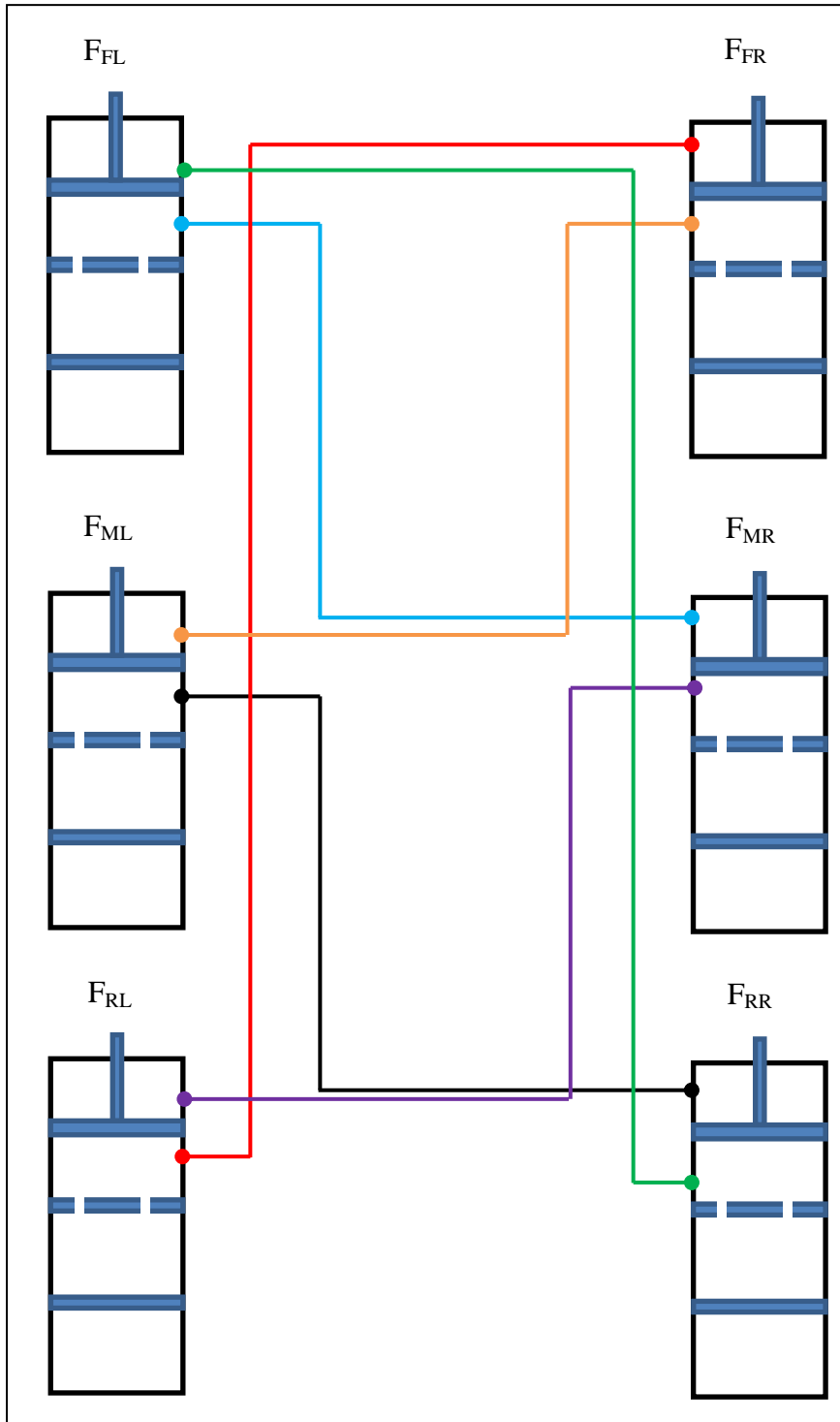


Figure 8.1: Interconnected HP Suspension System for a Three Axle Vehicle

However, the interconnected HP suspension unit shown in Figure 8.2 has roll interconnection between the intermediate and the rear suspension units, and thus is not pure X type.

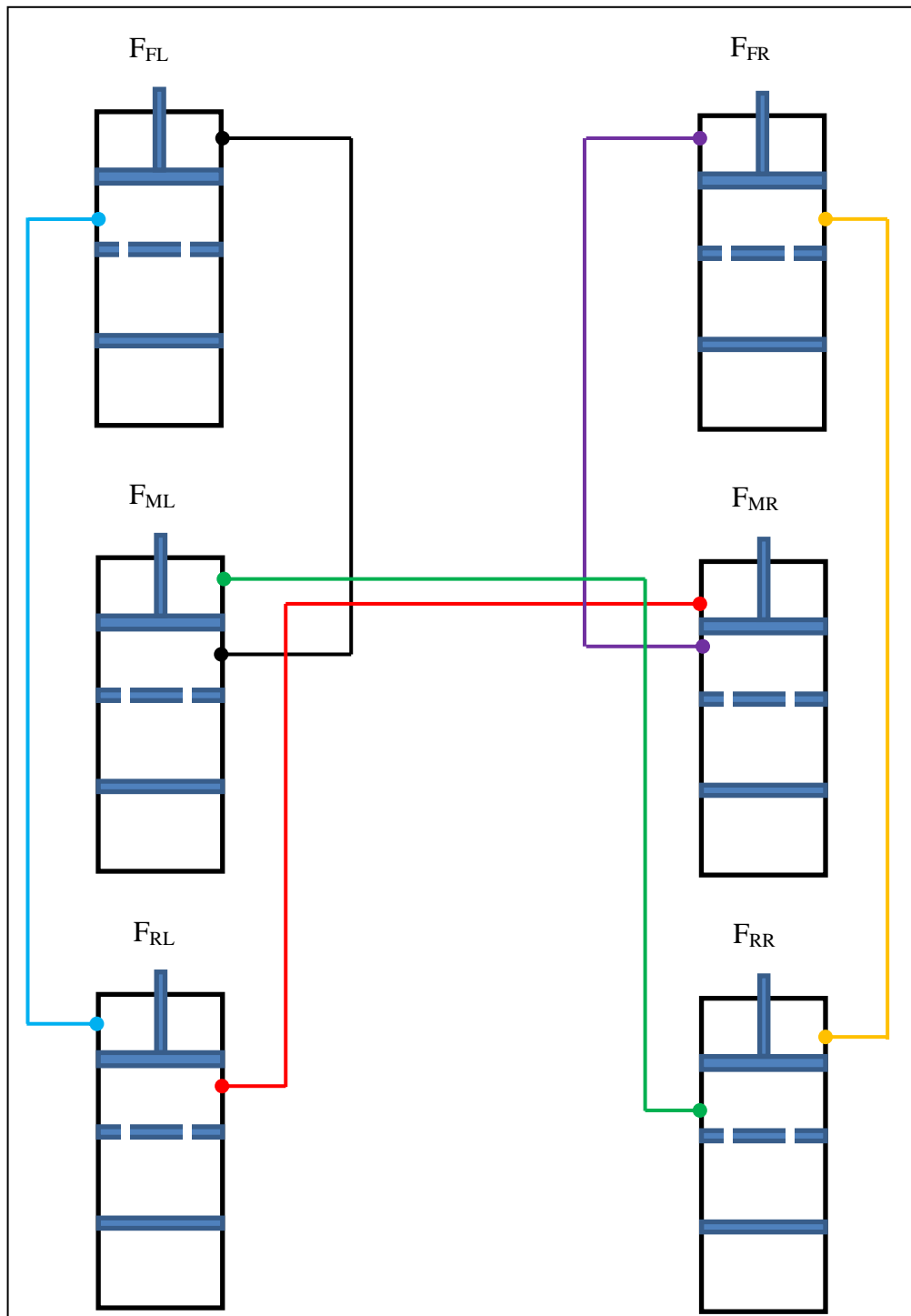


Figure 8.2: Interconnected HP Suspension System for a Three Axle Vehicle

In a summary, for a multi-axle vehicle, suspension units should be interconnected in the roll plane to form a pure X type connection to obtain higher roll stiffness and damping. Yet for the pitch plane, there are many possible interconnections. However as explained previously, interconnecting the suspension units which are far from each other in the pitch plane increases pitch stiffness and damping. According to these explanations, possible interconnections for multi-axle vehicles can be enumerated. After the possible type of the interconnected HP suspension system is determined, the next step is the determination of the initial suspension parameters. Important vehicle characteristics, such as suspension forces and the body bounce frequency are dependent on the vehicle suspension parameters at static equilibrium. Therefore, suspension parameters in static equilibrium are taken as the base parameters for the design. After the suspension parameters are determined, initial parameter sets before static equilibrium can be determined. Moreover, one of the special characteristics of the multi-axle vehicles is that the state of the vehicle at static equilibrium depends on the initial suspension parameters. This situation provides flexibility in the design of the suspension system. When the suspension initial parameters are changed, suspension parameters at static equilibrium also change. One of the possible ways of determining the suspension state at static equilibrium is specifying the suspension forces and the vehicle body bounce frequency. By this way, suspension parameters at static equilibrium can be determined.

A guideline for the design of the interconnected HP suspension system for two and for multi-axle vehicle for improved pitch and roll plane characteristics can be summarized in Figure 8.3 and Figure 8.4, respectively. The main difference between the design of the interconnected HP suspension system for two and multi-axle vehicles is the number of possible interconnections. For a vehicle with three and more axles, the number of the possible interconnections increases sharply. This provides flexibility in suspension design and different suspension systems with different characteristics can thus be obtained.

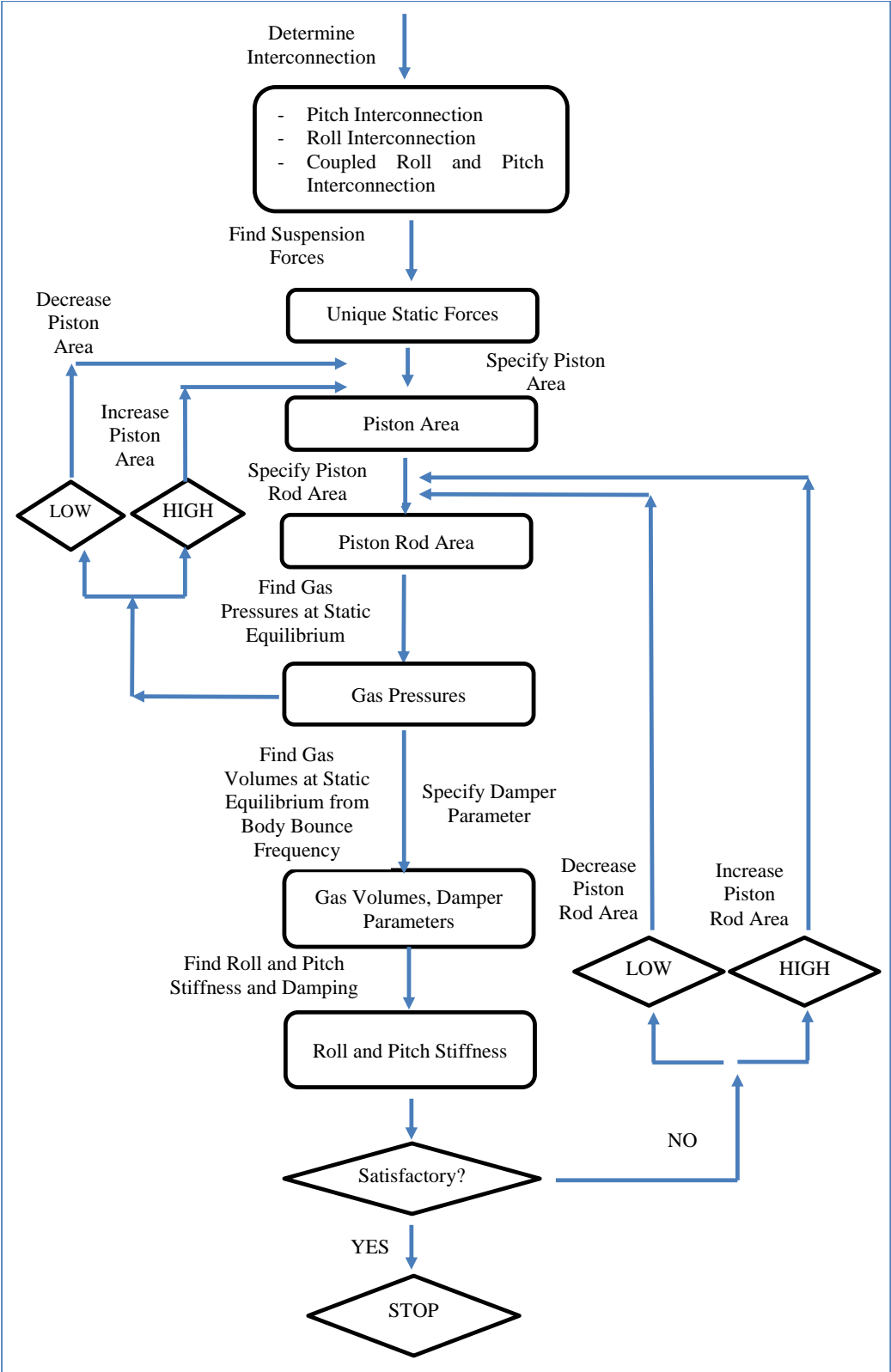


Figure 8.3: Interconnected Suspension Design Layout

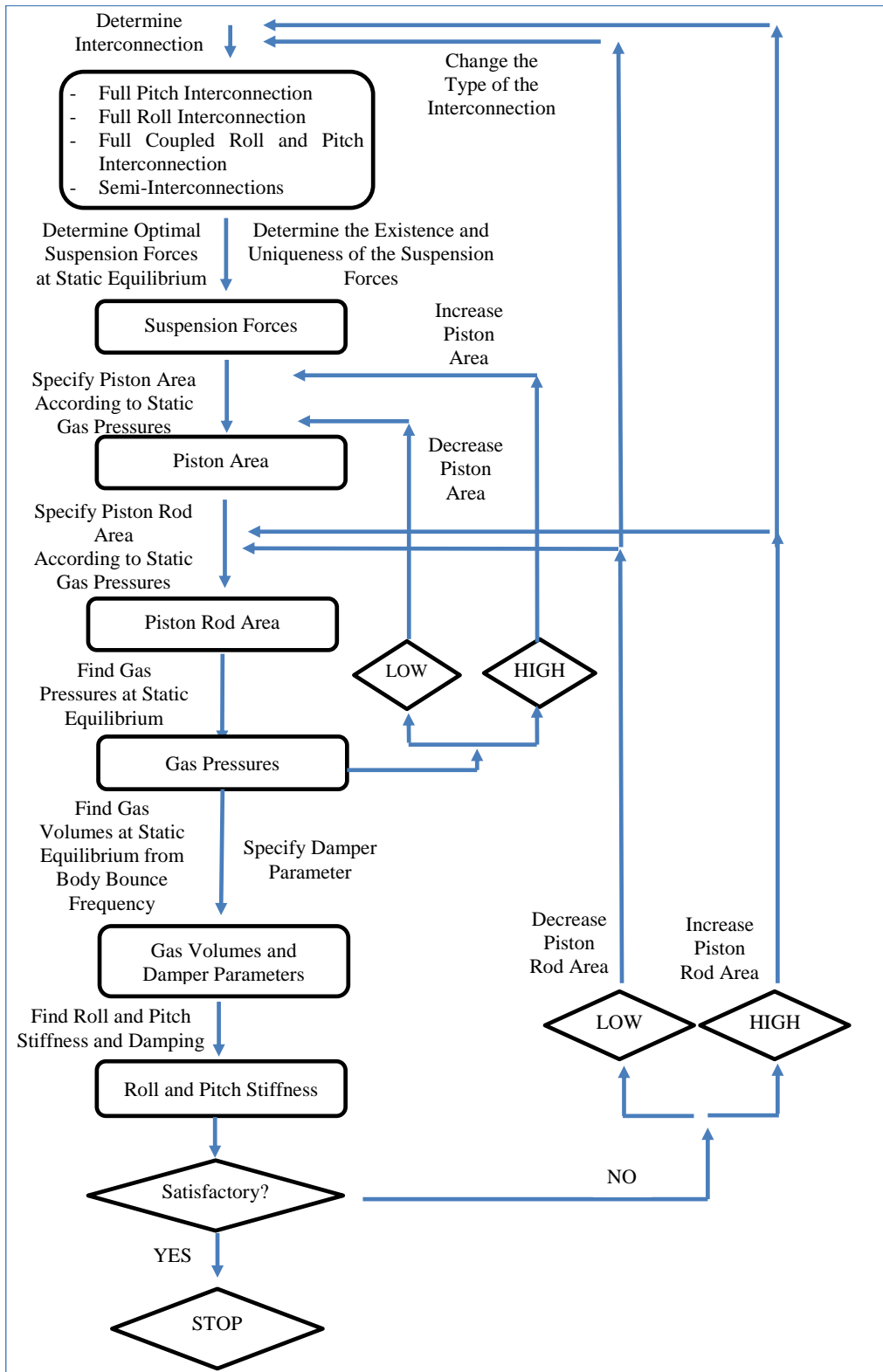


Figure 8.4: Interconnected Suspension Design Layout

As can be seen from Figure 8.4, the design of the interconnected HP suspension system can be summarized as,

- ❖ Determine the type of the interconnection as fully roll interconnected; fully pitch interconnected, fully coupled roll or pitch interconnection, or semi-interconnected. Vehicle with the fully roll interconnection has the highest roll stiffness and damping, vehicle with the fully pitch interconnection has highest pitch stiffness and damping, and vehicle with coupled fully roll and pitch interconnection has higher roll and pitch stiffness. When interconnection is converted from full to semi-interconnection, the roll and/or pitch stiffness decreases.
- ❖ Examine the feasibility of the interconnected suspension configurations by analyzing the consistency of the equations. Perform a static analysis to find the suspension forces at static equilibrium. For a vehicle with two axles, assuming left and right symmetry of vehicle, suspension forces at static equilibrium can be determined uniquely. For a vehicle with three and more axles, suspension forces at static equilibrium should be determined from the initial suspension configurations and static equilibrium. However, initial suspension configurations can be adjusted to obtain desired suspension parameters. For instance, suspension forces which are as close as to each other can be taken as the desired suspension forces, and suspension forces can be found uniquely.
- ❖ Specify the piston area. Piston area can be specified according to the gas and oil pressures at the static equilibrium. Moreover, while the vehicle is in operation, oil and gas pressures increases too. High oil pressures may increase the leakage across the piston and/or cylinder and/or from other connections. Thus according to the applications, the piston area should be selected according to reasonable oil pressures.
- ❖ Specify a piston rod area. When the piston rod area is low, the strength of the interconnection decreases and when the piston rod area increases the interconnection loses its strength. Oil and gas pressures at static equilibrium

change with the piston and piston rod areas. Therefore, piston rod area should be specified both according to the pressures at static equilibrium and desired stiffness and damping characteristics.

- ❖ Once the piston area, piston rod area, and the type of interconnection are determined, gas volumes at static equilibrium can be determined from the desired body bounce frequency.
- ❖ After the gas volumes are found and damper parameters are specified, the vertical, roll and pitch stiffness, and damping characteristics can be found. If the roll and pitch characteristics are found to be insufficient, the type of the interconnection can be changed such that higher roll and pitch stiffness can be obtained and/or the piston rod area can be decreased. If the roll and pitch stiffness and damping characteristic are too high, the suspension type can be changed into semi-interconnections and/or piston rod area can be increased.

If the suspension configuration is unconnected, the roll and pitch stiffness and damping can be increased by increasing suspension stiffness and damping. However, increasing suspension stiffness and damping also increases vertical stiffness and damping. This results in degraded vertical vehicle characteristics. However, in interconnected suspension configurations, the pitch and roll stiffness and damping can be increased by decreasing piston rod area without changing vertical stiffness and damping characteristics of the vehicle.

8.3. CONCLUSION

Interconnected HP suspension systems provide considerable flexibility for the performance improvements of multi-axle vehicles. Proper interconnected in the roll and/or pitch planes with suitable suspension parameters, handling and braking/acceleration and firing performance of the vehicle can be improved. Moreover, due to high number of possible interconnections, more design flexibility is offered to the designer.

CHAPTER 9

OPTIMIZATION OF HP SUSPENSION SYSTEMS

9.1. INTRODUCTION

In the previous chapters, HP suspension system integrated in different vehicle models analyzed and the active suspension applications of HP suspension systems are investigated. To be able to improve the roll and pitch performance of the HP suspension system in a complete vehicle model, interconnected HP suspension systems have been modeled. In all these studies, the nominal parameters of the HP suspension system have been used. In this chapter, to be able to satisfy the predefined vehicle performance consideration, optimum parameters of the HP suspension system are going to be determined.

Vehicle dynamics is a complex subject. It is customary to classify vehicle dynamics under three sub areas [82]:

- ❖ Vehicle Handling
- ❖ Vehicle Ride
- ❖ Vehicle Longitudinal Performance

These three characteristics of a vehicle are related to each other with the complex suspension dynamics. A well designed suspension system should improve the performance under these sub areas as much as possible. Even though the relations of the vehicle ride comfort with the suspension is obvious, the relation of the

suspension with the vehicle handling and the vehicle longitudinal performance are not so clear. When the vehicle is cornering, there is a lateral load transfer from the inner wheels to outer wheels. Lateral load transfer is due to many vehicle parameters one of which is the suspension stiffness. As can be understood from the tire models, tire cornering force increases with the increasing vertical load. Therefore when the vehicle is cornering, the outer tire cornering forces increase and the inner tire cornering forces are reduced. However, the total cornering force of the vehicle decreases with the increasing lateral load transfer. Moreover, tire deflections, due to road disturbances, result in the fluctuations of the tire vertical load and hence the effectiveness of traction, braking, and cornering will be variable. Therefore, it is desired to decrease the tire deflection fluctuations from the static equilibrium as much as possible to obtain better road holding.

Wong [40] examined the effects of the stiffness, damping, and the unsprung mass on the ride comfort, suspension packaging, and the road holding performance for a quarter car model. His results can be used as basic guidelines in the design of suspension systems.

- ❖ High suspension stiffness is required for better vibration isolation below the body bounce frequency,
- ❖ Low suspension stiffness is required for better vibration isolation between the body bounce and wheel hop frequencies,
- ❖ High damping is required for better vibration isolation around the body bounce frequency,
- ❖ Low damping is required for better vibration isolation between the body bounce and wheel hop frequencies,
- ❖ Lower damping ratio is required for better vibration isolation above the wheel hop frequency.
- ❖ Higher suspension stiffness is required for better suspension packaging at frequencies below body bounce frequency.

- ❖ Lower suspension stiffness is required for better suspension packaging between the body bounce frequency and the crossover frequency,
- ❖ Higher suspension stiffness is required for better suspension packaging between the crossover frequency and the wheel hop frequency.
- ❖ Higher damping ratio is required for better suspension packaging.
- ❖ Lower suspension stiffness is required for better road holding.
- ❖ Around wheel hop frequency, higher suspension stiffness is required for better road holding.
- ❖ Higher damping ratio is required for better road holding around the body bounce and the wheel hop frequencies.
- ❖ Lower damping ratio is required for better road holding between the body bounce and wheel hop frequencies

In order to design a suspension system for the desired vehicle performance characteristics, a detailed suspension optimization study is going to be performed in the following sections. The aim of this chapter is to determine the optimum parameters of the HP suspension system for the desired ride comfort and the vehicle handling performance. The parameters of the interconnected HP suspension system are optimized to get a compromise vehicle ride and handling performance. The objective function is defined as the weighted vertical acceleration of the driver and passengers. A maximum value of the roll angle is imposed in the optimization as an optimization constraint.

9.2. SUSPENSION OPTIMIZATION

As stated in Chapter I, the HP suspension system has certain advantages with respect to mechanical suspension systems. The fact that HP suspension units can be interconnected to each other easily improves the flexibility for the design of the suspension system for ride comfort, handling, and vehicle mobility. Thus in this chapter, the parameters of the interconnected and the unconnected HP suspensions are optimized to improve the vehicle ride comfort. To consider driving safety as well,

a constraint on vehicle handling is imposed in the process. Evaluation of the ride comfort is a subjective and the international standard ISO 2631 “Guide for the Evaluation of Human Exposure to Whole-Body Vibrations” [83] and BS6841 “Guide to Measurement and Evaluation of Human Exposure to Whole-Body Mechanical Vibration and Repeated Shock” [84] have been commonly used for this purpose. These standards provide a quantitative manner of evaluation of human exposure to vehicle accelerations in different directions. Human sensitivity to vibration changes with vibration amplitude, direction, duration, and frequency content. According to the ISO 2631, human exposure to vibrations can be evaluated in a quantitative manner by the so called reduced comfort boundaries. These reduced comfort boundaries provide the rms values of the limiting vibration values in different directions at different exposure durations and in a range of frequencies. For this reason, frequency shaping filters are used to evaluate the results of vibration exposure. In the study by Zuo and Nayfeh [85], low-order continuous time filters for the ride comfort frequency weighting curves are obtained. These filters are used in this study. The frequency weighting filter for vertical direction is given in Figure 9.1.

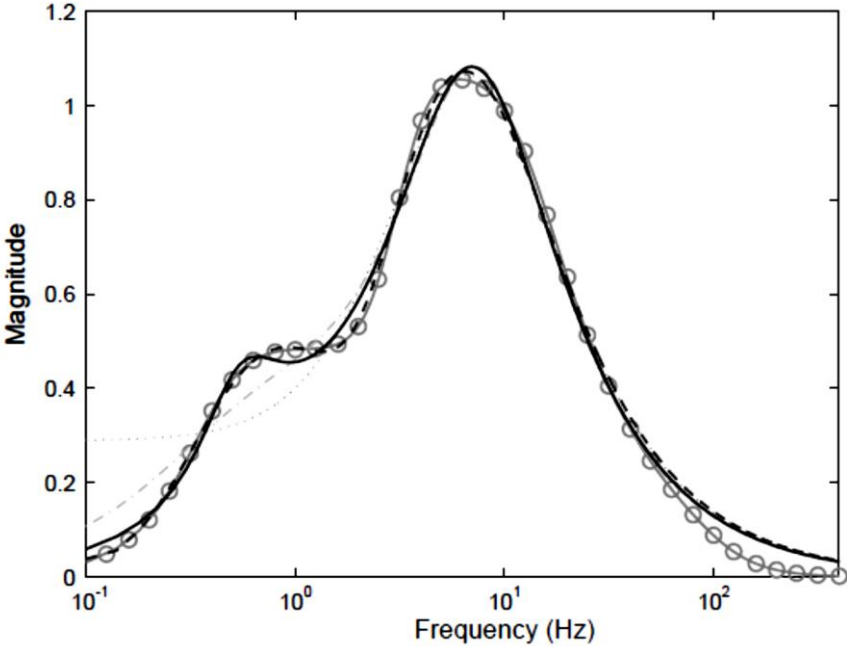


Figure 9.1: Weighting Frequency Approximation of the ISO-2631 Weighting Curve for Vertical Acceleration [85]

Third order mathematical representation of this weighing filter (dashed line in Figure 9.1) is given as [85],

$$W_k(s) = \frac{80.03s^2 + 989.0s + 0.02108}{s^3 + 78.92s^2 + 2412s + 5614} \quad (9-1)$$

The stiffness of the single one-sided HP suspension system depends on the initial gas volume and the piston area. Similarly, the damping of the HP suspension system depends on the piston area and the orifice opening. When the suspension units are interconnected to each other, the vertical, pitch, and roll stiffness depend on the piston areas, rod areas, initial gas volumes, and the type of the interconnection. Similarly, the vertical, roll, and the pitch damping depend on the piston areas, rod areas, orifice parameters, and the type of the interconnection. Among these parameters, the piston rod area is the main parameter of the interconnection and determines the effect of the interconnection dynamics on the whole suspension dynamics. The parameters of the interconnection connectors also affect suspension damping and also stiffness to a small extent. However, for the simplicity and brevity, these parameters are not included in the suspension design parameters. The design parameters to be optimized in the study are selected as the initial gas volume and the piston rod area for the stiffness, and the orifice parameters and the rod area for the damping. The piston area affects both the stiffness and damping and thus it is not included in the design parameters to simplify optimization. The piston area and the piston rod area change the initial oil pressure in the suspension units and they can be used for this purpose. The piston rod area is used in the optimization when the interconnected suspension configuration is considered. In summary, the suspension parameters, the optimized parameters, and the related vehicle dynamics are summarized in Table 9.1.

Table 9.1: Optimized and Design Parameters

	Suspension Parameters	Optimized Parameters
Vertical Stiffness	A_p, A_r, V_{30}	A_r, V_{30}
Roll Stiffness	A_p, A_r, V_{30}	A_r, V_{30}
Pitch Stiffness	A_p, A_r, V_{30}	A_r, V_{30}
Vertical Damping	$A_p, A_r, \text{Orifice Parameters, Connector Parameters}$	$A_r, \text{Orifice Parameters}$
Roll Damping	$A_p, A_r, \text{Orifice Parameters, Connector Parameters}$	$A_r, \text{Orifice Parameters}$
Pitch Damping	$A_p, A_r, \text{Orifice Parameters, Connector Parameters}$	$A_r, \text{Orifice Parameters}$

To examine the effects of the design parameters on the suspension performance, a sensitivity study is performed. The variation of the vertical, roll, and the pitch accelerations, and the variation of the roll and the pitch angles with the suspension design parameters are examined. Instead of using the design parameters directly in the optimization, dimensionless design parameters are used. These parameters are defined as,

$$n_{V_{30}} = \frac{V_{30n}}{V_{30}} \quad (9-2)$$

$$n_{\text{Damp}} = \frac{PQ_n}{PQ} \quad (9-3)$$

$$n_{A_r} = \frac{A_{rn}}{A_p} \quad (9-4)$$

where $n_{V_{30}}$ is the scaled initial gas volume, V_{30n} is the initial gas volume to be optimized, V_{30} is the nominal value of the initial gas volume, n_{Damp} is the scaled orifice damping, PQ_n is the orifice damping to be optimized, PQ is the nominal orifice damping, n_{A_r} is the scaled piston rod area, A_{rn} is the piston rod area to be optimized, and the A_p is the nominal piston area. The range of the scaled design parameters are,

$$n_{V_{30}} \in \{0.4, 2.5\}$$

$$n_{\text{Damp}} \in \{0.4, 2.5\}$$

$$n_{A_r} \in \{0.6, 1\}$$

When n_{Ar} is equal to 1, the suspension configuration becomes unconnected, and when n_{Ar} is not equal to 1, the suspension configuration become interconnected. Thus, n_{Ar} determines the strength of the interconnection. The optimized function is the weighted summation of the vertical, roll, and pitch accelerations of the sprung mass. To be able to take driving safety into consideration, constraint on the roll angle is imposed. As stated earlier, ride comfort is associated with the vertical, roll, and the pitch accelerations, and vehicle handling is associated with the maximum roll angle. Therefore the optimization process is formed as,

$$\arg \min_{n_{V30}, n_{Damp}, n_{Ar}} \left\{ \mathbf{W}_k (f) \left[\ddot{z}_{FL} + \ddot{z}_{FR} + \ddot{z}_{ML} + \ddot{z}_{MR} + \ddot{z}_{RL} + \ddot{z}_{RR} \right] \right\}$$

subject to

$$\begin{aligned} n_{V30} &\in \{ n_{V30min}, n_{V30max} \} \\ n_{Damp} &\in \{ n_{Dampmin}, n_{Dampmax} \} \\ n_{Ar} &\in \{ n_{Armin}, n_{Armax} \} \\ \phi &< \phi_{max} \end{aligned}$$

Roll angle constraint on the optimization was imposed as a new objective function as,

$$C(\phi) = \left(\frac{\phi}{\phi_{max}} \right)^{2n} \quad (9-5)$$

Roll angle constraint function used in the optimization study is given in Figure 9.2.

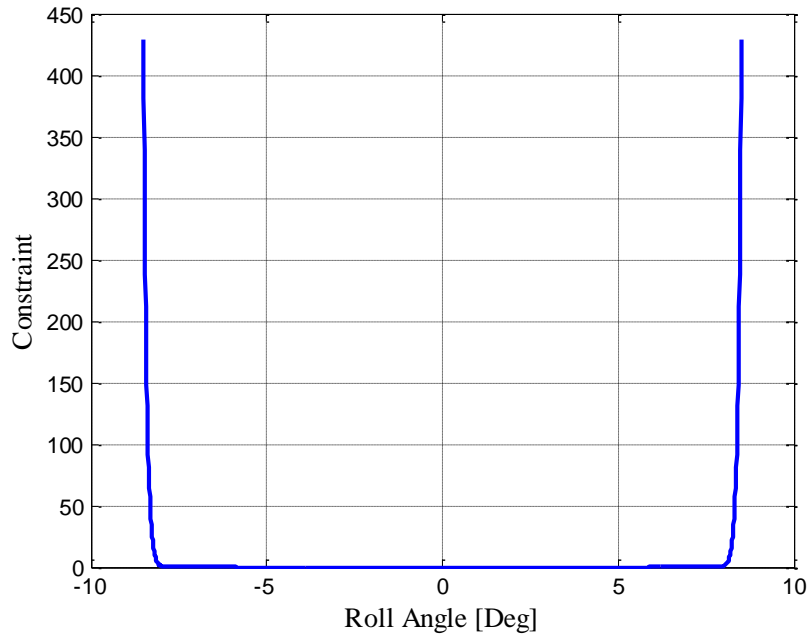


Figure 9.2: Roll Angle Constraint

In optimization study, the same random road displacement input used in section 4.2.4.1 is used for the ride comfort optimization, and the double lane change is used for the handling optimization.

9.3. SENSITIVITY STUDY

To get an initial insight into the optimization study, a sensitivity study is performed first. The variations of the vertical, roll, and pitch accelerations with the suspension design parameters are given in Figure 9.3 to Figure 9.5.

As can be seen from Figure 9.3 to Figure 9.5, when the ratio of the gas volumes to the nominal gas volumes are lower, suspension stiffness increases and vertical, pitch, and roll accelerations also increase. This causes deterioration in ride comfort.

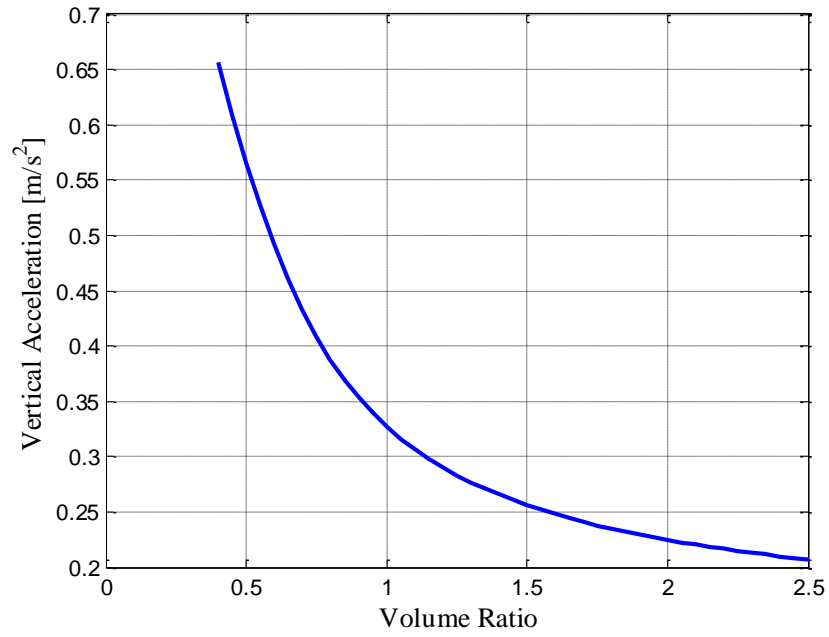


Figure 9.3: rms of Vertical Acceleration

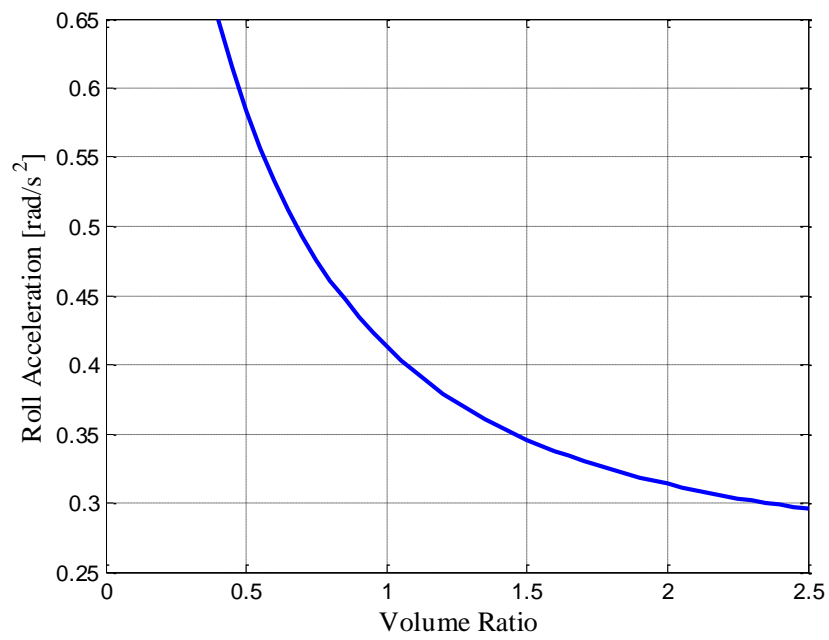


Figure 9.4: rms of Roll Acceleration

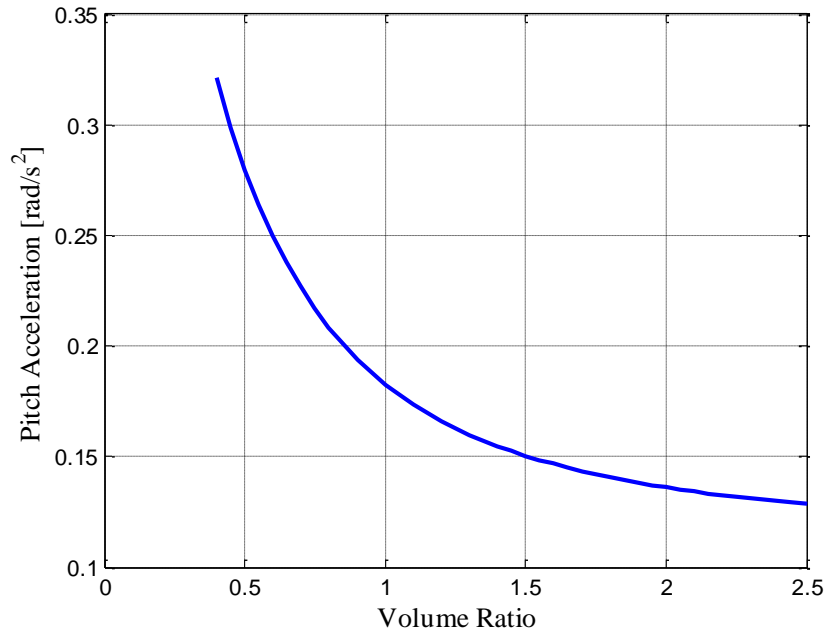


Figure 9.5: rms of Pitch Acceleration

Variation of the vertical, roll, and pitch accelerations with damping ratio are given in Figure 9.6 to Figure 9.8. The effects of the damping ratio on the accelerations are variable. As can be seen from Figure 9.6 to Figure 9.8, in the low damping ratio region, when the damping ratio increases accelerations are reduced. When a certain damping ratio threshold is exceeded, increasing the damping ratio results in increased accelerations. Finally, the effects of the piston ratio on the acceleration responses are examined. Variation of the vertical, roll, and pitch accelerations with the piston rod area are given in Figure 9.9 to Figure 9.11.

The variation of the accelerations with the piston ratio is not as obvious as the change of the accelerations with the volume ratio or with the damping ratio, since the piston ratio affects both the stiffness and the damping characteristics simultaneously. With regard to stiffness, when the piston ratio is reduced, the vertical stiffness decreases. However, when the piston ratio is reduced, tendency of increasing pitch and the roll stiffness appear. With regard to damping characteristics, when the piston ratio decreases, vertical damping is reduced. Similarly, there is a tendency of the increasing pitch and the roll damping when the piston ratio is reduced. Therefore,

increasing piston ratio results in lower vertical ride comfort performance and higher roll and pitch ride comfort performances.

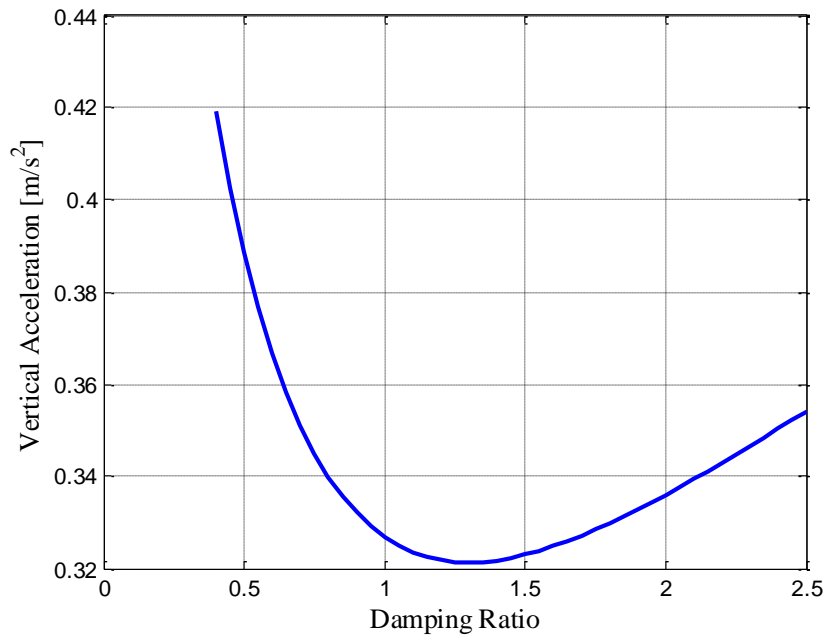


Figure 9.6: rms of Vertical Acceleration

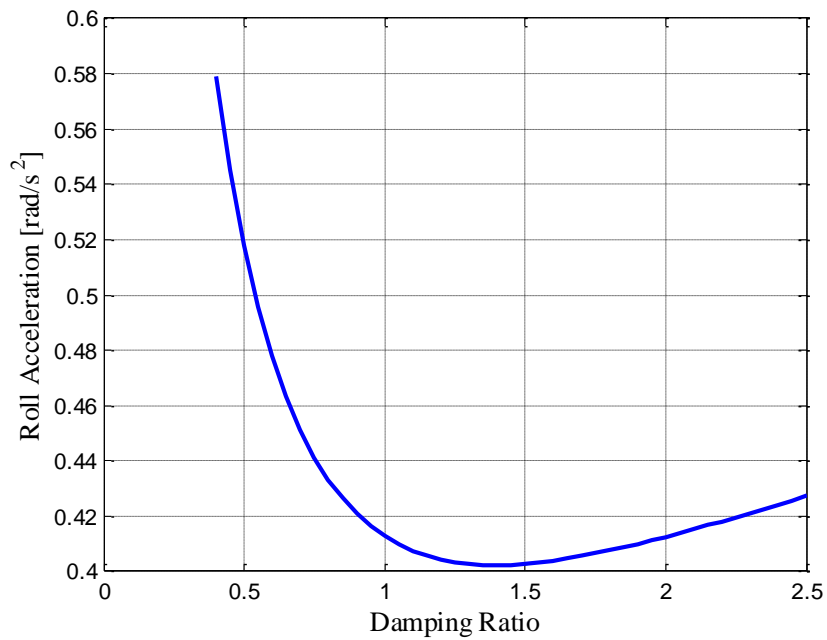


Figure 9.7: rms of Roll Acceleration

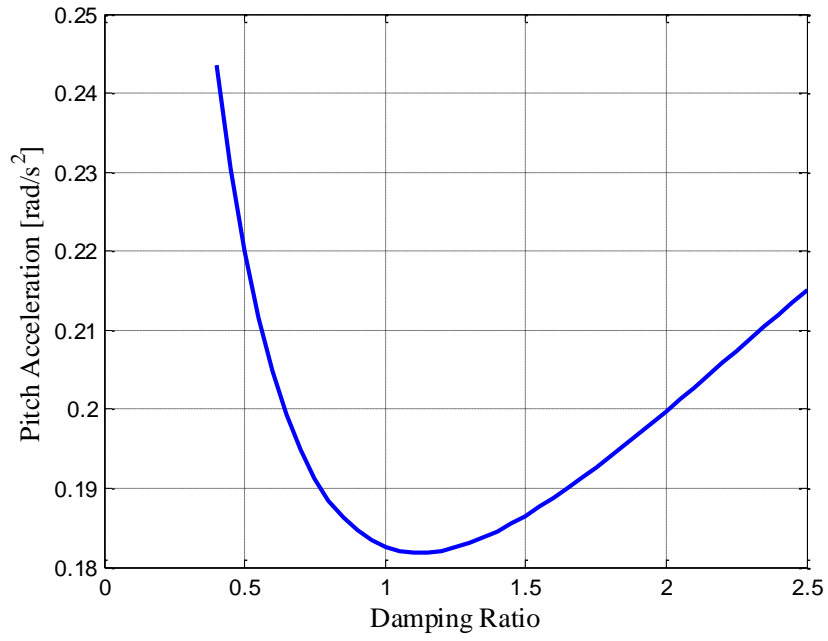


Figure 9.8: rms of Pitch Acceleration

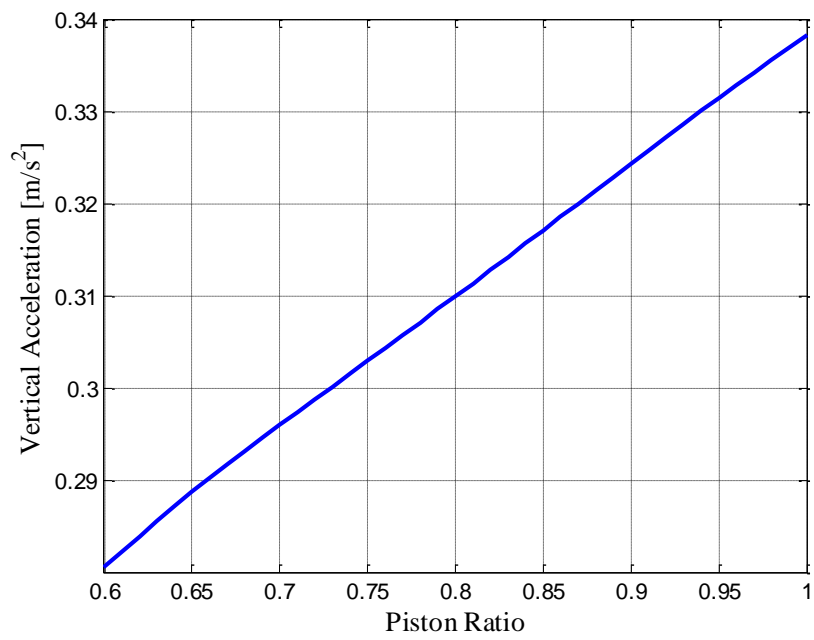


Figure 9.9: rms of Vertical Acceleration

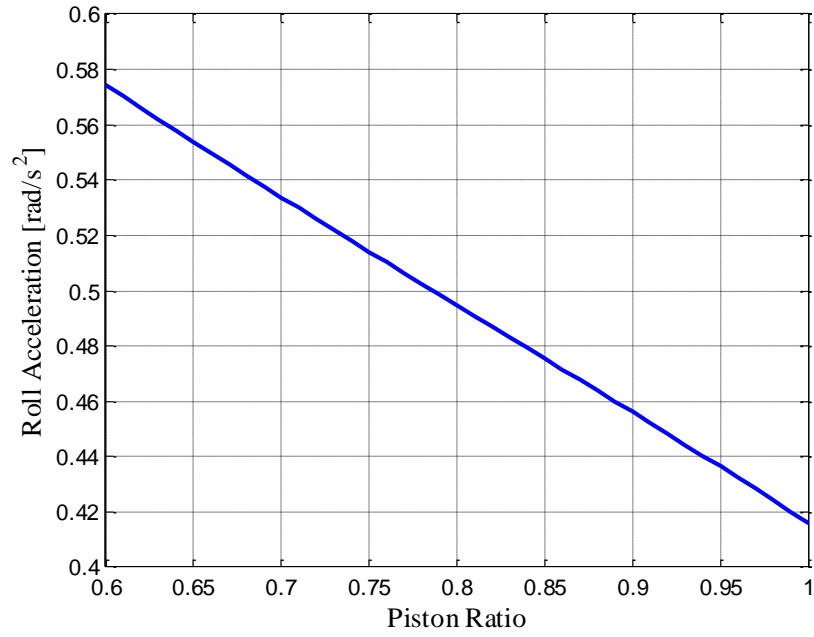


Figure 9.10: rms of Roll Acceleration

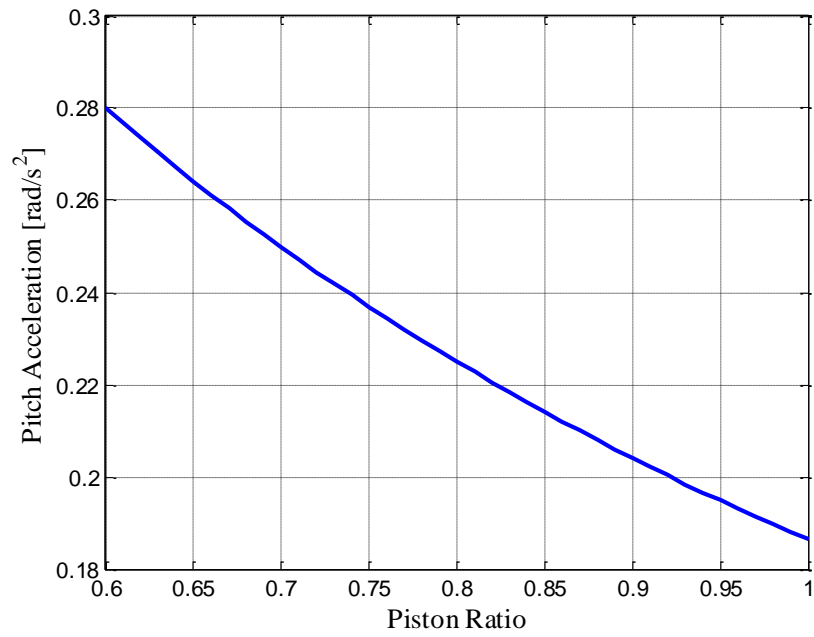


Figure 9.11: rms of Pitch Acceleration

After the variation of the vertical, roll, and the pitch accelerations with the suspension design parameters are examined, the variation of the handling variable

which is the roll angle with respect to the suspension design parameters are going to be examined. For simulations with the steering input, a linear two degrees of freedom bicycle with three axles are used. Then the roll moment disturbance is formed using the lateral acceleration data. Steering wheel input used for double lane change simulation is given in Figure 9.12. Figure 9.13 to Figure 9.15 show the variation of the maximum roll angle with respect to the volume ratio, damping ratio, and the piston ratio. When the volume ratio is reduced, the suspension stiffness increases, and the roll angle is reduced. When the damping ratio increases, maximum value of the roll angle decreases. The volume ratio has a stronger influence on the roll angle response than the damping ratio. When the piston ratio decreases, the roll stiffness increases, and the roll angle gets smaller.

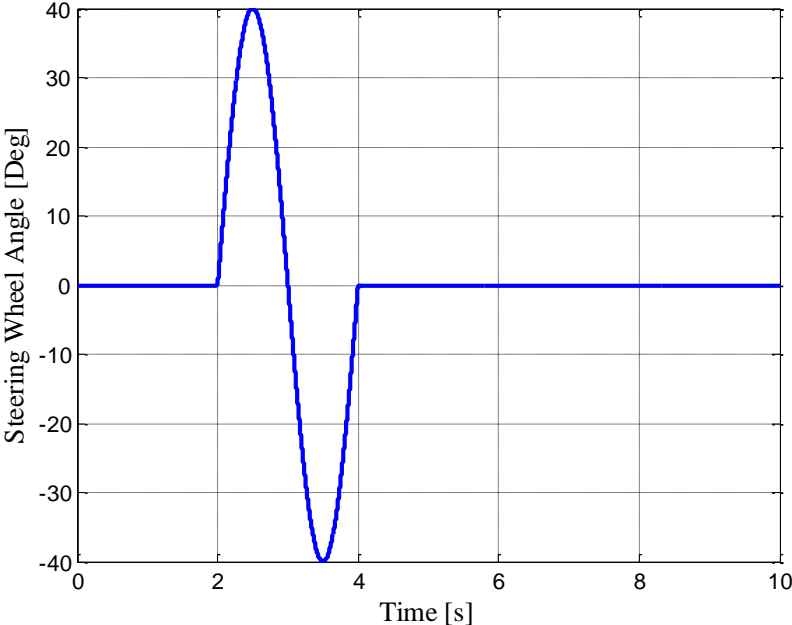


Figure 9.12: Steering Wheel Input for Double Lane Change Maneuver

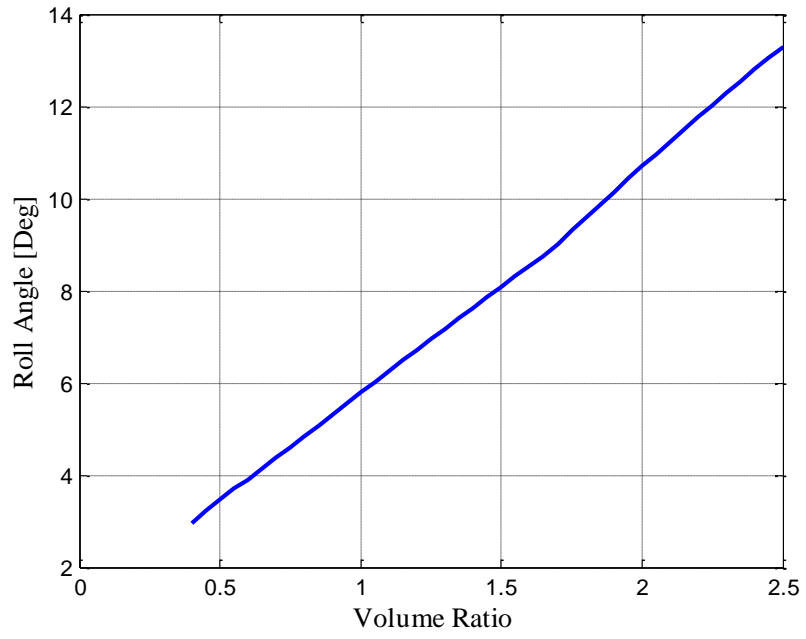


Figure 9.13: Roll Angle versus Volume Ratio

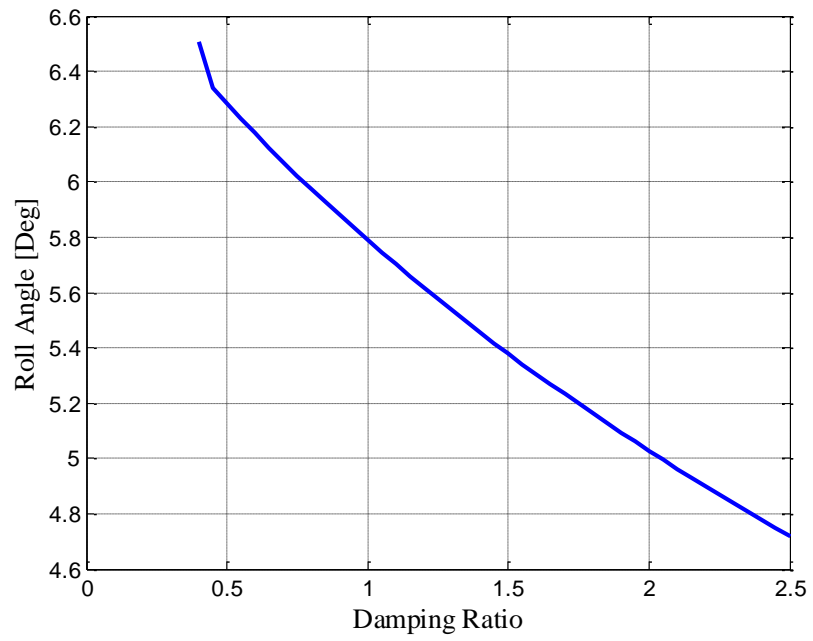


Figure 9.14: Roll Angle versus Damping Ratio

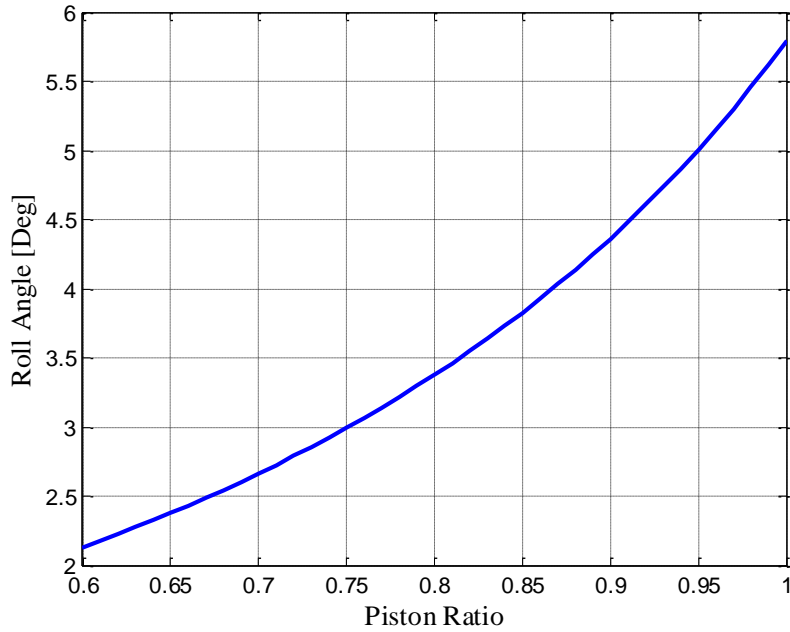


Figure 9.15: Roll Angle versus Piston Ratio

In summary, as expected, making the suspension stiffer by reducing the gas volumes improves handling, but deteriorates ride comfort. When the suspension configuration is changed from unconnected to the interconnected configuration, suspension stiffness and damping also change. Increasing the piston ratio reduces the vertical stiffness and damping and vice versa.

Therefore, there has to be a compromise between the vehicle ride comfort and handling performances. Making the suspension stiffer increases handling performance yet deteriorates the ride comfort performance. Thus, a compromise optimal solution should be found in order to improve both ride comfort and handling performance.

The aim of the optimization is to improve the ride comfort and constrain the maximum roll angle to a specified value for safe driving. When the suspension configuration is unconnected, the volume ratio and the damping ratio are set to optimum values which minimize the accelerations and the roll angle is set to a value lower than the limiting roll angle. However, when the suspension configuration is interconnected, the volume ratio, damping ratio, and the piston ratio are set to

optimum values to minimize the accelerations and the roll angle is set to the maximum roll angle. Thus, interconnected suspension configuration has one more design parameter which is the piston rod area. For the completeness of the study, suspension optimization is to be performed for both the unconnected and the interconnected suspensions.

9.4. OPTIMIZATION RESULTS

As a first step optimization is carried out by taking the identical front, intermediate, and rear suspension gas volumes, damping ratios, and piston rod area ratio. Optimization is performed for improved ride comfort and improved handling. As stated in previous section, vehicle handling is imposed as the constraint in the optimization. For the ride comfort optimization, the maximum constraint on the roll angle is specified as the 8 degrees and for the handling optimization the constraint on the roll angle is specified as 4 degrees for the double lane change maneuvers at the specified longitudinal velocity. For the optimization, a well-known heuristics global optimization algorithm, the Matlab Genetic Algorithm toolbox [86] is used.

The optimization results are given in Table 9.2 and the optimum parameter sets are given in Table 9.3.

Table 9.2: Optimization Results

	Ride Comfort ($\theta=8$ Deg)			Handling($\theta=4$ Deg)		
	Uncon.	Intercon.	%	Uncon.	Intercon.	%
Acceleration [m/s^2]	0.90	0.43	55	1.32	0.48	62
Roll Angle [Deg]	7.9	4.4	35	4.0	4.0	0

Table 9.3: Optimum Parameter Sets

	Ride Comfort ($\theta=8$ Deg)		Handling($\theta=4$ Deg)	
	Uncon.	Intercon.	Uncon.	Intercon.
Volume Ratio	1.47	2.50	0.76	2.26
Damping Ratio	0.83	0.40	1.73	0.50
Piston Area Ratio	-	0.60	-	0.60

As can be seen from Table 9.3, vehicle with the unconnected HP suspension system has a volume ratio of 1.31 and a damping ratio of 1.06 for the best ride comfort performance and in order to constrain the maximum roll angle to 8 degrees. For the vehicle with the interconnected HP suspension system, the volume ratio is set to the upper limit and the damping ratio is set to the lower limit in order to minimize the weighted vertical accelerations. However, the piston rod area is set to the possible minimum value for the roll angle constraint. Even though, 8 degrees roll angle constraint is imposed at the optimization, after optimization, 5.2 degree roll angle is obtained. When the optimization results for unconnected and interconnected HP suspension systems are compared to each other, it is seen that the vehicle with the interconnected HP suspension system has lower acceleration than the acceleration of the vehicle with the unconnected suspension system. The vehicle with the interconnected HP suspension system has a lower maximum roll angle as compared with the maximum roll angle of the vehicle with the unconnected suspension system.

For the improved handling behavior of the vehicle 4 degrees roll angle constraint is imposed during the optimization. As Table 9.3 illustrates, the vehicle with the interconnected HP suspension system has a somewhat higher volume ratio and lower damping ratio. These parameters result from the need to lower the vertical acceleration and thus increasing the ride comfort. However, the piston rod area is again set to its lower limit in order to reduce the roll angle. For the vehicle with the unconnected HP suspension system, a low value of the volume ratio and a high value of the damping ratio are obtained in order to limit the roll angle to 4 degrees. Thus the suspension stiffness is increased and thus ride comfort is degraded. Since the vehicle with the interconnected HP suspension system has lower acceleration, it has better ride comfort performance. In order to reduce the roll angle and improve the handling performance, roll stiffness and damping should be high. For a vehicle with the unconnected suspension system, the only way of achieving high roll stiffness and damping is to reduce the gas volume and increase the suspension damping. While increasing the roll stiffness and damping, vertical stiffness and damping are also increased and thus ride comfort is deteriorated. However, for a vehicle with the interconnected HP suspension system, the roll stiffness and damping can be

increased either by reducing gas volumes, increasing the suspension damping, or by reducing the piston rod area. In the first case both roll and vertical stiffness as well as damping are increased. However in the second case, vertical stiffness and damping characteristics can be kept constant, while increasing pitch stiffness and damping. As a result, more than 50 % improvement in ride comfort is obtained with equal handling performance by using the interconnected HP suspension system.

The same optimization procedure is also repeated with independent front, intermediate, and rear suspension parameters and the results in Table 9.4 to Table 9.6 are obtained.

Table 9.4: Optimization Results

	Ride Comfort ($\sigma=8$ Deg)			Handling($\sigma=4$ Deg)		
	Uncon.	Intercon.	%	Uncon.	Intercon.	%
Acceleration [m/s²]	0.77	0.46	40	1.00	0.48	52
Roll Angle [Deg]	7.7	5.0	35	4.0	3.9	3

Table 9.5: Optimum Parameter Sets for Ride Comfort Optimization

	Unconnected	Interconnected
Parameter	Value	Value
Front Volume Ratio	1.00	2.45
Front Damping Ratio	1.61	0.76
Front Piston Rod Ratio	-	0.63
Intermediate Volume Ratio	1.47	2.45
Intermediate Damping Ratio	0.41	0.43
Intermediate Piston Rod Ratio	-	0.62
Rear Volume Ratio	2.50	2.50
Rear Damping Ratio	0.42	0.41
Rear Piston Rod Ratio	-	0.63

Table 9.6: Optimum Parameter Sets for Handling Optimization

	Unconnected	Interconnected
Parameter	Value	Value
Front Volume Ratio	0.50	2.39
Front Damping Ratio	2.50	1.28
Front Piston Rod Ratio	-	0.65
Intermediate Volume Ratio	0.44	1.82
Intermediate Damping Ratio	0.77	0.41
Intermediate Piston Rod Ratio	-	0.61
Rear Volume Ratio	2.50	2.47
Rear Damping Ratio	0.41	0.50
Rear Piston Rod Ratio	-	0.60

As can be seen from Table 9.4, both unconnected and interconnected suspensions improve the ride comfort and handling performances of the vehicle. Similar to the previous results, interconnected HP suspension system have better ride comfort performance than the unconnected suspension.

As Table 9.5 and Table 9.6 illustrate, for minimized acceleration, optimized parameters for front, intermediate, and the rear suspension units are set to different values. For the unconnected HP suspension system to satisfy the roll angle constraint the initial gas volume of the front suspension unit is set to an intermediate value and initial gas volumes of the intermediate and the rear suspension units are set to somewhat higher values for ride comfort optimization. On the other hand, for the interconnected HP suspension system, roll angle constraint is satisfied by lower piston rod ratios for ride comfort optimization. By this way, initial gas volumes of front, intermediate, and the rear suspension units are optimized to their upper values for ride comfort performance.

For handling optimization, initial gas volumes of the front and intermediate suspension units are set to their lower limits in order to constrain the roll angle. However, initial gas volume of the rear suspension unit is set to its upper limit for reduced vertical acceleration. Interconnected HP suspension system minimizes the vertical acceleration by raising the initial gas volumes to their upper limits and lowering the damping ratios to their lower limits. Roll angle constraint is satisfied by

piston rod ratios set to their lower limits for the interconnected HP suspension systems.

9.5. CONCLUSION

In this chapter, suspension design parameters of the vehicle with the unconnected and interconnected HP suspension systems were optimized. The main aim of the optimization is to improve the ride comfort together with driving safety. The optimized suspension parameters for the unconnected HP suspension system are the gas volumes and the suspension damping. For the interconnected HP suspension system, the piston rod area is also an optimized suspension parameter. In the optimization normalized values of the suspension design parameters are used. The objective function was formed as the weighted rms of the sum of the vertical accelerations at different locations on the vehicle, and the maximum roll angle was imposed as the optimization constraint. Upper and lower limits were set to the optimized parameters in order to get physical parameter set. In the optimization, a well-known heuristic optimization algorithm, genetic algorithm is used. Optimization is performed for two different vehicle performance, first of which is the improved ride comfort and the second of which is the improved vehicle handling for both the unconnected and interconnected HP suspension systems. According to the optimization results, the vehicle with the interconnected HP suspension system has better ride comfort and handling performances with respect to vehicle with the unconnected HP suspension system. For the unconnected HP suspension system, the roll angle is lowered by reducing gas volumes and by increasing the suspension damping, which degrades the ride comfort. However, for the interconnected HP suspension system, the roll angle can be reduced by reducing the piston rod area. Therefore, suspension stiffness and damping in the vertical direction are not increased, so that ride comfort is not affected. As a result, vehicle with the interconnected HP suspension system has better ride comfort and vehicle handling performance as compared to the vehicle with the unconnected HP suspension system.

CHAPTER 10

CONCLUSION

In this study, the main subject has been the design and analysis of the HP suspension systems for road vehicles. At the beginning a single gas chamber HP suspension system is modeled and the model is validated by laboratory experiments and a detailed parametric analysis of HP suspension system is performed. Then active control of HP suspension system for the vehicle ride comfort, attitude, and handling has been performed. Various active suspension controllers with different complexity have been designed for the quarter, half, and full vehicle models. Performance of the active HP suspension systems have been examined by time and frequency domain simulations. Simulation results show that, the active controllers improve ride comfort and vehicle attitude performance considerably, by maintaining adequate vehicle handling response.

In the second part of the study, interconnected HP suspension systems for multi-axle vehicles have been studied. For a vehicle with three-axles, various roll and pitch coupled HP suspension systems have been modeled, their stiffness and damping characteristics have been derived. Various simulations have been performed to examine the performance of the interconnected suspension system. Simulation results show that properly selected interconnected HP suspension systems improve vehicle handling considerably while maintaining the ride comfort performance as compared with unconnected HP suspension systems. Finally, optimization of the connected and unconnected HP suspension systems has been performed for ride

comfort performance with adequate vehicle handling. Optimization results show that both the unconnected and interconnected HP suspension system improve the ride comfort while satisfying the handling constraint. However, the interconnected HP suspension system has better ride comfort and handling performance than the unconnected HP suspension system. This is basically due to higher roll and pitch stiffness and damping characteristics of the interconnected HP suspension systems.

Some of the specific conclusions related to the passive and HP suspension characteristics, design and control of the unconnected and interconnected suspension for multi axle vehicles are listed below.

- ❖ Stiffness characteristic of the HP suspension system with single gas chamber depends on the piston area and initial gas volume. Damping characteristics, on the other hand is governed by the piston area and orifice opening.
- ❖ A large piston area increases both the stiffness and the damping characteristics of the HP suspension, a large initial gas volume on the contrary lowers the suspension stiffness. Similarly an increased orifice opening results in a reduction in the suspension damping and vice versa.
- ❖ The main difference between the double gas chamber and the single gas chamber HP suspension systems is in their stiffness characteristics. In the single gas chamber HP suspension system, compression of the suspension increases stiffness and expansion of the suspension lowers the suspension stiffness. On the other hand, in a double gas chamber HP suspension system, both expansion and compression of the suspension increases suspension stiffness in general.
- ❖ By tuning the orifice areas of the single and double gas chamber HP suspension systems, similar damping characteristics can be obtained.

By using the derived model of the HP suspension system, active HP suspension control can be designed. After the active controller has been designed and performance it has been analyzed, the following specific conclusions have been reached:

- ❖ Since the HP suspension system has inherently nonlinear characteristics, nonlinear control methods should be used to design the active HP suspension controller. The SDRE control method is suitable for this purpose
- ❖ In order to design the controller with the SDRE control method, state space model of the HP suspension system with state dependent matrices is derived. In the implementation of the SDRE control, direct parameterization of the gas and orifice model is obtained by fitting a polynomial model to the polytropic gas equation.
- ❖ Active suspension controller can successfully improve the ride comfort performance.
- ❖ For certain types of road inputs, a steady state suspension deflection in the active suspension system should be reduced to zero and the active suspension controller should be designed with the suspension deflection integral constraint.
- ❖ Active suspension controller designed with the suspension deflection integral controller improves both the ride comfort and vehicle attitude performance.
- ❖ There has to be a compromise between the vehicle ride comfort and the vehicle attitude control performance of the active suspension control since these two objectives are conflicting.
- ❖ Suspension deflection integral weighting parameter has an important effect on the vehicle attitude performance. In order to improve the vehicle attitude performance, suspension deflection integral weighting parameters should be high.
- ❖ Ride comfort and vehicle attitude performance can be further improved with the adaptive controller using the state constraints formulation. By adaptation of the suspension deflection integral weighting parameter both ride comfort and vehicle attitude performances can be improved. With the adaptive controller, improvement of the ride comfort is emphasized at low suspension deflection, and lowering the suspension deflection is emphasized at high suspension deflection. By switching continuously between the different

values of the weighing parameters, different controllers can be implemented online.

- ❖ By using SDRE control, oil flow rate saturation and bump or hard stop can be incorporated into the active suspension control formulation.

After active suspension control has been performed, another important application of the HP suspension control, interconnected HP suspension systems for multi axle vehicles has been studied. Related to the applications of the interconnected HP suspension systems, the following specific conclusions can be stated:

- ❖ By connecting different HP suspension units using hydraulic connectors, significant improvements in the main characteristics of the HP suspension system can be obtained.
- ❖ For a vehicle with three axles, different interconnected HP suspension systems can be formed in the pitch plane, as full or semi-interconnection according to the degree of freedom of the interconnections.
- ❖ In order to compare the pitch stiffness and the damping characteristics of the different interconnected HP suspension systems, vertical stiffness and damping characteristics of the configurations should be equalized to each other.
- ❖ Vertical stiffness of different interconnections can be equalized to each other by optimizing the initial gas volumes. Similarly, vertical damping characteristics can be made similar by optimizing the damping parameters.
- ❖ The interconnections which connect front and rear suspension units have higher pitch stiffness. Moreover, all interconnections either full or semi-interconnection have pitch stiffness higher than the unconnected suspension.
- ❖ Simulation result show that vehicle with different suspension configurations have similar vertical accelerations response. However, the interconnected HP suspension systems bring about higher pitch accelerations due to their high stiffness.

- ❖ Interconnected HP suspension systems improve the pitch performance of the vehicle considerably by decreasing the pitch angle during braking maneuvers or firing situation.
- ❖ For a full vehicle model with three axles, numerous interconnected HP suspension systems for pitch and roll plane can be enumerated. However, in order to obtain physically appropriate interconnected HP suspension systems, a feasibility study should be performed.
- ❖ Interconnected HP suspension systems which have full roll interconnections have higher roll stiffness. On the other hand, for an interconnected HP suspension system to have higher pitch stiffness, front and rear suspension units should be connected to each other. Thus the fully interconnected HP suspension systems in pitch plane have the highest pitch stiffness.
- ❖ Simulation results show that interconnected HP suspension systems improve the roll and pitch performance of the vehicle considerably in braking in turn, and firing tests.
- ❖ The interconnected HP suspensions systems improve handling and pitch performance, and slightly degrade ride comfort performance.

Finally optimization studies have been performed in order to improve the ride comfort with safe driving. Optimization is performed for both the unconnected and interconnected HP suspension systems. According to the optimization results, the following conclusions have been reached:

- ❖ When the suspension damping is increased starting from the lower value, vertical, roll, and the pitch accelerations are reduced till some value and then they start increasing indicating the presence of an optimum value.
- ❖ Increasing piston ratio decreases roll and pitch accelerations, yet increase vertical acceleration. Roll angle decreases with a decrease in piston ratio.
- ❖ Sensitivities of the roll angle to initial gas volumes and piston rod area are higher than the sensitivity of roll angle to damping.
- ❖ As a result, in order to control the roll angle, initial gas volumes and the piston rod area should be optimized.

- ❖ For ride comfort optimization, the unconnected HP suspension system minimizes the accelerations by increasing the initial gas volumes and by decreasing the damping to somewhat lower values. However, the interconnected HP suspension system minimizes the acceleration by increasing the initial gas volume to its upper limit, by reducing the damping and the piston rod area to their lower limits. Since the effects of the initial gas volume and the damping on accelerations are stronger than the effects of the piston rod area, with the interconnected HP suspension systems lower accelerations can be obtained.
- ❖ For ride comfort optimization, unconnected HP suspension system controls the maximum roll angle by tuning the initial gas volumes and damping ratio. However, interconnected HP suspension system controls the maximum roll angle directly by optimizing the piston rod area.
- ❖ For handling optimization, unconnected suspension systems controls the maximum roll angle by reducing the initial gas volumes to its lower limits and by increasing the damping to its upper limit. On the other hand, the interconnected HP suspension system controls the roll angle mainly by setting the piston rod area to its lower limit. Initial gas volume and damping are close to their upper and lower limits, respectively. Therefore, the interconnected HP suspension system controls the roll angle by reducing the piston rod area and lowers the vertical accelerations by increasing initial gas volume and by reducing damping.
- ❖ Both the unconnected and interconnected suspension systems can improve the ride comfort by satisfying the handling constraint.
- ❖ The interconnected suspension system can lower the vertical accelerations to lower values than the unconnected HP suspension system.
- ❖ Thus, the interconnected HP suspension configuration can be implemented to improve the ride comfort to higher levels than that can be reached with the unconnected HP suspension systems.

REFERENCES

- [1]. Bauer, W., “Hydropneumatic Suspension Systems”, Springer, 2011.
- [2]. Deprez, K., Maertens, K., Ramon, H., “Comfort Improvement by Passive and Semi-active Hydropneumatic Suspension Using Global Optimization Technique”, Proceeding of the American Control Conference, Anchorage, May 2002.
- [3]. Shi, J-W., Li, X-W., Zhang, J-W., “Feedback Linearization and Sliding Mode Control for Active Hydropneumatic Suspension of a Special-purpose Vehicle”, Proc. ImechE Vol. 224 Part D: J. Automobile Engineering, 2010.
- [4]. Gao, B., Darling, J., Tilley, D., G., Williams, R., A., “Modeling and Simulation of a Semi-Active Suspension System”, In 18th Int. Conf. on Systems Engineering, ICSE, 2006-01-01, Coventry University.
- [5]. Beno, J., H., Weeks, D., A., Mock, J., R., “Simulation Based Design for Actively Controlled Suspension Systems”.
- [6]. Gao, B., Darling, J., Tilley, D., G., Williams, R., A., Bean, A., Donahue, J., “Non-linear Modeling of a Gas Strut Used in Ground Vehicle Suspensions”, Transactions of the Institute of Measurement and Control 2007; 29; 159.
- [7]. Gao, B., Darling, J., Tilley, D., G., Williams, R., A., Bean, A., Donahue, J., “Control of a Hydropneumatic Active Suspension Based on a Non-linear Quarter-Car Model”, Proc. IMechE Vol. 220 Part I: J. Systems and Control Engineering, 2006.
- [8]. Giliomee, C., L., Els, P., S., “Semi-active Hydropneumatic Spring and Damper Systems” Journal of Terramechanics 35, 1998, 109-117.
- [9]. Abd, El-Tawwab, A., M., “Advanced Hydro-Pneumatic Semi-Active Suspension System”, Journal of Low Frequency Noise, Vibration and Active Control, Pages 93 – 103, 2009.

- [10]. Sihong, Z., Baozhan, L., “Simulation on Output Force Characteristics of Damping-Adjustable Hydro-pneumatic Suspension”, Intelligent Vehicles Symposium, IEEE, 2009.
- [11]. Purdy, D., J. and Kumar, J., R., “Mathematical Modeling of a Hydro-Gas Suspension Unit for Tracked Military Vehicles”, Journal of Battlefield Technology Vol. 8, No 3, November 2005.
- [12]. Siminski, P., “Aspect of Simulation and Experimental Research Studies on Wheeled Armored Fighting Vehicles with Hydropneumatic Suspension”, SAE International, 2010-01-0651 Published 04/12/2010.
- [13]. Ryu, H., Choi, J., Bae, D., “Dynamic Modeling and Experiment of Military Tracked Vehicle” SAE International, 2006 World Congress Detroit, Michigan April 3-6, 2006.
- [14]. Becker, M., Jaker, K., P., Fruhauf, F., Rutz, R., “Development of an Active Suspension System for a Mercedes-Benz Coach (O404)”, Proceedings of the 1996 IEEE International Symposium on Computer-Aided Control System Design Dearborn, MI September 15-18, 1996.
- [15]. El-Demerdash, S., M., Crolla D., A., “Hydro-pneumatic Slow-active Suspension with Preview Control”, Vehicle System Dynamics, v.25, pp. 369-386, 1996.
- [16]. Rosam, N., Darling, J., “Development and Simulation of a Novel Roll Control System for the Interconnected Hydragas® Suspension”, Vehicle System Dynamics: International Journal of Vehicle Mechanics and Mobility, v.27, No.1, pp. 1-18, 1997.
- [17]. Schumann, A., R., Anderson, R., J., “Optimal Control of an Active Anti Roll Suspension for an Off-Road Utility Vehicle Using Interconnected Hydragas Suspension Units”, Vehicle System Dynamics Supplement 37, pp 145-156, 2002.
- [18]. Joo, F., R., “Dynamic Analysis of a Hydro-pneumatic Suspension System” Concordia University, Unpublished M.Sc. Thesis, Mechanical Engineering Department, 1991.

- [19]. Cao, D., “Theoretical Analyses of Roll-And Pitch-Coupled Hydro-pneumatic Strut Suspensions”, Ph.D. Thesis, 2008, Concordia University, Canada.
- [20]. Wu, L., “Analysis of Hydro-Pneumatic Interconnected Suspension Struts in the Roll Plane Vehicle Model”, M.Sc. Thesis, 2003, Concordia University, Canada.
- [21]. Chaudhary, S., “Ride and Roll Performance Analysis of a Vehicle with Spring Loaded Interconnected Hydro-Pneumatic Suspension”, M.Sc. Thesis, 1998, Concordia University, Canada.
- [22]. Smith, W., A., Zhang, N., & Jeyakumaran J. “Hydraulically Interconnected Vehicle Suspension: Theoretical and Experimental Ride Analysis”, *Vehicle System Dynamics: International Journal of Vehicle Mechanics and Mobility*, 48:1, 41-64. 2010.
- [23]. Smith, W., A., Zhang, N., & Hu, W., *Hydraulically Interconnected Vehicle Suspension: Handling Performance*, *Vehicle System Dynamics: International Journal of Vehicle Mechanics and Mobility*, 49:1-2, 87-106, 2011.
- [24]. Ding, F., Han, X., Luo, Z., & Zhang, N., “Modeling and Characteristic Analysis of Tri-Axle Trucks with Hydraulically Interconnected Suspensions”, *Vehicle System Dynamics: International Journal of Vehicle Mechanics and Mobility*, 50:12, 1877-1904, DOI, 2012.
- [25]. Karnopp, D., Heess, G., “Electronically Controllable Vehicle Suspension”, *Vehicle System Dynamics*, v.20, pp. 207-217,1991.
- [26]. Butsuen, T., “The Design of Semi-active Suspensions for Automotive Vehicles”, PhD Thesis, Massachusetts Institute of Technology, 1989.
- [27]. Elmadany, M., M., “Optimal Linear Active Suspensions with Multivariable Integral Control”, *Vehicle System Dynamics*, v.19, pp. 313-329, 1990.
- [28]. Alleyne, A., Neuhaus, P., D., Hedrick, J., K., “Application of Nonlinear Control Theory to Electronically Controlled Suspensions”, *Vehicle System Dynamics*, v.22, pp. 309-320, 1993.
- [29]. Pielbeam, C., Sharp, R., S., “Performance Potential and Power Consumption of Slow-Active Suspension with Preview”, *Vehicle System Dynamics*, v.25, pp. 169-183, 1996.

- [30]. Thompson, A., G., Chaplin, P., M., “Force Control in Electrohydraulic Active Suspensions”, *Vehicle System Dynamics*, v.25, pp. 185-202, 1996.
- [31]. Sharp, R., S., Peng, H., “Vehicle Dynamics Applications of Optimal Control Theory”, *Vehicle System Dynamics, International Journal of Vehicle Mechanics and Mobility*, v.49, No.7, pp. 1073-1111, 2011.
- [32]. Hudha, H., Jamaluddin, H., and Samin, P., M., “Disturbance Rejection Control of a Light Armoured Vehicle Using Stability Augmentation Based Active Suspension System”, *Int. J. Heavy Vehicle Systems*, Vol.15 Nos. 2/3/4, 2008.
- [33]. Youn, I., Im, J., and Tomizuka, M., “Level and Attitude Control of the Active Suspension System with Integral and Derivative Action”, *Vehicle System Dynamics: International Journal of Vehicle Mechanics and Mobility*, Vol. 44:9, pp. 659-674, 2006
- [34]. Wang, J. and Shen, S., ‘Integrated Vehicle Ride and Roll Control via Active Suspensions’, *Vehicle System Dynamics: International Journal of Vehicle Mechanics and Mobility*, Vol. 46:S1, pp. 495-508, 2008.
- [35]. Li, H., Jing X., Karimi H., R., “Output-Feedback-Based H_{∞} Control for Vehicle Suspensions With Control Delay”, *IEEE Transactions on Industrial Electronics*, v. 61, No. 1, pp. 436-446, 2014.
- [36]. Du, H., Zhang, N., Wang, L., “Switched Control of Vehicle Suspension Based on Motion-Mode Detection”, *Vehicle System Dynamics, International Journal of Vehicle Mechanics and Mobility*, v.52, No.1, pp. 142-165, 2014.
- [37]. Montazeri-Gh, M., Kavianipour, O., “Investigation of the Active Electromagnetic Suspension System Considering Hybrid Control Strategy”, *Proceedings of the Institution of Mechanical Engineers, Part C: Journal of Mechanical Engineering Science*, v. 228, No.10, pp. 1658-1669, 2014.
- [38]. LiQiang, J., Yue, L., “Study on Self-tuning Control Strategy of Suspension Systems for Improving Vehicle Ride Performance”, *International Journal of Control and Automation*, v.7, No. 6, pp. 129-142, 2014.

- [39]. Cooke, R., Crolla, D., A., Abe, M., “Modelling Combined Ride and Handling Maneuvers for a Vehicle with Slow-Active Suspension”, *Vehicle System Dynamics*, 27:5,457-476, 1997.
- [40]. Wong, J., Y., “Theory of Ground Vehicles”, 3rd Edition, John Wiley and Sons, 2001.
- [41]. Thoresson, M., J., “Mathematical Optimization of the Suspension System of an Off-Road Vehicle for Ride Comfort and Handling”, M.Sc. Thesis, University of Pretoria, November 2003.
- [42]. Els, Ps, S., and Uys, P., E., “Investigation of the Applicability of the Dynamic-Q Optimization Algorithm to Vehicle Suspension Design”, *Mathematical and Computer Modelling*, 37, pp 1029-1046, 2003.
- [43]. Drehmer, L., R., C., Casas, W., J., P., & Gomes, H., M., “Parameters Optimisation of a Vehicle Suspension System Using a Particle Swarm Optimisation Algorithm”, *Vehicle System Dynamics*, 53:4, 449-474, 2015. DOI: 10.1080/00423114.2014.1002503.
- [44]. Naude, A., F., and Snyman, J., A., “Optimization of Road Vehicle Passive Suspension Systems. Part 1. Optimisation Algorithm and Vehicle Model”, *Applied Mathematical Modelling*, Volume 27, 249-261, 2003.
- [45]. Naude, A., F., and Snyman, J., A., “Optimization of Road Vehicle Passive Suspension Systems. Part 2. Qualification and Case Study”, *Applied Mathematical Modelling*, Volume 27, 263-274, 2003.
- [46]. Thoresson, M., J., Uys, P., E., and Snyman, J., A., “Efficient Optimization of a Vehicle Suspension System Using a Gradient-based Approximation method, Part 1: Mathematical Modelling”, *Mathematical and Computer Modelling*, 50, 1421-1436, 2009.
- [47]. Thoresson, M., J., Uys, P., E., and Snyman, J., A., “Efficient Optimization of a Vehicle Suspension System Using a Gradient-based Approximation method, Part 2: Optimization Results”, *Mathematical and Computer Modelling*, 50, 1437-1447, 2009.

- [48]. Choi, E-H., Ryoo, J-B., Cho, J-R., and Lim, O-K., “Optimum Suspension Unit Design for Enhancing the Mobility of Wheeled Armored Vehicles”, *Journal of Mechanical Science and Technology* 24 (2010) 323-330.
- [49]. Dixon, J., C., “The Shock Absorber Handbook”, Second Edition, John Wiley & Sons, 2007.
- [50]. <http://www.fox.it/eng/schedaprodotto.asp?ID=12>, 20.01.2016 [Last Accessed on 19.01.2016].
- [51]. <http://ph.parker.com/us/en/mv-9mv-needle-valve/9mv600s>, 20.01.2016 [Last Accessed on 19.01.2016].
- [52]. Friedland, B. “Advanced Control System Design”, Prentice Hall, Englewood Cliffs, N.J., 1996.
- [53]. Mracek, C., P., Cloutier, J., R., “Control Designs for the Nonlinear Benchmark Problem via the State-Dependent Riccati Equation Method”, *International Journal of Robust and Nonlinear Control*, v.8, pp. 401-433, 1998.
- [54]. Bank, H., T., Lewis, B., M., Tran, H., T., “Nonlinear Feedback Controllers and Compensators- A State Dependent Riccati Equation Approach”, *Comput. Optim. Appl.*, v.37, pp. 177-218, 2007.
- [55]. Çimen, T., “State-Dependent Riccati Equation Control- A Survey”, *Proceedings of the 17th World Congress, The International Federation of Automatic Control*, Seoul, Korea, July 6-11, 2008.
- [56]. Kanarachos, S., Alirezai, M., Jansen, S., Maurice, J-P., “Control Allocation for Regenerative Braking of Electric Vehicles with an Electric Motor at the Front Axle Using the State-Dependent Riccati Equation Control Technique”, *Proceedings of the Institution of Mechanical Engineers, Part D: Journal of Automobile Engineering*, v.228, No.2, pp. 129-143, 2014.
- [57]. Jansen, S., Alirezai, M., Kanarachos, S., “Adaptive Regenerative Braking for Electric Vehicles with an Electric Motor at the Front Axle Using the State Dependent Riccati Equation Control Technique”, *Wseas Transactions on Systems and Control*, v.9, pp. 434-447, 2014.

- [58]. Alirezai, M., Kanarachos, B., Scheepers, B., Maurice, J., P., “Experimental Evaluation of Optimal Vehicle Dynamic Control Based on the State Dependent Riccati Equation Technique”, American Control Conference (ACC) Washington, DC, USA, 2013.
- [59]. Do, T., D., Kwak, S., Choi, H., H., Jung, J., W., “Suboptimal Control Scheme Design for Interior Permanent-Magnet Synchronous Motors: An SDRE-Based Approach”, IEEE Transaction on Power Electronics, v.29, No 6, pp. 3020-3031, 2014.
- [60]. Massari, M., Zamaro, M., “Application of SDRE Technique to Orbital and Attitude Control of Spacecraft Formation Flying”, Acta Astronautica, v.94, pp. 409-420, 2014.
- [61]. Korayem, M., H., Zehfroosh, A., Tourajizadeh, H., Manteghi, S., “Optimal Motion Planning of Non-linear Dynamic Systems in the Presence of Obstacles and Moving Boundaries Using SDRE: Application on Cable-Suspended Robot”, Nonlinear Dyn v. 76, pp. 1423-1441, 2014.
- [62]. Cloutier, J., R., and Cockburn, J., C., “The State-Dependent Nonlinear Regulator with State Constraints”, Proceedings of the American Control Conference, Arlington, VA June 25-27, Vol. 1, pp. 390-395, 2001.
- [63]. Friedland, B., “On Controlling Systems with State-Variable Constraints”, Proceedings of the American Control Conference, Philadelphia, Pennsylvania, Vol. 4, pp. 2123 - 2127, June 1998.
- [64]. Kılıç, V., “Determination of Road Surface Characteristics and Random Road Surface Generation”, Unpublished ME 513 Course Term Project, Mechanical Engineering Department, Middle East Technical University, 2006.
- [65]. Terrell, W., T., “Stability and Stabilization: An Introduction”, Princeton University Press, 2009.
- [66]. Esmailzadeh, E., Fahimi, F., “Optimal Adaptive Active Suspensions for a Full Car Model”, Vehicle System Dynamics: International Journal of Vehicle Mechanics and Mobility, 27:2, 89-107, 1997.
- [67]. <https://www.otokar.com.tr/tr-tr/urunler/Sayfalar/arma-6x6.aspx> [Last Accessed on 20.09.2015].

- [68]. Arınç, F., “ME210 Applied Mathematics”, Unpublished Lecture Notes, Mechanical Engineering Department, Middle East Technical University.
- [69]. Sağlam, F., Ünlüsoy, Y., S., “Birbirine Bağlı Hidro-Pnömatik Süspansiyon Sistemlerinin Araç Performansına Etkisi”, Uluslararası Katılımlı 17. Makina Teorisi Sempozyumu, İzmir, 14-17 Haziran 2015.
- [70]. Bakker, E., Nyborg, L., and Pacejka, H., B., “Tire Modeling for Use in Vehicle Dynamics Studies”, SAE paper 870421, 1987.
- [71]. Bakker, E., Pacejka, H., B., and Lidner, L., “A New Tire Model with an Application in Vehicle Dynamics Studies”, SAE paper 890087, 1989.
- [72]. Koopman, P., “Automated Highway Systems Document Archive”, 1995, https://users.ece.cmu.edu/~koopman/ahs/ahs_objectives/ [Last Accessed on 28.02.2016].
- [73]. Shim, T., and Ghike, C., “Understanding the Limitations of Different Vehicle Models for Roll Dynamics Studies”, *Vehicle System Dynamics*, 45:3, 191-216, 2007, DOI: 10.1080/00423110600882449.
- [74]. Wang, W., and Song, Y., “A New High Dimension Nonlinear Dynamics Simulation Model for Four-Wheel-Steering Vehicle”, *Proc IMechE Part C: J Mechanical Engineering Science*, 227(1) 29–37, 2012.
- [75]. Setiawan, J., D., Safarudin, M., Singh, A., “Modelling, Simulation and Validating of 14 DOF Full Vehicle Model”, Faculty of Engineering, Diponegoro University, Semarang, Indonesia, Faculty of Mechanical Engineering, University Teknikal Malaysia Melaka, Malaysia, 2009.
- [76]. Kadir, Z., A., Hudka, K., Ahmad, F., Abdullah, M., F., Norwazan, A., R., Mohd, Fazli, M., Y., Khalid, A., J., Gunasilan, M., “Verification of 14 DOF Full Vehicle Model Based on Steering Wheel Input”, *Applied Mechanics and Materials* Vol. 165 pp 109-113, 2012.
- [77]. Vaddi, P., KR, and Kumar, C., S., “A Non-Linear Vehicle Dynamics Model for Accurate Representation of Suspension Kinematics”, *Proceedings of the Institution of Mechanical Engineers, Part C: Journal of Mechanical Engineering Science*, April 2015, vol. 229, no. 6, 1002-1014.

- [78]. Guiggiani, M., “The Science of vehicle Dynamics: Handling, Braking, and Ride of Road and Race Cars”, Springer, 2013.
- [79]. Huh, K., Kim, J., Hong, J., “Handling and Driving Characteristics for Six-Wheeled Vehicles”, Proc. Instn mech Engrs, Vol. 214, Part D, 2000.
- [80]. Williams, D., E., “Generalised Multi-Axle Vehicle Handling”, Vehicle System Dynamics: International Journal of Vehicle Mechanics and Mobility, 50:1, 149-166, 2012. DOI: 10.1080/00423114.2011.577225.
- [81]. Wang, S., Zhang, J., li, H., “Steering Performance Simulation of Three-Axle Vehicle with Multi-Axle Dynamic Steering”, IEEE Vehicle Power and Propulsion Conference [VPPC], September 3-5, 2008, Harbin, China.
- [82]. Unlusoy, Y. S., “ME513 Vehicle Dynamics”, Lecture Notes, Middle East Technical University, Mechanical Engineering Department.
- [83]. ISO, International Organization for Standardization, “ISO 2631: Evaluation of Human Exposure to Whole-Body Vibration”, 1997.
- [84]. BSI, British Standard Institution, “Guide to Measurement and Evaluation of Human Exposure to Whole-Body Mechanical Vibration and Repeated Shock”, 1987.
- [85]. Zuo, L., Nayfeh, S., A., “Low Order Continuous-Time Filters for Approximation of the ISO-2631-1 Human Vibration Sensitivity Weightings”, Journal of Sound and Vibration, 265, pp.459-465, 2003.
- [86]. The Mathworks Inc., 2013, “Matlab Global Optimization Toolbox, Genetic Algorithm”

APPENDIX A

STATE DEPENDENT MATRICES OF HALF VEHICLE MODEL WITH ACTIVE HP SUSPENSION SYSTEM

A.1. HALF VEHICLE MODEL

State space representation of the half vehicle model with HP suspension system is,

$$\dot{x} = Ax + Bu$$

State vector is

$$x = [x_1 \quad x_2 \quad x_3 \quad x_4 \quad x_5 \quad x_6 \quad x_7 \quad x_8 \quad x_9 \quad x_{10} \quad x_{11} \quad x_{12}]^T$$

Elements of the system matrix are,

$$a_{11} = \frac{-(f_{2L} + f_{2R})}{M}$$

$$a_{12} = -\frac{t(f_{2L} - f_{2R})}{2M}$$

$$a_{13} = \frac{f_{1L}}{M}$$

$$a_{14} = \frac{f_{1R}}{M}$$

$$a_{19} = \frac{f_{2L}}{M}$$

$$a_{1_{-10}} = \frac{f_{2R}}{M}$$

$$a_{21} = \frac{-t(f_{2L} - f_{2R})}{2I_{xx}}$$

$$a_{22} = \frac{-t^2(f_{2L} + f_{2R})}{4I_{xx}}$$

$$a_{23} = \frac{tf_{1L}}{2I_{xx}}$$

$$a_{24} = -\frac{tf_{1R}}{2I_{xx}}$$

$$a_{29} = \frac{tf_{2L}}{2I_{xx}}$$

$$a_{2_{-10}} = -\frac{tf_{2R}}{2I_{xx}}$$

$$a_{31} = 1$$

$$a_{32} = \frac{t}{2}$$

$$a_{39} = -1$$

$$a_{41} = 1$$

$$a_{42} = -\frac{t}{2}$$

$$a_{4_{-10}} = -1$$

$$a_{51} = 1$$

$$a_{52} = \frac{t}{2}$$

$$a_{59} = -1$$

$$a_{61} = 1$$

$$a_{62} = -\frac{t}{2}$$

$$a_{6_{-10}} = -1$$

$$a_{79} = 1$$

$$a_{8_{-10}} = 1$$

$$a_{91} = \frac{f_{2L}}{M_t}$$

$$a_{92} = \frac{tf_{2L}}{2M_t}$$

$$a_{93} = -\frac{f_{1L}}{M_t}$$

$$a_{97} = -\frac{k_t}{M_t}$$

$$a_{99} = -\frac{f_{2L}}{M_t}$$

$$a_{10_{-1}} = \frac{f_{2R}}{M_t}$$

$$a_{10_{-2}} = -\frac{tf_{2R}}{2M_t}$$

$$a_{10_{-4}} = -\frac{f_{1R}}{M_t}$$

$$a_{10_{-8}} = -\frac{k_t}{M_t}$$

$$a_{10_{-10}} = -\frac{f_{2R}}{M_t}$$

$$a_{11_{-5}} = 1$$

$$a_{12_{-6}} = 1$$

Other elements, which are not written here, are zero. Control input matrix is

$$\mathbf{B} = \begin{bmatrix} 0 & 0 & -\frac{1}{A_p} & 0 & 0 & 0 & 0 & 0 & 0 & 0 & 0 & 0 \\ 0 & 0 & 0 & -\frac{1}{A_p} & 0 & 0 & 0 & 0 & 0 & 0 & 0 & 0 \end{bmatrix}^T$$

Control input vector is

$$\mathbf{u} = [Q_{inL} \quad Q_{inR}]^T$$

CURRICULUM VITAE

FERHAT SAĞLAM

CONTACT INFORMATION:

Residence Address: Ergazi Mahallesi, Akkent Yuvam Sitesi, C/11, 06370 Batıkent, Yenimahalle, Ankara-Turkey

Work Address: ASELSAN Inc., Yenimahalle, Ankara-Turkey

Home Tel: (312) 251 6580 **Work Tel:** **Mobile:** (535) 421 6948

E-mail: fesaglam@gmail.com

PERSONAL INFORMATION:

Date of Birth : 02.05.1984

Place of Birth : Ankara-Turkey

Marital Status : Single

EDUCATION:

B.Sc:

2002-2007 : Middle East Technical University, Mechanical Engineering Department 3.70/4.00

M.Sc

2007-2010 : Middle East Technical University, Mechanical Engineering Department 3.71/4.00

Thesis: Identification of Low Order Vehicle Handling Models from Multibody Dynamics Vehicle Models

Ph.D

2010-2016 : Middle East Technical University, Mechanical Engineering Department 3.94/4.00

Thesis: Optimization of Ride Comfort for Vehicles Equipped with Passive and Active Hydro-Pneumatic Suspensions

WORK EXPERIENCE:

2013- : ASELSAN Inc., Mechanical Design Engineer

2007-2013: Research and Teaching Assistant, Middle East Technical University, Mechanical Engineering Department

July 2006 : Summer Practice, Barış Elektrik A.Ş.

July 2005 : Summer Practice, Türk Traktör ve Ziraat Makinaları A.Ş.

FOREIGN LANGUAGES

English Reading: Advanced
 Writing: Advanced
 Speaking: Advanced

German: Reading: Beginner
 Writing: Beginner
 Speaking: Beginner

COMPUTER SKILLS:

Matlab : Advanced
Matlab/Simulink : Advanced
Mathcad : Advanced
MSC ADAMS : Advanced

PUBLICATIONS:

Journals

- 1) Sağlam, F. and Unlusoy, Y. S. "State Dependent Riccati Equation Control of an Active Hydro-Pneumatic Suspension System", Journal of Automation and Control Research, Vol. 1, pp. 1-10, 2014.
- 2) Sağlam F., Unlusoy, Y. S., "Adaptive Ride Comfort and Attitude Control of Vehicles Equipped With Active Hydro-Pneumatic Suspension", International Journal of Vehicle Design, (Accepted and Waiting for Publication)

Conferences

- 1) Sağlam, F., Ünlüsoy, Y. S., "Identification of Low Order Vehicle Handling Models from Multibody Vehicle Dynamics Models", ICM 2011 IEEE International Conference on Mechatronics, April 2011, İstanbul.
- 2) Sağlam, F., Ünlüsoy, Y. S., "Hidro-Pnömatik Süspansiyon Sistemlerinin Modellenmesi", VI. Ulusal Hidrolik Pnömatik Kongresi ve Sergisi (HPKON) Bildiri Kitabı, s. 245-259, 12-15 Ekim 2011, İzmir.
- 3) Sağlam, F., Ünlüsoy, Y. S., "Optimization of Hydropneumatic Suspension System Parameters for Ride Comfort", 2nd International Scientific Conference on Engineering "Manufacturing and Advanced Technologies", MAT 2012, pp. 173-176, 22-24 November, 2012, Antalya.
- 4) Sağlam, F., Ünlüsoy, Y. S., "A Hybrid Skyhook-Groundhook Control for Semi-Active Quarter Car Model with Hydropneumatic Suspension". 20th International Congress on Sound and Vibration, ICSV20 Bangkok, Thailand, 7-11 July 2013.
- 5) Sağlam, F., Ünlüsoy, Y. S., "Modelling and State Dependent Riccati Equation Control of an Active Hydro-Pneumatic Suspension System." Proceedings of the International Conference of Control, Dynamic Systems, and Robotics Ottawa, Ontario, Canada, May 15-16 2014 Paper No. 31
- 6) Sağlam, F., Ünlüsoy, Y. S., "Hidro-Pnömatik Süspansiyonlu Araçlar İçin Tümüleşik Sürüş Konforu Ve Yükseklik Kontrolü" OTEKON'14 7. Otomotiv Teknolojileri Kongresi 26 – 27 Mayıs 2014, BURSA.

- 7) Saęlam, F., Ünlüsoy, Y., S., “Birbirine Baęlı Hidro-Pnömatik Süspansiyon Sistemlerinin Araç Performansına Etkisi”, Uluslararası Katılımlı 17. Makina Teorisi Sempozyumu, İzmir, 14-17 Haziran 2015.
- 8) Saęlam, F., Ünlüsoy, Y., S., “Analysis and Design of Passive and Active Interconnected Hydro-Pneumatic Suspension Systems in Roll Plane”, ICENS 2015, International Conference on Engineering and natural Science, 15-19 May 2015, Skopje.

INTEREST:

Basketball, swimming, reading, travelling,